In vitro and *in vivo* Characterization of FimH Antagonists for Anti-Adhesion Therapy – An Alternative Therapeutic Approach Against Urinary Tract Infection

Inauguraldissertation
zur
Erlangung der Würde eines Doktors der Philosophie
vorgelegt der
Philosophisch-Narurwissenschaftlichen Fakultät
der Universität Basel

von

Daniela Abgottspon

aus
Staldenried, Wallis, Schweiz

Basel, 2014

Genehmigt von der Philosophisch-Naturwissenschaftlichen Fakultät

Auf Antrag von

Prof. Dr. Beat Ernst, Universität Basel
Prof. Dr. med. Niels Frimodt-Møller, Hvidovre Hospital, Denmark

Basel, den 11. Dezember 2012

Prof. Dr. Jörg Schibler

ACKNOWLEDGEMENTS

There are numerous people that I gratefully would like to acknowledge for their contributions and support through my dissertation in the past four years.

First, my sincere thanks go to my supervisor Prof. Dr. Beat Ernst for his valuable support, guidance and enthusiastic encourgement during my projects, and for giving me the freedom to explore my own ideas throughout my work. I am also very thankful that I got the opportunities to collaborate and to meet with other scientist during conferences all over the world. It gave me valuable insights and knowledge for the progress of my projects and also for my future.

I would like to thank Prof. Dr. Niels Frimodt-Møller for giving me the opportunity to stay in his lab at the Statens Serum Institute in Copenhagen where I was introduced into the UTI mouse model. Although it was in January I had an excellent time there, especially because of the great hospitalit of the people in your lab.

A special thank goes to Prof. Dr. Skoda who took over the responsibility for the *in vivo* studies at the Departement of Biomedicine at the University Hospital in Basel. His help was essential for the studies throughout my work.

I would also like to thank the co-authors for their help, discussions, contributions and encouragements during the writing phase of to the publications, which were part of my project and presented in this dissertation.

Furthermore, I would like to thank all present and past members of the IMP for the fantastic working and social environment.
I would like to thank Meike Scharenberg for her great help during our common projects and also for beeing a good, patient and helpful friend. I thank Simon Kleeb and Matthias Wittwer for their endless patience explaining and helping me during the MS measurements. Many thanks also to Roland Preston, who helped me establishing a B2 lab at the IMP. Furthermore, I would like to thank the chemists Xiaohua Jiang, Oliver Schwardt, Lijuang Pang and Wojciech Schönemann who provided me with huge amounts of compounds for the *in vivo* experiments. I would

also like to thank Martin Smiesko for his help when I had problems with computer programs or with my camera.

I wish to acknowledge my former master students Gina Rölli, Evelin Cicek, Sirin Zur Werra, Sabine Zimmermann and Pasqual Bichsel for their great commitment, support and patience during their work.

I also wish to thank my former supervisor Dr. Andrej Trampuz and colleagues in Lab 314 at the Departement of Biomedicine at the University Hospital in Basel. Daniela Baldoni, Anne-Kathrin Woischnig, Ivana Cvjietic-Majic, Andrea Steinhuber I would like to thank for their great help and intruduction into the work with B2 pathogens. I wish to thank Brigitte Schneider and Zarko Rajacic for their valuable technical support and suggestions on my project. Furthermore, I would like to thank all my former colleagues for the great working atmosphere in the tiny lab we shared.

I would like to offer my special thanks to Dr. Klaus Jensen who helped me planing and evaluating the *in vivo* PK/PD studies and who patiently discussed and answered all my questions.

I would also like to thank Ueli Schneider and his team in the animal facility at the Departement of Biomedicine at the University Hospital in Basel for taking care of the mice and for helping me when I needed their advice.

Finally, on a more personal level, I would like to thank my family and friends for their never einding patience, support and understanding during busy times at my work. I would like to express my deepest gratitute to Marc for his patient love, support, encouragement and help during the past few years and during stressful times. In the same way I would like to thank my family for their unresting support and understanding during the last few years with everything I did. Thank you!

TABLE OF CONTENTS

ABBREVIATIONS

AHL	Acyl-homoserine lactone
CFU	Colony forming unit
CRD	Carbohydrate recognition domain
EAEC	Enteroaggregative *Escherichia coli*
EF	Edema factor
EHEC	Enterohaemorrhagic *Escherichia coli*
EIEC	Enteroinvasive *Escherichia coli*
EPEC	Enteropathogenic *Escherichia coli*
ETEC	Enterotoxigenic *Escherichia coli*
ExPEC	Extraintestinal pathogenic *Escherichia coli*
DAEC	Diffusely adherent *Escherichia coli*
ELISA	Enzyme linked immunosorbent assay
GFP	Green fluorescence protein
HRP	Horseradish peroxidase
ICU	Intensive care unit
IDSA	Infectious Diseases Society of America
i.p.	Intraperitoneal
i.v.	Intravenous
ITC	Isothermal titration calorimetry
LF	Lethal factor
MDR	Multidrug-resistant
NMEC	Neonatal meningitis *Escherichia coli*
PAI	Pathogenicity island
PD	Pharmacodynamic
PDR	Pandrug-resistant
PK	Pharmacokinetic
p.o.	Peroral
QS	Quorum sensing
s.c.	Subcutaneous
SPR	Surface plasmon resonance
T3SS	Type III secretion system
TEM	Transmission electron microscopy

THP	Tamm-horsfall protein
TMP-SMZ	Trimethoprim-sulfamethoxazole
UPIa	Uroplakin Ia
UPEC	Uropathogenic *Escherichia coli*
UTI	Urinary tract infection

LIST OF PUBLISHED PAPERS, REVIEWS AND MANUSCRIPTS

The present dissertation is based on the following papers and unpublished manuscripts, which are presented in the results and discussion chapter.

Paper I

Abgottspon D, Rölli G, Hosch L, Steinhuber A, Jiang X, Schwardt O, Cutting B, Smiesko M, Jenal U, Ernst B, Trampuz A. Development of an Aggregation Assay to Screen FimH Antagonists. *J. Microbiol. Methods* **2010**, 82, 249.

Paper II

Klein T*, Abgottspon D*, Wittwer M*, Rabbani S*, Herold J*, Jiang X, Kleeb S, Lüthi C, Scharenberg M, Bezençon J, Gubler E, Pang L, Smiesko M, Cutting B, Schwardt O, Ernst B. FimH Antagonists for the Oral Treatment of Urinary Tract Infections: From Design and Synthesis to *in vitro* and *in vivo* Evaluation. *J. Med. Chem.* **2010**, 53, 8627.

* These authors contributed equally to the project.

Paper III

Scharenberg M, Abgottspon D, Ciceck E, Jiang X, Schwardt O, Rabbani S, Ernst B. A Flow Cytometry-Based Assay for Screeining FimH Antagonists. *Assay Drug Dev. Technol.* **2011**, 9, 455.

Paper IV

Schwardt O, Rabbani S, Hartmann M, Abgottspon D, Wittwer M, Kleeb S, Zalewski A, Smiesko M, Cutting B, Ernst B. Design, Synthesis and Biological Evaluation of Mannosyl Triazoles as FimH Antagonists. *Bioorg. Med. Chem.* **2011**, 19, 6454.

Paper V

Jiang X*, Abgottspon D*, Kleeb S*, Rabbani S, Scharenberg M, Wittwer M, Haug M, Schwardt O, Ernst B. Antiadhesion Therapy for Urinary Tract Infections – A Balanced PK/PD Pofile Proved to be Key for Success. *J. Med. Chem.* **2012**, 55, 4700.

* These authors contributed equally to the project.

Review

Abgottspon D, Ernst B. *In vivo* Evaluation of FimH Antagonists – A Novel Class of Antimicrobials for the Treatment of Urinary Tract Infection. *Chimia (Aarau)* **2012**, 66, 166.

Submitted manuscript

Simon Kleeb*, Lijuan Pang*, Katharina Mayer*, Deniz Eris*, Anja Sigl, Roland C. Preston, Pascal Zihlmann, Timothy Sharpe, Roman P. Jakob, Daniela Abgottspon, Aline S. Hutter, Meike Scharenberg, Xiaohua Jiang, Giulio Navarra, Said Rabbani, Martin Smiesko, Nathalie Lüdin, Jacqueline Bezencon, Oliver Schwardt, Timm Maier, Beat Ernst. FimH Antagonists - Bioisosteres to Improve the *in vitro* and *in vivo* PK/PD Profile. Manuscript submitted to: J. of Medicinal Chemistry (October 2014).
*These authors contributed equally tot he project.

Manuscript I

Abgottspon D, Schwardt O, Kleeb S, Scharenberg M, Ernst B. Anti-Adhesion Beats Killing - *In vivo* Activity of a FimH Antagonist Against UTI in Comparison to Antibiotic Treatment.

Manuscript II

Abgottspon D, Skovbo Jensen K, Jiang X, Ernst B. *In vivo* Pharmacokinetic/Pharmacodynamic Evaluation of JXH2372 – A Biphenyl FimH Antagonist for the Prevention of Urinary Tract Infection.

Manuscript III

Scharenberg M*, Abgottspon D*, Zimmermann S, zur Werra S, Preston R, Rabbani S, Ernst B. Characterization of Type 1 Pili-Dependent Binding Properties of Clinical Uropathogenic *Escherichia coli* Isolates.
* These authors contributed equally to the project.

ABSTRACT AND AIM

Uropathogenic *Escherichia coli* (UPEC) are the major cause of urinary tract infections (UTI), which is one of the most common infectious disease worldwide. Women belong to the most affected population, with every second woman experiencing at least one symptomatic UTI during her lifetime. Additionally, UTI is a major problem in the clinics, being the most common hospital acquired infection. To avoid complications like kidney infections, irreversible kidney damage or urosepsis, all symptomatic infections should be treated with antibiotics. The use of antibiotics for the treatment of UTI, is continuosly increasing the development of resistant pathogens against most of the currently available antimicrobials. Therefore, new treatment strategies targeting alternative mechanisms are urgently needed, avoiding selection pressure on bacteria and thereby implying a reduced risk of resistance.

An alternative approach for the treatment of UTI is the anti-adhesion therapy using FimH antagonists. FimH is an adhesin, located on the distal tip of type 1 pili, expressed on the surface of UPEC. The type 1 pilus contains a carbohydrate recognition domain, binding to mannose glycans expressed on urothelial cells. This allows UPEC to adhere to and to invade host cells within the urinary tract epithelium and is the initial step for a successful establishment of a UTI.

FimH antagonists are highly active anti-adhesion molecules, targeting the virulence factor FimH. *In vitro* and *in vivo* studies clearly indicate the potential of FimH antagonists for the prevention and treatment of UTI, with a higher therapeutic efficacy compared to antibiotics.

The anti-adhesion therapy is focusing on the development of a new class of antimicrobials exhibiting less selection pressure and therefore a reduced potential for the emergence of resistance. In addition, a reduction of the antibiotic associated side effects (e.g. the disruption of the commensal microbiota) is expected. Thus, the availability of a novel class of antimicrobials based on an alternative mode of action would have a huge impact on the treatment of UTI, being a substantial contribution to public health.

The aim of this thesis was to evaluate the therapeutic potential of FimH antagonists in the UTI mouse model. In order to select a candidate for *in vivo* studies, the activity in cell-based assays had to be evaluated first. Following aims were investigated throughout my thesis:

- The development of a cell-based assay, quantitatively measuring the aggregation potency of UPEC with yeast or guinea pig erythrocytes, respectively.

- The development of a cell-based assay, measuring the adhesion rate of GFP-labeled *E. coli* with human bladder carcinoma cells.

- The establishment of the UTI mouse model followed by the evaluation of the therapeutic efficacy of selected FimH antagonists for their *in vivo* pharmacokinetic and pharmacodynamic properties.

- Evaluation of the PK/PD profile of a FimH antagonist in the UTI mouse model.

INTRODUCTION

Antimicrobial Chemotherapy – History and Current Problems

The discovery of β-lactam antibiotics in the 1930s as well as the introduction of hygienic standards in hospitals (hand washing, use of disinfectants) were incisive steps in the development of public healthcare. Humans gained control over a 10^7 times smaller organism and the mortality from bacterial infections rapidly diminished and concomitantly also the interest to develop new antimicrobials. However, shortly after it was assumed that bacterial infections are under control, the first emergence of resistant strains evolved. The ability of our tiny cohabitants to adapt to new living conditions was severely underrated and only insufficient efforts were undertaken to contain the emerging bacterial threat with new antibiotics [1]. Therefore, since the 1990s, infectious diseases developed to the top five causes of death in high-income countries [2].

The majority of the classes of antimicrobials still used today have their origin in the 1940s to 1970s (Figure 1 top) [3]. Although numerous chemically modified derivatives entered the market in recent years, real innovation only occurred in the last 10 years when new classes of antibiotics were approved for clinical use (oxazolidinones, lipopeptides and mutilins) [4, 5]. The diminished interest to develop new antibiotics and the rapidly increasing emergence of resistance led to the highly prevalent problem that for an increasing number of multidrug-resistant (MDR) and pandrug-resistant (PDR) bacteria no effective therapeutic treatment is available [5].

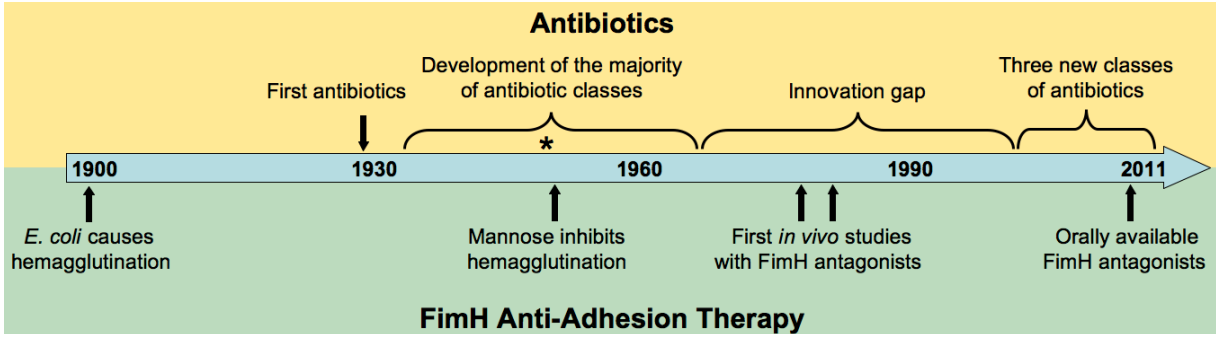

Figure 1. Timeline of the major steps of the development of antibiotics (top [5]) and the FimH anti-adhesion therapy for the treatment of urinary tract infection (UTI) (bottom [6 – 9, **Paper II**, 10]). The asterisk (*) is indicating the time when the first pharmacokinetic/pharmacodynamic (PK/PD) concept was described [11].

Originally, antibiotics were developed to kill or inhibit bacterial growth, by targeting functions, which are essential for their survival (Figure 2 A). Although the traditional mode of action of antibiotics proved to be highly effective, their threat forced bacteria to evolve survival strategies like the development of resistance [12]. An essential cause for the emergence of antimicrobial resistance is the extensive use of antibiotics, leading to treatment failure, a reduced range of therapeutic options for consecutive bacterial infections and ultimately a serious threat for the patient [13, 14]. Thus, there is an alarming rise of antimicrobial resistance against fluoroquinolones, which are highly effective and commonly used as a 3-day standard treatment for acute uncomplicated urinary tract infection (UTI). Therefore, the Infectious Diseases Society of America (IDSA), recommend to limit the use of fluoroquinolones for more severe infections than uncomplicated UTIs. With this guideline the IDSA hope to reduce not only fluoroquinolone resistant uropathogens, but also other more pathogenic and difficult-to-treat microorganisms [15]. Therefore, the search for alternative treatment options against infectious diseases is indispensable.

Bacterial Virulence – A Target for Antimicrobial Chemotherapy

A successful pathogen-host interaction is crucial for microorganisms to survive in the hostile host environment and to establish an infection. Bacteria have developed multiple virulence factors to ensure their survival in various and varying environments (e.g. quorum sensing, adhesins, toxins, iron acquisition systems, protectins, lipopolysaccharide proteases, biofilms, hemolysins, secretion systems, capsules [16, 17]). Many virulence factors are involved in the initial steps of the bacterial interaction with the host and they are essential for the establishment of an infection. Therefore virulence mechanisms are potential new targets for the development of antibacterial agents [18]. Selected currently pursued approaches and perspectives of anti-virulence therapies are listed below.

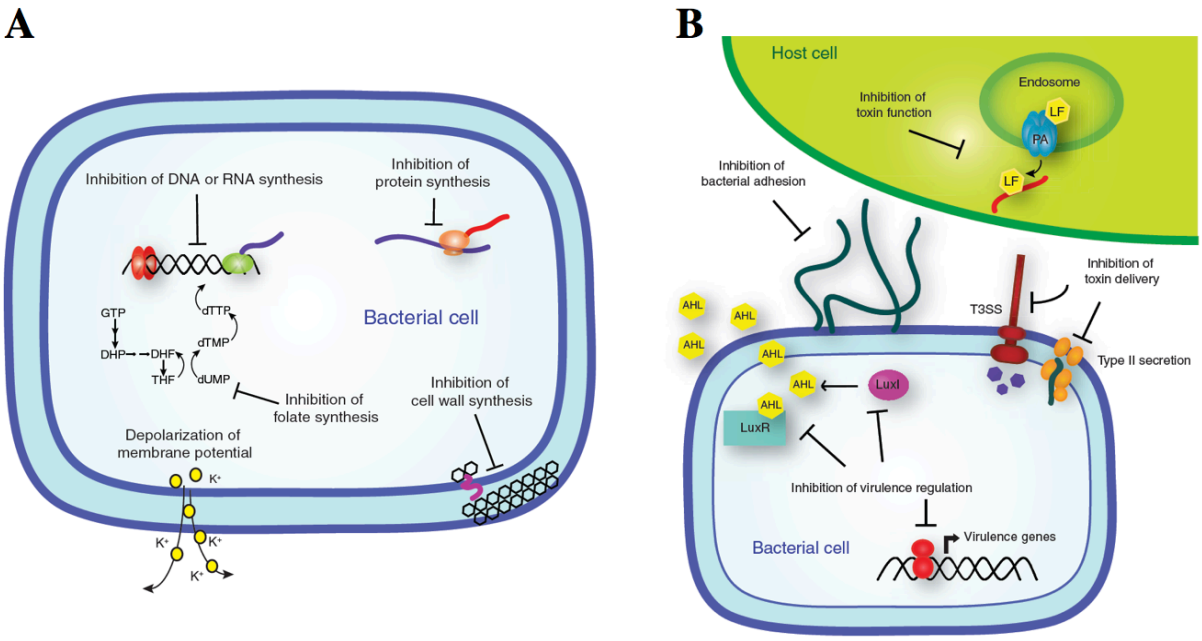

Figure 2. Targets for antimicrobial chemotherapy. **A.** Traditional antimicrobial targets, either acting bacteriocidal or bacteriostatic. They inhibit essential bacterial functions: cell wall synthesis (e.g. β-lactams), DNA replication (e.g. flouroquinolones), RNA transcription (e.g. tetracyclines), protein (e.g. aminoglycosides) or folate (e.g. sulfa drugs) synthesis. **B.** Targets for anti-virulence therapy. Toxin function and delivery can be prevented by inhibition of type II or type III (T3SS) secretion, respectively or by inhibition of the effect of lethal factor (LF), edema factor (EF) and protective antigen (PA). Disturbance of virulence gene regulation can either be achieved by quorum sensing (QS) alteration (e.g. acyl-homoserine lactone (AHL)-mediated QS by interference with LuxI or LuxR homologs) or by down-regulation of virulence gene expression on the transcriptional level. Bacterial adhesion to host cells can either be inhibited by pilus degradation (e.g. pilicides) or by inhibition of bacterial adhesion (e.g. FimH antagonists for type 1 pili mediated adhesion) [12].

Targeting toxin function and delivery. Toxins are proteins produced by bacteria to damage host cells and usually result in cell death or disruption of signal transduction. Three approaches are pursued in targeting bacterial toxins; first, attenuation of the toxin activity using antibodies (e.g. against *Corynebacterium diphteriae*, *Clostridium botulinum* or *Clostridium tetani* toxins) [12] or small molecules (e.g. hydroxymate from Merck, inhibiting lethal factor (LF) protease activity against *Bacillus anthracis* toxin [19]); second, modification of the host response to the toxin (e.g. thiazolidinone to inhibit Cl^- dependent intestinal fluid secretion against the effect of *Vibrio cholerae*

toxin) and third, inhibition of toxin delivery to the target site (e.g. cholestyramine binding and inactivating *Clostridium difficile* toxin) [20] (Figure 2 B).

Targeting virulence expression. A further approach in anti-virulence therapy is to directly inhibit the expression of the essential structures or mechanisms needed by microorganisms to establish an infection. A widely used target is the interference with bacterial quorum sensing (QS). QS is a chemically mediated cell-cell signaling mechanism, that enables bacteria to interact with their environment and to react upon changes with the expression of different genes (e.g. for bioluminescence, biofilm formation, signaling) or virulence factors (e.g. proteases, adhesins, toxins) [12, 21, 22] (Figure 2 B). Three approaches are used for targeting QS mechanisms; first, inhibition of the QS molecules producing enzymes (e.g. LuxI homologs in *Pseudomonas aeruginosa*) [23]; second, degradation of QS molecules (e.g. acyl-homoserine lactone (AHL) in *Bacillus* spp.) [24] and third, antagonizing the QS initiated transcription cascade (e.g. LuxR homologs in *P. aeruginosa*) (Figure 2 B) [25, 26].
Additional targets are transcriptional regulators, which are involved in the expression of various genes, e.g. adhesins, toxin production or secretion. One example is the small molecule virstatin, inhibiting two virulence mechanisms of *V. cholerae*, toxin-coregulated pili and cholera toxin, respectively, protecting mice from intestinal colonization [27].

Targeting adhesion. An important virulence mechanism for infecting bacteria are adhesive structures (fimbriae or pili), being the first direct cell-cell contact of the invading pathogen with the host (Figure 2 B and Figure 5 infection step 1.). Several well-known adhesins, recognizing carbohydrate structures on mucosal epithelial cell surfaces, are essential for pathogenesis in many bacterial species (e.g. *Helicobacter pylori, P. aeruginosa, Escherichia coli, Klebsiella pneumoniae*) [28 - 30]. Two approaches are followed in the development of anti-adhesive strategies; either, inhibition of pili or fimbriae formation (e.g. inhibition of the chaperone usher pathway in *E. coli* using bicyclic 2-pyridones as pilicides) [31] or inhibition of pili mediated pathogen-host interaction (e.g. inhibition of type 1 pili mediated bacterial adhesion using FimH antagonists) [32].

Urinary Tract Infection and Uropathogenic *Escherichia coli*

Urinary tract infection (UTI) is one of the most common bacterial infection worldwide. Women are the most affected population and every second woman will experience at least one UTI during her lifetime. Furthermore, catheter-associated UTI accounts for the most common hospital acquired (nosocomial) infection and UTI is the third most acquired infection in intensive care units (ICUs) in Europe [33]. Although UTI is not a life threatening disease, all symptomatic infections should be treated with antibiotics to prevent potential devastating complications, like kidney infections (pyelonephritis), irreversible kidney damage and dissemination from the kidneys to the bloodstream (urosepsis) [34].

The leading pathogen causing UTI is uropathogenic *E. coli* (UPEC), responsible for over 90% of all infections [35]. Bacteria invade the bladder via the urethra from outside. The most common source for *E. coli* is the host's own bowel flora [36], furthermore UPEC may be transmitted via ingestion of contaminated food [37, 38] or occasionally also by sexual transmission [39].

Although *E. coli* is a symbiotic inhabitant of the gastrointestinal tract, it is able to shape its genome by horizontal gene transfer in a pathogenic manner to cause various diseases in different niches. The gain and loss of mobile genetic elements like pathogenicity islands (PAIs), transferring virulence genes, can shape the genome of *E. coli* into different pathovars. Eight intensively studied *E. coli* pathovars are known, which can be divided in two main groups; diarrhoeagenic *E. coli* (responsible for intestinal diseases) and extraintestinal pathogenic *E. coli* (ExPEC). The following pathovars belong to the first group: enteropathogenic *E. coli* (EPEC), enterohaemorrhagic *E. coli* (EHEC), enteroinvasive *E. coli* (EIEC), enterotoxigenic *E. coli* (ETEC), enteroaggregative *E. coli* (EAEC) and diffusely adherent *E. coli* (DAEC). Two pathovars, uropathogenic *E. coli* (UPEC) and neonatal meningitis *E. coli* (NMEC), are responsible for extraintestinal infections [40]. All of the above mentioned pathovars have their origin in the commensal flora of the intestinal tract and, depending on their acquired PAIs, they can diverge into different pathovars and colonize different niches in the human host (Figure 3).

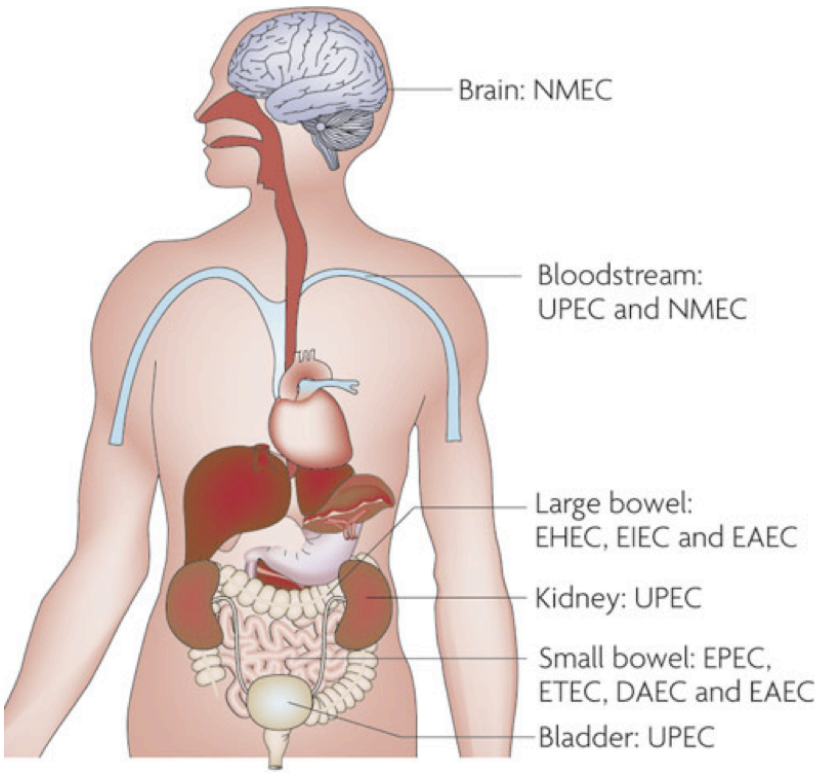

Figure 3: Sites of infection of different *E. coli* pathovars in humans. Extraintestinal pathogenic *E. coli* (ExPEC) cause diseases outside the intestinal tract: uropathogenic *E. coli* (UPEC) express distinctive adhesins to colonize the urinary tract and if left untreated can lead to urosepsis; neonatal meningitis *E. coli* (NMEC) is able to cross the blood brain barrier and cause meningitis in newborn children. Diarrhoeagenic *E. coli* cause intestinal diseases: enterohaemorrhagic *E. coli* (EHEC) and enteroinvasive *E. coli* (EIEC) colonize the large bowel; enteroaggregative *E. coli* (EAEC) colonize both, the large and the small bowel; enteropathogenic *E. coli* (EPEC), enterotoxigenic *E. coli* (ETEC) and diffusely adherent *E. coli* (DAEC) colonize the small bowel, causing diarrhea [40].

UPEC colonize the normally sterile urinary tract in an ascending manner. The decisive virulence mechanism of UPEC colonization is their adhesion capability, using filamentous multi-subunit membrane proteins (pili or fimbriae) [41]. The first and most important pili employed for the initial entry into the urethra (urethritis) and the bladder (cystitis) are type 1 pili (Figure 4 and Figure 6), where the mannose-dependent attachment to the glycosylated uroplakin Ia (UPIa) present on bladder cells is mediated by the fimbrial adhesin H (FimH) (Figure 5, infection step 1.). Furthermore, expression of flagella is important for the continuative ascension through the urethers into the kidneys (pyelonephritis) [42], where the adhesion is specifically mediated via P pili in a galactose dependent manner [40, 43, 44].

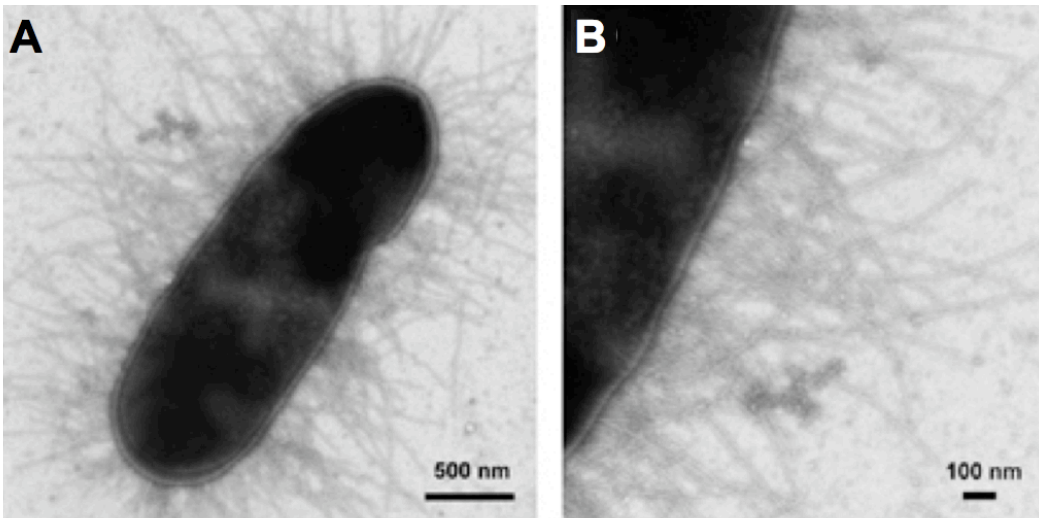

Figure 4: Uropathogenic *E. coli* (UPEC) expressing type 1 pili (transmission electron micrographs, **A** at a magnification of 34'000 and **B** at a magnification of 64'000) [45].

Adhesion can enhance the fitness of UPEC in multiple ways. First, the initial attachment prevents the rapid clearance of *E. coli* from the urinary tract by the bulk flow of urine and at the same time initiates the infection process [29]. Second, adhesion is activating bacterial cell signaling and third, it enables the transfer of bacterial products to the host cells, which finally leads to the bacterial invasion into the superficial bladder cells (Figure 5, infection step 2.) [46]. Once within the bladder cells, bacteria can either start to replicate or to form intracellular biofilms (Figure 5, infection step 3.), where they are well-protected from host defense and antibiotic treatment. Bacteria can persist in the intracellular biofilms for weeks or months and are a possible source for recurrent UTIs. In a later stage, bacteria are able to either efflux from superficial bladder cells and at the same time disseminate and invade other cells or penetrate deeper into the underlying tissue cells (Figure 5, infection steps 4. and 5.) [47].

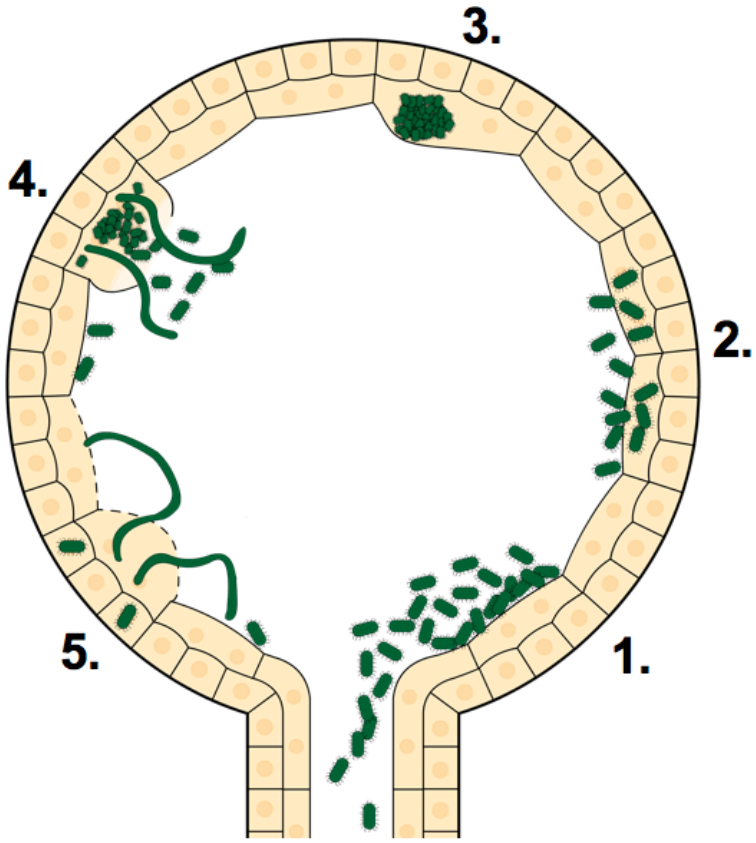

Figure 5. Schematic overview of the urinary tract infection cycle. 1. The first and most important step in the development of UTI is the type 1 pili dependent adhesion of UPEC (green) to uroplakin Ia (UPIa) on urothelial cells. 2. Adhesion triggers the invasion of the bacteria into the superficial bladder cells, lining the urinary tract. Once inside the cells, bacteria start to replicate and form 3. intracellular biofilms, where they are well protected from the host defense mechanisms and antibiotic treatment. 4. Later on, cells start to exfoliate and bacteria exit the cells in filamentous structures and 5. disperse in the environment ready to infect new cells (infection cycle adapted from Ref 47).

UPEC employ various virulence mechanisms to ensure their persistence in the urinary tract, which are upregulated during the infection process in the host. Although the most extensively studied virulence factor are type 1 pili, UPEC evolved further survival strategies, like the release of various toxins (hemolysin, cytotoxic necrotizing factor 1 and secreted autotransporter toxin) to damage the host epithelium [48], the production of polysaccharide capsules and immunosuppressive proteins to evade host immune response [49], and the expression of iron acquisition systems (e.g. iron uptake transport IutA) to survive in the iron-limited environment of the urinary tract [17, 50].

Also host defense evolved several self-protecting mechanisms for the defence against invading microorganisms. The main host strategies to defend the urinary tract are the bulk flow of urine to clear unattached bacteria, FimH dependent exfoliation of infected umbrella cells lining the bladder and production of inflammatory cells by activation of proinflammatory genes [51].

FimH – A Target for Anti-Adhesion Therapy

Adhesion of UPEC to carbohydrate structures on urothelial cell surfaces is mediated via the lectin FimH. Lectins are carbohydrate-binding proteins, being an evolutionary conserved cell-cell recognition strategy [52, 53]. The four subunits FimA, FimF, FimG and FimH compose a type 1 pilus, which is approximately 1 – 2 μm long (Figure 6) [54]. The pilus is built by a 6.9 nm wide rod, formed by a series of right-handed, helical sequences of FimA subunits. The tip fibrillum is composed of several copies of FimF and FimG subunits, concluding with a FimH subunit. As a part of the FimH subunit, a carbohydrate-recognition domain (CRD) is responsible for bacterial attachment to oligomannosides of the integral membrane glycoprotein uroplakin Ia (UPIa) located on the surface of the urinary bladder cells [55, 56]. Type 1 pili are assembled by the chaperone-usher pathway (Figure 6) [57]. The periplasmatic biogenesis is mediated via a protein-folding catalyst, the chaperone FimC, binding and transporting the pilus subunits to the outer membrane. On the assembly platform in the outer membrane, subunits dissociate from FimC, followed by the assembly of the subunits via the usher FimD, translocating and anchoring the pili to the bacterial cell surface [58].

Bacterial adhesins usually exhibit a relatively low affinity to their target structures in the millimolar range. Therefore, bacteria developed several mechanisms to overcome the low adhesion capability by clustering of adhesins on their surface, or in the case of UPEC by expression of a high number of adhesins (100 - 400 pili per bacterium) as well as sheer force enhanced binding capacity [59, 60]. The latter enables UPEC to resist the first line defense of the host, the urine flow, generating sheer stress for the bacteria, which tightens their FimH dependent attachment to UPIa on the bladder cells [61].

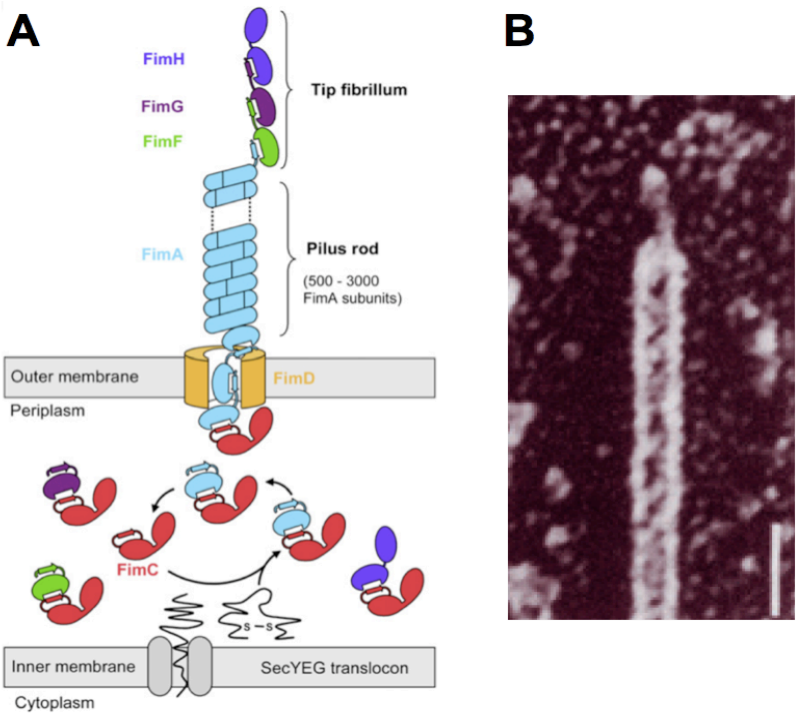

Figure 6. A. Schematic representation of the type 1 pilus assembly by the chaperone-usher pathway. The long and rigid fibrillum rod is composed of thousands of FimA subunits. The thin and flexibal tip fibrillum consists of the subunits FimF, FimG, and the adhesin FimH. The periplasmatic chaperone FimC binds intracellular to each subunit, catalyzing folding of the subunits, which are translocated by the Sec apparatus, located in the inner membrane. The subunits are delivered to the assembly platform FimD (usher) in the outer membrane, which forms a channel, allowing the pilus subunits to be assembled and expressed on the bacterial surface [62, 63]. **B.** Electron microscopic picture of a type 1 pilus (magnification = 300'000; bar = 20 nm) [55].

Previous studies clearly demonstrated that type 1 pili deficient UPEC strains are not able to initiate an infection in mice [43]. Furthermore, the immunization of mice, with antibodies directed against FimH, protected animals from bladder-colonization with UPEC [41]. These findings strongly suggest that the inhibition of the initial host-pathogen interaction with FimH antagonists is a suitable approach to prevent and treat UTI.

The host defense system exerts a FimH related mechanism to protect the sterile urinary tract from invading UPECs. The most abundant protein in the urine is the Tamm-Horsfall protein (THP; also called uromodulin). It is a high-mannosylated glycoprotein and is exclusively produced in the kidneys. It is able to neutralize UPEC

by binding to their type 1 pili and it thereby prevents the adhesion to urothelial cells [54]. Interestingly, it is highly conserved during evolution and THP-deficient mice are more susceptible to UTI [56]. Once the bacteria are trapped by THP, the THP/bacteria cluster is eliminated by the urine flow from the urinary tract. FimH antagonists would support the host defense mechanism to clear excessively invading bacteria. In addition, type 1 pili exhibit several important target-qualities for the development of an anti-adhesion therapy:

(i) they are the most prevalent fimbriae encoded by UPEC,
(ii) they are highly conserved during evolution,
(iii) they mediate the adhesion, which is the first and most important step for the establishment of the infection cycle (Figure 5) and
(iv) they target specific bacterial structures and are therefore expected to cause less side effects.

In vitro and *in vivo* Evaluation of FimH Antagonists

In the 1970s, Sharon and coworkers pioneered the discovery of anti-adhesion molecules targeting FimH (Figure 1 bottom). They reported on the *in vitro* inhibitory potential of methyl α-D-mannopyranoside (**1a**) [29] (Figure 8) and *p*-nitrophenyl α-D-mannopyranoside [64] and investigated (*in vitro* and *in vivo*) the FimH lectin as a potential target for anti-adhesion therapy (Figure 7). Since no crystal structure was available, they explored the FimH binding site (CRD) by testing a series of simple α-D-mannopyranosides with varying aglycons [65]. The structure-activity relationship investigations showed that substitutions on the aromatic ring have a favorable effect on the binding affinity of the α-D-mannopyranosides with an over 700-fold increase in affinity for *o*-chlorophenyl-*p*-nitrophenyl-α-D-mannopyranoside compared to methyl α-D-mannopyranoside (**1a**) (Figure 8).

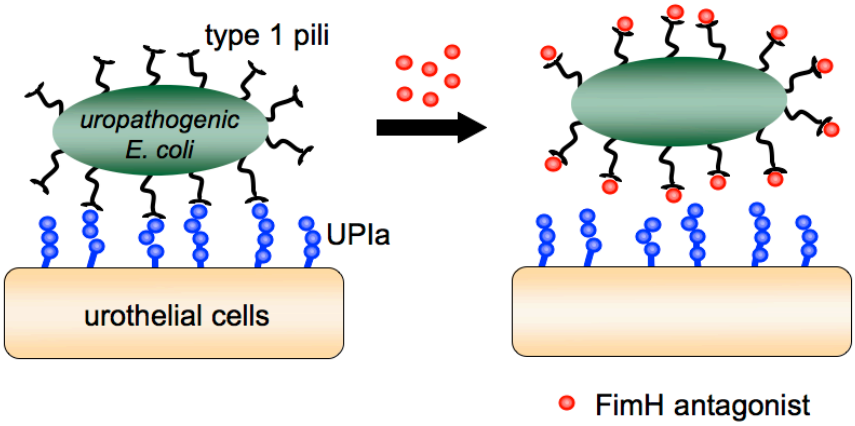

Figure 7. Principle of the anti-adhesion therapy. In the presence of FimH antagonists, type 1 pili expressing UPECs are not able to adhere to urothelial cells and are therefore washed out with the flow of urine. As a result, the infection cycle (Figure 5) can not be initiated.

After crystal structures of FimH and FimH co-crystallized with antagonists became available [66 a-c, 67, 68], research focused on the rational design of more potent antagonists following two major directions. First, multivalent FimH antagonists were investigated [69], showing that tri- and tetravalent glycoclusters exhibit the highest activities with an up to 780-fold increase in affinity compared to methyl α-D-mannopyranoside (**1a**). In a second approach, monovalent, high-affinity antagonists were designed and synthesized [32, 70]. Three main classes show a promising profile for affinity and *in vitro* pharmacokinetics and were therefore intensively investigated (*in vitro* and *in vivo*): (i) long-chain alkyl α-D-mannopyranosides [66 b, 71, 72] (e.g. Figure 8, **1**), (ii) α-D-mannopyranosides with aromatic aglycons [66 d, 68, 71, 73, **Paper II**, **Manuscript I**] (e.g. Figure 8, **2**, **5** and **6**) and (iii) α-D-mannopyranosides with extended aglycons [66 b, 68, 71, **Paper IV**, **Paper V**] (e.g. Figure 8, **3** and **4**).

Although both, mono- and multivalent FimH antagonists were designed and tested for their *in vitro* potencies, only with monovalent α-D-mannopyranosides (small-molecules) the hurdle to *in vivo* studies was taken, due to their favorable drug-like properties (solubility, permeability through enterocytes, metabolic stability, renal excretion).

In vitro Target-Based and Cell-Based Assays

At the beginning of the 20th century it was first discovered that *E. coli* cause hemagglutination (the ability to agglutinate erythrocytes) (Figure 1 bottom) [6]. Later on, correlation between agglutination capability and filamentous appendages present on the bacterial surface was identified and in the middle of the 20th century the ability of mannose to inhibit *E. coli* hemagglutination was first described [7]. Since then, the agglutination capability was used in most *in vitro* assays to evaluate the potential of FimH antagonists and is still used today (65, 72, 74 - 76, **Paper I**).

Later on, more complex assay set-ups were developed for the quantitative determination of the inhibitory potency of FimH antagonists (Table 1). The *in vitro* assays can be divided in two main groups: either whole *E. coli* cells or isolated type 1 pili or recombinant FimH protein, respectively are used for measurements. Furthermore, the assay either requires the immobilization of one of the binding partners on a specialized surface (e.g. enzyme linked immunosorbent assay (ELISA), surface plasmon resonance (SPR), human cell-based assays) or both partners are in solution (e.g. agglutination, hemagglutination, isothermal titration calorimetry (ITC), imaging and radioactive assays) (Table 1).

Besides agglutination, the enzyme linked immunosorbent assay (ELISA) is a further frequently used method to evaluate the binding potential of FimH antagonists. Traditionally, the assay format is based on the addition of a monoclonal antibody, followed by incubation of a secondary antibody, which is conjugated with horseradish peroxidase (HRP) to allow an optical detection [67, 77, 78]. To avoid the need of a specific primary monoclonal antibody, further ELISA set-ups have been developed with alternative, easier and direct detection methods. Direct detection without the need of antibodies was allowed by the use of biotinylated type 1 fimbriated *E. coli* [79], or in a cell-free competitive binding assay, by the interactions of a biotinylated polyacrylamide glycopolymer (trimannose-polyacrylamide) with the mannose receptors [80]. For both approaches, the complexation of the biotinylated glycompolymer with streptavidin coupled to HRP allows for the quantification of the binding potencies of the tested FimH antagonists. In a further approach, GFP labeled bacteria were used, to allow a fluorescence read-out [79].

Table 1: *In vitro* assays for the evaluation of the inhibitory potencies of FimH antagonists. BSA: bovine serum albumin; CRD: carbohydrate recognition domain; GFP: green fluorescence protein; HRP: horseradish peroxidase.

Method	Target/Ligand	Detection	Ref
Agglutination	Yeast (*Candida albicans, Streptomyces cerevisiae)*/ *E. coli*	Aggregometry	74, **Paper I**
Hemagglutination	Guinea pig erythrocytes/ *E. coli*	Visual (by eye)	68 72
		Aggregometry	74, **Paper I**
		Microtiter plate mirror	76
Enzyme linked immunosorbent assay (ELISA)	Mannan coated polystyrene surface/ *E. coli*	Immunostaining (405 nm)	77
	D-Mannose coated polystyrene surface/ isolated type 1 fimbriae	Immunostaining (415 nm)	78
	Mannose-BSA/ isolated FimCH	Immunostaining (450 nm)	67
	Mannan-coated plates/ biotinylated *E. coli*	Streptavidin-HRP conjugation, detection by enzymatic staining (415 nm)	79
	Isolated FimH-CRD-Th-6His/ Trimannose polymer coupled to HRP		80
	Mannan-coated plates/ GFP expressing *E. coli*	Fluorescence (485 nm)	79
Surface plasmon resonance (SPR)	Immobilized anti-FimH antibody/ isolated FimH	Residence units (RUs)	66 b
	Immobilized BSA-mannoside conjugate/ isolated FimH		66 b
	Immobilized low-molecular-weight FimH antagonist/ isolated FimH		71

Continuation of table 1:

Method	Target/Ligand	Detection	Ref
Human cell-based assays	Human granulocytes/ biotinylated type 1 fimbriae	Flow cytometric detection of fluorescently labeled streptavidin	81
	Human urothelial cells/ *E. coli*	Colony forming units (CFU) after cell lysis	66 c
	Human bladder cells/ GFP labeled *E. coli*	Flow cytometry	**Paper III**
Isothermal titration calorimetry (ITC)	Mannosylated ligands/ isolated FimH	Temperature changes (K_d)	71
	FimH antagonists/ isolated FimH CRD		82
Imaging	Mannose-encapsuled gold nanoparticles/ *E. coli*	Transmission electron microscopy (TEM)	83
	Mannose functionalized hematite (iron oxide)/ *E. coli*		84
Radioactive assays	Mannosides coupled with ^{125}I-labelled human serum albumin/ *E. coli*	Radioactivity	72
	^{3}H-labelled mannose/ isolated FimH		66 b

UTI Mouse Model - The Therapeutic Potential of FimH Antagonists

In the first *in vivo* proof of concept study, FimH antagonist **1a** was pre-incubated with type 1 pili expressing UPEC strains and the mixture was instilled transurethral into the bladder of mice (Figure 1 bottom and Figure 8) [8]. Urine samples were analyzed for bacterial counts, resulting in a significant reduction of bacteriuric mice after 5-16 days. In a second experiment, an additional dose of **1a** was injected intraperitoneal (i.p.) two and three days after infection with the bacteria/antagonist mixture, leading to no significant supplemental benefit. As mentioned by Sharon and coworkers [8], a major drawback of the UTI mouse model is the spontaneous clearance of bacteria from the urinary tract 14 days after infection (up to 45%). Nevertheless, when the sampling of urine was conducted for up to 16 days, a significant reduction of bacteriuric mice treated with the FimH antagonist compared to the control group was observed.

After the initial *in vivo* investigations of the therapeutic potential of FimH antagonists [8, 9], no further *in vivo* studies, testing the efficacy of antagonists were published for almost three decades (Figure 1 bottom). At the same time, however, based on the promising *in vivo* experiments, research directed to the identification of improved FimH antagonists [32]. Furthermore, the UTI mouse model was extensively used for the elucidation of the underlying mechanisms of this host-pathogen interaction (e.g. type 1 and P-pili [85], phase variation of type 1 pili [86], immune response [87] etc.) and the evaluation of antibiotic efficacy [46, 88].

The ascending UTI mouse model is the primarily used *in vivo* model, sharing following similarities to humans:

- The **infection route**, starting in the urethra, ascending to the bladder and finally infecting the kidneys [85, 89].
- The expression of the **uroplakin Ia (UPIa) receptor** on the urothelial cells, responsible for the type 1 pili dependent adhesion of UPEC [90].
- Equal **susceptibility** of bacterial strains used [85].
- No **vesicourethral reflux** [91].
- Similar **intracellular bacterial communities (IBC) formation** in urothelial cells [91].

Orally Available FimH Antagonists

Recently, the *in vivo* investigations of potential FimH antagonists were resumed and the initial treatment experiments, where bacteria/antagonist mixtures were directly applied into the bladder [8, 9] were replaced by a therapeutically more relevant protocol. In further *in vivo* studies, FimH antagonists were either applied orally (p.o.) or intravenously (i.v.), which closer simulates conditions used for later patient application [**Paper II**, **Paper V**, **Manuscript I**, **Manuscript II**, 10, 92]. More in depth investigations of high affinity antagonists according to their *in vitro* and *in vivo* pharmacokinetic (PK) profile were conducted, aiming an oral application of the drug.

In vitro and *in vivo* PK data of small molecule FimH antagonists showed that an optimal balance between solubility, permeability and lipophilicity is required for oral availability (**Paper II, Paper V**). In addition, to ensure the availability of the antagonist at the target organ (bladder), a prodrug approach was applied. The ester **2a** of a biphenyl α-D-mannopyranoside is orally absorbed and hydrolyzed to the renally excretable acid **2b** (Figure 8). When a single dose of 50 mg/kg is orally applied to the UTI mouse model ten minutes prior to infection (prevention study), a substantial reduction of 4 $\log_{10}$ of colony forming units (CFU) in the bladder could be detected (**Paper II**).
In a further prevention study, newly designed indolylphenyl (**3**) and indolinylphenyl (**4**) derivatives were investigated for their PK and pharmacodynamic (PD) profile in the UTI mouse model after i.v. application of 1 mg/kg and 0.05 mg/kg, respectively. They exhibited an availability in bladder for over eight hours, leading to a reduction of bacterial counts by -3.7 $\log_{10}$ CFU (**4**), being equally potent as the standard therapeutic, ciprofloxacin (**Paper V**).

The potential of biphenyl α-D-mannopyranosides for the treatment as well as prevention of UTI in mice was also evaluated by Cusumano *et al.* [10]. For treatment studies, animals with a two weeks chronic infection received a single oral dose of **5a** (100 mg/kg), **5b** and **6** (both 50 mg/kg), resulting in an 3 $\log_{10}$ CFU reduction of bladder counts for **5a** and up to 4 $\log_{10}$ CFU reduction for **5b** and **6** six hours after treatment. In comparison, the antibiotic trimethoprim-sulfamethoxazole (TMP-SMZ, applied in the drinking water) only reduced bacterial counts by 1.5 $\log_{10}$ CFU. Furthermore, antagonists applied together with antibiotics were reported to have a

synergistic effect on the treatment outcome. In a 24 hours multiple dosage study (three times 50 mg/kg p.o. of **6**, every eight hours) for the treatment of chronic infections, bacterial counts in the bladder were reduced by 4.5 $\log_{10}$ CFU. For prevention studies, a single oral dose of **5a** (50 mg/kg) was applied 30 minutes prior to infection, resulting in a 1.5 $\log_{10}$ CFU reduction of bladder counts, 6 h after infection.

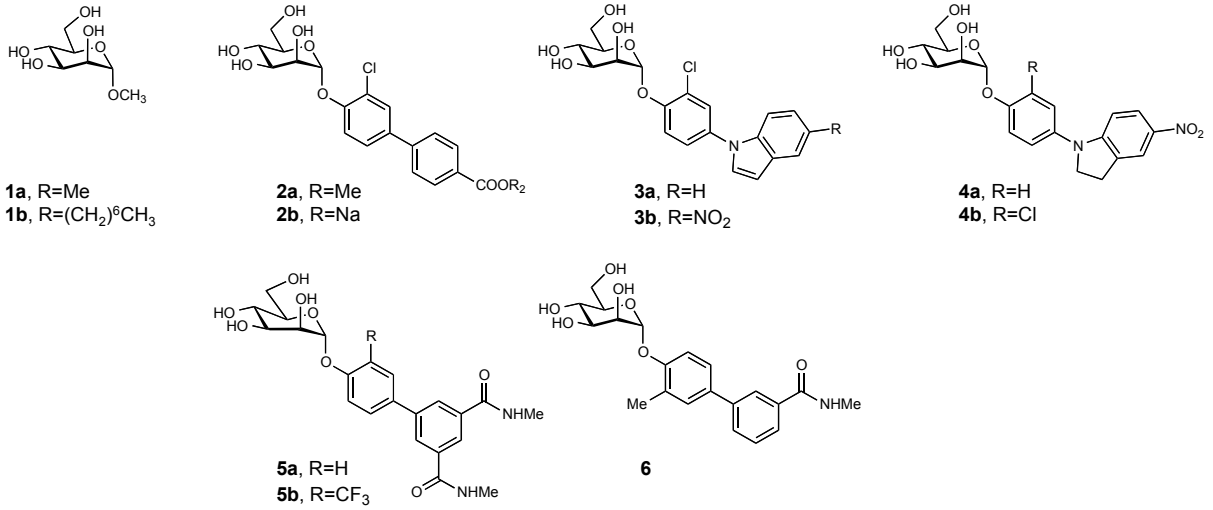

Figure 8: α-D-Mannopyranosides tested in the UTI mouse model. Methyl and *n*-heptyl α-D-mannopyranosides (**1a** & **1b)** [8, 9, **Paper II**], biphenyl α-D-mannopyranosides **2a** and **2b** [**Paper II**], indoline and indolinyl α-D-mannopyranosides **3** & **4**, diamidobiphenyl α-D-mannopyranosides **5a** and **5b** [10] and monoamidobiphenyl α-D-mannopyranoside **6** [10].

Additionally, the treatment with FimH antagonists prevented invasion of UPECs into the bladder cells leading to a reduction of biofilm formation, which was further evaluated in a mouse catheter model using optimized biphenyl α-D-mannopyranoside FimH antagonists (higher potency and improved PK properties) [10, 92, 93]. They showed that intraperitoneal (i.p.) applied mannopyranosides were able to improve the efficacy of TMP-SMZ treatment on catheter associated UTI.

Several *in vivo* studies confirmed the promising potential of orally applied FimH antagonists for both, prevention and treatment of UTI in mice. In addition, FimH antagonists proofed to be equally effective than antibiotics. Both aspects highlight the great potential of anti-adhesives for further clinical development (e.g. PK/PD studies).

Pharmacokinetic/Pharmacodynamic Studies – The Effect Profile of FimH Antagonists

A central aspect in antimicrobial development is the prediction of the efficacy for each individual antibiotic agent and the corresponding disease under varying concentrations, application time points and exposure times. The pharmacology of an antimicrobial determines its behavior in the organism and is composed of two main components, pharmacokinetics and pharmacodynamics (Figure 9) [94]. The first component, pharmacokinetics (PK), defines the absorption, distribution and elimination of a drug, determining the time course of drug concentration at the site of infection (tissue or body fluids). The second component, pharmacodynamics (PD), describes the correlation between serum concentration of a drug and its treatment efficacy. Together, they allow the simulation of the varying drug concentration over time in combination with efficacy, using pharmacokinetic/pharmacodynamic (PK/PD) modeling. PK/PD studies are important during drug development to find the optimal dosage regimen for later clinical trials and to minimize antimicrobial resistance development (by ensuring total bacterial eradication) [95, 96].

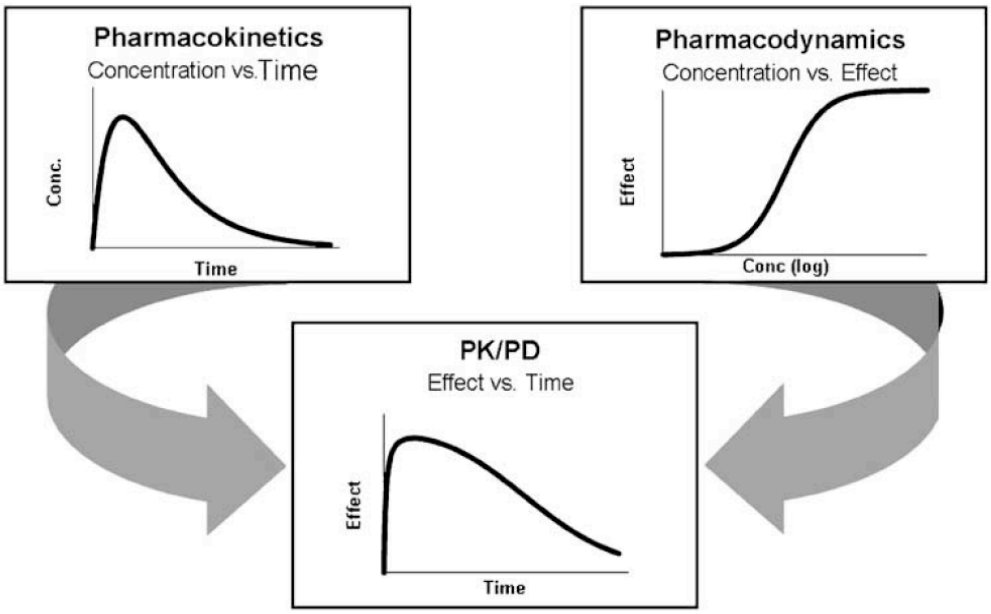

Figure 9: The concept of pharmacokinetic/pharmacodynamic (PK/PD) modeling. PK/PD studies combine the knowledge of the concentration-time profile (PK) of a drug with its efficacy-concentration (PK) profile, resulting in an efficacy over time (PK/PD) profile. The PK/PD profile is used to predict further dosage regimens and the therapeutic outcome *in vivo* (mouse model and human clinical trials) [97].

In the 1950s a time-dependent bactericidal efficacy of penicillin was first described in a rodent model, being the hour of birth for the PK/PD concept [11] (Figure 1 asterisk). However, the significance from the initial PK/PD investigations were understood only two decades later and the research was successfully revived. Hence, today patients profit from the gained PK/PD knowledge, incorporating virtually every antimicrobial class [95].

The three predictive PK/PD dosing indices for antimicrobials are (Figure 10) [94 - 96, 98]:

i) The duration of time a drug concentration remains above the minimal inhibitory concentration (MIC) (T>MIC), indicating the time-dependent activity. The bactericidal activity increases with a longer exposure time, but not with higher concentrations (e.g. penicillins, cephalosporins, carbapenems, vancomycin, clarithromycin, linezolid, doxycycline).

ii) The maximal reached drug concentration above the MIC (C_{max}/MIC or Peak/MIC), indicating the concentration-dependent activity. The bactericidal activity increases with higher drug concentration, but not with prolonged exposure time (e.g. aminoglycosides, daptomycin, streptomycin, metronidazole, fluoroquinolones).

iii) The area under the concentration time curve (AUC) over a time range of 24 hours above the MIC (AUC_{0-24}/MIC), indicating both, time- and concentration-dependent activity (e.g. aminoglycosides, fluoroquinolones, tetracyclines, vancomycin).

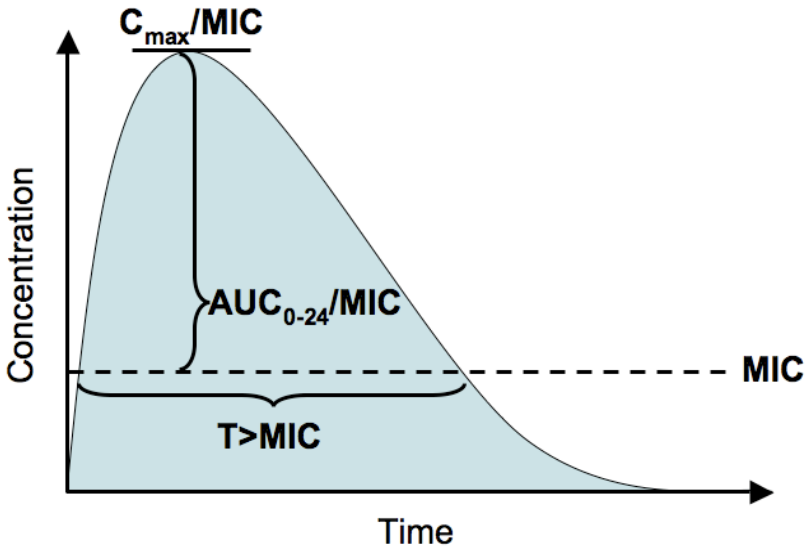

Figure 10: Pharmacokinetic/pharmacodynamic (PK/PD) indices of a drug used for the prediction of the therapeutic outcome *in vivo* [adapted from 96]. C_{max}: maximal concentration in the tested site (tissue or body fluids); MIC: minimal inhibitory concentration; AUC_{0-24}: area under the curve over a time period of 24 hours; T: time.

Several static and dynamic *in vitro* assay set-ups have been developed to determine the PK/PD measures for each drug [Refs 99]. However, *in vivo* studies remain indispensable, because they allow the evaluation of the efficacy of a drug at the infection site under changing time courses of drug availability and other host influence factors (e.g. immune system). To identify the PK/PD profile most closely correlated with efficacy, dose-fraction studies (same total drug-concentration administered in different dosing intervals) are performed [94, 95, 98]. Such experimental studies are usually easily conducted in animal models and decrease the risk (dose guessing in patients) and cost in drug development. They provide information for the selection of dose and dosing-intervals for human clinical trials and recent studies suggest that the PK/PD index most predictive for the efficacy of an antimicrobial agent in animal infection models correlate well with human infections [94]. Therefore, the preclinical determination of the PK/PD indices for FimH antagonists (**Manuscript II**) could provide valuable information for the later on clinical outcome of an anti-adhesive therapy against UTI.

References

1 Ofek I, Hasty DL, Doyle RJ, ‚Bacterial Adhesion to Animal Cells and Tissues', ASM Press. **2003**.

2 WHO statistics, ‚The top 10 causes of death', Fact sheet N°310, updated June **2011**.

3 Simmons KJ, Chopra I, Fishwick CWG, *Nat. Rev. Microbiol.* **2010**, 8, 501.

4 Hamad B, *Nat. Rev. Drug Discov.* **2010**, 9, 675.

5 Fischbach MA and Walsh CT, *Science* **2009**, 325, 1089.

6 Guyot G, *Zentbl. Bacteriol. Abt. I Orig.* **1908**, 47, 640.

7 Collier WA and deMiranda JC, *Antonie Leeuwenhoek* **1955**, 21, 133.

8 Aronson M, Medalia O, Schori L, Mirelman D, Sharon N, Ofek I, *J Infect. Dis.* **1979**, 139, 329.

9 Svanborg Edén C, Freter R, Hagberg L, Hull R, Hull S, Leffler H, Schoolnik G, *Nature* **1982**, 298, 560.

10 Cusumano CK, Pinkner JS, Han Z, Greene SE, Ford BA, Crowley JR, Henderson JP, Janetka JW, Hultgren SJ, *Sci. Transl. Med.* **2011**, 3, 109.

11 a) Eagle H, Fleischman R, Musselman AD, *J. Bacteriol.* **1950**, 59, 625. b) Eagle H, Fleischman R, Musselman AD, *Am. J. Med.* **1950**, 9, 280. c) Eagle H, FleischmanR, Levy M, *N. Engl. J. Med.* **1953**, 248, 481.

12 Clatworthy AE, Pierson E, Hung DT, *Nat. Chem. Biol.* **2007**, 9, 541.

13 Kresse H, Belsey MJ, Rovini H, *Nat. Rev. Drug Discov.* **2007**, 6, 19.

14 Allen HK, Donato J, Wang HH, Cloud-Hansen KA, Davies J, Handelsmann L, *Nat. Rev. Microbiol.* **2010**, 8, 251.

15 Hooton TM, Roberts PL, Stapleton AE, *JAMA*, **2012**, 307, 583.

16 Lee YM, Almqvist F, Hultgren SC, *Curr. Opin. Pharmacol*. **2003**, 3, 513.

17 Mühldorfer I and Hacker J, *Microb. Pathog.* **1994**, 16, 171.

18 Alksne LE, Projan SJ, *Curr. Opin. in Biotech*. **2000**, 11, 625.

19 Shoop WL, Xiong Y, Wiltsie J, Woods A, Guo J, Pivnichny JV, Felcetto T, Michael BF, Bansal A, Cummings RT, Cunningham BR, Friedlander AM, Douglas CM, Patel SB, Wisniewski D, Scapin G, Salowe SP, Zaller DM, Chapman KT, Scolnick EM, Schmatz DM, Bartizal K, MacCoss M, Hermes JD, *Proc. Natl. Acad. Sci. USA* **2005**, 102, 7958.

20 Hing CY and Barriere SL, *Antimicrob. Agents Chemother.* **1981**, 19, 326.

21 Miller MB and Bassler BL, *Annu. Rev. Microbiol.* **2001**, 55, 165.

22 Rasko DA and Sperandio V, *Nat. Rev. Drug Discov.* **2010**, 9, 117.

23 Parsek MR, Val DL, Hanzelka BL, Cronan JE, *Proc. Natl. Acad. Sci. USA* **1999**, 96, 4360.

24 Dong YH, Wang LH, Xu JL, Zhang HB, Zhang XF, Zhang LH, *Nature* **2001**, 411, 813.

25 Müh U, Schuster M, Heim R, Singh A, Olson ER, Greenberg EP, *Antimicrob. Agents Chemother.* **2006**, 50, 3674.

26 Geske GD, Wezeman RJ, Siegel AP, Blackwell HE, *J. Am. Chem. Soc.* **2005**, 127, 12762.

27 Hung DT, Shakhnovich EA, Pierson E, Mekalanos JJ, *Science* **2005**, 310, 670.

28 Bavington C and Page C, *Respiration* **2005**, 72, 335.

29 Ofek I, Mirelman D, Sharon N, *Nature* **1977**, 265, 623.

30 Duguid JP, *J. Gen. Microbiol.* **1959**, 21, 271.

31 Pinkner JS, Remaut H, Buelens F, Miller E, Aberg V, Pemberton N, Hedenström M, Larsson A, Seed P, Waksman G, Hultgren SJ, Almqvist F, *Proc. Natl. Acad. Sci. USA* **2006**, 103, 17897.

32 Hartmann M and Lindhorst TK, *Eur. J. Org. Chem.* **2011**, 3583.

33 Foxman B, *Am. J. Med.* **2002**, 113, 5S.

34 Sharon N, *Biochim. Biophysi. Acta* **2006**, 1760, 527.

35 Wiles TJ, Kulesus RR, Mulvey MA, *Exp. Mol. Pathol.* **2008**, *85*, 11.

36 Mitsumori K, Terai A, Yamamoto S, Yoshida O, *J. Urol.* **1997**, 158, 2329.

37 Manges AR, Johnson JR, Foxman B, O'Bryan, TT, Fullerton KE, Riley LW, *N. Engl. J. Med.* **2001**, 345, 1007.

38 Jakobsen L, Garneau P, Bruant G, Harel J, Olsen SS, Porsbo LJ, Hammerum AM, Frimodt-Møller N, *Eur. J. Clin. Microbiol. Infect. Dis.* **2012**, 31, 1121.

39 Foxman B, Manning SD, Tallman P, Bauer R, Zhang L, Koopman JS, Gillespie B, Sobel JD, Marrs CF, *Am. J. Epidemiol.* **2002**, 156, 1133.

40 Croxen MA and Finlay BB, *Nat. Rev. Microbiol.* **2010**, 8, 26.

41 Langermann S, Palaszynski S, Barnhart M, Auguste G, Pinkner JS, Burlein J, Barren P, Koenig S, Leath S, Jones CH, Hultgren SJ, *Science* **1997**, 276, 607.

42 Lane MG, Alteri CJ, Smith SN, Mobley HL, *Proc. Natl. Acad. Sci. USA* **2007**, 104, 16669.

43 Connell H, Agace W, Klemm P, Schembri M, Mårild S, Svanborg C, *Proc. Natl. Acad. Sci. USA* **1996**, 93, 9827.

44 Hunstad DA and Justice SS, *Annu. Rev. Microbiol.* **2010**, 64, 203.

45 Lane MC and Mobley HLT, *Kidney Int.* **2007**, 72, 19.

46 Mulvey MA, *Cell. Microbiol.* **2002**, *4*, 257.

47 Mulvey MA, Schilling JD, Martinez JJ, Hultgren SJ, *Proc. Natl. Acad. Sci. USA* **2000**, 97, 8829.

48 a) Smith YC, Rasmussen SB, Grande KK, Conran RM, O'Brien AD, *Infect. Immun.* **2008**, 76, 2978. b) Mills M, Meysick KC, O'Brien AD, *Infect. Immun.* **2000**, 68, 5869. c) Guyer DM, Radulovic S, Jones FE, Mobley HL, *Infect. Immun.* **2002**, 70, 4539.

49 a) Buckles EL, Wang X, Lane MC, Lockatell CV, Johnson DE, Rasko DA, Mobley HL, Donnenberg MS, *J. Infect. Dis.* **2009**, 199, 1689. b) Lloyd AL, Smith SN, Eaton KA, Mobley HL, *Infect. Immun.* **2009**, 77, 5322.

50 Torres AG, Redford P, Welch RA, Payne SM, *Infect. Immun.* **2001**, 69, 6179.

51 Bien J, Sokolova O, Bozko P, *Int. J. Nephrol.* **2012**, 2012, 681473.

52 Goldstein IJ and Hayes CE, *Adv. Carbohydr. Chem.Biochem.* **1978**, 35, 127.

53 Beuth J, Ko HL, Pulverer G, Uhlenbruck G, Pichlmaier H, *Glycoconj. J.* **1995**, 12, 1.

54 Pak J, Pu Y, Zhang Z, Hasty DL, Wu X, *J. Biol. Chem.* **2001**, 276, 9924.

55 Jones CH, Pinkner JS, Roth R, Heuser J, Nicholes AV, Abraham SN, Hultgren SJ, *Proc. Natl. Acad. Sci. USA* **1995**, 92, 2081.

56 Bates JM, Raffi HM, Prasadan K, Mascarenhas R, Laszik Z, Maeda N, Hultgren SJ, Kumar S, *Kidney Int.* **2004**, 65, 791.

57 Sauer FG, Barnhart M, Choudhury D, Knight SD, Waksman G, Hultgren SJ, *Curr. Opin. Struc. Biol.* **2000**, 10, 548.

58 Jones CH, Pinkner JS, Nicholes AV, Slonim LN, Abraham SN, Hultgren SJ, *Proc. Natl. Acad. Sci. USA* **1993**, 90, 8397.

59 Pieters RJ, *Trends Glycosci. Glycotechnol.* **2004**, 16, 243.

60 a) Yakovenko O, Sharma S, Forero M, Tchesnokova V, Aprikian P, Kidd B, Mach A, Vogel V, Sokurenko E, Thomas WE, *J Biol Chem*. **2008,** 283, 11596. b) Tchesnokova V, Aprikian P, Yakovenko O, Larock C, Kidd B, Vogel V, Thomas W, Sokurenko E, *J Biol Chem* **2008**, 283, 7823.

61 Aprikian P, Trinchina E, Thomas WE, Tchesnokova V, Nilsson LM, Vogel V, Sokurenke EV, *Abstr. Gen. Meet. Am. Soc. Microbiol.* **2004**, 104, 52.

62 Puorger C, Eidam O, Capitani G, Erilov D, Grutter MG, Glockshuber R, *Structure* **2008**, 16, 631.

63 Le Bouguénec C, *Int. J. Med. Microbiol.* **2005**, 295, 471.

64 Eshdat Y, Ofek I, Yashouv-Gan Y, Sharon N, Mirelman D, *Biochem. Biophys. Res. Commun.* **1978**, 85, 1551.

65 Firon N, Ashkenazi S, Mirelman D, Ofek I, Sharon N, *Infect. Immun*. **1987**, 55, 472.

66 a) Choudhury D, Thompson A, Stojanoff V, Langermann S, Pinkner J, Hultgren SJ, Knight SD, *Science* **1999**, 285, 1061. b) Bouckaert J, Berglund J, Schembri M, Genst ED, Cools L, Wuhrer M, Hung CS, Pinkner J, Slättergard R, Zavialov A, Choudhury D, *Mol. Microbiol.* **2005**, 55, 441. c) Wellens A, Garofalo C, Nguyen H, Van Gerven N, Slättergârd R, Hernalsteens J-P, Wyns L, Oscarson S, De Greve H, Hultgren S, Bouckaert J, *PLos One* **2008**, 3, 4. d) Han Z, Pinker JS, Ford B, Obermann R, Nolan W, Wildman SA, Hobbs D, Ellenberger T, Cusumano CK, SJ, Janetka JW, *J. Med. Chem.* **2010**, 53, 4779.

67 Hung C-S, Bouckaert J, Hung D, Pinkner J, Widberg C, DeFusco A, Auguste CG, Strouse R, Langermann S, Waksman G, Hultgren SJ, *Mol. Microbiol.* **2002**, 44, 903.

68 Hultgren SJ, Schwan WR, Schaeffer AJ, Duncan JL, *Infect. Immun.* **1986**, 54, 613.

69 a) Pieters RJ, *Org. Biomol. Chem.* **2009**, 7, 2013. b) Imberty A, Chabre YM, Roy R, *Chem. Eur. J.* **2008**, 14, 7490.

70 Ernst B and Magnani JL, *Nat. Rev. Drug Discov.* **2009**, 8, 661.

71 Durka M, Buffet K, Lejl J, Holler M, Nierengarten J-F, Taganna J, Bouckaert J, Vincent SP, *Chem. Commun.* **2011**, 47, 1321.

72 Nagahori N, Lee RT, Nishimura S-I, Pagé D, Roy R, Lee YC, *ChemBioChem* **2002**, 2, 836.

73 Sperling O, Fuchs A, Lindhorst TK, *Org. Biomol. Chem.* **2006**, 4, 3913.

74 Firon N, Ofek I, Sharon N, *Carbohydr. Res.* **1983**, 120, 235.

75 Sokurenko EV, Courtney HS, Ohman DE, Klemm P, Hasty DL, *J. Bacteriol.* **1994**, 176, 748.

76 Lindhorst TK, Kieburg C, Krallmann-Wenzel U, *Glycoconjugate J.* **1998**, 15, 605.

77 a) Lindhorst TK, Kötter S, Krallmann-Wenzel U, *J. Chem. Soc. Perkin Trans 1* **2001**, 823. b) Dubber M, Sperling O, Lindhorst TK, *Org. Biomol. Chem.* **2006**, 4, 3901. c) Sperling O, Dubber M, Lindhorst TK, *Carbohydr. Res.* **2007**, 342, 696. d) Heidecke C, Dubber M, Lindhorst TK, *Chem. Eur. J.* **2007**, 13, 9056.

78 Chessa D, Dorsey CW, Winter M, Bäumler AJ, *J. Biol. Chem.* **2008**, 283, 8118.

79 Hartmann M, Horst AK, Klemm P, Lindhorst TK, *Chem. Commun.* **2010**, 46, 330.

80 Rabbani S, Jiang X, Schwardt O, Ernst B, *Anal. Biochem.* **2010**, 15, 188.

81 Horst A, Kötter S, Lindhorst TK, Ludwig A, Brandt E, Wagener C, *Med. Microbiol. Immunol.* **2001**, 90, 145.

82 Pang L, Kleeb S, Lemme K, Rabbani S, Scharenberg M, Zalewski A, Schädler F, Schwardt O, Ernst B, *ChemMedChem* **2012**, 7, 1404.

83 Lin C-C, Yeh Y-C, Yang C-Y, Chen C-L, Chen G-F, Chen C-C, Wu Y-C, *J. Am. Chem. Soc.* **2002**, 124, 3508.

84 Liu L-H, Dietsch H, Schurtenberger P, Yan M, *Bioconjugate Chem.* **2009**, 20, 1349.

85 Hagberg L, Hull R, Hull S, Falkow S, Freter R, Svanborg Edén C, *Infect. Immun.* **1983**, 40, 265.

86 a) Eisenstein BI, *Science* **1981**, 214, 337. b) Hultgren SJ, Porter TN, Schaeffer AJ, Duncan JL, *Infect. Immun.* **1985**, 50, 370.

87 de Man P, van Kooten C, Aarden L, Engberg I, Linder H, Svanborg Edén C, *Infect. Immun.* **1989**, 57, 3383.

88 Kerrn MB, Frimodt-Møller N, Espersen F, *Antimicrob. Agents Chemother.* **2003**, 47, 1002.

89 Hvidberg H, Struve C, Krogfelt KA, Christensen N, Rasmussen SN, Frimodt-Møller N, *Antimicrob. Agents Chemother.* **2000**, 44, 156.

90 Zhou G, Mo WJ, Sebbel P, Min G, Neubert TA, Glockshuber R, Wu XR, Sun TT, Kong XP, *J. Cell Science* **2001**, 114, 4095.

91 Rosen DA, Hooton TM, Stamm WE, Humphrey PA, Hultgren SJ, *PLoS Medicine* **2007**, 4, 1949.

92 Han Z, Pinkner JS, Ford B, Chorell E, Crowley, Cusumano CK, Campbell S, Henderson JP, Hultgren JS, *J. Med. Chem.* **2012**, 55, 3945.

93 Guiton PS, Cusumano CK, Kline KA, Dodson KW, Han Z, Janetka JW, Henderson JP, Caparon MG, Hultgren SJ, *Antimicrob. Agents Chemother.* **2012**, 56, 4738.

94 Craig WA, *Clin. Infect. Dis.* **1998**, 26, 1.

95 Ambrose PG, Bhavnani SM, Rubino CM, Louie A, Gumbo T, Forrest A, Drusano GL, *Clin. Infect. Dis.* **2007**, 44, 79.

96 Frimodt-Møller N, *Int. J. Antimicrob. Agents* **2002**, 19, 333.

97 Derendorf H and Meibohm B, *Pharm. Res.* **1999**, 16, 176.

98 Andes D and Craig WA, *Int. J. Antimicrob. Agents* **2002**, 19, 261.

RESULTS AND DISCUSSION

Paper I

Development of an Aggregation Assay to Screen FimH Antagonists.

Abgottspon D, Rölli G, Hosch L, Steinhuber A, Jiang X, Schwardt O, Cutting B, Smiesko M, Jenal U, Ernst B, Trampuz A.

J. Microbiol. Methods **2010**.

My contributions:

Establishment of the aggregometry assay and screening of FimH antagonists together with the master student Rölli G.

Manuscript preparation.

Journal of Microbiological Methods 82 (2010) 249–255

Contents lists available at ScienceDirect

Journal of Microbiological Methods

journal homepage: www.elsevier.com/locate/jmicmeth

Development of an aggregation assay to screen FimH antagonists

Daniela Abgottspon [a,b], Gina Rölli [a,b], Lucie Hosch [c], Andrea Steinhuber [a], Xiaohua Jiang [a], Oliver Schwardt [a], Brian Cutting [a], Martin Smiesko [a], Urs Jenal [c], Beat Ernst [a,*], Andrej Trampuz [b,d,*]

[a] Institute of Molecular Pharmacy, Pharmacenter, University of Basel, Switzerland
[b] Infectious Diseases Research Laboratory, Department of Biomedicine, University Hospital, Basel, Switzerland
[c] Molecular Microbiology, Biozentrum, University of Basel, Switzerland
[d] Infectious Diseases Service, Department of Internal Medicine, University Hospital and University of Lausanne, Switzerland

ARTICLE INFO

Article history:
Received 13 April 2010
Received in revised form 19 June 2010
Accepted 29 June 2010
Available online 8 July 2010

Keywords:
Aggregation
E. coli
FimH antagonist
Type 1 pili
Urinary tract infection (UTI)

ABSTRACT

α-D-Mannopyranosides are potent FimH antagonists, which inhibit the adhesion of *Escherichia coli* to highly mannosylated uroplakin Ia on the urothelium and therefore offer an efficient therapeutic opportunity for the treatment and prevention of urinary tract infection. For the evaluation of the therapeutic potential of FimH antagonists, their effect on the disaggregation of *E. coli* from *Candida albicans* and guinea pig erythrocytes (GPE) was studied.

The mannose-specific binding of *E. coli* to yeast cells and erythrocytes is mediated by type 1 pili and can be monitored by aggregometry. Maximal aggregation of *C. albicans* or GPE to *E. coli* is reached after 600 s. Then the FimH antagonist was added and disaggregation determined by light transmission over a period of 1400 s. A FimH-deleted mutant of *E. coli*, which does not induce any aggregation, was used in a control experiment. The activities of FimH antagonists are expressed as IC_{50}s, the half maximal inhibitory concentration of the disaggregation potential. *n*-Heptyl α-D-mannopyranoside (**1**) was used as a reference compound and exhibits an IC_{50} of 77.14 μM, whereas methyl α-D-mannopyranoside (**2**) does not lead to any disaggregation at concentrations up to 800 μM. *o*-Chloro-*p*-[*N*-(2-ethoxy-3,4-dioxocyclobut-1-enyl)amino]phenyl α-D-mannopyranoside (**3**) shows a 90-fold and 2-chloro-4-nitrophenyl α-D-mannopyranoside (**4**) a 6-fold increased affinity compared to **1**. Finally, 4-nitrophenyl α-D-mannopyranoside (**5**) exhibits an activity similar to **1**. As negative control, D-galactose (**6**) was used.

The standardized aggregation assay generates concentration-dependent, reproducible data allowing the evaluation of FimH antagonists according to their potency to inhibit *E. coli* adherence and can therefore be employed to select candidates for experimental and clinical studies for treatment and prevention of urinary tract infections.

1. Introduction

Urinary tract infection (UTI) is one of the most common infections, affecting millions of people each year. Particularly affected are women, who have a 40–50% risk to experience at least one symptomatic UTI episode at some time during their life. Furthermore, more than half of them experience a relapse of the infection within 6 months (Fihn, 2003; Hooton, 2001).

Although UTI rarely cause severe disease such as pyelonephritis or urosepsis, it is associated with high morbidity and consumes considerable healthcare resources (Wiles et al., 2008). Uropathogenic *Escherichia coli* (UPEC) is the primary cause of UTIs accounting for 70–95% of the reported cases. Symptomatic UTIs require antimicrobial treatment, often resulting in the emergence of resistant microbial flora. As a consequence, treatment of consecutive infections becomes increasingly difficult, since the number of antibiotics is limited and the resistance in *E. coli* is increasing, especially in patients with diabetes, urinary tract anomaly, paraplegy and those with permanent urinary catheter. Therefore, a new approach for the prevention and treatment of UTI with inexpensive, orally applicable therapeutics with a low potential for resistance would have a great impact on patient care, public healthcare and medical expenses.

UPEC strains express a number of well-studied virulence factors used for a successful colonization of their host (Gouin et al., 2009; Rosen et al., 2008; Wiles et al., 2008). One important virulence factor is located on type **1** pili, allowing UPEC to adhere and invade host cells within the urinary tract. It enables UPEC to attach to oligomannosides, which are part of the glycoprotein uroplakin Ia on the urinary bladder

* Corresponding authors. B. Ernst is to be contatcted at Institute of Molecular Pharmacy, Pharmacenter, University of Basel, Klingelbergstrasse 50, CH-4056 Basel, Switzerland. Tel.: +41 61 267 1551; fax: +41 61 267 1552. Trampuz, Infectious Diseases Service, Department of Internal Medicine, University Hospital and University of Lausanne, Rue du Bugnon 46, CH-1011 Lausanne, Switzerland. Tel.: +41 21 314 3992; fax: +41 21 314 2876.
E-mail addresses: beat.ernst@unibas.ch (B. Ernst), andrej.trampuz@chuv.ch (A. Trampuz).

0167-7012/$ – see front matter © 2010 Elsevier B.V. All rights reserved.
doi:10.1016/j.mimet.2010.06.015

mucosa. This initial step prevents the rapid clearance of *E. coli* from the urinary tract by the bulk flow of urine and at the same time, enables the invasion of the host cells (Mulvey, 2002; Wiles et al., 2008).

Type 1 pili are the most prevalent fimbriae encoded by UPEC, consisting of the four subunits FimA, FimC, FimG and FimH, the latter located at the tip of the pili (Capitani et al., 2006). As a part of the FimH subunit, a carbohydrate-recognizing domain (CRD) is responsible for bacterial interactions with the host cells within the urinary tract (Mulvey, 2002). The crystal structure of the FimH-CRD was solved (Choudhury et al., 1999) and its complex with *n*-butyl α-D-mannopyranoside (Bouckaert et al., 2005) and Manα(1-3)[Manα(1-6)]Man (Wellens et al., 2008) recently became available.

Previous studies showed that vaccination with FimH adhesin inhibits colonization and subsequent *E. coli* infection of the urothelium in humans (Langermann et al., 1997; Langermann et al., 2000). In addition, adherence and invasion of host cells by *E. coli* can also be prevented by α-D-mannopyranosides, which are potent antagonists of type 1 pili interactions (Bouckaert et al., 2006). Whereas α-D-mannopyranosides efficiently prevent adhesion of *E. coli* to human urothelium, they are not exhibiting a selection pressure to provoke antimicrobial resistance. Furthermore, environmental contamination is less problematic compared to antibiotics (Sharon, 2006).

For the evaluation of the inhibitory potential of FimH antagonists various target-based (Bouckaert et al., 2005; Sperling et al., 2006) and function-based assays (Ofek and Beachey, 1978; Firon et al., 1987) were previously described. In this contribution, we present an advanced and validated approach to evaluate the antagonistic potential of α-mannopyranosides by a function-based aggregation assay. The FimH-dependent adhesion of *E. coli* to the urothelium can be mimicked by the interaction with mannan-presenting yeast cells (e.g. *Candida albicans*) or with the glycocalyx of guinea pig erythrocytes (GPE), respectively. Both interactions can be specifically inhibited with α-mannopyranosides (e.g. Giampapa et al., 1988; Gouin et al., 2009).

Originally, Ofek and Beachey, 1978 and Firon et al., 1982, monitored the aggregation of mannan-containing yeast cells and various strains of *E. coli* by aggregometry, i.e. as a function of the reduced turbidity caused by the aggregation event. They quantified the rate of aggregation by the steepest slope in the curve produced by increasing light transmission (Baumgartner and Born, 1968). In this communication, various parameters of the aggregometry assay were optimized and the potential of FimH antagonists quantified by the AUC (area under the curve) of the disaggregation curves. As a result, the hitherto predominantly visual examination of the aggregation event can now be quantitatively detected and reported by IC_{50}-values. The assay is standardized and allows the accurate, rapid and reproducible high-throughput screening of compound libraries to identify FimH antagonists qualified for an evaluation in a disease model (Hvidberg et al., 2000).

2. Materials and methods

2.1. Test and control microorganisms

The clinical *E. coli* isolate UTI89 (Mulvey et al., 2001) and the *C. albicans* strain ATCC 60193 were used. Microorganisms were stored at −70 °C and before experiment incubated at 37 °C in 10 ml medium using 50 ml tubes. Prior to each experiment, the microorganisms were washed twice and re-suspended in phosphate buffered saline (PBS) at pH 7.4 to reach the desired concentration. Bacterial and yeast concentrations were determined by plating serial 1:10 dilutions on blood agar, followed by colony counting on plates with 20–200 colonies after overnight incubation at 37 °C.

As control, a *E. coli* UTI89 *fimA-H:kan* mutant strain, lacking FimH-specific aggregation, was constructed. For this purpose, the parent *E. coli* UTI89 strain was transformed with the temperature sensitive plasmid pKM208 (Addgene plasmid 13077) containing the *red* recombination genes (Murphy and Campellone, 2003). Transformants carrying pKM208 were grown in LB medium without NaCl, supplemented with ampicillin (100 μg/ml) at 30 °C to late logarithmic phase. The *red* gene expression was induced for 30 min with 1 mM IPTG at 37 °C. Bacteria were subjected to a 15 min heat shock at 42 °C and rapidly cooled in an ice slurry before washing twice with PBS and concentrating 100-fold in 10 % glycerol. A kanamycin resistance cassette was PCR amplified from pKD3 (Datsenko and Wanner, 2000) with primer 2145-fimA_KO_P1 (gcc cat gtc gat tta gaa ata gtt ttt tga aag gaa agc agc ATG AAA ATt gta ggc tgg agc tgc ttc g) and primer 2146-fimH_KO_P2 (gta ata ttg cgt acc agc att agc aat gtc ctg tga ttt ctT TAT TGA TAc ata tga ata tcc tcc tta g). PCR fragments were gel purified (MN Nucleospin Extract II, Machery Nagel, Oensingen, Switzerland) and 10–100 ng purified DNA was mixed with 65 μl recombination competent UTI89 cells followed by electroporation in 1 mm Gene Pulser Cuvettes using a Gene Pulser (BioRad, Reinach, Switzerland) set to 1.75 V, 25 μF and 400 Ω. Shocked cells were mixed with cold (4 °C) salt optimized broth (2 % (w/v) bacto trypton; 0.5 % (w/v) yeast extract; 10 mM NaCl and 2.5 mM KCl), incubated for 1.5 h at 37 °C and plated out on LB agar plates containing 20 μg/ml kanamycin. Resistant clones were colony purified on LB medium containing kanamycin, tested by PCR and sequenced for correct insertion of the resistance cassette into the *fimA-H* locus.

2.2. Nutrients and solutions

The following media were used to investigate the optimal growth conditions for the microorganisms: Luria-Bertani broth (LB),

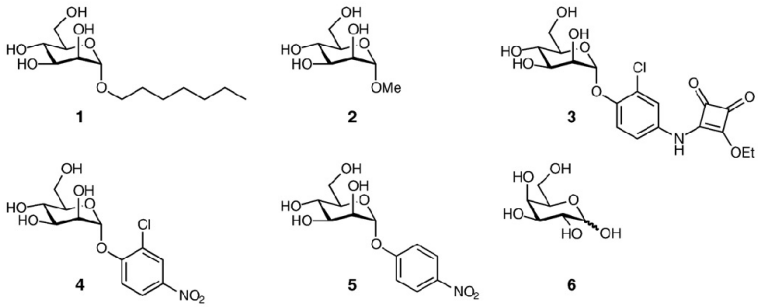

Fig. 1. Structures of the tested FimH antagonists **1**–**5** and the negative control D-galactose (**6**). *n*-Heptyl α-D-mannopyranoside (**1**), methyl α-D-mannopyranoside (**2**), *o*-chloro-*p*-[*N*-(2-ethoxy-3,4-dioxocyclobut-1-enyl)amino]phenyl α-D-mannopyranoside (**3**), 2-chloro-4-nitrophenyl α-D-mannopyranoside (**4**) and 4-nitrophenyl α-D-mannopyranoside (**5**).

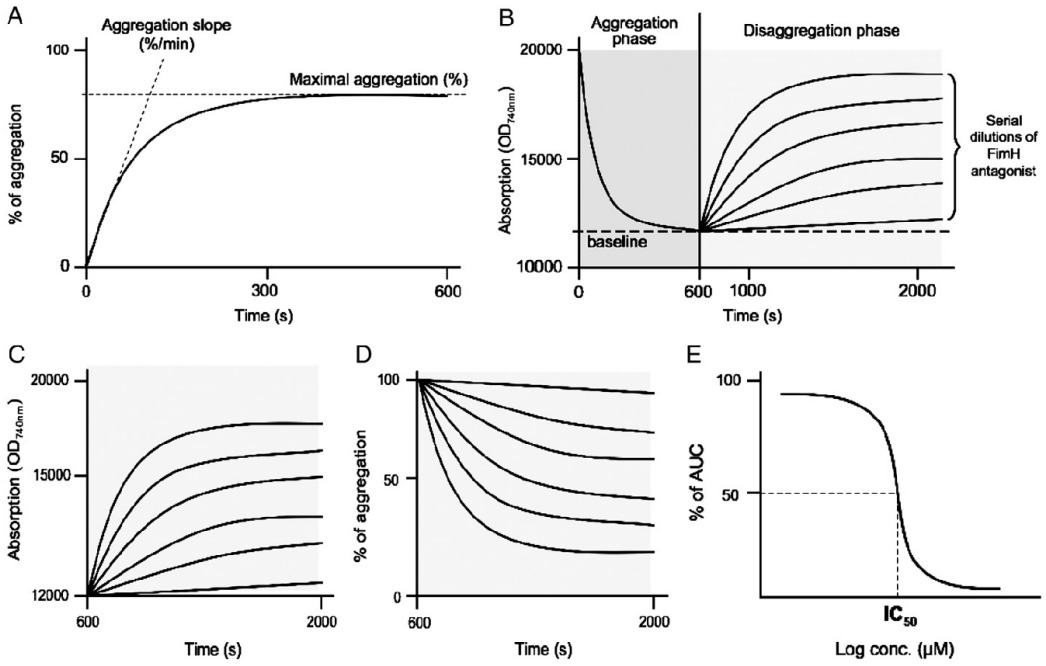

Fig. 2. Schematic overview of the evaluation process of the aggregometer data. (A) During measurements, the aggregometer software is plotting the aggregation curve as % of aggregation over time. For establishment of the method, the aggregation slope and the maximal aggregation were optimized. (B) The data exported from the aggregometer is plotted as absorbance (OD_{740}) over time. The aggregation phase is identical for all measurements whereas the disaggregation phase depends on the potency of FimH antagonists. For further evaluation only the disaggregation curves were taken into consideration. (C) Disaggregation curves of a serial dilution of a FimH antagonist after subtraction of the baseline. (D) For visualization purposes the disaggregation curves were inverted and normalized. At 100% of aggregation cells were maximally aggregated and disaggregation was monitored over 1400 s. (E) The AUC of the disaggregation curves are plotted against the concentration to determine the IC_{50}.

trypticase soy broth (TSB), Mueller-Hinton broth (MHB) and nutrient broth (NB). Media were dissolved in deionized water, autoclaved at 121 °C for 15 min and the pH was adjusted to 7.3. All media were purchased from Becton, Dickinson and Company (Le Pont de Claix, France). Autoclaved, endotoxin-free phosphate buffered saline (PBS), pH 7.4 was purchased from the Hospital Pharmacy at the University Hospital Basel, Switzerland.

2.3. Guinea pig erythrocytes (GPE)

Guinea pig blood was purchased from Charles River Laboratories, Sulzfeld, Germany. To separate GPE from other blood components, 1 ml of guinea pig blood was carefully added to 1 ml of Histopaque (density of 1.077 g/ml at 24 °C, Sigma-Aldrich, Buchs, Switzerland) and centrifuged at 24 °C for 30 min at 400 g. GPE were diluted in PBS to an OD_{600} of 4 and their number was determined using an automated cell counter (Invitrogen AG, Basel, Switzerland) resulting in 2.2×10^6 cells/ml.

2.4. Synthesis of the FimH antagonists

The FimH antagonists tested are listed in Fig. 1. The synthesis of *n*-heptyl α-D-mannopyranoside (1) is described in the supplementary content. Methyl α-D-mannopyranoside (2) was purchased from Fluka Chemie GmbH (Buchs, Switzerland). *o*-Chloro-*p*-[*N*-(2-ethoxy-3,4-dioxocyclobut-1-enyl)amino]phenyl α-D-mannopyranoside (3) and 2-chloro-4-nitrophenyl α-D-mannopyranoside (4) were synthesized as previously described (Sperling et al., 2006). 4-Nitrophenyl α-D-mannopyranoside (5) and D-galactose (6) were purchased from Sigma (Buchs, Switzerland).

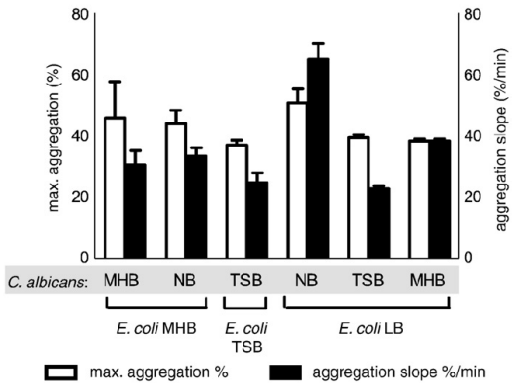

Fig. 3. Aggregation of *E. coli* with *C. albicans*, previously incubated in different cultivation media. Bars in black are representing the maximal aggregation (in %) and the white bars are showing the aggregation slope (in %/min). The bars represent means ± SD. MHB, Mueller-Hinton broth; TSB, trypticase soy broth; LB, Luria-Bertani broth; NB, nutrient broth. The highest values for the aggregation phase were obtain with *C. albicans* grown in NB and *E. coli* in LB, resulting in a maximal aggregation slope of 64.15 %/min (± 6.0 %/min) and a maximal aggregation of 54.65 % (± 4.6 %).

Table 1
Influence of *E. coli* and *C. albicans* concentrations on aggregation measurements. The values represent means ± SD of the maximal aggregation and the aggregation slope.

	C. albicans			
	OD_{600} of 2[a]		OD_{600} of 3[b]	
E. coli	Maximal aggregation (%)	Aggregation slope (%/min)	Maximal aggregation (%)	Aggregation slope (%/min)
OD_{600} 2[c]	50.68 ± 4.61	64.15 ± 6.02	–	–
OD_{600} 3[d]	40.99 ± 5.11	53.34 ± 22.19	41.77 ± 2.41	65.95 ± 6.53

[a] OD_{600} of 2 for *C. albicans* corresponds to 2×10^8 CFU/ml.
[b] OD_{600} of 3 for *C. albicans* corresponds to 3×10^8 CFU/ml.
[c] OD_{600} of 2 for *E. coli* corresponds to 9.6×10^7 CFU/ml.
[d] OD_{600} of 3 for *E. coli* corresponds to 1.4×10^8 CFU/ml.

2.5. Aggregation assay

The percentage of aggregation of *E. coli* with *C. albicans* or GPE was quantitatively determined by measuring the optical density at 740 nm, 37 °C under stirring at 1000 rpm using an APACT 4004 aggregometer (Endotell AG, Allschwil, Switzerland). Bacteria and yeast were statically incubated overnight (12 h) in TSB at 37 °C. Prior to the measurements, the cell densities were adjusted to OD_{600} of 2, corresponding to 9.6×10^7 CFU *E. coli*/ml and 2×10^8 CFU *C. albicans*/ml, respectively. For the calibration of the instrument, the aggregation of protein poor plasma (PPP) using PBS alone was set as 100% and the aggregation of protein rich plasma (PRP) as 0%. After calibration, measurements were performed with 250 µl *C. albicans* or GPE and 50 µl bacterial suspension and the aggregation monitored over 600 s. To optimize the assay, different bacterial and yeast growth conditions and measurement conditions were evaluated for the aggregation phase.

With the optimized assay parameters, the disaggregation potential of FimH antagonists was evaluated. After an aggregation phase of 600 s, 25 µl of antagonist was added to each cuvette and disaggregation was monitored for 1400 s. A two-fold serial dilution of a stock solution of the FimH antagonists **1** to **5** and the negative control D-galactose (**6**), starting at 769 µM, was tested in triplicates.

2.6. Data analysis

The data for the aggregation and the disaggregation phase were plotted using the APACT 4 LPC software version 1.21c from Labor BioMedical Technologies (LABiTec GmbH, Ahrensburg, Germany). For the aggregation phase, the initial slope (in %/min) and the maximal aggregation (in %) were determined (Fig. 2A). Values for the absorption at 740 nm were measured with the aggregometer every 0.2 s. For the disaggregation phase, the baseline was determined by calculating the average value between 530 and 590 s and subtracted from the disaggregation curves (Fig. 2B and C). The curves were then inverted and the baseline before addition of the antagonist was set as 100% aggregation (Fig. 2D). For calculating the potency of FimH antagonists, the area under each disaggregation curve from 600 s until 2000 s ($AUC_{600-2000\ s}$) was determined and plotted against the concentration of the antagonist to obtain the half maximal inhibitory concentration (IC_{50}) (Fig. 2E). Mean values, standard deviation (SD), AUC and the plots were calculated and plotted using GraphPad Prism 5.0a (GraphPad Software, La Jolla, CA).

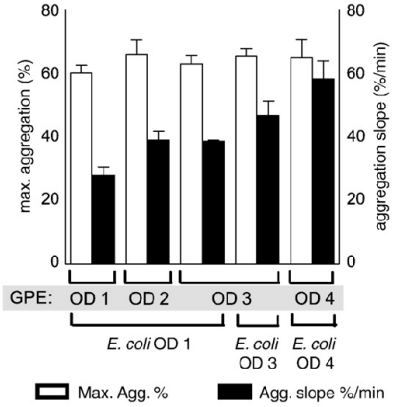

Fig. 4. Evaluation of the best aggregation conditions using *E. coli* and GPE at different concentrations, measured as OD_{600}. Bars in black are representing the maximal aggregation (in %) and the white bars are showing the aggregation slope (in %/min). The bars represent means ± SD. For *E. coli*, OD_{600} of 1 corresponds to 4.7×10^7 CFU/ml, OD_{600} of 3 to 1.4×10^8 CFU/ml and OD_{600} of 4 to 1.9×10^8 CFU/ml. For GPE, OD_{600} of 1 corresponds to 5.5×10^5 cells/ml, OD_{600} of 2 to 1.1×10^6 cells/ml, OD_{600} of 3 to 1.7×10^6 cells/ml and OD_{600} of 4 to 2.2×10^6 cells/ml.

3. Results

3.1. Optimization of the aggregation assay

3.1.1. Initial growth and measurement conditions

Bacteria and yeast were incubated overnight (12 h) in TSB at 37 °C without shaking, leading to a maximal aggregation slope for *E. coli* with *C. albicans* of 23.78 %/min (±4.09 %/min) and a maximal aggregation of 36.89 % (± 1.63 %). With the *E. coli* Δ*fimA-H* mutant, virtually no aggregation was observed with *C. albicans*, resulting in a maximal aggregation slope of 0.25 %/min (±0.29 %/min) and a maximal aggregation of 0.02 % (± 0.1 %) (Fig. 2A). After 600 s of measurement, a stable baseline was achieved, a prerequisite for a reliable determination of the disaggregation potency of FimH antagonists (Fig. 2B).

3.1.2. Shaking versus static incubation

Compared to static incubation (see above), *E. coli* and *C. albicans* incubated overnight under shaking conditions (250 rpm) exhibited a 13-fold lower aggregation slope of 1.82 %/min (±0.61 %/min) and a 5-fold lower aggregation maximum of 8.38 % (±0.69 %). In the optimized assay format, *E. coli* was therefore incubated overnight under static conditions whereas *C. albicans* was agitated at 250 rpm.

3.1.3. Bacterial and yeast growth media

In Fig. 3, the maximal aggregation (%) and the aggregation slope (%/min) of *E. coli* and *C. albicans* incubated in different growth media are presented. The best values were obtained when *E. coli* was cultivated in LB broth and *C. albicans* in NB medium, resulting in an aggregation slope of 64.15 %/min (±6.0 %/min) and a maximal aggregation of 54.65 % (±4.6 %). These conditions were therefore applied for all further measurements.

Fig. 5. Disaggregation curves and corresponding IC_{50} values, calculated using the $AUC_{600\ 2000s}$ of the disaggregation curves. Values represent the mean ± SD of triplicate measurements. (A) **1** shows an IC_{50} of 77.14 µM and represents the reference antagonist. (B) **2** does not exhibit a measurable disaggregation potency at concentrations up to 769 µM. (C) **3** exhibits the best inhibitory potential of all measured FimH antagonists with an IC_{50} of 0.87 µM. (D) **4** has an IC_{50} of 13.92 µM. (E) **5** shows almost the same inhibitory potential as **2**, resulting in an IC_{50} 62.96 µM.

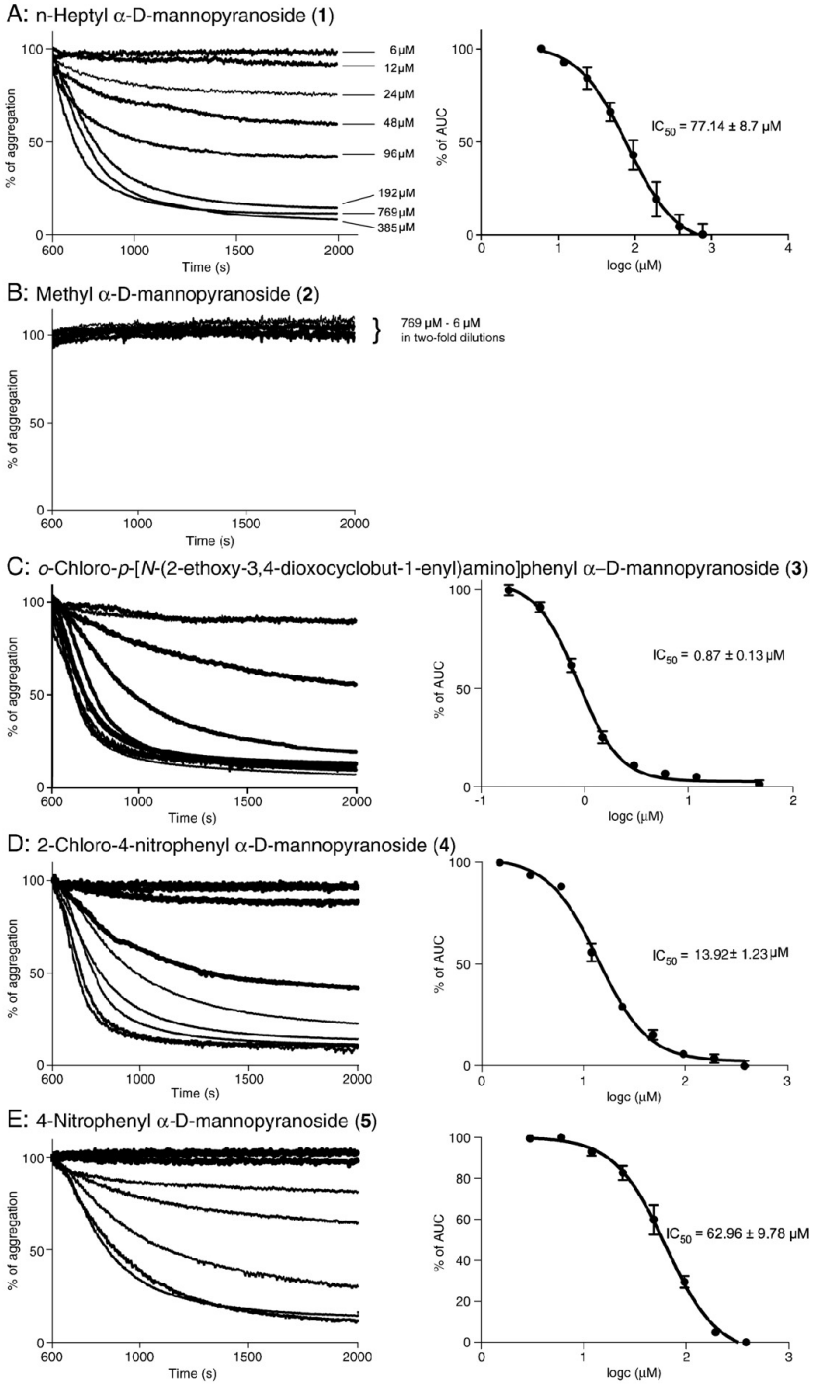
A: n-Heptyl α-D-mannopyranoside (1)
6 µM
12 µM
24 µM
48 µM
96 µM
192 µM
769 µM
385 µM
% of aggregation
Time (s)
% of AUC
IC50 = 77.14 ± 8.7 µM
logc (µM)
B: Methyl α-D-mannopyranoside (2)
769 µM - 6 µM
in two-fold dilutions
C: o-Chloro-p-[N-(2-ethoxy-3,4-dioxocyclobut-1-enyl)amino]phenyl α–D-mannopyranoside (3)
IC50 = 0.87 ± 0.13 µM
D: 2-Chloro-4-nitrophenyl α-D-mannopyranoside (4)
IC50 = 13.92± 1.23 µM
E: 4-Nitrophenyl α-D-mannopyranoside (5)
IC50 = 62.96 ± 9.78 µM

3.1.4. Concentration of E. coli and C. albicans

For both *E. coli* and *C. albicans*, the highest maximal aggregation of 50.68 % (±4.61 %) was obtained at an OD_{600} of 2 (Table 1). This concentration represents a bacteria to yeast ratio of 10:1 (4.8×10^6 CFU/50 µl: 5×10^7 CFU/250 µl). When the concentration of *E. coli* exceeds this ratio, a reduction of the maximal aggregation was observed.

3.1.5. Incubation time

For the optimization of the incubation time, cultures of *E. coli* and *C. albicans* incubated overnight, for 24 h and 48 h were compared. For *C. albicans*, the incubation time did not influence the aggregation behavior (data not shown). However, for *E. coli* the aggregation slope was increased by approx. 10 % and the maximal aggregation by approximately 5 % after incubation for 24 h compared to those incubated overnight. Incubation for 48 h resulted in a 16.1 % increase of the aggregation slope, but a 6.3 % reduction of the maximal aggregation. Since a 24 h incubation period resulted in the best maximal aggregation, it was applied for all further measurements.

3.1.6. Ratio of GPE and E. coli

To obtain an optimal aggregation phase, different ratios of *E. coli* and GPE were tested (Fig. 4). For both, an OD_{600} of 4 showed the best aggregation potential [aggregation slope of 62.2 %/min (±2.4 %/min) and a maximal aggregation of 65.1 % (±5.6 %)]. This concentration represents a bacteria to GPE ratio of 17:1 (9.6×10^6 CFU/50 µl: 5.8×10^5 cells/250 µl).

Since the aggregation of *E. coli* with GPE showed less variability and a higher reproducibility than those of *E. coli* with *C. albicans* (data not shown), they were exclusively employed for evaluation of the disaggregation potential of FimH antagonists.

3.2. Disaggregation potential of FimH antagonists

The disaggregation potential of five α-D-mannopyranosides and D-galactose was determined with the optimized conditions (see section 3.1). Fig. 5 shows the disaggregation curves for two-fold serial dilutions of the antagonists and the corresponding IC_{50} curves, calculated using the $AUC_{600-2000\ s}$. The AUC of each curve was calculated and plotted against the concentration. The reference compound **1** exhibits an IC_{50} of 77.14±8.7 µM. For compound **2** no disaggregation could be observed up to 769 µM. Compounds **4** and **5** showed IC_{50}s of 13.92±1.23 µM and 62.96±9.78 µM, respectively. The best disaggregation potential was achieved with compound **3**, resulting in an IC_{50} of 0.87±0.13 µM. Compound **6** was used as negative control and showed no disaggregation up to 769 µM.

In order to optimize the measurement time, the effect of a shorter disaggregation period was evaluated. When the AUC for a disaggregation phase of 700 s ($AUC_{600-1300\ s}$) and 1400 s ($AUC_{600-2000\ s}$) were compared, no significant difference of the IC_{50}s (± SD) for the antagonists **1**, **3** and **4** was observed. However, for compound **5** (Fig. 5E), an approx. 50 % higher IC_{50}-value was obtained with a 700 s disaggregation phase, because the baseline is not reached at that time point (IC_{50} of 92.86 µM vs. 62.96±9.78 µM). Therefore, a standard disaggregation phase of 1400 s ($AUC_{600-2000\ s}$) was applied.

4. Discussion

In the initially reported aggregometry assay by Ofek and Beachey in 1978, *E. coli* and yeast cells were used and the potential of FimH antagonists was evaluated and quantified based on the slope of the *E. coli*-yeast disaggregation curve. Since for our investigation a different assay set-up, other *E. coli* strains, and different aggregation cells were applied, the measurement settings had to be re-evaluated and validated.

Due to the suppression of type 1 pili expression under shaking incubation (Hultgren, 1986), a significant decrease in aggregation was observed using *E. coli* cultures agitated overnight. *C. albicans* showed no reduction of aggregation after shaking incubation, indicating that the mannan-structures on the cell wall are constantly expressed. Due to a higher yield of microorganisms grown under shaking conditions, *C. albicans* was incubated at 250 rpm for all further experiments. With the Δ*fimA-H* deletion mutant of *E. coli*, we could demonstrate that the aggregation depends exclusively on type 1 pili mediated adherence to *C. albicans* and GPE, respectively.

To determine the optimal nutrient conditions for type 1 pili expression, various growth media were investigated. With *E. coli* incubated in LB broth and *C. albicans* grown in NB medium, the highest aggregation values were achieved (Hultgren, 1986; Ofek and Beachey, 1978). In addition, optimal aggregation conditions were obtained when *E. coli* and *C. albicans* samples with an OD_{600} of 2 were used. As recommended (Blood and Curtis, 1995; Firon et al., 1983; Giampapa et al., 1988) the best results were obtained when the cultures were incubated for at least 24 h. Whereas overnight incubation led to less aggregation, similar values were obtained with cultures incubated for 48 h.

The majority of the disaggregation data reported in literature were obtained by a visual and therefore only semiquantitative interpretation of the disaggregation potential of the investigated FimH antagonists (e.g. Nagahori et al., 2002; Gouin et al., 2009). In addition, quantitative disaggregation data were also determined with an aggregometry assay reported by Ofek and Beachey, 1978 and Firon et al., 1983. In contrast, in this communication IC_{50} values were determined from the AUCs of the disaggregation curves obtained of serially diluted antagonists. In addition, the various assay parameters as growth and measurement conditions, cell types were thoroughly optimized.

Optimization experiments clearly showed the advantages of blood cells (GPE, Fig. 4) over yeast (*C. albicans*, Fig. 3). With GPE the maximal aggregation is independent on the OD_{600}s within 60–66 %, whereas the aggregation slope is heavily depending on the OD_{600} of both GPE and *E. coli*. The present format leads to a substantial improvement of the maximal aggregation (from 36.9 % to 65.1 %) and the ascending slope (from 23.8 %/min to 62.2 %/min).

The aggregometry assay was validated with five FimH antagonists (**1**–**5**) and a negative control (**6**) measured in serial dilutions starting with a concentration of 769 µM (Table 2). The determination of the dependence of the AUCs from the antagonist concentration (Fig. 5) leads to the IC_{50}-values. *n*-Heptyl α-D-mannopyranoside (**1**) was employed as reference compound. Methyl α-D-mannopyranoside (**2**) exhibited no disaggregation at a concentration up to 769 µM. Furthermore, **3** showed the lowest IC_{50} of all tested antagonists. **4** exhibited a slight improvement of activity compared to reference compound **1**, whereas **5** was equally active as **1**. With D-galactose (**6**) disaggregation could not be enforced and was therefore used as negative control (e.g. Clegg et al., 1984; Nagahori et al., 2002).

In Table 2 the IC_{50}-values are summarized and compared to those reported in literature. A direct comparison, however, is not possible, since the antagonistic potencies were measured in different assay formats and are reported relative to methyl α-D-mannopyranoside (**2**), which does not contribute to disaggregation up to a concentration of 769 µM in our aggregometry assay. Since the literature values for the disaggregation potencies are expressed as relative inhibitory potentials (rIPs) compared to **2**, the IC_{50}s were transformed into rIPs (Table 2). Except for **5**, our rIPs correlate well with values found in literature. Whereas **5** showed equal activity than the reference compound **1** in the aggregometry assay, a 6-fold lower activity is reported in literature.

Compared to previously described aggregation- and hemagglutination assays (Firon et al., 1983; Nagahori et al., 2002; Gouin et al., 2009) the presented aggregometry assay was optimized and standardized allowing the accurate and reproducible high-throughput screening of FimH antagonists. Instead of a visual and therefore only semi-quantitative analysis of the disaggregation event, a

Table 2
IC_{50} values determined with the aggregometry assay using *E. coli* with GPE. The relative IC_{50} (rIC_{50}) of the reference compound 1 was defined as 1. The rIP of each substance was calculated by dividing the IC_{50} of the reference compound 1 by the IC_{50} of the compound of interest. This results in rIPs above 1.00 for derivatives binding better than 1 and rIPs below 1.00 for compounds with a lower affinity than 1. (n.d.: not determinable).

FimH antagonist	Aggregometry assay			Literature
	IC_{50} [μM]	rIC_{50}	rIP	rIP
n-Heptyl α-D-mannopyranoside (**1**)	77.14 ± 8.7	1	1	440[a]
Methyl α-D-mannopyranoside (**2**)	n.d.	n.d.	n.d.	1[a,b,c]
o-Chloro-*p*-[*N*-(2-ethoxy-3, 4-dioxocyclobut-1-enyl)amino]phenyl α-D-mannopyranoside (**3**)	0.87 ± 0.13	0.011	90	6900[b]
2-Chloro-4-nitrophenyl α-D-mannopyranoside (**4**)	13.92 ± 1.23	0.18	6	717[c]
4-Nitrophenyl α-D-mannopyranoside (**5**)	62.96 ± 9.8	0.82	1	70[c]

[a] RIP determined by surface plasmon resonance measurements (Bouckaert et al., 2005).
[b] RIP determined by ELISA measurements (Sperling et al., 2006).
[c] RIP determined by aggregometer measurements (Firon et al., 1987).

quantitative method to determine the inhibitory potential of FimH antagonists was developed. The results (IC_{50}) of this function-based assay can be applied to determine the therapeutic dosage for in vivo studies.

The potential of anti-virulence therapies for UTI is investigated for a long period of time (Collier and De Miranda, 1955; Old, 1972; Ofek and Beachey, 1978; Firon et al., 1983; Bouckaert et al., 2005; Ernst and Magnani, 2009) and is still actively pursued (Cegelski et al., 2008). The reported new assay format will hopefully contribute to this endeavor by supporting the identification of carbohydrate-derived FimH antagonists with a therapeutic potential.

Acknowledgments

This study was supported by the Swiss National Science Foundation (SNF interdisciplinary grant K-32 K1-120904). Part of the results were presented at the 49th Interscience Conference of Antimicrobial Agents and Chemotherapy, San Francisco, CA, September 12 to 15 2009 (B-040).

Appendix A. Supplementary data

Supplementary data associated with this article can be found, in the online version, at doi:10.1016/j.mimet.2010.06.015.

References

Baumgartner, H.R., Born, G.V.R., 1968. Effect of 5-hydroxytryptamine on platelet aggregation. Nature 218, 137–141.
Blood, R.M., Curtis, G.D., 1995. Media for 'total' Enterobacteriaceae, coliforms and *Escherichia coli*. Int. J. Food Microbiol. 26, 93–115.
Bouckaert, J., Berglund, J., Schembri, M., De Genst, E., Cools, L., Wuhrer, M., Hung, C.S., Pinkner, J., Slattegard, R., Zavialov, A., Choudhury, D., Langermann, S., Hultgren, S.J., Wyns, L., Klemm, P., Oscarson, S., Knight, S.D., De Greve, H., 2005. Receptor binding studies disclose a novel class of high-affinity inhibitors of the *Escherichia coli* FimH adhesin. Mol. Microbiol. 55, 441–455.
Bouckaert, J., Mackenzie, J., de Paz, J.L., Chipwaza, B., Choudhury, D., Zavialov, A., Mannerstedt, K., Anderson, J., Pierard, D., Wyns, L., Seeberger, P.H., Oscarson, S., De Greve, H., Knight, S.D., 2006. The affinity of the FimH fimbrial adhesin is receptor-driven and quasi-independent of *Escherichia coli* pathotypes. Mol. Microbiol. 61, 1556–1568.
Capitani, G., Eidam, O., Glockshuber, R., Grutter, M.G., 2006. Structural and functional insights into the assembly of type 1 pili from *Escherichia coli*. Microbes Infect. 8, 2284–2290.
Cegelski, L., Marshall, G.R., Eldridge, G.R., Hultgren, S.J., 2008. The biology and future prospects of antivirulence therapies. Nat. Rev. Microbiol. 6, 17–27.
Choudhury, D., Thompson, A., Stojanoff, V., Langermann, S., Pinkner, J., Hultgren, S.J., Knight, S.D., 1999. X-ray structure of the FimC–FimH chaperone–adhesin complex from uropathogenic *Escherichia coli*. Science 285, 1061–1066.
Clegg, H., Guerina, N., Langermann, S., Kessler, T.W., Guerina, V., Goldmann, D., 1984. Pilus-mediated adherence of *Escherichia coli* K1 to human oral epithelial cells. Infect. Immun. 45, 299–301.
Collier, W.A., De Miranda, J.C., 1955. Bacterial hemagglutination. III. Mannose inhibition of *E. coli* hemagglutination. Antonie Leeuwenhoek 21, 133–140.
Datsenko, K.A., Wanner, B.L., 2000. One-step inactivation of chromosomal genes in *Escherichia coli* K-12 using PCR products. Proc. Natl Acad. Sci. USA 97, 6640–6645.
Ernst, B., Magnani, J.L., 2009. From carbohydrate leads to glycomimetic drugs. Nat. Rev. Drug Discov. 8, 661–677.
Fihn, S.D., 2003. Clinical practice. Acute uncomplicated urinary tract infection in women. N Engl J. Med. 349, 259–266.
Firon, N., Ofek, I., Sharon, N., 1982. Interaction of mannose-containing oligosaccharides with the fimbrial lectin of *Escherichia coli*. Biochem. Biophys. Res. Commun. 105, 1426–1432.
Firon, N., Ofek, I., Sharon, N., 1983. Carbohydrate specificity of the surface lectins of *Escherichia coli*, *Klebsiella pneumoniae*, and *Salmonella typhimurium*. Carbohydr. Res. 120, 235–249.
Firon, N., Ashkenazi, S., Mirelman, D., Ofek, I., Sharon, N., 1987. Aromatic alpha-glycosides of mannose are powerful inhibitors of the adherence of type 1 fimbriated *Escherichia coli* to yeast and intestinal epithelial cells. Infect. Immun. 55, 472–476.
Giampapa, C.S., Abraham, S.N., Chiang, T.M., Beachey, E.H., 1988. Isolation and characterization of a receptor for type 1 fimbriae of *Escherichia coli* from guinea pig erythrocytes. J. Biol. Chem. 263, 5362–5367.
Gouin, S.G., Wellens, A., Bouckaert, J., Kovensky, J., 2009. Synthetic multimeric heptyl mannosides as potent antiadhesives of uropathogenic *Escherichia coli*. Chem. Med. Chem. 4, 749–755.
Hvidberg, H., Struve, C., Krogfelt, K.A., Christensen, N., Rasmussen, S.N., Frimodt-Møller, N., 2000. Development of a long-term ascending urinary tract infection mouse model for antibiotic treatment studies. Antimicrob. Agents Chemother. 44, 156–163.
Hooton, T.M., 2001. Recurrent urinary tract infection in women. Int. J. Antimicrob. Agents 17, 259–268.
Hultgren, S.J., 1986. Regulation of production of type 1 pili among urinary tract isolates of *Escherichia coli*. Infect. Immun. 54, 613–620.
Langermann, S., Palaszynski, S., Barnhart, M., Auguste, G., Pinkner, J.S., Burlein, J., Barren, P., Koenig, S., Leath, S., Jones, C.H., Hultgren, S.J., 1997. Prevention of mucosal *Escherichia coli* infection by FimH-adhesin-based systemic vaccination. Science 276, 607–611.
Langermann, S., Mollby, R., Burlein, J.E., Palaszynski, S.R., Auguste, C.G., DeFusco, A., Strouse, R., Schenerman, M.A., Hultgren, S.J., Pinkner, J.S., Winberg, J., Guldevall, L., Soderhall, M., Ishikawa, K., Normark, S., Koenig, S., 2000. Vaccination with FimH adhesin protects cynomolgus monkeys from colonization and infection by uropathogenic *Escherichia coli*. J. Infect. Dis. 181, 774–778.
Mulvey, M.A., 2002. Adhesion and entry of uropathogenic *Escherichia coli*. Cell. Microbiol. 4, 257–271.
Mulvey, M.A., Schilling, J.D., Hultgren, S.J., 2001. Establishment of a persistent *Escherichia coli* reservoir during the acute phase of a bladder infection. Infect. Immun. 69, 4572–4579.
Murphy, K.C., Campellone, K.G., 2003. Lambda Red-mediated recombinogenic engineering of enterohemorrhagic and enteropathogenic *E. coli*. BMC Mol. Biol. 4, 11.
Nagahori, N., Lee, R.T., Nishimura, S., Page, D., Roy, R., Lee, Y.C., 2002. Inhibition of adhesion of type 1 fimbriated *Escherichia coli* to highly mannosylated ligands. Chembiochem 3, 836–844.
Ofek, I., Beachey, E.H., 1978. Mannose binding and epithelial cell adherence of *Escherichia coli*. Infect. Immun. 22, 247–254.
Old, D.C., 1972. Inhibition of the interaction between fimbrial haemagglutinins and erythrocytes by d-mannose and other carbohydrates. J. Gen. Microbiol. 71, 149–157.
Rosen, D.A., Hung, C.S., Kline, K.A., Hultgren, S.J., 2008. Streptozocin-induced diabetic mouse model of urinary tract infection. Infect. Immun. 76, 4290–4298.
Sharon, N., 2006. Carbohydrates as future anti-adhesion drugs for infectious diseases. Biochim. Biophys. Acta 1760, 527–537.
Sperling, O., Fuchs, A., Lindhorst, T.K., 2006. Evaluation of the carbohydrate recognition domain of the bacterial adhesin FimH: Design, synthesis and binding properties of mannoside ligands. Org. Biomol. Chem. 4, 3913–3922.
Wellens, A., Garofalo, C., Nguyen, H., Van Gerven, N., Slättergård, R., Hernalsteens, J.-P., Wyns, L., Oscarson, S., De Greve, H., Hultgren, S., Bouckaert, J., 2008. Intervening with urinary tract infections using anti adhesives based on the crystal structure of the FimH oligomannose 3 complex. PLoS ONE 3, 4–13.
Wiles, T.J., Kulesus, R.R., Mulvey, M.A., 2008. Origins and virulence mechanisms of uropathogenic *Escherichia coli*. Exp. Mol. Pathol. 85, 11–19.

RESULTS AND DISCUSSION

Paper II

FimH Antagonists for the Oral Treatment of Urinary Tract Infections: From Design and Synthesis to *in vitro* and *in vivo* Evaluation.

Klein T*, Abgottspon D*, Wittwer M*, Rabbani S*, Herold J*, Jiang X, Kleeb S, Lüthi C, Scharenberg M, Bezençon J, Gubler E, Pang L, Smiesko M, Cutting B, Schwardt O, Ernst B.

J. Med. Chem. **2010**.

* These authors contributed equally to the project.

My contributions:

In vitro evaluation of the inhibitory potency of the FimH antagonists in the aggregometry assay.

In vivo pharmacokinetic and infection studies in the UTI mouse model.

Manuscript preparation.

Journal of Medicinal Chemistry Article

J. Med. Chem. **2010,** *53,* 8627–8641 **8627**
DOI: 10.1021/jm101011y

FimH Antagonists for the Oral Treatment of Urinary Tract Infections: From Design and Synthesis to in Vitro and in Vivo Evaluation

Tobias Klein,[†] Daniela Abgottspon,[†] Matthias Wittwer,[†] Said Rabbani,[†] Janno Herold,[†] Xiaohua Jiang, Simon Kleeb, Christine Lüthi, Meike Scharenberg, Jacqueline Bezençon, Erich Gubler, Lijuan Pang, Martin Smiesko, Brian Cutting, Oliver Schwardt, and Beat Ernst*

Institute of Molecular Pharmacy, Pharmacenter, University of Basel, Klingelbergstrasse 50, CH-4056 Basel, Switzerland.
[†]*These authors contributed equally to the project*

Received August 4, 2010

Urinary tract infection (UTI) by uropathogenic *Escherichia coli* (UPEC) is one of the most common infections, particularly affecting women. The interaction of FimH, a lectin located at the tip of bacterial pili, with high mannose structures is critical for the ability of UPEC to colonize and invade the bladder epithelium. We describe the synthesis and the in vitro/in vivo evaluation of α-D-mannosides with the ability to block the bacteria/host cell interaction. According to the pharmacokinetic properties, a prodrug approach for their evaluation in the UTI mouse model was explored. As a result, an orally available, low molecular weight FimH antagonist was identified with the potential to reduce the colony forming units (CFU) in the urine by 2 orders of magnitude and in the bladder by 4 orders of magnitude. With FimH antagonist **16b**, the great potential for the effective treatment of urinary tract infections with a new class of orally available antiinfectives could be demonstrated.

Introduction

Urinary tract infection (UTI[a]) is one of the most common infections, affecting millions of people each year. Particularly affected are women, who have a 40−50% risk to experience at least one symptomatic UTI episode at some time during their life. In addition, more than half of them experience a relapse of the infection within 6 months.[1,2]

Although UTIs rarely cause severe diseases such as pyelonephritis or urosepsis, they are associated with high incidence rate and consume considerable healthcare resources.[3] Uropathogenic *Escherichia coli* (UPEC) are the primary cause of UTIs, accounting for 70−95% of the reported cases. Symptomatic UTIs require antimicrobial treatment, often resulting in the emergence of resistant microbial flora. As a consequence, treatment of consecutive infections becomes increasingly difficult because the number of antibiotics is limited and the resistance of *E. coli* is increasing, especially in patients with diabetes, urinary tract anomaly, paraplegy, and those with permanent urinary catheter. Therefore, a new approach for the prevention and treatment of UTI with inexpensive, orally applicable therapeutics with a low potential for resistance would have a great impact on patient care, public health care, and medical expenses.

UPEC strains express a number of well-studied virulence factors used for a successful colonization of their host.[3−5] One important virulence factor is located on type 1 pili, allowing UPEC to adhere and invade host cells within the urinary tract. It enables UPEC to attach to oligomannosides, which are part of the glycoprotein uroplakin Ia on the urinary bladder mucosa. This initial step prevents the rapid clearance of *E. coli* from the urinary tract by the bulk flow of urine and at the same time enables the invasion of the host cells.[3,6]

Type 1 pili are the most prevalent fimbriae encoded by UPEC, consisting of the four subunits FimA, FimF, FimG, and FimH, the latter located at the tip of the pili.[7] As a part of the FimH subunit, a carbohydrate-recognizing domain (CRD) is responsible for bacterial interactions with the host cells within the urinary tract.[6] The crystal structure of the FimH-CRD was solved[8] and its complexes with *n*-butyl α-D-mannopyranoside[9] and Manα(1−3)[Manα(1−6)]Man[10] recently became available.

Previous studies showed that vaccination with FimH adhesin inhibits colonization and subsequent *E. coli* infection of the urothelium in humans.[11,12] In addition, adherence and invasion of host cells by *E. coli* can also be prevented by α-D-mannopyranosides, which are potent antagonists of interactions mediated by type 1 pili.[13] Whereas α-D-mannopyranosides efficiently prevent adhesion of *E. coli* to human urothelium, they are not exhibiting a selection pressure to induce antimicrobial resistance. Furthermore, environmental contamination is less problematic compared to antibiotics.[14]

More than two decades ago, Sharon and co-workers have investigated various mannosides and oligomannosides as

*To whom correspondence should be addressed. Phone: +41 61 267 1551. Fax: +41 61 267 1552. E-mail: beat.ernst@unibas.ch.

[a]Abbreviations: AUC, area under the curve; Caco-2 cells, Caucasian colon adenocarcinoma cells; CFU, colony forming units; CRD, carbohydrate recognition domain; DC-SIGN, dendritic cell-specific intercellular adhesion molecule-3-grabbing nonintegrin; CES, carboxylesterase; IC_{50}, half maximal inhibitory concentration; iv, intravenous; D, distribution coefficient; GPE, guinea pig erythrocytes; LC-MS, liquid chromatography−mass spectrometry; MBP, mannose-binding protein; PAMPA, parallel artificial membrane permeation assay; P_{app}, apparent permeability; P_e, effective permeation; po, peroral; PPB, plasma protein binding; PSA, polar surface area; *S*, solubility; SAR, structure−activity relationship; sGF, simulated gastric fluid; sIF, simulated intestinal fluid; TEER, transepithelial resistance; UPEC, uropathogenic *E. coli*; UTI, urinary tract infection.

Published on Web 11/24/2010

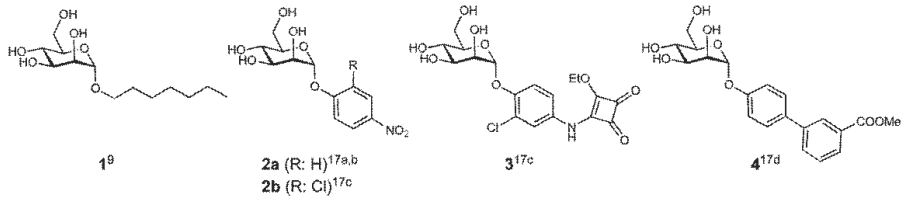

Figure 1. Known alkyl (**1**) and aryl (**2**–**4**) α-D-mannosides exhibiting nanomolar affinities.

Scheme 1. Phenyl α-D-Mannosides **7a**–**7d** with Spacers of Different Lengths between the Carbohydrate Moiety and the Phenyl Substituent[a]

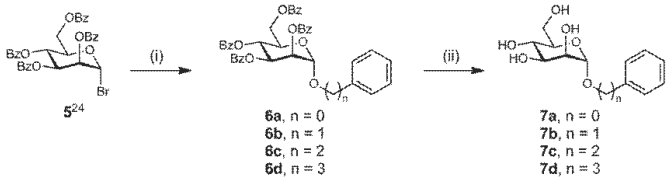

[a] (i) $Ph(CH_2)_nOH$, $Hg(CN)_2$, $HgBr_2$, DCM, 2 h to 7 d, rt, 57–99%; (ii) NaOMe, MeOH, 6–16 h, rt, 48–91%.

potential antagonists for type 1 fimbriae-mediated bacterial adhesion.[15] However, for these mannosides, only weak interactions in the milli- to micromolar range were observed. In contrast, numerous reports on glycoconjugate dendrimers with nanomolar affinities have been published.[16] However, on the basis of their large molecular weight and high polarity, they are predicted to exhibit only poor intestinal absorption and are therefore not amenable for oral dosing. Recently, some isolated reports on high affinity monovalent FimH antagonists were published[17] and, in one case, a systematic structure–activity relationship (SAR) profile was established.[17d] In summary,[8,9,15–19] long chain alkyl and aryl mannosides (selected examples are presented in Figure 1) displayed the highest affinity, likely due to hydrophobic interactions with two tyrosines and one isoleucine forming the entrance to the binding site, the so-called "tyrosine gate".[18] Because binding affinities were obtained from diverse assay formats,[9,17c,20] a direct comparison of the affinities is difficult. On the basis of various crystal structures of methyl-[8] and *n*-butyl α-D-mannoside[18] as well as oligomannose-3[9] bound to FimH, Han et al. recently presented a rationale for the design of arylmannosides with increased affinities.[17d]

To date, a few reports on the in vivo potential of methyl α-D-mannoside[10,21,22] and *n*-heptyl α-D-mannoside (**1**)[10] are available. In all cases, the FimH antagonists were directly instilled into the bladder concomitantly with uropathogenic *E. coli* (UPEC). In this communication, we present for the first time nanomolar FimH antagonists exhibiting appropriate pharmacokinetic properties for iv and oral treatment of urinary tract infections.

Results and Discussion

Identification of Lead Mannoside. In most of the reported FimH antagonists, aromatic aglycones have been applied.[17] However, only limited information on the optimal spacer length between the mannose moiety and the aromatic substituent is available. Generally, the aromatic moiety is directly fused to the anomeric oxygen.[17a–d] Extended spacers containing one[17b,d] or two[17c] methylene moieties were also reported, however, the corresponding antagonists are not really comparable to each other because different assay formats were used for their evaluation. For the identification of the optimal spacer length, we therefore synthesized mannosides **7a**–**d** (Scheme 1). In a competitive binding assay,[23] mannoside **7a** showed a slightly higher affinity (Table 1, entry 2) compared with **7b**–**7d** (see Table 1, entries 3–5), confirming recent data for **7a** and **7b**.[17d]

From the crystal structure of *n*-butyl α-D-mannoside bound to FimH,[18] it becomes obvious that the hydrophobic rim formed by Tyr48, Tyr137, and Ile52 is not reached by an anomeric phenyl group. An extension by a second aromatic ring, i.e. a biphenyl α-D-mannoside, however, should be compatible for π–π staking. Indeed, some recently published representatives of this compound class show excellent affinities.[17d]

To achieve an optimal fit with the hydrophobic binding site of FimH, the conformation of the biphenyl aglycone in **i** was modified by different substitution patterns on ring A (Figure 2). Because electron poor aromatic rings substantially improve the binding affinities of FimH antagonists (a 10-fold improvement is reported for **2B** vs **2A**[17c]), chloro substituents on ring A were used for the spatial exploration of the binding site. With substituents in *ortho*-position, only a minor change of the dihedral angle Φ_1 is observed (−3.3° to −0.7°). However, by an increased rotational barrier, the conformational flexibility is limited. The dihedral angle Φ_2 between the conjugated aromatic rings results from an interplay between π-conjugation and steric effects.[24,25] By migrating the substituent to the *meta*-position, the torsion angle Φ_2 is substantially influenced. Whereas unsubstituted biphenyls show a global twisted minimum at a torsion angle Φ_2 of approximately 39°,[26] substituents in the *meta*-position favor an increase of Φ_2 to 60°. Details of the conformational analyses are summarized in the Supporting Information.

Design Strategy for Intestinal Absorption and Renal Elimination. Besides high affinity, drug-like pharmacokinetic properties are a prerequisite for a successful in vivo application. In the present case, orally available FimH antagonists

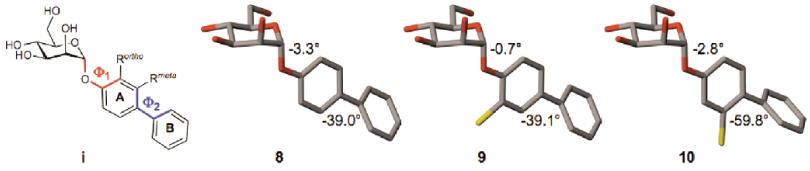

Figure 2. Conformational changes of the biphenyl aglycone by chloro substitutions in *ortho*- and *meta*-position of ring A.

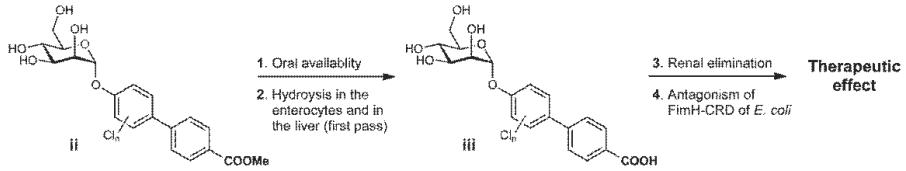

Figure 3. FimH antagonists with the pharmacodynamic and pharmacokinetic properties required for a therapeutic application. (1) For the prediction of oral availability, the PAMPA[30] and the Caco-2 cell assay[31] are applied. (2) The hydrolysis of ester **ii** to carboxylate **iii** is evaluated by mouse liver microsomes. (3) Renal excretion is estimated based on a positive correlation with polar descriptors (polar surface area, H-bond donors, H-bond acceptors, rotatable bonds).[32] (4) The potential of FimH antagonists is assessed with a target-based assay[23] and a function-based cellular assay.[33] For the evaluation of the therapeutic effect, a urinary tract infection mouse model (UTI mouse model in C3H/HeN mice) is applied.

that, once in circulation, are metabolically stable and undergo fast renal elimination, are required. This pharmacokinetic profile results from various serial and/or simultaneous processes that include dissolution, intestinal absorption, plasma protein binding, metabolic clearance, body distribution as well as renal and other clearance mechanisms. Because intestinal absorption and renal elimination are related to opposed properties, i.e. lipophilicity for intestinal absorption and hydrophilicity for renal elimination, a prodrug approach[27] was envisaged (Figure 3). Ester **ii** is expected to undergo intestinal absorption[28] and, later on, efficient hydrolysis to carboxylate **iii** by esterases[29] present in enterocytes lining the small intestine and in the liver.

For renal clearance, the net result of glomerular filtration, active tubular secretion, and reabsorption, carboxylate **iii** should exhibit low lipophilicity (log $D_{7.4}$) and favorable polar descriptor values (polar surface area (PSA), H-bond capacity and rotatable bonds).[32] By contrast, lipophilic compounds are efficiently reabsorbed (as the passive reabsorption process occurs throughout the length of the nephron, whereas the secretion predominantly occurs at the proximal tubule). The estimated negative log $D_{7.4}$ for antagonists of type **iii** is expected to fulfill these specifications for an efficient renal elimination and a low reabsoption. Finally, once arrived at the site of action in the bladder, the antagonist binds to the carbohydrate recognition domain (CRD) located on the bacterial pili, thus interfering with the adhesion of *E. coli* to oligosaccharide structures on urothelial cells.[34] To identify antagonists with the pharmacokinetic properties required for oral absorption and fast renal elimination, it was planned to determine PK parameters such as log $D_{7.4}$, pK_a, solubility, plasma protein binding, metabolic stability, and oral availability using the parallel artificial membrane permeation assay (PAMPA)[30] and the Caco-2 cell assay.[31]

Synthesis of FimH Antagonists. The aglycone in the α-1-position of D-mannose plays a ternary role, i.e. it mediates the lipophilic contact with the hydrophobic tyrosine gate, contains the elements required for intestinal absorption and, after metabolic cleavage of the prodrug, for a fast renal elimination.

The syntheses of the *para*-substituted biphenyls **16a−e** and **17a−c,e** are outlined in Scheme 2. Lewis acid promoted glycosylation of the halogenated phenols **13a−e** with trichloroacetimidate **12**[35] yielded the phenyl α-D-mannosides **14a−e**. In a palladium-catalyzed Suzuki coupling with 4-methoxycarbonylphenylboronic acid, the biphenyls **15a−e** were obtained. For the deprotection of the mannose moiety, Zemplén conditions were applied (→ **16a−e**). Finally, the methyl esters were saponified, yielding the sodium salts **17a−c,e**.

In a similar approach, two *meta*-substituted biphenyls in their ester form (→ **21a,b**) and as free acids (→ **22a,b**) were obtained (see Scheme 3).

Binding Affinities and Activities. For the biological in vitro evaluation of the FimH antagonists, two assay formats have been developed. For an initial characterization, a cell-free competitive binding assay[23] and, later on, a cell-based aggregation assay,[33] were applied. Whereas in the cell-free competitive binding assay only the CRD of the pili was used, the complete pili are present in the cell-based assay format. Furthermore, both formats are competitive assays, i.e. the analyzed antagonists compete with mannosides for the binding site. In the cell-free competitive binding assay, the competitors are polymer-bound trimannosides, whereas in the aggregation assay, the antagonist competes with more potent oligo- and polysaccharide chains present on the surface of erythrocytes.[36] Therefore, lower IC_{50} values are expected for the cell-free competitive binding assay. In addition, switching from the cell-free target-based assay to the function-based assay generally leads to a reduction of potency by several orders of magnitude. The interaction is further complicated by the existence of a high- and a low-affinity state of the CRD of FimH. Aprikian et al. experimentally demonstrated that in full-length fimbriae the pilin domain stabilizes the CRD domain in the low-affinity state, whereas the CRD domain alone adopts the high-affinity state.[37] It was recently shown that the pilin domain allosterically causes a twist in the β-sandwich fold of the CRD domain, resulting in a loosening of the binding pocket.[38] On

Scheme 2[a]

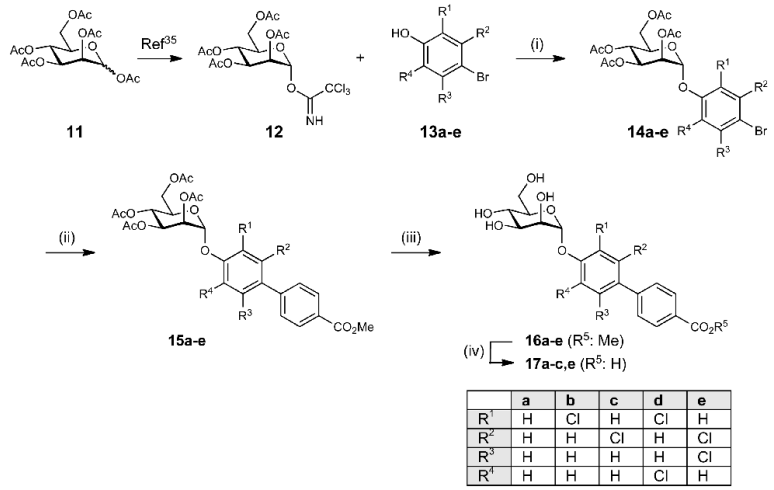

	a	b	c	d	e
R^1	H	Cl	H	Cl	H
R^2	H	H	Cl	H	Cl
R^3	H	H	H	H	Cl
R^4	H	H	H	Cl	H

[a] (i) TMSOTf, toluene, rt, 5 h (42−77%); (ii) 4-methoxycarbonylphenylboronic acid, Cs_2CO_3, $Pd(PPh_3)_4$, dioxane, 120°C, 8 h (28−85%); (iii) NaOMe, MeOH, rt, 4−24 h (22−86%); (iv) NaOMe, MeOH, rt, then NaOH/H_2O, rt, 16−24 h (63−94%).

Scheme 3[a]

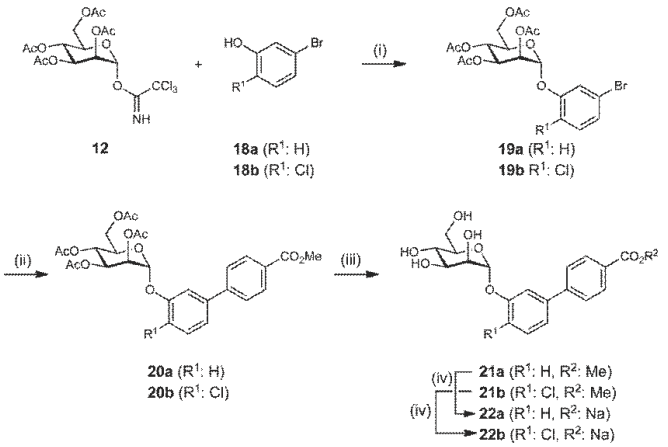

[a] (i) TMSOTf, toluene, rt, 5 h (67−70%); (ii) 4-methoxycarbonylphenylboronic acid, Cs_2CO_3, $Pd(PPh_3)_4$, dioxane, 120°C, 8 h or $Pd_2(dba)_3$, *S*-Phos, dioxane, 80°C, overnight (46−56%); (iii) NaOMe, MeOH, rt, 24 h (52−67%); (iv) NaOMe, MeOH, rt, then NaOH/H_2O, rt, 24 h (75−95%).

the basis of these findings, we expect a loss of affinity of our antagonists toward full-length fimbriae, when compared to the CRD domain alone.

Cell-Free Competitive Binding Assay. The cell-free inhibition assay is based on the interaction of a biotinylated polyacrylamide glycopolymer with the FimH-CRD as previously reported.[23] A recombinant protein consisting of the carbohydrate recognition domain of FimH linked with a thrombin cleavage site to a 6His-tag (FimH-CRD-Th-6His) was expressed in *E. coli* strain HM125 and purified by affinity chromatography. The IC_{50} values of the test compounds were determined in microtiter plates coated with FimH-CRD-Th-6His. Complexation of the biotinylated glycopolymer with streptavidin coupled to horseradish peroxidase allowed the quantification of the binding properties of FimH antagonists (Figure 4a). To ensure comparability with different antagonists, the reference compound *n*-heptyl α-D-mannopyranoside (**1**)[33] was tested in parallel in each individual microtiter plate. The affinities are reported relative to *n*-heptyl α-D-mannopyranoside (**1**) as rIC_{50} in Table 1.

The most active representatives from the ester group are **16a** (Table 1, entry 6) and **16b** (entry 8) with affinities in the low nanomolar range, which is an approximately 10-fold improvement compared to reference compound **1**. The

Table 1. Pharmacodynamic and Pharmacokinetic Parameters of FimH Antagonists[a,b]

		IC_{50} binding assay [nM]	rIC_{50}	IC_{50} Aggregometry assay [μM]	PAMPA log P_e [log10⁻⁶ cm/s]/ %Mm	Caco-2 P_{app} [10⁻⁶ cm/s]	log $D_{7.4}$	pK_a	log S [μg/mL]/ pH	PPB [%]
1	 **1**	73±7.9	1.0	77.14±8.7	-4.89/21	nd	1.65	-	>3000	81
2	 **7a**	150±11.5	1.9	nd	nd/nd	nd	nd	-	>3000	nd
3	 **7b**	364±16.8	4.6	nd	nd/nd	nd	nd	-	nd	nd
4	 **7c**	210±11.2	2.6	nd	nd/nd	nd	nd	-	nd	nd
5	 **7d**	253±13.4	3.2	nd	nd/nd	nd	nd	-	nd	nd
6	 **16a**[7d]	10.4±1.2	0.14	42±7	-4.7/<20%	4.23	2.14	-	33.8/6.51	93
7	 **17a**	17.1±2.2	0.15	45±8	np	nd	<-1.5	3.88	>3000/6.61	73
8	 **16b**	4.8±1.2	0.06	9±2.7	-4.6/41.00	2.05	2.32	-	11.9/6.53	94
9	 **17b**	6.7±2.1	0.09	10±2.3	np/3.5	nd	-0.77	3.98	>3000/6.50	89
10	 **16c**	22.0±8.4	0.30	41[2]	-4.72/67.6	nd	2.42	-	11.5/6.50	95
11	 **17c**	27.6±3.9	0.38	17[2]	np	nd	-1.33	3.95	>3000/6.50	82
12	 **16d**	16.0±0.8	0.22	14[2]	-4.29/54.3	3.32	2.31	-	4.6/6.53	98
13	 **16e**	15.3±0.4	0.07	nd	-4.40/70.2	5.81	3.10	-	22.7/6.53	94
14	 **17e**	23.9±2.2	0.19	nd	nd/nd	nd	nd	nd	nd	nd
15	 **21a**[7d]	20.0±4.3	0.27	33[3]	-5.01/60.7	4.88	2.02	-	37.6/6.52	92
16	 **22a**	38.7±5.2	0.53	45[3]	np/9.7	nd	<-1.5	3.69	>3000/6.50	81
17	 **21b**	11.8±0.1	0.16	31[3]	-4.69/51.7	1.63	1.70	-	24.3/6.54	96
18	 **22b**	29.2±0.7	0.40	nd	np/nr	0.55	<-1.5	3.41	>3000/6.5	87

[a] Single determination; P_e,effective permeation; P_{app}, apparent permeability; np, no permeation; nr, no retention; nd, not determined. [b] The IC_{50}s were determined with the cell-free competitive binding assay.[23] The rIC_{50} of each substance was calculated by dividing the IC_{50} of the compound of interest by the IC_{50} of the reference compound **1** (entry 1). This leads to rIC_{50} values below 1.00 for derivatives binding better than **1** and rIC_{50} values above 1.00 for compounds with a lower affinity than **1**. The aggregation of *E. coli* and GPE were determined in the aggregometry assay.[33] Passive permeation through an artificial membrane and retention therein was determined by PAMPA (parallel artificial membrane permeation assay).[30] The permeation through cell monolayers was assessed by a Caco-2 assay.[31] Distribution coefficients (log *D* values) were measured by a miniaturized shake flask procedure.[44] pK_a values were determined by NMR spectroscopy.[45] Plasma protein binding (PPB) was assessed by a miniaturized equilibrium dialysis protocol.[46] Thermodynamic solubility (S) was measured by an equilibrium shake flask approach.[47]

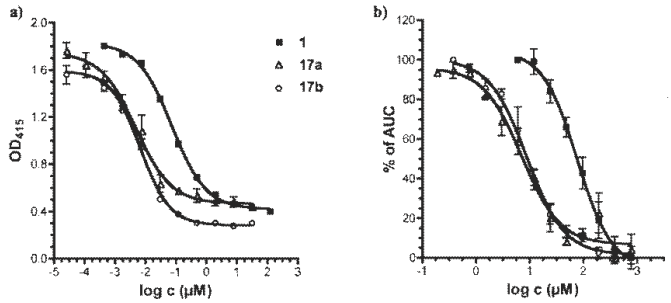

Figure 4. Affinities were determined in two different competitive assay formats. (a) a cell-free competitive binding assay[23] and (b) a cell-based aggregometry assay.[33] For antagonists **17a**, **17b**, and the reference compound **1**, IC_{50} values in the nM and μM range, respectively, were obtained. The 1000-fold difference between the two assay formats is due to the different competitors used as well as the different affinity states present in FimH, i.e. the high-affinity state present in the CRD used in the cell-free competitive binding assay and the low-affinity state present in the pili of *E. coli* used in the aggregometry assay.

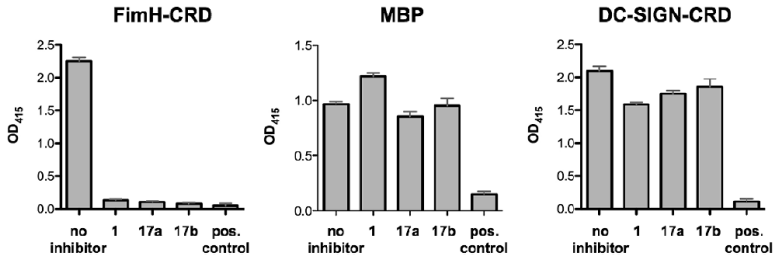

Figure 5. Competitive binding assay using FimH-CRD-Th-6His, DC-SIGN-CRD-IgG-Fc,[43] and MBP to evaluate the selectivity of compounds **1**, **17a**, and **17b**. Inhibitory capacities of the compounds were tested at a concentration of 1 mM. As positive control, D-mannose at a concentration of 50 mM was used.

corresponding carboxylic acids **17a** (entry 7) and **17b** (entry 9) exhibited a small reduction in affinity but are still 5-fold more active than reference compound **1**. All the remaining antagonists listed in Table 1 are slightly less active. For the in vivo examination, antagonists **17a** and **17b** were therefore foreseen for iv application and the prodrug **16b** for oral application.

Target selectivity is a further important issue. Mammalian mannose receptors are part of various biological processes, e.g. in cell−cell adhesion (DC-SIGN, dendritic cell-specific intercellular adhesion molecule-3-grabbing nonintegrin),[39] in the regulation of serum glycoprotein homeostasis (mannose receptor)[40] or in the innate and adaptive immune system by recognizing molecular patterns on pathogens (e.g., mannose-binding protein, mannose receptor, DC-SIGN).[39,41,42] Nonspecific interactions to the various mannose receptors by FimH inhibitors would have a profound impact on these processes. We therefore determined the affinity of reference compound **1** and the two antagonists **17a** and **17b** for two additional mannose binding proteins, DC-SIGN,[39,43] and MBP (mannose-binding protein)[42] (Figure 5). In both cases, affinities above 1 mM, i.e. a decrease of more than 5 orders of magnitude, was detected.

Aggregometry Assay. The potential of the biphenyl mannosides to disaggregate *E. coli* from guinea pig erythrocytes (GPE) was determined by a function-based aggregometry assay.[33] Antagonists were measured in triplicates, and the corresponding IC_{50} values were calculated by plotting the area under the curve (AUC) of disaggregation against the concentration of the antagonists. *n*-Heptyl α-D-mannopyranoside (**1**) was used again as reference compound and exhibits an IC_{50} of 77.14 ± 8.7 μM. Antagonists **17a** and **17b** showed IC_{50} values of 45 ± 8 μM and 10 ± 2.3 μM, respectively (Figure 4b). In general, the activities obtained from the aggregometry assay are approximately 1000-fold lower than the affinities determined in the target-based competitive assay (discussion see above).

In Vitro Pharmacokinetic Characterization of FimH Antagonists. For an application in the UTI mouse model, iv or po available FimH antagonists are required that, once absorbed to circulation, are metabolically stable and undergo fast renal elimination. Sufficient bioavailability requires a combination of high solubility and permeability to maximize absorption and low hepatic clearance to minimize first pass extraction. Furthermore, for efficient renal elimination, active and/or passive membrane permeability and low reabsorption in the renal tubuli is required. From the series of FimH antagonists with nanomolar in vitro activities (see Table 1), representatives with appropriate pharmacokinetic properties were selected for in vivo experiments based on the parameters shown below.

Oral Absorption and Renal Excretion. For the evaluation of oral absorption and renal excretion of the esters **16** and **21** as well as the acids **17** and **22** physicochemical parameters such as pK_a values, lipophilicity (distribution coefficients, log $D_{7.4}$), solubility, and permeability were determined

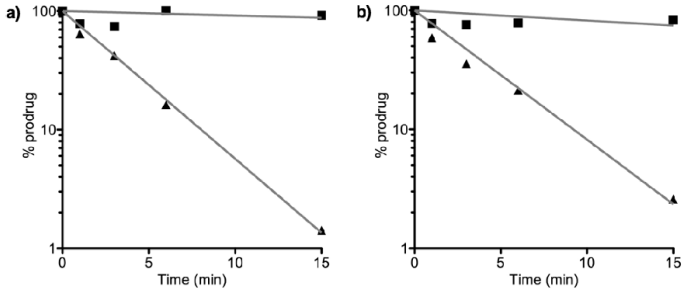

Figure 6. Incubation of (a) **16a** and (b) **16b** with pooled mouse liver microsomes (0.25 mg of protein/mL), in absence (▲) and in presence (■) of the specific carboxylesterase inhibitor bis(4-nitrophenyl) phosphate (BNPP).

(Table 1). Not surprisingly, the acids **17** and **22** showed log $D_{7.4}$ values in the range of −1 to −2 and pK_a values of approximately 4. While these parameters are beneficial for renal excretion,[32] oral absorption by passive diffusion seems unlikely. Indeed, when the permeation through an artificial membrane (PAMPA[30]) was studied, neither significant permeation (log P_e, P_e: effective permeation) nor membrane retention could be detected. Whereas for a successful oral absorption log P_e should be above −5.7 and/or the membrane retention above 80%,[48] the corresponding values for the carboxylic acids **17** and **22** are far from being in this range (see Table 1, e.g. entries 7 and 9). However, log $D_{7.4}$ values and PAMPA results were markedly improved for the esters **16** and **21** (Table 1, e.g. entries 6 and 8), suggesting that these FimH antagonists are orally absorbed. This assumption was fully confirmed in a cell-based permeation assay with Caco-2 cells.[31] For renal excretion, Varma et al.[31] correlated low lipophilicity and the presence of a charged state at physiological pH positively with enhanced elimination. On the basis of log $D_{7.4}$ and pK_a summarized in Table 1, the carboxylates **17** and **22** fulfill these requirements. Overall, these results support the prodrug approach: (i) oral application of the esters **16** and **21** and (ii) renal elimination of the corresponding acids **17** and **22**.

Solubility. A major problem of the antagonists **16** and **21** is their insufficient solubility, ranging from 4.6 to 37.6 μg/mL. Even though the solubility issue can be addressed by appropriate formulations, further structural modifications to improve solubility are necessary. Opposite to the esters, the corresponding carboxylates **17** and **22** showed excellent solubility (> 3 mg/mL). This enables their iv application in physiological solutions (PBS) in the UTI model without further needs to develop suitable formulations (see below).

Stability in Simulated Gastrointestinal Fluids. To exclude degradation in the gastrointestinal tract prior to absorption, the stability of **1**, **16b**, and **17b** in simulated gastric fluid (sGF) and simulated intestinal fluid (sIF) was determined. All three antagonists proved to be sufficiently stable with more than 80% of the initial concentrations found after two hours.

Metabolic Stability. Because the prodrug approach is only applicable when the esters **16a** and **16b** are rapidly metabolically cleaved into the corresponding acids, their propensity to enzymatic hydrolysis by carboxylesterase (CES) was studied. Mammalian CESs are localized in the endoplasmatic reticulum of the liver and most other organs.[29] Because of the excellent affinity of the corresponding acids **17a** and **17b** to FimH, we concentrated our metabolic studies on the ester prodrugs **16a** and **16b**, which were incubated with pooled male mouse liver microsomes to study the hydrolysis and the release of the metabolites. Preliminary experiments involving low substrate concentrations (2 μM) and a concentration of the microsomal protein of 0.25 mg/mL showed a fast degradation of the ester prodrugs (Figure 6). Addition of the specific CES inhibitor bis(4-nitrophenyl) phosphate (BNPP) prevented ester degradation, suggesting that the metabolic transformation can be attributed to CESs.[49]

On the basis of these in vitro results, we also expect fast hydrolysis of the esters in vivo at the first liver passage. Current studies are focusing on the kinetic parameters of the enzymatic ester cleavage.

To reach the minimal therapeutic concentration in the bladder (approximately 1 μg/mL, as estimated from a cell-based infection assay[50]), the FimH antagonists **17a** and **17b** should be efficiently renally eliminated and not further metabolically processed. Therefore, the metabolic fate of the free carboxylic acids **17a** and **17b** was examined. A common method to predict a compound's propensity to phase I metabolism is its incubation with liver microsomes in presence of NADPH.[51] Under these conditions, in vitro incubations of the free carboxylic acids **17a** and **17b** with pooled male mouse liver microsomes (0.5 mg microsomal protein/mL) did not show significant compound depletion over a period of 30 min, suggesting a high stability against cytochrome P450 mediated metabolism in vivo. However, phase II metabolic pathways such as glucuronidation remain to be studied in details.

Plasma Protein Binding (PPB). Compared to the corresponding esters **16** and **21**, the antagonists **17** and **22** exhibit 5−20% lower plasma protein binding, typically in the range of 73−89%. This rather low PPB beneficially influences renal excretion because, in line with the free drug hypothesis,[52] molecules bound to plasma proteins evade metabolism and excretion. However, for a concluding statement, the kinetics of PPB, i.e. association and dissociation rate constants, have to be determined because PPB alone is not necessarily predictive for distribution, metabolism, and clearance.[53,54]

In Vivo Pharmacokinetics and Treatment Studies. The two mannose derivatives methyl α-D-mannoside and *n*-heptyl α-D-mannoside (**1**) were previously tested in the UTI mouse model.[10,21,22] In all three studies, the FimH antagonists were first preincubated with the bacterial suspension, followed by transurethral inoculation. To efficiently reduce infection,

Antagonist	Compartement	C_{max} (μg/mL)	AUC_{0-24} (μg x h/mL)	PPB
1	plasma	35 ± 14.1	34.3 ± 33.3	81%
	urine	951.4 ± 249.6	2469.3 ± 636.4	
17a	plasma	34.4 ± 11.8	19.3 ± 6.2	73%
	urine	509.6 ± 427.5	139.9 ± 118.8	
17b	plasma	39.4 ± 15.7	20.8 ± 7.3	89%
	urine	588.4 ± 218.2	209.6 ± 72.3	

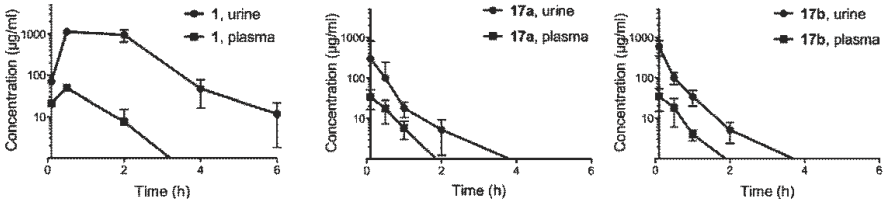

Figure 7. Determination of antagonist concentration in urine and plasma after a single iv application of 50 mg/kg. The data (table and graphs) show time-dependent urine and plasma concentrations of **1**, **17a**, and **17b**.

large amounts of methyl α-D-mannoside had to be applied (up to 1 M).[21] For *n*-heptyl α-D-mannoside (**1**), an approximately one $\log_{10}$ unit reduction of bacterial counts in the bladder was reached with lower, but still millimolar, concentration.[10] In the previously presented studies, the FimH antagonists were exclusively instilled into the bladder, which is obviously not suitable for a therapeutic application. The aim of our project was therefore the identification of FimH antagonists suitable for iv or preferably po applications. Before infection studies in a mouse disease model could be performed, the in vivo pharmacokinetic parameters (C_{max}, AUC) had to be determined to ensure the antagonists availability in the target organ (bladder).

Pharmacokinetics of a Single iv Application in C3H/HeN Mice. Plasma and urine concentrations of the FimH antagonists **1**, **17a**, and **17b** after iv application were determined. With a single dose of 50 mg/kg, the control compound **1** exhibited availability in the bladder over a period of 6 h after administration (n = 4), whereas at similar doses, **17a** and **17b** showed lower urine concentrations over a reduced time period (max 2 h) (n = 6). In Figure 7, the pharmacokinetic parameters are summarized. Overall, for all three compounds, higher availability of the antagonists in the urine was observed compared to the plasma. Because plasma protein binding is of comparable scale for the three compounds (see Table 1 and Figure 7), it similarly influences urine concentrations.

Pharmacokinetics of a Single po Application in C3H/HeN Mice. Aiming for an orally available FimH antagonist, the prodrug **16b** and its metabolite **17b** were tested. Because of the in vitro pharmacokinetic properties of **17b** (Table 1, entry 9), its low oral bioavailability after the administration of a single po dose (50 mg/kg) was not surprising. For the determination of the availability of a similar dose of **16b** at the target organ (bladder), plasma and urine concentrations were determined over a period of 24 h (n = 6) (Figure 8). Because **16b** was designed as a prodrug expected to be rapidly hydrolyzed, plasma and urine samples were analyzed not only for **16b** but also for its metabolite **17b**. **16b** was present only in minor concentrations in both plasma and urine. However, although the AUC of metabolite **17b** in urine is reduced by 90% compared to the iv application, its minimal therapeutic concentration can be maintained over a period of 2 to 3 h.

Antagonist applied	Antagonist detected	Compartment	$AUC_{0-24\ p.o.}$ (μg x h/mL)
17b	**17b**	Plasma	n.d.
		Urine	2.7 ± 3.2
16b	**16b**	Plasma	1.02 ± 0.32
		Urine	1.89 ± 0.37
	17b	Plasma	2.1 ± 0.61
		Urine	21.69 ± 3.88

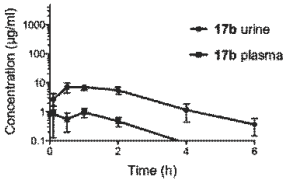

Figure 8. Determination of antagonist concentration in urine and plasma after a single po application of 50 mg/kg of antagonists **16b** and **17b**. The data (table and graph) show their time-dependent urine and plasma concentrations. When **17b** was orally applied, its plasma concentration was below the detection level, and only a small portion was present in the urine. However, after the application of the prodrug **16b**, metabolite **17b** was predominantly detected due to fast metabolic hydrolysis of **16b**. However, minor amounts of **16b** are still traceable in plasma as well as urine; nd, not detectable.

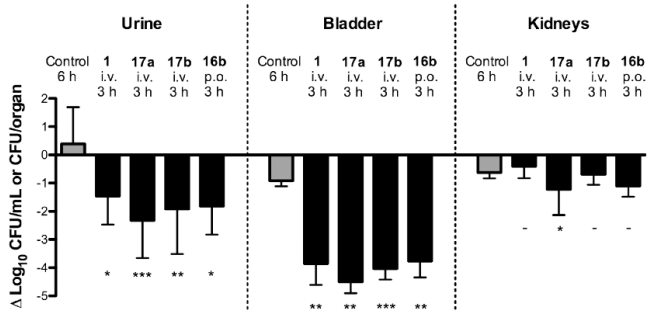

Figure 9. Treatment efficacy of the reference compound (**1**) and three FimH antagonists (**17a**, **17b**, **16b**) at a dosage of 50 mg/kg in the UTI mouse model after 3 h of infection, compared to a 6 h infection study ($n = 6$). **1**, **17a**, and **17b** were applied iv into the tail vein, whereas **16b** was applied orally. As baseline (reference), the mean counts of the 3 h infection were subtracted from the results of the tested antagonists and the 6 h control group. P values were calculated by comparing the treatment groups with the 3 h control group. (*) $P < 0.05$, (**) $P < 0.01$, (***) $P < 0.001$, (−) not significant (determined by Mann−Whitney test).

UTI Mouse Model: Treatment Study. Before treatment studies were started, the optimal infection profile was established. A 3 h infection exhibited the highest infection level in the C3H/HeN mouse strain. At longer infection times, e.g. 6 h, the control group showed indeed higher bacterial counts in the urine, however, the bladder and kidney counts already decreased due to self-clearance of the infection in the UTI mouse model.[55] For the in vivo UTI treatment studies (Figure 9), antagonists **1**, **17a**, **17b**, and **16b** were applied followed by infection with UPEC (UTI89). For each antagonist, a group of six animals was used. The animals were sacrificed 3 h after inoculation and urine and homogenized organs (bladder, kidneys) were examined for bacterial counts. The mean value in the untreated reference group ($n = 6$) showed 1.8×10^6 CFU/mL in the urine, 1.4×10^8 CFU in the bladder and 9.7×10^6 CFU in the kidneys. The bar diagram in Figure 9 summarizes the bacterial counts after iv (**1**, **17a**, and **17b**) and po (**16b**) treatment. The baseline represents the values obtained for the control group after 3 h and was used as reference for CFU reductions. **1** showed the lowest inhibition of growth in the urine with 1.5 $\log_{10}$ CFU reduction and an approximately 4 $\log_{10}$ reduction of bacterial counts in the bladder. After iv application of **17a**, a substantial decrease in the bacterial count was obtained (> 2 $\log_{10}$ CFU reduction in the urine and 4.5 $\log_{10}$ reduction in the bladder). A slightly lower reduction was observed when **17b** was applied iv (a decrease of 2 $\log_{10}$ CFU in the urine and 4 $\log_{10}$ for bladder counts). Interestingly, almost the same reduction of the bacterial count was detected with orally applied **16b**.

In general, urine samples showed higher bacterial counts compared to the bladder. This could be due to the difficulties during urine sampling. We observed that infected C3H/HeN mice void considerably less urine (5−50 μL) compared to healthy mice (50−100 μL). As a consequence, the lower urine volume leads to a higher concentration of bacteria in the collected urine and therefore to higher bacterial counts compared to the bladder.

In all treated animals, bacterial counts were only marginally reduced in the kidneys. This lower response to the treatment with FimH antagonists is probably due to different bacterial adhesion mechanisms in bladder and kidney. Whereas in the bladder adhesion is mediated by type 1 pili (via the CRD of FimH), P pili-dependent interactions are crucial for the adhesion in the kidneys.[6]

Summary and Conclusions

With the objective to develop an oral treatment of urinary tract infections, we have synthesized a series of potent small molecular weight FimH antagonists. Starting from the known antagonist phenyl α-D-mannopyranoside (**7a**), two equally potent classes of biphenyl α-D-mannopyranoside, those with an ester function (**16** and **21**) and those with a carboxylate (**17** and **22**) on the terminal aromatic ring, were synthesized. According to their pharmacokinetic properties, the acids **17** and **22** were not expected to be orally absorbed, a prediction that was also confirmed by an in vivo PK study. Therefore, a prodrug approach was envisaged. On the basis of permeation assays (PAMPA and Caco-2), the esters **16** and **22** were expected to exhibit oral availability. Moreover, metabolic studies with mouse liver microsomes proposed fast in vivo hydrolysis of orally applied **16b** to the corresponding carboxylate **17b**. In vivo PK studies in mice finally confirmed the in vitro prediction of a fast renal elimination of **17b** to the target organ, the bladder. When orally applied **16b** was tested in the UTI mouse model, it reduced the colony forming units (CFU) in the urine by 2 orders of magnitude and in the bladder by 4 orders of magnitude. As a result, a low molecular weight FimH antagonist suitable for the oral treatment of urinary tract infections was identified.

However, a number of parameters remain to be improved. Because the solubilities of the esters **16** and **22** are in the low μg/mL range, an iv application was impossible and the suspension in DMSO/1% Tween 80 used for oral dosing is not optimal. In addition, due to fast renal elimination, the minimal therapeutic concentration of **17b** in the bladder could only be maintained for 2−3 h. Because high plasma protein binding was observed, an unfavorable kinetic of dissociation of the active principle from plasma proteins followed by fast renal elimination might be the reason for these findings. An improvement of the corresponding pharmacokinetic parameters should positively influence the duration of action. Furthermore, a detailed analysis of the metabolic pathway of **16b** and its metabolite **17b** will elucidate their overall metabolic fate. Finally, a detailed PK/PD profile in the mouse model will elucidate the full potential of FimH antagonists for the therapy of urinary tract infections (UTI).

Experimental Section

General Methods. NMR spectra were recorded on a Bruker Avance DMX-500 (500 MHz) spectrometer. Assignment of ^{1}H

and ^{13}C NMR spectra was achieved using 2D methods (COSY, HSQC, TOCSY). Chemical shifts are expressed in ppm using residual $CHCl_3$, CHD_2OD, and HDO as references. Optical rotations were measured using Perkin-Elmer polarimeter 341. Electron spray ionization mass spectra (ESI-MS) were obtained on a Waters micromass ZQ. HRMS analysis were carried out using a Bruker Daltonics micrOTOF spectrometer equipped with a TOF hexapole detector. Microanalyses were performed at the Department of Chemistry, University of Basel, Switzerland. Microwave-assisted reactions were carried out with a CEM Discover and Explorer. Reactions were monitored by TLC using glass plates coated with silica gel 60 F_{254} (Merck) and visualized by using UV light and/or by heating to 140 °C for 5 min with a molybdate solution (a 0.02 M solution of ammonium cerium sulfate dihydrate and ammonium molybdate tetrahydrate in aqueous 10% H_2SO_4). Column chromatography was performed on a CombiFlash Companion (Teledyne-ISCO, Inc.) using RediSep normal phase disposable flash columns (silica gel). Reversed phase chromatography was performed on LiChroprepRP-18 (Merck, 40−63 μm). Commercially available reagents were purchased from Fluka, Aldrich, Merck, AKSci, ASDI, or Alfa Aesar. Methanol (MeOH) was dried by refluxing with sodium methoxide and distilled immediately before use. Toluene was dried by filtration over Al_2O_3 (Fluka, type 5016 A basic). Dioxane was dried by distillation from sodium/benzophenone.

4-Bromophenyl 2,3,4,6-Tetra-*O*-acetyl-α-D-mannopyranoside (14a). To a stirred solution of **12** (1.17 g, 3.00 mmol) and 4-bromophenol (**13a**, 623 mg, 3.60 mmol) in toluene (12 mL), TMSOTf (65 μL, 0.36 mmol) was added dropwise under argon. The mixture was stirred at rt for 5 h and then diluted with toluene (15 mL) and washed with satd aq $NaHCO_3$. The organic layer was separated, and the aqueous layer was extracted three times with toluene. The combined organic layers were dried over Na_2SO_4 and concentrated in vacuo. The residue was purified by flash chromatography on silica (petroleum ether/EtOAc, 19:1 to 1.5:1) to yield **14a** (1.17 g, 74%) as a white solid.

^1H NMR (500 MHz, $CDCl_3$): δ 2.06 (s, 9H, 3 $COCH_3$), 2.19 (s, 3H, $COCH_3$), 4.06 (m, 2H, H-5, H-6a), 4.27 (dd, J = 5.6, 12.4 Hz, 1H, H-6b), 5.36 (t, J = 10.2 Hz, 1H, H-4), 5.43 (dd, J = 1.8, 3.5 Hz, 1H, H-2), 5.48 (d, J = 1.7 Hz, 1H, H-1), 5.53 (dd, J = 3.5, 10.1 Hz, 1H, H-3), 6.98, 7.41 (AA′, BB′ of AA′BB′, J = 9.0 Hz, 4H, C_6H_4). ^{13}C NMR (125 MHz, $CDCl_3$): δ 20.71, 20.73, 20.74, 20.9 (4 $COCH_3$), 62.1 (C-6), 65.9 (C-4), 68.8 (C-3), 69.2 (C-2), 69.3 (C-5), 95.9 (C-1), 115.6, 118.3, 132.6, 154.7 (6C, C_6H_4), 170.0 (4C, 4 CO).

4-Bromo-2-chlorophenyl 2,3,4,6-tetra-*O*-acetyl-α-D-mannopyranoside (14b). According to the procedure described for **14a**, compound **12** (2.38 g, 4.84 mmol) and 4-bromo-2-chlorophenol (**13b**, 1.20 g, 5.80 mmol) were treated with TMSOTf (107 mg, 0.484 mmol) to yield **14b** (1.54 g, 59%) as a white solid.

$[\alpha]_D$ +60.6 (c 0.40, $CHCl_3$). ^1H NMR (500 MHz, $CDCl_3$): δ 2.02, 2.04, 2.18 (3s, 12H, 4 $COCH_3$), 4.05 (dd, J = 2.3, 12.2 Hz, 1H, H-6a), 4.10 (ddd, J = 2.7, 5.3, 9.6 Hz, 1H, H-5), 4.24 (dd, J = 5.4, 12.2 Hz, 1H, H-6b), 5.35 (t, J = 10.1 Hz, 1H, H-4), 5.48 (m, 2H, H-1, H-2), 5.56 (dd, J = 3.2, 10.1 Hz, 1H, H-3), 7.03 (d, J = 8.8 Hz, 1H, C_6H_3), 7.30 (dd, J = 2.4, 8.8 Hz, 1H, C_6H_3), 7.53 (d, J = 2.4 Hz, 1H, C_6H_3). ^{13}C NMR (125 MHz, $CDCl_3$): δ 20.9, 21.1 (4C, 4 $COCH_3$), 62.3 (C-6), 65.9 (C-4), 68.9 (C-3), 69.4 (C-2), 70.1 (C-5), 96.9 (C-1), 115.9, 118.4, 125.7, 130.8, 133.3, 150.6 (C_6H_3), 169.9, 170.0, 170.1, 170.7 (4 CO). ESI-MS calcd for $C_{20}H_{22}BrClNaO_{10}$ $[M + Na]^+$ 559.0; found 559.0; Anal. Calcd for $C_{20}H_{22}BrClO_{10}$: C 44.67, H 4.12. Found: C 45.08, H 4.14.

Methyl 4′-(2,3,4,6-Tetra-*O*-acetyl-α-D-mannopyranosyloxy)-biphenyl-4-carboxylate (15a). A Schlenk tube was charged with **14a** (503 mg, 1.00 mmol), 4-methoxycarbonylphenylboronic acid (224 mg, 1.24 mmol), *S*-Phos (20.5 mg, 0.05 mmol), cesium carbonate (1.17 g, 3.6 mmol), $Pd_2(dba)_3$ (10.4 mg, 0.01 mmol), and a stirring bar. The tube was closed with a rubber septum and was evacuated and flushed with argon. This procedure was repeated once, and then freshly degassed dioxane (5 mL) was added under a stream of argon. The reaction tube was quickly sealed and the contents were stirred at 80 °C overnight. The reaction mixture was cooled to rt, diluted with EtOAc (10 mL), washed with satd aq $NaHCO_3$ (5 mL) and brine (5 mL), and dried over Na_2SO_4. The solvents were removed in vacuo, and the residue was purified by flash chromatography on silica (petroleum ether/EtOAc, 3:1 to 3:2) to give **15a** (474 mg, 85%) as a white solid.

$[\alpha]_D$ +80.8 (c 1.00, $CHCl_3$). ^1H NMR (500 MHz, $CDCl_3$): δ 2.02, 2.03, 2.04, 2.19 (4s, 12H, $COCH_3$), 3.91 (s, 3H, OCH_3), 4.08 (m, 2H, H-6a, H-5), 4.27 (dd, J = 5.2, 12.2 Hz, 1H, H-6b), 5.37 (t, J = 10.1 Hz, 1H, H-4), 5.45 (dd, J = 1.8, 3.4 Hz, 1H, H-2), 5.56 (m, 2H, H-1, H-3), 7.16 (AA′ of AA′BB′, J = 8.7 Hz, 2H, C_6H_4), 7.57 (m, 4H, C_6H_4), 8.07 (BB′ of AA′BB′, J = 8.4 Hz, 2H, C_6H_4). ^{13}C NMR (125 MHz, $CDCl_3$): δ 20.74, 20.75, 20.77, 21.0 (4 $COCH_3$), 52.2 (OCH_3), 62.1 (C-6), 65.9 (C-4), 68.9 (C-3), 69.3, 69.4 (C-2, C-5), 95.8 (C-1), 116.9, 126.7, 128.5, 128.7, 130.2, 134.8, 144.8, 155.7 (12C, 2 C_6H_4), 167.0, 169.8, 170.0, 170.1, 170.6 (5 CO). ESI-MS calcd for $C_{28}H_{30}NaO_{12}$ $[M + Na]^+$ 581.2; found 581.0.

Methyl 4′-(2,3,4,6-Tetra-*O*-acetyl-α-D-mannopyranosyloxy)-3′-chlorobiphenyl-4-carboxylate (15b). A microwave tube was charged with bromide **14b** (720 mg, 1.34 mmol), 4-methoxycarbonylphenylboronic acid (289 mg, 1.61 mmol), cesium carbonate (1.31 g, 4.02 mmol), and $Pd(PPh_3)_4$ (77.4 mg, 0.067 mmol). The tube was sealed with a Teflon septum, evacuated through a needle, and flushed with argon. Degassed dioxane (1.5 mL) was added and the closed tube was degassed in an ultrasonic bath for 15 min, flushed again with argon for 20 min, and exposed to microwave irradiation at 120 °C for 500 min. The solvent was evaporated in vacuo. The residue was dissolved in DCM (10 mL), washed with brine (2 × 10 mL), dried over Na_2SO_4, and concentrated in vacuo. The residue was purified by flash chromatography on silica (petroleum ether/EtOAc, 5:1 to 0.5:1) to yield **15b** (333 mg, 42%) as a white foam.

$[\alpha]_D$ +66.3 (c 1.06, $CHCl_3$). ^1H NMR (500 MHz, $CDCl_3$): δ 2.03, 2.06, 2.20 (3s, 12H, $COCH_3$), 3.92 (s, 3H, OCH_3), 4.08 (dd, J = 2.4, 12.3 Hz, 1H, H-6a), 4.17 (m, 1H, H-5), 4.28 (dd, J = 5.4, 12.3 Hz, 1H, H-6b), 5.39 (t, J = 10.6 Hz, 1H, H-4), 5.54 (dd, J = 1.9, 3.4 Hz, 1H, H-2), 5.59 (d, J = 1.8 Hz, 1H, H-1), 5.62 (dd, J = 3.5, 10.1 Hz, 1H, H-3), 7.24 (s, 1H, C_6H_3), 7.44 (dd, J = 2.2, 8.5 Hz, 1H, C_6H_3), 7.57 (AA′ of AA′BB′, J = 8.5 Hz, 2H, C_6H_4), 7.65 (d, J = 2.2 Hz, 1H, C_6H_3), 8.08 (BB′ of AA′BB′, J = 8.5 Hz, 2H, C_6H_4). ^{13}C NMR (125 MHz, $CDCl_3$): δ 20.9, 21.0, 21.1 (4C, 4 $COCH_3$), 52.5 (OCH_3), 62.3 (C-6), 66.0 (C-4), 69.0 (C-3), 69.5 (C-2), 70.0 (C-5), 96.8 (C-1), 117.4, 126.7, 126.9, 129.5, 130.5, 136.4, 143.6, 151.3 (12C, C_6H_3, C_6H_4), 167.0, 169.9, 170.0, 170.2, 170.7 (5 CO). ESI-MS calcd for $C_{28}H_{29}ClNaO_{12}$ $[M + Na]^+$ 615.1; found 615.2. Anal. Calcd for $C_{28}H_{29}ClO_{12}$: C 56.71, H 4.93. Found: C 56.79, H 4.92.

Methyl 4′-(α-D-Mannopyranosyloxy)-biphenyl-4-carboxylate (16a).[17d] To a solution of **15a** (170 mg, 0.304 mmol) in MeOH (3 mL) was added freshly prepared 1 M NaOMe in MeOH (100 μL) under argon. The mixture was stirred at rt until the reaction was complete (monitored by TLC), then neutralized with Amberlyst-15 (H^+) ion-exchange resin, filtered, and concentrated in vacuo. The residue was purified by reversed-phase chromatography (RP-18, H_2O/MeOH, 1:0−1:1) to give **16a** (90 mg, 76%) as white solid.

$[\alpha]_D$ +82.8 (c 0.2, MeOH). ^1H NMR (500 MHz, CD_3OD): δ 3.62 (m, 1H, H-5), 3.72 (m, 3H, H-4, H-6a, H-6b), 3.92 (m, 4H, H-3, OCH_3), 4.03 (s, 1H, H-2), 5.55 (s, 1H, H-1), 7.24 (AA′ of AA′BB′, J = 8.0 Hz, 2H, C_6H_4), 7.64 (AA′ of AA′BB′, J = 7.5 Hz, 2H, C_6H_4), 7.71 (BB′ of AA′BB′, J = 8.0 Hz, 2H, C_6H_4), 8.07 (BB′ of AA′BB′, J = 7.5 Hz, 2H, C_6H_4). ^{13}C NMR (125 MHz, CD_3OD): δ 52.6 (OCH_3), 62.7 (C-6), 68.3 (C-4), 72.0 (C-2), 72.4 (C-3), 75.5 (C-5), 100.1 (C-1), 118.2, 127.7, 131.1, 135.1, 146.6, 158.2, 160.3 (12C, 2 C_6H_4), 166.1 (CO). HR-MS calcd for $C_{20}H_{22}NaO_8$ $[M + Na]^+$ 413.1212; found 413.1218.

Methyl 3′-Chloro-4′-(α-D-mannopyranosyloxy)-biphenyl-4-carboxylate (16b). According to the procedure described for **16a**, compound **16b** was prepared from **15b** (764 mg, 1.29 mmol). Yield: 69 mg, 12%.

$[\alpha]_D$ +97.4 (*c* 1.01, MeOH). ^{1}H NMR (500 MHz, CD_3OD): δ 3.64 (m, 1H, H-5), 3.72 (m, 1H, H-6a), 3.78 (m, 2H, H-4, H-6b), 3.91 (s, 3H, OCH_3), 4.00 (dd, *J* = 3.4, 9.5 Hz, 1H, H-3), 4.11 (dd, *J* = 1.8, 3.1 Hz, 1H, H-2), 5.60 (d, *J* = 1.1 Hz, 1H, H-1), 7.46 (d, *J* = 8.6 Hz, 1H, C_6H_3), 7.58 (dd, *J* = 2.2, 8.6 Hz, 1H, C_6H_3), 7.69 (AA′ of AA′BB′, *J* = 8.4 Hz, 2H, C_6H_4), 7.72 (d, *J* = 2.2 Hz, 1H, C_6H_3), 8.08 (BB′ of AA′BB′, *J* = 8.4 Hz, 2H, C_6H_4). ^{13}C NMR (125 MHz, CD_3OD): δ 52.7 (OCH_3), 62.8 (C-6), 68.3 (C-4), 71.9 (C-2), 72.5 (C-3), 76.2 (C-5), 100.8 (C-1), 118.7, 125.58, 127.8, 127.9, 129.9, 130.3, 131.3, 136.4, 145.3, 153.5 (12C, C_6H_3, C_6H_4), 168.4 (CO). HR-MS calcd for $C_{20}H_{21}ClNaO_8$ [M + Na]$^+$ 447.0823; found 447.082.

Sodium 4′-(α-D-Mannopyranosyloxy)-biphenyl-4-carboxylate (17a). To a solution of **15a** (228 mg, 0.408 mmol) in MeOH (6.0 mL) was added 1 M NaOMe in MeOH (60 μL) at rt. The reaction mixture was stirred at rt for 4 h, and then NaOH (82 mg) in water (6 mL) was added and stirring was continued at rt overnight. The reaction mixture was concentrated in vacuo, and the residue was purified by reversed-phase chromatography (RP-18, H_2O/MeOH, 1:0−1:1) to afford **17a** (96 mg, 63%) as a white solid.

$[\alpha]_D$ +103 (*c* 0.10, MeOH). ^{1}H NMR (500 MHz, CD_3OD): δ 3.60 (m, 1H, H-5), 3.72 (m, 3H, H-6a, H-6b, H-4), 3.89 (dd, *J* = 3.4, 9.5 Hz, 1H, H-3), 4.00 (dd, *J* = 1.8, 3.3 Hz, 1H, H-2), 5.51 (s, 1H, H-1), 7.19, 7.60 (AA′, BB′ of AA′BB′, *J* = 8.7 Hz, 4H, C_6H_4), 8.01(d, *J* = 8.2 Hz, 2H, C_6H_4), 8.46 (s, 2H, C_6H_4). ^{13}C NMR (125 MHz, CD_3OD): δ 63.2 (C-6), 68.9 (C-4), 72.6 (C-2), 73.0 (C-3), 76.1 (C-5), 100.7 (C-1), 118.7, 128.0, 129.9, 131.8 (12C, 2 C_6H_4). HR-MS calcd for $C_{19}H_{20}NaO_8$ [M + H]$^+$ 399.1056; found 399.1052.

Sodium 3′-Chloro-4′-(α-D-mannopyranosyloxy)-biphenyl-4-carboxylate (17b). To a solution of **15b** (380 mg, 0.641 mmol) in MeOH (10 mL) was added 1 M NaOMe in MeOH (300 μL). After stirring at rt for 24 h, 0.5 M aq NaOH (18 mL) was added and stirring continued for another 24 h. The solution was concentrated in vacuo and the residue was purified by reversed-phase chromatography (RP-18, H_2O/MeOH, 1:0−1:1) to yield **17b** (222 mg, 80%) as a white solid.

$[\alpha]_D$ +61.6 (*c* 1.00, H_2O). ^{1}H NMR (500 MHz, D_2O): δ 3.66 (m, 1H, H-5), 3.73 (m, 2H, H-6a, H-6b), 3.79 (t, *J* = 9.8 Hz, 1H, H-4), 4.07 (dd, *J* = 3.4, 9.8 Hz, 1H, H-3), 4.14 (d, *J* = 1.4 Hz, 1H, H-2), 5.47 (bs, 1H, H-1), 7.04 (d, *J* = 8.6 Hz, 1H, C_6H_3), 7.24 (d, *J* = 8.6 Hz, 1H, C_6H_3), 7.37 (AA′ of AA′BB′, *J* = 8.1 Hz, 2H, C_6H_4), 7.41 (bs, 1H, C_6H_3), 7.86 (BB′ of AA′BB′, *J* = 8.1 Hz, 2H, C_6H_4). ^{13}C NMR (125 MHz, D_2O): δ 60.6 (C-6), 66.5 (C-4), 69.0 (C-2), 70.5 (C-3), 73.9 (C-5), 98.6 (C-1), 117.5, 123.9, 126.2, 126.4, 128.4, 129.6, 135.2, 135.3, 141.0, 150.4 (12C, C_6H_3, C_6H_4), 175.0 (CO). HR-MS calcd for $C_{19}H_{18}ClNaO_8$ [M + H]$^+$ 433.0666; found 433.0670.

Competitive Binding Assay. A recombinant protein consisting of the CRD of FimH linked with a thrombin cleavage site to a 6His-tag (FimH-CRD-Th-6His) was expressed in *E. coli* strain HM125 and purified by affinity chromatography.[23] To determine the affinity of the various FimH antagonists, a competitive binding assay described previously[23] was applied. Microtiter plates (F96 MaxiSorp, Nunc) were coated with 100 μL/well of a 10 μg/mL solution of FimH-CRD-Th-6His in 20 mM HEPES, 150 mM NaCl, and 1 mM $CaCl_2$, pH 7.4 (assay buffer) overnight at 4 °C. The coating solution was discarded and the wells were blocked with 150 μL/well of 3% BSA in assay buffer for 2 h at 4 °C. After three washing steps with assay buffer (150 μL/well), a 4-fold serial dilution of the test compound (50 μL/well) in assay buffer containing 5% DMSO and streptavidin-peroxidase coupled Man-α(1-3)-[Man-α(1-6)]-Man-β(1-4)-Glc*N*Ac-β(1-4)-Glc*N*Acβ polyacrylamide (TM-PAA) polymer (50 μL/well of a 0.5 μg/mL solution) were added. On each individual microtiter plate, *n*-heptyl α-D-mannopyranoside (**1**) was tested in parallel. The plates were incubated for 3 h at 25 °C and 350 rpm and then carefully washed four times with 150 μL/well assay buffer. After the addition of 100 μL/well of 2,2′-azino-di-(3-ethylbenzthiazoline-6-sulfonic acid) (ABTS)-substrate, the colorimetric reaction was allowed to develop for 4 min and then stopped by the addition of 2% aqueous oxalic acid before the optical density (OD) was measured at 415 nm on a microplate-reader (Spectramax 190, Molecular Devices, California, USA). The IC_{50} values of the compounds tested in duplicates were calculated with prism software (GraphPad Software, Inc., La Jolla, California, USA). The IC_{50} defines the molar concentration of the test compound that reduces the maximal specific binding of TM-PAA polymer to FimH-CRD by 50%. The relative IC_{50} (rIC_{50}) is the ratio of the IC_{50} of the test compound to the IC_{50} of *n*-heptyl α-D-mannopyranoside (**1**).

Selectivity for FimH vs Mannose-Binding Protein and DC-SIGN. Recombinant FimH-CRD-Th-6His (10 μg/mL), DC-SIGN-CRD-Fc-IgG[39] (2.5 μg/mL), and mannose-binding protein[42] (MBP, 10 μg/mL, R&D Systems, Minneapolis, MN) were each diluted in assay buffer (20 mM HEPES, pH 7.4, 150 mM NaCl, and 10 mM $CaCl_2$) and were coated on microtiter plates (F96 MaxiSorp, Nunc) with 100 μL/well overnight at 4 °C. The further steps were performed as described above.

Aggregometry Assay. The aggregometry assay was carried out as previously described.[33] In short, the percentage of aggregation of *E. coli* UTI89 with guinea pig erythrocytes (GPE) was quantitatively determined by measuring the optical density at 740 nm and 37 °C under stirring at 1000 rpm using an APACT 4004 aggregometer (Endotell AG, Allschwil, Switzerland). Bacteria were cultivated as described below (see in vivo models). GPE were separated from guinea pig blood (Charles River Laboratories, Sulzfeld, Germany) using Histopaque (density of 1.077 g/mL at 24 °C, Sigma-Aldrich, Buchs, Switzerland). Prior to the measurements, the cell densities of *E. coli* and GPE were adjusted to an OD_{600} of 4, corresponding to 1.9×10^8 CFU/mL and 2.2×10^6 cells/mL, respectively. For the calibration of the instrument, the aggregation of protein-poor plasma (PPP) using PBS alone was set as 100% and the aggregation of protein-rich plasma (PRP) using GPE as 0%. After calibration, measurements were performed with 250 μL of GPE and 50 μL of bacterial suspension and the aggregation monitored over 600 s. After the aggregation phase of 600 s, 25 μL of antagonist in PBS was added to each cuvette and disaggregation was monitored for 1400 s. UTI89 Δ*fimA-H* was used as negative control.

Determination of the Pharmacokinetic Parameters. Materials. Dimethyl sulfoxide (DMSO), 1-octanol, pepsin, pancreatin, reduced nicotinamide adenine dinucleotide phosphate (NADPH), Dulbecco's Modified Eagle's Medium (DMEM) high glucose, and bis(4-nitrophenyl) phosphate (BNPP) were purchased from Sigma-Aldrich (Sigma-Aldrich, St. Louis MO, USA). PAMPA System Solution, GIT-0 Lipid Solution, and Acceptor Sink Buffer were ordered from pIon (pIon, Woburn MA, USA). L-Glutamine-200 mM (100×) solution, MEM nonessential amino acid (MEM-NEAA) solution, fetal bovine serum (FBS), and DMEM without sodium pyruvate and phenol red were bought from Invitrogen (Invitrogen, Carlsbad CA, USA). Human plasma was bought from Biopredic (Biopredic, Rennes, France) and acetonitrile (MeCN) from Acros (Acros Organics, Geel, Belgium). Pooled male mouse liver microsomes were purchased from BD Bioscience (BD Bioscience, Woburn, MA, USA). Magnesium chloride was bought from Fluka (Fluka Chemie GmbH, Buchs, Switzerland). Tris(hydroxymethyl)-aminomethane (TRIS) was obtained from AppliChem (AppliChem, Darmstadt, Germany). The Caco-2 cells were kindly provided by Prof G. Imanidis, FHNW, Muttenz, and originated from the American Type Culture Collection (Rockville, MD, USA).

log $D_{7.4}$ Determination. The in silico prediction tool ALOGPS 2.1[56] was used to estimate the log *P* values of the compounds. Depending on these values, the compounds were classified into three categories: hydrophilic compounds (log *P*

Table 2

compound type	log *P*	ratios (1-octanol:buffer)
hydrophilic	< 0	30:140, 40:130
moderately lipophilic	0−1	70:110, 110:70
lipophilic	> 1	3:180, 4:180

below zero), moderately lipophilic compounds (log *P* between zero and one) and lipophilic compounds (log *P* above one). For each category, two different ratios (volume of 1-octanol to volume of buffer) were defined as experimental parameters (Table 2):

Equal amounts of phosphate buffer (0.1 M, pH 7.4) and 1-octanol were mixed and shaken vigorously for 5 min to saturate the phases. The mixture was left until separation of the two phases occurred, and the buffer was retrieved. Stock solutions of the test compounds were diluted with buffer to a concentration of 1 μM. For each compound, six determinations, i.e., three determinations per 1-octanol:buffer ratio, were performed in different wells of a 96-well plate. The respective volumes of buffer containing analyte (1 μM) were pipetted to the wells and covered by saturated 1-octanol according to the chosen volume ratio. The plate was sealed with aluminum foil, shaken (1350 rpm, 25 °C, 2 h) on a Heidoph Titramax 1000 plate-shaker (Heidolph Instruments GmbH & Co. KG, Schwabach, Germany) and centrifuged (2000 rpm, 25 °C, 5 min, 5804 R Eppendorf centrifuge, Hamburg, Germany). The aqueous phase was transferred to a 96-well plate for analysis by liquid chromatography−mass spectrometry (LC-MS).

log $D_{7.4}$ was calculated from the 1-octanol:buffer ratio (o:b), the initial concentration of the analyte in buffer (1 μM), and the concentration of the analyte in buffer (c_B) with equilibration:

$$\log D_{7.4} = \log\left(\frac{1\ \mu\text{M} - c_B}{c_B} \times \frac{1}{o:b}\right)$$

The average of the three log $D_{7.4}$ values per 1-octanol:buffer ratio was calculated. If the two mean values obtained for a compound did not differ by more than 0.1 unit, the results were accepted.

Parallel Artificial Membrane Permeation Assay (PAMPA). log P_e was determined in a 96-well format with the PAMPA[30] permeation assay. For each compound, measurements were performed at three pH values (5.0, 6.2, 7.4) in quadruplicates. For this purpose, 12 wells of a deep well plate, i.e., four wells per pH value, were filled with 650 μL of System Solution. Samples (150 μL) were withdrawn from each well to determine the blank spectra by UV-spectroscopy (SpectraMax 190, Molecular Devices, Silicon Valley CAa, USA). Then, analyte dissolved in DMSO was added to the remaining System Solution to yield 50 μM solutions. To exclude precipitation, the optical density was measured at 650 nm, with 0.01 being the threshold value. Solutions exceeding this threshold were filtrated. Afterward, samples (150 μL) were withdrawn to determine the reference spectra. A further 200 μL were transferred to each well of the donor plate of the PAMPA sandwich (pIon, Woburn MA, USA, P/N 110 163). The filter membranes at the bottom of the acceptor plate were impregnated with 5 μL of GIT-0 Lipid Solution and 200 μL of Acceptor Sink Buffer were filled into each acceptor well. The sandwich was assembled, placed in the GutBox, and left undisturbed for 16 h. Then, it was disassembled and samples (150 μL) were transferred from each donor and acceptor well to UV-plates. Quantification was performed by both UV-spectroscopy and LC-MS. log P_e values were calculated with the aid of the PAMPA Explorer Software (pIon, version 3.5).

Colorectal Adenocarcinoma Cells (Caco-2 Cells) Permeation Assay. The cells were cultivated in tissue culture flasks (BD Biosciences, Franklin Lakes NJ, USA) with DMEM high glucose medium, containing 1% L-glutamine solution, 1% MEM-NEAA solution, and 10% FBS. The cells were kept at 37 °C in humidified air containing 8% CO_2, and the medium was changed every second to third day. When approximately 90% confluence was reached, the cells were split in a 1:10 ratio and distributed to new tissue culture flasks. At passage numbers between 60 and 65, they were seeded at a density of 5.33×10^5 cells per well to Transwell 6-well plates (Corning Inc., Corning NY, USA) with 2.5 mL of culture medium in the basolateral compartment and 1.5 mL (days 1−10) or 1.8 mL (from day 10 on) in the basolateral compartment. The medium was renewed on alternate days. Experiments were performed between days 19 and 21 postseeding. DMEM without sodium pyruvate and phenol red was used as transport medium for experiments. Previous to the experiment, the integrity of the Caco-2 monolayers was evaluated by measuring the transepithelial resistance (TEER) in transport medium (37 °C) with an Endohm tissue resistance instrument (World Precision Instruments Inc., Sarasota, FL, USA). Only wells with TEER values higher than 300 Ωcm^2 were used. Experiments were performed in triplicates. Transport medium (10 μL) from the apical compartments of three wells were replaced by the same volume of compound stock solutions (10 mM). The Transwell plate was then shaken (250 rpm) in the incubator. Samples (100 μL) were withdrawn after 5, 15, 30, 60, and 120 min from the basolateral compartment and concentrations were analyzed by HPLC. Apparent permeability coefficients (P_{app}) were calculated according to the following equation

$$P_{app} = \frac{dQ}{dt} \times \frac{1}{A \times c_0}$$

where dQ/dt is the permeability rate, A the surface area of the monolayer, and c_0 the initial concentration in the donor compartment.[31] After the experiment, TEER values were assessed again for every well and results from wells with values below 300 Ωcm^2 were discarded.

pK_a Values. The pK_a values were determined as described elsewhere.[45] Briefly, the pH of a sample solution was gradually changed and the chemical shift of protons adjacent to ionizable centers was monitored by ^{1}H nuclear magnetic resonance (NMR) spectroscopy. The shift was plotted against the pH of the respective sample, and the pK_a was read out from the inflection point of the resulting sigmoidal curve.

Plasma Protein Binding (PPB). The dialysis membranes (HTDialysis LCC, Gales Ferry, CT, USA; MWCO 12−14 K) were prepared according to company instructions. The human plasma was centrifuged (5800 rpm, 25 °C, 10 min), the pH of the centrifugate (without floating plasma lipids) was adjusted to 7.5, and analyte was added to yield 10 μM solutions. Equal volumes (150 μL) of phosphate buffer (0.1 M, pH 7.5) and analyte-containing plasma were transferred to the separated compartments of the assembled 96-well high throughput dialysis block (HTDialysis LCC, Gales Ferry, CT, USA). Measurements were performed in triplicates. The plate was covered with a sealing film and incubated (5 h, 37 °C). Buffer and plasma compartment were processed separately. From the buffer compartments, 90 μL were withdrawn and 10 μL of blank plasma were added. From the plasma compartments, 10 μL were withdrawn and 90 μL of blank buffer were added. After protein precipitation with 300 μL ice-cooled MeCN, the solutions were mixed, centrifuged (3600 rpm, 4 °C, 11 min), and 50 μL of the supernatant were retrieved. Analyte concentrations were determined by LC-MS. The fraction bound (f_b) was calculated as follows:

$$f_b = 1 - \frac{c_b}{c_p}$$

where c_b is the concentration in the buffer and c_p the concentration in the plasma compartment. Values were accepted if the recovery of analyte was between 80 and 120%.

Thermodynamic Solubility. Microanalysis tubes (Labo-Tech J. Stofer LTS AG, Muttenz, Switzerland) were charged with

1 mg of solid substance and 250 μL of phosphate buffer (50 mM, pH 6.5). The samples were briefly shaken by hand and then sonicated for 15 min and vigorously shaken (600 rpm, 25 °C, 2 h) on a Eppendorf Thermomixer Comfort. Afterward, the samples were left undisturbed for 24 h. After measuring the pH, the saturated solutions were filtered through a filtration plate (MultiScreen HTS, Millipore, Billerica MA, USA) by centrifugation (1500 rpm, 25 °C, 3 min). Prior to concentration determination by LC-MS, the filtrates were diluted (1:1, 1:10 and 1:100 or, if the results were outside of the calibration range, 1:1000 and 1:10000). The calibration was based on six values ranging from 0.1 to 10 μg/mL.

Stability in Simulated Gastrointestinal Fluids. Simulated gastric fluid (sGF) and simulated intestinal fluid (sIF) were prepared according to the United States Pharmacopeia (USP 28). sGF contained sodium chloride (200 mg), pepsin (320 mg), and 37% aq HCl (0.7 mL) in bidistilled water (100 mL). sIF consisted of monopotassium phosphate (680 mg), 0.2 M NaOH (7.7 mL), and pancreatin (1 g) in bidistilled water (100 mL). sIF was adjusted to pH 6 by adding 0.2 M NaOH. sGF and sIF were preheated (37 °C), and the compounds were added to yield 10 μM solutions. Incubations were performed on a Eppendorf Thermomixer Comfort (500 rpm, 37 °C). Before starting the experiment ($t = 0$ min) and after an incubation time of 15, 30, 60, and 120 min, samples (20 μL) were withdrawn, precipitated with ice-cooled MeCN, and centrifuged (3600 rpm, 4 °C, 10 min). The concentrations of analyte in the supernatant were analyzed by LC-MS. Stability was expressed as percentage remaining compound relative to the initial concentration.

In Vitro Metabolism: Ester Hydrolysis. Incubations were performed in a 96-well format on a Eppendorf Thermomixer Comfort. Each compound was incubated with a reaction mixture (270 μL) consisting of pooled male mouse liver microsomes in the presence of TRIS buffer (0.1 M, pH 7.4) and $MgCl_2$ (2 mM). After preheating (37 °C, 500 rpm, 10 min), the incubation was initiated by adding 30 μL of compound solution (20 μM) in TRIS buffer. The final concentration of the compounds was 2 μM, and the microsomal concentration was 0.25 mg/mL. At the beginning of the experiment ($t = 0$ min) and after an incubation time of 1, 3, 6, and 15 min, samples (50 μL) were transferred to 150 μL of ice-cooled MeCN, centrifuged (3600 rpm, 4 °C, 10 min), and 80 μL of supernatant were transferred to a 96-well plate for LC-MS analysis. Metabolic degradation was assessed as percentage remaining compound versus incubation time. Control experiments were performed in parallel by preincubating the microsomes with the specific carboxylesterase inhibitor BNPP (1 mM) for 5 min before addition of the antagonists.

In Vitro Metabolism: Cytochrome P450-Mediated Metabolism. Incubations consisted of pooled male mouse liver microsomes (0.5 mg microsomal protein/mL), compounds (2 μM), $MgCl_2$ (2 mM), and NADPH (1 mM) in a total volume of 300 μL TRIS buffer (0.1 M, pH 7.4) and were performed in a 96-well plate on a Thermomixer Comfort. Compounds and microsomes were preincubated (37 °C, 700 rpm, 10 min) before NADPH was added. Samples (50 μL) at $t = 0$ min and after an incubation time of 5, 10, 20, and 30 min were quenched with 150 μL of ice-cooled acetonitrile, centrifuged (3600 rpm, 4 °C, 10 min), and 80 μL of each supernatant were transferred to a 96-well plate for LC-MS analysis. Control experiments without NADPH were performed in parallel.

LC-MS Measurements. Analyses were performed using a 1100/1200 series HPLC system coupled to a 6410 triple quadrupole mass detector (Agilent Technologies, Inc., Santa Clara, CA, USA) equipped with electrospray ionization. The system was controlled with the Agilent MassHunter Workstation Data Acquisition software (version B.01.04). The column used was an Atlantis T3 C18 column (2.1 mm × 50 mm) with a 3 μm particle size (Waters Corp., Milford, MA, USA). The mobile phase consisted of two eluents: solvent A (H_2O, containing 0.1% formic acid, v/v) and solvent B (acetonitrile, containing 0.1% formic acid, v/v), both delivered at 0.6 mL/min. The gradient was ramped from 95% A/5% B to 5% A/95% B over 1 min, and then held at 5% A/95% B for 0.1 min. The system was then brought back to 95% A/5% B, resulting in a total duration of 4 min. MS parameters such as fragmentor voltage, collision energy, polarity were optimized individually for each drug, and the molecular ion was followed for each compound in the multiple reaction monitoring mode. The concentrations of the analytes were quantified by the Agilent Mass Hunter Quantitative Analysis software (version B.01.04).

In Vivo Pharmacokinetic and Disease Model. Bacteria. The clinical *E. coli* isolate UTI89[55] (UTI89wt) were kindly provided by the group of Prof. Urs Jenal, Biocenter, University of Basel. Microorganisms were stored at −70 °C and before experiment incubated for 24 h under static conditions at 37 °C in 10 mL of Luria−Bertani broth (Becton, Dickinson and Company, Le Pont de Claix, France) using 50 mL tubes. Prior to each experiment, the microorganisms were washed twice and resuspended in phosphate buffered saline (PBS, Hospital Pharmacy at the University Hospital Basel, Switzerland). Bacterial concentrations were determined by plating serial 1:10 dilutions on blood agar, followed by colony counting with 20−200 colonies after overnight incubation at 37 °C.

Animals. Female C3H/HeN mice weighting between 19 and 25 g were obtained from Charles River (Sulzfeld, Germany) and were housed four to a cage. Mice were kept under specific-pathogen-free conditions in the Animal House of the Department of Biomedicine, University Hospital Basel, and animal experimentation guidelines according to the regulations of Swiss veterinary law were followed. After seven days of acclimatization, 9- to 10-week old mice were used for the PK and infection studies. During the studies, animals were allowed free access to chow and water. Three days before infection studies and during infection, 5% D-(+)-glucose (AppliChem, Baden-Dättwil, Switzerland) was added to the drinking water to increase the number of bacterial counts in the urine and kidneys.[57]

Pharmacokinetic Studies. Single-dose pharmacokinetic studies were performed by iv and po application of the FimH antagonists at a concentration of 50 mg/kg followed by urine and plasma sampling. For iv application, the antagonists (**1**, **17a**, **17b**) were diluted in 100 μL of PBS and injected into the tail vein. For po application, antagonist **1** was diluted in 200 μL of PBS and antagonists **17b** and **16b** were first dissolved in DMSO (20×) and then slowly diluted to the final concentration (1×) in 1% Tween-80/PBS to obtain a suspension. Antagonists were applied iv by injection into the tail vein and po using a gavage followed by blood and urine sampling (10 μL) after 6 min, 30 min, 1 h, 2 h, 4 h, 6 h, 8 h, and 24 h. Before analysis, proteins in blood and urine samples were precipitated using methanol (Acros Organics, Basel, Switzerland) and centrifuged for 11 min at 13000 rpm. The supernatant was transferred into a 96-well plate (0.5 mL, polypropylene, Agilent Technologies, Basel, Switzerland) and analyzed by LC-MS as described above.

UTI Mouse Model. Mice were infected as previously described.[57] In brief, before infection, all remaining urine was depleted form the bladder by gentle pressure on the abdomen. Mice were anesthetized with 2.5 vol% isoflurane/oxygen mixture (Attane, Minrad Inc., Buffalo, NY, USA) and placed on their back. Anesthetized mice were inoculated transurethrally with the bacterial suspension by use of a 2 cm polyethylene catheter (Intramedic polyethylene tubing, inner diameter 0.28 mm, outer diameter 0.61 mm, Beckton Dickinson, Allschwil, Switzerland), which was placed on a syringe (Hamilton Gastight Syringe 50 μL, removable 30G needle, BGB Analytik AG, Boeckten, Switzerland). The catheter was gently inserted through the urethra until it reached the top of the bladder, followed by slow injection of 50 μL of bacterial suspension at a concentration of approximately 10^9 to 10^{10} CFU/mL.

Antagonist Treatment Studies. FimH antagonists were applied iv in 100 μL of PBS into the tail vein or po as a suspension by the help

of a gavage, 10 min (**17a**, **17b**, **16b**) or 1 h before infection (**1**). Three h after the onset of infection, urine was collected by gentle pressure on the abdomen and then the mouse was sacrificed with CO_2. Organs were removed aseptically and homogenized in 1 mL of PBS by using a tissue lyser (Retsch, Haan, Germany). Serial dilutions of urine, bladder, and kidneys were plated on Levine Eosin Methylene Blue Agar plates (Beckton Dickinson, Le Pont de Claix, France). CFU counts were determined after overnight incubation at 37 °C and expressed as CFU/mL for the urine and CFU/bladder and CFU/2 kidneys for the organs.

Acknowledgment. We thank Professor Rudi Glockshuber (ETH Zürich, Switzerland) for gratefully providing the plasmid pNT-FimH used for the cloning of the FimH CRD and *E. coli* strain HM 125. We thank Dr. Manfred Kansy and Dr. Christoph Funk, F. Hoffmann-La Roche AG, Basel, Switzerland, for supporting us with their expertise when we established the PADMET platform, and to Prof. Angelo Vedani, University of Basel, Switzerland, for fruitful discussions on conformational issues. We further appreciate the support by Prof. Dr. med. Radek Skoda, Department of Biomedicine, University Hospital Basel, Switzerland, for giving us access to the animal facility and Prof. Niels Frimodt-Moller. Statens Serum Institut, Copenhagen, Denmark for the introduction to the in vivo model. We thank Prof G. Imanidis, FHNW, Muttenz, Switzerland, for providing the Caco-2 cells, and Dr. M. Schneider, Department of Pharmaceutical Sciences, University of Basel, Switzerland, for his help during the assay build-up. We are grateful to Prof. Urs Jenal, Biocenter of the University of Basel, Switzerland, for the clinical *E. coli* isolate UTI89 and the FimH knock out strain UTI89Δ*fimA-H*. Finally, we thank the Swiss National Science Foundation (project K-32K1-120904) for their financial support.

Supporting Information Available: ^{1}H NMR spectra and HPLC traces for the target compounds **16a**−**c**, **17a**−**c**,**e**, **21a**,**b**, and **22a**,**b** and experimental and spectroscopic details for compounds **6a**−**d**, **7a**−**d**, **14c**−**e**, **15c**−**e**, **16c**−**e**, **17c**,**e**, **19a**,**b**, **20a**,**b**, and **21a**,**b**. This material is available free of charge via the Internet at http://pubs.acs.org.

References

(1) Fihn, S. D. Clinical practice. Acute uncomplicated urinary tract infection in women. *N. Engl. J. Med.* **2003**, *349*, 259–266.
(2) Hooton, T. M. Recurrent urinary tract infection in women. *Int. J. Antimicrob. Agents* **2001**, *17*, 259–268.
(3) Wiles, T. J.; Kulesus, R. R.; Mulvey, M. A. Origins and virulence mechanisms of uropathogenic *Escherichia coli*. *Exp. Mol. Pathol.* **2008**, *85*, 11–19.
(4) Gouin, S. G.; Wellens, A.; Bouckaert, J.; Kovensky, J. Synthetic Multimeric Heptyl Mannosides as Potent Antiadhesives of Uropathogenic *Escherichia coli*. *ChemMedChem* **2009**, *4*, 749–755.
(5) Rosen, D. A.; Hung, C. S.; Kline, K. A.; Hultgren, S. J. Streptozocin-induced diabetic mouse model of urinary tract infection. *Infect. Immun.* **2008**, *76*, 4290–4298.
(6) Mulvey, M. A. Adhesion and entry of uropathogenic *Escherichia coli*. *Cell Microbiol.* **2002**, *4*, 257–271.
(7) Capitani, G.; Eidam, O.; Glockshuber, R.; Grutter, M. G. Structural and functional insights into the assembly of type 1 pili from *Escherichia coli*. *Microbes Infect.* **2006**, *8*, 2284–2290.
(8) Choudhury, D.; Thompson, A.; Stojanoff, V.; Langermann, S.; Pinkner, J.; Hultgren, S. J.; Knight, S. D. X-ray structure of the FimC−FimH chaperone−adhesin complex from uropathogenic *Escherichia coli*. *Science* **1999**, *285*, 1061–1066.
(9) Bouckaert, J.; Berglund, J.; Schembri, M.; Genst, E. D.; Cools, L.; Wuhrer, M.; Hung, C. S.; Pinkner, J.; Slättergard, R.; Zavialov, A.; Choudhury, D.; Langermann, S.; Hultgren, S. J.; Wyns, L.; Klemm, P.; Oscarson, S.; Knight, S. D.; Greve, H. D. Receptor binding studies disclose a novel class of high-affinity inhibitors of the *Escherichia coli* FimH adhesin. *Mol. Microbiol.* **2005**, *55*, 441–455.
(10) Wellens, A.; Garofalo, C.; Nguyen, H.; Van Gerven, N.; Slättergard, R.; Hernalsteens, J.-P.; Wyns, L.; Oscarson, S.; De Greve, H.; Hultgren, S.; Bouckaert, J. Intervening with urinary tract infections using anti-adhesives based on the crystal structure of the FimH−oligomannose-3 complex. *PLoS ONE* **2008**, *3*, 4–13.
(11) Langermann, S.; Mollby, R.; Burlein, J. E.; Palaszynski, S. R.; Auguste, C. G.; DeFusco, A.; Strouse, R.; Schenerman, M. A.; Hultgren, S. J.; Pinkner, J. S.; Winberg, J.; Guldevall, L.; Soderhall, M.; Ishikawa, K.; Normark, S.; Koenig, S. Vaccination with FimH adhesin protects cynomolgus monkeys from colonization and infection by uropathogenic *Escherichia coli*. *J. Infect. Dis.* **2000**, *181*, 774–778.
(12) Langermann, S.; Palaszynski, S.; Barnhart, M.; Auguste, G.; Pinkner, J. S.; Burlein, J.; Barren, P.; Koenig, S.; Leath, S.; Jones, C. H.; Hultgren, S. J. Prevention of mucosal *Escherichia coli* infection by FimH-adhesin-based systemic vaccination. *Science* **1997**, *276*, 607–611.
(13) Bouckaert, J.; Mackenzie, J.; de Paz, J. L.; Chipwaza, B.; Choudhury, D.; Zavialov, A.; Mannerstedt, K.; Anderson, J.; Pierard, D.; Wyns, L.; Seeberger, P. H.; Oscarson, S.; De Greve, H.; Knight, S. D. The affinity of the FimH fimbrial adhesin is receptor-driven and quasi-independent of *Escherichia coli* pathotypes. *Mol. Microbiol.* **2006**, *61*, 1556–1568.
(14) Sharon, N. Carbohydrates as future anti-adhesion drugs for infectious diseases. *Biochim. Biophys. Acta* **2006**, *1760*, 527–537.
(15) (a) Firon, N.; Ofek, I.; Sharon, N. Interaction of mannose-containing oligosaccharides with the fimbrial lectin of *Escherichia coli*. *Biochem. Biophys. Res. Commun.* **1982**, *105*, 1426–1432. (b) Firon, N.; Ofek, I.; Sharon, N. Carbohydrate specificity of the surface lectins of Escherichia coli, Klebsiella pneumoniae and Salmonella typhimurium. *Carbohydr. Res.* **1983**, *120*, 235–249. (c) Sharon, N. Bacterial lectins, cell−cell recognition and infectious disease. *FEBS Lett.* **1987**, *217*, 145–157.
(16) (a) Neeser, J.-R.; Koellreutter, B.; Wuersch, P. Oligomannoside-type glycopeptides inhibiting adhesion of *Escherichia coli* strains mediated by type 1 pili: preparation of potent inhibitors from plant glycoprteins. *Infect. Immun.* **1986**, *52*, 428–436. (b) Lindhorst, T. K. Artificial multivalent sugar ligands to understand and manipulate carbohydrate−protein interactions. *Top. Curr. Chem.* **2002**, *218*, 201−235 (review); (c) Patel, A.; Lindhorst, T. K. A modular approach for the synthesis of oligosaccharide mimetics. *Carbohydr. Res.* **2006**, *341*, 1657–1668. (d) Nagahori, N.; Lee, R. T.; Nishimura, S.-I.; Pagé, S.; Roy, R.; Lee, Y. C. Inhibition of adhesion of type 1 fimbriated Escherichia coli to highly mannosylated ligands. *ChemBioChem* **2002**, *3*, 836–844. (e) Appeldoorn, C. C. M.; Joosten, J. A. F.; Maate, F. A.; Dobrindt, U.; Hacker, J.; Liskamp, R. M. J.; Khan, A. S.; Pieters, R. J. Novel multivalent mannose compounds and their inhibition of the adhesion of type 1 fimbriated uropathogenic E. coli. *Tetrahedron Asymmetry* **2005**, *16*, 361–372. (f) Touaibia, M.; Wellens, A.; Shiao, T. C.; Wang, Q.; Sirois, S.; Bouckaert, J.; Roy, R. Mannosylated G(0) dendrimers with nanomolar affinities to Escherichia coli FimH. *ChemMedChem* **2007**, *2*, 1190–1201.
(17) (a) Firon, N.; Ashkenazi, S.; Mirelman, D.; Ofek, I.; Sharon, N. Aromatic alpha-glycosides of mannose are powerful inhibitors of the adherence of type 1 fimbriated *Escherichia coli* to yeast and intestinal epithelial cells. *Infect. Immun.* **1987**, *55*, 472–476. (b) Lindhorst, T. K.; Kötter, S.; Kubisch, J.; Krallmann-Wenzel, U.; Ehlers, S.; Kren, V. Effect of p-substitution of aryl α-D-mannosides on inhibiting mannose-sensitive adhesion of Escherichia coli—synthesis and testing. *Eur. J. Org. Chem.* **1998**, 1669–1674. (c) Sperling, O.; Fuchs, A.; Lindhorst, T. K. Evaluation of the carbohydrate recognition domain of the bacterial adhesin FimH: design, synthesis and binding properties of mannoside ligands. *Org. Biomol. Chem.* **2006**, *4*, 3913–3922. (d) Han, Z.; Pinker, J. S.; Ford, B.; Obermann, R.; Nolan, W.; Wildman, S. A.; Hobbs, D.; Ellenberger, T.; Cusumano, C. K.; Hultgren, S. J.; Janetka, J. W. Structure-Based Drug Design and Optimization of Mannoside Bacterial FimH Antagonists. *J. Med. Chem.* **2010**, *53*, 4779–4792. (e) Berglund, J.; Bouckaert, J.; De Greve, H.; Knight, S. Anti-adhesive compounds to prevent and treat bacterial infections. International Patent Application PCT/US 2005/089733, 2005.
(18) Hung, C. S.; Bouckaert, J.; Hung, D.; Pinkner, J.; Widberg, C.; Defusco, A.; Auguste, C. G.; Strouse, R.; Langermann, S.; Waksman, G.; Hultgren, S. J. Structural basis of tropism of *Escherichia coli* to the bladder during urinary tract infection. *Mol. Microbiol.* **2002**, *44*, 903–918.
(19) Ernst, B.; Magnani, J. L. From carbohydrate leads to glycomimetic drugs. *Nature Rev. Drug Discovery* **2009**, *8*, 661–677.
(20) (a) Lindhorst, T. K.; Kieburg, C.; Krallmann-Wenzel, U. Inhibition of the type 1 fimbriae-mediated adhesion of *Escherichia coli* to erythrocytes by multiantennary α-mannosyl clusters: the effect of multivalency. *Glycoconjugate J.* **1998**, *15*, 605–613. (b) Dubber, M.; Sperling, O.; Lindhorst, T. K. Oligomannoside mimetics by glycosylation of 'octopus glycosides' and their investigation as inhibitors of type 1

fimbriae-mediated adhesion of Escherichia coli. *Org. Biomol. Chem.* **2006**, *4*, 3901–3912. (c) Touaibia, M.; Wellens, A.; Shiao, T. C.; Wang, Q.; Sirois, S.; Bouckaert, J.; Roy, R. Mannosylated G0 dendrimers with nanomolar affinities to Escherichia coli FimH. *ChemMedChem* **2007**, *2*, 1190–1201.

(21) Aronson, M.; Medalia, O.; Schori, L.; Mirelman, D.; Sharon, N.; Ofek, I. Prevention of colonization of the urinary tract of mice with *Escherichia coli* by blocking of bacterial adherence with methyl α-D-mannopyranoside. *J. Infect. Dis.* **1979**, *139*, 329–332.

(22) Svanborg Eden, C.; Freter, R.; Hagberg, L.; Hull, R.; Leffler, H.; Schoolnik, G. Inhibition of experimental ascending urinary tract infection by an epithelial cell-surface receptor analog. *Nature* **1982**, *298*, 560–562.

(23) Rabbani, S.; Jiang, X.; Schwardt, O.; Ernst, B. Expression of the carbohydrate recognition domain of FimH and development of a competitive binding assay. *Anal. Biochem.* **2010**, *407*, 188–195.

(24) Ness, R. K.; Fletcher, H. G.; Hudson, C. S. Reaction of 2,3,4,6-tetrabenzoyl-α-D-glucopyranosyl bromide and 2,3,4,6-tetrabenzoyl-α-D-mannopyranosyl bromide with methanol. Certain benzoylated derivatives of D-glucose and D-mannose. *J. Am. Chem. Soc.* **1950**, *72*, 2200–2205.

(25) Sancho-Garcia, J. C.; Cornil, J. Anchoring the Torsional Potential of Biphenyl at the ab Initio Level: The Role of Basis Set versus Correlation Effects. *J. Chem. Theory Comput.* **2005**, *1*, 581–589.

(26) Eaton, V. J.; Steele, D. Dihedral angle of biphenyl in solution and the molecular force field. *J. Chem. Soc., Faraday Trans. 2* **1973**, 1601–1608.

(27) Albert, A. Chemical aspects of selective toxicity. *Nature* **1958**, *182*, 421–422.

(28) Winiwarter, S.; Bonham, N. M.; Ax, F.; Hallberg, A.; Lennernäs, H.; Karlén, A. Correlation of Human Jejunal Permeability (in Vivo) of Drugs with Experimentally and Theoretically Derived Parameters. A Multivariate Data Analysis Approach. *J. Med. Chem.* **1998**, *41*, 4939–4949.

(29) Taketani, M.; Shii, M.; Ohura, K.; Ninomiya, S.; Imai, T. Carboxylesterase in the liver and small intestine of experimental animals and human. *Life Sci.* **2007**, *81*, 924–932.

(30) Kansy, M.; Senner, F.; Gubernator, K. Physicochemical High Throughput Screening: Parallel Artificial Membrane Permeation Assay in the Description of Passive Absorption Processes. *J. Med. Chem.* **1998**, *41*, 1007–1010.

(31) Artursson, P.; Karlsson, J. Correlation between oral drug absorption in humans and apparent drug permeability coefficients in human intestinal epithelial (Caco-2) cells. *Biochem. Biophys. Res. Com.* **1991**, *175*, 880–885.

(32) Varma, M. V. S.; Feng, B.; Obach, R. S.; Troutman, M. D.; Chupka, J.; Miller, H. R.; El-Kattan, A. Physicochemical Determinants of Human Renal Clearance. *J. Med. Chem.* **2009**, *52*, 4844–4852.

(33) Abgottspon, D.; Rölli, G.; Hosch, L.; Steinhuber, A.; Jiang, X.; Schwardt, O.; Cutting, B.; Smiesko, M.; Jenal, U.; Ernst, B.; Trampuz, A. Development of an Aggregation Assay to Screen FimH Antagonists. *J. Microbiol. Methods* **2010**, *82*, 249–255.

(34) Zhou, G.; Mo, W.-J.; Sebbel, P.; Min, G.; Neubert, T. A.; Glockshuber, R.; Wu, X.-R.; Sun, T.-T.; Kong, X.-P. Uroplakin Ia is the urothelial receptor for uropathogenic *Escherichia coli*: evidence from in vitro FimH binding. *J. Cell Sci.* **2001**, *114*, 4095–4103.

(35) (a) Kartha, K. P. R; Field, R. A. Iodine: a versatile reagent in carbohydrate chemistry. IV. Per-*O*-acetylation, regioselective acylation and acetolysis. *Tetrahedron* **1997**, *53*, 11753–11766. (b) Chittaboina, S.; Hodges, B.; Wang, Q. A facile route for the regioselective deacetylation of peracetylated carbohydrates at anomeric position. *Lett. Org. Chem.* **2006**, *3*, 35–38. (c) Mori, M.; Ito, Y.; Ogawa, T. Total synthesis of the mollu-series glycosyl ceramides α-D-Manp-(1→3)-β-D-Manp-(1→4)-β-D-Glcp-(1→1)-Cer and α-D-Manp-(1→3)-[β-D-Xylp-(1→2)]-β-D-Manp-(1→4)-β-D-Glcp-(1→1)-Cer. *Carbohydr. Res.* **1990**, *195*, 199–224. (d) Egusa, K.; Kusumoto, S.; Fukase, K. Solid-phase synthesis of a phytoalexin elicitor pentasaccharide using a 4-azido-3-chlorobenzyl group as the key for temporary protection and catch-and-release purification. *Eur. J. Org. Chem.* **2003**, 3435–3445.

(36) Giampapa, C. S.; Abraham, S. N.; Chiang, T. M.; Beachey, E. H. Isolation and characterization of a receptor for type 1 fimbriae of *Escherichia coli* from guinea pig erythrocytes. *J. Biol. Chem.* **1988**, *263*, 5362–5367.

(37) Aprikian, P.; Tchesnokova, V.; Kidd, B.; Yakovenko, O.; Yarov-Yarovoy, V.; Trinchina, E.; Vogel, V.; Thomas, W.; Sokurenko, E. Interdomain interaction in the FimH adhesin of *Escherichia coli* regulates the affinity to mannose. *J. Biol. Chem.* **2007**, *282*, 23437–23446.

(38) Trong, I. L.; Aprikian, P.; Kidd, B. A.; Forero-Shelton, M.; Tchesnokova, V.; Rajagopal, P.; Rodriguez, V.; Interlandi, G.; Klevit, R.; Vogel, V.; Stenkamp, R. E.; Sokurenko, E. V.; Thomas, W. E. Structural basis for mechanical force regulation of the adhesin FimH via finger trap-like beta sheet twisting. *Cell* **2010**, *141*, 645–655.

(39) Khoo, U. S.; Chan, K. Y. K.; Chan, V. S. F.; Lin, C. L. S. DC-SIGN and L-SIGN: the SIGNs for infection. *J. Mol. Med.* **2008**, *86*, 861–874.

(40) Lee, S. J.; Evers, S.; Roeder, D.; Parlow, A. F.; Risteli, J.; Risteli, L.; Lee, Y. C.; Feizi, T.; Langen, H.; Nussenzweig, M. C. Mannose receptor-mediated regulation of serum glycoprotein homeostasis. *Science* **2002**, *295*, 1898–1901.

(41) East, L.; Isacke, C. M. The mannose receptor family. *Biochim. Biophys. Acta* **2002**, *1572*, 364–386.

(42) Dommett, R. M.; Klein, N.; Turner, M. W. Mannose-binding lectin in innate immunity: past, present and future. *Tissue Antigens* **2006**, *68*, 193–209.

(43) Scharenberg, M. Expression and purification of DC-SIGN-CRD-Fc-IgG. Unpublished results .

(44) Dearden, J. C.; Bresnen, J. G. M. The measurement of partition coefficients. *QSAR Comb. Sci.* **1988**, *7*, 133–144.

(45) Wittwer, M.; Bezençon, J.; Cutting, B.; Wagner, B.; Kansy, M.; Ernst, B. pK_a determination by ^{1}H-NMR spectroscopy—an old methodology revisited. Unpublished results .

(46) Banker, M. J.; Clark, T. H.; Williams, J. A. Development and validation of a 96-well equilibrium dialysis apparatus for measuring plasma protein binding. *J. Pharm. Sci.* **2003**, *92*, 967–974.

(47) Kerns, E. H. High throughput physicochemical profiling for drug discovery. *J. Pharm. Sci.* **2001**, *90*, 1838–1858.

(48) Avdeef, A.; Bendels, S.; Di, L.; Faller, B.; Kansy, M.; Sugano, K.; Yamauchi, Y. Parallel artificial membrane permeability assay (PAMPA)-critical factors for better predictions of absorption. *J. Pharm. Sci.* **2007**, *96*, 2893–2909.

(49) Brandt, E.; Heymann, E.; Mentlein, R. Selective inhibition of rat liver carboxylesterases by various organophosphorus diesters in vivo and in vitro. *Biochem. Pharamcol.* **1980**, *29*, 1927–1931.

(50) Scharenberg, M.; Abgottspon, D. Personal communication .

(51) Obach, R. S. Prediction of human clearance of twenty-nine drugs from hepatic microsomal intrinsic clearance data: an examination of in vitro half-life approach and nonspecific binding to microsomes. *Drug Metab. Dispos.* **1999**, *27*, 1350–1359.

(52) Trainor, G. L. The importance of plasma protein binding in drug discovery. *Expert Opin. Drug Discovery* **2007**, *2*, 51–64.

(53) Weisiger, R. A. Dissociation from albumin: a potentially rate-limiting step in the clearance of substances by the liver. *Proc. Natl. Acad. Sci. U.S.A.* **1985**, *82*, 1563–1567.

(54) Urien, S.; Tillement, J.-P.; Barre, J., The significance of plasma protein binding in drug research. In *Pharmacokinetic Optimization in Drug Research: Biological, Physicochemical, and Computational Strategies*; Wiley-VCH: Weinheim, Germany, 2001; pp 189–197.

(55) Mulvey, M. A.; Schilling, J. D.; Hultgren, S. J. Establishment of a persistent *Escherichia coli* reservoir during the acute phase of a bladder infection. *Infect. Immun.* **2001**, *69*, 4572–4579.

(56) (a) *VCCLAB, Virtual Computational Chemistry Laboratory*; http://www.vcclab.org, 2005; (b) Tetko, I. V.; Gasteiger, J.; Todeschini, R.; Mauri, A.; Livingstone, D.; Ertl, P.; Palyulin, V. A.; Radchenko, E. V.; Zefirov, N. S.; Makarenko, A. S.; Tanchuk, V. Y.; Prokopenko, V. V. Virtual computational chemistry laboratory—design and description. *J. Comput.-Aided Mol. Des.* **2005**, *19*, 453–463.

(57) Kerrn, M. B.; Frimodt-Møller, N.; Espersen, F. Effects of Sulfomethizole and Amdinocillin against *Escherichia coli* Strains (with Various Susceptibilities) in an Ascending Urinary Tract Infection Model. *Antimicrob. Agents Chemother.* **2003**, *47*, 1002–1009.

RESULTS AND DISCUSSION

Paper III

A Flow Cytometry-Based Assay for Screeining FimH Antagonists.

Scharenberg M, Abgottspon D, Ciceck E, Jiang X, Schwardt O, Rabbani S, Ernst B.

Assay Drug Dev. Technol. **2011**.

My contributions:

Establishment of the flow cytometry infection assay and secreening of FimH antagonists together with Scharenberg M. and the mater student Ciceck E.

A Flow Cytometry-Based Assay for Screening FimH Antagonists

Meike Scharenberg, Daniela Abgottspon, Evelin Cicek, Xiaohua Jiang, Oliver Schwardt, Said Rabbani, and Beat Ernst

Institute of Molecular Pharmacy, Pharmacenter, University of Basel, Basel, Switzerland.

ABSTRACT

Urinary tract infections (UTIs), including cystitis and pyelonephritis, affect a large proportion of the population and account for significant medical costs. In more than 80% of UTIs, uropathogenic Escherichia coli (UPEC) is the causative pathogen. The initial step in the pathogenesis of the infection is the adherence of UPEC to the human bladder epithelium, enabling the invasion into the host cells and the development of UTIs. This process is mediated by the lectin FimH located on type I pili and enables UPECs to attach to oligomannosides of the glycoprotein uroplakin Ia presented on uroepithelial cells. FimH antagonists such as α-D-mannopyranosides have been shown to interfere with the attachment of UPEC to their host cells, thus providing a novel therapeutic opportunity for the treatment and prevention of UTIs. In this article, we report a flow cytometry-based assay to evaluate the potential of FimH antagonists for the prevention of the infection of the human urinary bladder cell line 5637 by UPEC strain UTI89. The assay was optimized and validated, and the inhibitory potency of different α-D-mannopyranosides was determined. Finally, the IC_{50} values measured by the flow cytometry-based assay were compared with those reported for other assay formats.

INTRODUCTION

Urinary tract infection (UTI) is one of the most common infections, affecting millions of people each year. Particularly affected are women, who have a 40%–50% risk to experience at least one symptomatic UTI episode at some time during their life.[1] In more than 80% of the reported cases, invasive uropathogenic *Escherichia coli* strains (UPEC) are the etiological agent. A nontreated UTI can lead to bladder (cystitis) and kidney infection (pyelonephritis).[2] The antibiotic treatment does not always eradicate UPEC and often results in the emergence of microbial resistance and consequently in recurrent infections.[3] Further, more than half of patients experience a relapse of the infection within 6 months.[2,4]

The initial step in the pathogenesis of UPEC infection is the adherence of bacteria to the bladder epithelium (urothelium), which thereby slows down their clearance from the urinary tract. At the same time, the attachment enables the pathogens to invade the host cells.[5,6] The attachment is mediated by 1–3 μm long, filamentous, oligomeric organelles called type 1 pili,[7,8] which are helical rods with a diameter of 7 nm and composed of FimA, FimF, FimG, and FimH subunits. The adhesin FimH, which is located at the distal end of the linear fibrillum, contains an amino-terminal, mannose-specific carbohydrate recognition domain (FimH-CRD).[9–11] FimH-CRD binds to mannose residues provided by the glycoprotein uroplakin Ia (UPIa).[12–14] The adherence of UPEC to the urothelium activates the innate immune defense, triggering the exfoliation of infected bladder cells, the influx of neutrophils, and other inflammatory responses.[15] Nevertheless, UPEC can resist innate host defense mechanisms, invade deeper into the tissue, and adopt a quiescent state, probably the reason for the high incidence of recurrence of UTIs.[15]

Because of increasing antibiotic resistance, efforts are underway to identify new and inexpensive orally available therapeutics, which inhibit bacterial adhesion with a low potential for generating resistance. New studies are focusing on carbohydrate-based FimH antagonists.[16–22] For the evaluation of such antagonists, several *in vitro* assays have been reported, although most of them measure the effect of antagonists on the hemagglutination of erythrocytes[18,23,24] or the aggregation of yeast cells in the presence of UPEC.[25–27] In addition, FimH antagonists were evaluated with an enzyme-linked immunosorbent based assay[20,27] and with bacterial adhesion assays using green fluorescence protein (GFP)-tagged bacteria,[28] radiolabeled mannose,[16] or radiolabeled bacteria.[29] The inhibition of the binding of purified type 1 fimbriae to human granulocytes was investigated utilizing the flow cytometry technology.[30] In surface plasmon resonance experiments, the binding of FimH to an anti-FimH blocking antibody covalently linked to the sensor chip enabled the determination of the affinity of antagonists.[16] Depending on the applied assay format, the reported inhibitory potencies of the reference compounds D-mannose (1) and methyl α-D-mannopyranoside (2) vary between millimolar[18,26] and micromolar.[16,31] The discrepancies noticed in aggregation and hemagglutination assays are mainly due to the variability in the levels of FimH expressed by different

ABBREVIATIONS: BSA, bovine serum albumin; CFSE, 5-(6)-carboxyfluorescein *N*-succinimidylester; CRD, carbohydrate recognition domain; DMSO, dimethylsulfoxide; FCS, fetal calf serum; GFP, green fluorescent protein; FSC, forward scatter; GPE, guinea pig erythrocytes; LB, Luria-Bertani; MFI, mean fluorescent intensity; MOI, multiplicity of infection; OD, optical density; PBS, phosphate-buffered saline; RPMI, Roswell Park Memorial Institute medium; SSC, side scatter; UPEC, uropathogenic *Escherichia coli*; UPIa, uroplakin Ia; UTI, urinary tract infection.

bacterial strains[25,26] as well as significant differences in the sensitivity of erythrocytes to type 1 pili-mediated hemagglutination.[23] Further, FimH located at the tip of the pili mediates weak binding at low shear stress, but shifts to strong binding at high shear.[32] The isolated CRD, which is often used in target-based assays, always adopts the high-affinity state and therefore mediates strong binding to mannose even under static conditions.[33]

Recently, we reported two new assay formats for the evaluation of FimH antagonists, a cell-free target-based assay[34] and function-based aggregation assay.[24] Both formats are competitive assays, where the analytes compete with oligomannosides for the binding site. In the cell-free competitive binding assay, the competitors are polymer-bound trimannosides,[34] whereas in the aggregation assay, the antagonist competes with more potent oligo- and polysaccharide chains present on the surface of erythrocytes.[24]

In this article, we describe the development of a function-based flow cytometry assay that allows to quantify the effect of FimH antagonists on the adhesion of UPEC (UTI89) to human epithelial bladder cells 5637. The results are compared with those reported for the various assay formats mentioned earlier. The reproducibility, sensitivity, and assay conditions close to the physiological situation make this assay format suitable for the estimation of the minimal therapeutic concentration for *in vivo* UTI treatment studies.

MATERIALS AND METHODS

Cell Culture

The human epithelial bladder carcinoma cell line 5637 was obtained from the German Collection of Microorganisms and Cell Cultures (DSMZ). The cells were grown in Roswell Park Memorial Institute medium (RPMI) 1640 medium, supplemented with 10% fetal calf serum (FCS), 100 U/mL penicillin, and 100 µg/mL streptomycin, at 37°C under 5% CO_2. All solutions were purchased from Invitrogen. The cells were subcultured 1:5 twice per week (using Trypsin/EDTA [Sigma] for the detachment) for six passages before using them in the infection assay. Two days before infection, 1.8×10^5 cells were seeded in each well of a 24-well plate in RPMI 1640 containing 10% FCS without antibiotics. The cell density was approximately $3–5 \times 10^5$ cells/well prior the infection.

Bacterial Strains

The clinical *E. coli* isolate UTI89[35] (UTI89 *wt*) and the FimA-H knock-out strain UTI89 Δ*fimA-H* were kindly provided by Prof. Urs Jenal (Biocenter, University of Basel, Switzerland). The bacteria were frozen at −70°C and, before the experiment, incubated for 24 h under static conditions at 37°C in 10 mL Luria-Bertani (LB) broth (Becton, Dickinson and Company). The bacterial suspension was washed twice and resuspended either in phosphate-buffered saline (PBS; Sigma) for staining and aggregometry measurements or in RPMI 1640 without supplements for infection experiments. The bacterial concentration was determined by plating serial 1:10 dilutions on blood agar plates (Becton, Dickinson and Company), followed by colony counting after overnight incubation at 37°C.

GFP Staining

Plasmid pBR322GFP encoding GFP was transformed into bacterial strains (UTI89 *wt* and UTI89 Δ*fimA-H*) by electroporation. Briefly, purified DNA (10–100 ng) was mixed with bacterial suspension (80 µL), followed by electroporation in 1 mm cuvettes using a Gene Pulser (BioRad) set to 1.75 V, 25 µF, and 400 Ω. Electroporated cells were mixed with 1 mL superoptimal broth medium (2% bacto tryptone, 0.5% yeast extract, 10 mM NaCl, and 2.5 mM KCl), incubated for 30 min at 37 °C, and plated on LB agar plates containing 20 µg/mL ampicillin (AppliChem). Single clones were cultured and tested in the flow cytometer for the expression of GFP. Non–GFP-transformed cells were used as negative control.

5-(6)-Carboxyfluorescine *N*-succinimidylester Staining

5-(6)-Carboxyfluorescine *N*-succinimidylester (CFSE; Lubio Science) in PBS, 7.5 µM, was added to an equal volume of bacterial suspension (OD_{600} of 0.5) and incubated for 30 min at 37°C, under constant shaking (80 rpm) and protected from light. The staining was blocked by the addition of 20 mL ice-cold 2.5% human serum albumin (CSL Behring). Subsequently, CFSE-labeled bacteria were washed four times with PBS prior to use. Unstained cells were used as negative control.

FimH Antagonists

D-Mannoside (**1**), methyl α-D-mannopyranoside (**2**), 4-nitrophenyl α-D-mannopyranoside (**4**), and D-galactose (**13**) were purchased from Fluka Chemie GmbH. *n*-Heptyl α-D-mannopyranoside (**3**) was synthesized as previously described.[24,36] 2-Chloro-4-nitrophenyl α-D-mannopyranoside (**5**) and *o*-chloro-*p*-[*N*-(2-ethoxy-3,4-dioxocyclobut-1-enyl)amino]phenyl α-D-mannopyranoside (**6**) were synthesized as previously described.[20] The biphenyl α-D-mannopyranosides **7**–**12** were synthesized as described elsewhere[21,37] (see *Fig. 1*).

Aggregometry Assay

The aggregometry assay was carried out as described by Abgottspon *et al.*[24] Briefly, the aggregation of *E. coli* with guinea pig erythrocytes (GPE) was quantitatively determined using an APACT 4004 aggregometer (Endotell AG). Bacteria were cultivated as described earlier. GPE were isolated from guinea pig blood (Charles River Laboratories) using Histopaque (Sigma-Aldrich) (density of 1.077 g/mL at 24°C). Before the assay, the cell densities of *E. coli* and GPE were adjusted to an optical density (OD) at 600 nm of 4 (1.9×10^8 CFU/mL and 2.2×10^6 cells/mL, respectively). To calibrate the instrument, the aggregation of protein-poor plasma in PBS was set at 100% and the aggregation of protein-rich plasma in the presence of GPE at 0%. After calibration, measurements were performed with 250 µL GPE and 50 µL bacterial suspension. After an aggregation phase of 600 s, 25 µL of a twofold serial dilution of the antagonist in PBS was added to each cuvette and disaggregation was monitored for 1,400 s (*Fig. 2*). UTI89 Δ*fimA-H* was used as negative control.

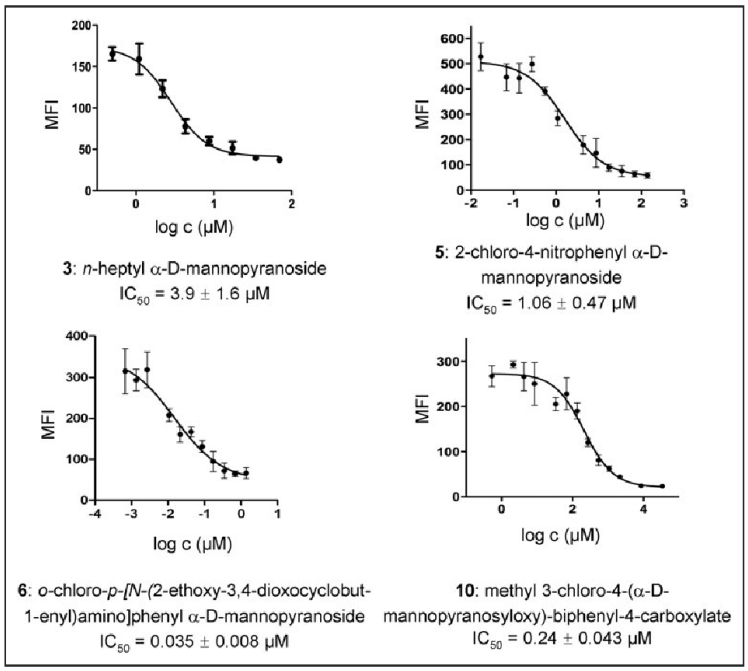

Fig. 1. Determination of the IC_{50} values for FimH antagonists (using an MOI of 1:50). Examples of sigmoidal inhibition curves obtained from the competitive flow cytometry assay for compound **3**, **5**, **6**, and **10**. Error bars represent standard error of $n = 2–3$ values. Assays were repeated at least twice.

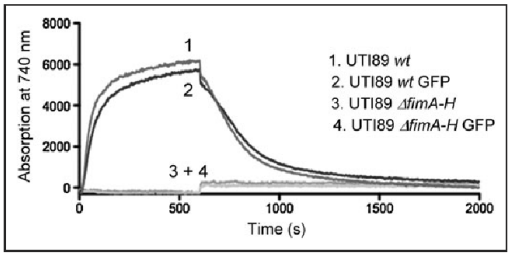

Fig. 2. The aggregation of guinea pig erythrocytes with GFP-expressing UTI89 strains (*wt* and Δ*fimA-H*) and unlabeled strains was recorded at OD_{750}. After 600 s, the disaggregation was initiated by the addition of a single concentration of 5 mM *n*-heptyl α-D-mannopyranoside (**3**).

Competitive Binding Assay

The competitive binding assay was carried out as described by Rabbani *et al.*[34] A recombinant protein consisting of the CRD of FimH linked with a thrombin cleavage site to a 6His-tag (FimH-CRD-Th-6His) was expressed in *E. coli* strain HM125 and purified on a Ni-NTA column. Microtiter plates (F96 MaxiSorp; Nunc) were coated with 100 μL/well of a 10 μg/mL solution of FimH-CRD-Th-6His in assay buffer (20 mM HEPES, 150 mM NaCl, and 1 mM $CaCl_2$ [pH 7.4]) overnight at 4°C. The coating solution was discarded and the wells were blocked with 150 μL/well of 3% bovine serum albumin (BSA) in assay buffer for 2 h at 4°C. After three washing steps with assay buffer (150 μL/well), a fourfold serial dilution of the test compound (50 μL/well) in assay buffer containing 5% dimethylsulfoxide (DMSO) and streptavidin-peroxidase–coupled Manα1-3(Manα1-6)Manβ1-4GlcNAcβ1-4GlcNAcβ-polymer (50 μL/well of a 0.5 μg/mL solution) were added. On each individual microtiter plate, *n*-heptyl α-D-mannopyranoside (3) was tested in parallel. The plates were incubated for 3 h at 25°C and 350 rpm and then carefully washed four times with 150 μL/well assay buffer. After the addition of 100 μL/well of 2,2′-azino-bis-(3-ethylbenzthiazoline-6-sulfonic acid) substrate, the colorimetric reaction was allowed to develop for 4 min and then stopped by the addition of 2% aqueous oxalic acid before the OD was measured at 415 nm on a microplate reader (Spectramax 190; Molecular Devices).

UPIa Immunoblotting

Human epithelial bladder 5637 cells from different passage numbers were grown at confluence and lysed with 1% Triton X-100 (Sigma). Cell lysates were resolved on a 12% sodium dodecyl sulfate–polyacrylamide gel electrophoresis under reducing conditions and transferred onto a nitrocellulose membrane (BioRad). The membrane was blocked with 3% BSA (Sigma) in PBS and incubated with a polyclonal goat anti-UPIa antibody (Santa Cruz Biotechnology). As secondary antibody an alkaline phosphatase–coupled donkey anti-goat IgG (Santa Cruz Biotechnology) was used. After three washing steps, the membrane was developed with the nitro blue tetrazolium chloride/5-bromo-4-chloro-3-indolylphosphate *p*-toluidine salt solution (Fluka).

Quantification of Bacterial Adhesion on 5637 Cells: Infection Assay

The 5637 cells, grown in 24-well plates, were infected with 200 µL bacterial suspension at a multiplicity of infection (MOI) of 1:20, 1:50, and 1:100 (cell:bacteria). To homogenize the infection, plates were centrifuged at room temperature for 3 min at 600 *g*. After an incubation of 1.5 h at 37°C, infected cells were washed four times with RPMI 1640 medium and suspended in ice-cold PBS for 5–20 min (treatment with ice-cold PBS results in the detachment of the infected cells). The cells were then kept in the dark until analysis. All measurements were made within 1 h after the termination of the infection. Samples were measured with a CyAn ADP flow cytometer (Beckman-Coulter) and analyzed by gating on the eukaryotic cells based on forward (FSC) and side scatter (SSC), which excludes unbound labeled bacteria and debris from analysis. A total of 10^4 cells were measured per sample. Data were acquired in a linear mode for the SSC and in a logarithmic mode for FSC and the green fluorescent channel FL1-H (*e.g.*, GFP, CFSE). The mean fluorescence intensity (MFI) of FL1-H was counted as a surrogate marker for the adherence of bacteria. Quantification of adhesion was evaluated with the FlowJo software 9.0.1 (Tree Star, Inc.).

Inhibition Assay (Flow Cytometry Assay)

To evaluate FimH antagonists, a serial dilution in 5% DMSO was prepared. Before infection, bacterial suspension (200 µL) and 25 µL of the test compound were preincubated for 10 min at room temperature. The bacteria–antagonist mixture was then added to the monolayer of 5637 cells. Infection, measurement, and quantification of adhesive bacteria were performed as described earlier. IC_{50} values were determined by plotting the concentration of the antagonist in a logarithmic mode versus the MFI and by fitting the curve with the prism software (GraphPad; inhibition curve, variable slope) ($n = 2–3$, in duplicates/triplicates). The protocol of the inhibition assay is summarized in *Table 1*.

Internalization (Invasion) Assay

Invasion assays were performed essentially as described by Elsinghorst (gentamicin protection assay).[38] Briefly, the 5637 cells were grown in 24-well plates to confluence and infected with 200 µL bacterial suspension at an MOI of 1:50. To homogenize the infection, plates were centrifuged at room temperature for 3 min at 600 *g*. After an incubation time of 1.5 h at 37°C, the infected cells were washed four times with PBS. To determine the total of extra- and intracellular bacteria, the cells were directly lysed by the addition of 0.2 mL lysis buffer (ddH_2O and 0.1% Triton X-100 [Sigma]) and plated on blood agar plates in 1:10 dilutions. To determine only intracellular bacteria, infected cells were treated with gentamicin (100 µg/mL; Essex Chemie AG) for 30 min after the initial washing step. Then, the cells were washed three times with PBS and lysed with 0.2 mL lysis buffer. The number of intracellular bacteria surviving the gentamicin treatment was determined by plating serial 1:10 dilutions on blood agar plates.

Table 1. Protocol Table of the Flow Cytometry Inhibition Assay

Step	Parameter	Value	Description
1	Plate cells	1.8×10^5 cells/well	5637 cells
2	OD_{600}	According to cells/well	UTI89 GFP density (MOI 1:50)
3	Antagonists	225 µL	25 µL antagonist (serial dilution) to 200 µL UTI89 GFP
4	Preincubation time	10 min	UTI89 GFP with antagonist (serial dilution)
5	Infection	225 µL	Bacteria–antagonist mixture to 5637 cells
6	Centrifugation	3 min	600 *g*
7	Incubation time	1.5 h	37°C
8	Wash step	200 µL	4 × with PBS
9	Incubation time	200 µL, 10 min	Ice-cold PBS
10	Read-out	10^4 cells	Flow cytometry measurements, MFI in green fluorescent channel

Step Notes

1. 24-well tissue culture plate.
2. OD_{600} 1 equivalent to 48×10^6 bacteria.
3. Serial dilution of antagonists (stock concentration 10 mM) in PBS, 5% DMSO.
4. 200 µL bacterial solution with 25 µL antagonist solution.
6. For homogenization of infection.
8. Clearance from nonadherent bacteria.
9. Leads to loosening of the cells from the culture tissue.
10. Gating on mammalian cells in FSC and SSC; IC_{50} is obtained by plotting the MFI versus log[antagonist]; fit: inhibition curve with variable slope.

OD, optical density; GFP, green fluorescent protein; MOI, multiplicity of infection; PBS, phosphate-buffered saline; MFI, mean fluorescent intensity; DMSO, dimethylsulfoxide; FSC, forward scatter; SSC, side scatter.

RESULTS

Analysis of UPIa Expression in 5637 Cells

The adhesion of *E. coli* UTI89 to bladder epithelial cells depends on the uroplakin receptor complex on the surface of the host cells, containing the protein UPIa.[13] To verify whether the human urinary bladder carcinoma cell line 5637 expresses UPIa, a western blot analysis was performed using cell lysates after different cell passage numbers and a polyclonal anti-UPIa antibody. The result clearly showed that the UPIa receptor on 5637 cells was efficiently expressed with the expected molecular weight (27 kDa), independent of the number of cell passages (*Fig. 3*). Weak additional signals were observed probably because of cross-reaction with other uroplakin family members.

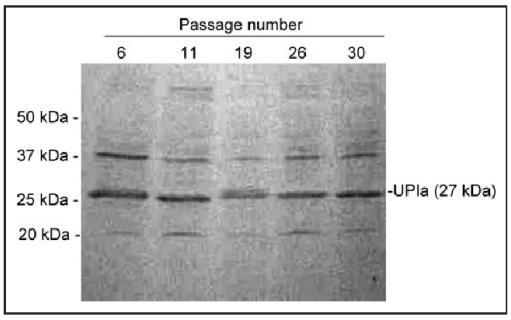

Fig. 3. Western blot analysis of UPIa. The expression of UPIa in 5637 cells from passage numbers 6 to 30 was analyzed by immunoblotting. The primary antibody was a polyclonal goat anti-UPIa (C-18) immunoglobulin G and secondary antibody a donkey anti-goat immunoglobulin G coupled to alkaline phosphatase. UPIa, uroplakin Ia.

Fluorescent Staining of UTI89 Bacteria

For visualization, UTI89 *wt* and the UTI89 Δ*fimA-H* strains were either transformed with a GFP-encoding plasmid or stained with CFSE directly before infection. Cell growth measurement and colony-plating assays demonstrated that the bacteria were not affected by labeling (data not shown). In the flow cytometry analysis, CFSE-treated bacteria showed an inhomogeneous staining profile, with fluorescently active and inactive subpopulations, although a high concentration of the fluorescent agent was used (final concentration: 7.5 μM) (*Fig. 4A*). In addition, we observed differences in fluorescent intensities between the UTI89 *wt* and UTI89 Δ*fimA-H* strains, that is, CFSE uptake into the wild-type strain was much more efficient than into the pilus-deficient strain.

In contrast to CFSE-labeled bacteria, GFP-expressing bacteria showed a uniform, intense fluorescence profile (*Fig. 4B*). Further, the stable expression of GFP by the bacteria made this labeling technique suitable for subsequent experiments. To test the binding ability of GFP-expressing bacteria to GPE, the aggregometry assay[21] using 384 μM *n*-heptyl α-D-mannopyranoside (3) was carried out, using GFP-labeled and nonlabeled strains. The result clearly indicated that the GFP expression did not alter the ability of the bacteria to interact with GPEs (*Fig. 2*), and thus, the expression of bacterial adhesins remains unaffected by GFP expression.

Infection Assay

For the optimization of the infection assay, three different MOI ratios (20:1, 50:1, and 100:1, bacteria:cell) were tested (*Fig. 5*). The fluorescence emitted from unbound bacteria was discriminated from fluorescence emitted from cell-bound bacteria by selecting the appropriate fluorescence-activated cell sorting size gate, which was determined by measuring uninfected cells and labeled bacteria alone. For the UTI89 *wt* strain, the fluorescence signal was proportional to the MOI ratio and was in the optimal range of MFI of >200. For all subsequent experiments, an MOI of 50:1 was used.

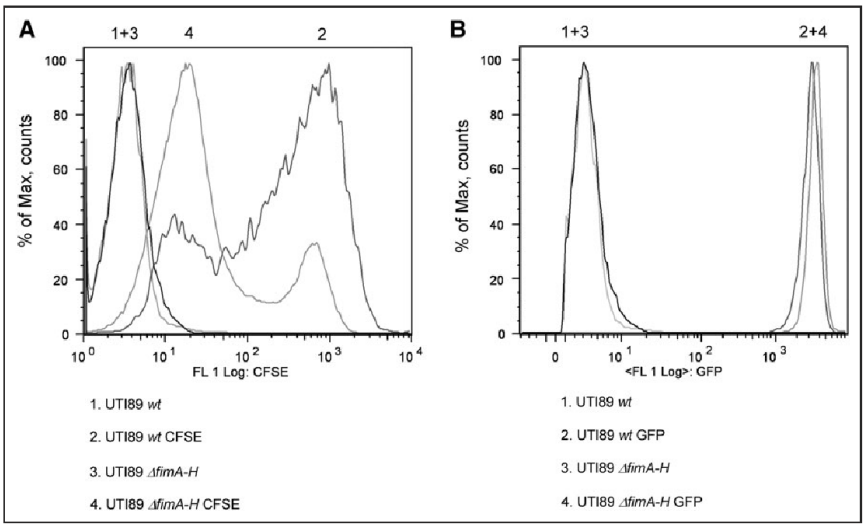

Fig. 4. Flow cytometry analysis of CFSE-stained **(A)** and GFP-expressing **(B)** UTI89 *wt* and UTI89 Δ*fimA-H* strains. The analysis was carried out as described in the Materials and Methods section. CFSE, 5-(6)-carboxyfluorescein *N*-succinimidylester; GFP, green fluorescent protein.

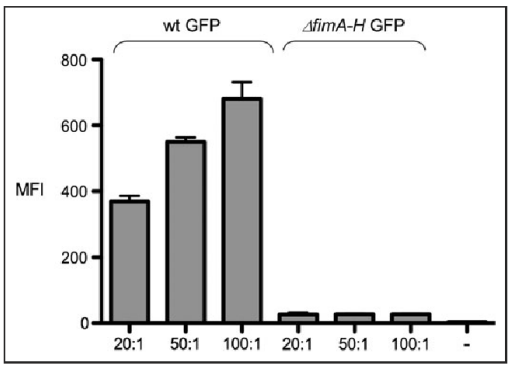

Fig. 5. Infection assay: MFI of 5637 cells infected with different ratios of GFP-expressing UTI89 strains (wt and Δ*fimA-H* strain); MOIs: 20:1, 50:1, and 100:1 (bacteria:cell). (−) indicates uninfected 5637 cells. Assay and analysis were performed as described in the Materials and Methods section. Error bars represent standard error of $n=3$ values. MFI, mean fluorescent intensity; MOI, multiplicity of infection.

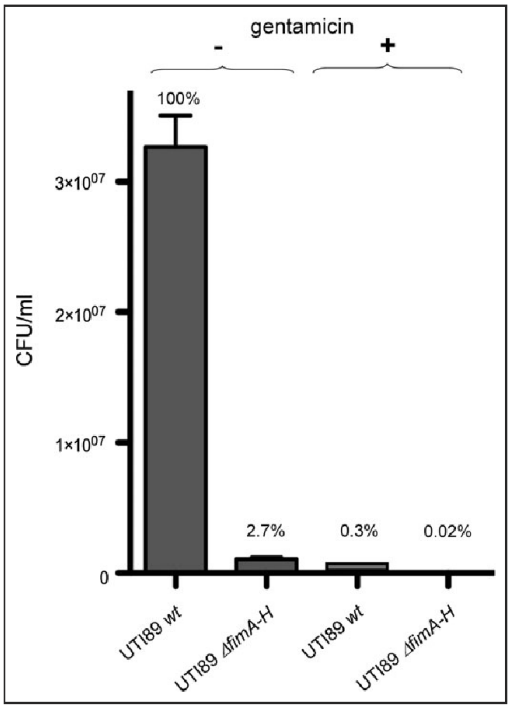

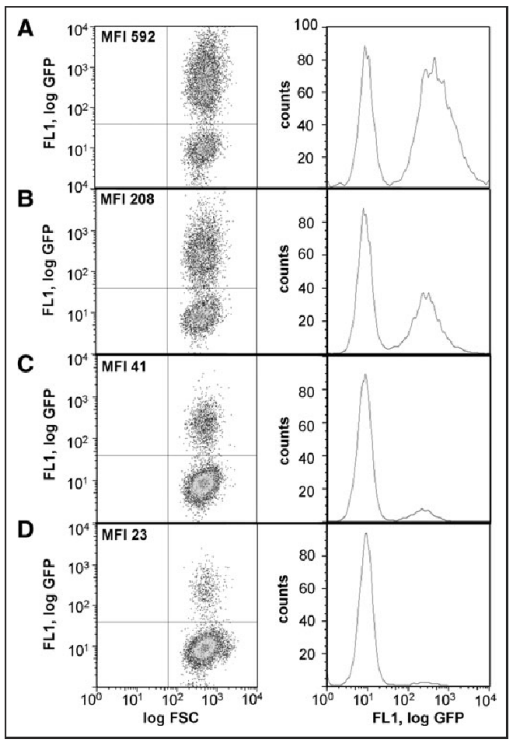

Fig. 7. Flow cytometry analysis of 5637 cells infected with GFP-expressing UTI89 strains (MOI 50:1, bacteria:cell). Histograms show the green fluorescence intensity of cells infected with UTI89 *wt* **(A)**, pretreated UTI89 *wt* with 7 μM **(B)** and 111 μM **(C)** *n*-heptyl α-D-mannopyranoside (**3**) before infection, and UTI89 Δ*fimA-H* **(D)**.

At this MOI, an intensive fluorescence profile without saturation, because of an excess of bacteria, was obtained. Bladder cells infected with the FimH-deficient strain UTI89 Δ*fimA-H* displayed a weak fluorescence signal, similar to that of uninfected cells (MFI below 30), confirming that the adhesion of UTI89 is exclusively type 1 pili dependent. Pils *et al.*[39] reported that trypan blue can be used to quench

Fig. 6. Internalization (invasion) assay: CFU/mL of UTI89 *wt* and UTI89 Δ*fimA-H* after infection (1.5 h) of 5637 cells with and without subsequent gentamicin (100 μg/mL) treatment. CFU/mL of the adhesive UTI89 *wt* was set to 100%. Assay and analysis were performed as described in the Material and Methods section. Error bars represent standard error of $n=6$ values.

extracellular fluorescence signals of CFSE-labeled bacteria. Therefore, infected cells treated with trypan blue emit light specifically from internalized bacteria. In our assay, the application of this method to GFP-labeled bacteria turned out to be not successful (data not shown), because the fluorescence emitted by GFP-labeled, extracellular bacteria could not be quenched. Consequently, GFP labeling could not be used to investigate the internalization of bacteria by flow cytometry via trypan blue treatment.

Therefore, the extent of internalization of bacteria within an incubation time of 1.5 h (*Fig. 6*) was determined according to the internalization assay published by Elsinghorst.[38] The observed CFU/mL of extra- and intracellular adhesive UTI89 *wt* before gentamicin treatment was set to 100%. As less than 1% of the adhesive UTI89 *wt* bacteria (representing internalized bacteria) survived the gentamicin treatment, the internalization occurrence during 1.5 h of infection is negligible. As expected, the mutant UTI89 Δ*fimA-H* was nonadhesive and noninvasive under similar conditions.

Inhibition Assay (Flow Cytometry Assay)

To evaluate the applicability of the assay for the evaluation of FimH antagonists, two different concentrations (7 and 111 μM) of *n*-heptyl α-D-mannopyranoside (3) were added to the bacterial suspension before infection. *Figure 7* shows that compound 3 successfully antagonized the adhesion of bacteria to 5637 cells. The MFI of cells infected with the UTI89 *wt* strain in the absence of compound 3 was 592 (*Fig. 7A*) and decreased in the presence of compound 3 at 7 and 111 μM to 208 and 41, respectively (*Fig. 7B, C*). Cells treated with the UTI89 Δ*fimA-H* mutant strain (*Fig. 7D*) exhibited only a low MFI

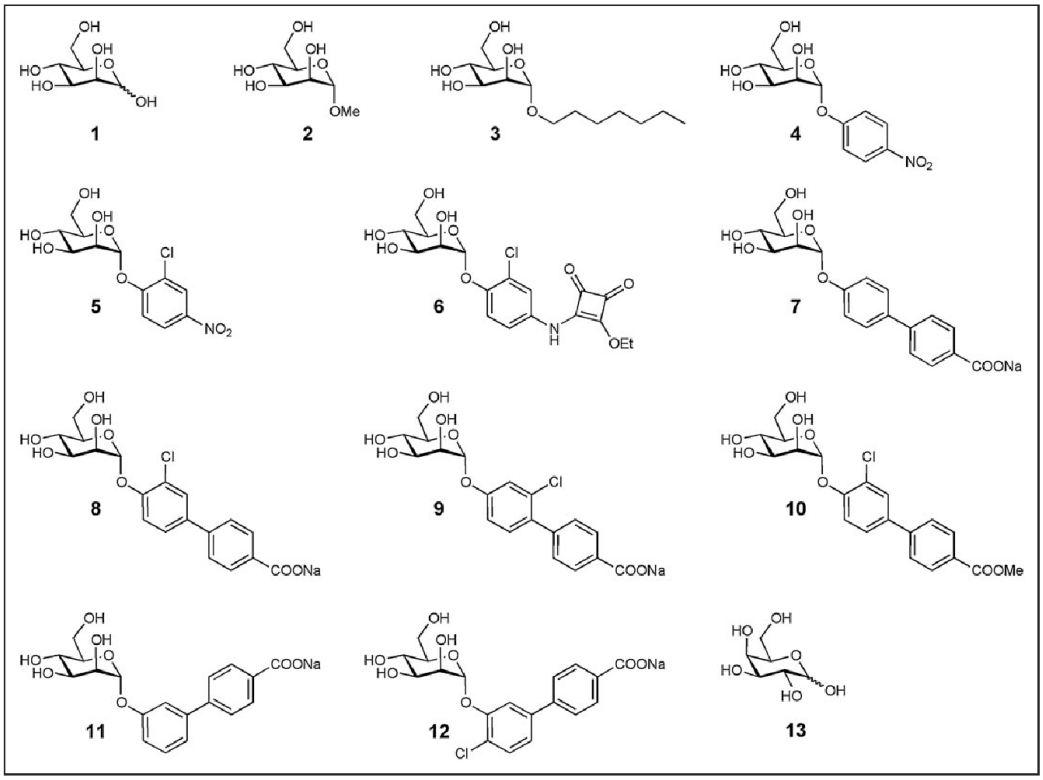

Fig. 8. Structures of FimH antagonists and the negative control D-galactose (**13**). D-Mannopyranoside (**1**), methyl α-D-mannopyranoside (**2**), *n*-heptyl α-D-mannopyranoside (**3**),[24,36] 4-nitrophenyl α-D-manno-pyranoside (**4**), 2-chloro-4-nitrophenyl α-D-mannopyranoside (**5**),[20] *o*-chloro-*p*-[*N*-(2-ethoxy-3,4-dioxocyclobut-1-enyl)amino]phenyl α-D-mannopyranoside (**6**),[20] and the biphenyl α-D-mannopyranoside derivatives **7**–**12**.[21,37]

Table 2. Inhibitory Potencies of FimH Antagonists

FimH Antagonist	Flow Cytometry Inhibition Assay		Aggregometry Assay [24]	Competitive Binding Assay [34]
	IC_{50} [μM]	rIC_{50}	rIC_{50}	rIC_{50}
2	249.2 ± 62.3	59.6	n.d.	29.2
3 (ref. compound)	3.9 ± 1.6	1	1	1
4	3.2 ± 0.69	0.76	0.84	1.57
5	1.06 ± 0.47	0.25	0.18	0.32
6	0.035 ± 0.008	0.008	0.01	0.15
7	0.86 ± 0.56	0.22	0.58	0.15
8	0.33 ± 0.05	0.08	0.13	0.09
9	0.53 ± 0.06	0.13	0.22	0.38
10	0.24 ± 0.043	0.06	0.12	0.06
11	4.45 ± 1.9	1.14	0.58	0.53
12	0.79 ± 0.16	0.2	n.d.	0.4
13	> 5500	–	n.d.	n.d.

IC_{50} values (using an MOI of 1:50) were determined with the flow cytometry assay as described in the Materials and Methods section and compared with rIC_{50} values obtained with the aggregometry and competition binding assays (values for compound **2**–**6** derive from literature,[24,34] whereas compounds **7**–**13** were newly tested). rIC_{50}s were calculated by dividing the IC_{50} of the compound of interest by the IC_{50} of the reference compound **3**. This leads to in rIC_{50} values below 1.0 for derivatives with higher activity than **3** and rIC_{50} values above 1.0 for compounds with lower activity than **3**.

n.d., not determined.

of 23. In a next step, the bacteria were treated with a serial dilution of inhibitor prior to infection. By measuring the MFI values, an IC_{50} value could be derived from the sigmoid inhibition curve (MFI vs. log[antagonist]) (*Fig. 1*). The reproducible IC_{50} value for the reference compound **3** was in the low μM range (3.9 ± 1.6 μM). To validate the assay, different FimH antagonists (*Fig. 8*) were evaluated. The assay was performed in duplicates/triplicates and repeated two or three times. Examples of inhibition curves of the antagonists **5**, **6**, and **10** are shown in *Figure 1*. Affinities were compared with affinity data obtained with the aggregometry assay[24] and competitive binding assay[34] (*Table 2*). Relative IC_{50} values (rIC_{50}) were calculated using *n*-heptyl α-D-mannopyranoside (**3**) as reference compound. As expected, methyl α-D-mannopyranoside (**2**) exhibited the weakest inhibitory potential, with an IC_{50} value of 249.2 ± 62.3 μM. The best inhibitor turned out to be the squaric acid derivative compound **6**, with an IC_{50} value of 35 ± 8 nM. The other phenyl and biphenyl derivatives (**4**, **5**, **7**–**12**), except for compound **11**, which had a similar IC_{50} value as **3**, exhibited slightly higher inhibitory potentials than reference compound **3**. D-Galactose (**13**), used as negative control, did not show any inhibitory effect up to a concentration of 5.5 mM.

DISCUSSION

On epithelial bladder cells, α-mannosides are the primary ligands for UPEC. For their attachment, FimH lectins located at the tip of bacterial fimbriae are required. To prevent UTI, inhibition of this type 1 fimbriae-mediated bacterial adhesion to the bladder epithelium is a promising therapeutic approach.[10]

Various mannose derivatives[16–18,20,21] and oligomannosides[19,40] have been shown to antagonize FimH. For the evaluation of these antagonists, cell-based inhibition assays were mainly applied, using the properties of UPEC to agglutinate GPE[18,23,24] or to aggregate mannan-expressing yeast cells.[25–27] The results of these functional assays vary significantly because of the differential expression of FimH[25,26] and depend strongly on both source and batch of erythrocytes.[23] Further, GPE do not display the natural receptors for FimH, as the uroplakin proteins are exclusively expressed on bladder epithelial cells.[14]

Using GFP-labeled UPECs and human epithelial carcinoma bladder 5637 cells, a function-based flow cytometry assay was established. The assay allows a highly accurate analysis of bacterial adhesion, as more than 10,000 epithelial cells can be analyzed within a short time period. By investigating a large number of cells, variations caused by naturally occurring outliers are minimized. Further, easy handling reduces the effect of factors that influence reproducibility and reliability of the assay. In addition, the cumbersome fluorescent labeling prior to each experiment is not necessary when GFP-expressing bacteria are used.

It could be demonstrated with the UTI89 Δ*fimA-H* mutant strain that the adherence of the UPEC strain UTI89 to epithelial cells exclusively depends on type 1 pili. This result emphasizes the pivotal role of these pili for the pathogenesis of UPEC infection. Further, it validates FimH as a target for a therapeutic approach. The assay was first optimized with *n*-heptyl α-D-mannopyranoside (**3**), a potent FimH antagonist.[16] For the validation of the assay, the IC_{50} values of different FimH antagonists were determined (*Figs. 1* and *8*) and compared with affinity data obtained by two other assay formats[24,34] (*Table 2*). As expected, methyl α-D-mannopyranoside (**2**) showed the lowest affinity (IC_{50} = 249 ± 62.3 μM). For mannosides with aromatic aglycones such as *p*-nitrophenyl α-D-mannopyranoside (**4**) and 2-chloro-4-nitrophenyl α-D-mannopyranoside (**5**),[20] affinity was enhanced, thus confirming the beneficial effect of lipophilic interactions between the aromatic aglycone and the tyrosine gate of the binding site of the protein. The squaric acid derivative **6**[20] showed the best inhibitory potential of all tested antagonists (IC_{50} = 35 ± 8 nM), a more than 100-fold increased activity compared with **3**. For the biphenyl mannosides **7**–**12**,[37] the best activities were obtained with an *ortho*-chloro substituent on the aromatic ring adjacent to the anomeric oxygen and *para*-substitution of the biphenyl (**8**–**10**). Antagonists with a *meta*-substituted biphenyl aglycone exhibited a two- to fivefold lower activity (**7** vs. **11**, **8** vs. **12**). A similar effect was found for an additional

chloro-substituent (11 vs. 12). Finally, for D-galactose (13), which was used as negative control, no inhibition of FimH-mediated adhesion at concentrations up to 5.5 mM was detected.

In *Table 2*, rIC_{50} values obtained with the flow cytometry assay are compared with those obtained with the competitive binding assay[31] and the aggregometry assay.[24] However, a direct comparison of the IC_{50} values is not possible, as the inhibition potencies were measured in different assay formats. For the competitive binding assay, we used the isolated CRD of FimH, which adopts the high-affinity state even under static conditions.[33] In contrast, in the cell-based aggregometry and flow cytometry assays, the bacteria display full-length fimbriae, representing the FimH low-affinity state under low shear stress.[33] However, when affinity data relative to a reference compound (rIC_{50}) were compared, the rIC_{50} values from the flow cytometry assay, in general, correlate well with values measured with the aggregometry assay[24] and the cell-free competitive binding assay[31] (*Table 2*). One exception is the squaric acid derivative **6**, which gave similar results in the flow cytometry and aggregometry assays, but a much higher rIC_{50} in the cell-free competitive binding assay. Further, the affinities of compounds **2**, **4**, and **5** agree very well with reported values.[16,31]

The assay was optimized for an infection time of 1.5 h. At this time point, the degree of internalization of bacteria by 5637 cells is below 1% and therefore negligible, as determined by an internalization assay[38] (*Fig. 6*). However, when the contact time between bacteria and cells is prolonged, internalization of bacteria may occur to a higher extent and will therefore falsify the readout of the assay.

In the target- and function-based assays published to date, the affinities of antagonists to purified lectin[16,30,34] or whole bacteria[23,24,28] are measured by competition assays with either immobilized/soluble D-mannose derivatives[16,28,34] or glycans present on cell surfaces of yeast,[25–27] erythrocytes,[18,23,24] or granulocytes.[30] In the presented flow cytometry assay, the antagonists compete with oligomannosides of the endogenously expressed physiological ligand UPIa on bladder epithelial cells for binding to type 1 fimbriae of the clinical isolate UTI89. Therefore, the new *in vitro* assay allows to estimate the inhibitory potential of antagonists *in vivo*.

In summary, we developed a reproducible and sensitive function-based assay that allows the quantitative analysis of FimH-mediated bacterial adhesion to mammalian cells and, further, the determination of the inhibitory potential of compounds that block the adhesion. Easy handling makes it a valuable tool for the evaluation of novel FimH antagonists. Moreover, the obtained IC_{50} value can serve as a guidance value for the minimal therapeutic concentration in the bladder necessary for a successful treatment of UTI in *in vivo* studies.

ACKNOWLEDGMENTS

The authors thank Prof. Urs Jenal, Biocenter of the University of Basel, for the clinical *E. coli* isolate UTI89 and the FimH knock-out strain UTI89Δ*fimA-H*. The financial support by the Swiss National Science Foundation (SNF interdisciplinary grant K-32K1-120904) is gratefully acknowledged.

DISCLOSURE STATEMENT

No competing financial interests exist.

REFERENCES

1. Foxman B, Barlow R, D'Arcy H, Gillespie B, Sobel JD: Urinary tract infection: self reported incidence and associated costs. *Ann Epidemiol* 2000;10:509–515.
2. Ronald A: The etiology of urinary tract infection: traditional and emerging pathogens. *Acad Med* 2002;113:14S–19S.
3. Foxman B, Brown P: Epidemiology of urinary tract infections—transmission and risk factors, incidence, and costs. *Infect Dis Clin North Am* 2003;17:227–241.
4. Foxman B: Recurring urinary tract infection: incidence and risk factors. *Am J Public Health* 1990;80:331–333.
5. Mulvey MA: Adhesion and entry of uropathogenic *Escherichia coli*. *Cell Microbiol* 2002;4:257–271.
6. Wiles TJ, Kulesus RR, Mulvey MA: Origins and virulence mechanisms of uropathogenic *Escherichia coli*. *Clin Mol Pathol* 2008;85:11–19.
7. Russell PW, Orndorff PE: Lesions in two *Escherichia coli* type 1 pilus genes alter pilus number and length without affecting receptor binding. *J Bacteriol* 1992; 174:5923–5935.
8. Jones CH, Pinkner JS, Roth R, Heuser J, Nicholes AV, Abraham SN, *et al.*: FimH adhesin of type 1 pili is assembled into a fibrillar tip structure in the Enterobacteriaceae. *Proc Natl Acad Sci U S A* 1995;92:2081–2085.
9. Hung C, Bouckaert J, Hung DL, Pinkner J, Widberg C, DeFusco A, *et al.*: Structural basis of tropism of *Escherichia coli* to the bladder during urinary tract infection. *Abstr Gen Meet Am Soc Microbiol* 2002;102:41.
10. Hanson MS, Brinton CC: Identification and characterization of *E. coli* type-1 pilus tip adhesion protein. *Nature* 1988;332:265–268.
11. Choudhury D, Thompson A, Stojanoff V, Langermann S, Pinkner J, Hultgren SJ, *et al.*: X-ray structure of the FimC-FimH chaperone-adhesin complex from uropathogenic *Escherichia coli*. *Science* 1999;285:1061–1066.
12. Xie B, Zhou G, Chan SY, Shapiro E, Kong XP, Wu XR, *et al.*: Distinct glycan structures of uroplakins Ia and Ib - Structural basis for the selective binding of FimH adhesin to uroplakin Ia. *J Biol Chem* 2006;281:14644–14653.
13. Zhou G, Mo WJ, Sebbel P, Min GW, Neubert TA, Glockshuber R, *et al.*: Uroplakin Ia is the urothelial receptor for uropathogenic *Escherichia coli*: evidence from *in vitro* FimH binding. *J Cell Sci* 2001;114:4095–4103.
14. Wu XR, Sun TT, Medina JJ: *In vitro* binding of type 1-fimbriated *Escherichia coli* to uroplakins Ia and Ib: relation to urinary tract infections. *Proc Natl Acad Sci U S A* 1996;93:9630–9635.
15. Mulvey MA, Lopez-Boado YS, Wilson CL, Roth R, Parks WC, Heuser J, *et al.*: Induction and evasion of host defenses by type 1-piliated uropathogenic *Escherichia coli*. *Science* 1998;282:1494–1497.
16. Bouckaert J, Berglund J, Schembri M, De Genst E, Cools L, Wuhrer M, *et al.*: Receptor binding studies disclose a novel class of high-affinity inhibitors of the *Escherichia coli* FimH adhesin. *Mol Microbiol* 2005;55:441–455.
17. Imberty A, Chabre YM, Roy R: Glycomimetics and glycodendrimers as high affinity microbial anti-adhesins. *Chemistry* 2008;14:7490–7499.
18. Lindhorst TK, Kieburg C, Krallmann-Wenzel U: Inhibition of the type 1 fimbriae-mediated adhesion of *Escherichia coli* to erythrocytes by multiantennary alpha-mannosyl clusters: the effect of multivalency. *Glycoconj J* 1998;15:605–613.
19. Dubber M, Sperling O, Lindhorst TK: Oligomannoside mimetics by glycosylation of 'octopus glycosides' and their investigation as inhibitors of type 1 fimbriae-mediated adhesion of *Escherichia coli*. *Org Biomol Chem* 2006;4:3901–3912.
20. Sperling O, Fuchs A, Lindhorst TK: Evaluation of the carbohydrate recognition domain of the bacterial adhesin FimH: design, synthesis and binding properties of mannoside ligands. *Org Biomol Chem* 2006;4:3913–3922.
21. Han Z, Pinker JS, Ford B, Obermann R, Nolan W, Wildman SA, Hobbs D, Ellenberger T, Cusumano CK, Hultgren SJ, Janetka JW: Structure-based drug design and optimization of mannoside bacterial FimH antagonists. *J Med Chem* 2010;53:4779–4792.

22. Ernst B, Magnani JL: From carbohydrate leads to glycomimetic drugs. *Nat Rev Drug Discov* 2009;8:661–677.
23. Nagahori N, Lee RT, Nishimura S, Page D, Roy R, Lee YC: Inhibition of adhesion of type 1 fimbriated *Escherichia coli* to highly mannosylated ligands. *Chembiochem* 2002;3:836–844.
24. Abgottspon D, Rölli G, Hosch L, Steinhuber A, Jiang X, Schwardt O, Cutting B, Smiesko M, Jenal U, Ernst B, Trampuz A: Development of an aggrgation assay to screen FimH antagoists. *J Microbiol Methods* 2010;82:249–255.
25. Firon N, Ofek I, Sharon N: Carbohydrate specificity of the surface lectins of *Escherichia coli, Klebsiella pneumoniae*, and *Salmonella typhimurium*. *Carbohydr Res* 1983;120:235–249.
26. Firon N, Ashkenazi S, Mirelman D, Ofek I, Sharon N: Aromatic alpha-glycosides of mannose are powerful inhibitors of the adherence of type 1 fimbriated *Escherichia coli* to yeast and intestinal epithelial cells. *Infect Immun* 1987; 55:472–476.
27. Sokurenko EV, Courtney HS, Ohman DE, Klemm P, Hasty DL: FimH family of type 1 fimbrial adhesins: functional heterogeneity due to minor sequence variations among fimH genes. *J Bacteriol* 1994;176:748–755.
28. Hartmann M, Horst AK, Klemm P, Lindhorst TK: A kit for the investigation of live *Escherichia coli* cell adhesion to glycosylated surfaces. *Chem Commun* 2010; 46:330–332.
29. Schaeffer AJ, Amundsen SK, Schmidt LN: Adherence of *Escherichia coli* to human urinary tract epithelial cells. *Infect Immun* 1979;24:753–759.
30. Horst AK, Kotter S, Lindhorst TK, Ludwig A, Brandt E, Wagener C: Binding inhibition of type 1 fimbriae to human granulocytes: a flow cytometric inhibition assay using trivalent cluster mannosides. *Med Microbiol Immunol* 2001;190:145–149.
31. Touaibia M, Wellens A, Shiao TC, Wang Q, Sirois S, Bouckaert J, *et al.*: Mannosylated G(0) dendrimers with nanomolar affinities to *Escherichia coli* FimH. *ChemMedChem* 2007;2:1190–1201.
32. Yakovenko O, Sharma S, Forero M, Tchesnokova V, Aprikian P, Kidd B, Mach A, Vogel V, Sokurenko E, Thomas WE: FimH forms catch bonds that are enhanced by mechanical force due to allosteric regulation. *J Biol Chem* 2008;283, 11596–11605.
33. Aprikian P, Tchesnokova V, Kidd B, Yakovenko O, Yarov-Yarovoy V, Trinchina E, *et al.*: Interdomain interaction in the FimH adhesin of *Escherichia coli* regulates the affinity to mannose. *J Biol Chem* 2007;282:23437–23446.
34. Rabbani S, Jiang X, Schwardt O, Ernst B: Expression of the carbohydrate recognition domain of FimH and development of a competitive binding assay. *Anal Biochem* 2010;407:188–195.
35. Mulvey MA, Schilling JD, Hultgren SJ: Establishment of a persistent *Escherichia coli* reservoir during the acute phase of a bladder infection. *Infect Immun* 2001;69:4572–4579.
36. Oscarson S, Tiden AK: Syntheses of the octyl and tetradecyl glycosides of 3,6-di-o-alpha-deuteriummannopyranosyl-alpha-deuterium-mannopyranose and of 3,4-di-o-alpha-deuterium-mannopyranosyl-alpha-deuterium-mannopyranose a new way for 2,4-di-o-protection of mannopyranosides. *Carbohydr Res* 1993;247: 323–328.
37. Klein T, Abgottspon D, Wittwer M, Rabbani S, Herold J, Jiang X, Kleeb S, Lüthi C, Scharenberg M, Bezençon J, Gubler E, Pang L, Smiesko M, Schwardt O, Ernst B: FimH Antagonists for the oral treatment of urinary tract infections: from design and synthesis to *in vitro* and *in vivo* evaluation. *J Med Chem* 2010;53:8627–8641.
38. Elsinghorst EA: Measurement of invasion by gentamicin resistance. *Methods Enzymol* 1994;236:405–420.
39. Pils S, Schmitter T, Neske F, Hauck CR: Quantification of bacterial invasion into adherent cells by flow cytomet ry. *J Microbiol Methods* 2006;65:301–310.
40. Bouckaert J, Mackenzie J, de Paz JL, Chipwaza B, Choudhury D, Zavialov A, et al: The affinity of the FimH fimbrial adhesin is receptor-driven and quasi-independent of *Escherichia coli* pathotypes. *Mol Microbiol* 2006;61:1556–1568.

Address correspondence to:
Beat Ernst, PhD
Institute of Molecular Pharmacy
Pharmacenter
University of Basel
Klingelbergstrasse 50
CH-4056 Basel
Switzerland

E-mail: beat.ernst@unibas.ch

RESULTS AND DISCUSSION

Paper IV

Design, Synthesis and Biological Evaluation of Mannosyl Triazoles as FimH Antagonists.

Schwardt O, Rabbani S, Hartmann M, Abgottspon D, Wittwer M, Kleeb S, Zalewski A, Smiesko M, Cutting B, Ernst B.

Bioorg. Med. Chem. **2011**.

My contribution:

Aggregometry measurements of the mannosyl triazoles.

Bioorganic & Medicinal Chemistry 19 (2011) 6454–6473

Contents lists available at SciVerse ScienceDirect

Bioorganic & Medicinal Chemistry

journal homepage: www.elsevier.com/locate/bmc

Design, synthesis and biological evaluation of mannosyl triazoles as FimH antagonists

Oliver Schwardt, Said Rabbani, Margrit Hartmann, Daniela Abgottspon, Matthias Wittwer, Simon Kleeb, Adam Zalewski, Martin Smieško, Brian Cutting, Beat Ernst *

Institute of Molecular Pharmacy, Pharmacenter, University of Basel, Klingelbergstrasse 50, CH-4056 Basel, Switzerland

ARTICLE INFO

Article history:
Received 22 April 2011
Revised 24 August 2011
Accepted 25 August 2011
Available online 31 August 2011

Keywords:
Uropathogenic *Escherichia coli*
Urinary tract infections
Bacterial adhesin FimH
FimH antagonists
Competitive binding assay
Aggregometry assay
NMR spectroscopy

ABSTRACT

Urinary tract infection (UTI) caused by uropathogenic *Escherichia coli* (UPEC) is one of the most prevalent infectious diseases. Particularly affected are women, who have a 40–50% risk to experience at least one symptomatic UTI episode at some time during their life. In the initial step of the infection, the lectin FimH, located at the tip of bacterial pili, interacts with the high-mannosylated uroplakin Ia glycoprotein on the urinary bladder mucosa. This interaction is critical for the ability of UPEC to colonize and invade the bladder epithelium. X-ray structures of FimH co-crystallized with two different ligands, the physiological binding epitope oligomannose-3 and the antagonist biphenyl α-D-mannoside **4a** revealed different binding modes, an *in-docking-mode* and an *out-docking-mode*, respectively. To accomplish the *in-docking-mode*, that is the docking mode where the ligand is hosted by the so-called tyrosine gate, FimH antagonists with increased flexibility were designed and synthesized. All derivatives **5–8** showed nanomolar affinities, but only one representative, the 4-pyridiyl derivative **5j**, was as potent as the reference compound *n*-heptyl α-D-mannoside (**1b**). Furthermore, a loss of affinity was observed for *C*-glycosides and derivatives where the triazole aglycone is directly *N*-linked to the anomeric center. A conformational analysis by NMR revealed that the triazolyl-methyl-*C*-mannosides **8** adopt an unusual $^{1}C_{4}$ chair conformation, explaining the comparably lower affinity of these compounds. Furthermore, to address the drug-likeness of this new class of FimH antagonists, selected pharmacokinetic parameters, which are critical for oral bioavailability (lipophilicity, solubility, and membrane permeation), were determined.

1. Introduction

Urinary tract infections (UTIs) are among the most common infections, affecting millions of people each year. Although UTIs rarely cause severe diseases such as pyelonephritis or urosepsis, they are associated with extensive morbidity and generate considerable medical expenses.[1] Uropathogenic *Escherichia coli* (UPEC) are the primary cause of UTIs accounting for 70–95% of the reported cases. Particularly affected are women, who have a 40–50% risk to suffer from a symptomatic UTI episode at some time during their life.[2,3] Symptomatic UTIs require antimicrobial treatment, resulting in selection and development of bacterial resistance. Consequently, treatment of consecutive infections becomes increasingly difficult. Especially patients with diabetes, urinary tract anomaly, paraplegia and those with permanent urinary catheter experience repeated UTIs with resistant strains. Therefore, a new approach for the treatment and prevention of UTI with non-antibiotic and orally applicable therapeutics with a low potential for resistance would have a great impact on patient care, public healthcare, and medical expenses.

UPEC express a number of well-studied virulence factors for successful colonization of and survival within the host.[1,4,5] One important virulence factor, the mannose-specific FimH adhesin, is located at the tip of bacterial type **1** pili.[6] Type **1** pili are the most prevalent fimbriae encoded by UPEC, consisting of the four subunits FimA, FimF, FimG and FimH. The FimH lectin enables UPEC to attach to high-mannosylated uroplakin Ia glycoproteins on the urinary bladder mucosa, thus enabling adherence and invasion of host cells and at the same time preventing the rapid clearance of

Abbreviations: ABTS, 2,2′-azino-di-(3-ethylbenzthiazoline-6-sulfonic acid); AUC, area under the curve; BSA, bovine serum albumin; CRD, carbohydrate recognition domain; D, distribution coefficient; DCM, dichloromethane; DMSO, dimethyl sulfoxide; GIT, gastrointestinal tract; GPE, guinea pig erythrocytes; HEPES, 4-(2-hydroxyethyl)-piperazine-1-ethanesulfonic acid; IC_{50}, half maximal inhibitory concentration; iv, intravenous; Man, D-mannose; NMR, nuclear magnetic resonance; NOESY, nuclear Overhauser enhancement spectroscopy; PAA, polyacrylamide; PAMPA, parallel artificial membrane permeation assay; P_{app}, apparent permeability; P_e, effective permeation; po, peroral; rIC_{50}, relative inhibitory concentration; SAR, structure–activity relationship; THF, tetrahydrofurane; TM-PAA, Manα(1-3)-[Manα(1-6)]-Manβ(1-4)-GlcNAcβ(1-4)-GlcNAcβ-PAA; UPEC, uropathogenic *E. coli*; UTI, urinary tract infection.

* Corresponding author. Tel.: +41 61 2 67 15 51; fax: +41 61 2 67 15 52.
E-mail address: beat.ernst@unibas.ch (B. Ernst).

0968-0896/$ - see front matter © 2011 Elsevier Ltd. All rights reserved.
doi:10.1016/j.bmc.2011.08.057

E. coli from the UTI by the bulk flow of urine.[1,7] As a part of the FimH subunit, a carbohydrate-recognition domain (CRD) is responsible for bacterial interactions with the host cells within the urinary tract.[7] The crystal structure of methyl α-D-mannopyranoside bound to the FimH-CRD was solved[8] and the structures of the corresponding complexes with *n*-butyl α-D-mannopyranoside,[9] Manα(1-3)-[Manα(1-6)]-Manβ(1-4)-Glc*N*Acβ-(1-4)Glc*N*Ac (oligomannose-3)[10] and biphenyl α-D-mannopyranoside[11] recently became available.

Previous studies showed that colonization and subsequent *E. coli* infection of the human urothelium can be prevented by vaccination with FimH adhesin.[12,13] Furthermore, adherence and invasion of host cells by *E. coli* can also be inhibited by oligomannosides representing the glycosylation of uroplakin **1a**.[14] For some α-D-mannosides it was shown that they prevent type **1** pili mediated adhesion, that is, they do not act by killing or arresting the growth of the pathogen as antibiotics do. Therefore, the spread of strains resistant to such agents are expected to be significantly delayed as compared to that of strains resistant to antibiotics.[15] In addition, environmental contamination is less problematic compared to antibiotics.[15a]

More than two decades ago, various oligomannosides and aromatic α-D-mannosides that antagonize type **1** fimbriae-mediated bacterial adhesion were identified.[15,16] However, for these mannosides only weak interactions in the milli- to micromolar range were observed. To improve their affinity, the multivalent presentation of the α-mannoside epitope,[17] and the rational design of ligands guided by structural information were explored.[9–11] Recently, various reports on high affinity monovalent FimH antagonists were published.[11,18,19]

The CRD of the FimH protein consists of amino acids with hydrophilic side chains and can therefore establish a perfect network of hydrogen bonds with the hydroxyl groups at the 2-, 3-, 4- and 6-positions of D-mannose. The entrance to this mannose-binding pocket, the so-called 'tyrosine gate', is shaped by two tyrosines (Tyr48 and Tyr137), and one isoleucine (Ile52) which support hydrophobic contacts.[20] Generally, long chain alkyl and aryl mannosides (for selected examples see Fig. 1) displayed the highest affinities.[8,9,11,16–21]

Recently, we reported the synthesis, the critical pharmacokinetic properties and affinity data of low molecular weight α-D-mannosides with the ability to block the FimH-mediated bacterial adhesion in a mouse infection model.[19] The orally available, nanomolar FimH antagonist **4b** (Fig. 1) exhibited the potential to reduce the colony forming units (CFU) in the urine and in the bladder by two and four orders of magnitude, respectively, demonstrating the therapeutic potential of this new class of anti-infectives for the effective treatment of urinary tract infections.

However, a potential drawback of FimH antagonists with aglycons consisting of biphenyls directly linked to the carbohydrate moiety is their limited conformational flexibility, which could hamper an optimal fit with the tyrosine gate.[11] To increase the conformational flexibility, the spacers between the mannose moiety and the first aromatic ring of the biphenyl moiety in **i** (Fig. 2) as well as between the aromatic rings was extended. Furthermore, the rotational barrier of the biphenyl[25] was reduced by replacing one of the rings by a triazole (for the torsion profile see Fig. 2). Overall, these modifications should lead to a reduction of the conformational restraints and therefore an optimized spatial arrangement of the aglycone in the tyrosine gate.

Oligomannose-3 is present on the high-mannosylated uroplakin Ia located on urothelial cells and is supposed to interact with UPEC. The crystal structure of the FimH-CRD[10] complexed with oligomannose-3 (PDB code 2VCO, Fig. 3A) clearly shows the important role of the tyrosine gate hosting this physiological ligand in the so-called *in-docking-mode*. Interestingly, for **4a** complexed with FimH-CRD a different binding mode outside of the tyrosine gate was reported (*out-docking-mode*, see Fig. 3B).[11] In analogy to oligomannose-3, docking of triazole derivative **5b** to the crystal structure of the FimH lectin domain (PDB code 3MCY)[11] led – as a result of the increased flexibility of the aglycone – to the *in-docking-mode*. Thus, in contrast to the biphenyl aglycone present in **4a**, the phenyl-triazole **5b** is expected to be hosted by the tyrosine gate. The three-dimensional structure **5b** was generated using Glide 5.5[26] and the kinetic stability of the protein–ligand complex was then assessed with a 2 ns molecular-dynamics simulation using Desmond.[27]

A comparison of the docking modes of oligomannose-3, **4a** and **5b** reveals that the interaction of the mannose moiety is highly conserved for all three compounds. However, in contrast to oligomannose-3 and **5b**, the biphenyl moiety in **4a** is not able to reach the tyrosine gate due to its rigid structure. Instead, a π-π-stacking interaction of the second aromatic ring of the biphenyl aglycone with Tyr48 outside of the tyrosine gate[11] (*out-docking-mode*, Fig. 3B) is achieved by induced fit, that is, a substantial move of Tyr48. In addition, a further stabilization of the protein–ligand complex by a hydrogen bond between the ester in the *meta*-position of **4a** and the side-chain of Arg98 was assumed.[11]

Based on these evidences, a library of derivatives according to the criteria summarized in Figure 2 was designed. Here, we describe synthesis, biological evaluation, and determination of pharmacokinetic parameters of triazole derivatives.

2. Results and discussion

2.1. Synthesis of triazolyl-methyl and -ethyl α-D-mannopyranosides

In a first approach, the phenyl ring adjacent to the anomeric center (see Fig. 2) was replaced by a triazolyl-methyl moiety to increase the conformational flexibility. To avoid solubility problems as well as to take advantage of additional polar interactions, for

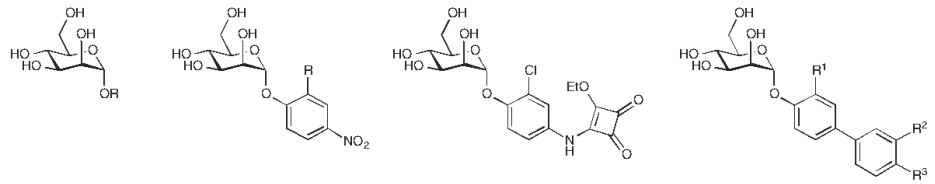

1a (R: Me)
1b (R: *n*-heptyl)[9]
2a (R: H)[18a,b]
2b (R: Cl)[18c]
3[18c]
4a (R^1: H, R^2: CO_2Me, R^3: H)[11]
4b (R^1: Cl, R^2: H, R^3: CO_2Me)[19]
4c (R^1: Cl, R^2: H, R^3: CO_2Na)[19]

Figure 1. Known alkyl (**1**) and aryl (**2**–**4**) α-D-mannosides exhibiting micro- to nanomolar affinities.

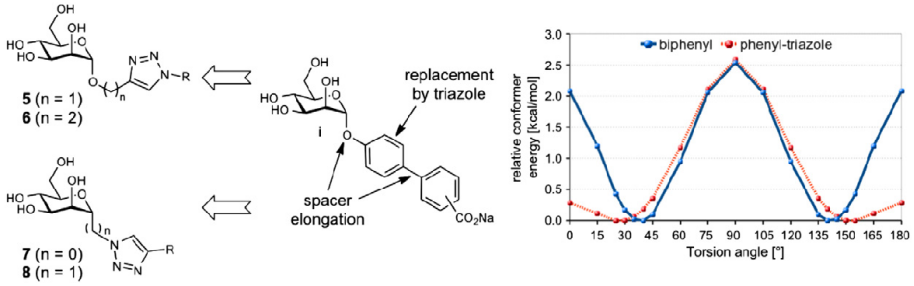

Figure 2. Design of FimH antagonists with aglycons of increased flexibility. Spacer elongations and replacement of one phenyl ring by a triazole should reduce the conformational restraints and lead to an improved fit in the tyrosine gate. The torsion profiles for biphenyl and 1-phenyl-1,2,3-triazole were calculated at the B3LYP level of theory[22,23] with 6-31G(d,p) basis set in the gas phase using Gaussian 03.[24]

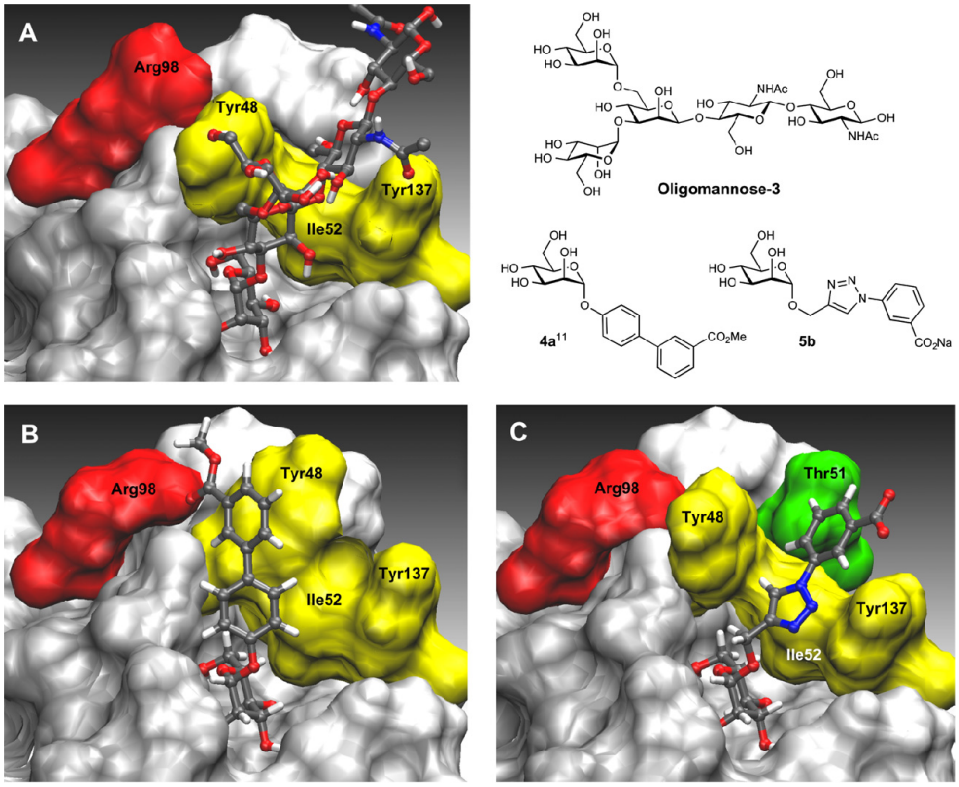

Figure 3. (A) & (B) Crystal structures of oligomannose-3 (A, PDB code 2VCO)[19] and biphenyl **4a** (B, PDB code 3MCY)[11] bound to the FimH-CRD. C) Automated docking of triazole **5b** into the lectin domain of FimH (PDB code 3MCY).[11] The images have been generated using VMD.[28] The ligands are depicted colored by atom (C: dark grey, H: white, O: red, N: blue); the tyrosine gate (residues Tyr48, Tyr137 and Ile52) is shown in yellow, residue Thr51 in green and residue Arg98 in red. While **4a** binds in the *out-docking-mode*, compound **5b**, like oligomannose-3, is inserted into the tyrosine gate (*in-docking-mode*).

example, H-bonds with the hydroxyl-groups of Thr51 or Tyr137 (Fig. 3C), the second aromatic ring was substituted with a carboxylate in *para*- or *meta*-position (→**5a**–**c**, Scheme 1).

For the synthesis of mannosyl triazoles **5a**–**c**, alkyne **10**[29] readily available from peracetylated D-mannose (**9**) was reacted with the known aryl azides **11a**,[30] **11b**,[31] and **11c**[32] in a copper(I)-catalyzed Huisgen 1,3-dipolar cycloaddition[33,34] using *tert*-butanol/water/THF (**1**:**1**:**1**) as solvent.[35] The saponification of the *anti*-substituted triazoles **12a**–**c** yielded the test compounds **5a**–**c** (Table 1).

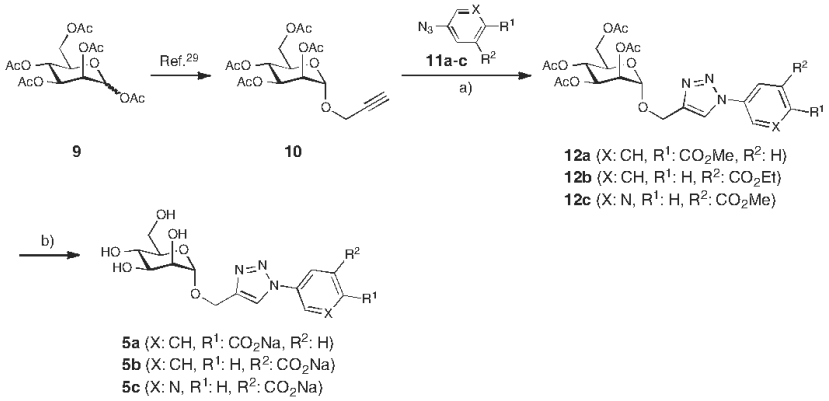

Scheme 1. Reagents and conditions: (a) $CuSO_4{\cdot}5H_2O$, Na-ascorbate, *t*-BuOH/H_2O/THF (1:1:1), rt, 24 h, 73–97%; (b) (i) NaOMe, MeOH, rt, 3 h; (ii) 1 M NaOH, H_2O/dioxane (1:1), 16 h, 78–91%.

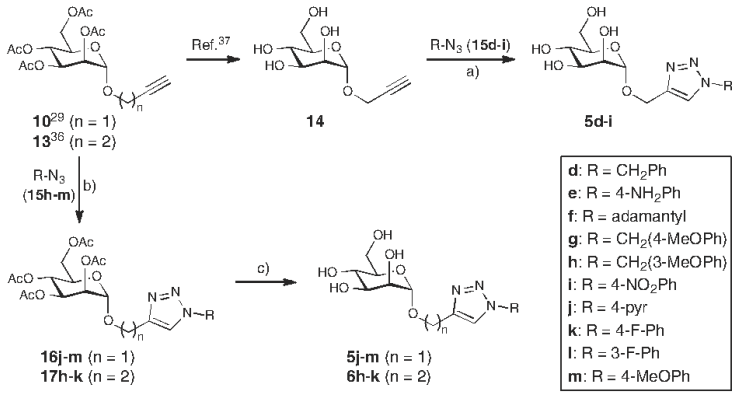

Scheme 2. Reagents and conditions: (a) $CuSO_4{\cdot}5H_2O$, Na-ascorbate, *t*-BuOH/H_2O (1:1), rt, 24 h, (**5d–i**: 27–77%); (b) $CuSO_4{\cdot}5H_2O$, Na-ascorbate, *t*-BuOH/H_2O/THF (1:1:1), rt, 24 h (**16j–m**: 85–94%, **17h–k**: 83–96%); (c) NaOMe, MeOH, rt, 2–6 h, (**5j–m**: 75–85%, **6h–k**: 73–90%).

In a second approach, the terminal aromatic ring was replaced by various substituents like (hetero)aryl, benzyl, and adamantyl groups (→**5d–i** & **5j–m**). Furthermore, in compounds **6h–k** the spacer between the carbohydrate moiety and the triazole ring was elongated from methyl to ethyl allowing for a higher conformational flexibility (Scheme 2).

The mannosyl triazoles **5d–m** and **6h–k** were obtained by reacting the known mannosyl alkynes **10**,[29] **13**[36] and **14**[37] with the azides **15d–m**. Whereas the azides **15d–f** are commercially available, **15g**,[38] **15h**,[39] **15i**,[40] **15j–l**,[41] and **15m**[40] were obtained by known procedures.

The cycloaddition of alkyne **14** and azides **15d–i** under Cu(I)-catalyzed click conditions[33,34] yielded directly the *anti*-substituted triazoles **5d–i** in 27–77% (Table 1). However, due to the cumbersome purification of the unprotected mannosyl triazoles, test compounds **5j–m** were obtained by an alternative sequence starting from the protected alkyne **10** and azides **15j–m** followed by saponification of the intermediates **16j–m**. The analogous cycloaddition of butinyl mannoside **13** with azides **15h–k** yielded the protected triazoles **17h–k** in 83–96%. Final deacetylation under Zemplén conditions gave the test compounds **6h–k**, which contain a linker extended by an additional carbon between mannose and aglycone (Table 1).

2.2. Synthesis of FimH antagonists modified at the anomeric center

To avoid the low metabolic stability of *O*-mannosides like compounds **5** and **6** due to potential cleavage by mannosidases, the corresponding *N*-linked mannosyl triazoles **7** and *C*-mannosides **8** were prepared (Scheme 3). Mannosyl azide **18** was obtained according to published procedures.[42] The Cu(I)-catalyzed click reaction of **18** with the commercially available acetylenes **19n–s** gave exclusively the anomerically pure *anti*-substituted α-D-mannosyl-triazoles **20n–s** in 84–98% yield and after deacetylation the test compounds **7n–s** (Table 1).

Finally, the synthesis of triazolyl-methyl-*C*-mannosides **8n–s** (Scheme 3) started from mannosyl cyanide **21**, which was obtained

Table 1
Pharmacodynamic and pharmacokinetic parameters of mannosylated triazoles **5–8**

Entry	Ligand	R	Competitive binding assay		$logD_{7.4}$	PAMPA $logP_e$ [$log10^{-6}$ cm/s]/%Mm	Solubility [μg/mL]
			IC_{50} [μM]	rIC_{50}			
1	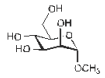	**1a**[45]	1.9	29	n.d.	n.d./n.d.	n.d.
2	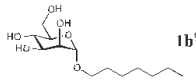	**1b**[9]	0.0656	**1.0**	1.65	-4.89/21.0	> 3000
3		**5a** 	0.207	3.2	n.d.	n.d./n.d.	> 3000
4		**5b** 	0.296	4.5	n.d.	n.d./n.d.	> 3000
5		**5c** 	0.169	2.6	n.d.	n.d./n.d.	> 3000
6		**5d** 	0.667	10.2	-0.33	-8.60/3.0	> 3000
7		**5e** 	0.420	6.4	0.20	-10/4.0	> 2000
8		**5f** 	0.135	2.1	0.07	-7.42/9.8	> 3000
9	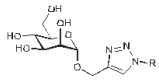	**5g** 	0.511	7.8	-0.40	-8.21/3.1	> 3000
10		**5h** 	0.452	6.9	-0.38	-8.18/4.0	> 3000
11		**5i** 	0.397	6.1	-0.16	-9.40/4.9	2600
12		**5j** 	0.070	1.1	0.24	-8.70/9.2	> 3000
13		**5k** 	0.778	11.9	-0.15	-10/4.6	> 3000
14		**5l** 	0.348	5.3	0.18	-8.80/5.4	> 3000
15		**5m** 	0.161	2.5	-0.05	-8.90/7.9	2600

(*continued on next page*)

Table 1. (*continued*)

Entry	Ligand	R	Competitive binding assay IC_{50} [μM]	rIC_{50}	$logD_{7.4}$	PAMPA $logP_e$ [$log10^{-6}$ cm/s]/%Mm	Solubility [μg/mL]
16		**6h**	0.229	3.5	< -1	-8.70/11.8	> 3000
17		**6i**	0.112	1.7	-0.30	-9.20/2.9	> 3000
18		**6j**	0.153	2.3	< -1.5	-9.10/4.3	> 3000
19		**6k**	0.196	3.0	-0.21	-10/4.0	> 3000
20		**7n**	0.250	3.8	0.21	-8.6/6.4	> 3000
21		**7o**	0.248	3.8	0.91	-8.1/11.5	445
22		**7p**	0.331	5.1	1.22	-7.8/13.2	705
23		**7q**	0.144	2.2	1.45	-7.7/17.2	159
24		**7r**	0.216	3.3	-1.04	-10/10.3	1378
25		**7s**	0.493	7.5	-0.18	-9.0/5.5	> 3000
26		**8n**	0.560	8.5	-0.36	-9.1/7.8	> 3000
27		**8o**	0.565	8.6	0.23	-9.3/6.3	1489
28		**8p**	0.639	9.7	0.68	-9.7/n.p.	> 3000
29		**8q**	0.194	3.0	1.07	-9.3/n.p.	525
30		**8r**	0.333	5.1	< -1.5	-10/n.p.	1877
31		**8s**	0.327	5.0	-0.83	-10/n.p.	n.d.

The IC_{50}s were determined with a cell-free competitive binding assay.[45] Relative IC_{50}s (rIC_{50}) were calculated by dividing the IC_{50} of the substance of interest by the IC_{50} of the reference compound **1b** (entry 2). Passive permeation through an artificial membrane and retention therein was determined by PAMPA (parallel artificial membrane permeation assay).[50] Distribution coefficients ($logD_{7.4}$ values) were measured by a miniaturized shake flask procedure.[51] Thermodynamic solubility was measured by an equilibrium shake flask approach.[52] P_e effective permeation; n.p. not permeable; n.d. not determined.

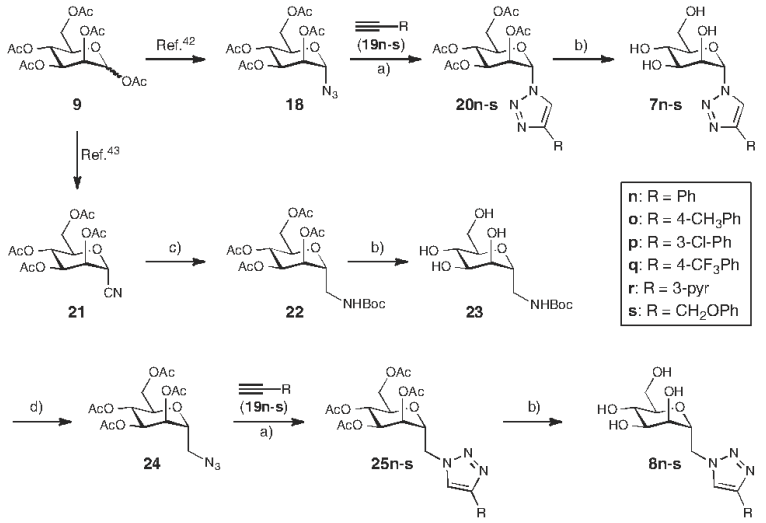

Scheme 3. Reagents and conditions: (a) $CuSO_4{\cdot}5H_2O$, Na-ascorbate, *t*-BuOH/H_2O/THF (1:1:1), rt, 1–2 d (**20n–s**: 84–98%, **25n–s**: 93–98%); (b) NaOMe, MeOH, rt, 3–6 h, (**7n–s**: 65–92%, **8n–s**: 83–87%, **23**: 95%); (c) H_2 (4 bar), cat. Pd/C, Boc_2O, EtOAc, 1 d (72%); d) (i) concd HCl, dioxane/H_2O (2:1), 4 h; (ii) TfN_3, $NaHCO_3$, cat. $CuSO_4{\cdot}5H_2O$, PhMe/H_2O/MeOH, rt, 20 h; (iii) Ac_2O, pyridine, rt, 4 h (81%).

from **9** as reported earlier.[43] Catalytic hydrogenation in the presence of Boc_2O (→**22**) followed by deacetylation led to the Boc-protected amine **23**. Cleavage of the Boc-group, amine-azide exchange[44] and subsequent re-acetylation yielded azide **24** in 81% over three steps. The cycloaddition of **24** and the acetylenes **19n–s** gave the *anti*-substituted triazoles **25n–s** in excellent yields. Final deprotection afforded the test compounds **8n–s** (Table 1).

2.3. Biological evaluation

For an initial biological in vitro characterization, a cell-free competitive binding assay[45] and later on, a cell-based aggregation assay[46] were applied. Whereas for the cell-free competitive binding assay only the CRD of the pili was expressed, the complete pili are present in the cell-based assay format. Furthermore, both formats are competitive assays, that is, the analyzed antagonists compete with mannosides for the binding site. In the cell-free competitive binding assay, the competitors are polymer-bound trimannosides, whereas in the aggregation assay the antagonist competes with more potent oligo- and polysaccharide chains[14] present on the surface of erythrocytes.[47] The interaction is further complicated by the existence of a high- and a low-affinity state of the CRD of FimH. Aprikian et al. experimentally demonstrated that in full-length fimbriae the pilin domain stabilizes the CRD domain in the low-affinity state, whereas the CRD domain alone adopts the high-affinity state.[48] Furthermore, it was recently shown that shear stress can induce a conformational switch (twist in the β-sandwich fold of the CRD domain) resulting in improved affinity.[49] Therefore, different affinities are expected when - as in the cell-based aggregometry assay - full-length fimbriae are present, when compared to the CRD domain alone.

2.4. Cell-free competitive binding assay

The cell-free inhibition assay is based on the interaction of a biotinylated polyacrylamide glycopolymer with the carbohydrate recognition domain (CRD) of FimH as previously reported.[45] A soluble recombinant protein consisting of the FimH-CRD (amino acid residues 1–156), a C-terminal thrombin cleavage site and a 6His-tag (FimH-CRD-Th-6His) was expressed in *E. coli* strain HM125 and purified by affinity chromatography on a Ni-NTA column. For the determination of IC_{50} values, a microtiter plate coated with FimH-CRD-Th-6His was incubated with biotinylated Manα(1-3)-[Manα(1-6)]-Manβ(1-4)-Glc*N*Acβ(1-4)-Glc*N*Acβ-polyacrylamide (TM-PAA) polymer conjugated to streptavidin-horseradish peroxidase and the FimH antagonist in fourfold serial dilution (Fig. 4). The assay was performed in duplicates and repeated twice for each compound. To ensure comparability of different antagonists, the reference compound *n*-heptyl α-D-mannopyranoside (**1b**)[9,46] was tested in parallel on each individual microtiter plate. The affinities are reported relative to **1b** as rIC_{50} in Table 1. The relative IC_{50} (rIC_{50}) is the ratio of the IC_{50} of the test compound to the IC_{50} of **1b** (entry 2).

Interestingly, all antagonists in Table 1 except methyl α-D-mannoside (**1a**) exhibit nanomolar affinities. When compared to **1a**, an up to 30-fold improvement was obtained. In the first series, containing a triazolyl-methyl moiety (**5a–m**, entries 3–15), **5j** (entry 12) exhibits the highest affinity with an IC_{50} of 70 nM. This is in the range of *n*-heptyl α-D-mannoside (**1b**), however, compared to the biphenyl derivative **4b**[19] (Fig. 1), this in fact represents a 18-fold reduction of affinity (rIC_{50} 0.06[19] for **4b** vs. rIC_{50} 1.1 for **5j**). At this point, we should recollect that **4b** and **5j** address different docking modes (*out-* and *in-docking-mode*) and therefore also different structural environments.

Antagonists where the linker between the anomeric center and the triazole is extended by an additional carbon (→**6h–k**, entries 16–19) show affinities in the range of 200 nM and therefore - with the exception of 4-pyridyl derivative **6j** (entry 18) - two- to fourfold higher affinity compared to their counterparts with the shorter linker. When the triazole is directly linked to the anomeric center (→**7n–s**, entries 20–25) affinities are 2- to 8-fold reduced, probably as a consequence of the reduced flexibility preventing an optimal

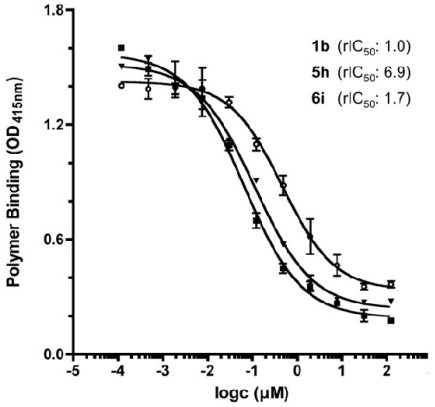

Figure 4. Examples of inhibition curves obtained from the cell-free competitive binding assay.[45] Each assay was run in duplicate and was repeated at least twice. For antagonists **5h**, **6i** and the reference compound **1b** IC_{50} values in the nM range were obtained.

interaction of the aglycone with the tyrosine gate. Finally, the *C*-mannosides **8n**–**s** (entries 26–31), which do not exhibit the exo-anomeric effect of the *O*-mannosides and therefore can more easily adopt the optimal orientation within the tyrosine gate, surprisingly show a twofold reduction in affinity.

2.5. Aggregometry assay

The potential to disaggregate *E. coli* from guinea pig erythrocytes (GPE) was determined for a variety of the mannosylated triazoles in a function-based aggregometry assay.[46] The measurements were performed in triplicates and the corresponding IC_{50} values were calculated by plotting the area under the curve (AUC) of disaggregation against the concentration of the antagonists. *n*-Heptyl α-D-mannopyranoside (**1b**) was again used as reference compound with an IC_{50} of 77.1 µM (Table 2, entry 1). While the antagonists **5e**, **6j**, **6k**, **7o** and **7q** showed IC_{50} values in the range of 200–300 µM, surprisingly no activities could be determined for compounds **5j**, **8q** and **8r** up to a concentration of 700 µM. As earlier observed,[46] the activities obtained from the aggregometry assay are approximately 1000-fold lower than the affinities determined in the target-based competitive assay.

2.6. Conformational analysis of mannosyl triazoles

Compared to their counterparts **7**, where the triazole is directly linked to the anomeric center, most of the *C*-mannosides **8** exhibit a lower affinity. By applying NMR techniques, it was investigated whether this loss of affinity originates from distorted ring conformations. Due to signal overlap, the unprotected mannosides **7** and **8** were not suited for the conformational analysis. However, for the peracetylated derivatives **20n** and **25n** the ring conformation could be assigned based on coupling constants and NOESY experiments. First, the observed ^3J coupling constants for their ring protons were strikingly different. In **20n**, they were in agreement with those expected for a regular $^4C_1$ chair conformation of an α-D-mannopyranosyl ring, with small $J_{1,2}$ and $J_{2,3}$ couplings and large values for $J_{3,4}$ and $J_{4,5}$ (Fig. 5A). In contrast, the large $J_{1,2}$ coupling constant (8.4 Hz) and small to medium values for $J_{2,3}$, $J_{3,4}$ and $J_{4,5}$ found for **25n**, are in agreement with a ring flip of the α-D-mannopyranosyl chair from the common $^4C_1$ to the unusual $^1C_4$ conformation (Fig. 5B). A similar conformational switch has also been observed for α-CF_2-mannosides.[53] As a consequence, the triazolyl-methyl group now is oriented equatorially in *C*-mannoside **25n**, while in **20n** the triazole moiety adopts an axial position.

Subsequent 2D-NOESY measurements (Fig. 5C and D) confirmed this analysis. For both compounds a sequence of seven 2D-NOESY experiments with increasing mixing times from 0.5 s to 2.0 s in steps of 0.25 s was recorded. The intensity of the positive signals grows with increasing mixing time and indicates the relative spatial proximity of a particular proton to that of the source proton. The NOEs of the proton of interest (int_{cross}) were normalized to the intensity of the diagonal peak of the source proton (int_{diag}). Plotting these normalized intensities against the mixing time results in a straight line for each pair of protons. The distances r_{ij} were then calculated from the slopes σ of the linear regression according to $r_{ij} = r_{ref}\,(\sigma_{ref}/\sigma_{ij})^{1/6}$, were r_{ref} is the average distance of the geminal protons H-6a and H-6b, which was chosen as reference (r_{ref} = 1.78 Å).[54,55]

Typically, in the chair conformation of carbohydrates the vicinal proton–proton distances are approx. 2.95 ± 0.15 Å for a diaxial, 2.45 ± 0.15 Å for an axial-equatorial and 2.50 ± 0.20 Å for a diequatorial orientation.[56] As shown in Figure 5A and B, the distances of the ring protons in **20n** and **25n** determined from NOE experiments correlate well with the theoretical values and support the results obtained from the analysis of the coupling constants. In summary, NMR spectroscopic data indicate that the mannopyranosyl chairs in these compounds adopt different conformations, depending on the substituent at C-1.

This conformational analysis offers an explanation for the twofold reduction of affinity found for most of the *C*-mannosides **8** compared to the corresponding *N*-linked triazoles **7**. Due to the inversion of the ring conformation in **8** ($^1C_4$ vs $^4C_1$), the optimal fit into the hydrophilic mannose-binding pocket of FimH is disturbed.

2.7. Pharmacokinetic properties of mannosyl triazoles

Finally, the druglikeness of this new class of FimH antagonists was addressed. For a successful po application in our UTI mouse model,[19] FimH antagonists have to exhibit oral bioavailability, metabolic stability and fast renal elimination to the urinary tract, their place of action. For the evaluation of oral absorption and renal excretion of the triazoles **5–8** physicochemical parameters such as solubility, lipophilicity (distribution coefficients, log $D_{7.4}$) and permeability were determined (Table 1). The mannosides of all four compound families (**5–8**) are all highly soluble (159 µg/mL to > 3 mg/mL) and therefore fulfill a first prerequisite for absorption in the gastrointestinal tract (GIT). All compounds showed low to moderate log $D_{7.4}$ values in the range of < -1.5 to 1.45. While these parameters are beneficial for renal excretion,[57] oral absorption by passive diffusion can only be expected to a minor extent. Indeed, for none of the tested compounds a significant permeation through an artificial membrane (PAMPA,[50] log P_e, P_e: effective permeation) nor membrane retention could be detected. Whereas for a successful oral absorption a log P_e >−5.7 and/or a membrane retention %Mm > 80 % are required,[58] the corresponding values for all triazoles are far from being in this range. Overall, only poor absorption from the GIT can be therefore expected.

3. Conclusions

Crystal structures indicate that the natural ligand oligomannose-3[10] inserts into the tyrosine gate formed by Tyr48, Tyr137 and Ile52 of the carbohydrate recognition domain of FimH (*in-docking-mode*). In contrast, the recently reported high-affinity

Table 2
IC_{50} values of mannosylated triazoles determined in the aggregometry assay[46]

Entry	Ligand		R	Aggregometry assay	
				IC_{50} [μM]	rIC_{50}
1	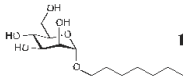	**1b**[9]		77.1	1.0
2	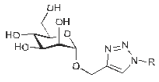	**5e**		299	3.9
3		**5j**		n.a.	-
5	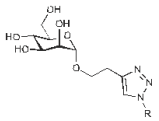	**6j**		277	3.6
6		**6k**		216	2.8
8	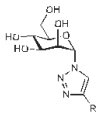	**7o**		289	3.7
9		**7q**		249	3.2
10	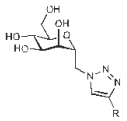	**8q**		n.a.	-
11		**8r**		n.a.	-

The relative IC_{50} (rIC_{50}) was calculated by dividing the IC_{50} of the substance of interest by the IC_{50} of the reference compound **1b**. n.a., not active.

biphenyl mannoside **4c** was shown to bind in the *out-docking-mode*, that is, it establishes a π-π-stacking interaction with Tyr48 from the outside of the tyrosine gate.[11] Based on docking studies, we designed a series of low molecular weight mannosyl triazoles, which exhibit an increased conformational flexibility of the aglycone and therefore should allow for binding to the tyrosine gate in the *in-docking-mode*. For their pharmacodynamical evaluation two assay formats, a target-based binding assay[45] and a function-based aggregation assay,[46] were applied. In general, all triazoles **5–8** showed nanomolar affinities, but only one representative, the 4-pyridyl derivative **5j**, was as potent as the reference compound *n*-heptyl mannoside (**1b**). Obviously, the high flexibility of the *n*-heptyl aglycone in **1b** optimally fulfills the spatial requirements of the tyrosine gate. In addition, the hydrophobic contacts established by the substituted triazole aglycone within the tyrosine gate in the *in-docking-mode* are less favorable than the π-π-stacking interaction of biphenyl derivatives[11,19] with Tyr48 in the *out-docking-mode*.

Furthermore, the reduced affinities of the triazolyl-methyl-*C*-mannosides **8** can be rationalized by a disturbed interaction of the mannose moiety. A conformational analysis by ^{1}H NMR and NOESY NMR revealed that in contrast to the other three classes of mannosyl triazoles (compounds **5**, **6** and **7**), the *C*-mannosides **8** do not adopt the common $^4C_1$ but an unusual $^1C_4$ chair conformation, thus preventing an optimal fit of the mannosyl moiety into the hydrophilic mannose-binding pocket of FimH.

Finally, for a successful therapeutic application, FimH antagonists have to exhibit appropriate pharmacokinetic properties, that is, oral bioavailability and fast renal elimination to the urinary tract, their place of action. One prerequisite for absorption in the GIT is sufficient solubility, a property, which is fulfilled by all synthesized antagonists. However, according to their lipophilicity and membrane permeation properties, the mannosyl triazoles are not expected to be orally absorbed. Possible improvements of the pharmacokinetic profiles of mannosyl triazoles are currently studied.

4. Experimental part

4.1. Chemistry

General. NMR spectra were recorded on a Bruker Avance DMX-500 (500 MHz) spectrometer. Assignment of ^{1}H and ^{13}C NMR spectra was achieved using 2D methods (COSY, HSQC). Chemical shifts are expressed in ppm using residual $CHCl_3$ and CD_2HOD as references. Optical rotations were measured using a Perkin-Elmer Polarimeter 341. Electron spray ionization mass

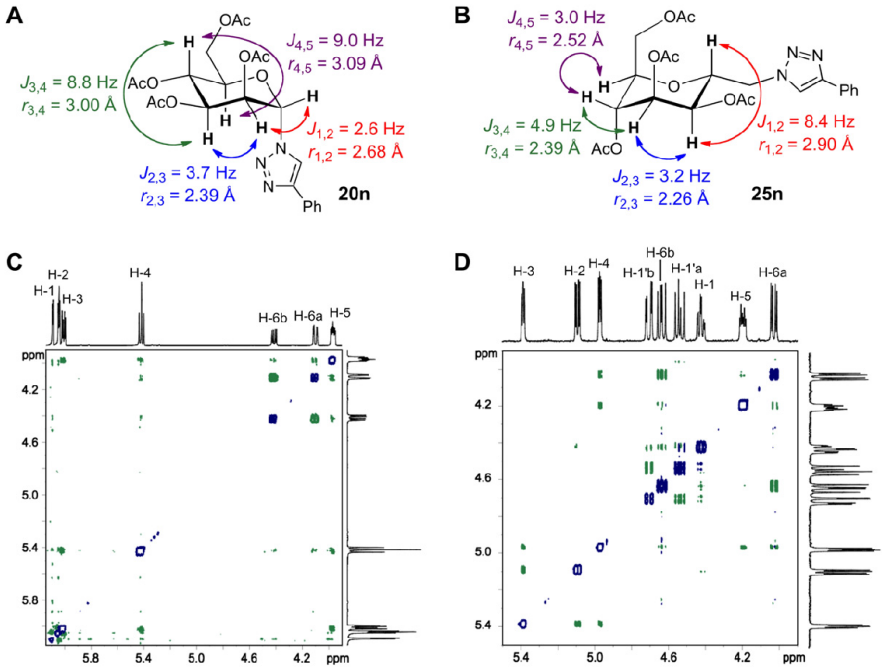

Figure 5. Coupling constants and proton-proton distances for peracetylated triazoles **20n** (A) and **25n** (B) determined by ^{1}H NMR and 2D-NOESY experiments; 2D-NOESY spectra of **20n** (C) and **25n** (D) in $CDCl_3$ with mixing times of 1.5 s (C) and 750 ms (D).

spectra (ESI-MS) were obtained on a Waters micromass ZQ. The HRMS analyses were carried out using a Bruker QTOF. Reactions were monitored by TLC using glass plates coated with silica gel 60 F_{254} (Merck) and visualized by using UV light and/or by charring with a molybdate solution (a 0.02 M solution of ammonium cerium sulfate dihydrate and ammonium molybdate tetrahydrate in aqueous 10% H_2SO_4). MPLC separations were carried out on a Combi-Flash Companion from Teledyne Isco equipped with RediSep normal-phase or C_{18} reversed-phase flash columns. Tetrahydrofurane (THF) was freshly distilled under argon over sodium and benzophenone. Methanol (MeOH) was dried by refluxing with sodium methoxide and distilled immediately before use. Dichloromethane (DCM), ethyl acetate (EtOAc), and toluene were dried by filtration over Al_2O_3 (Fluka, type 5016 A basic).

4.1.1. General procedure A for the synthesis of mannosyl triazoles 5d–i

A mixture of acetylene **14**[37] (1.0 eq), azide **15d–i** (1.5 eq), $CuSO_4{\cdot}5H_2O$ (0.25 eq) and sodium ascorbate (0.5 eq) was dissolved in degassed *tert*-BuOH/H_2O (1:1, 2 mL/0.1 mmol **14**) under argon. After stirring for 1 d the solvents were removed in vacuo and the crude product was first purified by MPLC on silica (DCM/MeOH) and then by reversed-phase chromatography (RP-18, H_2O/MeOH) to yield **5d–i** as colorless solids.

4.1.2. General procedure B for the synthesis of mannosyl triazoles 12a–c, 16j–m and 17h–k

Acetylene **10**[29] or **13**[36] (1.0 eq) and azide **11a–c** or **15h–m** (1.5–2 eq) were dissolved in THF/*tert*-BuOH/H_2O (1:1:1, 1.5 mL/0.1 mmol **10** or **11**). The mixture was degassed in an ultrasound bath under a flow of argon for 20 min. Then 0.5 M aq $CuSO_4{\cdot}5H_2O$ (0.25 eq) and 1 M aq sodium ascorbate (0.5 eq) were added under argon at rt. After stirring overnight the solvents were removed in vacuo and the crude product was purified by MPLC on silica (petrol ether/EtOAc) to yield **12a–c**, **16j–m** and **17h–k** as colorless oils.

4.1.3. General procedure C for the synthesis of mannosyl triazoles 20n–s and 25n–s

Azide **18**[42] or **24** (1.0 eq) and acetylene **19n–s** (2.0 eq) were dissolved in THF/*tert*-BuOH/H_2O (1:1:1, 3 mL/0.1 mmol **18** or **24**). The mixture was degassed in an ultrasound bath under a flow of argon for 20 min. Then 0.2 M aq $CuSO_4{\cdot}5H_2O$ (0.2 eq) and 1 M aq sodium ascorbate (0.4 eq) were added under argon at rt. After stirring for 1–2 d the solvents were removed in vacuo and the crude product was purified by MPLC on silica (petrol ether/EtOAc) to yield **20n–s** and **25n–s** as colorless oils.

4.1.4. General procedure D for deacetylation

To a solution of the acetylated compound (38–50 mg) in MeOH (3 mL) was added 1 M NaOMe/MeOH (0.3 mL). The mixture was stirred at rt for 3–6 h. The solution was concentrated and the residue was purified by MPLC on reversed phase (RP-18 column, H_2O/MeOH) and P2 size-exclusion chromatography to afford the target molecule as a colorless solid after a final lyophilization from water/dioxane.

4.1.5. Synthesis of azide 24

4.1.5.1. (2,3,4,6-Tetra-*O*-acetyl-α-D-mannopyranosyl)-*N*-*tert*-butoxycarbonyl-methylamine (22). Cyanide **21**[43] (1.63 g, 4.57 mmol), Boc_2O (1.49 g, 6.86 mmol) and Pd/C (10%, 250 mg) were suspended in EtOAc (25 mL) and hydrogenated (4 bar H_2) at rt for 4 h. After filtration over Celite, fresh Pd/C (10%, 750 mg)

was added and the mixture was hydrogenated (4 bar H_2) for additional 17 h. The suspension was filtered over Celite and concentrated. The residue was purified by MPLC on silica (petrol ether/EtOAc) to give **22** (1.51 g, 72%) as a colorless solid.

^{1}H NMR (500 MHz, $CDCl_3$): δ 1.44 (s, 9H, $C(CH_3)_3$), 2.07, 2.10, 2.10 (3 s, 12H, 4 $COCH_3$), 3.38 (m, 2H, H-1′), 3.99–4.05 (m, 2H, H-1, H-5), 4.07 (dd, J = 3.8, 11.8 Hz, 1H, H-6a), 4.54 (dd, J = 6.9, 11.7 Hz, 1H, H-6b), 4.79 (m, 1H, NH), 5.07 (dd, J = 5.3, 6.4 Hz, 1H, H-4), 5.10 (dd, J = 3.3, 6.0 Hz, 1H, H-2), 5.26 (dd, J = 3.3, 6.5 Hz, 1H, H-3); ^{13}C NMR (125 MHz, $CDCl_3$): δ 20.70, 20.73, 20.76, 20.81 (4 $COCH_3$), 28.3 ($C(CH_3)_3$), 39.7 (C-1′), 61.2 (C-6), 67.50, 67.51 (C-2, C-4), 68.0 (C-3), 71.1 (C-1), 72.2 (C-5), 79.7 ($C(CH_3)_3$), 155.8 (NCO), 169.5, 169.6, 169.9, 170.7 (4 $COCH_3$); ESI-MS Calcd for $C_{20}H_{31}NNaO_{11}$ $[M+Na]^+$: 484.18, Found: 484.11.

4.1.5.2. *N-tert*-Butoxycarbonyl-(α-D-mannopyranosyl)methylamine (23). A solution of **22** (1.47 g, 3.19 mmol) in MeOH (20 mL) was treated with 1 M methanolic NaOMe (2 mL) under argon at rt for 3 h. The reaction mixture was neutralized with acetic acid and concentrated. The residue was purified by MPLC on silica (DCM/MeOH) to give **23** (925 mg, 99%) as a colorless solid.

^{1}H NMR (500 MHz, CD_3OD): δ 1.44 (s, 9H, $C(CH_3)_3$), 3.32 (m, 2H, H-1′), 3.54 (m, 1H, H-5), 3.63 (t, J = 7.6 Hz, 1H, H-4), 3.68 (dd, J = 3.1, 7.8 Hz, 1H, H-3), 3.74 (dd, J = 2.8, 11.8 Hz, 1H, H-6a), 3.77 (m, 1H, H-2), 3.79 (dd, J = 6.4, 11.8 Hz, 1H, H-6b), 3.86 (m, 1H, H-1), 6.72 (m, 1H, NH); ^{13}C NMR (125 MHz, CD_3OD): δ 28.8 ($C(CH_3)_3$), 40.6 (C-1′), 62.7 (C-6), 69.6 (C-4), 70.2 (C-2), 72.7 (C-3), 76.9 (C-1), 77.4 (C-5), 80.2 ($C(CH_3)_3$), 158.6 (NCO); ESI-MS Calcd for $C_{12}H_{23}NNaO_7$ $[M+Na]^+$: 316.14, Found: 316.03.

4.1.5.3. (2,3,4,6-Tetra-*O*-acetyl-α-D-mannopyranosyl)methylazide (24). *Triflyl azide stock solution preparation*:[44] Sodium azide (796 mg, 12.2 mmol) was dissolved in water (2 mL). Toluene (2 mL) was added, and the mixture was cooled to 0 °C with stirring. Then triflic anhydride (1.31 mL, 6.12 mmol) was added dropwise. The biphasic reaction mixture was stirred vigorously at 0 °C for 30 min and at 10 °C for another 2 h. The reaction mixture was neutralized with satd aq $NaHCO_3$. The phases were separated, and the aqueous phase extracted with toluene (2 × 2 mL). The organic layers were combined to give the triflyl azide stock solution. *Amine-azide exchange*: A solution of **23** (430 mg, 1.47 mmol) in dioxane/water (2:1, 15 mL) was treated with concentrated HCl (5 mL) under argon at rt for 4 h. The mixture was concentrated and the residue was dried in high vacuo. Then, the crude amine hydrochloride (341 mg), $NaHCO_3$ (492 mg, 5.86 mmol) and $CuSO_4{\cdot}5H_2O$ (14.1 mg, 61 μmol) were dissolved in water (1.91 mL). The triflyl azide stock solution (3.25 mL, 3.3 mmol) was added and the biphasic reaction mixture was made homogenous by the addition of MeOH (12.6 mL). The mixture was stirred at rt for 20 h. The solvents were removed in vacuo and the residue was taken up in dry pyridine (10 mL), and acetic anhydride (4 mL) was added. The reaction mixture was stirred at rt under argon for 4 h. The solvents were removed in vacuo and the crude product was purified by MPLC on silica (petrol ether/EtOAc) to yield **24** (459 mg, 81%) as a colorless oil.

IR (film) 2102 (vs, N_3), 1747 (vs, CO) cm^{-1}; ^{1}H NMR (500 MHz, $CDCl_3$): δ 2.04, 2.07, 2.08, 2.10 (4 s, 12H, 4 $COCH_3$), 3.29 (dd, J = 3.3, 13.4 Hz, 1H, H-1′a), 3.49 (dd, J = 7.3, 13.4 Hz, 1H, H-1′b), 4.05–4.09 (m, 2H, H-5, H-6a), 4.15 (dt, J = 3.2, 7.1 Hz, 1H, H-1), 4.60 (m, 1H, H-6b), 5.01 (dd, J = 4.4, 6.0 Hz, 1H, H-4), 5.14 (dd, J = 3.4, 6.9 Hz, 1H, H-2), 5.27 (dd, J = 3.4, 6.0 Hz, 1H, H-3); ^{13}C NMR (125 MHz, $CDCl_3$): δ 20.61, 20.63, 20.65, 20.74 (4 $COCH_3$), 50.1 (C-1′), 60.8 (C-6), 67.0 (C-2), 67.5 (C-3), 67.6 (C-4), 70.5 (C-1), 72.9 (C-5), 169.3, 169.5, 169.6, 170.6 (4 $COCH_3$); ESI-MS Calcd for $C_{15}H_{21}N_3NaO_9$ $[M+Na]^+$: 410.12, Found: 410.04.

4.1.6. Synthesis of peracetylated mannosyl triazoles

4.1.6.1. Methyl 4-[4-((2,3,4,6-tetra-*O*-acetyl-α-D-mannopyranosyloxy)methyl)-1*H*-1,2,3-triazol-1-yl]-benzoate (12a). Following general procedure B, **10** (40.0 mg, 0.103 mmol) was reacted with methyl 4-azidobenzoate (**11a**,[30] 36.5 mg, 0.206 mmol), 0.5 M $CuSO_4$ (52 μL, 26 μmol) and 1 M sodium ascorbate (52 μL, 52 μmol) to yield **12a** (55.8 mg, 96%).

$[\alpha]_D$ +45.0 (c 1.03, $CHCl_3$); IR (film) 1747 (vs, CO) cm^{-1}; ^{1}H NMR (500 MHz, $CDCl_3$): δ 1.99, 2.04, 2.12, 2.16 (4 s, 12H, 4 $COCH_3$), 3.97 (s, 3H, OMe), 4.10 (ddd, J = 2.2, 5.1, 9.5 Hz, 1H, H-5), 4.14 (dd, J = 2.3, 12.2 Hz, 1H, H-6a), 4.32 (dd, J = 5.2, 12.2 Hz, 1H, H-6b), 4.79, 4.95 (A, B of AB, J = 12.6 Hz, 2H, H-1′), 5.01 (d, J = 1.1 Hz, 1H, H-1), 5.28 (dd, J = 1.7, 3.1 Hz, 1H, H-2), 5.32 (t, J = 9.8 Hz, 1H, H-4), 5.36 (dd, J = 3.2, 10.0 Hz, 1H, H-3), 7.88 (AA′ of AA′BB′, J = 8.7 Hz, 2H, C_6H_4), 8.11 (s, 1H, C_2N_3H), 8.23 (BB′ of AA′BB′, J = 8.7 Hz, 2H, C_6H_4); ^{13}C NMR (125 MHz, $CDCl_3$): δ 20.7, 20.8, 20.9 (4C, 4 $COCH_3$), 52.5 (OMe), 61.0 (C-1′), 62.4 (C-6), 66.0 (C-4), 68.8, 69.0, 69.4 (C-2, C-3, C-5), 97.0 (C-1), 120.0 (2C, C_6H_4), 121.0 (C_2N_3H–C5), 130.4 (C_6H_4–C1), 131.4 (2C, C_6H_4), 139.9 (C_6H_4–C4), 144.7 (C_2N_3H–C4), 169.7, 170.0, 170.1, 170.7 (5C, 5 CO); ESI-MS Calcd for $C_{25}H_{29}N_3NaO_{12}$ $[M+Na]^+$: 586.02, Found: 586.16.

4.1.6.2. Ethyl 3-[4-((2,3,4,6-tetra-*O*-acetyl-α-D-mannopyranosyloxy)methyl)-1*H*-1,2,3-triazol-1-yl]-benzoate (12b). Following general procedure B, **10** (50.0 mg, 0.129 mmol) was reacted with ethyl 3-azidobenzoate (**11b**,[31] 49.3 mg, 0.258 mmol), 0.5 M $CuSO_4$ (64 μL, 32 μmol) and 1 M sodium ascorbate (64 μL, 64 μmol) to yield **12b** (72.7 mg, 97%).

$[\alpha]_D$ +40.2 (c 1.04, $CHCl_3$); IR (film) 1749 (vs, CO) cm^{-1}; ^{1}H NMR (500 MHz, $CDCl_3$): δ 1.43 (t, J = 7.2 Hz, 1H, CH_3), 1.99, 2.04, 2.12, 2.16 (4 s, 12H, 4 $COCH_3$), 4.09–4.15 (m, 2H, H-5, H-6a), 4.32 (dd, J = 5.0, 12.1 Hz, 1H, H-6b), 4.44 (q, J = 7.2 Hz, 2H, OCH_2), 4.79, 4.95 (A, B of AB, J = 12.4 Hz, 2H, H-1′), 5.02 (d, J = 1.4 Hz, 1H, H-1), 5.28 (dd, J = 1.7, 3.2 Hz, 1H, H-2), 5.31 (m, 1H, H-4), 5.36 (dd, J = 3.3, 9.9 Hz, 1H, H-3), 7.64 (t, J = 8.0 Hz, 1H, C_6H_4–H5), 8.02 (ddd, J = 0.9, 2.1, 8.0 Hz, 1H, C_6H_4–H4), 8.11 (s, 1H, C_2N_3H), 8.14 (d, J = 7.9 Hz, 1H, C_6H_4-H6), 8.38 (t, J = 1.7 Hz, 1H, C_6H_4-H2); ^{13}C NMR (125 MHz, $CDCl_3$): δ 14.3 (CH_3), 20.67, 20.69, 20.78, 20.88 (4 $COCH_3$), 60.9 (C-1′), 61.7 (OCH_2), 62.4 (C-6), 66.0 (C-4), 68.8 (C-3), 69.0 (C-5), 69.4 (C-2), 96.9 (C-1), 121.2 (C_6H_4), 121.3 (C_2N_3H–C5), 124.8, 129.9, 130.0, 132.3, 137.0 (C_6H_4), 144.5 (C_2N_3H–C4), 165.2, 169.7, 169.9, 170.1, 170.7 (5 CO); ESI-MS Calcd for $C_{26}H_{32}N_3O_{12}$ $[M+H]^+$: 578.20, Found: 578.19.

4.1.6.3. Methyl 5-[4-((2,3,4,6-tetra-*O*-acetyl-α-D-mannopyranosyloxy)methyl)-1*H*-1,2,3-triazol-1-yl]-nicotinate (12c). Following general procedure B, **10** (40.0 mg, 0.103 mmol) was reacted with methyl 5-azidonicotinate (**11c**,[32] 32.5 mg, 0.182 mmol), 0.5 M $CuSO_4$ (52 μL, 26 μmol) and 1 M sodium ascorbate (52 μL, 52 μmol). The crude product was dissolved in DCM (10 mL) and washed with 0.1 M aq EDTA (5 mL). The aqueous phase was extracted with DCM (2 × 10 mL) and the combined organic layers were dried with Na_2SO_4 and evaporated to dryness. The residue was purified by MPLC on silica (petrol ether/EtOAc) to give **12c** (42.4 mg, 73%).

$[\alpha]_D$ +39.7 (c 1.06, $CHCl_3$); IR (film) 1733 (vs, CO) cm^{-1}; ^{1}H NMR (500 MHz, $CDCl_3$): δ 1.98, 2.03, 2.11, 2.15 (4 s, 12H, 4 $COCH_3$), 4.01 (s, 3H, OCH_3), 4.09 (m, 1H, H-5), 4.14 (dd, J = 2.4, 12.2 Hz, 1H, H-6a), 4.31 (dd, J = 5.2, 12.3 Hz, 1H, H-6b), 4.79, 4.96 (A, B of AB, J = 12.5 Hz, 2H, H-1′), 5.01 (d, J = 1.4 Hz, 1H, H-1), 5.27 (dd, J = 1.7, 3.0 Hz, 1H, H-2), 5.30 (t, J = 9.8 Hz, 1H, H-4), 5.34 (dd, J = 3.3, 9.9 Hz, 1H, H-3), 8.17 (s, 1H, C_2N_3H), 8.69 (t, J = 2.0 Hz, 1H, C_5H_3N-H2), 9.27, 9.30 (2 s, 2H, C_5H_3N-H4, H6); ^{13}C NMR (125 MHz, $CDCl_3$): δ 20.63, 20.65, 20.75, 20.84 (4 $COCH_3$), 52.9 (OMe), 60.8 (C-1′), 62.4 (C-6), 66.0 (C-4), 68.8, 68.9 (C-3, C-5), 69.3 (C-2), 97.0 (C-1), 121.2 (C_2N_3H–C5), 126.9, 128.6, 133.3

(C_5H_3N), 145.1 (2C, C_5H_3N, (C_2N_3H–C4), 150.7 (C_5H_3N), 164.4, 169.7, 169.9, 170.1, 170.7 (5 CO); ESI-MS Calcd for $C_{24}H_{29}N_4O_{12}$ $[M+H]^+$: 565.18, Found: 565.15.

4.1.6.4. [1-(Pyridin-4-yl)-1,2,3-triazol-4-yl]methyl 2,3,4,6-tetra-*O*-acetyl-α-D-mannopyranoside (16j). Following general procedure B, **10** (100 mg, 0.26 mmol) was reacted with 4-azidopyridine (**15j**,[41] 47 mg, 0.39 mmol), 0.5 M $CuSO_4$ (130 μL, 65 μmol) and 1 M sodium ascorbate (130 μL, 130 μmol). The crude product was dissolved in DCM (20 mL) and washed with 0.1 M aq EDTA (10 mL). The aqueous phase was extracted with DCM (2 × 20 mL) and the combined organic layers were dried with Na_2SO_4 and evaporated to dryness. The residue was purified by MPLC on silica (DCM/MeOH) to give **16j** (114 mg, 87%).

$[\alpha]_D$ +52.1 (*c* 2.26, DCM); IR (film) 1748 (vs, CO) cm^{-1}; ^1H NMR (500 MHz, $CDCl_3$): δ 1.92, 1.97, 2.05, 2.09 (4s, 12H, 4 $COCH_3$), 3.96–4.14 (m, 2H, H-5, H-6a), 4.24 (dd, *J* = 4.8, 12.1 Hz, 1H, H-6b), 4.73, 4.89 (A, B of AB, *J* = 12.5 Hz, 2H, H-1′), 4.94 (s, 1H, H-1), 5.14–5.33 (m, 3H, H-2, H-3, H-4), 7.70 (m, 2H, C_5H_4N), 8.15 (s, 1H, C_2N_3H), 8.73 (m, 2H, C_5H_4N); ^{13}C NMR (125 MHz, $CDCl_3$): δ 20.77, 20.78, 20.88, 20.96 (4 $COCH_3$), 61.0 (C-1′), 62.5 (C-6), 66.1, 68.9, 69.0, 69.5 (C-2, C-3, C-4, C-5), 97.1 (C-1), 113.9 (2C, C_5H_4N), 120.7 (C_2N_3H–C5), 143.0 (C_5H_4N–C1), 145.2 (C_2N_3H–C4), 151.9 (2C, C_5H_4N), 169.8, 170.1, 170.2, 170.8 (4 $COCH_3$); ESI-MS Calcd for $C_{22}H_{26}N_4NaO_{10}$ $[M+Na]^+$: 529.16, Found: 529.07.

4.1.6.5. [1-(4′-Fluorophenyl)-1,2,3-triazol-4-yl]methyl 2,3,4,6-tetra-*O*-acetyl-α-D-mannopyranoside (16k). Following general procedure B, **10** (100 mg, 0.26 mmol) was reacted with 1-azido-4-fluorobenzene (**15k**,[41] 53 mg, 0.39 mmol), 0.5 M $CuSO_4$ (130 μL, 65 μmol) and 1 M sodium ascorbate (130 μL, 130 μmol) to yield **16k** (127 mg, 94%).

$[\alpha]_D$ +42.0 (*c* 1.00, DCM); IR (film) 1749 (vs, CO) cm^{-1}; ^1H NMR (500 MHz, $CDCl_3$): δ 1.96, 2.01, 2.09, 2.13 (4s, 12H, 4 $COCH_3$), 4.07 (m, 1H, H-5), 4.11 (dd, *J* = 2.4, 12.2 Hz, 1H, H-6a), 4.28 (dd, *J* = 5.2, 12.2 Hz, 1H, H-6b), 4.75, 4.91 (A, B of AB, *J* = 12.4 Hz, 2H, H-1′), 4.98 (d, *J* = 1.6 Hz, 1H, H-1), 5.24–5.31 (m, 2H, H-2, H-4), 5.33 (dd, *J* = 3.3, 10.0 Hz, 1H, H-3), 7.21 (m, 2H, C_6H_4), 7.71 (m, 2H, C_6H_4), 7.97 (s, 1H, C_2N_3H); ^{13}C NMR (125 MHz, $CDCl_3$): δ 20.87, 20.88, 20.98, 21.07 (4 $COCH_3$), 61.3 (C-1′), 62.6 (C-6), 66.3, 69.0, 69.2, 69.7 (C-2, C-3, C-4, C-5), 97.2 (C-1), 117.0 (d, *J* = 22.5 Hz, 2C, C_6H_4), 121.6 (C_2N_3H–C5), 122.9 (d, *J* = 8.8 Hz, 2C, C_6H_4), 133.4 (d, *J* = 3.8 Hz, C_6H_4–C1), 145.0 (C_2N_3H–C4), 163.8 (d, *J* = 247.5 Hz, C_6H_4–C4), 169.9, 170.2, 170.3, 170.9 (4 $COCH_3$); ESI-MS Calcd for $C_{23}H_{26}FN_3NaO_{10}$ $[M+Na]^+$: 546.16, Found: 546.15.

4.1.6.6. [1-(3′-Fluorophenyl)-1,2,3-triazol-4-yl]methyl 2,3,4,6-tetra-*O*-acetyl-α-D-mannopyranoside (16l). Following general procedure B, **10** (100 mg, 0.26 mmol) was reacted with 1-azido-3-fluorobenzene (**15l**,[41] 53 mg, 0.39 mmol), 0.5 M $CuSO_4$ (130 μL, 65 μmol) and 1 M sodium ascorbate (130 μL, 130 μmol) to yield **16l** (115 mg, 85%).

$[\alpha]_D$ +47.5 (*c* 2.14, DCM); IR (film) 1748 (vs, CO) cm^{-1}; ^1H NMR (500 MHz, $CDCl_3$): δ 1.96, 2.01, 2.09, 2.13 (4s, 12H, 4 $COCH_3$), 4.02–4.15 (m, 2H, H-5, H-6a), 4.29 (dd, *J* = 5.1, 12.2 Hz, 1H, H-6b), 4.75, 4.91 (A, B of AB, *J* = 12.5 Hz, 2H, H-1′), 4.98 (s, 1H, H-1), 5.22–5.36 (m, 3H, H-2, H-3, H-4), 7.14 (m, 1H, C_6H_4), 7.44–7.59 (m, 3H, C_6H_4), 8.02 (s, 1H, C_2N_3H); ^{13}C NMR (125 MHz, $CDCl_3$): δ 20.86, 20.88, 20.97, 21.07 (4 $COCH_3$), 61.2 (C-1′), 62.6 (C-6), 66.2, 69.0, 69.2, 69.6 (C-2, C-3, C-4, C-5), 97.2 (C-1), 108.6 (d, *J* = 26.3 Hz, C_6H_4), 116.0 (d, *J* = 17.5 Hz, C_6H_4), 116.1 (m, C_6H_4), 121.3 (C_2N_3H–C5), 131.5 (d, *J* = 8.8 Hz, C_6H_4), 138.2 (d, *J* = 10.0 Hz, C_6H_4–C1), 144.7 (C_2N_3H–C4), 163.3 (d, *J* = 247.5 Hz, C_6H_4–C4), 169.9, 170.1, 170.3, 170.9 (4 $COCH_3$); ESI-MS Calcd for $C_{23}H_{26}FN_3NaO_{10}$ $[M+Na]^+$: 546.16, Found: 546.15.

4.1.6.7. [1-(4′-Methoxyphenyl)-1,2,3-triazol-4-yl]methyl 2,3,4,6-tetra-*O*-acetyl-α-D-mannopyranoside (16m). Following general procedure B, **10** (100 mg, 0.26 mmol) was reacted with 1-azido-4-methoxybenzene (**15m**,[40] 58 mg, 0.39 mmol), 0.5 M $CuSO_4$ (130 μL, 65 μmol) and 1 M sodium ascorbate (130 μL, 130 μmol) to yield **16m** (128 mg, 92%).

$[\alpha]_D$ +45.0 (*c* 2.26, DCM); IR (film) 1749 (vs, CO) cm^{-1}; ^1H NMR (500 MHz, $CDCl_3$): δ 1.93, 1.98, 2.06, 2.10 (4s, 12H, 4 $COCH_3$), 3.81 (s, 3H, OCH_3), 3.99–4.12 (m, 2H, H-5, H-6a), 4.26 (dd, *J* = 5.3, 12.4 Hz, 1H, H-6b), 4.71, 4.87 (A, B of AB, *J* = 12.4 Hz, 2H, H-1′), 4.95 (d, *J* = 1.4 Hz, 1H, H-1), 5.20–5.28 (m, 2H, H-2, H-4), 5.30 (dd, *J* = 3.2, 10.0 Hz, 1H, H-3), 6.97 (m, 2H, C_6H_4), 7.58 (m, 2H, C_6H_4), 7.91 (s, 1H, C_2N_3H); ^{13}C NMR (125 MHz, $CDCl_3$): δ 20.78, 20.80, 20.89, 20.98 (4 $COCH_3$), 55.7 (OCH_3), 61.2 (C-1′), 62.5 (C-6), 66.1, 68.9, 69.1, 69.5 (C-2, C-3, C-4, C-5), 97.0 (C-1), 114.9 (2C, C_6H_4), 121.5 (C_2N_3H–C5), 122.4 (2C, C_6H_4), 130.4 (C_6H_4–C1), 144.1 (C_2N_3H–C4), 160.0 (C_6H_4–C4), 169.8, 170.0, 170.2, 170.8 (4 $COCH_3$); ESI-MS Calcd for $C_{24}H_{29}N_3NaO_{11}$ $[M+Na]^+$: 558.18, Found: 558.18.

4.1.6.8. [1-(3′-Methoxybenzyl)-1,2,3-triazol-4-yl]ethyl 2,3,4,6-tetra-*O*-acetyl-α-D-mannopyranoside (17h). Following general procedure B, **13** (55 mg, 0.14 mmol) was reacted with 3-methoxybenzylazide (**15h**,[39] 34 mg, 0.21 mmol), 0.5 M $CuSO_4$ (70 μL, 35 μmol) and 1 M sodium ascorbate (70 μL, 70 μmol) to yield **17h** (65 mg, 83%).

$[\alpha]_D$ +36.5 (*c* 1.00, DCM); IR (film) 1748 (vs, CO) cm^{-1}; ^1H NMR (500 MHz, $CDCl_3$): δ 1.85, 1.88, 1.93, 1.99 (4s, 12H, 4 $COCH_3$), 2.86 (tt, *J* = 4.8, 9.9 Hz, 2H, H-2′), 3.56 (dt, *J* = 6.6, 9.5 Hz, 1H, H-1′a), 3.63 (s, 3H, OCH_3), 3.69 (m, 1H, H-5), 3.83 (dt, *J* = 6.6, 9.5 Hz, 1H, H-1′b), 3.91 (dd, *J* = 2.4, 12.3 Hz, 1H, H-6a), 4.09 (dd, *J* = 5.2, 12.3 Hz, 1H, H-6b), 4.65 (d, *J* = 1.7 Hz, 1H, H-1), 5.03 (dd, *J* = 1.8, 3.0 Hz, 1H, H-2), 5.07–5.16 (m, 2H, H-3, H-4), 5.33 (s, 2H, CH_2Ar), 6.68, 6.72, 7.13 (m, 4H, C_6H_4), 7.68 (s, 1H, C_2N_3H); ^{13}C NMR (125 MHz, $CDCl_3$): δ 20.85, 20.88, 21.02 (4C, 4 $COCH_3$), 26.4 (C-2′), 54.1 (CH_2Ar), 55.4 (OCH_3), 62.5 (C-6), 66.2 (C-4), 67.2 (C-1′), 68.9, 69.2, 69.7 (C-2, C-3, C-5), 97.6 (C-1), 113.9, 114.2, 120.4, 130.3 (C_6H_4, C_2N_3H–C5), 136.5 (C_6H_4–C1), 144.8 (C_2N_3H–C4), 160.2 (C_6H_4–C3), 169.8, 170.1, 170.2, 170.8 (4 $COCH_3$); ESI-MS Calcd for $C_{26}H_{33}N_3NaO_{11}$ $[M+Na]^+$: 586.21, Found 586.29.

4.1.6.9. [1-(4′-Nitrophenyl)-1,2,3-triazol-4-yl]ethyl 2,3,4,6-tetra-*O*-acetyl-α-D-mannopyranoside (17i). Following general procedure B, **13** (55 mg, 0.14 mmol) was reacted with 1-azido-4-nitrobenzene (**15i**,[40] 34 mg, 0.21 mmol), 0.5 M $CuSO_4$ (70 μL, 35 μmol) and 1 M sodium ascorbate (70 μL, 70 μmol) to yield **17i** (74 mg, 94%).

$[\alpha]_D$ +28.1 (*c* 1.00, DCM); IR (film) 1748 (vs, CO) cm^{-1}; ^1H NMR (500 MHz, $CDCl_3$): δ 1.92, 1.99, 2.06, 2.11 (4s, 12H, 4 $COCH_3$), 3.12 (m, 2H, H-2′), 3.69–3.82 (m, 2H, H-5, H-1′a), 3.99–4.09 (m, 2H, H-6a, H-1′b), 4.19 (dd, *J* = 5.3, 12.3 Hz, 1H, H-6b), 4.84 (d, *J* = 1.6 Hz, 1H, H-1), 5.17–5.27 (m, 2H, H-2, H-4), 5.30 (dd, *J* = 3.3, 10.2 Hz, 1H, H-3), 8.03 (s, 1H, C_2N_3H), 8.06, 8.37 (m, 4H, C_6H_4); ^{13}C NMR (125 MHz, $CDCl_3$): δ 20.75, 20.89, 20.91, 21.02 (4 $COCH_3$), 26.3 (C-2′), 62.5 (C-6), 66.1 (C-4), 66.6 (C-1′), 69.1, 69.2, 69.6 (C-2, C-3, C-5), 97.5 (C-1), 120.6 (C_2N_3H–C5), 120.6 (2C, C_6H_4), 125.6 (2C, C_6H_4), 141.5 (C_6H_4–C1), 146.2 (C_2N_3H–C4), 147.2 (C_6H_4–C4), 169.7, 170.3, 170.4, 170.8 (4 $COCH_3$); ESI-MS Calcd for $C_{26}H_{33}N_3NaO_{11}$ $[M+Na]^+$: 587.17, Found 587.25.

4.1.6.10. [1-(Pyridin-4′-yl)-1,2,3-triazol-4-yl]ethyl 2,3,4,6-tetra-*O*-acetyl-α-D-mannopyranoside (17j). Following general procedure B, **13** (60 mg, 0.15 mmol) was reacted with 4-azidopyridine (**15j**,[41] 28 mg, 0.23 mmol), 0.5 M $CuSO_4$ (75 μL, 38 μmol) and 1 M sodium ascorbate (75 μL, 75 μmol). The crude product was dissolved in DCM (20 mL) and washed with 0.1 M aq EDTA

(10 mL). The aqueous phase was extracted with DCM (2 × 20 mL) and the combined organic layers were dried with Na_2SO_4 and evaporated to dryness. The residue was purified by MPLC on silica (petrol ether/EtOAc) to give **17j** (74 mg, 94%).

$[\alpha]_D$ +32.6 (*c* 0.99, DCM); IR (film) 1748 (vs, CO) cm^{-1}; ^1H NMR (500 MHz, $CDCl_3$): δ 1.88, 1.97, 2.05, 2.10 (4s, 12H, 4 $COCH_3$), 3.10 (m, 2H, H-2′), 3.64–3.79 (m, 2H, H-5, H-1′a), 3.96–4.06 (m, 2H, H-6a, H-1′b), 4.17 (dd, *J* = 5.3, 12.3 Hz, 1H, H-6b), 4.83 (d, *J* = 1.6 Hz, 1H, H-1), 5.16–5.26 (m, 2H, H-2, H-4), 5.28 (dd, *J* = 3.4, 10.1 Hz, 1H, H-3), 7.78 (dd, *J* = 1.6, 4.7 Hz, 2H, C_5H_4N), 8.04 (s, 1H, C_2N_3H), 8.72 (dd, *J* = 1.4, 4.9 Hz, 2H, C_5H_4N); ^{13}C NMR (125 MHz, $CDCl_3$): δ 20.68, 20.88, 21.0 (4C, 4 $COCH_3$), 26.3 (C-2′), 62.5 (C-6), 66.0 (C-4), 66.5 (C-1′), 69.0, 69.2, 69.7 (C-2, C-3, C-5), 97.4 (C-1), 113.9 (2C, C_5H_4N), 120.0 (C_2N_3H–C5), 143.3 (C_5H_4N–C1), 146.1 (C_2N_3H–C4), 151.8 (2C, C_5H_4N), 169.7, 170.3, 170.4, 170.8 (4 $COCH_3$); ESI-MS Calcd for $C_{26}H_{33}N_3$ NaO_{11} $[M+Na]^+$: 543.18, Found: 543.14.

4.1.6.11. [1-(4′-Fluorophenyl)-1,2,3-triazol-4-yl]ethyl 2,3,4,6-tetra-*O*-acetyl-α-D-mannopyranoside (17k). Following general procedure B, **13** (60 mg, 0.15 mmol) was reacted with 1-azido-4-fluorobenzene (**15k**,[41] 32 mg, 0.23 mmol), 0.5 M $CuSO_4$ (77 μL, 38 μmol) and 1 M sodium ascorbate (75 μL, 75 μmol) to yield **17k** (77 mg, 96%).

$[\alpha]_D$ +32.0 (*c* 1.01, DCM); IR (film) 1751 (vs, CO) cm^{-1}; ^1H NMR (500 MHz, $CDCl_3$): δ 1.90, 1.96, 2.05, 2.10 (4s, 12H, 4 $COCH_3$), 3.07 (m, 2H, H-2′), 3.67–3.79 (m, 2H, H-5, H-1′a), 3.96–4.06 (m, 2H, H-6a, H-1′b), 4.18 (dd, *J* = 5.2, 12.3 Hz, 1H, H-6b), 4.82 (d, *J* = 1.6 Hz, 1H, H-1), 5.16–5.24 (m, 2H, H-2, H-4), 5.28 (dd, *J* = 3.4, 10.1 Hz, 1H, H-3), 7.16, 7.73 (m, 4H, C_6H_4), 7.85 (s, 1H, C_2N_3H); ^{13}C NMR (125 MHz, $CDCl_3$): δ 20.71, 20.85, 20.88, 21.01 (4 $COCH_3$), 26.3 (C-2′), 62.5 (C-6), 66.1 (C-4), 66.8 (C-1′), 68.9, 69.2, 69.7 (C-2, C-3, C-5), 97.4 (C-1), 116.8 (d, *J* = 22.5 Hz, 2C, C_6H_4), 120.7 (C_2N_3H–C5), 122.6 (d, *J* = 8.8 Hz, 2C, C_6H_4), 133.6 (d, *J* = 2.5 Hz, C_6H_4–C1), 145.4 (C_2N_3H–C4), 162.5 (d, *J* = 247.5 Hz, C_6H_4–C4), 169.7, 170.2, 170.3, 170.8 (4 $COCH_3$); ESI-MS Calcd for $C_{26}H_{33}N_3NaO_{11}$ $[M+Na]^+$: 560.18, Found 560.17.

4.1.6.12. 1-(2,3,4,6-Tetra-*O*-acetyl-α-D-mannopyranosyl)-4-phenyl-1,2,3-triazole (20n). Following general procedure C, **18** (102 mg, 0.273 mmol) was reacted with phenylacetylene (**19n**, 60 μL, 0.55 mmol), 0.2 M $CuSO_4$ (273 μL, 54.6 μmol) and 1 M sodium ascorbate (109 μL, 109 μmol) to yield **20n** (110 mg, 84%).

$[\alpha]_D$ +65.5 (*c* 1.01, $CHCl_3$); ^1H NMR (500 MHz, $CDCl_3$): δ 2.07, 2.07, 2.09, 2.20 (4 s, 12H, 4 $COCH_3$), 3.94 (ddd, *J* = 2.5, 5.4, 9.0 Hz, 1H, H-5), 4.08 (dd, *J* = 2.5, 12.5 Hz, 1H, H-6a), 4.39 (dd, *J* = 5.4, 12.5 Hz, 1H, H-6b), 5.39 (t, *J* = 8.9 Hz, 1H, H-4), 5.98 (dd, *J* = 3.7, 8.8 Hz, 1H, H-3), 6.02 (dd, *J* = 2.7, 3.7 Hz, 1H, H-2), 6.07 (d, *J* = 2.6 Hz, 1H, H-1), 7.32–7.39, 7.44–7.47, 7.85–7.87 (m, 5H, C_6H_5), 7.96 (s, 1H, C_2N_3H); ^{13}C NMR (125 MHz, $CDCl_3$): δ 20.5, 20.6, 20.6, 20.7 (4 $COCH_3$), 61.5 (C-6), 66.0 (C-4), 68.2 (C-2), 68.7 (C-3), 72.1 (C-5), 83.5 (C-1), 119.7 (C_2N_3H–C5), 125.8, 128.6, 128.9, 129.6 (6C, C_6H_5), 148.2 (C_2N_3H–C4), 169.2, 169.6, 169.6, 170.4 (4 $COCH_3$); ESI-MS Calcd for $C_{22}H_{25}N_3NaO_9$ $[M+Na]^+$: 498.15, Found: 498.20.

4.1.6.13. 1-(2,3,4,6-Tetra-*O*-acetyl-α-D-mannopyranosyl)-4-(4-methylphenyl)-1,2,3-triazole (20o). Following general procedure C, **18** (50 mg, 0.13 mmol) was reacted with *p*-tolylacetylene (**19o**, 34 μL, 0.27 mmol), 0.2 M $CuSO_4$ (134 μL, 27 μmol) and 1 M sodium ascorbate (54 μL, 54 μmol) to yield **20o** (64 mg, 98%).

$[\alpha]_D$ +62.4 (*c* 1.09, $CHCl_3$); ^1H NMR (500 MHz, $CDCl_3$): δ 2.06, 2.07, 2.09, 2.19 (4 s, 12H, 4 $COCH_3$), 2.39 (s, 3H, $PhCH_3$), 3.94 (ddd, *J* = 2.4, 5.3, 9.0 Hz, 1H, H-5), 4.07 (dd, *J* = 2.4, 12.5 Hz, 1H, H-6a), 4.38 (dd, *J* = 5.4, 12.5 Hz, 1H, H-6b), 5.39 (t, *J* = 8.9 Hz, 1H, H-4), 5.98 (dd, *J* = 3.7, 8.7 Hz, 1H, H-3), 6.01 (dd, *J* = 2.6, 3.7 Hz, 1H, H-2), 6.05 (d, *J* = 2.4 Hz, 1H, H-1), 7.26, 7.74 (AA′, BB′ of AA′BB′, *J* = 7.9 Hz, 4H, C_6H_4), 7.90 (s, 1H, C_2N_3H); ^{13}C NMR (125 MHz, $CDCl_3$): δ 20.6, 20.7, 20.8 (4C, 4 $COCH_3$), 21.3 ($PhCH_3$), 61.6 (C-6), 66.1 (C-4), 68.3 (C-2), 68.8 (C-3), 72.1 (C-5), 83.6 (C-1), 119.3 (C_2N_3H–C5), 125.8, 126.8, 129.6, 138.6 (6C, C_6H_4), 148.4 (C_2N_3H–C4), 169.3, 169.7, 169.7, 170.5 (4 $COCH_3$); ESI-MS Calcd for $C_{23}H_{27}N_3NaO_9$ $[M+Na]^+$: 512.16, Found: 512.15.

4.1.6.14. 1-(2,3,4,6-Tetra-*O*-acetyl-α-D-mannopyranosyl)-4-(3-chlorophenyl)-1,2,3-triazole (20p). Following general procedure C, **18** (50 mg, 0.13 mmol) was reacted with 3-chloro-1-ethinylbenzene (**19p**, 33 μL, 0.27 mmol), 0.2 M $CuSO_4$ (134 μL, 27 μmol) and 1 M sodium ascorbate (54 μL, 54 μmol) to yield **20p** (59 mg, 86%).

$[\alpha]_D$ +56.3 (*c* 1.03, $CHCl_3$); ^1H NMR (500 MHz, $CDCl_3$): δ 2.07, 2.08, 2.09, 2.19 (4 s, 12H, 4 $COCH_3$), 3.95 (m, 1H, H-5), 4.08 (dd, *J* = 2.1, 12.5 Hz, 1H, H-6a), 4.41 (dd, *J* = 5.4, 12.5 Hz, 1H, H-6b), 5.38 (t, *J* = 8.7 Hz, 1H, H-4), 5.95 (dd, *J* = 3.6, 8.6 Hz, 1H, H-3), 6.00 (m, 1H, H-2), 6.07 (d, *J* = 2.4 Hz, 1H, H-1), 7.34–7.40 (m, 2H, C_6H_4–H5, H6), 7.75 (d, *J* = 7.4 Hz, 1H, C_6H_4–H4), 7.85 (s, 1H, C_6H_4–H2), 7.98 (s, 1H, C_2N_3H); ^{13}C NMR (125 MHz, $CDCl_3$): δ 20.6, 20.7, 20.7, 20.8 (4 $COCH_3$), 61.5 (C-6), 66.1 (C-4), 68.2 (C-2), 68.7 (C-3), 72.4 (C-5), 83.5 (C-1), 120.1 (C_2N_3H–C5), 124.0 (C_6H_4–C4), 126.0 (C_6H_4–C2), 128.7, 130.3 (C_6H_4–C5, C6), 131.5 (C_6H_4–C3), 134.9 (C_6H_4–C1), 147.2 (C_2N_3H–C4), 169.3, 169.6, 169.7, 170.5 (4 $COCH_3$); ESI-MS Calcd for $C_{22}H_{24}ClN_3NaO_9$ $[M+Na]^+$: 532.11, Found: 532.13.

4.1.6.15. 1-(2,3,4,6-Tetra-*O*-acetyl-α-D-mannopyranosyl)-4-(4-trifluoromethylphenyl)-1,2,3-triazole (20q). Following general procedure C, **18** (50 mg, 0.13 mmol) was reacted with 1-ethinyl-4-trifluoromethylbenzene (**19q**, 44 μL, 0.27 mmol), 0.2 M $CuSO_4$ (134 μL, 27 μmol) and 1 M sodium ascorbate (54 μL, 54 μmol) to yield **20q** (62 mg, 85%).

$[\alpha]_D$ +54.5 (*c* 0.95, $CHCl_3$); ^1H NMR (500 MHz, $CDCl_3$): δ 2.08, 2.09, 2.19 (3 s, 12H, 4 $COCH_3$), 3.97 (ddd, *J* = 2.5, 5.4, 8.7 Hz, 1H, H-5), 4.09 (dd, *J* = 2.5, 12.5 Hz, 1H, H-6a), 4.41 (dd, *J* = 5.5, 12.5 Hz, 1H, H-6b), 5.39 (t, *J* = 8.8 Hz, 1H, H-4), 5.95 (dd, *J* = 3.7, 8.7 Hz, 1H, H-3), 6.00 (dd, *J* = 3.1, 3.4 Hz, 1H, H-2), 6.09 (d, *J* = 2.8 Hz, 1H, H-1), 7.71, 7.98 (AA′, BB′ of AA′BB′, *J* = 8.1 Hz, 4H, C_6H_4), 8.05 (s, 1H, C_2N_3H); ^{13}C NMR (125 MHz, $CDCl_3$): δ 20.60, 20.69, 20.70, 20.73 (4 $COCH_3$), 61.4 (C-6), 66.0 (C-4), 68.2 (C-2), 68.7 (C-3), 72.5 (C-5), 83.5 (C-1), 120.6 (C_2N_3H–C5), 124.0 (q, *J* = 272 Hz, CF_3), 126.0 (q, *J* = 3.8 Hz, 2C, C_6H_4–C3, C5), 126.1 (2C, C_6H_4–C2, C6), 130.5 (d, *J* = 32.6 Hz, C_6H_4–C4), 133.1 (C_6H_4–C1), 147.0 (C_2N_3H–C4), 169.3, 169.6, 169.7, 170.5 (4 $COCH_3$); ESI-MS Calcd for $C_{23}H_{24}F_3N_3NaO_9$ $[M+Na]^+$: 566.14, Found: 566.10.

4.1.6.16. 1-(2,3,4,6-Tetra-*O*-acetyl-α-D-mannopyranosyl)-4-(3-pyridyl)-1,2,3-triazole (20r). Following general procedure C, **18** (50 mg, 0.13 mmol) was reacted with 3-ethinylpyridine (**19r**, 27.6 mg, 0.27 mmol), 0.2 M $CuSO_4$ (134 μL, 27 μmol) and 1 M sodium ascorbate (54 μL, 54 μmol). Then the reaction mixture was diluted with DCM (20 mL) and extracted with 25 mM aq EDTA (10 mL). The organic layer was dried (Na_2SO_4), concentrated and the residue was purified by MPLC on silica (petrol ether/EtOAc) to yield **20r** (61 mg, 96%).

$[\alpha]_D$ +56.0 (*c* 0.70, $CHCl_3$); ^1H NMR (500 MHz, $CDCl_3$): δ 2.06, 2.06, 2.07, 2.17 (4 s, 12H, 4 $COCH_3$), 3.95 (ddd, *J* = 2.6, 5.5, 8.8 Hz, 1H, H-5), 4.07 (dd, *J* = 2.6, 12.5 Hz, 1H, H-6a), 4.40 (dd, *J* = 5.6, 12.5 Hz, 1H, H-6b), 5.38 (t, *J* = 8.8 Hz, 1H, H-4), 5.92 (dd, *J* = 3.7, 8.8 Hz, 1H, H-3), 6.00 (dd, *J* = 3.2, 3.5 Hz, 1H, H-2), 6.11 (d, *J* = 2.9 Hz, 1H, H-1), 7.45 (dd, *J* = 4.9, 7.2 Hz, 1H, C_5H_4N-H5), 8.11 (s, 1H, C_2N_3H), 8.28 (d, *J* = 7.9 Hz, 1H, C_5H_4N-H6), 8.62 (m, 1H, C_5H_4N-H4), 9.06 (br s, 1H, C_5H_4N–H2); ^{13}C NMR (125 MHz, $CDCl_3$): δ 20.56, 20.66, 20.68, 20.70 (4 $COCH_3$), 61.4 (C-6), 66.0 (C-4), 68.1 (C-2), 68.6 (C-3), 72.5 (C-5), 83.6 (C-1), 120.4 (C_2N_3H–C5), 124.1

(C_5H_4N–C5), 126.3 (C_5H_4N–C1), 133.7 (C_5H_4N–C6), 145.0 (C_2N_3H–C4), 146.5 (C_5H_4N–C2), 148.9 (C_5H_4N–C4), 169.3, 169.6, 169.6, 170.5 (4 $COCH_3$); ESI-MS Calcd for $C_{21}H_{24}N_4NaO_9$ $[M+Na]^+$: 477.16, Found: 477.08.

4.1.6.17. 1-(2,3,4,6-Tetra-*O*-acetyl-α-D-mannopyranosyl)-4-phenoxymethyl-1,2,3-triazole (20s). Following general procedure C, **18** (50 mg, 0.13 mmol) was reacted with phenylpropargyl ether (**19s**, 34 μL, 0.27 mmol), 0.2 M $CuSO_4$ (134 μL, 27 μmol) and 1 M sodium ascorbate (54 μL, 54 μmol) to yield **20s** (58 mg, 85%).

$[\alpha]_D$ +38.8 (*c* 0.61, $CHCl_3$); ^1H NMR (500 MHz, $CDCl_3$): δ 2.06, 2.07, 2.09, 2.18 (4 s, 12H, 4 $COCH_3$), 3.90 (m, 1H, H-5), 4.05 (dd, *J* = 2.0, 12.5 Hz, 1H, H-6a), 4.37 (dd, *J* = 5.4, 12.5 Hz, 1H, H-6b), 5.26 (s, 2H, CH_2OPh), 5.37 (t, *J* = 8.9 Hz, 1H, H-4), 5.93 (dd, *J* = 3.6, 8.8 Hz, 1H, H-3), 5.97 (dd, *J* = 2.7, 3.3 Hz, 1H, H-2), 6.00 (d, *J* = 2.3 Hz, 1H, H-1), 6.98–7.00, 7.30–7.32 (m, 5H, C_6H_5), 7.81 (s, 1H, C_2N_3H); ^{13}C NMR (125 MHz, $CDCl_3$): δ 20.59, 20.67, 20.69, 20.73 (4 $COCH_3$), 61.5 (C-6), 61.8 (CH_2OPh), 66.0 (C-4), 68.2 (C-2), 68.7 (C-3), 72.2 (C-5), 83.6 (C-1), 114.7 (2C, C_6H_5–C2, C6), 121.4 (C_6H_5–C4), 123.0 (C_2N_3H–C5), 129.6 (2C, C_6H_5–C3, C5), 145.2 (C_2N_3H–C4), 158.0 (C_6H_5–C1), 169.3, 169.6, 169.7, 170.5 (4 $COCH_3$); ESI-MS Calcd for $C_{23}H_{27}N_3NaO_{10}$ $[M+Na]^+$: 528.16, Found: 528.14.

4.1.6.18. 1-(2,3,4,6-Tetra-*O*-acetyl-α-D-mannopyranosyl)methyl-4-phenyl-1,2,3-triazole (25n). Following general procedure C, **24** (40 mg, 0.10 mmol) was reacted with phenylacetylene (**19n**, 23 μL, 0.21 mmol), 0.2 M $CuSO_4$ (103 μL, 21 μmol) and 1 M sodium ascorbate (41 μL, 41 μmol) to yield **25n** (47 mg, 93%).

$[\alpha]_D$ -1.76 (*c* 1.50, $CHCl_3$); ^1H NMR (500 MHz, $CDCl_3$): δ 1.83, 2.08, 2.11, 2.12 (4 s, 12H, 4 $COCH_3$), 4.00 (dd, *J* = 3.9, 12.2 Hz, 1H, H-6a), 4.16 (dt, *J* = 3.5, 9.0 Hz, 1H, H-5), 4.39 (dt, *J* = 2.6, 8.6 Hz, 1H, H-1), 4.50 (dd, *J* = 8.8, 14.3 Hz, 1H, H-1′a), 4.59 (dd, *J* = 9.2, 12.1 Hz, 1H, H-6b), 4.66 (dd, *J* = 2.4, 14.3 Hz, 1H, H-1′b), 4.94 (dd, *J* = 3.0, 4.9 Hz, 1H, H-4), 5.06 (dd, *J* = 3.2, 8.4 Hz, 1H, H-2), 5.35 (t, *J* = 4.0 Hz, 1H, H-3), 7.32 (t, *J* = 7.4 Hz, 1H, C_6H_5-H4), 7.41 (t, *J* = 7.4 Hz, 2H, C_6H_5-H3, H5), 7.83 (d, *J* = 8.0 Hz, 2H, C_6H_5-H2, H6), 7.92 (s, 1H, C_2N_3H); ^{13}C NMR (125 MHz, $CDCl_3$): δ 20.4, 20.6, 20.7, 20.8 (4 $COCH_3$), 50.3 (C-1′), 60.0 (C-6), 66.8 (C-2), 66.9 (C-3), 68.0 (C-4), 68.4 (C-1), 73.4 (C-5), 120.9 (C_2N_3H–C5), 125.6, 128.2, 128.8, 130.5 (6C, C_6H_5), 148.0 (C_2N_3H–C4), 169.1, 169.4, 169.6, 170.4 (4 $COCH_3$); ESI-MS Calcd for $C_{23}H_{28}N_3O_9$ $[M+H]^+$: 490.18, Found: 490.17.

4.1.6.19. 1-(2,3,4,6-Tetra-*O*-acetyl-α-D-mannopyranosyl)methyl-4-(4-methylphenyl)-1,2,3-triazole (25o). Following general procedure C, **24** (40 mg, 0.10 mmol) was reacted with *p*-tolylacetylene (**19o**, 26 μL, 0.21 mmol), 0.2 M $CuSO_4$ (103 μL, 21 μmol) and 1 M sodium ascorbate (41 μL, 41 μmol) to yield **25o** (50 mg, 97%).

$[\alpha]_D$ -1.57 (*c* 1.26, $CHCl_3$); ^1H NMR (500 MHz, $CDCl_3$): δ 1.83, 2.07, 2.10, 2.11 (4 s, 12H, 4 $COCH_3$), 2.36 (s, 3H, $PhCH_3$), 3.99 (dd, *J* = 4.0, 12.2 Hz, 1H, H-6a), 4.15 (dt, *J* = 3.5, 9.0 Hz, 1H, H-5), 4.38 (dt, *J* = 2.7, 8.6 Hz, 1H, H-1), 4.50 (dd, *J* = 8.8, 14.4 Hz, 1H, H-1′a), 4.58 (dd, *J* = 9.1, 12.2 Hz, 1H, H-6b), 4.64 (dd, *J* = 2.8, 14.4 Hz, 1H, H-1′b), 4.94 (dd, *J* = 3.1, 5.0 Hz, 1H, H-4), 5.06 (dd, *J* = 3.3, 8.3 Hz, 1H, H-2), 5.34 (dd, *J* = 3.5, 4.8 Hz, 1H, H-3), 7.21, 7.70 (AA′, BB′ of AA′BB′, *J* = 8.0 Hz, 4H, C_6H_4), 7.87 (s, 1H, C_2N_3H); ^{13}C NMR (125 MHz, $CDCl_3$): δ 20.41, 20.62, 20.64, 20.74 (4 $COCH_3$), 21.2 ($PhCH_3$), 50.2 (C-1′), 60.0 (C-6), 66.8 (C-2), 66.9 (C-3), 68.0 (C-4), 68.5 (C-1), 73.3 (C-5), 120.5 (C_2N_3H–C5), 125.5, 127.6, 129.5, 138.0 (6C, C_6H_4), 147.8 (C_2N_3H–C4), 169.1, 169.4, 169.6, 170.4 (4 $COCH_3$); ESI-MS Calcd for $C_{24}H_{30}N_3O_9$ $[M+H]^+$: 504.20, Found: 504.20.

4.1.6.20. 1-(2,3,4,6-Tetra-*O*-acetyl-α-D-mannopyranosyl)methyl-4-(3-chlorophenyl)-1,2,3-triazole (25p). Following general procedure C, **24** (40 mg, 0.10 mmol) was reacted with 3-chloro-1-ethinylbenzene (**19p**, 25 μL, 0.21 mmol), 0.2 M $CuSO_4$ (103 μL, 21 μmol) and 1 M sodium ascorbate (41 μL, 41 μmol) to yield **25p** (51 mg, 94%).

$[\alpha]_D$ -2.55 (*c* 1.27, $CHCl_3$); ^1H NMR (500 MHz, $CDCl_3$): δ 1.84, 2.07, 2.10, 2.11 (4 s, 12H, 4 $COCH_3$), 3.99 (dd, *J* = 4.0, 12.2 Hz, 1H, H-6a), 4.15 (dt, *J* = 3.4, 9.0 Hz, 1H, H-5), 4.38 (dt, *J* = 2.7, 8.6 Hz, 1H, H-1), 4.51 (dd, *J* = 8.7, 14.4 Hz, 1H, H-1′a), 4.60 (dd, *J* = 9.2, 12.2 Hz, 1H, H-6b), 4.65 (dd, *J* = 2.7, 14.4 Hz, 1H, H-1′b), 4.93 (dd, *J* = 2.9, 4.9 Hz, 1H, H-4), 5.03 (dd, *J* = 3.3, 8.5 Hz, 1H, H-2), 5.34 (dd, *J* = 3.6, 4.6 Hz, 1H, H-3), 7.27 (m, 1H, C_6H_4-H6), 7.33 (t, *J* = 7.8 Hz, 1H, C_6H_4–H5), 7.72 (d, *J* = 7.7 Hz, 1H, C_6H_4–H4), 7.81 (t, *J* = 1.7 Hz, 1H, C_6H_4-H2), 7.94 (s, 1H, C_2N_3H); ^{13}C NMR (125 MHz, $CDCl_3$): δ 20.41, 20.60, 20.64, 20.73 (4 $COCH_3$), 50.4 (C-1′), 59.9 (C-6), 66.7 (C-2), 66.8 (C-3), 68.0 (C-4), 68.3 (C-1), 73.5 (C-5), 121.3 (C_2N_3H–C5), 123.6, 125.6, 128.1, 130.1, 132.3, 134.8 (C_6H_4), 146.5 (C_2N_3H–C4), 169.1, 169.3, 169.5, 170.3 (4 $COCH_3$); ESI-MS Calcd for $C_{23}H_{27}ClN_3O_9$ $[M+H]^+$: 524.14, Found: 524.04.

4.1.6.21. 1-(2,3,4,6-Tetra-*O*-acetyl-α-D-mannopyranosyl)methyl-4-(4-trifluoromethylphenyl)-1,2,3-triazole (25q). Following general procedure C, **24** (40 mg, 0.10 mmol) was reacted with 1-ethinyl-4-trifluoromethylbenzene (**19q**, 34 μL, 0.21 mmol), 0.2 M $CuSO_4$ (103 μL, 21 μmol) and 1 M sodium ascorbate (41 μL, 41 μmol) to yield **25q** (56 mg, 98%).

$[\alpha]_D$ +0.47 (*c* 1.19, $CHCl_3$); ^1H NMR (500 MHz, $CDCl_3$): δ 1.82, 2.08, 2.10, 2.12 (4 s, 12H, 4 $COCH_3$), 3.97 (dd, *J* = 4.0, 12.2 Hz, 1H, H-6a), 4.15 (dt, *J* = 3.4, 9.0 Hz, 1H, H-5), 4.40 (dt, *J* = 2.5, 8.6 Hz, 1H, H-1), 4.53 (dd, *J* = 8.7, 14.4 Hz, 1H, H-1′a), 4.63 (dd, *J* = 9.2, 12.2 Hz, 1H, H-6b), 4.67 (dd, *J* = 2.7, 14.4 Hz, 1H, H-1′b), 4.93 (dd, *J* = 2.9, 4.7 Hz, 1H, H-4), 5.04 (dd, *J* = 3.2, 8.6 Hz, 1H, H-2), 5.34 (t, *J* = 4.0 Hz, 1H, H-3), 7.66, 7.95 (AA′, BB′ of AA′BB′, *J* = 8.2 Hz, 4H, C_6H_4), 8.00 (s, 1H, C_2N_3H); ^{13}C NMR (125 MHz, $CDCl_3$): δ 20.42, 20.63, 20.67, 20.76 (4 $COCH_3$), 50.4 (C-1′), 59.9 (C-6), 66.7 (C-2), 66.8 (C-3), 68.0 (C-4), 68.2 (C-1), 73.5 (C-5), 121.7 (C_2N_3H–C5), 124.0 (q, *J* = 272 Hz, CF_3), 125.7 (2C, C_6H_4–C2, C6), 125.8 (q, *J* = 3.8 Hz, 2C, C_6H_4–C3, C5), 129.9 (q, *J* = 32.5 Hz, C_6H_4–C4), 133.9 (C_6H_4–C1), 146.4 (C_2N_3H–C4), 169.1, 169.4, 169.6, 170.3 (4 $COCH_3$); ESI-MS Calcd for $C_{24}H_{27}F_3N_3O_9$ $[M+H]^+$: 558.17, Found: 558.22.

4.1.6.22. 1-(2,3,4,6-Tetra-*O*-acetyl-α-D-mannopyranosyl)methyl-4-(3-pyridyl)-1,2,3-triazole (25r). Following general procedure C, **24** (40 mg, 0.10 mmol) was reacted with 3-ethinylpyridine (**19r**, 21.2 mg, 0.206 mmol), 0.2 M $CuSO_4$ (103 μL, 21 μmol) and 1 M sodium ascorbate (41 μL, 41 μmol) to yield **25r** (50 mg, 98%).

$[\alpha]_D$ -0.08 (*c* 1.04, $CHCl_3$); ^1H NMR (500 MHz, $CDCl_3$): δ 1.83, 2.07, 2.09, 2.10 (4 s, 12H, 4 $COCH_3$), 3.97 (dd, *J* = 4.0, 12.2 Hz, 1H, H-6a), 4.14 (dt, *J* = 3.4, 8.9 Hz, 1H, H-5), 4.39 (dt, *J* = 2.6, 8.6 Hz, 1H, H-1), 4.54 (dd, *J* = 8.6, 14.4 Hz, 1H, H-1′a), 4.60 (dd, *J* = 9.1, 12.2 Hz, 1H, H-6b), 4.66 (dd, *J* = 2.7, 14.4 Hz, 1H, H-1′b), 4.92 (dd, *J* = 2.9, 4.8 Hz, 1H, H-4), 5.02 (dd, *J* = 3.3, 8.5 Hz, 1H, H-2), 5.33 (m, 1H, H-3), 7.37 (m, 1H, C_5H_4N-H5), 8.02 (s, 1H, C_2N_3H), 8.21 (d, *J* = 7.9 Hz, 1H, C_5H_4N-H6), 8.56 (s, 1H, C_5H_4N-H2), 9.00 (m, 1H, C_5H_4N-H4); ^{13}C NMR (125 MHz, $CDCl_3$): δ 20.44, 20.61, 20.65, 20.74 (4 $COCH_3$), 50.4 (C-1′), 59.9 (C-6), 66.6 (C-2), 66.8 (C-3), 67.9 (C-4), 68.3 (C-1), 73.5 (C-5), 121.3 (C_2N_3H–C5), 123.8 (C_5H_4N–C5), 126.8 (C_5H_4N–C1), 133.0 (C_5H_4N–C6), 144.6 (C_2N_3H–C4), 146.7 (C_5H_4N–C2), 149.0 (C_5H_4N–C4), 169.1, 169.3, 169.5, 170.3 (4 $COCH_3$); ESI-MS Calcd for $C_{22}H_{27}N_4O_9$ $[M+H]^+$: 491.18, Found: 491.17.

4.1.6.23. 1-(2,3,4,6-Tetra-*O*-acetyl-α-D-mannopyranosyl)methyl-4-phenoxymethyl-1,2,3-triazole (25s). Following general procedure C, **24** (40 mg, 0.10 mmol) was reacted with phenylpropargyl ether (**19s**, 26 μL, 0.21 mmol), 0.2 M $CuSO_4$ (103 μL, 21 μmol) and 1 M sodium ascorbate (41 μL, 41 μmol) to yield **25s** (51 mg, 96%).

$[\alpha]_D$ +2.34 (*c* 1.03, $CHCl_3$); ^1H NMR (500 MHz, $CDCl_3$): δ 2.00, 2.08, 2.12, 2.13 (4 s, 12H, 4 $COCH_3$), 4.04 (dd, J = 4.1, 12.1 Hz, 1H, H-6a), 4.15 (m, 1H, H-5), 4.37 (dt, J = 2.4, 8.6 Hz, 1H, H-1), 4.50 (dd, J = 8.7, 14.4 Hz, 1H, H-1′a), 4.55 (dd, J = 9.0, 12.1 Hz, 1H, H-6b), 4.63 (dd, J = 2.5, 14.4 Hz, 1H, H-1′b), 4.96 (dd, J = 3.2, 4.9 Hz, 1H, H-4), 5.04 (dd, J = 3.3, 8.3 Hz, 1H, H-2), 5.34 (m, 1H, H-3), 6.96–6.99, 7.29–7.31 (m, 5H, C_6H_5), 7.80 (s, 1H, C_2N_3H); ^{13}C NMR (125 MHz, $CDCl_3$): δ 20.49, 20.62, 20.66, 20.74 (4 $COCH_3$), 50.2 (C-1′), 60.0 (C-6), 61.9 (CH_2OPh), 66.7 (C-2), 66.9 (C-3), 67.8 (C-4), 68.5 (C-1), 73.3 (C-5), 114.6, 121.2 (3C, C_6H_5), 123.8 (C_2N_3H–C5), 129.5 (2C, C_6H_5), 144.3 (C_2N_3H–C4), 158.1 (C_6H_4–C1), 169.1, 169.4, 169.6, 170.4 (4 $COCH_3$); ESI-MS Calcd for $C_{24}H_{30}N_3O_9$ $[M+H]^+$: 520.19, Found: 520.16.

4.1.7. Synthesis of mannosyl triazoles

4.1.7.1. Sodium 4-[4-((α-D-mannopyranosyloxy)methyl)-1*H*-1,2,3-triazol-1-yl]-benzoate (5a). To a solution of **12a** (48.0 mg, 85.2 μmol) in MeOH (4 mL) was added freshly prepared 1 M NaOMe in MeOH (0.4 mL) under argon. The mixture was stirred at rt for 3 h and then evaporated to dryness. The remains were dissolved in H_2O/dioxane (1:1, 5 mL) and treated with 1 M aq. NaOH (0.5 mL) for 16 h. The solution was concentrated and the residue purified by MPLC on RP-18 (H_2O/MeOH) and P2 size exclusion chromatography to give **5a** (31.2 mg, 91%) as white powder after a final lyophilization from water.

$[\alpha]_D$ +41.7 (*c* 0.60, H_2O); IR (KBr) 3413 (vs b, OH), 1607 (vs, CO) cm^{-1}; ^1H NMR (500 MHz, D_2O): δ 3.60–3.66 (m, 2H, H-4, H-5), 3.72 (dd, J = 5.5, 12.1 Hz, 1H, H-6a), 3.78 (dd, J = 3.4, 9.4 Hz, 1H, H-3), 3.82 (dd, J = 1.4, 12.2 Hz, 1H, H-6b), 3.93 (dd, J = 1.7, 3.4 Hz, 1H, H-2), 4.71 (m, 1H, H-1′a), 4.82 (m, 1H, H-1′b), 4.97 (s, 1H, H-1), 7.68 (m, 2H, C_6H_4), 7.94 (m, 2H, C_6H_4), 8.41 (m, 1H, C_2N_3H); ^{13}C NMR (125 MHz, D_2O): δ 59.7 (C-1′), 60.8 (C-6), 66.6 (C-4), 69.9 (C-2), 70.4 (C-3), 72.9 (C-5), 99.5 (C-1), 120.2 (2C, C_6H_4), 123.3 (C_2N_3H–C5), 130.3, 137.0, 137.7 (4C, C_6H_4), 144.2 (C_2N_3H–C4), 174.1 (CO); HR-MS Calcd for $C_{16}H_{19}N_3NaO_8$ $[M+H]^+$: 404.1070, Found: 404.1071.

4.1.7.2. Sodium 3-[4-((α-D-mannopyranosyloxy)methyl)-1*H*-1,2,3-triazol-1-yl]-benzoate (5b). According to the procedure described for **5a**, **12b** (67.0 mg, 0.116 mmol) was subsequently treated with 1 M methanolic NaOMe (0.5 mL) in MeOH (5 mL) and 1 M aq. NaOH (0.5 mL) in H_2O/dioxane (1:1, 6 mL) to yield **5b** (37.7 mg, 81%).

$[\alpha]_D$ +44.4 (*c* 0.89, H_2O); IR (KBr) 3401 (vs b, OH), 1610 (vs, CO) cm^{-1}; ^1H NMR (500 MHz, D_2O): δ 3.61–3.66 (m, 2H, H-4, H-5), 3.72 (dd, J = 5.4, 12.2 Hz, 1H, H-6a), 3.78 (dd, J = 3.5, 9.5 Hz, 1H, H-3), 3.82 (dd, J = 1.5, 12.2 Hz, 1H, H-6b), 3.92 (dd, J = 1.7, 3.3 Hz, 1H, H-2), 4.69 (A of AB, J = 12.8 Hz, 1H, H-1′a), 4.80 (m, 1H, H-1′b), 4.96 (s, 1H, H-1), 7.51 (m, 1H, C_6H_4-H5), 7.69 (d, J = 7.0 Hz, 1H, C_6H_4-H4), 7.87 (d, J = 7.7 Hz, 1H, C_6H_4-H6), 8.01 (s, 1H, C_6H_4-H2), 8.36 (m, 1H, C_2N_3H); ^{13}C NMR (125 MHz, D_2O): δ 59.7 (C-1′), 60.8 (C-6), 66.7 (C-4), 69.9 (C-2), 70.4 (C-3), 72.9 (C-5), 99.5 (C-1), 120.8 (C_6H_4), 123.0 (C_2N_3H–C5), 123.3, 129.5, 129.8, 135.9, 138.1 (C_6H_4), 144.1 (C_2N_3H–C4), 173.6 (CO); HR-MS Calcd for $C_{16}H_{19}N_3NaO_8$ $[M+H]^+$: 404.1070, Found: 404.1068.

4.1.7.3. Sodium 5-[4-((α-D-mannopyranosyloxy)methyl)-1*H*-1,2,3-triazol-1-yl]-nicotinate (5c). According to the procedure described for **5a**, **12c** (41.0 mg, 72.6 μmol) was subsequently treated with 1 M methanolic NaOMe (0.4 mL) in MeOH (4 mL) and 1 M aq. NaOH (0.4 mL) in H_2O/dioxane (1:1, 4 mL) to yield **5c** (23.0 mg, 78%).

$[\alpha]_D$ +36.0 (*c* 0.69, H_2O); IR (KBr) 3413 (vs b, OH), 1616 (vs, CO) cm^{-1}; ^1H NMR (500 MHz, D_2O): δ 3.61–3.66 (m, 2H, H-4, H-5), 3.73 (dd, J = 5.4, 12.1 Hz, 1H, H-6a), 3.79 (dd, J = 3.5, 9.4 Hz, 1H, H-3), 3.83 (d, J = 12.0 Hz, 1H, H-6b), 3.94 (dd, J = 1.7, 3.2 Hz, 1H, H-2), 4.76, 4.87 (A, B of AB, J = 12.6 Hz, 1H, H-1′), 4.99 (d, J = 0.7 Hz, 1H, H-1), 8.47 (t, J = 2.0 Hz, 1H, C_5H_3N-H2), 8.56 (m, 1H, C_2N_3H), 8.96 (d, J = 2.1 Hz, 1H, C_5H_3N-H6), 8.97 (d, J = 1.4 Hz, 1H, C_5H_3N-H4); ^{13}C NMR (125 MHz, D_2O): δ 59.7 (C-1′), 60.8 (C-6), 66.7 (C-4), 69.9 (C-2), 70.4 (C-3), 73.0 (C-5), 99.5 (C-1), 123.6 (C_2N_3H–C5), 129.5, 133.1, 133.4, 142.6 (C_5H_3N), 144.6 (C_2N_3H–C4), 149.7 (C_5H_3N), 171.1 (CO); HR-MS Calcd for $C_{15}H_{17}N_4Na_2O_8$ $[M+Na]^+$: 427.0842, Found: 427.0844.

4.1.7.4. (1-Benzyl-1,2,3-triazol-4-yl)methyl α-D-mannopyranoside (5d). Following general procedure A, **14** (40 mg, 0.18 mmol) was reacted with benzyl azide (**15d**, 34 μL, 0.27 mmol), $CuSO_4$ (11 mg, 45 μmol) and sodium ascorbate (18 mg, 90 μmol) to yield **5d** (57 mg, 71%).

$[\alpha]_D$ +53.3 (*c* 1.03, MeOH); ^1H NMR (500 MHz, CD_3OD): δ 3.50 (m, 1H, H-5), 3.56 (t, J = 9.4 Hz, 1H, H-4), 3.60–3.68 (m, 2H, H-3, H-6a), 3.73 (m, 1H, H-2), 3.79 (dd, J = 1.7, 11.7 Hz, 1H, H-6b), 4.60, 4.75 (A, B of AB, J = 12.4 Hz, 2H, H-1′), 4.80 (d, J = 1.6 Hz, 1H, H-1), 5.56 (s, 2H, CH_2Ph), 7.24–7.41 (m, 5H, C_6H_5), 7.97 (s, 1H, C_2N_3H); ^{13}C NMR (125 MHz, CD_3OD): δ 55.1 (CH_2Ph), 60.8 (C-1′), 63.1 (C-6), 68.7 (C-4), 72.1 (C-2), 72.6 (C-3), 75.1 (C-5), 100.9 (C-1), 125.5 (C_2N_3H–C5), 129.3, 129.8, 130.2, 136.9 (6C, C_6H_5), 145.9 (C_2N_3H–C4); HR-MS Calcd for $C_{16}H_{21}N_3NaO_6$ $[M+Na]^+$: 374.1328, Found: 374.1334.

4.1.7.5. [1-(4′-Aminophenyl)-1,2,3-triazol-4-yl]methyl α-D-mannopyranoside hydrochloride (5e). Following general procedure A, **14** (40 mg, 0.18 mmol) was reacted with 4-azidoaniline hydrochloride (**15e**, 46 mg, 0.27 mmol), $CuSO_4$ (11 mg, 45 μmol) and sodium ascorbate (18 mg, 90 μmol) to yield **5e** (19 mg, 27%).

$[\alpha]_D$ +55.2 (*c* 1.00, MeOH); ^1H NMR (500 MHz, CD_3OD): δ 3.55–3.60 (m, 2H, H-4, H-5), 3.64–3.72 (m, 2H, H-3, H-6a), 3.78 (m, 1H, H-2), 3.83 (m, 1H, H-6b), 4.68, 4.82 (A, B of AB, J = 12.4 Hz, 2H, H-1′), 4.86 (m, 1H, H-1), 6.78, 7.45 (AA′, BB′ of AA′BB′, J = 8.7 Hz, 4H, C_6H_4), 8.33 (s, 1H, C_2N_3H); ^{13}C NMR (125 MHz, CD_3OD): δ 60.8 (C-1′), 63.2 (C-6), 68.8 (C-4), 72.2 (C-2), 72.6 (C-3), 75.2 (C-5), 100.9 (C-1), 116.2 (2C, C_6H_4), 123.3 (2C, C_6H_4), 123.7 (C_2N_3H–C5), 128.8 (C_6H_4–C1), 145.8 (C_2N_3H–C4), 150.8 (C_6H_4–C4); HR-MS Calcd for $C_{15}H_{21}N_4O_6$ $[M+H]^+$: 353.1461, Found: 353.1463.

4.1.7.6. (1-Adamantyl-1,2,3-triazol-4-yl)methyl α-D-mannopyranoside (5f). Following general procedure A, **14** (40 mg, 0.18 mmol) was reacted with 1-azidoadamantane (**15f**, 48 mg, 0.27 mmol), $CuSO_4$ (11 mg, 45 μmol) and sodium ascorbate (18 mg, 90 μmol) to yield **5f** (20 mg, 28%).

$[\alpha]_D$ +50.5 (*c* 1.04, MeOH); ^1H NMR (500 MHz, CD_3OD): δ 1.76–1.88 (m, 6H, Ad), 2.24 (s, 9H, Ad), 3.50–3.60 (m, 2H, H-4, H-5), 3.61–3.70 (m, 2H, H-3, H-6a), 3.75 (dd, J = 1.7, 3.3 Hz, 1H, H-2), 3.82 (m, 1H, H-6b), 4.60, 4.76 (A, B of AB, J = 12.3 Hz, 2H, H-1′), 4.80 (d, J = 1.4 Hz, 1H, H-1), 8.09 (s, 1H, C_2N_3H); ^{13}C NMR (125 MHz, CD_3OD): δ 31.1, 37.1, 44.0 (10 C, Ad), 60.9 (C-1′), 63.2 (C-6), 68.8 (C-4), 72.2 (C-2), 72.6 (C-3), 75.1 (C-5), 100.9 (C-1), 122.2 (C_2N_3H–C5), 144.6 (C_2N_3H–C4); HR-MS Calcd for $C_{19}H_{29}N_3NaO_6$ $[M+Na]^+$: 418.1954, Found: 418.1951.

4.1.7.7. [1-(4′-Methoxybenzyl)-1,2,3-triazol-4-yl]methyl α-D-mannopyranoside (5g). Following general procedure A, **14** (50 mg, 0.23 mmol) was reacted with 4-methoxybenzylazide (**15g**,[38] 57 mg, 0.35 mmol), $CuSO_4$ (15 mg, 60 μmol) and sodium ascorbate (24 mg, 120 μmol) to yield **5g** (64 mg, 73%).

$[\alpha]_D$ +66.6 (*c* 1.01, MeOH); ^1H NMR (500 MHz, CD_3OD): δ 3.50 (m, 1H, H-5), 3.57 (t, J = 9.4 Hz, 1H, H-4), 3.61–3.69 (m, 2H, H-3, H-6a), 3.74 (m, 4H, H-2, OCH_3), 3.78 (dd, J = 1.7, 11.7 Hz, 1H, H-6b), 4.58, 4.73 (A, B of AB, J = 12.4 Hz, 2H, H-1′), 4.79 (m, 1H, H-1), 5.46 (s, 2H, CH_2Ar), 6.88, 7.25 (AA′, BB′ of AA′BB′, J = 8.6 Hz, 4H, C_6H_4), 7.91 (s, 1H, C_2N_3H);

^{13}C NMR (125 MHz, CD_3OD): δ 54.6 (CH_2Ar), 55.8 (OCH_3), 60.7 (C-1′), 63.0 (C-6), 68.6 (C-4), 72.0 (C-2), 72.5 (C-3), 75.0 (C-5), 100.8 (C-1), 115.4 (2C, C_6H_4), 125.1 (C_2N_3H–C5), 128.6 (2C, C_6H_4), 130.8 (C_6H_4–C1), 145.6 (C_2N_3H–C4), 161.4 (C_6H_4–C4); HR-MS Calcd for $C_{17}H_{23}N_3NaO_7$ [M+Na]$^+$: 404.1434, Found: 404.1431.

4.1.7.8. [1-(3′-Methoxybenzyl)-1,2,3-triazol-4-yl]methyl α-D-mannopyranoside (5h). Following general procedure A, **14** (50 mg, 0.23 mmol) was reacted with 3-methoxybenzylazide (**15h**,[39] 57 mg, 0.35 mmol), $CuSO_4$ (15 mg, 60 μmol) and sodium ascorbate (24 mg, 120 μmol) to yield **5h** (68 mg, 77%).

$[\alpha]_D$ +62.2 (*c* 1.00, MeOH); ^{1}H NMR (500 MHz, CD_3OD): δ 3.52 (m, 1H, H-5), 3.58 (t, *J* = 9.4 Hz, 1H, H-4), 3.61–3.70 (m, 2H, H-3, H-6a), 3.70–3.84 (m, 5H, H-2, H-6b, OCH_3), 4.60, 4.75 (A, B of AB, *J* = 12.3 Hz, 2H, H-1′), 4.81 (m, 1H, H-1), 5.52 (s, 2H, CH_2Ar), 6.85 (s, 3H, C_6H_4), 7.24 (t, *J* = 7.9 Hz, 1H, C_6H_4), 7.98 (s, 1H, C_2N_3H); ^{13}C NMR (125 MHz, CD_3OD): δ 55.5 (CH_2Ar), 55.9 (OCH_3), 60.8 (C-1′), 63.0 (C-6), 68.7 (C-4), 72.1 (C-2), 72.6 (C-3), 75.1 (C-5), 100.9 (C-1), 114.9, 115.2, 121.4 (3C, C_6H_4), 125.6 (C_2N_3H–C5), 131.3 (C_6H_4), 138.2 (C_6H_4–C1), 145.8 (C_2N_3H–C4), 161.7 (C_6H_4–C3); HR-MS Calcd for $C_{17}H_{23}N_3NaO_7$ [M+Na]$^+$: 404.1434, Found: 404.1435.

4.1.7.9. [1-(4′-Nitrophenyl)-1,2,3-triazol-4-yl]methyl α-D-mannopyranoside (5i). Following general procedure A, **14** (40 mg, 0.18 mmol) was reacted with 1-azido-4-nitrobenzene (**15i**,[40] 44 mg, 0.27 mmol), $CuSO_4$ (11 mg, 45 μmol) and sodium ascorbate (18 mg, 90 μmol) to yield **5i** (31 mg, 44%).

$[\alpha]_D$ +50.4 (*c* 1.02, MeOH); ^{1}H NMR (500 MHz, CD_3OD): δ 3.56–3.60 (m, 2H, H-4, H-5), 3.64–3.72 (m, 2H, H-3, H-6a), 3.80 (dd, *J* = 1.7, 3.3 Hz, 1H, H-2), 3.84 (dd, *J* = 1.0, 11.7 Hz, 1H, H-6b), 4.75 (A of AB, *J* = 12.5 Hz, 1H, H-1′a), 4.88–4.91 (m, 2H, H-1, H-1′b), 8.16 (m, 2H, C_6H_4), 8.44 (m, 2H, C_6H_4), 8.75 (s, 1H, C_2N_3H); ^{13}C NMR (125 MHz, CD_3OD): δ 60.9 (C-1′), 63.2 (C-6), 68.8 (C-4), 72.1 (C-2), 72.6 (C-3), 75.3 (C-5), 101.2 (C-1), 122.0 (2C, C_6H_4), 123.9 (C_2N_3H–C5), 126.7 (2C, C_6H_4), 142.7 (C_6H_4–C1), 147.1 (C_2N_3H–C4), 148.9 (C_6H_4–C4); HR-MS Calcd for $C_{15}H_{18}N_4NaO_8$ [M+Na]$^+$: 405.1022, Found: 405.1020.

4.1.7.10. [1-(Pyridin-4′-yl)-1,2,3-triazol-4-yl]methyl α-D-mannopyranoside (5j). Prepared from **16j** (102 mg, 0.20 mmol) according to general procedure D. Yield: 58 mg, 85%.

$[\alpha]_D$ +70.3 (*c* 1.00, MeOH); ^{1}H NMR (500 MHz, CD_3OD): δ 3.53–3.63 (m, 2H, H-4, H-5), 3.64–3.74 (m, 2H, H-3, H-6a), 3.77–3.87 (m, 2H, H-2, H-6b), 4.73 (A of AB, *J* = 12.6 Hz, 1H, H-1′a), 4.84–4.92 (m, 2H, H-1, H-1′b), 7.96, 8.67 (m, 4H, C_5H_4N), 8.77 (s, 1H, C_2N_3H); ^{13}C NMR (125 MHz, CD_3OD): δ 60.9 (C-1′), 63.1 (C-6), 68.7 (C-4), 72.1 (C-2), 72.6 (C-3), 75.2 (C-5), 101.2 (C-1), 115.5 (2C, C_5H_4N), 123.5 (C_2N_3H–C5), 145.2 (C_2N_3H–C4), 147.2 (C_5H_4N–C1), 152.5 (2C, C_5H_4N); HR-MS Calcd for $C_{14}H_{19}N_4O_6$ [M+H]$^+$: 339.1305, Found: 339.1302.

4.1.7.11. [1-(4′-Fluorophenyl)-1,2,3-triazol-4-yl]methyl α-D-mannopyranoside (5k). Prepared from **16k** (106 mg, 0.20 mmol) according to general procedure D. Yield: 56 mg, 78%.

$[\alpha]_D$ +78.5 (*c* 1.00, MeOH); ^{1}H NMR (500 MHz, CD_3OD): δ 3.60–3.69 (m, 2H, H-4, H-5), 3.71–3.78 (m, 2H, H-3, H-6a), 3.86 (dd, *J* = 1.7, 3.4 Hz, 1H, H-2), 3.89 (dd, *J* = 1.8, 11.8 Hz, 1H, H-6b), 4.77, 4.91 (A, B of AB, *J* = 12.5 Hz, 2H, H-1′), 4.94 (d, *J* = 1.6 Hz, 1H, H-1), 7.34, 7.89 (m, 4H, C_6H_4), 8.56 (s, 1H, C_2N_3H); ^{13}C NMR (125 MHz, CD_3OD): δ 60.9 (C-1′), 63.2 (C-6), 68.8 (C-4), 72.2 (C-2), 72.6 (C-3), 75.2 (C-5), 101.1 (C-1), 117.8 (d, *J* = 23.8 Hz, 2C, C_6H_4), 124.0 (2C, C_6H_4), 124.0 (C_2N_3H–C5), 134.9 (d, *J* = 3.8 Hz, C_6H_4–C1), 146.5 (C_2N_3H–C4), 164.1 (d, *J* = 246.3 Hz, C_6H_4–C4); HR-MS Calcd for $C_{15}H_{18}FN_3NaO_6$ [M+Na]$^+$: 378.1077, Found: 378.1079.

4.1.7.12. [1-(3′-Fluorophenyl)-1,2,3-triazol-4-yl]methyl α-D-mannopyranoside (5l). Prepared from **16l** (105 mg, 0.20 mmol) according to general procedure D. Yield: 58 mg, 81%.

$[\alpha]_D$ +73.8 (*c* 1.00, MeOH); ^{1}H NMR (500 MHz, CD_3OD): δ 3.51–3.62 (m, 2H, H-4, H-5), 3.62–3.73 (m, 2H, H-3, H-6a), 3.78 (dd, *J* = 1.6, 3.1 Hz, 1H, H-2), 3.84 (m, 1H, H-6b), 4.71 (A of AB, *J* = 12.4 Hz, 1H, H-1′a), 4.82–4.89 (m, 2H, H-1, H-1′b), 7.23 (m, 1H, C_6H_4), 7.57 (m, 1H, C_6H_4), 7.64–7.74 (m, 2H, C_6H_4), 8.61 (s, 1H, C_2N_3H); ^{13}C NMR (125 MHz, CD_3OD): δ 60.8 (C-1′), 63.1 (C-6), 68.8 (C-4), 72.1 (C-2), 72.6 (C-3), 75.2 (C-5), 101.1 (C-1), 109.1 (d, *J* = 26.3 Hz, C_6H_4), 116.9 (d, *J* = 21.3 Hz, C_6H_4), 117.3 (d, *J* = 3.8 Hz, C_6H_4), 123.8 (C_2N_3H–C5), 132.9 (d, *J* = 10.0 Hz, C_6H_4), 139.7 (d, *J* = 10.0 Hz, C_6H_4–C1), 146.6 (C_2N_3H–C4), 161.7 (d, *J* = 245.0 Hz, C_6H_4–C3); HR-MS Calcd for $C_{15}H_{18}FN_3NaO_6$ [M+Na]$^+$: 378.1077, Found: 378.1081.

4.1.7.13. [1-(4′-Methoxyphenyl)-1,2,3-triazol-4-yl]methyl α-D-mannopyranoside (5m). Prepared from **16m** (113 mg, 0.21 mmol) according to general procedure D. Yield: 58 mg, 75%.

$[\alpha]_D$ +37.4 (*c* 1.01, MeOH); ^{1}H NMR (500 MHz, CD_3OD): δ 3.54–3.64 (m, 2H, H-4, H-5), 3.65–3.74 (m, 2H, H-3, H-6a), 3.80 (dd, *J* = 1.6, 3.2 Hz, 1H, H-2), 3.81–3.87 (m, 4H, H-6b, OCH_3), 4.69, 4.83 (A, B of AB, *J* = 12.4 Hz, 2H, H-1′), 4.87 (m, 1H, H-1), 7.05, 7.68 (AA′, BB′ of AA′BB′, *J* = 9.0 Hz, 4H, C_6H_4), 8.42 (s, 1H, C_2N_3H); ^{13}C NMR (125 MHz, CD_3OD): δ 56.3 (OCH_3), 60.8 (C-1′), 63.1 (C-6), 68.8 (C-4), 72.2 (C-2), 72.6 (C-3), 75.2 (C-5), 101.0 (C-1), 116.0 (2C, C_6H_4), 123.4 (2C, C_6H_4), 123.8 (C_2N_3H–C5), 131.7 (C_6H_4–C1), 146.1 (C_2N_3H–C4), 161.7 (C_6H_4–C4); HR-MS Calcd for $C_{16}H_{21}N_3NaO_7$ [M+Na]$^+$: 390.1277, Found: 390.1279.

4.1.7.14. [1-(3′-Methoxybenzyl)-1,2,3-triazol-4-yl]ethyl α-D-mannopyranoside (6h). Prepared from **17h** (53 mg, 94 μmol) according to general procedure D. Yield: 30 mg, 81%.

$[\alpha]_D$ +45.9 (*c* 1.00, MeOH); ^{1}H NMR (500 MHz, CD_3OD): δ 2.99 (t, *J* = 6.6 Hz, 2H, H-2′), 3.41 (m, 1H, H-5), 3.57–3.75 (m, 4H, H-3, H-4, H-6a, H-1′a), 3.71 (dd, *J* = 1.7, 3.1 Hz, 1H, H-2), 3.78–3.83 (m, 4H, H-6b, OCH_3), 3.97 (dt, *J* = 6.7, 9.7 Hz, 1H, H-1′b), 4.77 (d, *J* = 1.6 Hz, 1H, H-1), 5.54 (s, 2H, CH_2Ar), 6.80–6.96, 7.29 (m, 4H, C_6H_4), 7.79 (s, 1H, C_2N_3H); ^{13}C NMR (125 MHz, CD_3OD): δ 27.2 (C-2′), 54.9 (CH_2Ar), 55.9 (OCH_3), 63.0 (C-6), 67.6 (C-1′), 68.7 (C-4), 72.2 (C-2), 72.7 (C-3), 74.9 (C-5), 101.7 (C-1), 114.8, 115.1, 121.2 (3C, C_6H_4), 124.2 (C_2N_3H–C5), 131.3 (C_6H_4), 138.4 (C_6H_4–C1), 146.7 (C_2N_3H–C4), 161.7 (C_6H_4–C3); HR-MS Calcd for $C_{18}H_{25}N_3NaO_7$ [M+Na]$^+$: 418.1590, Found: 418.1591.

4.1.7.15. [1-(4′-Nitrophenyl)-1,2,3-triazol-4-yl]ethyl α-D-mannopyranoside (6i). Prepared from **17i** (61 mg, 0.11 mmol) according to general procedure D. Yield: 37 mg, 86%.

$[\alpha]_D$ +44.4 (*c* 1.00, MeOH); ^{1}H NMR (500 MHz, CD_3OD): δ 3.13 (t, *J* = 6.5 Hz, 2H, H-2′), 3.42 (m, 1H, H-5), 3.60 (t, *J* = 9.5 Hz, 1H, H-4), 3.64–3.73 (m, 2H, H-3, H-6a), 3.78–3.88 (m, 3H, H-2, H-6b, H-1′a), 4.09 (dt, *J* = 6.6, 9.8 Hz, 1H, H-1′b), 4.83 (d, *J* = 1.5 Hz, 1H, H-1), 8.18, 8.48 (m, 4H, C_6H_4), 8.55 (s, 1H, C_2N_3H); ^{13}C NMR (125 MHz, CD_3OD): δ 27.3 (C-2′), 63.1 (C-6), 67.4 (C-1′), 68.7 (C-4), 72.2 (C-2), 72.8 (C-3), 75.0 (C-5), 101.8 (C-1), 122.0 (2C, C_6H_4), 122.5 (C_2N_3H–C5), 126.6 (2C, C_6H_4), 142.8 (C_6H_4–C1), 148.1 (C_2N_3H–C4), 148.9 (C_6H_4–C4); HR-MS Calcd for $C_{16}H_{20}N_4NaO_8$ [M+Na]$^+$: 419.1179, Found: 419.1177.

4.1.7.16. [1-(Pyridin-4′-yl)-1,2,3-triazol-4-yl]ethyl α-D-mannopyranoside (6j). Prepared from **17j** (63 mg, 0.12 mmol) according to general procedure D. Yield: 31 mg, 73%.

$[\alpha]_D$ +48.3 (*c* 1.00, MeOH); ^{1}H NMR (500 MHz, CD_3OD): δ 3.12 (t, *J* = 6.5 Hz, 2H, H-2′), 3.43 (m, 1H, H-5), 3.61 (t, *J* = 9.5 Hz, 1H, H-4),

3.64–3.73 (m, 2H, H-3, H-6a), 3.77–3.87 (m, 3H, H-2, H-6b, H-1′a), 4.08 (dt, J = 6.6, 9.8 Hz, 1H, H-1′b), 4.83 (d, J = 1.5 Hz, 1H, H-1), 7.99 (dd, J = 1.6, 4.8 Hz, 2H, C_5H_4N), 8.58 (s, 1H, C_2N_3H), 8.74 (m, 2H, C_5H_4N); ^{13}C NMR (125 MHz, CD_3OD): δ 27.2 (C-2′), 63.1 (C-6), 67.3 (C-1′), 68.7 (C-4), 72.2 (C-2), 72.7 (C-3), 75.0 (C-5), 101.8 (C-1), 115.5 (2C, C_5H_4N), 122.0 (C_2N_3H–C5), 145.3 (C_5H_4N–C1), 148.1 (C_2N_3H–C4), 152.4 (2C, C_5H_4N); HR-MS Calcd for $C_{15}H_{21}N_4O_6$ $[M+H]^+$: 353.1461, Found: 353.1460.

4.1.7.17. [1-(4′-Fluorophenyl)-1,2,3-triazol-4-yl]ethyl α-D-mannopyranoside (6k). Prepared from **17k** (65 mg, 0.12 mmol) according to general procedure D. Yield: 40 mg, 90%.

$[\alpha]_D$ +50.7 (c 1.00, MeOH); ^1H NMR (500 MHz, CD_3OD): δ 3.10 (t, J = 6.5 Hz, 2H, H-2′), 3.43 (m, 1H, H-5), 3.61 (t, J = 9.5 Hz, 1H, H-4), 3.65–3.74 (m, 2H, H-3, H-6a), 3.77–3.87 (m, 3H, H-2, H-6b, H-1′a), 4.07 (dt, J = 6.6, 9.8 Hz, 1H, H-1′b), 4.82 (d, J = 1.6 Hz, 1H, H-1), 7.34, 7.88 (m, 4H, C_6H_4), 8.33 (s, 1H, C_2N_3H); ^{13}C NMR (125 MHz, CD_3OD): δ 27.2 (C-2′), 63.1 (C-6), 67.5 (C-1′), 68.7 (C-4), 72.2 (C-2), 72.8 (C-3), 75.0 (C-5), 101.8 (C-1), 117.8 (d, J = 23.8 Hz, 2C, C_6H_4), 122.6 (C_2N_3H–C5), 124.0 (d, J = 8.8 Hz, 2C, C_6H_4), 135.0 (d, J = 2.5 Hz, C_6H_4–C1), 147.4 (C_2N_3H–C4), 164.1 (d, J = 246.3 Hz, C_6H_4–C4); HR-MS Calcd for $C_{16}H_{20}FN_3NaO_6$ $[M+Na]^+$: 392.1234, Found: 392.1238.

4.1.7.18. 1-(α-D-Mannopyranosyl)-4-phenyl-1,2,3-triazole (7n). Prepared from **20n** (50 mg, 0.11 mmol) according to general procedure D. Yield: 29 mg, 89%.

$[\alpha]_D$ +98.0 (c 1.34, MeOH); ^1H NMR (500 MHz, CD_3OD): δ 3.38 (ddd, J = 2.5, 6.6, 8.9 Hz, 1H, H-5), 3.76–3.80 (m, 2H, H-4, H-6a), 3.85 (dd, J = 2.5, 12.1 Hz, 1H, H-6b), 4.12 (dd, J = 3.5, 8.5 Hz, 1H, H-3), 4.76 (t, J = 3.1 Hz, 1H, H-2), 6.08 (d, J = 2.7 Hz, 1H, H-1), 7.34–7.38, 7.43–7.46, 7.84–7.85 (m, 5H, C_6H_5), 8.51 (s, 1H, C_2N_3H); ^{13}C NMR (125 MHz, CD_3OD): δ 62.6 (C-6), 68.7 (C-4), 70.1 (C-2), 72.6 (C-3), 78.7 (C-5), 88.5 (C-1), 122.1 (C_2N_3H–C5), 126.8, 129.5, 130.0, 131.4 (6C, C_6H_5), 149.0 (C_2N_3H–C4); HR-MS Calcd for $C_{14}H_{17}N_3NaO_5$ $[M+Na]^+$: 330.1066, Found: 330.1060.

4.1.7.19. 1-(α-D-Mannopyranosyl)-4-(4-methylphenyl)-1,2,3-triazole (7o). Prepared from **20o** (46 mg, 94 μmol) according to general procedure D. Yield: 20 mg, 65%.

$[\alpha]_D$ +84.6 (c 0.63, MeOH); ^1H NMR (500 MHz, CD_3OD): δ 2.36 (s, 3H, PhCH_3), 3.36 (ddd, J = 2.3, 6.7, 8.9 Hz, 1H, H-5), 3.74–3.78 (m, 2H, H-4, H-6a), 3.84 (dd, J = 2.4, 12.1 Hz, 1H, H-6b), 4.10 (dd, J = 3.5, 8.5 Hz, 1H, H-3), 4.74 (t, J = 3.0 Hz, 1H, H-2), 6.05 (d, J = 2.6 Hz, 1H, H-1), 7.25, 7.72 (AA′, BB′ of AA′BB′, J = 8.0 Hz, 4H, C_6H_4), 8.45 (s, 1H, C_2N_3H); ^{13}C NMR (125 MHz, CD_3OD): δ 21.3 (PhCH_3), 62.6 (C-6), 68.7 (C-4), 70.1 (C-2), 72.6 (C-3), 78.7 (C-5), 88.5 (C-1), 121.7 (C_2N_3H–C5), 126.7, 128.6, 130.6, 139.6 (6C, C_6H_5), 149.2 (C_2N_3H–C4); HR-MS Calcd for $C_{15}H_{18}N_3NaO_5$ $[M+Na]^+$: 344.1222, Found: 344.1215.

4.1.7.20. 4-(3-Chlorophenyl)-1-(α-D-mannopyranosyl)-1,2,3-triazole (7p). Prepared from **20p** (43 mg, 84 μmol) according to general procedure D. Yield: 25 mg, 87%.

$[\alpha]_D$ +89.2 (c 0.50, MeOH); ^1H NMR (500 MHz, CD_3OD): δ 3.37 (ddd, J = 2.4, 6.7, 8.7 Hz, 1H, H-5), 3.77 (dd, J = 6.6, 12.2 Hz, 1H, H-6a), 3.78 (t, J = 8.6 Hz, 1H, H-4), 3.87 (dd, J = 2.4, 12.1 Hz, 1H, H-6b), 4.11 (dd, J = 3.5, 8.3 Hz, 1H, H-3), 4.75 (t, J = 3.1 Hz, 1H, H-2), 6.07 (d, J = 2.6 Hz, 1H, H-1), 7.37 (d, J = 8.1 Hz, 1H, C_6H_4-H6), 7.44 (t, J = 7.9 Hz, 1H, C_6H_4–H5), 7.79 (d, J = 7.7 Hz, 1H, C_6H_4–H4), 7.90 (s, 1H, C_6H_4-H2), 8.58 (s, 1H, C_2N_3H); ^{13}C NMR (125 MHz, CD_3OD): δ 62.6 (C-6), 68.7 (C-4), 70.1 (C-2), 72.6 (C-3), 78.7 (C-5), 88.6 (C-1), 122.7 (C_2N_3H–C5), 125.0, 126.6, 129.4, 131.6, 133.5, 136.0 (C_6H_4), 147.7 (C_2N_3H–C4); HR-MS Calcd for $C_{14}H_{16}ClN_3NaO_5$ $[M+Na]^+$: 364.0676, Found: 364.0676.

4.1.7.21. 4-(4-Trifluoromethylphenyl)-1-(α-D-mannopyranosyl)-1,2,3-triazole (7q). Prepared from **20q** (46 mg, 85 μmol) according to general procedure D. Yield: 27 mg, 86%.

$[\alpha]_D$ +83.4 (c 0.34, MeOH); ^1H NMR (500 MHz, CD_3OD): δ 3.38 (m, 1H, H-5), 3.77–3.81 (m, 2H, H-4, H-6a), 3.85 (dd, J = 1.9, 12.0 Hz, 1H, H-6b), 4.11 (dd, J = 3.3, 8.4 Hz, 1H, H-3), 4.76 (t, J = 2.7 Hz, 1H, H-2), 6.10 (d, J = 2.3 Hz, 1H, H-1), 7.76, 8.06 (AA′, BB′ of AA′BB′, J = 8.0 Hz, 4H, C_6H_4), 8.66 (s, 1H, C_2N_3H); ^{13}C NMR (125 MHz, CD_3OD): δ 62.6 (C-6), 68.7 (C-4), 70.1 (C-2), 72.6 (C-3), 78.8 (C-5), 88.6 (C-1), 123.2 (C_2N_3H–C5), 125.6 (q, J = 272 Hz, CF_3), 127.0 (q, J = 3.7 Hz, 2C, C_6H_4–C3, C5), 127.2 (2C, C_6H_4–C2, C6), 131.2 (d, J = 32.4 Hz, C_6H_4–C4), 135.5 (C_6H_4–C1), 147.6 (C_2N_3H–C4); HR-MS Calcd for $C_{15}H_{16}F_3N_3NaO_5$ $[M+Na]^+$: 398.0940, Found: 398.0942.

4.1.7.22. 1-(α-D-Mannopyranosyl)-4-(3-pyridyl)-1,2,3-triazole (7r). Prepared from **20r** (47 mg, 98 μmol) according to general procedure D. Yield: 28 mg, 92%.

$[\alpha]_D$ +86.7 (c 0.93, MeOH); ^1H NMR (500 MHz, CD_3OD): δ 3.40 (ddd, J = 2.3, 6.6, 8.6 Hz, 1H, H-5), 3.77–3.82 (m, 2H, H-4, H-6a), 3.86 (dd, J = 2.4, 12.1 Hz, 1H, H-6b), 4.11 (dd, J = 3.5, 8.4 Hz, 1H, H-3), 4.76 (t, J = 3.1 Hz, 1H, H-2), 6.11 (d, J = 2.7 Hz, 1H, H-1), 7.54 (dd, J = 5.0, 7.8 Hz, 1H, C_5H_4N-H5), 8.31 (m, 1H, C_5H_4N-H6), 8.53 (dd, J = 1.4, 4.9 Hz, 1H, C_5H_4N-H4), 8.68 (s, 1H, C_2N_3H), 9.04 (d, J = 1.5, 1H, C_5H_4N–H2); ^{13}C NMR (125 MHz, CD_3OD): δ 62.6 (C-6), 68.7 (C-4), 70.1 (C-2), 72.6 (C-3), 78.8 (C-5), 88.6 (C-1), 123.1 (C_2N_3H–C5), 125.6 (C_5H_4N–C5), 128.5 (C_5H_4N–C1), 135.0 (C_5H_4N–C6), 145.6 (C_2N_3H–C4), 147.3 (C_5H_4N–C2), 149.7 (C_5H_4N–C4); HR-MS Calcd for $C_{13}H_{16}N_4NaO_5$ $[M+Na]^+$: 331.1018, Found: 331.1013.

4.1.7.23. 1-(α-D-Mannopyranosyl)-4-phenoxymethyl-1,2,3-triazole (7s). Prepared from **20s** (46 mg, 90 μmol) according to general procedure D. Yield: 27 mg, 89%.

$[\alpha]_D$ +57.0 (c 0.90, MeOH); ^1H NMR (500 MHz, CD_3OD): δ 3.30 (m, 1H, H-5), 3.70–3.74 (m, 2H, H-4, H-6a), 3.78 (dd, J = 1.8, 12.1 Hz, 1H, H-6b), 4.04 (dd, J = 3.2, 8.4 Hz, 1H, H-3), 4.67 (m, 1H, H-2), 5.14 (s, 2H, CH_2OPh), 6.00 (d, J = 1.7 Hz, 1H, H-1), 6.91 (t, J = 7.3 Hz, 1H, C_6H_5–H4), 6.96 (d, J = 8.1 Hz, 2H, C_6H_5–H2, H6), 7.24 (t, J = 7.8 Hz, 2H, C_6H_5–H3, H5), 8.20 (s, 1H, C_2N_3H); ^{13}C NMR (125 MHz, CD_3OD): δ 62.2 (CH_2OPh), 62.5 (C-6), 68.6 (C-4), 70.1 (C-2), 72.5 (C-3), 78.6 (C-5), 88.4 (C-1), 115.8 (2C, C_6H_5–C2, C6), 122.3 (C_6H_5–C4), 125.3 (C_2N_3H–C5), 130.5 (2C, C_6H_5–C3, C5), 145.4 (C_2N_3H–C4), 159.7 (C_6H_5–C1); HR-MS Calcd for $C_{15}H_{19}N_3NaO_5$ $[M+Na]^+$: 360.1172, Found: 360.1171.

4.1.7.24. 1-(α-D-Mannopyranosyl)methyl-4-phenyl-1,2,3-triazole (8n). Prepared from **25n** (38 mg, 78 μmol) according to general procedure D. Yield: 22 mg, 87%.

$[\alpha]_D$ +30.6 (c 0.91, MeOH); ^1H NMR (500 MHz, CD_3OD): δ 3.73–3.75 (m, 2H, H-4, H-6a), 3.79–3.85 (m, 3H, H-2, H-3, H-5), 3.88 (dd, J = 7.2, 11.5 Hz, 1H, H-6b), 4.25 (dt, J = 4.8, 7.9 Hz, 1H, H-1), 4.73 (dd, J = 8.0, 14.4 Hz, 1H, H-1′a), 4.76 (dd, J = 4.5, 14.3 Hz, 1H, H-1′b), 7.33 (t, J = 7.7 Hz, 1H, C_6H_5-H4), 7.42 (t, J = 7.8 Hz, 2H, C_6H_5-H3, H5), 7.81 (d, J = 8.0 Hz, 2H, C_6H_5-H2, H6), 8.45 (s, 1H, C_2N_3H); ^{13}C NMR (125 MHz, CD_3OD): δ 50.9 (C-1′), 62.1 (C-6), 69.1 (C-2), 70.0 (C-4), 72.5 (C-3), 74.9 (C-1), 78.5 (C-5), 123.4 (C_2N_3H–C5), 126.7, 129.3, 129.9, 131.8 (6C, C_6H_5), 148.8 (C_2N_3H–C4); HR-MS Calcd for $C_{15}H_{19}NaN_3O_5$ $[M+Na]^+$: 344.1222, Found: 344.1222.

4.1.7.25. 1-(α-D-Mannopyranosyl)methyl-4-(4-methylphenyl)-1,2,3-triazole (8o). Prepared from **25o** (42 mg, 84 μmol) according to general procedure D. Yield: 25 mg, 87%.

$[\alpha]_D$ +33.8 (c 1.12, MeOH); ^1H NMR (500 MHz, CD_3OD): δ 2.35 (PhCH_3), 3.72–3.76 (m, 2H, H-4, H-6a), 3.80 (dt, J = 3.2, 7.1 Hz, 1H, H-5), 3.81–3.85 (m, 2H, H-2, H-3), 3.87 (dd, J = 7.1, 11.5 Hz,

1H, H-6b), 4.24 (dt, J = 5.1, 7.4 Hz, 1H, H-1), 4.72–4.75 (m, 2H, H-1′), 7.24, 7.69 (AA′, BB′ of AA′BB′, J = 8.0 Hz, 4H, C_6H_4), 8.40 (s, 1H, C_2N_3H); ^{13}C NMR (125 MHz, CD_3OD): δ 21.3 ($PhCH_3$), 50.8 (C-1′), 62.0 (C-6), 69.1 (C-2), 69.9 (C-4), 72.4 (C-3), 75.0 (C-1), 78.4 (C-5), 123.0 (C_2N_3H–C5), 126.6, 128.9, 130.5, 139.3 (6C, C_6H_5), 148.9 (C_2N_3H–C4); HR-MS Calcd for $C_{16}H_{21}NaN_3O_5$ [M+Na]$^+$: 358.1379, Found: 358.1380.

4.1.7.26. 4-(3-Chlorophenyl)-1-(α-D-mannopyranosyl)methyl-1,2,3-triazole (8p). Prepared from **25p** (40 mg, 77 μmol) according to general procedure D. Yield: 23 mg, 83%.

$[\alpha]_D$ +31.5 (c 1.05, MeOH); ^1H NMR (500 MHz, CD_3OD): δ 3.73 (m, 1H, H-4), 3.74 (dd, J = 3.0, 11.5 Hz, 1H, H-6a), 3.79–3.82 (m, 2H, H-3, H-5), 3.83 (dd, J = 3.4, 8.7 Hz, 1H, H-2), 3.89 (dd, J = 7.4, 11.6 Hz, 1H, H-6b), 4.24 (dt, J = 4.7, 7.9 Hz, 1H, H-1), 4.73 (dd, J = 8.0, 14.4 Hz, 1H, H-1′a), 4.77 (dd, J = 4.4, 14.5 Hz, 1H, H-1′b), 7.33 (dd, J = 0.9, 8.1 Hz, 1H, C_6H_4-H6), 7.41 (t, J = 7.9 Hz, 1H, C_6H_4–H5), 7.74 (d, J = 7.8 Hz, 1H, C_6H_4–H4), 7.90 (t, J = 1.6 Hz, 1H, C_6H_4-H2), 8.51 (s, 1H, C_2N_3H); ^{13}C NMR (125 MHz, CD_3OD): δ 50.9 (C-1′), 62.0 (C-6), 69.0 (C-2), 70.0 (C-4), 72.4 (C-3), 74.7 (C-1), 78.5 (C-5), 124.0 (C_2N_3H–C5), 124.9, 126.5, 129.1, 131.5, 133.9, 135.9 (6C, C_6H_4), 147.4 (C_2N_3H–C4); HR-MS Calcd for $C_{15}H_{18}ClNaN_3O_5$ [M+Na]$^+$: 378.0833, Found: 378.0833.

4.1.7.27. 4-(4-Trifluoromethylphenyl)-1-(α-D-mannopyranosyl)methyl-1,2,3-triazole (8q). Prepared from **25q** (47 mg, 84 μmol) according to general procedure D. Yield: 28 mg, 86%.

$[\alpha]_D$ +32.6 (c 1.03, MeOH); ^1H NMR (500 MHz, CD_3OD): δ 3.73–3.76 (m, 2H, H-4, H-6a), 3.81–3.86 (m, 3H, H-2, H-3, H-5), 3.89 (dd, J = 7.5, 11.5 Hz, 1H, H-6b), 4.25 (dt, J = 4.8, 7.9 Hz, 1H, H-1), 4.76 (dd, J = 8.0, 14.5 Hz, 1H, H-1′a), 4.79 (dd, J = 4.4, 14.5 Hz, 1H, H-1′b), 7.72, 8.01 (AA′, BB′ of AA′BB′, J = 8.2 Hz, 4H, C_6H_4), 8.60 (s, 1H, C_2N_3H); ^{13}C NMR (125 MHz, CD_3OD): δ 51.0 (C-1′), 62.0 (C-6), 69.0 (C-2), 70.0 (C-4), 72.4 (C-3), 74.7 (C-1), 78.6 (C-5), 124.5 (C_2N_3H–C5), 125.6 (q, J = 271 Hz, CF_3), 126.9 (q, J = 3.7 Hz, 2C, C_6H_4–C3, C5), 127.0 (2C, C_6H_4–C2, C6), 130.9 (q, J = 32.4 Hz, C_6H_4–C4), 135.7 (C_6H_4–C1), 147.2 (C_2N_3H–C4); HR-MS Calcd for $C_{16}H_{18}F_3NaN_3O_5$ [M+Na]$^+$: 412.1096, Found: 412.1095.

4.1.7.28. 1-(α-D-Mannopyranosyl)methyl-4-(3-pyridyl)-1,2,3-triazole (8r). Prepared from **25r** (44 mg, 90 μmol) according to general procedure D. Yield: 24 mg, 83%.

$[\alpha]_D$ +31.2 (c 0.99, MeOH); ^1H NMR (500 MHz, CD_3OD): δ 3.71–3.74 (m, 2H, H-4, H-6a), 3.80–3.83 (m, 3H, H-2, H-3, H-5), 3.89 (dd, J = 7.7, 11.6 Hz, 1H, H-6b), 4.23 (dt, J = 4.6, 8.6 Hz, 1H, H-1), 4.76 (dd, J = 8.4, 14.4 Hz, 1H, H-1′a), 4.80 (dd, J = 4.2, 14.4 Hz, 1H, H-1′b), 7.53 (dd, J = 5.0, 7.9 Hz, 1H, C_5H_4N-H5), 8.28 (d, J = 8.0 Hz, 1H, C_5H_4N-H6), 8.51 (d, J = 4.8 Hz, 1H, C_5H_4N-H4), 8.63 (s, 1H, C_2N_3H), 9.02 (s, 1H, C_5H_4N–H2); ^{13}C NMR (125 MHz, CD_3OD): δ 48.1 (C-1′), 60.6 (C-6), 67.2 (C-2), 68.5 (C-4), 70.6 (C-3), 75.1 (C-1), 76.2 (C-5), 123.2 (C_2N_3H–C5), 124.5 (C_5H_4N–C5), 126.82 (C_5H_4N–C1), 134.3 (C_5H_4N–C6), 144.4 (C_2N_3H–C4), 145.7 (C_5H_4N–C2), 148.4 (C_5H_4N–C4); HR-MS Calcd for $C_{14}H_{18}NaN_4O_5$ [M+Na]$^+$: 345.1175, Found: 345.1175.

4.1.7.29. 1-(α-D-Mannopyranosyl)methyl-4-phenoxymethyl-1,2,3-triazole (8s). Prepared from **25s** (41 mg, 79 μmol) according to general procedure D. Yield: 23 mg, 83%.

$[\alpha]_D$ +22.8 (c 1.01, MeOH); ^1H NMR (500 MHz, CD_3OD): δ 3.69–3.76 (m, 3H, H-4, H-5, H-6a), 3.79–3.82 (m, 2H, H-2, H-3), 3.83 (dd, J = 6.5, 11.5 Hz, 1H, H-6b), 4.19 (dt, J = 5.0, 7.0 Hz, 1H, H-1), 4.69 (dd, J = 7.5, 14.5 Hz, 1H, H-1′a), 4.72 (dd, J = 5.0, 14.5 Hz, 1H, H-1′b), 5.15 (s, 2H, CH_2OPh), 6.94 (t, J = 7.4 Hz, 1H, C_6H_5-H4), 7.00 (d, J = 8.1 Hz, 2H, C_6H_5-H2, H6), 7.27 (m, 2H, C_6H_5-H3, H5), 8.17 (s, 1H, C_2N_3H); ^{13}C NMR (125 MHz, CD_3OD): δ 50.9 (C-1′), 62.0 (C-6), 62.3 (CH_2OPh), 69.0 (C-2), 69.8 (C-4), 72.4 (C-3), 74.9 (C-1), 78.4 (C-5), 115.9 (2C, C_6H_5–C2, C6), 122.2 (C_6H_5–C4), 126.4 (C_2N_3H–C5), 130.5 (2C, C_6H_5–C3, C5), 145.0 (C_2N_3H–C4), 159.8 (C_6H_5–C1); HR-MS Calcd for $C_{16}H_{21}N_3NaO_5$ [M+Na]$^+$: 374.1328, Found: 374.1328.

4.2. Biological evaluation

4.2.1. Competitive binding assay

A recombinant protein consisting of the CRD of FimH linked with a thrombin cleavage site to a 6His-tag (FimH-CRD-Th-6His) was expressed in *E. coli* strain HM125 and purified by affinity chromatography.[45] To determine the affinity of the various FimH antagonists, an competitive binding assay described previously[45] was applied. Microtiter plates (F96 MaxiSorp, Nunc) were coated with 100 μL/well of a 10 μg/mL solution of FimH-CRD-Th-6His in 20 mM HEPES, 150 mM NaCl and 1 mM $CaCl_2$, pH 7.4 (assay buffer) overnight at 4 °C. The coating solution was discarded and the wells were blocked with 150 μL/well of 3% BSA in assay buffer for 2 h at 4 °C. After three washing steps with assay buffer (150 μL/well), a four-fold serial dilution of the test compound (50 μL/well) in assay buffer containing 5% DMSO and streptavidin-peroxidase coupled TM-PAA polymer (50 μL/well of a 0.5 μg/mL solution) were added. On each individual microtiter plate *n*-heptyl α-D-mannopyranoside (**1b**) was tested in parallel. The plates were incubated for 3 h at 25 °C and 350 rpm and then carefully washed four times with 150 μL/well assay buffer. After the addition of 100 μL/well of ABTS-substrate, the colorimetric reaction was allowed to develop for 4 min, then stopped by the addition of 2% aqueous oxalic acid before the optical density (OD) was measured at 415 nm on a microplate-reader (Spectramax 190, Molecular Devices, California, USA). The IC_{50} values of the compounds tested in duplicates were calculated with prism software (GraphPad Software, Inc., La Jolla, USA). The IC_{50} defines the molar concentration of the test compound that reduces the maximal specific binding of TM-PAA polymer to FimH-CRD by 50%. The relative IC_{50} (rIC_{50}) is the ratio of the IC_{50} of the test compound to the IC_{50} of **1b**.

4.2.2. Aggregometry assay

The aggregometry assay was carried out as previously described.[46] In short, the percentage of aggregation of *E. coli* UTI89[59] (UTI89wt) with guinea pig erythrocytes (GPE) was quantitatively determined by measuring the optical density at 740 nm and 37 °C under stirring at 1000 rpm using an APACT 4004 aggregometer (Endotell AG, Allschwil, Switzerland). GPE were separated from guinea pig blood (Charles River Laboratories, Sulzfeld, Germany) using Histopaque (density of 1.077 g/mL at 24 °C, Sigma-Aldrich, Buchs, Switzerland). Prior to the measurements, the cell densities of *E. coli* and GPE were adjusted to an OD_{600} of 4, corresponding to 1.9×10^8 CFU/mL and 2.2×10^6 cells/mL respectively. For the calibration of the instrument, the aggregation of protein poor plasma (PPP) using PBS alone was set as 100% and the aggregation of protein rich plasma (PRP) using GPE as 0%. After calibration, measurements were performed with 250 μL GPE and 50 μL bacterial suspension and the aggregation monitored over 600 s. After the aggregation phase of 600 s, 25 μL of antagonist in PBS were added to each cuvette and disaggregation was monitored for 1400 s. UTI89 Δ*fimA-H* was used as negative control.

4.3. Determination of the pharmacokinetic parameters

4.3.1. Materials

Dimethyl sulfoxide (DMSO) and 1-octanol were purchased from Sigma-Aldrich (St. Louis MI, USA). PAMPA System Solution, GIT-0 Lipid Solution, and Acceptor Sink Buffer were ordered from pion (Woburn MA, USA). Acetonitrile (MeCN) was bought from Acros Organics (Geel, Belgium).

4.3.2. LC–MS measurements

Analyses were performed using an Agilent 1100/1200 Series HPLC System coupled to a 6410 Triple Quadrupole mass detector (Agilent Technologies, Inc., Santa Clara CA, USA) equipped with electrospray ionization. The system was controlled with the Agilent MassHunter Workstation Data Acquisition software (version B.01.04). The column used was an Atlantis® T3 C18 column (2.1 x 50 m) with a 3 μm particle size (Waters Corp., Milford MA, USA). The mobile phase consisted of two eluents: solvent A (H_2O, containing 0.1% formic acid, v/v) and solvent B (MeCN, containing 0.1% formic acid, v/v), both delivered at 0.6 mL/min. The gradient was ramped from 95% A/5% B to 5% A/95% B over 1 min, and then hold at 5% A/95% B for 0.1 min. The system was then brought back to 95% A/5% B, resulting in a total duration of 4 min. MS parameters such as fragmentor voltage, collision energy and polarity were optimized individually for each compound, and the molecular ion was followed for each compound in the multiple reaction monitoring mode. The concentrations of the analytes were quantified by the Agilent Mass Hunter Quantitative Analysis software (version B.01.04).

4.3.3. log $D_{7.4}$ determination

The *in silico* prediction tool ALOGPS[60] was used to estimate the log *P* values. Depending on these values, the compounds were classified into three categories: hydrophilic compounds (log *P* below zero), moderately lipophilic compounds (log *P* between zero and one) and lipophilic compounds (log *P* above one). For each category, two different ratios (volume of 1-octanol to volume of buffer) were defined as experimental parameters:

Compound type	log *P*	Ratios (1-octanol:buffer)
Hydrophilic	<0	30:140, 40:130
Moderately lipophilic	0–1	70:110, 110:70
Lipophilic	>1	3:180, 4:180

Equal amounts of phosphate buffer (0.1 M, pH 7.4) and 1-octanol were mixed and shaken vigorously for 5 min to saturate the phases. The mixture was left until separation of the two phases occurred, and the buffer was retrieved. Stock solutions of the test compounds were diluted with buffer to a concentration of 1 μM. For each compound, six determinations, that is, three determinations per 1-octanol : buffer ratio, were performed in different wells of a 96-well plate. The respective volumes of buffer containing analyte (1 μM) were pipetted to the wells and covered by saturated 1-octanol according to the chosen volume ratio. The plate was sealed with aluminium foil, shaken (1350 rpm, 25 °C, 2 h) on a Heidoph Titramax 1000 plate-shaker (Heidolph Instruments GmbH & Co. KG, Schwabach, Germany) and centrifuged (2000 rpm, 25 °C, 5 min, 5804 R Eppendorf centrifuge, Hamburg, Germany). The aqueous phase was transferred to a 96-well plate for analysis by liquid chromatography-mass spectrometry (LC-MS).

log $D_{7.4}$ was calculated from the 1-octanol : buffer ratio (o:b), the initial concentration of the analyte in buffer (1 μM), and the concentration of the analyte in buffer (c_B) with equilibration:

$$\log D_{7.4} = \left(\frac{1\mu M - c_B}{c_B} \times \frac{1}{o:b} \right)$$

The average of the three log $D_{7.4}$ values per 1-octanol:buffer ratio was calculated. If the two mean values obtained for a compound did not differ by more than 0.1 unit, the results were accepted.

4.3.4. Parallel artificial membrane permeation assay (PAMPA)

log P_e was determined in a 96-well format with the PAMPA[50] permeation assay. For each compound, measurements were performed at three pH values (5.0, 6.2 and 7.4) in quadruplicates. For this purpose, 12 wells of a deep well plate, that is, four wells per pH-value, were filled with 650 μL PAMPA System Solution. Samples (150 μL) were withdrawn from each well to determine the blank spectra by UV-spectroscopy (SpectraMax 190, Molecular Devices, Silicon Valley Ca, USA). Then, analyte dissolved in DMSO was added to the remaining PAMPA System Solution to yield 50 μM solutions. To exclude precipitation, the optical density was measured at 650 nm, with 0.01 being the threshold value. Solutions exceeding this threshold were filtrated. Afterwards, samples (150 μL) were withdrawn to determine the reference spectra. Further 200 μL were transferred to each well of the donor plate of the PAMPA sandwich (pIon, Woburn MA, USA, P/N 110 163). The filter membranes at the bottom of the acceptor plate were impregnated with 5 μL of GIT-0 Lipid Solution and 200 μL of Acceptor Sink Buffer were filled into each acceptor well. The sandwich was assembled, placed in the GutBox™, and left undisturbed for 16 h. Then, it was disassembled and samples (150 μL) were transferred from each donor and acceptor well to UV-plates. Quantification was performed by both UV-spectroscopy and LC-MS. log P_e-values were calculated with the aid of the PAMPA Explorer Software (pIon, version 3.5).

4.3.5. Thermodynamic solubility

Microanalysis tubes (Labo-Tech J. Stofer LTS AG, Muttenz, Switzerland) were charged with 1 mg of solid substance and 250 μL of phosphate buffer (50 mM, pH 6.5). The samples were briefly shaken by hand, then sonicated for 15 min and vigorously shaken (600 rpm, 25 °C, 2 h) on a Eppendorf Thermomixer comfort. Afterwards, the samples were left undisturbed for 24 h. After measuring the pH, the saturated solutions were filtered through a filtration plate (MultiScreen® HTS, Millipore, Billerica MA, USA) by centrifugation (1500 rpm, 25 °C, 3 min). Prior to concentration determination by LC-MS, the filtrates were diluted (1:1, 1:10 and 1:100 or, if the results were outside of the calibration range, 1:1000 and 1:10000). The calibration was based on six values ranging from 0.1 to 10 μg/mL.

Acknowledgement

We thank the Swiss National Science Foundation (project K-32KI-120904) for their support.

Supplementary data

Supplementary data (HRMS and HPLC data of target compounds **5**–**8**) associated with this article can be found, in the online version, at doi:10.1016/j.bmc.2011.08.057.

References and notes

1. Wiles, T. J.; Kulesus, R. R.; Mulvey, M. A. *Exp. Mol. Pathol.* **2008**, *85*, 11.
2. Finn, S. D. *N. Engl. J. Med.* **2003**, *349*, 259.
3. Hooton, T. M. *Int. J. Antimicrob. Agents* **2001**, *17*, 259.
4. Gouin, S. G.; Wellens, A.; Bouckaert, J.; Kovensky, J. *ChemMedChem* **2009**, *4*, 749.
5. Rosen, D. A.; Hung, C. S.; Kline, K. A.; Hultgren, S. J. *Infect. Immun.* **2008**, *76*, 4290.
6. Capitani, G.; Eidam, O.; Glockshuber, R.; Grutter, M. G. *Microbes Infect.* **2006**, *8*, 2284.
7. Mulvey, M. A. *Cell Microbiol.* **2002**, *4*, 257.
8. Choudhury, D.; Thompson, A.; Stojanoff, V.; Langermann, S.; Pinkner, J.; Hultgren, S. J.; Knight, S. D. *Science* **1999**, *285*, 1061.
9. Bouckaert, J.; Berglund, J.; Schembri, M.; Genst, E. D.; Cools, L.; Wuhrer, M.; Hung, C. S.; Pinkner, J.; Slättergärd, R.; Zavialov, A.; Choudhury, D.; Langermann, S.; Hultgren, S. J.; Wyns, L.; Klemm, P.; Oscarson, S.; Knight, S. D.; Greve, H. D. *Mol. Microbiol.* **2005**, *55*, 441.
10. Wellens, A.; Garofalo, C.; Nguyen, H.; Van Gerven, N.; Slättergärd, R.; Hernalsteens, J.-P.; Wyns, L.; Oscarson, S.; De Greve, H.; Hultgren, S.; Bouckaert, J. *PLoS ONE* **2008**, *3*, 4.

11. Han, Z.; Pinker, J. S.; Ford, B.; Obermann, R.; Nolan, W.; Wildman, S. A.; Hobbs, D.; Ellenberger, T.; Cusumano, C. K.; Hultgren, S. J.; Janetka, J. W. *J. Med. Chem.* **2010**, *53*, 4779.
12. Langermann, S.; Mollby, R.; Burlein, J. E.; Palaszynski, S. R.; Auguste, C. G.; DeFusco, A.; Strouse, R.; Schenerman, M. A.; Hultgren, S. J.; Pinkner, J. S.; Winberg, J.; Guldevall, L.; Soderhall, M.; Ishikawa, K.; Normark, S.; Koenig, S. *J. Infect. Dis.* **2000**, *181*, 774.
13. Langermann, S.; Palaszynski, S.; Barnhart, M.; Auguste, G.; Pinkner, J. S.; Burlein, J.; Barren, P.; Koenig, S.; Leath, S.; Jones, C. H.; Hultgren, S. J. *Science* **1997**, *276*, 607.
14. Bouckaert, J.; Mackenzie, J.; de Paz, J. L.; Chipwaza, B.; Choudhury, D.; Zavialov, A.; Mannerstedt, K.; Anderson, J.; Pierard, D.; Wyns, L.; Seeberger, P. H.; Oscarson, S.; De Greve, H.; Knight, S. D. *Mol. Microbiol.* **2006**, *61*, 1556.
15. (a) Sharon, N. *Biochim. Biophys. Acta* **2006**, *1760*, 527; (b) Ofek, I.; Hasty, D. L.; Sharon, N. *FEMS Immun. Med. Microbiol.* **2003**, *38*, 181; (c) Sharon, N.; Ofek, I. In *Protein-Carbohydrate Interactions in Infectious Diseases*; Bewley, C. A., Ed.; RSC Biomolecular Sciences: Cambridge, UK, 2006; pp 49–72.
16. (a) Firon, N.; Ofek, I.; Sharon, N. *Biochem. Biophys. Res. Commun.* **1982**, *105*, 1426; (b) Firon, N.; Ofek, I.; Sharon, N. *Carbohydr. Res.* **1983**, *120*, 235; (c) Sharon, N. *FEBS Lett.* **1987**, *217*, 145.
17. (a) Neeser, J.-R.; Koellreutter, B.; Wuersch, P. *Infect. Immun.* **1986**, *52*, 428; (b) Lindhorst, T. K. *Top. Curr. Chem.* **2002**, *218*, 201. review; (c) Patel, A.; Lindhorst, T. K. *Carbohydr. Res.* **2006**, *341*, 1657; (d) Nagahori, N.; Lee, R. T.; Nishimura, S.-I.; Pagé, S.; Roy, R.; Lee, Y. C. *ChemBioChem* **2002**, *3*, 836; (e) Appeldoorn, C. C. M.; Joosten, J. A. F.; Maate, F. A.; Dobrindt, U.; Hacker, J.; Liskamp, R. M. J.; Khan, A. S.; Pieters, R. J. *Tetrahedron: Asymmetry* **2005**, *16*, 361; (f) Touaibia, M.; Wellens, A.; Shiao, T. C.; Wang, Q.; Sirois, S.; Bouckaert, J.; Roy, R. *ChemMedChem* **2007**, *2*, 1190.
18. (a) Firon, N.; Ashkenazi, S.; Mirelman, D.; Ofek, I.; Sharon, N. *Infect. Immun.* **1987**, *55*, 472; (b) Lindhorst, T. K.; Kötter, S.; Kubisch, J.; Krallmann-Wenzel, U.; Ehlers, S.; Kren, V. *Eur. J. Org. Chem.* **1998**, 1669; (c) Sperling, O.; Fuchs, A.; Lindhorst, T. K. *Org. Biomol. Chem.* **2006**, *4*, 3913; (d) Berglund, J.; Bouckaert, J.; De Greve, H.; Knight, S. PCT/US 2005/089733, 2005.
19. Klein, T.; Abgottspon, D.; Wittwer, M.; Rabbani, S.; Herold, J.; Jiang, X.; Kleeb, S.; Lüthi, C.; Scharenberg, M.; Bezençon, J.; Gubler, E.; Pang, L.; Smiesko, M.; Cutting, B.; Schwardt, O.; Ernst, B. *J. Med. Chem.* **2010**, *53*, 8627.
20. Hung, C. S.; Bouckaert, J.; Hung, D.; Pinkner, J.; Widberg, C.; Defusco, A.; Auguste, C. G.; Strouse, R.; Langermann, S.; Waksman, G.; Hultgren, S. J. *Mol. Microbiol.* **2002**, *44*, 903.
21. Ernst, B.; Magnani, J. L. *Nat. Rev. Drug Disc.* **2009**, *8*, 661.
22. Becke, A. D. *J. Chem. Phys.* **1993**, *98*, 5648.
23. Stephens, P. J.; Devlin, F. J.; Chabalowski, C. F.; Frisch, M. J. *J. Phys. Chem.* **1994**, *98*, 11623.
24. Frisch, M. J.; Trucks, G. W.; Schlegel, H. B.; Scuseria, G. E.; Robb, M. A.; Cheeseman, J. R.; Montgomery, J., J.A.; Vreven, T.; Kudin, T. K. N.; Burant, J. C. et al. *Gaussian 2003*, Gaussian Inc: Pittsburgh, PA, 2003.
25. Sancho-Garcia, J. C.; Cornil, J. *J. Chem. Theory Comput.* **2005**, *1*, 581.
26. *Glide*, version 5.5; Schrödinger, LLC: New York, NY, 2009.
27. *Desmond Molecular Dynamics System*, version 2.2; D. E. Shaw Research: New York, NY, 2009.
28. Humphrey, W.; Dalke, A.; Schulten, K. *J. Mol. Graphics* **1996**, *14*, 33.
29. Kaufman, R. J.; Sidhu, R. S. *J. Org. Chem.* **1982**, *47*, 4941.
30. (a) Lamara, K.; Smalley, R. K. *Tetrahedron* **1991**, *47*, 2277; (b) Li, Y.; Gao, L.-X.; Han, F.-S. *Chem. Eur. J.* **2010**, *16*, 7969.
31. Hu, M.; Li, J.; Yao, S. Q. *Org. Lett.* **2008**, *10*, 5529.
32. (a) Sawanishi, H.; Tajima, K.; Tsuchiya, T. *Chem. Pharm. Bull.* **1987**, *35*, 4101; (b) Sapountzis, I.; Ettmayer, P.; Klein, C.; Mantoulidis, A.; Steegmaier, M.; Steurer, S.; Waizenegger, I. PCT/EP2008/058432, 2008.
33. (a) Tornøe, C. W.; Meldal, M. In *Peptides: The Wave of the Future: Proceedings of the Second International and the Seventeenth American Peptide Symposium*; Lebl, M., Houghten, R. A., Eds.; Springer, 2001; p 263; (b) Tornøe, C. W.; Christensen, C.; Meldal, M. *J. Org. Chem.* **2002**, *67*, 3057.
34. Kolb, H. C.; Sharpless, K. B. *Angew. Chem., Int. Ed.* **2001**, *40*, 2004.
35. Palomo, C.; Aizpurua, J. M.; Balentová, E.; Azcune, I.; Santos, J. I.; Jiménez-Barbero, J.; Cañada, J.; Miranda, J. I. *Org. Lett.* **2008**, *10*, 2227.
36. (a) Tietze, L.; Bothe, U. *Chem. Eur. J.* **1998**, *4*, 1179; (b) Gouin, S. G.; Vanquelef, E.; García Fernández, J. M.; Ortiz Mellet, C.; Dupradeau, F.-Y.; Kovensky, J. *J. Org. Chem.* **2007**, *72*, 9032.
37. Fernández-Megía, E.; Correa, J.; Rodríguez-Meizoso, I.; Riguera, R. *Macromolecules* **2006**, *39*, 2113.
38. Buckle, D. R.; Rockell, C. J. M. *J. Chem. Soc., Perkin Trans. 1* **1982**, 627.
39. Stefely, J. A.; Palchaudhuri, R.; Miller, P. A.; Peterson, R. J.; Moraski, G. C.; Hergenrother, P. J.; Miller, M. J. *J. Med. Chem.* **2010**, *53*, 3389.
40. Benati, L.; Bencivenni, G.; Leardini, R.; Minozzi, M.; Nanni, D.; Scialpi, R.; Spagnolo, P.; Zanardi, G. *J. Org. Chem.* **2006**, *71*, 5822.
41. Ito, S.; Satoh, A.; Nagatomi, Y.; Hirata, Y.; Suzuki, G.; Kimura, T.; Satow, A.; Maehara, S.; Hikichi, H.; Hata, M.; Kawamoto, H.; Ohta, H. *Bioorg. Med. Chem.* **2008**, *16*, 9817.
42. (a) Kunz, H.; Pfrengle, W.; Rück, K.; Sager, W. *Synthesis* **1991**, *103*, 1039; (b) Györgydeak, Z.; Szilagyi, L.; Paulsen, H. *J. Carbohydr. Chem.* **1993**, *12*, 139.
43. (a) Myers, R. W.; Lee, Y. C. *Carbohydr. Res.* **1986**, *154*, 145; (b) Köll, P.; Förtsch, A. *Carbohydr. Res.* **1987**, *171*, 301.
44. Titz, A.; Radic, Z.; Schwardt, O.; Ernst, B. *Tetrahedron Lett.* **2006**, *47*, 2383.
45. Rabbani, S.; Jiang, X.; Schwardt, O.; Ernst, B. *Anal. Biochem.* **2010**, *407*, 188.
46. Abgottspon, D.; Rölli, G.; Hosch, L.; Steinhuber, A.; Jiang, X.; Schwardt, O.; Cutting, B.; Smiesko, M.; Jenal, U.; Ernst, B.; Trampuz, A. *J. Microbiol. Methods* **2010**, *82*, 249.
47. Giampapa, C. S.; Abraham, S. N.; Chiang, T. M.; Beachey, E. H. *J. Biol. Chem.* **1988**, *263*, 5362.
48. Aprikian, P.; Tchesnokova, V.; Kidd, B.; Yakovenko, O.; Yarov-Yarovoy, V.; Trinchina, E.; Vogel, V.; Thomas, W.; Sokurenko, E. *J. Biol. Chem.* **2007**, *282*, 23437.
49. Trong, I. L.; Aprikian, P.; Kidd, B. A.; Forero-Shelton, M.; Tchesnokova, V.; Rajagopal, P.; Rodriguez, V.; Interlandi, G.; Klevit, R.; Vogel, V.; Stenkamp, R. E.; Sokurenko, E. V.; Thomas, W. E. *Cell* **2010**, *141*, 645.
50. Kansy, M.; Senner, F.; Gubernator, K. *J. Med. Chem.* **1998**, *41*, 1007.
51. Dearden, J. C.; Bresnen, J. G. M. *QSAR Comb. Sci.* **1988**, *7*, 133.
52. Kerns, E. H. *J. Pharm. Sci.* **2001**, *90*, 1838.
53. Poulain, F.; Serre, A.-L.; Lalot, J.; Leclerc, E.; Quirion, J.-C. *J. Org. Chem.* **2008**, *73*, 2435.
54. Kessler, H.; Gehrke, M.; Griesinger, C. *Angew. Chem.* **1988**, *100*, 507; *Angew. Chem. Int. Ed.* **1988**, *27*, 490.
55. Reid, B. R.; Banks, K.; Flynn, P.; Nerdalt, W. *Biochemistry* **1989**, *28*, 10001.
56. Szilágyi, L.; Forgó, P. *Carbohydr. Res.* **1993**, *247*, 129.
57. Varma, M. V. S.; Feng, B.; Obach, R. S.; Troutman, M. D.; Chupka, J.; Miller, H. R.; El-Kattan, A. *J. Med. Chem.* **2009**, *52*, 4844.
58. Avdeef, A.; Bendels, S.; Di, L.; Faller, B.; Kansy, M.; Sugano, K.; Yamauchi, Y. *J. Pharm. Sci.* **2007**, *96*, 2893.
59. Mulvey, M. A.; Schilling, J. D.; Hultgren, S. J. *Infect. Immun.* **2001**, *69*, 4572.
60. VCCLAB, Virtual Computational Chemistry Laboratory, http://www.vcclab.org, 2005.; (b) Tetko, I. V.; Gasteiger, J.; Todeschini, R.; Mauri, A.; Livingstone, D.; Ertl, P.; Palyulin, V. A.; Radchenko, E. V.; Zefirov, N. S.; Makarenko, A. S.; Tanchuk, V. Y.; Prokopenko, V. V. *J. Comput. Aid. Mol. Des.* **2005**, *19*, 453.

RESULTS AND DISCUSSION

Paper V

Antiadhesion Therapy for Urinary Tract Infections – A Balanced PK/PD Pofile Proved to be Key for Success.

Jiang X*, Abgottspon D*, Kleeb S*, Rabbani S, Scharenberg M, Wittwer M, Haug M, Schwardt O, Ernst B.

J. Med. Chem. **2012**.

*These authors contributed equally to the project.

My contribution:

In vitro evaluation of the inhibitory potency of the FimH antagonists in the flow cytometry infection assay together with Scharenberg M. and in the aggregometry assay.

In vivo pharmacokinetic and infection studies in the UTI mouse model.

Manuscript preparation.

Journal of Medicinal Chemistry

Article

pubs.acs.org/jmc

Antiadhesion Therapy for Urinary Tract Infections—A Balanced PK/PD Profile Proved To Be Key for Success

Xiaohua Jiang,[†] Daniela Abgottspon,[†] Simon Kleeb,[†] Said Rabbani, Meike Scharenberg, Matthias Wittwer, Martina Haug, Oliver Schwardt, and Beat Ernst*

Institute of Molecular Pharmacy, University of Basel, Klingelbergstrasse 50, 4056 Basel, Switzerland

Supporting Information

ABSTRACT: The initial step for the successful establishment of urinary tract infections (UTIs), predominantly caused by uropathogenic *Escherichia coli*, is the adhesion of bacteria to urothelial cells. This attachment is mediated by FimH, a mannose-binding adhesin, which is expressed on the bacterial surface. To date, UTIs are mainly treated with antibiotics, leading to the ubiquitous problem of increasing resistance against most of the currently available antimicrobials. Therefore, new treatment strategies are urgently needed, avoiding selection pressure and thereby implying a reduced risk of resistance. Here, we present a new class of highly active antimicrobials, targeting the virulence factor FimH. When the most potent representative, an indolinylphenyl mannoside, was administered in a mouse model at the low dosage of 1 mg/kg (corresponding to approximately 25 μg/mouse), the minimal therapeutic concentration to prevent UTI was maintained for more than 8 h. In a treatment study, the colony-forming units in the bladder could be reduced by almost 4 orders of magnitude, comparable to the standard antibiotic treatment with ciprofloxacin (8 mg/kg, sc).

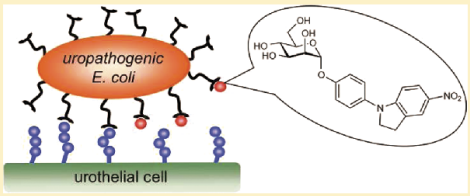

INTRODUCTION

Adhesion to target cells enables microorganisms to evade the natural clearing mechanisms and to ensure survival in the host environment. In urinary tract infections (UTIs), which are predominantly caused by uropathogenic *Escherichia coli* (UPEC), adhesion is accomplished by bacterial lectins, recognizing carbohydrate ligands located on the endothelial cells of the urinary tract.[1] For example, UPEC expressing P-pili cause pyelonephritis by binding to galabiose-containing ligands on the kidney epithelium, while mannose-binding type 1 piliated UPEC promote cystitis by targeting the glycoprotein uroplakin Ia (UPIa) on the mucosal surface of the urinary bladder. This initial step of the infection, the adhesion to the bacterial surface, prevents the rapid clearance of UPECs from the urinary tract by the bulk flow of urine and, at the same time, enables the invasion of host cells.[2,3] The most prevalent fimbriae encoded by UPEC consist of four subunits, FimA, FimF, FimG, and FimH.[4] The FimH lectin caps the fimbriae of type 1 pili and contains the carbohydrate recognition domain (CRD), mediating the crucial bacteria−cell interaction.[3]

UTIs affect a large proportion of the world population and account for significant morbidity and high medical costs.[2] Symptomatic UTIs should be treated with antibiotics to prevent potential devastating complications, like pyelonephritis and urosepsis. However, recurrent infections with subsequent antibiotic exposure can lead to emergence of antimicrobial resistance, which often results in treatment failure and reduces the range of therapeutic options. Hence, it is an urgent need for public health to develop an efficient, cost-effective, and nonantibiotic therapy to both prevent and treat UTIs without facilitating antimicrobial resistance.[5]

More than two decades ago, Sharon and co-workers have investigated various mannosides as antagonists for type 1 fimbriae-mediated bacterial adhesion.[6] For the further improvement of these FimH antagonists, two different approaches were explored. First, multivalent mannosides were investigated,[7,8] and second, monovalent high-affinity antagonists were designed (for representative examples, see Figure 1)[8] based on structural information obtained from crystal structures of the carbohydrate-recognition domain (CRD) of FimH cocrystallized with FimH antagonists.[9]

In this article, we present a new class of FimH antagonists. The binding affinities of these indolylphenyl and indolinylphenyl α-D-mannosides were determined in several target- and function-based assays. In addition, their in vitro pharmacokinetic properties were assigned, before the potential of selected compounds for in vivo application in a UTI mouse model was explored.

RESULTS AND DISCUSSION

Rational Design of FimH Antagonists. Crystal structures of FimH cocrystallized with various mannosides[9] disclosed a carbohydrate binding pocket with a hydrophobic entrance, the so-called tyrosine gate. The latter is formed by two tyrosines (Tyr48 and Tyr137) and an isoleucine (Ile52). Whereas *n*-butyl

Received: February 12, 2012
Published: April 23, 2012

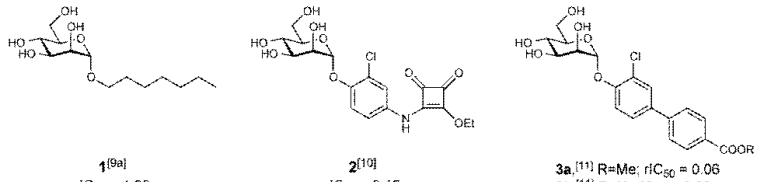

Figure 1. Alkyl (**1**) and aryl (**2** and **3**) α-D-mannopyranosides with nanomolar affinities. *n*-Heptyl α-D-mannoside (**1**) serves as a reference compound throughout our studies. Mannosides **2** and **3** exhibit low nanomolar affinities. Compound **3a** is the first reported orally available FimH antagonist that is hydrolyzed to the renally excretable acid **3b**. The IC_{50} values were determined with a cell-free binding assay.[12] Relative IC_{50} values (rIC_{50}) were calculated by dividing the IC_{50} of the substance of interest by the IC_{50} of the reference compound **1**.

α-D-mannoside populates the tyrosine gate and interacts with both tyrosines (in-docking mode),[9b,c] biphenyl α-D-mannosides, probably due to insufficient flexibility, adopt an out-docking mode, leading to an optimal $\pi-\pi$ stacking of their outer aromatic ring with Tyr48.[9d] In several recent publications, biphenyl α-D-mannosides with excellent affinities were reported.[9d,11,13]

Here, antagonists with (aza)indolylphenyl and indolinylphenyl aglycones (see Table 1) are explored. According to our docking studies, the increased volume of the outer aromatic ring (indolyl/indolinyl vs phenyl) leads to an improved fit. Details are given in the Supporting Information.

Synthesis of FimH Antagonists. Starting from trichloroacetimidate **5**, which was obtained from D-mannose (**4**) as reported earlier,[14] Lewis acid-promoted mannosylation of the phenols **6a–d** yielded the phenyl α-D-mannosides **7–10** (Scheme 1). In the subsequent copper-catalyzed Ullmann type coupling reaction[15] with the indoles **11e–j**, a partial deacetylation of the mannose moiety was observed due to the use of K_2CO_3 or K_3PO_4 as a base. Therefore, the crude products were reacetylated to give the substituted 4-(indol-1-yl)phenyl α-D-mannopyranosides **12–20** and **30**. Saponification afforded the test compounds **21–29**, **31**, and **32** (Table 1).

Careful reduction of the nitro group in **13** by catalytic hydrogenation with PtO_2 in the presence of catalytic amounts of morpholine[16] quantitatively yielded the corresponding amine **33** (Scheme 2). Acylation with 4-chlorobenzoyl chloride or methanesulfonyl chloride (→ **34** and **35**) and subsequent deacetylation under Zemplén conditions gave the amides **36** and **37** (Table 1).

Starting from phenyl mannoside **7**, 7-azaindole derivatives **39** and **40** (Scheme 3) were obtained by an Ullmann type coupling reaction as well. Final deprotection yielded the test compounds **41** and **42** (Table 1).

To further explore the contribution of the indole aglycone to binding, it was replaced by indoline moieties (→ **48a–d** and **52**, Scheme 4). The phenyl mannosides **44** and **50** were synthesized using the procedure as described for **7**. In a palladium-catalyzed Buchwald–Hartwig coupling[17] with 5-nitro-indoline (**45**) or indoline (**46**), the protected mannosides **47a–d** and **51** were obtained in 43–80% yield. Final deacetylation under Zemplén conditions gave the indoline derivatives **48a–d** and **52** (Table 1).

Finally, the synthesis of the 5-linked 7-aza-indole **57** and the imidazo-pyridine derivative **58** is outlined in Scheme 5. Palladium-catalyzed Suzuki–Miyaura coupling[18] of **7** with boronic esters **53** or **54** (→ **55** and **56**) and subsequent deprotection afforded the test compounds **57** and **58** (Table 1).

In Vitro Binding Affinities. To evaluate the potential of indolylphenyl and indolinylphenyl mannosides to prevent FimH-dependent adhesion of UPECs to urothelial cell surfaces, two different assay formats were applied. First, in the cell-free binding assay,[12] which is based on the interaction of a biotinylated polyacrylamide glycopolymer with the CRD of FimH, the inhibitory potency of FimH antagonists was measured. Second, in the cell-based aggregation assay,[19] the disaggregation of guinea pig erythrocytes (GPE) incubated with UPEC, strain UTI89 was determined as a function of various concentrations of FimH antagonists.

In the two assay formats, different affinities were expected. Whereas in the cell-free binding assay only the CRD of FimH is used, the complete pili are present in the cell-based aggregation assay. Furthermore, both formats are competitive assays, that is, the analyzed antagonists compete with mannosides for the binding site. In the cell-free binding assay, the competitor is a polymer-bound trimannoside, whereas in the aggregation assay, the antagonist competes with more potent oligo- and polysaccharide chains[20] present on the surface of erythrocytes.[21] The interaction is further complicated by the existence of a high- and a low-affinity state of the CRD of FimH. Aprikian et al. experimentally demonstrated that in full-length fimbriae the pilin domain stabilizes the CRD domain in the low-affinity state, whereas the CRD domain alone adopts the high-affinity state.[22] Furthermore, it was recently shown that shear stress can induce a conformational switch (twist in the β-sandwich fold of the CRD domain) resulting in improved affinity.[23] Despite these differences, the ranking of the half maximal inhibitory concentration (IC_{50}) values within the two assay formats is expected to be in a similar order.

According to molecular dynamics (MD) simulations, a cavity between the *ortho*-hydrogen of the phenyl ring adjacent to the anomeric center and the binding pocket offers the opportunity to improve binding with a substituent of appropriate size, leading to refined van der Waals interactions. We therefore replaced the *ortho*-hydrogen by a chloro (entries 3–7 and 12–17), fluoro (entries 8 and 9), or methoxy substituent (entry 10). The *ortho*-chloro substituted antagonist showed the best binding affinities in both assays (Table 1). When a second chloro substituent was introduced to the *ortho'*-position (**29**, entry 11), the binding affinity unexpectedly decreased in both assays, indicating that the entropic gain expected by symmetrization of the antagonist could not be realized, probably because of rotational constraints. Therefore, an *ortho*-chloro substituent in the first aromatic ring was retained when the indole/indoline moiety was further optimized (**48a–d**, entries 18–21). As compared to the reference compound **1**, the indoline derivative **48c** (entry 20) exhibited an

Scheme 1[a]

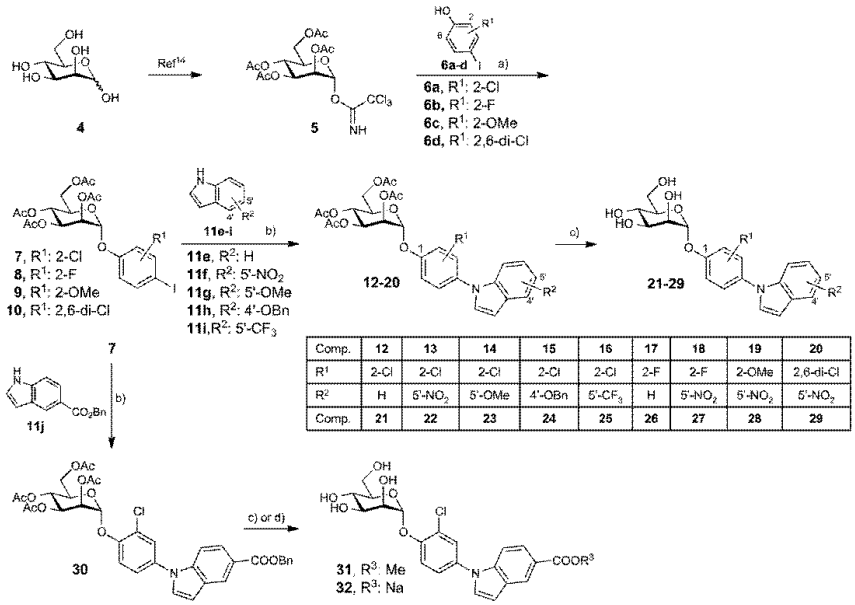

Comp.	12	13	14	15	16	17	18	19	20
R^1	2-Cl	2-Cl	2-Cl	2-Cl	2-Cl	2-F	2-F	2-OMe	2,6-di-Cl
R^2	H	5'-NO_2	5'-OMe	4'-OBn	5'-CF_3	H	5'-NO_2	5'-NO_2	5'-NO_2
Comp.	21	22	23	24	25	26	27	28	29

[a]Reagents and conditions: (a) 4 Å MS, TMSOTf, toluene, rt, 2 h (37−94%). (b) (i) CuI, K_2CO_3, L-proline, DMSO, 90°C, overnight or CuI, K_3PO_4, *trans*-1,2-cyclohexanediamine, dioxane, 105°C, overnight; (ii) Ac_2O/pyr, DMAP, 2−4 h. (c) 0.5 M NaOMe/MeOH, rt. (d) 2N NaOH, THF/MeOH/H_2O (5:5:2), 40 °C (→ **32**).

Scheme 2[a]

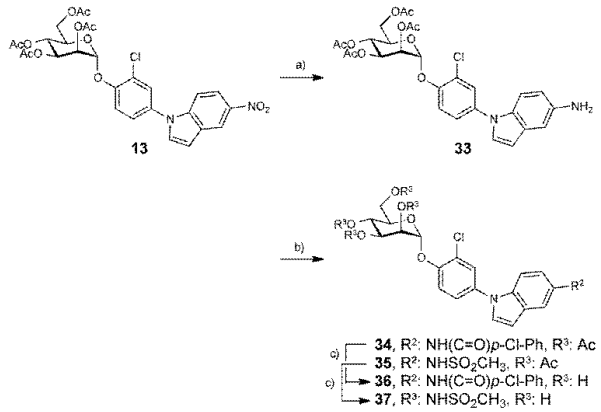

[a]Reagents and conditions: (a) H_2 (1 atm), PtO_2, cat. morpholine, MeOH/EtOAc (quant). (b) 4-Cl-BzCl or $MeSO_2Cl$, Et_3N, DCM, rt, 1 h (**34**, 94%; **35**, 82%). (c) 0.5 M NaOMe/MeOH, rt (**36**, 85%; **37**, 82%).

up to 30-fold improved affinity in the cell-free binding assay and the aggregometry assay. Finally, when the indolinyl substituent was introduced in the *meta*-position (→ **52**, entry 22) or aza-indolyl (→ **57**, entry 23) and imidazo-pyridyl substituents (→ **58**, entry 24) were introduced in the *para*-position of the first aromatic ring, a substantial reduction in affinity was observed.

Scheme 3[a]

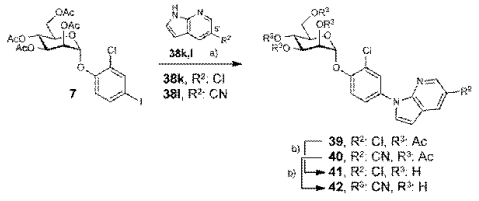

[a]Reagents and conditions: (a) (i) CuI, K_2CO_3, L-proline, DMSO, 90 °C, overnight or CuI, K_3PO_4, *trans*-1,2-cyclohexanediamine, dioxane, 105 °C, overnight; (ii) Ac_2O/pyr, DMAP, 2–4 h (**39**, 82%; **40**, 80%). (b) 0.5 M NaOMe/MeOH, rt (**41**, 63%; **42**, 91%).

Scheme 5[a]

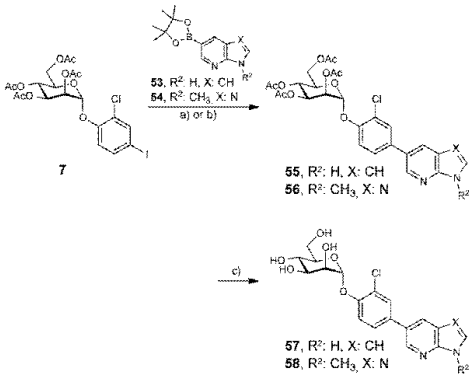

[a]Reagents and conditions: (a) K_3PO_4, $Pd(Ph_3P)_4$, dioxane, 100 °C, overnight (**55**, 56%). (b) K_3PO_4, $PdCl_2$(dppf), DMF, 100 °C, overnight (**56**, 96%). (c) 0.5 M NaOMe/MeOH, rt, 2–2.5 h (**57**, 42%; **58**, 37%).

In Vitro Pharmacokinetic Characterization. To reach their therapeutic target, orally applied FimH antagonists should be gastrointestinally absorbed and renally eliminated; that is, an optimal balance between solubility, permeability, and lipophilicity is required. To identify the most promising candidates among the high-affinity FimH antagonists for the in vivo validation, membrane permeability, thermodynamic solubility, octanol–water partition, and plasma protein binding (PPB) were therefore determined.

The parallel artificial membrane permeability assay (PAMPA) predicts a medium to high oral absorption potential for compounds with an effective permeability (log P_e) above −6.3,[24] a property fulfilled by most of the listed indole and indoline derivatives (Table 2). Apparently, elevated lipophilicity of most antagonists, that is, log $D_{7.4} > 2$, facilitates permeation

Scheme 4[a]

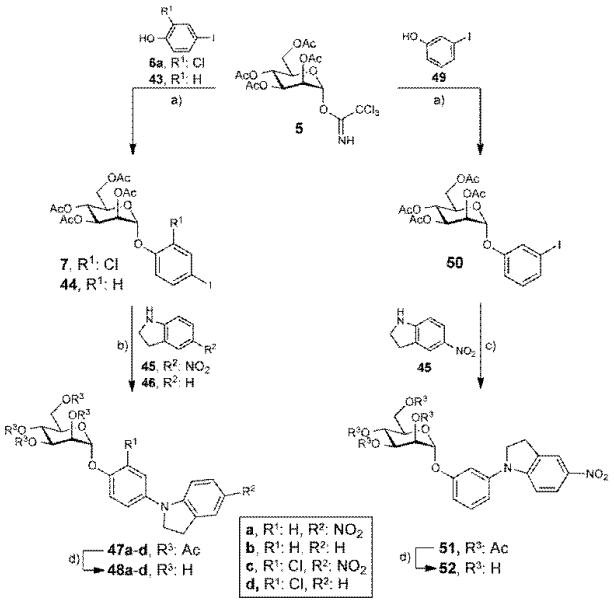

[a]Reagents and conditions: (a) 4 Å MS, TMSOTf, toluene or DCM, rt, 2 h (**7**, 73%; **44**, quant; **50**, 93%). (b) Cs_2CO_3, $Pd_2(dba)_3$, X-Phos, toluene, 80 °C, 140 h or microwave, 80 °C, 8 h (**47a–d**, 43–75%). (c) Cs_2CO_3, $Pd_2(dba)_3$, X-Phos, dioxane, Ac_2O, pyr, 80 °C, 53 h (80%). (d) NaOMe/MeOH, rt, 20–23 h, (**48a–d**, 37–77%; **52**, 60%).

dx.doi.org/10.1021/jm300192x | J. Med. Chem. 2012, 55, 4700–4713

Table 1. In Vitro Pharmacodynamic Parameters of FimH Antagonists[a]

Entry	Comp. No.	R^1	R^2	X	Cell-free binding assay		Aggregometry assay	
					IC_{50} [nM]	rIC_{50}	IC_{50} [μM]	rIC_{50}
1	**1**[9a,11]	*n*-Heptyl α-D-mannopyranoside			73	**1**	77.1	**1**
2	**3b**[11]	Sodium 3'-chloro-4'-(α-D-manno-pyranosyloxy)-biphenyl-4-carboxylate			6.7	0.09	10.0	0.13
		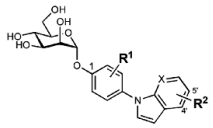						
3	**21**	2-Cl	H	CH	14.9	0.2	8.3	0.11
4	**22**	2-Cl	5'-NO_2	CH	7.7	0.1	1.3	0.01
5	**23**	2-Cl	5'-OMe	CH	59.0	0.81	n.d.	-
6	**24**	2-Cl	4'-OBn	CH	48.6	0.66	n.a.	-
7	**25**	2-Cl	5'-CF_3	CH	18.8	0.26	6.4	0.08
8	**26**	2-F	H	CH	35.3	0.48	29.5	0.38
9	**27**	2-F	5'-NO_2	CH	52.8	0.72	5	0.06
10	**28**	2-OMe	5'-NO_2	CH	18.7	0.26	4.1	0.05
11	**29**	2,6-di-Cl	5'-NO_2	CH	28.1	0.38	7.1	0.09
12	**31**	2-Cl	5'-COOMe	CH	8.0	0.11	n.d.	-
13	**32**	2-Cl	5'-COOH	CH	20.3	0.28	3.1	0.04
14	**36**	2-Cl	5'-NH(C=O)*p*Cl-Ph	CH	40.1	0.55	n.a.	-
15	**37**	2-Cl	5'-NHS(=O)$_2$Me	CH	20.7	0.28	5.6	0.07
16	**41**	2-Cl	5'-Cl	N	20.0	0.26	23.1	0.3
17	**42**	2-Cl	5'-CN	N	12.8	0.17	8.2	0.11
		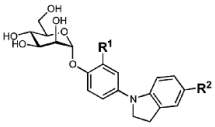						
18	**48a**	H	NO_2	-	20	0.27	26.9	0.35
19	**48b**	H	H	-	14.5	0.20	n.d.	-
20	**48c**	Cl	NO_2	-	2.4	0.03	3.4	0.04
21	**48d**	Cl	H	-	27.8	0.43	n.d.	-
		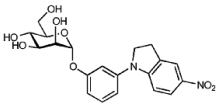						
22	**52**	-			15.1	0.32	19.2	0.25
		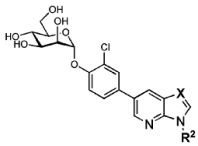						
23	**57**	-	H	CH	40.1	0.55	35.9	0.47
24	**58**	-	Me	N	15.1	0.21	25.3	0.33

[a]The IC_{50} values were determined with the cell-free binding assay[12] and the aggregometry assay.[19] The rIC_{50} values were calculated by dividing the IC_{50} of the compound of interest by the IC_{50} of the reference compound **1**. This leads to rIC_{50} values below 1 for derivatives binding better than **1** and rIC_{50} values above 1.00 for compounds with a lower affinity than **1**. n.a., not active; n.d., not determined.

across the artificial membrane. In contrast to the promising PAMPA results, thermodynamic solubility strongly limited the dosages, which could be applied for the in vivo pharmacokinetic (PK) studies (see below).[25,26]

Regarding their renal elimination, lipophilic FimH antagonists (log $D_{7.4}$ > 2) are expected to undergo considerable reabsorption in the renal tubules, leading overall only to a slow excretion into the bladder. On the contrary, hydrophilic

Table 2. Distribution Coefficients (log $D_{7.4}$ Values) Were Measured by a Miniaturized Shake Flask Procedure[29a]

entry	compd no.	log $D_{7.4}$	solubility/pH (μg/mL)	PAMPA log P_e (log 10^{-6} cm/s)	PPB (%)
25	**3b**[11]	−0.8	>3000	NP	89
26	**21**	1.8	31.5/6.5	−4.7	98
27	**22**	1.8	1.4/6.5	−4.9	99
28	**23**	3.0	9.6/6.6	−4.6	96
29	**24**	2.7	<0.1/6.5	NP	ND
30	**25**	ND	0.1/6.5	−4.6	>99
31	**26**	2.4	67/6.5	−4.7	98
32	**27**	1.9	4.0/6.5	−5.4	95
33	**31**	2.8	2.1/6.5	−4.4	99
34	**32**	1.1	1050/5.6	−6.4	93
35	**36**	ND	<0.001/6.5	−6	>99
36	**37**	1.8	279/6.3	NP	94
37	**41**	3.4	3.8/6.5	−5.0	96
38	**42**	1.6	8.5/6.3	−6.3	95
39	**48a**	1.9	24/6.5	−5.5	95
40	**48b**	2.3	31/6.5	−4.7	97
41	**48c**	1.9	3.6/6.5	−5.7	99
42	**48d**	2.8	21/6.5	−4.6	99
43	**57**	3.2	5.5/6.4	NP	90
44	**58**	1.3	2.4/6.3	−8.0	<30

[a]Thermodynamic solubility (S) was measured by an equilibrium shake flask approach.[30] Passive permeation through an artificial membrane and retention therein was determined by PAMPA.[24a] PPB was assessed following a miniaturized equilibrium dialysis protocol.[31] P_e, effective permeation; ND, not determined; NP, no permeation.

compounds (log $D_{7.4}$ < 0) are poorly reabsorbed and thus rapidly renally cleared, which leads to high initial compound levels in the urine but narrows the time range where a therapeutic concentration (T > $MIC_{adhesion}$, see below) is maintained.[27] Consequently, moderate lipophilicity, that is, log $D_{7.4}$ in the range of 1−2, is beneficial to maintain the drug concentration in the bladder over an extended time period. Most of the FimH antagonists listed in Table 2 show moderate to high lipophilicity and are therefore potentially affected by renal reabsorption. Moreover, PPB values ≥90% as found for most of the antagonists in Table 2 attenuate fast renal clearance, because, in line with the free drug hypothesis, molecules bound to plasma proteins evade excretion.[28] Compounds for the further evaluation were selected according to affinity (**22** and **48c**, Table 1) or their PK properties (**21** and **48a**, Table 2).

Determination of the Minimal Inhibitory Concentration of Adhesion ($MIC_{adhesion}$). Whereas in antimicrobial chemotherapy the MIC is defined as the lowest concentration of a drug that inhibits visible growth of an organism,[32] we defined a modified MIC for FimH antagonists because of their different mode of action (they neither kill nor inhibit the growth of bacteria). The $MIC_{adhesion}$ can be used for the determination of the therapeutic dosage in vivo and is defined as the concentration of antagonist leading to 90% inhibition of adhesion of the pathogen to the target cells (IC_{90}). To determine the $MIC_{adhesion}$, human bladder cells are infected with green fluorescent protein (GFP) labeled UPEC (strain UTI89) in the presence of different concentrations of FimH antagonists and analyzed by flow cytometry.[33] The half-maximal inhibitory concentration (IC_{50}) was calculated by plotting the mean fluorescent intensity (MFI) of the cells versus the concentration of the antagonist. From this plot, the concentration where 90% bacterial adhesion to human bladder cells is inhibited (IC_{90}) can be deduced. The corresponding concentration in μg/mL was defined as $MIC_{adhesion}$. IC_{50}, IC_{90}, and $MIC_{adhesion}$ values of the four selected FimH antagonists and of the previously reported biphenyl derivative **3b**[11] are listed in Figure 2.

Entry	Comp. No.	IC_{50} [μM]	IC_{90} [μM]	$MIC_{adhesion}$ [μg/mL]
45	**3b**	0.33 ± 0.05	1.4	0.61
46	**21**	20.14 ± 7.6	~350	~140
47	**22**	0.5 ± 0.29	2.9	1.32
48	**48a**	0.14 ± 0.05	1.16	0.49
49	**48c**	0.04 ± 0.02	0.3	0.14

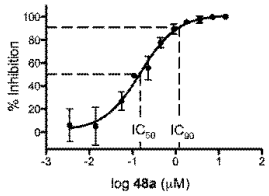

Figure 2. Determination of the $MIC_{adhesion}$. The table lists the half-maximal inhibitory concentration (IC_{50}), the 90% inhibitory concentration of adhesion [IC_{90} (μM)] and the $MIC_{adhesion}$ (μg/mL) of selected indolylphenyl (**21** and **22**) and indolinylphenyl (**48a** and **48c**) mannosides as well as the previously reported biphenyl derivative **3b**.[11] IC_{50} values were determined using the cell-based flow cytometry infection assay[33] (see the graph, representing results for **48a**). The $MIC_{adhesion}$ is the concentration in μg/mL of antagonist that inhibits adhesion of the pathogen to host cells by 90% (IC_{90}).

Pharmacokinetic Studies in C3H/HeN Mice with a Single iv Dose. In our previously reported study,[11] FimH antagonist **3b** was applied at a dosage of 50 mg/kg. For the in vivo characterization of the compounds of the new series, the dosage was adjusted according to their maximal solubility [in 5% aqueous dimethyl sulfoxide (DMSO)]. Plasma and urine concentrations of the selected FimH antagonists **3b**,[11] **21**, **22**, **48a**, and **48c** after single iv application are summarized in Figure 3. The $MIC_{adhesion}$ values are indicated in the individual graphs with a dotted line. An important parameter for the prediction of the therapeutic outcome in the UTI mouse model is the time period for which the antagonist concentration in the urine is above the $MIC_{adhesion}$ (T > $MIC_{adhesion}$), representing the therapeutic time range.

As a consequence of fast renal excretion, the $MIC_{adhesion}$ value for reference compound **3b** applied at a dosage of 50 mg/kg could be maintained for approximately 4 h (Figure 3A). When **21** and **22** were applied at dosages of 25 and 5 mg/kg, respectively, substantially lower urine concentrations were observed, for **21** below the $MIC_{adhesion}$ value and for **22** only marginally above (Figure 3B,C). Although compound **48a** was applied with a single dose of 1 mg/kg (50-fold reduced dosage as compared to **3b**), it exhibited the highest availability in the urine [area under the curve $(AUC)_{0-24}$] with a T > $MIC_{adhesion}$ of >8 h (Figure 3D). Finally, antagonist **48c** was applied at 0.05 mg/kg, which is a 1000-fold reduced dosage as compared to **3b**. Nevertheless, it still showed an improved therapeutic time range of 8 h (T > $MIC_{adhesion}$, Figure 3E).

Treatment Study in C3H/HeN Mice. For the in vivo UTI treatment study, antagonist **48a** was selected for iv application (1 mg/kg) into the tail vein, followed by infection with UPEC (UTI89). The animals were sacrificed 3 h after inoculation, and

dx.doi.org/10.1021/jm300192x | J. Med. Chem. 2012, 55, 4700−4713

Antagonist Dosage	Compartment	AUC_{0-24} [µg x h/mL]	T > $MIC_{Adhesion}$ [h]
3b 50 mg/kg	Plasma	20.8 ± 7.3	-
	Urine	209.6 ± 72.3	4
21 25 mg/kg	Plasma	8.2 ± 3.2	-
	Urine	19.3 ± 3.9	0
22 5 mg/kg	Plasma	2.3 ± 1.1	-
	Urine	13.2 ± 4.2	3
48a 1 mg/kg	Plasma	2.2 ± 0.8	-
	Urine	586.4 ± 251.6	> 8
48c 0.05 mg/kg	Plasma	3.5 ± 1.2	-
	Urine	33.4 ± 11	8

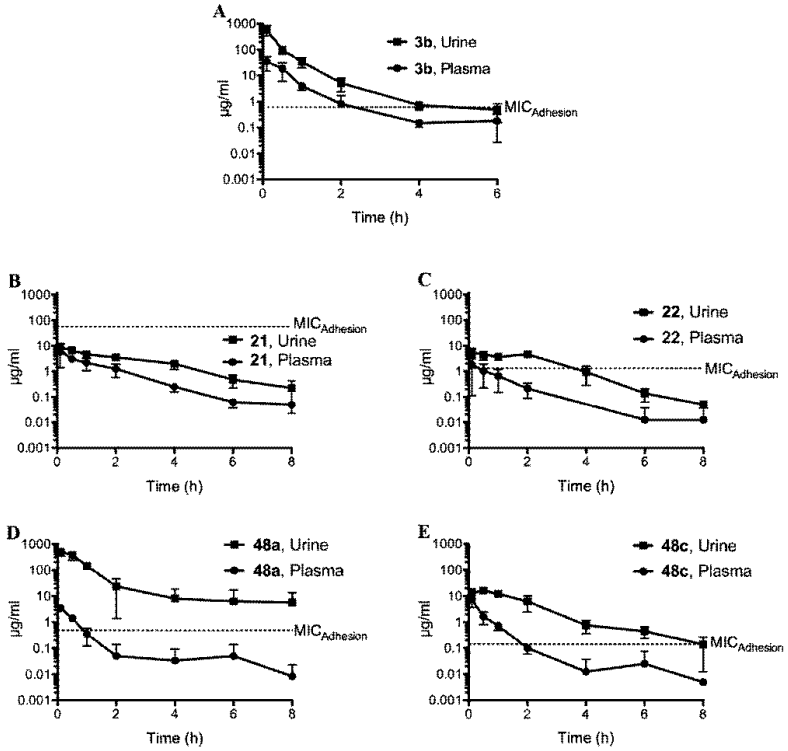

Figure 3. Determination of antagonist concentration in urine and plasma after a single iv application ($n = 4$). The data (table and graphs) show time-dependent urine and plasma concentrations and the $MIC_{adhesion}$ values as dotted lines for **3b** (reference compound[11]), **21**, **22**, **48a**, and **48c**. AUC_{0-24} is the AUC over 24 h; $MIC_{adhesion}$ is the minimal inhibitory concentration of adhesion.

homogenized organs (bladder and kidneys) were examined for bacterial counts. The results were compared to ciprofloxacin (CIP), used as standard antibiotic therapy against UTI[34]

The mean value in the untreated control group showed bacterial counts of 1.4×10^8 colony-forming units (CFU) in the bladder and 9.7×10^6 CFU in the kidneys. The bar diagram in Figure 4 summarizes the bacterial counts after treatment. The baseline represents the values obtained for the control group, which was used as reference for CFU reductions. After iv application of **48a**, a substantial decrease of the bacterial counts by 3.7 $\log_{10}$ CFU was observed in the bladder. Results were compared to the previously presented antagonist **3b**,[11] which was tested using the same protocol. With **3b**, a 50-fold higher dosage (50 mg/kg) had to be applied to obtain a comparable reduction of 4 $\log_{10}$ CFU for bladder counts. Mice treated with CIP (8 mg, sc) showed an almost identical reduction of bacterial counts in the bladder as the tested FimH antagonists **3b** (50 mg/kg) and **48a** (1 mg/kg). Furthermore, antagonist **48a** prevented bacteria from ascending into the kidneys (−1.3 $\log_{10}$ CFU) twice as efficiently as **3b** (−0.7 $\log_{10}$ CFU).

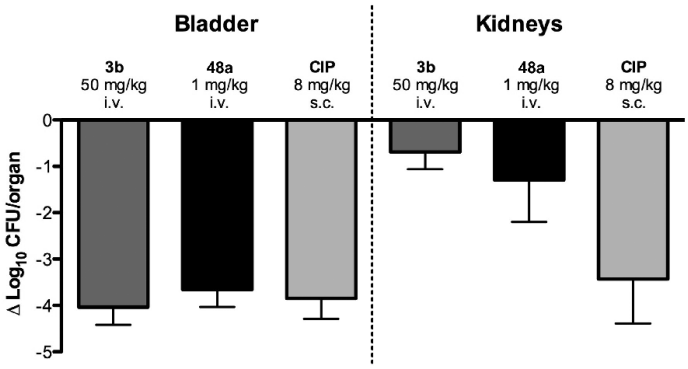

Figure 4. Treatment efficacy in the UTI mouse model 3 h after infection (n = 6). The bar diagram shows the reduction of bacterial counts of the indolinylphenyl mannoside **48a** at an iv dosage of 1 mg/kg, the biphenyl derivative **3b** at an iv dosage of 50 mg/kg, and ciprofloxacin (CIP) at an sc dosage of 8 mg/kg (representing the murine dose equivalent to a human standard dose).[35] The baseline represents the mean counts of the untreated control group; that is, the values of the control group were subtracted from the results of the tested antagonists.

As previously addressed,[11] urine samples show in general higher bacterial counts as compared to the bladder. A possible explanation is the varying urine volumes, leading to either a concentration or a dilution of bacteria in the urine samples. Therefore, results were limited to the evaluation of bladder and kidney counts. Furthermore, as compared to bladder counts, the bacterial counts in the kidneys were reduced to a smaller extent, probably due to different bacterial adhesion mechanisms in bladder and kidney (type 1 pili- vs P pili-dependent interactions).[3] Therefore, the considerable reduction of the bacterial counts in the kidney as observed for antagonist **48a** may originate from the inability of UPECs blocked by **48a** to adhere to bladder cells and their subsequent removal from the bladder by the urine flow. As a result, only a reduced population for ascending into the kidneys is available.

■ CONCLUSIONS

The FimH antagonists presented in this article exhibit an alternative mode of action as compared to antibiotics as they neither kill nor inhibit growth of bacteria. By blocking FimH, a lectin located at the tip of the bacterial fimbriae, they interfere with the adhesion of UPEC to the endothelial cells of the urinary tract and therewith the initial step of the infection. To select the most promising candidates for in vivo studies,[36] a thorough investigation of the in vitro potency and the physicochemical/PK properties of these FimH antagonists (Tables 1 and 2) was performed.

Starting from the known FimH antagonist biphenyl α-D-mannopyranoside (**3b**), we designed antagonists with spatially more demanding aglycones and therefore a better fit in the out-docking mode.[9a,13,37] Thus, a series of indolylphenyl and indolinylphenyl α-D-mannopyranosides were synthesized. For the initial evaluation of their affinities, a target-based, cell-free binding assay[12] and a cell-based aggregometry assay[19] were applied. In both series, an *ortho*-chloro substituent on the phenyl ring adjacent to the anomeric oxygen and an electron-withdrawing substituent on the indole/indoline moiety yielded the antagonists with the highest affinities/activities (see Table 1), presumably by favoring the $\pi-\pi$ stacking with the electron rich Tyr48.

The most important requirement for a successful treatment in the UTI mouse model is the maintenance of a $MIC_{adhesion}$ of the antagonist in the urine. To avoid a fast renal clearance as experienced with the biphenyl mannoside **3b**[11] (log $D_{7.4}$ of −0.8, PPB 89%) (Figure 3A), the indole derivatives **21** and **22** and the indoline derivatives **48a** and **48c** exhibiting higher lipophilicity (log $D_{7.4}$ values of 1.8 and 1.9) and PPB (>95%) were selected as candidates for the in vivo PK study. Whereas for the indole derivatives **21** and **22** only insufficient urine concentrations (Figure 3B,C) were obtained, **48a** and **48c** exhibited a substantially improved renal elimination profile with $T > MIC_{adhesion}$ of >8 and 8 h, respectively, although 50−1000-fold lower dosages were applied (Figure 3D,E).

On the basis of these results, **48a** was selected for the treatment study in the UTI mouse model (dosage of 1 mg/kg). It reduced the CFUs in the bladder by 3.7 orders of magnitude, which is almost comparable to **3b**, applied at a 50-fold higher dosage (50 mg/kg, −4 $\log_{10}$ CFU). Furthermore, **48a** led to a considerably better reduction of bacterial counts in the kidneys (−1.3 $\log_{10}$ CFU vs −0.7 $\log_{10}$ CFU for **3b**). Of additional interest is the fact that the FimH antagonist **48a** was able to reduce bacterial infection in the bladder comparably well as the standard antibiotic treatment with ciprofloxacin (CIP),[34] indicating a promising profile for the alternative treatment of UTIs with FimH antagonists. Overall, the indoline derivative **48a** is the most active antagonist tested in vivo to date.[11,13] Because the experimental setup used in this study is a prophylactic approach, an adopted protocol for the treatment of an established infection is currently developed.

According to the PAMPA values, most representatives of the indole and indoline series are expected to be orally available (Table 2). However, a major drawback is their low solubility, limiting, for example, the dosage of **48a** to 1 mg/kg and **48c** to 0.05 mg/kg. To evaluate the dosage dependence, that is, whether higher dosages will further reduce the bacterial counts in bladder and kidney, the physicochemical issue of solubility will be addressed by appropriate formulations and structural modifications (e.g., by disruption of the molecular planarity of the aromatic aglycone[26]).

Overall, these results clearly indicate the high therapeutic potential of this new series of FimH antagonists. Because of optimized PK properties, a substantial reduction of the dosage could be achieved. Thus, with the most promising representative to date, the indolinylphenyl α-D-mannoside **48a**, the infection can be successfully treated with a low dosage of 1 mg/kg (approximately 25 μg/mouse) without any additional administration of antibiotics.

EXPERIMENTAL SECTION

Synthesis. The synthesis of compounds **7**−**10**, **14**−**20**, **23**−**37**, **39**−**42**, 44, 47**b**,**d**, 48**b**,**d**, **50**−**52**, and **55**−**58**, including compound characterization data, can be found in the Supporting Information.

General Methods. Commercially available reagents were purchased from Fluka, Aldrich, Merck, AKSci, ASDI, or Alfa Aesar. Methanol (MeOH) was dried by distillation from sodium methoxide. Toluene and dioxane were dried by distillation from sodium/benzophenone. Optical rotations were measured at 20 °C on a Perkin-Elmer 341 polarimeter. Nuclear magnetic resonance (NMR) spectra were obtained on a Bruker Avance 500 UltraShield spectrometer at 500.13 MHz (^{1}H) or 125.76 MHz (^{13}C). Chemical shifts are given in ppm and were calibrated on residual solvent peaks or to tetramethylsilane as an internal standard. Multiplicities are specified as s (singlet), d (doublet), dd (doublet of a doublet), t (triplet), q (quartet), or m (multiplet). Assignment of the ^{1}H and ^{13}C NMR spectra was achieved using 2D methods (COSY, HSQC). ESI mass spectra were recorded on a Waters micromass ZQ instrument. High-resolution mass spectra were obtained on an ESI Bruker Daltonics micrOTOF spectrometer equipped with a TOF hexapole detector. Microwave-assisted reactions were carried out with CEM Discover and Explorer. Reactions were monitored by TLC using glass plates coated with silica gel 60 F_{254} and visualized by using UV light and/or by charring with a molybdate solution (a 0.02 M solution of ammonium cerium sulfate dihydrate and ammonium molybdate tetrahydrate in aqueous 10% H_2SO_4) with heating to 150 °C for 5 min. Column chromatography was performed on a CombiFlash Companion (ISCO, Inc.) using RediSep normal phase disposable flash columns (silica gel). Reversed phase chromatography was performed on LiChroprepRP-18 (Merck, 40−63 μm).

Compound Purity. Each test compound was purified by chromatography on silica (dichloromethane (DCM)/MeOH, 10:1) or reversed-phase chromatography (RP-18 column, H_2O/MeOH, gradient from 0 to 20% MeOH), followed by Bio-Gel P2 (exclusion limit 1800 Da, Bio-Rad Laboratories) size exclusion chromatography (elution with water containing up to 20% MeOH at 0.25 mL/min) prior to HPLC, HRMS, NMR, and activity testing. The purity of all test compounds was determined by NMR and HPLC [Beckman Coulter Gold, consisting of pump 126, DAD 168 (190−410 nm), and autosampler 508. Column: Waters Atlantis T3, 3 μm, 2.1 mm × 100 mm. A, H_2O + 0.1% TFA; B, MeCN + 0.1% TFA. Detection, 270 nm. Gradient, 5 → 95% B (22 min); flow rate, 0.5 mL/min] to be ≥95% (for ^{1}H NMR spectra and HPLC traces, see the Supporting Information).

*2-Chloro-4-(indol-1-yl)phenyl α-D-Mannopyranoside (**21**).* A resealable Schlenk tube, which was equipped with a magnetic stirring bar, was charged with 7 (146 mg, 0.25 mmol), CuI (10 mg, 0.05 mmol), indole (**11e**, 35.0 mg, 0.30 mmol), K_2CO_3 (86 mg, 0.63 mmol), and L-proline (11.5 mg, 0.10 mmol). The vessel was sealed with a rubber septum, evacuated, and backfilled with argon (this process was repeated twice). Then, DMSO (1 mL) was added under a stream of argon, the reaction tube was quickly sealed, and the suspension was stirred at 90 °C overnight. The reaction mixture was cooled to rt, diluted with EtOAc (5 mL), and filtered through a plug of Celite. The filtrate was concentrated in vacuo, and the residue was treated for 2 h with Ac_2O/pyridine (3 mL, 1:2) and a catalytic amount of DMAP. The reaction was quenched by the addition of MeOH and concentrated, and the residue was purified by chromatography on silica (petroleum ether/EtOAc, 4:1 to 1:1) to give slightly impure **12** (40 mg, 28%). Compound **12** (40 mg, 0.07 mmol) was dissolved in MeOH (1 mL) and treated at rt with 0.5 M NaOMe/MeOH (14 μL) until completion of the reaction. The reaction mixture was neutralized with amberlyst-15 (H^+) ion-exchange resin and filtered. The filtrate was concentrated, and the residue was purified by chromatography on silica (DCM/MeOH, 10:1) and P2 size exclusion chromatography to afford **21** (20 mg, 70%) as a white solid after a final lyophilization from water/dioxane. $[\alpha]_D^{20}$ +171.6 (*c* 0.18, MeOH). ^{1}H NMR (500 MHz, CD_3OD): δ 7.62−7.54 (m, 3H, Ar−H), 7.45−7.38 (m, 3H, Ar−H), 7.18 (t, *J* = 7.0 Hz, 1H, Ar−H), 7.11 (t, *J* = 7.0 Hz, 1H, Ar−H), 6.65 (s, 1H, Ar−H), 5.61 (s, 1H, H-1), 4.14 (m, 1H, H-2), 4.01 (dd, *J* = 9.0, 2.5 Hz, 1H, H-3), 3.81−3.69 (m, 4H, H-6a, H-4, H-6b, H-5). ^{13}C NMR (125 MHz, CD_3OD): δ 151.81, 137.30, 136.22, 130.81, 128.98, 127.04, 125.58, 124.98, 123.49, 122.06, 121.42, 119.23, 111.00, 104.71 (Ar−C), 101.03 (C-1), 76.11 (C-5), 72.38 (C-3), 71.84 (C-2), 68.22 (C-4), 62.70 (C-6). HRMS (ESI) *m*/*z* calcd for $C_{20}H_{20}ClNNaO_6$ [M + Na]$^+$, 428.0877; found, 428.0875.

*2-Chloro-4-(5-nitroindol-1-yl)phenyl α-D-Mannopyranoside (**22**).* According to the procedure described for **21**, compound **22** was prepared from 7 (117 mg, 0.20 mmol) and 5-nitroindole (**11f**, 39 mg, 0.24 mmol) via the acetylated intermediate **13**. After workup, the residue was purified by chromatography on silica (DCM/MeOH, 10:1) and P2 size exclusion chromatography to yield **22** (54 mg, 60%) as a yellow solid after a final lyophilization from water/dioxane. $[\alpha]_D^{20}$ +85.7 (*c* 0.25, MeOH). ^{1}H NMR (500 MHz, CD_3OD): δ 8.63 (d, *J* = 2.0 Hz, 1H, Ar−H), 8.11 (dd, *J* = 9.0, 2.0 Hz, 1H, Ar−H), 7.65−7.55 (m, 4H, Ar−H), 7.48 (dd, *J* = 8.5, 2.5 Hz, 1H, Ar−H), 6.91 (d, *J* = 3.0 Hz, 1H, Ar−H), 5.65 (s, 1H, H-1), 4.14 (m, 1H, H-2), 4.01 (dd, *J* = 9.5, 3.5 Hz, 1H, H-3), 3.83−3.72 (m, 3H, H-6a, H-4, H-6b), 3.66 (m, 1H, H-5). ^{13}C NMR (125 MHz, CD_3OD): δ 152.73, 143.52, 140.14, 134.75, 132.99, 130.01, 127.65, 125.75, 125.57, 119.11, 118.95, 118.79, 111.51, 106.68 (Ar−C), 100.90 (C-1), 76.19 (C-5), 72.37 (C-3), 71.78 (C-2), 68.18 (C-4), 62.69 (C-6). HRMS (ESI) *m*/*z* calcd for $C_{20}H_{19}ClN_2NaO_8$ [M + Na]$^+$, 473.0728; found, 473.0728.

*4-(5-Nitroindolin-1-yl)phenyl 2,3,4,6-Tetra-O-acetyl-α-D-mannopyranoside (**47a**).* In a Schlenk tube, a mixture of 2-dicyclohexylphosphino-2′,4′,6′-triisopropylbiphenyl (X-Phos) (9.1 mg, 0.019 mmol) and $Pd_2(dba)_3$ (3.85 mg, 0.0037 mmol) in dry toluene (3.5 mL) was stirred for 15 min at 40 °C under argon. Then, 44 (200 mg, 0.37 mmol), Cs_2CO_3 (364 mg 1.12 mmol), and 5-nitroindoline (**45**, 91.6 mg, 0.56 mmol) were added. The reaction mixture was degassed in an ultrasonic bath and stirred for 140 h at 80 °C. The reaction mixture was diluted with EtOAc (10 mL) and washed with aqueous saturated $NaHCO_3$ and brine. The aqueous layers were extracted with EtOAc (3 × 10 mL), and the combined organic layers were dried over Na_2SO_4, filtered, and concentrated under reduced pressure. The residue was purified by chromatography on silica (5−40% gradient of EtOAc in petrol ether) to give 47**a** (163 mg, 75%) as an orange solid. $[\alpha]_D^{20}$ +55.0 (*c* 1.00, $CHCl_3$). ^{1}H NMR (500 MHz, $CDCl_3$): δ 7.98 (dd, *J* = 2.3 Hz, 8.9 Hz, 1H, Ar−H), 7.95 (s, 1H, Ar−H), 7.21 (m, 1H, Ar−H), 7.13 (m, 3H, Ar−H), 6.73 (d, *J* = 8.9 Hz, 1H, Ar−H), 5.55 (dd, *J* = 10.1, 3.5 Hz, 1H, H-3), 5.50 (d, *J* = 1.6 Hz, 1H, H-1), 5.44 (dd, *J* = 3.5, 1.8 Hz, 1H, H-2), 5.38 (t, *J* = 10.1 Hz, 1H, H-4), 4.28 (dd, *J* = 12.5, 5.2 Hz, 1H, H-6a), 4.08 (m, 4H, CH_2, H-6b, H-5), 3.19 (t, *J* = 8.6 Hz, 2H, CH_2), 2.20, 2.18, 2.04, 2.02 (4s, 12H, OAc). ^{13}C NMR (125 MHz, $CDCl_3$): δ 170.70, 170.23, 170.19, 169.90 (4 CO), 137.21, 128.40, 126.27, 122.03, 121.32, 117.92, 117.81, 105.52 (Ar−C), 96.36 (C-1), 69.53 (C-5), 69.40 (C-2), 68.98 (C-3), 66.03 (C-4), 62.28 (C-6), 53.85 (CH_2), 27.27 (CH_3), 21.65, 21.09, 20.92, 20.90 (4 $COCH_3$). MS (ESI) *m*/*z* calcd for $C_{28}H_{31}N_2O_{12}$ [M + H]$^+$, 587.19; found, 587.29.

*2-Chloro-4-(5-nitroindolin-1-yl)phenyl 2,3,4,6-Tetra-O-acetyl-α-D-mannopyranoside (**47c**).* According to the procedure described for 47**a**, compound 7 (60 mg, 0.10 mmol) was microwave irradiated with Cs_2CO_3 (100 mg 0.30 mmol), X-Phos (4.9 mg, 0.010 mmol), $Pd_2(dba)_3$ (2.21 mg, 0.0020 mmol), and 5-nitroindoline (**45**, 50.5 mg, 0.30 mmol) in toluene (1 mL) to yield 47**c** (36 mg, 56%) as an orange solid. $[\alpha]_D^{20}$ +99.6 (*c* 0.08, $CHCl_3$). ^{1}H NMR (500 MHz, $CDCl_3$): δ 8.03 (dd, *J* = 8.8, 2.3 Hz, 1H, Ar−H), 7.99 (m, 1H, Ar−H), 7.30 (d, *J* = 2.7 Hz, 1H, Ar−H), 7.26−7.08 (m, 2H, Ar−H), 6.82 (d, *J* = 8.9 Hz, 1H, Ar−H), 5.59 (dd, *J* = 10.1, 3.4 Hz, 1H, H-3), 5.54−5.46 (m, 2H, H-2, H-1), 5.39 (t, *J* = 10.1 Hz, 1H, H-4), 4.28 (dd, *J* = 12.2, 5.1 Hz, 1H, H-6a), 4.21 (m, 1H, H-5), 4.10 (dd, *J* = 12.3, 2.2 Hz,

1H, H-6b), 4.06 (t, J = 9.0 Hz, 2H, CH_2), 3.20 (t, J = 8.6 Hz, 2H, CH_2), 2.19, 2.06, 2.05, 2.03 (4s, 12H, OAc). ^{13}C NMR (125 MHz, $CDCl_3$): δ 170.69, 170.21, 170.04, 169.94 (4 CO), 152.91, 147.91, 138.24, 131.61, 129.24, 128.43, 125.72, 122.33, 121.42, 119.52, 118.45, 106.00 (Ar–C), 97.42 (C-1), 70.00 (C-3), 69.53 (C-2), 68.90 (C-5), 65.99 (C-4), 62.31 (C-6), 53.70 (CH_3), 27.31 (CH_3), 21.11, 20.94, 20.92 (4C, 4 $COCH_3$). MS (ESI) m/z calcd for $C_{28}H_{39}ClN_2NaO_{12}$ $[M + Na]^-$, 643.13; found, 643.19.

4-(5-Nitroindolin-1-yl)phenyl α-D-Mannopyranoside (48a). Compound **47a** (218 mg, 0.37 mmol) was dissolved in MeOH (2 mL) and treated at rt with 0.5 M NaOMe/MeOH (1 mL) for 20 h. The reaction mixture was neutralized with amberlyst-15 (H^-) ion-exchange resin and filtered. The filtrate was concentrated, and the residue was purified by RP-18 chromatography (H_2O/MeOH, gradient from 0 to 20% MeOH), followed by P2 size exclusion chromatography to yield **48a** (77.7 mg, 50%) as a colorless solid after a final lyophilization from water/dioxane. $[\alpha]_D^{20}$ +57.0 (c 0.10, MeOH). ^1H NMR (500 MHz, CD_3OD): δ 8.00 (m, 2H, Ar–H), 7.31 (m, 2H, Ar–H), 7.21 (m, 2H, Ar–H), 6.78 (d, J = 8.5 Hz, 1H, Ar–H), 5.47 (d, J = 2.0 Hz, 1H, H-1), 4.12 (m, 2H, NCH_2), 4.02 (dd, J = 3.3, 1.8 Hz, 1H, H-2), 3.90 (dd, J = 9.4, 3.4 Hz, 1H, H-3), 3.79 (dd, J = 12.0, 6.4 Hz, 1H, H-6a), 3.73 (m, 2H, H-6b, H-4), 3.62 (ddd, J = 9.7, 5.3, 2.3 Hz, 1H, H-5), 3.21 (t, J = 8.5 Hz, 2H, CH_2). ^{13}C NMR (125 MHz, CD_3OD): δ 154.98, 137.95, 127.14, 123.52, 122.02, 119.08, 106.41 (Ar–C), 100.69 (C-1), 75.62 (C-5), 72.54 (C-3), 72.13 (C-2), 68.50 (C-4), 62.86 (C-6), 55.07 (CH_2), 28.03 (CH_2). HRMS (ESI) m/z calcd for $C_{20}H_{23}N_2O_8$ $[M + H]^-$, 419.1449; found, 419.1453.

2-Chloro-4-(5-nitroindolin-1-yl)phenyl α-D-Mannopyranoside (48c). According to the procedure described for **48a**, compound **47c** (36 mg, 0.058 mmol) was treated with 0.5 M NaOMe/MeOH (0.5 mL) in MeOH (1 mL) for 21 h. After workup, the residue was purified by RP-18 chromatography (H_2O/MeOH, gradient from 0 to 20% MeOH) and P2 size exclusion chromatography to yield **48c** (16.5 mg, 63%) as a colorless solid after a final lyophilization from water/dioxane. $[\alpha]_D^{20}$ +53.8 (c 0.21, MeOH/$CHCl_3$). ^1H NMR (500 MHz, CD_3OD): δ 8.05–8.01 (m, 2H, Ar–H), 7.42 (m, 2H, Ar–H), 7.28 (dd, J = 9.0, 2.5 Hz, 1H, Ar–H), 6.86 (d, J = 8.5 Hz, 1H, Ar–H), 5.51 (d, J = 1.5 Hz, 1H, H-1), 4.11 (m, 3H, NCH_2, H-2), 3.97 (dd, J = 9.3, 3.4 Hz, 1H, H-3), 3.81(dd, J = 11.7, 2.2 Hz, 1H, H-6a), 3.64 (ddd, J = 9.7, 5.6, 2.2 Hz, 1H, H-5), 3.23 (t, J = 8.6 Hz, 2H, CH_2). ^{13}C NMR (125 MHz, CD_3OD): δ 134.69, 133.05, 132.87, 130.67, 129.03, 126.83, 123.31, 121.97, 121.31, 119.65, 106.72 (Ar–C), 101.25 (C-1), 76.04 (C-5), 72.40 (C-3), 71.88 (C-2), 68.27 (C-4), 62.73 (C-6), 54.74 (CH_3), 27.93 (CH_2). HRMS (ESI) m/z calcd for $C_{20}H_{21}ClN_2NaO_8$ $[M + Na]^-$, 475.0879; found, 475.0875.

In Vitro Activity. *Cell-Free Binding Assay.* To determine the affinity of the various FimH antagonists, a cell-free binding assay described previously[12] was applied. A recombinant protein consisting of the CRD of FimH linked with a thrombin cleavage site to a 6His-tag (FimH-CRD-Th-6His) was expressed in *E. coli* strain HM125 and purified by affinity chromatography. Microtiter plates (F96 MaxiSorp, Nunc) were coated with 100 μL/well of a 10 μg/mL solution of FimH-CRD-Th-6His in 20 mM HEPES, 150 mM NaCl, and 1 mM $CaCl_2$, pH 7.4 (assay buffer), overnight at 4 °C. The coating solution was discarded, and the wells were blocked with 150 μL/well of 3% BSA in assay buffer for 2 h at 4 °C. After three washing steps with assay buffer (150 μL/well), a 4-fold serial dilution of the test compound (50 μL/well) in assay buffer containing 5% DMSO and streptavidin-peroxidase coupled biotinylated polyacrylamide (PAA) glycopolymers [Manα1−3(Manα1−6)Manβ1−4GlcNAcβ1−4GlcNAcβ-PAA-biotin, TM-PAA] (50 μL/well of a 0.5 μg/mL solution), was added. On each individual microtiter plate, *n*-heptyl α-D-mannopyranoside (**1**) was tested as a reference compound. The plates were incubated for 3 h at 25 °C and 350 rpm and then carefully washed four times with 150 μL/well assay buffer. After the addition of 100 μL/well of the horseradish peroxidase substrate 2,2′-azino-di(3-ethylbenzthiazoline-6-sulfonic acid) (ABTS), the colorimetric reaction was allowed to develop for 4 min, then stopped by the addition of 2% aqueous oxalic acid before the optical density (OD) was measured at 415 nm on a microplate-reader (Spectramax 190, Molecular Devices, CA). The IC_{50} values of the compounds tested in duplicates were calculated with the prism software (GraphPad Software, Inc., La Jolla, CA). The IC_{50} defines the molar concentration of the test compound that reduces the maximal specific binding of TM-PAA polymer to FimH-CRD by 50%. The relative IC_{50} (rIC_{50}) is the ratio of the IC_{50} of the test compound to the IC_{50} of *n*-heptyl α-D-mannopyranoside (**1**).

Bacteria and Growth. The clinical *E. coli* isolate UTI89[38] (UTI89wt) was kindly provided by the group of Prof. Urs Jenal, Biocenter, University of Basel, Switzerland. Microorganisms were stored at −70 °C and incubated for 24 h before the experiments under static conditions at 37 °C in 10 mL of Luria–Bertani broth (Becton, Dickinson and Company, Le Pont de Claix, France) using 50 mL tubes. Prior to each experiment, the microorganisms were washed twice and resuspended in phosphate-buffered saline (PBS, Sigma-Aldrich, Buchs, Switzerland). Bacterial concentrations were determined by plating serial 1:10 dilutions on blood agar, followed by colony counting with 20–200 colonies after overnight incubation at 37 °C.

Aggregometry Assay. The aggregometry assay was carried out as previously described.[19] In short, the percentage of aggregation of *E. coli* UTI89 with GPEs was quantitatively determined by measuring the optical density at 740 nm and 37 °C under stirring at 1000 rpm using an APACT 4004 aggregometer (Endotell AG, Allschwil, Switzerland). Bacteria were cultivated as described above. GPEs were separated from guinea pig blood (Charles River Laboratories, Sulzfeld, Germany) using Histopaque (density of 1.077 g/mL at 24 °C, Sigma-Aldrich). Prior to the measurements, the cell densities of *E. coli* and GPE were adjusted to an OD_{600} of 4, corresponding to 1.9×10^8 CFU/mL and 2.2×10^6 cells/mL, respectively. For the calibration of the instrument, the aggregation of platelet poor plasma (PPP) using PBS alone was set as 100%, and the aggregation of platelet rich plasma (PRP) using GPE was set as 0%. After calibration, measurements were performed with 250 μL of GPE and 50 μL of bacterial suspension, and the aggregation was monitored over 600 s. After the aggregation phase of 600 s, 25 μL of antagonist in PBS was added to each cuvette, and disaggregation was monitored for 1400 s.

Cultivation of 5637 Cells. The human epithelial bladder carcinoma cell line 5637 was obtained from the German Collection of Microorganisms and Cell Cultures (DSMZ, Braunschweig, Germany). The cells were grown in RPMI 1640 medium, supplemented with 10% fetal calf serum (FCS), 100 U/mL penicillin, and 100 μg/mL streptomycin at 37 °C, 5% CO_2. All solutions were purchased from Invitrogen (Basel, Switzerland). The cells were subcultured 1:5 twice per week for six passages before using them in the infection assay. Two days before infection, 1.8×10^5 cells were seeded in each well of a 24-well plate in RPMI 1640 containing 10% FCS without antibiotics. The cell density was approximately (3–5) $\times 10^5$ cells/well prior the infection.

Flow Cytometry Infection Assay. The infection assay was carried out as previously described.[33] Briefly, to evaluate FimH antagonists, a serial dilution of the antagonists in 5% DMSO was prepared. Before infection, a suspension of green fluorescently labeled (GFP) bacteria (UTI89, 200 μL) and 25 μL of the test compound were preincubated for 10 min at room temperature. The bacteria–antagonist mixture was then added to the monolayer of 5637 cells (grown in 24-well plates, as described above) at a multiplicity of infection (MOI) of 1:50 (cell:bacteria). To homogenize the infection, plates were centrifuged at room temperature for 3 min at 600g. After an incubation of 1.5 h at 37 °C, infected cells were washed four times with RPMI 1640 medium and suspended in ice-cold PBS for 5–20 min. Cells were then kept in the dark until analysis. All measurements were made within 1 h after the termination of the infection. Samples were acquired in a CyAn ADP flow cytometer (Becton, Dickinson and Company) and analyzed by gating on the eukaryotic cells based on forward (FSC) and side scatter (SSC), which excludes unbound GFP-labeled bacteria and debris from analysis. A total of 10^4 cells were measured per sample. Data were acquired in a linear mode for the side scatter (SSC) and in a logarithmic mode for the forward scatter (FSC) and the green

fluorescent channel FL1-H (e.g., GFP). The MFI of FL1-H was counted as a surrogate marker for the adherence of bacteria. Quantification of adhesion was evaluated with the FlowJo software 9.0.1 (Tree Star, Inc., Ashland, OR). IC_{50} values were determined by plotting the concentration of the antagonist in logarithmic mode versus the MFI and by fitting the curve with the prism software (GraphPad, inhibition curve, nonlinear regression, variable slope, $n = 4$). The IC_{90} ($F = 90$) was calculated from the determined IC_{50} value and the hill slope (H) as follows:

$$IC_F = \left(\frac{F}{100 - F}\right)^{1/H} \times IC_{50}$$

In Vitro Pharmacokinetic Parameters. *Materials.* DMSO and 1-octanol were purchased from Sigma-Aldrich. PAMPA System Solution, GIT-0 Lipid solution, and Acceptor Sink Buffer were ordered from pIon (Woburn, MA). Human plasma was bought from Biopredic (Rennes, France), and acetonitrile (MeCN) was from Acros Organics (Geel, Belgium).

Log $D_{7.4}$ Determination. The in silico prediction tool ALOGPS[39] was used to estimate the log P values of the compounds. Depending on these values, the compounds were classified into three categories: hydrophilic compounds (log P below zero), moderately lipophilic compounds (log P between zero and one), and lipophilic compounds (log P above one). For each category, two different ratios (volume of 1-octanol to volume of buffer) were defined as experimental parameters (Table 3).

Table 3

compd type	log P	ratios (1-octanol:buffer)
hydrophilic	<0	30:140, 40:130
moderately lipophilic	0−1	70:110, 110:70
lipophilic	>1	3:180, 4:180

Equal amounts of phosphate buffer (0.1 M, pH 7.4) and 1-octanol were mixed and shaken vigorously for 5 min to saturate the phases. The mixture was left until separation of the two phases occurred, and the buffer was retrieved. Stock solutions of the test compounds were diluted with buffer to a concentration of 1 μM. For each compound, six determinations, that is, three determinations per 1-octanol:buffer ratio, were performed in different wells of a 96-well plate. The respective volumes of buffer containing analyte (1 μM) were pipetted to the wells and covered by saturated 1-octanol according to the chosen volume ratio. The plate was sealed with aluminum foil, shaken (1350 rpm, 25 °C, 2 h) on a Heidolph Titramax 1000 plate-shaker (Heidolph Instruments GmbH & Co. KG, Schwabach, Germany), and centrifuged (2000 rpm, 25 °C, 5 min, 5804 R Eppendorf centrifuge, Hamburg, Germany). The aqueous phase was transferred to a 96-well plate for analysis by LC-MS (see below).

log $D_{7.4}$ was calculated from the 1-octanol:buffer ratio (o:b), the initial concentration of the analyte in buffer (1 μM), and the concentration of the analyte in the aqueous phase (c_B) with equation:

$$\log D_{7.4} = \log\left(\frac{1\ \mu M - c_B}{c_B} \times \frac{1}{o{:}\ b}\right)$$

The average of the three log $D_{7.4}$ values per 1-octanol:buffer ratio was calculated. If the two means obtained for a compound did not differ by more than 0.1 unit, the results were accepted.

PAMPA. Log P_e was determined in a 96-well format with the PAMPA[21a] permeation assay. For each compound, measurements were performed at three pH values (5.0, 6.2, and 7.4) in quadruplicates. For this purpose, 12 wells of a deep well plate, that is, four wells per pH value, were filled with 650 μL of System Solution. Samples (150 μL) were withdrawn from each well to determine the blank spectra by UV spectroscopy (SpectraMax 190, Molecular Devices). Then, analyte dissolved in DMSO was added to the remaining System Solution to yield 50 μM solutions. To exclude precipitation, the optical density was measured at 650 nm, with 0.01 being the threshold value. Solutions exceeding this threshold were filtrated. Afterward, samples (150 μL) were withdrawn to determine the reference spectra. Further samples (200 μL) were transferred to each well of the donor plate of the PAMPA sandwich (pIon, Woburn, MA, P/N 110 163). The filter membranes at the bottom of the acceptor plate were impregnated with 5 μL of GIT-0 Lipid Solution, and 200 μL of Acceptor Sink Buffer was filled into each acceptor well. The sandwich was assembled, placed in the GutBox, and left undisturbed for 16 h. Then, it was disassembled, and samples (150 μL) were transferred from each donor and acceptor well to UV plates. Quantification was performed by both UV spectroscopy and LC-MS (see below). log P_e values were calculated with the aid of the PAMPA Explorer Software (pIon, version 3.5).

Thermodynamic Solubility. Microanalysis tubes (LaboTech J. Stofer LTS AG, Muttenz, Switzerland) were charged with 1 mg of solid substance and 250 μL of phosphate buffer (50 mM, pH 6.5). The tubes were briefly shaken by hand, sonicated for 15 min, and vigorously shaken (600 rpm, 25 °C, 2 h) on an Eppendorf Thermomixer Comfort. Afterward, they were left undisturbed for 24 h. After the pH was measured, the compound solutions were filtered (MultiScreen HTS 96-well Filtration System, Millipore, Billerica, MA) by centrifugation (1500 rpm, 25 °C, 3 min). The filtrates were diluted (1:2, 1:10, and 1:100 or, if the results were outside of the calibration range, 1:1000 and 1:10000), and the concentrations were determined by LC-MS (see below). The calibration was based on six values ranging from 0.1 to 10 μg/mL.

PPB. The dialysis membranes (MWCO 12−14 K; HTDialysis LCC, Gales Ferry, CT) were prepared according to the instructions of the manufacturer. The human plasma was centrifuged (5800 rpm, 25 °C, 10 min), the pH of the supernatant (without floating plasma lipids) was adjusted to 7.5, and the analyte was added to yield 10 μM solutions. PPB determinations were performed in triplicate. Equal volumes (150 μL) of phosphate buffer (0.1 M, pH 7.4) and plasma containing the analyte were transferred to the separated compartments of the 96-well high throughput dialysis block (HTDialysis LCC). The plate was covered with a sealing film and incubated (5 h, 37 °C). Afterward, samples (90 μL) were withdrawn from the buffer compartments and diluted with plasma (10 μL). From the plasma compartments, samples (10 μL) were withdrawn and diluted with phosphate buffer (90 μL). The solutions were further diluted with ice-cooled MeCN (300 μL) to precipitate the proteins and centrifuged (3600 rpm, 4 °C, 11 min). The supernatants (50 μL) were retrieved, and the analyte concentrations were determined by LC-MS (see below). The fraction bound (f_b) was calculated as follows:

$$f_b = 1 - \frac{c_b}{c_p}$$

where c_b is the concentration of the analyte in the buffer compartment and c_p is the concentration in the plasma compartment. The values were accepted if the recovery of analyte was between 80 and 120% of the initial amount.

LC-MS Measurements. Analyses were performed using a 1100/1200 Series HPLC System coupled to a 6410 Triple Quadrupole mass detector (Agilent Technologies, Inc., Santa Clara, CA) equipped with electrospray ionization. The system was controlled with the Agilent MassHunter Workstation Data Acquisition software (version B.01.04). The column used was an Atlantis T3 C18 column (2.1 mm × 50 mm) with a 3 μm particle size (Waters Corp., Milford, MA). The mobile phase consisted of two eluents: solvent A (H_2O, containing 0.1% formic acid, v/v) and solvent B (acetonitrile, containing 0.1% formic acid, v/v), both delivered at a flow rate of 0.6 mL/min. The gradient was ramped from 95% A/5% B to 5% A/95% B over 1 min and then held at 5% A/95% B for 0.1 min. The system was then brought back to 95% A/5% B, resulting in a total duration of 4 min. MS parameters such as fragmentor voltage, collision energy, and polarity were optimized individually for each compound, and the molecular ion was followed for each compound in the multiple reaction monitoring

mode. The concentration of each analyte was quantified by the Agilent Mass Hunter Quantitative Analysis software (version B.01.04).

In Vivo Pharmacokinetic and Treatment Studies. *Animals.* Female C3H/HeN mice weighing between 19 and 25 g were obtained from Charles River Laboratories and were housed three or four to a cage. Mice were kept under specific pathogen-free conditions in the Animal House of the Department of Biomedicine, University Hospital Basel, and animal experimentation guidelines according to the regulations of Swiss veterinary law were followed. After 7 days of acclimatization, 9−10 week old mice were used for the PK and infection study. During the studies, animals were allowed free access to chow and water. Three days before infection studies and during infection, 5% D-(+)-glucose (AppliChem, Baden-Dättwil, Switzerland) was added to the drinking water, to increase the number of bacterial counts in the urine and kidneys.[10]

Pharmacokinetic Studies. Single-dose PK studies were performed by iv application of the FimH antagonist at the designated dosages followed by urine and plasma sampling. For iv application, the antagonists were diluted in 100 μL of PBS and injected into the tail vein. Blood and urine were sampled (10 μL) after 6 and 30 min and 1, 2, 4, 6, and 8 h. Before analysis, proteins in blood and urine samples were precipitated using methanol (Acros Organics) and centrifuged for 11 min at 13000 rpm. The supernatant was transferred into a 96-well plate (0.5 mL, polypropylene, Agilent Technologies) and analyzed by LC-MS as described above.

UTI Mouse Model. Mice were infected as previously described.[10] In brief, before infection, all remaining urine was depleted form the bladder by gentle pressure on the abdomen. Mice were anesthetized with 1.1 vol% isoflurane/oxygen mixture (Attane, Minrad Inc., Buffalo, NY) and placed on their backs. Anesthetized mice were inoculated transurethrally with the bacterial suspension by use of a 2 cm polyethylene catheter (Intramedic polyethylene tubing; inner diameter, 0.28 mm; outer diameter, 0.61 mm; Beckton, Dickinson and Company), which was placed on a syringe (Hamilton Gastight Syringe 50 μL, removable 30G needle, BGB Analytik AG, Boeckten, Switzerland). The catheter was gently inserted through the urethra until it reached the top of the bladder, followed by slow injection of 50 μL of bacterial suspension at a concentration of approximately 5×10^7 to 5×10^8 CFU.

Antagonist Treatment Studies. The FimH antagonists were applied iv in 100 μL of PBS into the tail vein 10 min before infection. Three hours after the onset of infection, mice were sacrificed with CO_2. Organs were removed aseptically and homogenized in 1 mL of PBS by using a tissue lyser (Retsch, Haan, Germany). Serial dilutions of bladder and kidneys were plated on Levine Eosin Methylene Blue Agar plates (Beckton, Dickinson and Company). CFU counts were determined after overnight incubation at 37 °C and expressed as CFU/organ, corresponding to CFU/bladder and CFU/2 kidneys.

■ ASSOCIATED CONTENT

Supporting Information

Synthesis of compounds **7−10**, **14−20**, **23−37**, **39−42**, **44**, **47b,d**, **48b,d**, **50−52**, and **55−58**; HRMS data, HPLC traces, and ^{1}H NMR spectra for the target compounds **21−29**, **31**, **32**, **36**, **37**, **41**, **42**, **48a−d**, **52**, **57**, and **58**. This material is available free of charge via the Internet at http://pubs.acs.org.

■ AUTHOR INFORMATION

Corresponding Author

*Tel: +41 61 267 15 51. Fax: +41 61 267 15 52. E-mail: beat.ernst@unibas.ch.

Author Contributions

†These authors contributed equally to the project.

Notes

The authors declare no competing financial interest.

■ ACKNOWLEDGMENTS

We thank Prof. Urs Jenal, Biocenter of the University of Basel, Switzerland, for the clinical *E. coli* isolate UTI89. We further appreciate the support by Prof. Dr. med. Radek Skoda, Department of Biomedicine, University Hospital Basel, Switzerland, for giving us access to the animal facility. The financial support by the Swiss National Science Foundation (SNF interdisciplinary grant K-32K1-120904) is gratefully acknowledged.

■ ABBREVIATIONS USED

ABTS, 2,2′-azino-di(3-ethylbenzthiazoline-6-sulfonic acid); AUC, area under the curve; CFU, colony-forming units; CRD, carbohydrate recognition domain; log $D_{7.4}$, distribution coefficient at pH 7.4; DCM, dichloromethane; dba, dibenzylideneacetone; DMSO, dimethyl sulfoxide; GFP, green fluorescent protein; GPE, guinea pig erythrocytes; IC_{50}, half maximal inhibitory concentration; IC_{90}, concentration where 90% of the maximal observed effect is obtained; iv, intravenous; $MIC_{adhesion}$, minimal inhibitory concentration of adhesion; Man, D-mannose; MD, molecular dynamics; MFI, mean fluorescent intensity; NMR, nuclear magnetic resonance; PAMPA, parallel artificial membrane permeation assay; P_e, effective permeation; PPB, plasma protein binding; PK, pharmacokinetic; PPP, platelet poor plasma; PRP, platelet rich plasma; rIC_{50}, relative inhibitory concentration; *S*, solubility; SAR, structure−activity relationship; sc, subcutaneous; $T > MIC_{adhesion}$, time over the minimal inhibitory concentration of adhesion; TM-PAA, Manα1−3(Manα1−6)Manβ1−4GlcNAcβ1−4GlcNAcβ-polyacrylamide-biotin; TMSOTf, trimethylsilyl trifluoromethanesulfonate; UPEC, uropathogenic *Escherichia coli*; UPIa, uroplakin Ia; UTI, urinary tract infection; X-Phos, 2-dicyclohexylphosphino-2′,4′,6′-triisopropylbiphenyl

■ REFERENCES

(1) (a) Berglund, J.; Knight, S. D. Structural basis for bacterial adhesion in the urinary tract. *Adv. Exp. Med. Biol.* **2003**, *535*, 33−52. (b) Westerlund-Wikström, B.; Korhonen, T. K. Molecular structure of adhesin domains in *Escherichia coli* fimbriae. *Int. J. Med. Microbiol.* **2005**, *295*, 479−486.

(2) Wiles, T. J.; Kulesus, R. R.; Mulvey, M. A. Origins and virulence mechanisms of uropathogenic *Escherichia coli*. *Exp. Mol. Pathol.* **2008**, *85*, 11−19.

(3) Mulvey, M. A. Adhesion and entry of uropathogenic *Escherichia coli*. *Cell Microbiol.* **2002**, *4*, 257−271.

(4) Capitani, G.; Eidam, O.; Glockshuber, R.; Grutter, M. G. Structural and functional insights into the assembly of type 1 pili from *Escherichia coli*. *Microbes Infect.* **2006**, *8*, 2284−2290.

(5) Sharon, N. Carbohydrates as future anti-adhesin drugs for infectious diseases. *Biochim. Biophys. Acta* **2006**, *1760*, 527−537.

(6) (a) Firon, N.; Ofek, I.; Sharon, N. Interaction of mannose-containing oligosaccharides with the fimbrial lectin of *Escherichia coli*. *Biochem. Biophys. Res. Commun.* **1982**, *105*, 1426−1432. (b) Firon, N.; Ofek, I.; Sharon, N. Carbohydrate specificity of the surface lectins of *Escherichia coli*, *Klebsiella pneumoniae* and *Salmonella typhimurium*. *Carbohydr. Res.* **1983**, *120*, 235−249. (c) Sharon, N. Bacterial lectins, cell-cell recognition and infectious disease. *FEBS Lett.* **1987**, *217*, 145−157.

(7) (a) Pieters, R. J. Maximising multivalency effects in protein-carbohydrate interactions. *Org. Biomol. Chem.* **2009**, *7*, 2013−2025. (b) Imberty, A.; Chabre, Y. M.; Roy, R. Glycomimetics and glycodendrimers as high affinity microbial anti-adhesins. *Chem.—Eur. J.* **2008**, *14*, 7490−7499.

(8) Hartmann, M.; Lindhorst, T. K. The bacterial lectin FimH, a target for drug discovery-carbohydrate inhibitors of type 1 fimbriae-mediated bacterial adhesin. *Eur. J. Org. Chem.* **2011**, 3583−3609.
(9) (a) Choudhury, D.; Thompson, A.; Stojanoff, V.; Langermann, S.; Pinkner, J.; Hultgren, S. J.; Knight, S. D. X-ray structure of the FimC-FimH chaperone-adhesin complex from uropathogenic *Escherichia coli*. *Science* **1999**, *285*, 1061−1066. (b) Bouckaert, J.; Berglund, J.; Schembri, M.; Genst, E. D.; Cools, L.; Wuhrer, M.; Hung, C. S.; Pinkner, J.; Slättergard, R.; Zavialov, A.; Choudhury, D.; Langermann, S.; Hultgren, S. J.; Wyns, L.; Klemm, P.; Oscarson, S.; Knight, S. D.; Greve, H. D. Receptor binding studies disclose a novel class of high-affinity inhibitors of the *Escherichia coli* FimH adhesin. *Mol. Microbiol.* **2005**, *55*, 441−455. (c) Wellens, A.; Garofalo, C.; Nguyen, H.; Van Gerven, N.; Slättergård, R.; Hernalsteens, J.-P.; Wyns, L.; Oscarson, S.; De Greve, H.; Hultgren, S.; Bouckaert, J. Intervening with urinary tract infections using anti-adhesives based on the crystal structure of the FimH-oligomannose-3 complex. *PLos One* **2008**, *3*, 4−13. (d) Han, Z.; Pinker, J. S.; Ford, B.; Obermann, R.; Nolan, W.; Wildman, S. A.; Hobbs, D.; Ellenberger, T.; Cusumano, C. K.; Hultgren, S. J.; Janetka, J. W. Structure-based drug design and optimization of mannoside bacterial FimH antagonists. *J. Med. Chem.* **2010**, *53*, 4779−4792.
(10) (a) Sperling, O.; Fuchs, A.; Lindhorst, T. K. Evaluation of the carbohydrate recognition domain of the bacterial adhesin FimH: design, synthesis and binding properties of mannoside ligands. *Org. Biomol. Chem.* **2006**, *4*, 3913−3922. (b) Grabosch, C.; Hartmann, M.; Schmidt-Lassen, J.; Lindhorst, T. K. Squaric acid monoamide mannosides as ligands for the bacterial lectin FimH: Covalent inhibition or not? *ChemBioChem* **2011**, *12*, 1066−1074.
(11) Klein, T.; Abgottspon, D.; Wittwer, M.; Rabbani, S.; Herold, J.; Jiang, X.; Kleeb, S.; Lüthi, C.; Scharenberg, M.; Bezençon, J.; Gubler, E.; Pang, L.; Smiesko, M.; Cutting, B.; Schwardt, O.; Ernst, B. FimH antagonist for the oral treatment of urinary tract infections: From design and synthesis to in vitro and in vivo evaluation. *J. Med. Chem.* **2010**, *53*, 8627−8641.
(12) Rabbani, S.; Jiang, X.; Schwardt, O.; Ernst, B. Expression of the carbohydrate recognition domain of FimH and development of a competitive binding assay. *Anal. Biochem.* **2010**, *407*, 188−195.
(13) Cusumano, C. K.; Pinkner, J. S.; Han, Z.; Greene, S. E.; Ford, B. A.; Crowley, J. R.; Henderson, J. P.; Janetka, J. W.; Hultgren, S. J. Treatment and prevention of urinary tract infection with orally active FimH inhibitors. *Sci. Transl. Med.* **2011**, *3*, 1−10.
(14) Kerékgyártó, J.; Kamerling, J. P.; Bouwstra, J. B.; Vliegenthasrt, J. F. G.; Liptak, A. Synthesis of four structural elements of xylose-containing carbohydrate chains from N-glycoproteins. *Carbohydr. Res.* **1989**, *186*, 51−62.
(15) (a) Ma, D.; Cai, Q. L-Proline promoted Ullmann type coupling reactions of aryl iodides with indoles, pyrroles, imidazoles or pyrazoles. *Synlett* **2004**, 128−130. (b) Ma, D.; Cai, Q. Copper/Amino acid catalyzed cross-couplings of aryl and vinyl halides with nucleophiles. *Acc. Chem. Res.* **2008**, *41*, 1450−1460. and the references thereof (c) Ley, S. V.; Thomas, A. W. Modern Synthetic methods for copper-mediated C(aryl)-O, C(aryl)-N, and C(aryl)-S bond formation. *Angew. Chem., Int. Ed.* **2003**, *42*, 5400−5449. (d) Antilla, J. C.; Klapars, A.; Buchwald, S. L. The copper-catalyzed N-arylation of indoles. *J. Am. Chem. Soc.* **2002**, *124*, 11684−11688.
(16) Kosak, J. R. Catalytic hydrogenation of aromatic halonitro compounds. *Ann. N.Y. Acad. Sci.* **1970**, *172*, 175−185.
(17) Wolfe, J. P.; Wagaw, S.; Marcoux, J.-F.; Buchwald, S. L. Rational development of practical catalysts for aromatic carbon-nitrogen bond formation. *Acc. Chem. Res.* **1998**, *31*, 805−818.
(18) Prieto, M; Zurita, E.; Rosa, E.; Muñoz, L.; Lloyd-Williams, P.; Giralt, E. Arylboronic acids and arylpinacolboronate esters in Suzuki-coupling reactions involving indoles. Partner role swapping and heterocycle protection. *J. Org. Chem.* **2004**, *69*, 6812−6820.
(19) Abgottspon, D.; Rölli, G.; Hosch, L.; Steinhuber, A.; Jiang, X.; Schwardt, O.; Cutting, B.; Smiesko, M.; Jenal, U.; Ernst, B.; Trampuz, A. Development of an aggregation assay to screen FimH antagonists. *J. Microbiol. Methods* **2010**, *82*, 249−255.
(20) Bouckaert, J.; Mackenzie, J.; de Paz, J. L.; Chipwaza, B.; Choudhury, D.; Zavialov, A.; Mannerstedt, K.; Anderson, J.; Pierard, D.; Wyns, L.; Seeberger, P. H.; Oscarson, S.; De Greve, H.; Knight, S. D. The affinity of the FimH fimbrial adhesin is receptor-driven and quasi-independent of *Escherichia coli* pathotypes. *Mol. Microbiol.* **2006**, *61*, 1556−1568.
(21) Giampapa, C. S.; Abraham, S. N.; Chiang, T. M.; Beachey, E. H. Isolation and characterization of a receptor for type 1 fimbriae of *Escherichia coli* from guinea pig erythrocytes. *J. Biol. Chem.* **1988**, *263*, 5362−5367.
(22) Aprikian, P.; Tchesnokova, V.; Kidd, B.; Yakovenko, O.; Yarov-Yarovoy, V.; Trinchina, E.; Vogel, V.; Thomas, W.; Sokurenko, E. Interdomain interaction in the FimH adhesin of *Escherichia coli* regulates the affinity to mannose. *J. Biol. Chem.* **2007**, *282*, 23437−23446.
(23) Trong, I. L.; Aprikian, P.; Kidd, B. A.; Forero-Shelton, M.; Tchesnokova, V.; Rajagopal, P.; Rodriguez, V.; Interlandi, G.; Klevit, R.; Vogel, V.; Stenkamp, R. E.; Sokurenko, E. V.; Thomas, W. E. Structural basis for mechanical force regulation of the adhesin FimH via finger trap-like beta sheet twisting. *Cell* **2010**, *141*, 645−655.
(24) (a) Kansy, M.; Senner, F.; Gubernator, K. Physicochemical high throughput screening: Parallel artificial membrane permeation assay in the description of passive absorption processes. *J. Med. Chem.* **1998**, *41*, 1007−1010. (b) Avdeef, A.; Bendels, S.; Di, L.; Faller, B.; Kansy, M.; Sugano, K.; Yamauchi, Y. Parallel artificial membrane permeability assay (PAMPA)-critical factors for better predictions of absorption. *J. Pharm. Sci.* **2007**, *96*, 2893−2909.
(25) Lipinski, C. A. Drug-like properties and the causes of poor solubility and poor permeability. *J. Pharmacol. Toxicol. Methods* **2000**, *44*, 235−249.
(26) Lovering, F.; Bikker, J.; Humblet, C. Escape from flatland: increasing saturation as an approach to improving clinical success. *J. Med. Chem.* **2009**, *52*, 6752−6756.
(27) van de Waterbeemd, H.; Smith, D. A.; Beaumont, K.; Walker, D. K. Property-based design: optimization of drug absorption and pharmacokinetics. *J. Med. Chem.* **2001**, *44*, 1313−1333.
(28) (a) Schmidt, S.; Gonzalez, D.; Derendorf, H. Significance of protein binding in pharmacokinetics and pharmacodynamics. *J. Pharm. Sci.* **2010**, *99*, 1107−1122. (b) Trainor, G. L. The importance of plasma protein binding in drug discovery. *Expert Opin. Drug Discovery* **2007**, *2*, 51−64. (c) Weisiger, R. A. Dissociation from albumin: a potentially rate-limiting step in the clearance of substances by the liver. *Proc. Natl. Acad. Sci. U.S.A.* **1985**, *82*, 1563−1567.
(29) Dearden, J. C.; Bresnen, J. G. M. The measurement of partition coefficients. *QSAR Comb. Sci.* **1988**, *7*, 133−144.
(30) Kerns, E. H. High throughput physicochemical profiling for drug discovery. *J. Pharm. Sci.* **2001**, *90*, 1838−1858.
(31) Banker, M. J.; Clark, T. H.; Williams, J. A. Development and validation of a 96-well equilibrium dialysis apparatus for measuring plasma protein binding. *J. Pharm. Sci.* **2003**, *92*, 967−974.
(32) Andrews, J. M. Determination of minimum inhibitory concentrations. *J. Antimicrob. Chemother.* **2001**, *48* (Suppl1), 5−16.
(33) Scharenberg, M.; Abgottspon, D.; Ciceck, E.; Jiang, X.; Schwardt, O.; Rabbani, S.; Ernst, B. Flow cytometry-based assay for screening FimH antagonists. *Assay Drug Dev. Technol.* **2011**, *9*, 455−464.
(34) Hooton, T. M. Fluoroquinolones and resistance in the treatment of uncomplicated urinary tract infection. *Int. J. Antimicrob. Agents* **2003**, *22*, 65−72.
(35) Jakobsen, L.; Cattoir, V.; Hammerum, A. M.; Nordmann, P.; Frimodt-Møller, N. Impact of low-level fluoroquinolone resistance genes qnrA1, qnrB19, and qnrS1 on ciprofloxacin treatment of *Escherichia coli* urinary tract infection in murine model. Poster presented at ICAAC 2010. 50th Interscience Conference on Antimicrobial Agents and Chemotharapy, 2010, Sep 12−15, Boston, MA.
(36) (a) Russell, W. M. S.; Burch, R. L. *The Principles of Humane Experimental Technique*; Methuen: London, 1959; reprinted: Universities Federation for Animal Welfare, Wheathampstead, United

Kingdom, 1992. (b) Demers, G.; Griffin, G.; De Vroey, G.; Haywood, J. R.; Zurlo, J.; Bédard, M. Harmonization of animal care and use guidance. *Science* **2006**, *312*, 700−701.
(37) Schwardt, O.; Rabbani, S.; Hartmann, M.; Abgottspon, D.; Wittwer, M.; Kleeb, S.; Zalewski, A.; Smiesko, M.; Cutting, B.; Ernst, B. Design, Synthesis and biological evaluation of mannosyl triazoles as FimH antagonists. *Bioorg. Med. Chem.* **2011**, *19*, 6454−6473.
(38) Mulvey, M. A.; Schilling, J. D.; Hultgren, S. J. Establishment of a persistent *Escherichia coli* reservoir during the acute phase of a bladder infection. *Infect. Immun.* **2001**, *69*, 4572−4579.
(39) (a) VCCLAB, Virtual Computational Chemistry Laboratory; http://www.vcclab.org, 2005. (b) Tetko, I. V.; Gasteiger, J.; Todeschini, R.; Mauri, A.; Livingstone, D.; Ertl, P.; Palyulin, V. A.; Radchenko, E. V.; Zefirov, N. S.; Makarenko, A. S.; Tanchuk, V. Y.; Prokopenko, V. V. Virtual computational chemistry laboratory—Design and description. *J. Comput.-Aided Mol. Des.* **2005**, *19*, 453−463.
(40) Kerrn, M. B.; Frimodt-Møller, N.; Espersen, F. Effects of sulfomethizole and amdinocillin against *Escherichia coli* strains (with various susceptibilities) in an ascending urinary tract infection model. *Antimicrob. Agents Chemother.* **2003**, *47*, 1002−1009.

RESULTS AND DISCUSSION

Review

In vivo Evaluation of FimH Antagonists – A Novel Class of Antimicrobials for the Treatment of Urinary Tract Infection.

Abgottspon D, Ernst B.

Chimia (Aarau) **2012**.

My contributions:

Writing of the review.

doi:10.2533/chimia.2012.166 Chimia 66 (2012) 166–169

In vivo Evaluation of FimH Antagonists – A Novel Class of Antimicrobials for the Treatment of Urinary Tract Infection

Daniela Abgottspon§* and Beat Ernst

§SCS-Metrohm Foundation Award for best oral presentation

Abstract: The discovery of antimicrobials as β-lactam antibiotics or aminoglycosides revolutionized the treatment of infectious diseases. However, the extensive use rapidly created the problem of resistant pathogens, which are increasingly difficult to treat. FimH antagonists are a new class of antimicrobials, which target the bacterial adhesion to urothelial cells, a crucial first step in the establishment of urinary tract infections. Because of their different mode of action, FimH antagonists neither kill nor inhibit the growth of bacteria, they should have a reduced potential to generate resistant strains. This mini-review outlines the main problems associated with increasing development of antimicrobial resistance. Furthermore, it summarizes the currently available *in vivo* studies in mice for the treatment of urinary tract infections conducted with FimH antagonists.

Keywords: FimH antagonists · α-D-Mannopyranoside · Type 1 pili · Urinary tract infection (UTI) · Uropathogenic *Escherichia coli* (UPEC)

1. Antibiotics and Resistance – The Microbiological Twins

The discovery of β-lactame antibiotics in the 1930s as well as the introduction of hygienic standards in hospitals (hand washing, use of disinfectants) was an incisive step in the development of public healthcare. Humans gained control over a 10^7 times smaller organism and the mortality from bacterial infections rapidly diminished and concomitantly also the interest to develop new antimicrobials. However, shortly after it was assumed that bacterial infections were under control, the first emergence of resistant strains evolved. The ability of our tiny cohabitants to adapt to new living conditions was severely underrated and only insufficient efforts were undertaken to contain the emerging bacterial threat with new antibiotics.[1] Therefore, since the 1990s, infectious diseases have non-surprisingly developed to become one of the top five causes of death in high-income countries.[2]

The majority of the classes of antimicrobials still used today have their origin in the 1940s to 1970s (Fig. 1).[3] Although numerous chemically modified derivatives entered the market in recent years, real innovation only occurred in the last 10 years when new classes of antibiotics were approved for clinical use (oxazolidinones, lipopeptides and mutilins).[4,11] The diminished interest to develop new antibiotics and the rapidly increasing emergence of resistance led to the highly prevalent problem that for an increasing number of multidrug-resistant (MDR) and pandrug-resistant (PDR) bacteria no effective therapeutic treatment is available.[4] An essential cause for the emergence of antimicrobial resistance is the extensive use of antibiotics, leading to treatment failure, a reduced range of therapeutic options for consecutive bacterial infections and ultimately a serious threat for the patient.[12,13]

The most common bacterial infectious diseases are respiratory tract infections and urinary tract infections (UTIs). Although UTI is not a life-threatening disease, all symptomatic infections should be treated with antibiotics to prevent potential devastating complications, like pyelonephritis and urosepsis. Thus, the availability of a novel class of antimicrobials based on an alternative mode of action would have a huge impact on the treatment of UTI, being a substantial contribution to public health.[14]

2. Adhesion and Infection – The Importance of the FimH Lectin for UTIs

The crucial step for the majority of infectious diseases is the initial contact (adhesion) of the infecting microorgan-

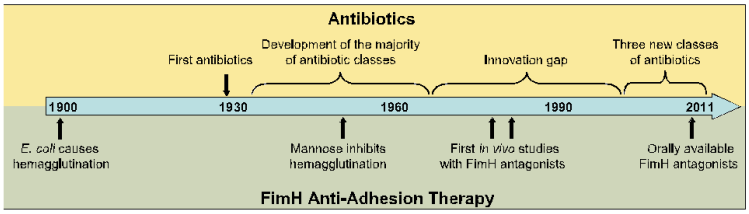

Fig. 1. Timeline of the major steps of the development of antibiotics (top[4]) and the FimH anti-adhesion therapy for the treatment of UTI (bottom[5–10]).

*Correspondence: D. Abgottspon
University of Basel
Institute of Molecular Pharmacy
Klingelbergstrasse 50
CH-4056 Basel
Tel.: +41 61 267 1561
Fax: +41 61 267 1552
E-mail: daniela.abgottspon@unibas.ch

ism with the target cells, enabling bacteria to avoid the natural clearing mechanisms and the immune system and thereby ensure survival in the host environment.[14] UTI is predominantly caused by uropathogenic *Escherichia coli* (UPEC) and strongly depends on the specific adhesion of the pathogen to carbohydrate-containing ligands on the host endothelium.[15] The ability of UPEC to adhere to and to ascend within the urinary tract is mediated *via* filamentous multi-subunit membrane proteins, so-called type 1 pili and P-pili.[16] Whereas P-pili account for the infection of the kidneys (pyelonephritis), type 1 pili are responsible for the initial colonization of the bladder (cystitis). The four subunits FimA, FimF, FimG and FimH compose a type 1 pilus, with FimH located at the tip.[17] As a part of the FimH subunit, a carbohydrate-recognition domain (CRD) is responsible for bacterial attachment to oligomannosides of the glycoprotein uroplakin Ia (UPIa) located on the urinary bladder mucosa.[18] This initial step prevents the rapid clearance of *E. coli* from the urinary tract by the bulk flow of urine and at the same time, initiates the infection process (Fig. 2A).[19]

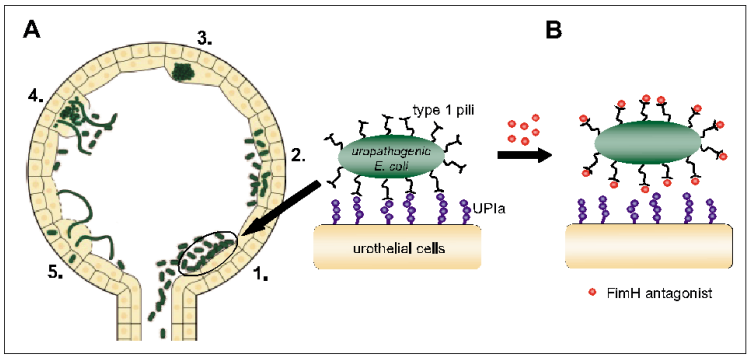

Fig. 2. A) Urinary tract infection cycle. 1. The first and most important step in the development of UTI is the type 1 pili dependent adhesion of UPEC to uroplakin Ia (UPIa) on urothelial cells. 2. Adhesion triggers the invasion of the bacteria into the superficial bladder cells, lining the urinary tract. Once inside the cells, bacteria start to replicate and form 3. intracellular biofilms, where they are well protected from the host defense mechanisms and antibiotic treatment. 4. Later on, cells start to exfoliate and bacteria exit the cells in filamentous structures and 5. disperse in the environment ready to infect new cells (infection cycle adapted from ref. [20]). B) In the presence of FimH antagonists, UPECs are not able to adhere to urothelial cells and are therefore washed out with the flow of urine. As a result, the infection cycle cannot be established.

3. Virulence and FimH – A Target for Anti-Adhesion Therapy

Previous studies clearly demonstrated that type 1 pili deficient UPEC strains are not able to initiate an infection in mice.[21] Furthermore, the immunization of mice with antibodies directed against FimH, protected animals from bladder-colonization with UPEC.[22] These findings strongly suggest that the inhibition of the initial host-pathogen interaction with FimH antagonists as a suitable approach to prevent and treat UTIs.

The host defense system exerts a FimH related mechanism to protect the sterile urinary tract from invading UPECs. The most abundant protein in the urine is the Tamm-Horsfall protein (THP; also called uromodulin). It is a high-mannosylated glycoprotein and is exclusively produced in the kidneys. It is able to neutralize UPEC by binding to their type 1 pili and it thereby prevents the adhesion to urothelial cells.[23] Interestingly, it is highly conserved during evolution and THP-deficient mice are more susceptible to UTI.[24] Once the bacteria are trapped by THP, the THP/bacteria cluster is eliminated by the urine flow from the urinary tract. FimH antagonists would support the host defense mechanism to clear excessively invading bacteria. In addition, type 1 pili exhibit several important target-qualities for the development of an anti-adhesion therapy: (i) they are the most prevalent fimbriae encoded by UPEC, (ii) they are highly conserved during evolution and (iii) they mediate the adhesion, which is the first and most important step for the establishment of the infection cycle (Fig. 2).

4. UTI Mouse Model and Treatment – The Therapeutic Potential of FimH Antagonists

4.1 *Initial in vivo Studies*

In the 1970s, Sharon and coworkers pioneered the discovery of anti-adhesion molecules targeting FimH. They reported on the *in vitro* inhibitory potential of methyl α-D-mannopyranoside (**1**)[25] (Fig. 3) and *p*-nitrophenyl α-D-mannopyranoside,[26] and investigated (*in vitro* and *in vivo*) the FimH lectin as a potential target for an anti-adhesion therapy. In the first *in vivo* proof of concept study, FimH antagonist **1** was pre-incubated with type 1 pili expressing UPEC strains and the mixture was instilled transurethrally into the bladder of mice.[7] Urine samples were analyzed every two to three days for bacterial counts, resulting in a significant reduction of bacteriuric mice after 5–16 days. In a second experiment, an additional dose of **1** was injected intraperitoneally two and three days after the infection with the bacteria/antagonist mixture, leading to no significant supplemental benefit. As mentioned by Sharon and coworkers,[7] a major drawback of the UTI mouse model is the spontaneous clearance of bacteria from the urinary tract 14 days after infection (up to 45%). Nevertheless, when the sampling of urine was conducted for up to 16 days, a significant reduction of bacteriuric mice treated with the FimH antagonist compared to the control group was observed. Based on this promising *in vivo* experiment, research directed to the identification of improved FimH antagonists[27] as well as the elucidation of the underlying mechanisms of this host-pathogen interaction (*e.g.* type 1 and P-pili,[28] phase variation of type 1 pili,[29] immune response,[30] *etc.*) was initiated.

In the 1980s, Svanborg Edén *et al.*[8] repeated the *in vivo* study[7] with methyl α-D-mannopyranoside (**1**) by instilling a higher concentration of bacteria/antagonist mixture into the bladder of mice. 2 and 16 h after the onset of infection, the animals were sacrificed to analyze their bladder and kidneys for bacterial counts. Surprisingly, they reported no reduction of bacterial load, although they used a higher

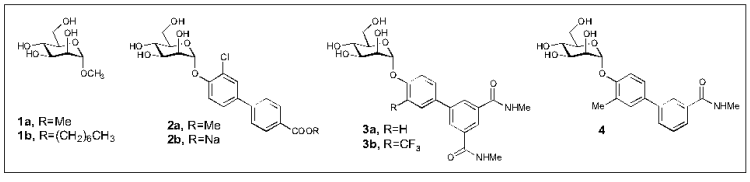

Fig. 3. α-D-Mannopyranosides tested in the UTI mouse model. Methyl and n-heptyl α-D-mannopyranosides **1a** and **1b**,[7–9] biphenyl α-D-mannopyranoside **2a** and **2b**,[9] diamidobiphenyl α-D-mannopyranoside **3a** and **3b**[10] and monoamidobiphenyl α-D-mannopyranoside **4**.[10]

inoculation concentration of **1** compared to the *in vivo* experiment of Sharon and coworkers[7] (5 mg/ml vs. 0.1 mg/ml). The different outcome of the two *in vivo* experiments could be related to the applied bacterial strains. Both groups used clinical UPEC isolates for their *in vivo* studies, however, Svanborg Edén *et al.*[8] subjected their strain to chemical mutagenesis by treatment with N-methyl-N-nitro-N-nitrosoguanidine, leading to random mutations.[31] Modified binding properties could therefore explain the different outcome of the two *in vivo* experiments. Furthermore, methyl α-D-mannopyranoside (**1**) is a low affinity antagonist[32] and would probably require much higher concentrations for the high level of inoculation (up to 10^9 UPECs per mouse,[8] compared to 10^6 UPECs by Sharon and coworkers[7]).

After these initial *in vivo* studies investigating the therapeutic potential of FimH antagonists,[7,8] no further *in vivo* studies were published for almost three decades (Fig. 1). At the same time, however, the UTI mouse model was extensively used for in depth investigations of the basic mechanisms of bacteria associated UTIs.[16] Simultaneously, the development of more potent FimH antagonists followed two major directions. First, multivalent FimH antagonists were investigated[33] and second, based on structural information obtained from the crystal structure of FimH co-crystallized with antagonists,[34] monovalent, high-affinity antagonists were designed[27] (the design, synthesis and *in vitro* evaluation of mono- and oligovalent mannosides is reviewed in detail by Hartmann and Lindhorst,[27] and Ernst and Magnani[35]).

4.2 *Orally Available FimH Antagonists*

Recently, Klein *et al.*[9] published for the first time *in vitro* and *in vivo* pharmacokinetic (PK) data of monovalend FimH antagonists. For oral availability, an optimal balance between solubility, permeability and lipophilicity is required. In addition, to ensure the availability of the antagonist at the target organ (bladder), a prodrug approach was applied. The ester **2a** is orally absorbed and hydrolyzed to the renally excretable acid **2b**. When applied to the UTI mouse model (single dose of 50 mg/kg, p.o.) ten minutes prior to infection, a substantial reduction of colony forming units (up to –4 $\log_{10}$ CFU) in the bladder could be detected.

In a recent study by Cusumano *et al.*[10] the FimH antagonists were evaluated for their potential to treat as well as to prevent UTI in mice. For this purpose, animals with a two-week chronic infection were treated with **3a** (single dose 100 mg/kg p.o.) or **3b** and **4** (single dose of 50 mg/kg p.o.), resulting in an 3 $\log_{10}$ CFU reduction of bladder counts for **3a** and up to –4 $\log_{10}$ CFU for **3b** and **4** six hours after treatment. In comparison, the antibiotic trimethoprim-sulfamethoxazole (TMP-SMZ, applied in the drinking water) only reduced bacterial counts by 1.5 $\log_{10}$ CFU. Furthermore, antagonists applied together with antibiotics were reported to have a synergistic effect on the treatment outcome. In a 24 hours multiple dosage study (3 times 50 mg/kg of **4**, every eight hours) for the treatment of chronic infections, bacterial counts in the bladder were reduced by –4.5 $\log_{10}$ CFU. Furthermore, to prevent infection, a single dose of **3a** (50 mg/kg) was applied 30 minutes prior to infection, resulting in a –1.5 $\log_{10}$ CFU reduction of bladder counts, 6 h after infection. Additionally, these authors reported that treatment with FimH antagonists prevented invasion of UPECs into the bladder cells leading to a reduction of biofilm formation.

In summary, both studies confirmed the promising potential of orally applied FimH antagonists for both prevention and treatment of UTIs *in vivo*. In addition, FimH antagonists proved to be equally effective as antibiotics. Whereas in the initial treatment experiments[7,8] bacteria/antagonist mixtures were directly applied into the bladder, the latter studies[9,10] used a therapeutically more relevant protocol by applying the FimH antagonists either p.o. or i.v., which closer simulates conditions used for later patient application. Furthermore, the higher potency of the newly developed FimH antagonists, further contributed to the positive therapeutic outcome in the UTI mouse model. However, the orally applied antagonists (**2a**, **3a**, **3b** & **4**) still exhibit unfavorable PK properties (*e.g.* low solubility, short exposure in plasma and urine), which both research teams aim to improve with further investigations.

5. Summary and Outlook

Although the development of resistant bacteria started shortly after the introduction of the first antimicrobial drugs,[13] the treatment paradigm only recently shifted from killing the pathogen to inhibiting its adhesion to the host cells. The anti-adhesion therapy is focusing on the development of a new class of antimicrobials exhibiting less selection pressure and therefore a reduced potential for the emergence of resistance. In addition, a reduction of the antibiotic associated side effects (*e.g.* the disruption of the commensal microbiota) is expected. A recent very promising example is the inhibition of the type 1 pili dependent adhesion of uropathogenic *Escherichia coli* (UPEC) to bladder cells for the treatment of urinary tract infections (UTIs). The *in vivo* studies reported to this day clearly indicate the potential of orally available FimH antagonists for the prevention and treatment of UTIs, with a higher therapeutic effect compared to treatment with antibiotics.

Received: January 23, 2012

[1] I. Ofek, D. L. Hasty, R. J. Doyle, 'Bacterial Adhesion to Animal Cells and Tissues', ASM Press, **2003**.
[2] WHO statistics, 'The top 10 causes of death', Fact sheet N°310, updated June **2011**.
[3] K. J. Simmons, I. Chopra, C. W. G. Fishwick, *Nat. Rev. Microbiol.* **2010**, *8*, 501.
[4] M. A. Fischbach, C. T. Walsh, *Science* **2009**, *325*, 1089.
[5] G. Guyot, *Zentbl. Bacteriol. Abt. I Orig.* **1908**, *47*, 640.
[6] W. A. Collier, J. C. deMiranda, *Antonie Leeuwenhoek* **1955**, *21*, 133.
[7] M. Aronson, O. Medalia, L. Schori, D. Mirelman, N. Sharon, I. Ofek, *J. Infect. Dis.* **1979**, *139*, 329.
[8] C. Svanborg Edén, R. Freter, L. Hagberg, R. Hull, S. Hull, H. Leffler, G. Schoolnik, *Nature* **1982**, *298*, 560.
[9] T. Klein, D. Abgottspon, M. Wittwer, S. Rabbani, J. Herold, X. Jiang, S. Kleeb, C. Lüthi, M. Scharenberg, J. Bezençon, E. Gubler, L. Pang, M. Smiesko, B. Cutting, O. Schwardt, B. Ernst, *J. Med. Chem.* **2010**, *53*, 8627.
[10] C. K. Cusumano, J. S. Pinkner, Z. Han, S. E. Greene, B. A. Ford, J. R. Crowley, J. P. Henderson, J. W. Janetka, S. J. Hultgren, *Sci. Transl. Med.* **2011**, *3*, 109.
[11] B. Hamad, *Nat. Rev. Drug Discov.* **2010**, *9*, 675.
[12] H. Kresse, M. J. Belsey, H. Rovini, *Nat. Rev. Drug Discov.* **2007**, *6*, 19.
[13] H. K. Allen, J. Donato, H. H. Wang, K. A. Cloud-Hansen, J. Davies, L. Handelsmann, *Nat. Rev. Microbiol.* **2010**, *8*, 251.
[14] N. Sharon, *Biochim. Biophysi. Acta* **2006**, *1760*, 527.
[15] J. Berglund, S. D. Knight, *Adv. Exp. Med. Biol.* **2003**, *535*, 33.
[16] M. A. Mulvey, *Cell Microbiol.* **2002**, *4*, 257.
[17] G. Capitani, O. Eidam, R. Glockshuber, M. G. Grütter, *Microbes Infect.* **2006**, *8*, 2284.
[18] M. A. Mulvey, *Cell Microbiol.* **2002**, *4*, 257.
[19] T. J. Wiles, R. R. Kulesus, M. A. Mulvey, *Exp. Mol. Pathol.* **2008**, *85*, 11.
[20] M. A. Mulvey, J. D. Schilling, J. J. Martinez, S. J. Hultgren, *PNAS* **2001**, *97*, 8829.
[21] H. Connell, W. Agace, P. Klemm, M. Schembri, S. Mårild, C. Svanborg, *PNAS* **1996**, *93*, 9827.
[22] S. Langermann, S. Palaszynski, M. Barnhart, G. Auguste, J. S. Pinkner, J. Burlein, P. Barren, S. Koenig, S. Leath, C. H. Jones, S. J. Hultgren, *Science* **1997**, *276*, 607.
[23] J. Pak, Y. Pu, Z. Zhang, D. L. Hasty, X. Wu, *J. Biol. Chem.* **2001**, *276*, 9924.
[24] J. M. Bates, H. M. Raffi, K. Prasadan, R. Mascarenhas, Z. Laszik, N. Maeda, S. J. Hultgren, S. Kumar, *Kidney Int.* **2004**, *65*, 791.
[25] I. Ofek, D. Mirelman, N. Sharon, *Nature* **1977**, *265*, 623.
[26] Y. Eshdat, I. Ofek, Y. Yashouv-Gan, N. Sharon, D. Mirelman, *Biochem. Biophys. Res. Commun.* **1978**, *85*, 1551.
[27] M. Hartmann, T. K. Lindhorst, *Eur. J. Org. Chem.* **2011**, 3583.
[28] L. Hagberg, R. Hull, S. Hull, S. Falkow, R. Freter, C. Svanborg Edén, *Infect. Immun.* **1983**, *40*, 265.
[29] a) B. I. Eisenstein, *Science* **1981**, *214*, 337; b) S. J. Hultgren, T. N. Porter, A. J. Schaeffer, J. L. Duncan, *Infect. Immun.* **1985**, *50*, 370.

[30] P. de Man, C. van Kooten, L. Aarden, I. Engberg, H. Linder, C. Svanborg Edén, *Infect. Immun.* **1989**, *57*, 3383.
[31] R. Arshad, S. Farooq, S. S. Ali, *Ann. Microbiol.* **2010**, *60*, 645.
[32] a) S. Rabbani, X. Jiang, O. Schwardt, B. Ernst, *Anal. Biochem.* **2010**, *407*, 188; b) D. Abgottspon, G. Rölli, L. Hosch, A. Steinhuber, X. Jiang, O. Schwardt, B. Cutting, M. Smiesko, U. Jenal, B. Ernst, A. Trampuz, *J. Microbiol. Methods* **2010**, *82*, 249; c) M. Scharenberg, D. Abgottspon, E. Ciceek, X. Jiang, O. Schwardt, S. Rabbani, B. Ernst, *Assay Drug Dev. Technol.* **2011**, *9*, 455.
[33] a) R. J. Pieters, *Org. Biomol. Chem.* **2009**, *7*, 2013. b) A. Imberty, Y. M. Chabre, R. Roy, *Chem. Eur. J.* **2008**, *14*, 7490.
[34] a) D. Choudhury, A. Thompson, V. Stojanoff, S. Langermann, J. Pinkner, S. J. Hultgren, S. D. Knight, *Science* **1999**, *285*, 1061; b) J. Bouckaert, J. Berglund, M. Schembri, E. D. Genst, L. Cools, M. Wuhrer, C. S. Hung, J. Pinkner, R. Slättergard, A. Zavialov, D. Choudhury, S. Langermann, S. J. Hultgren, L. Wyns, P. Klemm, S. Oscarson, S. D. Knight, H. D. Greve, *Mol. Microbiol.* **2005**, *55*, 441; c) A. Wellens, C. Garofalo, H. Nguyen, N. Van Gerven, R. Slättergård, J.-P. Hernalsteens, L. Wyns, S. Oscarson, H. De Greve, S. Hultgren, J. Bouckaert, *PLos One* **2008**, *3*, 4; d) Z. Han, J. S. Pinker, B. Ford, R. Obermann, W. Nolan, S. A. Wildman, D. Hobbs, T. Ellenberger, C. K. Cusumano, S. J. Hultgren, J. W. Janetka, *J. Med. Chem.* **2010**, *53*, 4779.
[35] B. Ernst, J. L. Magnani, *Nat. Rev. Drug Discov.* **2009**, *8*, 661.

RESULTS AND DISCUSSION

Submitted manuscript

FimH Antagonists - Bioisosteres to Improve the *in vitro* and *in vivo* PK/PD Profile.

Simon Kleeb*, Lijuan Pang*, Katharina Mayer*, Deniz Eris*, Anja Sigl, Roland C. Preston, Pascal Zihlmann, Timothy Sharpe, Roman P. Jakob, Daniela Abgottspon, Aline S. Hutter, Meike Scharenberg, Xiaohua Jiang, Giulio Navarra, Said Rabbani, Martin Smiesko, Nathalie Lüdin, Jacqueline Bezencon, Oliver Schwardt, Timm Maier, Beat Ernst.

*These authors contributed equally tot he project.

Manuscript submitted to: J. of Medicinal Chemistry (October 2014).

FimH Antagonists - Bioisosteres to Improve the *in vitro* and *in vivo* PK/PD Profile

Simon Kleeb,[a)]# Lijuan Pang,[a)]# Katharina Mayer,[a)]# Deniz Eris,[a)]# Anja Sigl,[a)] Roland C. Preston,[a)] Pascal Zihlmann,[a)] Timothy Sharpe,[c)] Roman P. Jakob,[b)] Daniela Abgottspon,[a)] Aline S. Hutter,[a)] Meike Scharenberg,[a)] Xiaohua Jiang,[a)] Giulio Navarra,[a)] Said Rabbani,[a)] Martin Smiesko,[a)] Nathalie Lüdin,[a)] Jacqueline Bezencon,[a)] Oliver Schwardt,[a)] Timm Maier,[b)] Beat Ernst [a)]*

# Equally contributed

a) Institute of Molecular Pharmacy, Pharmacenter, University of Basel, Klingelbergstrasse 50, CH-4056 Basel, Switzerland

b) Structural Biology, Biocenter, University of Basel, Klingelbergstrasse 70, CH-4056 Basel

c) Biophysical Facility, Biocenter, University of Basel, Klingelbergstrasse 70, CH-4056 Basel

* To whom correspondence should be addressed: Prof. Dr. Beat Ernst, Institute of Molecular Pharmacy, Pharmacenter, University of Basel, Klingelbergstrasse 50, CH-4056 Basel, Switzerland; Tel: +41 61 267 15 51, Fax: +41 61 267 15 52; E-mail: beat.ernst@unibas.ch

Keywords:

ABBREVIATIONS:

ΔH, change in enthalpy; ΔS, change in entropy; AUC, Area under the curve; BSA, bovine serum albumin; C_{max}, maximal concentration; Caco-2 cells, colorectal adenocarcinoma cells; CFU, colony forming units; CL_{tot}, total clearance; CRD, carbohydrate recognition domain; C_0, initial concentration; FITC, fluorescein isothiocyanate; FP, fluorescence polarization; ITC, isothermal titration calorimetry; K_D, dissociation constant; MAC_{90}, minimal anti-adhesion concentration to inhibit 90% adhesion; PAMPA, parallel artificial membrane permeation assay; P_{app}, apparent permeability; PD, pharmacodynamics; P_e, effective permeability; PK, pharmacokinetics; po, per os; UPEC, uropathogenic *Escherichia coli*; UTI, urinary tract infection; V_z, volume of distribution in terminal phase.

ABSTRACT

Urinary tract infections (UTIs), predominantly caused by uropathogenic *Escherichia coli* (UPEC) belong to the most prevalent infectious diseases worldwide. For the successful establishment of an UTI, the adhesion of bacteria to urothelial cells is a crucial first step, protecting the bacteria from the natural defense mechanisms as urine flow or the host immune system. The attachment of UPEC to host cells is mediated by FimH, a mannose-binding adhesin at the tip of type 1 pili, which are expressed on the bacterial surface. To date, UTIs are mainly treated with antibiotics, leading to the ubiquitous problem of increasing resistance against most of the currently available antimicrobials. Therefore, new treatment strategies are urgently needed, avoiding selection pressure and thereby affording a reduced risk of resistance. Here, we describe the development of an orally available FimH antagonist. Starting from the carboxylate substituted biphenyl α-D-mannoside **6** affinity as well as the relevant pharmacokinetic parameters (solubility, permeability, renal excretion) could be substantially improved by a bioisosteric approach. With 3'-chloro-4'-(α-D-mannopyranosyloxy)-biphenyl-4-carbonitrile (**11j**) a FimH antagonist with an optimal *in vitro* PK/PD profile was identified. The *para*-cyano substituent conferred lipophilicity and high binding to plasma proteins, which slowed down the rate of renal excretion. Despite higher lipophilicity, antagonist **11j** was insusceptible to CYP450 mediated metabolism, and as a consequence predominantly eliminated via the renal pathway. Finally, *in vivo* experiments confirmed the excellent PK-profile of **11j** with steady renal excretion for more than eight hours after oral application, suggesting a long-lasting anti-adhesive effect. Finally, orally applied **11j** was effective in a mouse model of UTI by reducing the bacterial load in the bladder by over 1000-fold.

INTRODUCTION

Urinary tract infection (UTI) is one of the most frequent infectious diseases worldwide and affects millions of people every year.[1] In more than 70% of the reported cases, uropathogenic *Escherichia coli* (UPEC) is the causal pathogen.[2] Acute, uncomplicated lower urinary tract infection, commonly referred to as cystitis, requires an antibiotic treatment for symptom relief (i.e. reduction of dysuria, frequent and urgent urination, bacteriuria, pyuria) and for prevention of more devastating or even life threatening complications like pyelonephritis and urosepsis.[3,4] However, the repeated use of antibacterial chemotherapeutics provokes antimicrobial resistance leading to treatment failure.[5] Hence, a new approach for the prevention and treatment of UTI with orally applicable therapeutics is urgently needed.[6]

UPEC undergo a well-defined infection cycle within the host.[7] The key step in pathogenesis is bacterial adhesion to the epithelial cells in the lower urinary tract.[8] This interaction prevents UPEC from clearance by the bulk flow of urine and enables the bacteria to colonize the epithelial cells. The adhesion is mediated by the virulence factor FimH located at the tip of bacterial type 1 pili.[9,10] FimH consists of two immunoglobulin-like domains: the N-terminal lectin domain and – connected by a short linker – the C-terminal pilin domain.[11] The lectin domain encloses the carbohydrate recognition domain (CRD) that binds to the oligomannosides of the glycoprotein uroplakin Ia on the epithelial cell surface.[12] The pilin domain anchors the adhesin to the pilus and regulates the switch between the two conformational states of the CRD with high and low affinity for mannosides, respectively.

More than three decades ago, Sharon and co-workers described various oligomannosides and aryl α-D-mannosides as potential antagonists of the FimH-mediated bacterial adhesion.[13,14] However, only weak interactions in the milli- to micromolar range were observed. In recent years, several high-affinity monovalent α-D-mannopyranosides have been reported.[15-24] Their improved affinities are based on optimal interactions with the main structural features of the CRD.[25-28] First, the mannose binding pocket accommodating the mannose moiety by means of an extended hydrogen bond network and, second, the entrance to the binding site composed of three hydrophobic amino acids (Tyr48, Tyr137, and Ile52) and therefore

referred to as 'tyrosine gate' hosting aliphatic and aromatic aglycones. As an example, *n*-heptyl α-D-mannopyranoside (**1**) exhibits nanomolar affinity due to hydrophobic contacts of the alkyl aglycone with the hydrophobic residues of the tyrosine gate.[15] Furthermore, aromatic aglycones, such as present in the mannosides **2**-**10** (Figure 1), provide strong π-π stacking interactions with the tyrosine gate. These interactions are further favored by the addition of an electron withdrawing substituent on the terminal ring of the biaryl portion.[18,19]

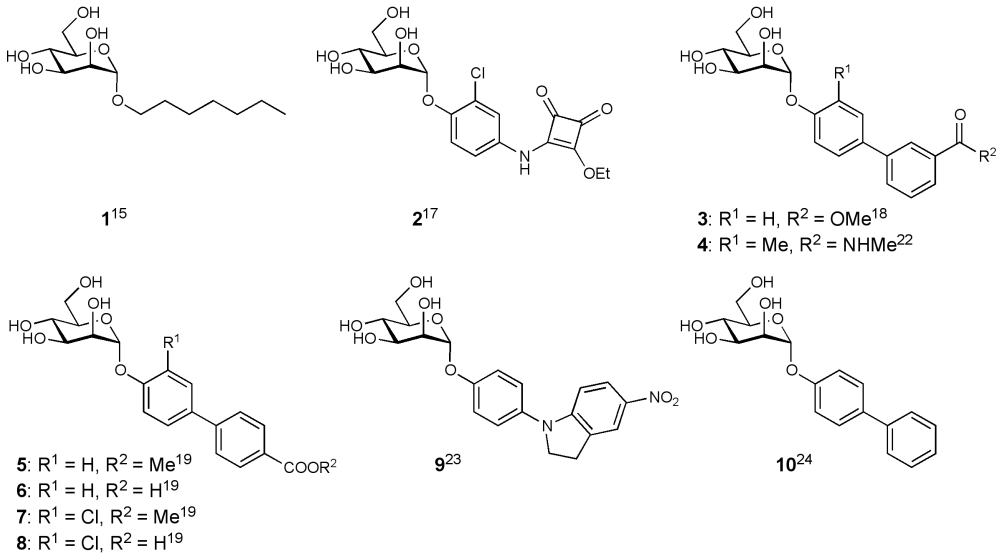

Figure 1. Monovalent FimH antagonists exhibiting nanomolar affinities.

Recent *in vivo* PK studies in mice proved the high potential of the biphenyl α-D-mannosides **4** and **7** for an oral treatment, although high doses (≥ 50 mg/kg) were necessary to achieve the minimal concentrations required for the anti-adhesive effect in the urinary bladder.[19,21,22] Moreover, the therapeutic effect could only be maintained for a few hours, i.e. four hours for a po (per os) single-dose application of **7** (50 mg/kg), because of rapid elimination by glomerular filtration and low reabsorption from the primary urine in the renal tubules.[19]

To date, the physicochemical properties affecting the rate of renal excretion, i.e. lipophilicity and plasma protein binding (PPB), or metabolic liabilities promoting non-renal elimination pathways have been barely investigated for FimH antagonists. The goal of the present study was to optimize the biphenyl α-D-mannoside with respect to oral bioavailability and renal excretion. Starting from antagonist **6**, we synthesized

new biphenyl derivatives, characterized their affinity to the CRD, structurally investigated their binding mode, and determined physicochemical and pharmacokinetic parameters predictive for intestinal absorption and renal elimination. Furthermore, we determined *in vivo* PK (pharmacokinetic) of the most promising new antagonists in a mouse model. The compound with the best PK profile proofed effective in reducing the bacterial loads upon bladder infection in a mouse model of UTI.

RESULTS AND DISCUSSION

As previously reported, the carboxylate substituent present in the biphenyl mannoside **6** – its electron withdrawing potential being essential for an enhanced drug target interaction – strongly decreases the lipophilicity of the antagonist (log $D_{7.4}$ < -1.5[19]) in comparison to the *n*-heptyl (→ **1**, log *P* = 1.7[19]) or the unsubstituted biphenyl aglycone (→ **10**, log *P* = 2.1[24]). Since low lipophilicity is a major reason for low intestinal absorption and rapid renal excretion of the systemically available antagonist,[19,23] we aspired to improve oral bioavailability as well as renal excretion by replacing the carboxylate in **6** with various bioisosteric groups[29] (Figure 2).

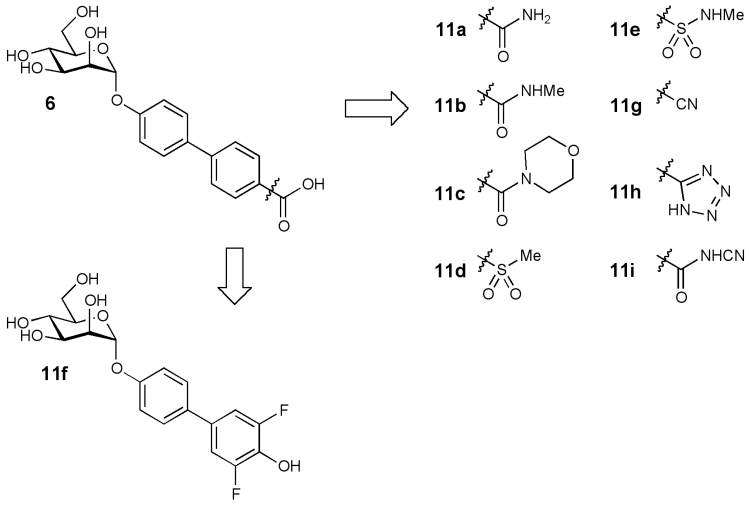

Figure 2. Bioisosteric replacement of the carboxylic acid substituent of biphenyl α-D-mannopyranoside **6**.

Synthesis. Iodide **12** was prepared from peracetylated mannose and 4-iodophenol in the presence of $BF_3 \cdot Et_2O$.[24] In a palladium-catalyzed Miyaura-Suzuki coupling[30] with

the boronic acid or boronate derivatives **13a-g**, the biphenyl derivatives **14a-g** were obtained in good to excellent yields. Final deprotection yielded the test compounds **11a-g**. Utilizing microwave-assisted reaction condition,[31] the conversion of arylnitrile **14g** to tetrazole **15** proceeded rapidly and with good yield. After deprotection of **15** using Zemplén conditions, the test compound **11h** was obtained (Scheme 1).

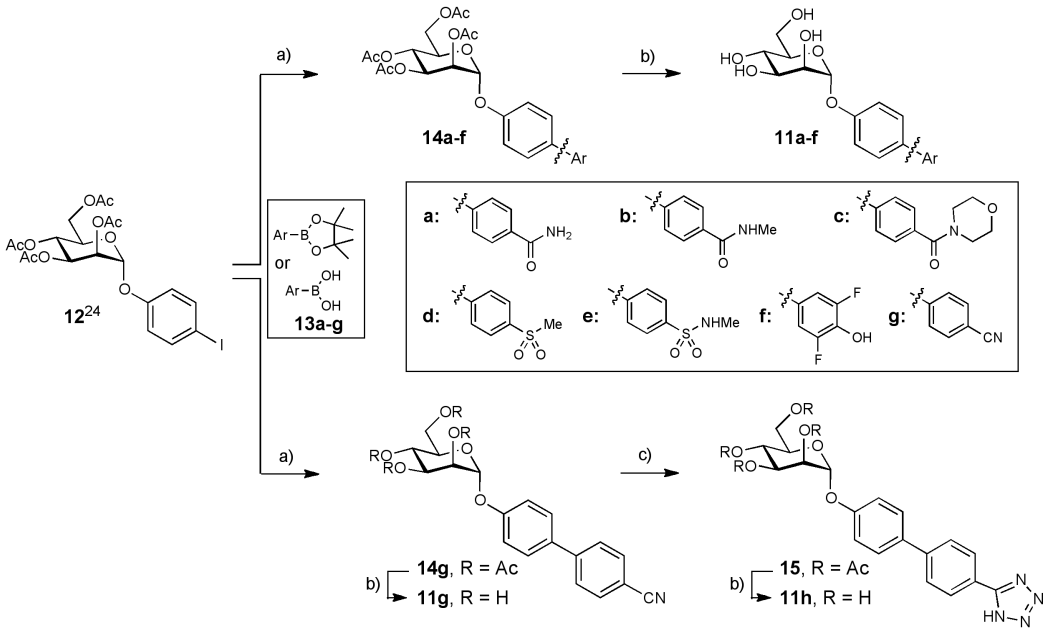

Scheme 1. a) $Pd(Cl_2)dppf{\cdot}CH_2Cl_2$, K_3PO_4, DMF, 80 °C, 4 h (**14a-g**, 44-99%); b) NaOMe, MeOH, rt, 4 h (**11a-h**, 29-86%); c) $TMSN_3$, $Bu_2Sn(O)$, DME, 150 °C, μW, 10 min, 81%.

The cyanobenzamide derivative **11i** (Scheme 2) was obtained from **6** by peracetylation (→ **16**) followed by conversion of the carboxylic acid into its acid chloride with 1-chloro-*N*,*N*,2-trimethyl-1-propenylamine.[32] Without isolation, the acid chloride was reacted with sodium hydrogen cyanamide in DMF followed by deacetylation under Zemplén conditions to yield the test compound **11i**.

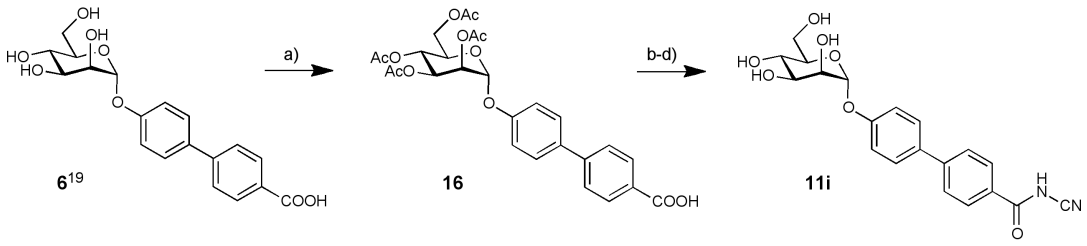

Scheme 2. a) i) Ac_2O, DMAP, pyridine, 0 °C to rt, overnight; ii) satd. $NaHCO_3$ aq., DCM, rt, 2 h (**16**, 53%); b) 1-chloro-*N*,*N*,2-trimethyl-1-propenylamine, toluene, 0 °C to rt, 2 h; c) NaH, NH_2CN, DMF, 0 °C to rt, overnight; d) NaOMe, MeOH, rt, 4 h (**11i**, 21% for three steps).

Finally, to further improve the pharmacokinetic properties of mannoside **11g** (see Table 3), a chloride substituent was introduced to the *ortho*-position of the aromatic ring adjacent to the anomeric oxygen. For its synthesis, peraceylated α-D-mannose (**17**) was coupled with 2-chloro-4-iodophenol (**18**) using $BF_3 \cdot Et_2O$ as promotor (→ **19**, 76%). After the introduction of the second aromatic ring by Miyaura-Suzuki coupling (→ **20**, 75%), deprotection yielded mannoside **11j** (Scheme 3).

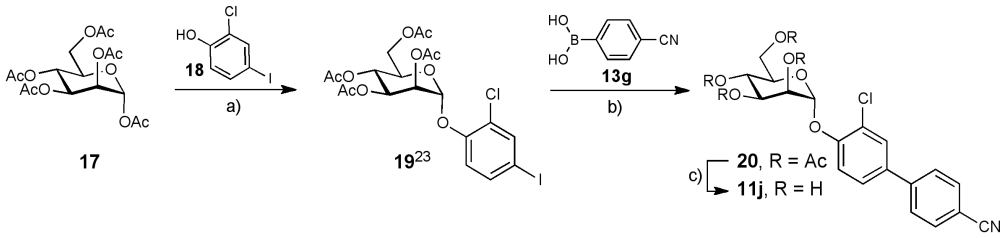

Scheme 3. a) $BF_3 \cdot Et_2O$, CH_2Cl_2, 40 °C (76%); b) $Pd(Cl_2)dppf \cdot CH_2Cl_2$, K_3PO_4, DMF, 80 °C (75%); c) NaOMe, MeOH, rt, 4 h (48%).

Binding Affinity. The binding affinity of heptyl mannoside **1**, the biphenyl mannosides **5**, **6**, **10**, and the bioisosteres **11a-j** was determined in a competitive fluorescence polarization assay (FP-assay) and with isothermal titration calorimetry (ITC). A protein construct consisting of the CRD with a C-terminal His-tag with a thrombin cleavage site (FimH-CRD-Th-His_6) was used for all experiments.[33]

Competitive Fluorescence Polarization Assay. For the rapid evaluation of binding affinity, we established a competitive binding assay based on fluorescence polarization (FP). Similar formats have been applied before for the detection of carbohydrate-lectin interactions.[18,34] In this assay, the antagonist of interest displaces a fluorescently labeled competitor from the binding site, thereby causing a reduction in fluorescence polarization.[35] To identify the optimal competitor, fluorescein isothiocyanate (FITC) was connected to the FimH ligand **8** by three linkers of different lengths (→ **21**-**23**, Scheme 4). For optimal sensitivity and signal-to-noise ratio, three main parameters need to be considered: (i) the affinity of the competitor should not be impaired by the fluorescent label, (ii) the conformational flexibility of the label upon binding of the competitor to the CRD should be low and (iii) the fluorescence properties of the label should not be affected by the connected ligand.[36-38] A change in fluorescence properties was observed for reporter ligand **21**

in which the label was linked to the biphenyl agylcone by an amide bond. The absorption spectrum revealed a lack of the characteristic fluorescein absorption peak at 494 nm (Scheme 4), likely due to an extension of the conjugated system to the biphenyl moiety of the ligand. The elongated saturated spacer groups in competitors **22** and **23** ensured that the expected spectral properties of the dye were retained (Scheme 4).

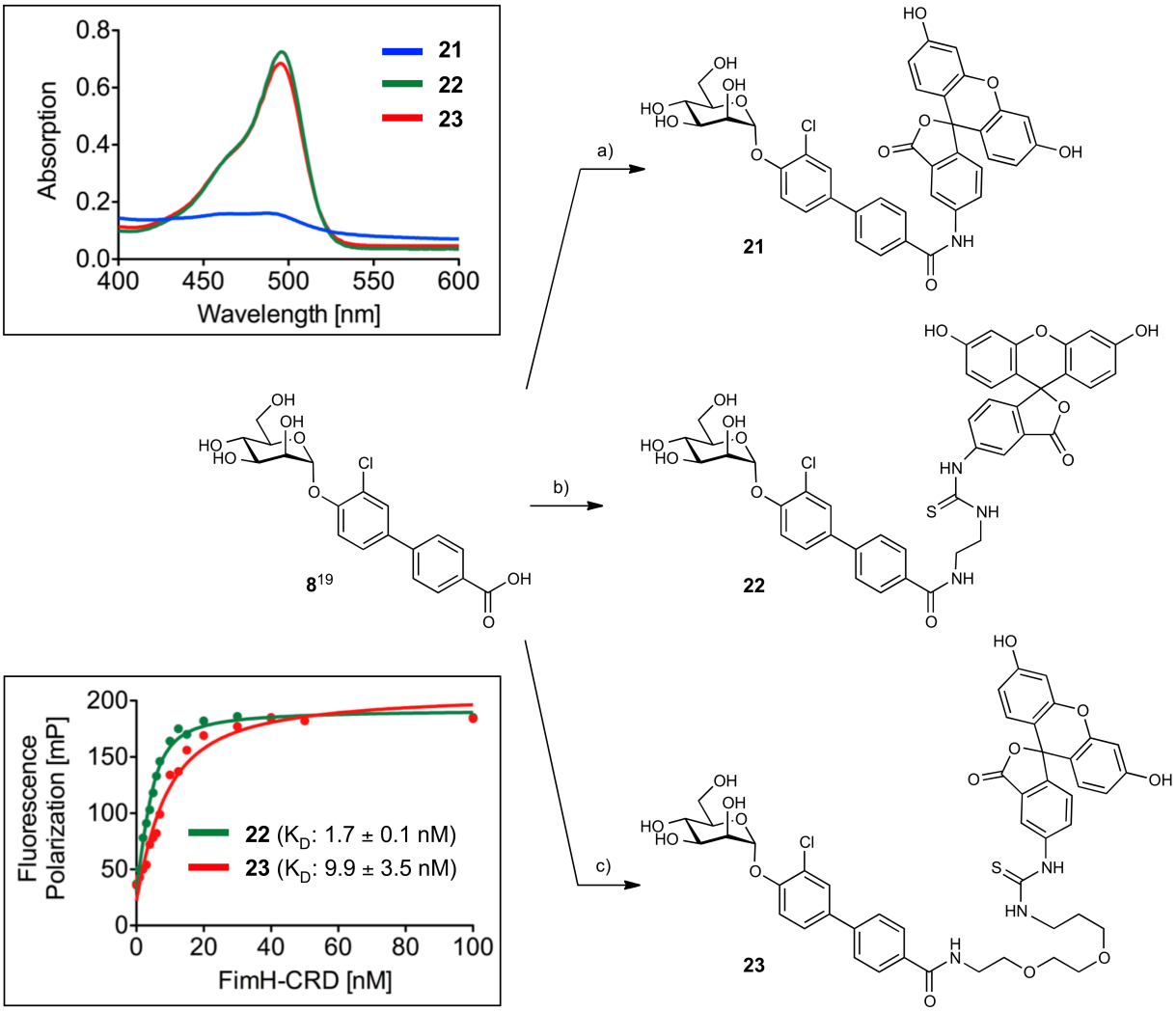

Scheme 4. a) 1-[(1-(Cyano-2-ethoxy-2-oxoethylideneaminooxy)-dimethylamino-morpholinomethylene)] methanaminium hexafluorophosphate (COMU), NEt_3, fluoresceinamine, DMF, rt, 7 h (**21**, 19%); b) i. DIC, NHS, *N*-Boc-ethylenediamine, DMF, rt, 12 h; ii. TFA, DCM, rt, 10 min (68% over two steps), iii. fluorescein isothiocyanate (FITC), NEt_3, DMF, rt, 3 h (**22**, 48%); c) i. DIC, NHS, *N*-Boc-PEG2-NH_2, DMF, rt, 14 h; ii. TFA, DCM, rt, 30 min (62% over two steps); iii. FITC, DMF, rt (**23**, 65%).

For the determination of their binding affinity, fixed concentrations of the reporter ligands **22** and **23** were incubated for 24 h with a linear dilution of the FimH-CRD (0-100 nM). FP was measured using a plate reader, with polarized excitation at 485 nm, and emission at 528 nm measured through appropriately oriented polarizers. Fitting the single-site binding function of Cooper[39] to the observed FP data resulted for compound **22** in a dissociation constant (K_D = 1.7 nM, Figure 3A) similar to that of the unlabeled parent compound **8**,[19] whereas **23** showed a five-fold lower affinity (9.9 nM) (Scheme 4). Therefore, the reporter ligand **22** fulfills all characteristics as an optimal competitor and was used for the FP assay.

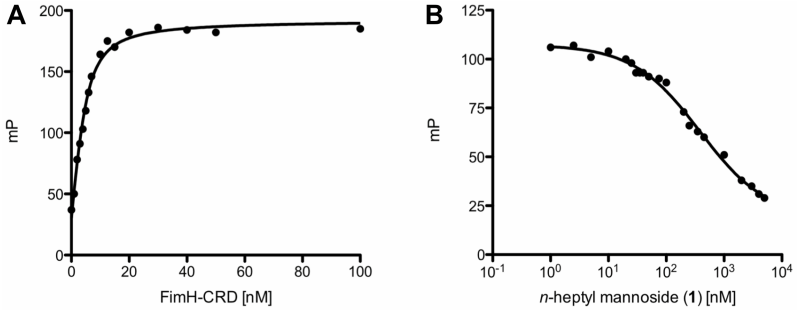

Figure 3. A) Direct binding curve of the labeled competitor **22** obtained by adding a linear dilution of FimH-CRD (0-100 nM) and a constant concentration of competitor **22** (5 nM). The K_D was determined by fitting the experimental data to a single-site binding fit that accounts for ligand depletion. In three FP based direct binding experiments the K_D of competitor **22** was determined to be 1.7 nM. B) Inhibition curve of *n*-heptyl mannoside (**1**) from the competitive FP assay. The IC_{50} value was determined by nonlinear least-squares fitting to a standard 4-parameter equation. A modified Cheng-Prusoff equation was used to calculate the corresponding K_D value (K_D = 28.3 nM).

For the test compounds **1**, **5**, **6**, **10**, and **11a-j**, a 24 h incubation time was applied before FP was measured due to the long residence time of FimH antagonists ($t_{1/2}$ > 3.5 h, Figure 3B[40]). The 24 h incubation period was empirically determined to be necessary to reach equilibrium between reporter ligand and compound of interest. IC_{50} values were obtained by nonlinear least-squares regression (standard four-parameter dose response curve) and converted to K_D values using a modified Cheng-Prusoff equation.[35] This equation accounts for the ligand depletion effect in competitive titrations involving high-affinity interaction partners present in similar concentrations. Under these conditions, the free concentration of an interacting species cannot be assumed to equal the total concentration.

The K_D values determined for the test compounds **1**, **5**, **6**, **10**, and **11a-j** are summarized in Table 1. Against our expectations, the biphenyl mannosides **6** and **10**

exhibit similar affinities (Table 1), despite the presence of an electron withdrawing carboxylate substituent in antagonist **6**. According to the crystal structure of FimH co-crystallized with the sulfonamide derivative **11e** (Figure 4A), the outer aromatic ring of the biphenyl aglycone forms π-π interactions with the electron rich Tyr48, which is part of the tyrosine gate of FimH.[15] A reduction of electron density of the aglycone by the electron withdrawing carboxylate was expected to enforce these π-π stacking interactions and lead to improved affinity. However, this beneficial effect might be compensated by an entropic penalty originating from the improved π-π stacking to Tyr48 that might lead to the reduced flexibility of both protein and antagonist. Furthermore, a beneficial enthalpy effect might be partially compensated by an enthalpy penalty originating from the desolvation of the charged **10** carboxylate[41] (see also experimental part). Although this substituent is solvent exposed, at least a partial desolvation may be necessary upon antagonist binding. To prove this assumption, we replaced the carboxylate by the corresponding methyl ester (→ **5**)[19] in order to reduce the desolvation penalty and, as predicted by the Hammett constant σ_p,[42] to further improve the π-π stacking. Indeed, a six-fold improvement in affinity was achieved. However, since the methyl ester undergoes rapid enzyme-mediated hydrolysis *in vivo*,[19] it will not be available at the place of action in the urinary bladder. The methyl ester was therefore replaced by metabolically stable bioisosteres[29] exhibiting comparable electron withdrawing properties[42] (Table 1, entries 5-13). The most potent derivatives **11d**, **11e** and **11g** showed affinities in the low nanomolar range.

As previously reported,[24] a chloro substituent in the *ortho*-position of the aromatic ring adjacent to the anomeric oxygen is favorable for affinity and improves the physicochemical properties relevant for oral bioavailability. Indeed, the corresponding antagonist **11j** was the most potent compound tested in this study.

Table 1. Affinities (K_D) of FimH antagonists to FimH-CRD-Th-His$_6$; dissociation constants (K_D) were determined in a competitive fluorescence polarization assay.

Entry	Compd	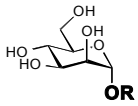	**Affinity** K_D [nM]
1	**1**	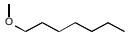	28.3 ± 5.0
2	**10**	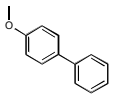	15.1 ± 2.2
3	**6**	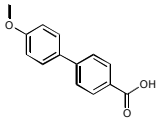	17.9 ± 1.5
4	**5**	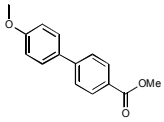	3.6 ± 0.9
5	**11a**	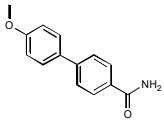	2.8 ± 0.3
6	**11b**	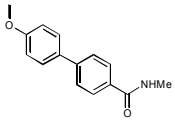	2.9 ± 0.5
7	**11c**	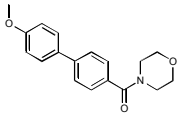	3.0 ± 0.1
8	**11d**	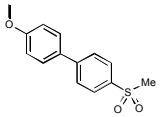	1.7 ± 0.2
9	**11e**	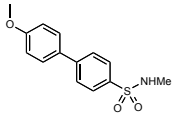	2.7 ± 0.4
10	**11f**	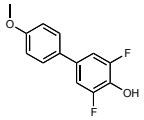	3.7 ± 0.2
11	**11g**	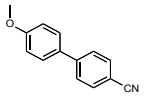	2.0 ± 0.6
12	**11h**	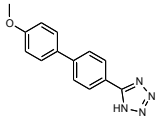	5.7 ± 0.1
13	**11i**	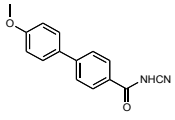	8.4 ± 0.3

14	**11j**	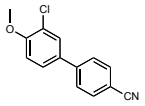	< 1[a)]

[a)] The K_D value of **11j** was approximated to be in the subnanomolar range. The IC_{50} value obtained in the competitive FP assay was equal to the lowest value that can be resolved by the assay, indicating stoichiometric titration of **11j** due to its high affinity. Consequently, its K_D must be below the K_D of competitor **22**.

Isothermal Titration Calorimetry (ITC). To further confirm our hypothesis regarding π-π stacking and desolvation, we performed ITC experiments with unsubstituted biphenyl mannoside **10**, the carboxylic acid **6**, and the bioisosteres **11b-e, g** and **j** (Table 2). ITC allows the simultaneous determination of the stoichiometry (*N*), the change in enthalpy (ΔH) and the dissociation constant (K_D) for ligand-protein binding.[43,44] The reliable determination of these three parameters requires well-defined sigmoidal titration curves characterized by the dimensionless Wiseman parameter *c* ($c = Mt(0)\ K_D^{-1}$, where *Mt*(0) is the initial macromolecule concentration).[45] To be sure that data can be fitted with confidence, the *c*-value should be between 1 and 1,000 (ideally between 5 and 500),[46] which could be achieved for the antagonists **6** and **10**. For titrations involving low micromolar *Mt*(0) and interactions in the low nanomolar or picomolar range, as suggested for the bioisosteres **11b-j**, *c*-values above 1,000 were expected. Since these conditions lead to steep titration curves that do not allow the determination of the curve slope representing $1/K_D$, we applied an alternative, competitive format referred to as displacement assay.[47,48] First, FimH-CRD-Th-His_6 was pre-incubated with the low affinity antagonist *n*-heptyl 2-deoxy-α-D-mannopyranoside (**24**, for synthesis see supporting information). The high-affinity bioisosteres of interest were titrated into the protein-ligand complex giving well-defined sigmoidal titration curves.

Table 2. Thermodynamic parameters from ITC for selected FimH-antagonists binding to FimH-CRD-Th-His_6; n, stoichiometric correction factor; CI, confidence interval from fitting.

Entry	Compd	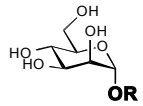	K_D [nM] (95 % CI)	ΔG [kJ/mol]	ΔH [kJ/mol] (95 % CI)	$-T\Delta S$ [kJ/mol]	n	Type of measurement
1	**10**	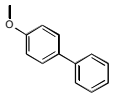	17.7 (14.1 – 22.3)	-44.2	-45.0 (-44.5 – -45.6)	0.8	1.07	direct
2	**6**	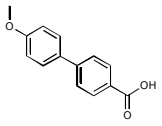	15.0 (13.4 – 16.7)	-44.7	-48.7 (-48.4 – -49.0)	4.0	1.05	direct
3	**11b**	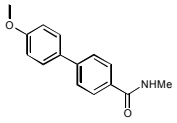	4.3 (3.2 – 5.6)	-47.8	-54.5 (-54.1 – -54.9)	6.7	1.02	competitive vs. **24**
4	**11c**	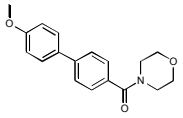	5.0 (3.8 – 6.6)	-47.4	-54.5 (-54.1 – -54.8)	7.1	0.97	competitive vs. **24**
5	**11d**	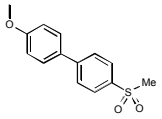	3.0 (2.1 – 4.2)	-48.7	-52.3 (-51.5 – -53.1)	3.6	0.99	competitive vs. **24**
6	**11e**	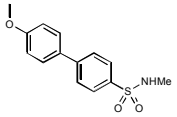	3.5 (2.9 – 4.3)	-48.2	-52.2 (-51.6 – -52.8)	3.9	1.06	competitive vs. **24**
7	**11g**	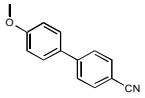	2.8 (2.3 – 3.3)	-48.8	-58.2 (-57.8 – -58.6)	9.4	1.00	competitive vs. **24**
8	**11j**	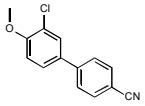	1.3 (1.1 – 1.6)	-50.7	-60.9 (-60.4 – -61.4)	10.1	1.01	competitive vs. **24**
9	**24**	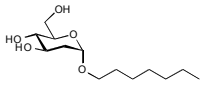	9’386 (8’555 – 10’287)	-28.7	-19.5 (-19.1 – -20.0)	-9.1	1.00	direct

The resulting *K*D values (Table 2) correspond well with the data obtained from the FP assay (Table 1). A comparison of the thermodynamic fingerprints of antagonists **10** and **6** reveals that the more favorable enthalpic contribution resulting from facilitated π-π stacking leads to a net enthalpy gain ($\Delta\Delta H$: -3.7 kJ/mol). However, an even greater increase in enthalpy is likely countered by the enthalpy costs for desolvation of the electron withdrawing carboxylate.

The gain in enthalpy is in turn compensated by an unfavorable entropy ($-T\Delta\Delta S$: 3.2 kJ/mol) as a result of the reduced flexibility of both the antagonist and the Tyr48 side-

chain caused by the improved interaction. This is not entirely outweighed by the beneficial entropy contribution related to the partial desolvation of the carboxylate and the related release of water into the bulk. Added together, the enthalpy and entropy contributions of antagonists **10** and **6** result in similar affinities (*K*D: 17.7 and 15.0 nM, respectively).

In contrast, the replacement of the carboxylate group by various neutral bioisosteres (entries 3-6) reduces the enthalpy costs for desolvation (see calculated free energies of desolvation, experimental part) and therefore leads to a markedly improved enthalpy (ΔΔ*H*: -3.5 to -5.8 kJ/mol). As a result, an up to fivefold improvement of the *K*D values was achieved. Finally, with a cyano substituent (entries 7 & 8), the enthalpy term was further improved (ΔΔ*H*: -3.7 kJ/mol) due to a reduced desolvation penalty and improved π-π stacking interactions. However, this beneficial component is again partially compensated by a decrease in entropy. This can be attributed, first, to the loss of flexibility of the tightly bound ligand (Figure 4B) and, second, to the smaller surface area of the cyano substituent compared to amide, sulfonamide and sulfone, which results in a smaller number of water molecules being released to bulk upon binding.

X-ray Crystallography. To determine the binding poses of the bioisosters, we co-crystallized the compounds **11e** or **11j** with FimH-CRD (Figure 4). Atomic resolution crystal structures were obtained at 1.07 Å (**11e**) and 1.10 Å (**11j**). As observed in previous mannoside co-crystal structures,[15,18,27] the mannose moiety forms an extensive hydrogen bond network to the well-defined binding site with all of its hydroxyl groups. The biphenyl aglycone is located between the tyrosine gate residues (Tyr48/Tyr137). The π-π stacking of the second aromatic ring of the aglycone to the side chain of Tyr48 contributes most to the interaction energy of the aglycone moiety. Interactions to the Tyr137 side-chain on the other hand are only limited. Whereas a previously published crystal structure of a biphenyl mannoside in complex with FimH-CRD suffers from crystal contacts of binding site residues (Tyr48 side-chain to backbone oxygen of Val27) possibly causing the distortion of the binding site,[18] the binding site of our structures are mostly solvent exposed. This revealed the flexibility of the aglycone in the FimH-CRD/**11e** structure, since the electron density towards the solvent-exposed sulfonamide indicates that there is not

one single orientation. Therefore, the aglycone was modeled in two distinct poses. In contrast, in the FimH-CRD/**11j** structure the amino acid side chain of Y48 can be modeled in two distinct rotamers, suggesting flexibility also of the receptor.

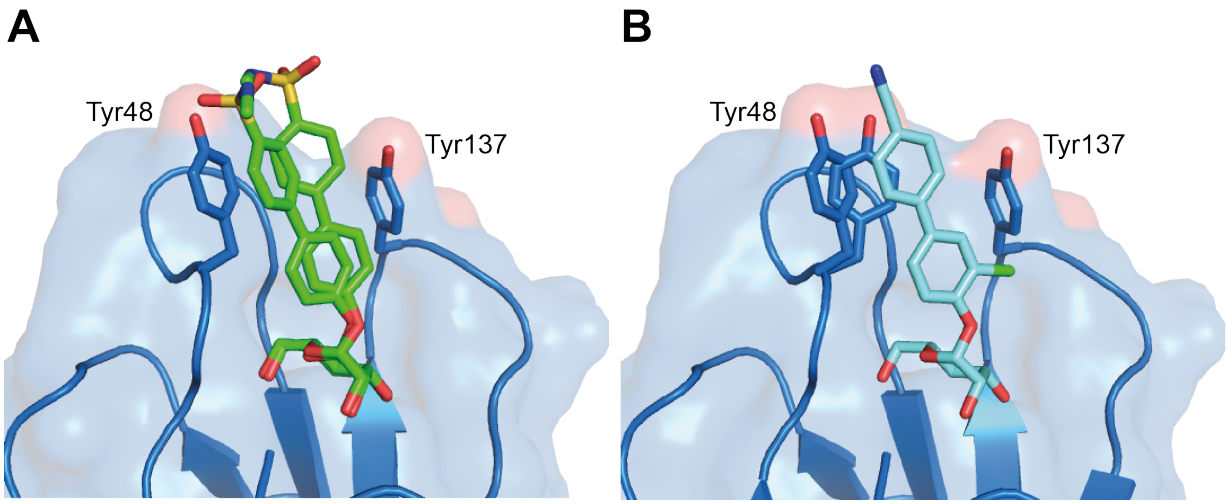

Figure 4. Ligand binding poses determined by X-ray co-crystallization with compounds **11e** resolved to 1.07 Å (**A**) and **11j** resolved to 1.10 Å (**B**). The electron density surrounding the aglycone of **11e** indicates flexibility of the aglycone and was modeled in two poses. Both compounds bind in a similar pose with a well-defined hydrogen network surrounding the mannose moiety and π-π stacking interactions between the second aromatic ring and Tyr48 side-chain (**A**). In contrast, in the FimH-CRD/**11j** structure the amino acid side chain of Y48 can be modeled in two distinct rotamers, suggesting flexibility also of the receptor (**B**).

Physicochemical Properties and *In Vitro* Pharmacokinetics. Intestinal absorption and renal excretion are prerequisites for a successful oral treatment of UTI with FimH antagonists. Furthermore, reabsorption of antagonist from the renal ultrafiltrate is desirable for maintaining the minimal anti-adhesive concentration in the target organ, namely the bladder, over an extended period of time. To estimate the influence of the bioisostere approach on oral bioavailability and the rate of renal excretion, we determined lipophilicity by means of the octanol-water distribution coefficient (log $D_{7.4}$),[49] aqueous solubility, and membrane permeability in the artificial membrane permeability assay (PAMPA)[50] and the colorectal adenocarcinoma (Caco-2) cell monolayer model.[51]

Table 3. Physicochemical and *in vitro* pharmacokinetic parameters.

Compd	pK_a[a]	log $D_{7.4}$[b]	Solubility [µg/mL] / pH[c]	PAMPA log P_e [cm/s] / pH[d]	Caco-2 P_{app}, [10^{-6} cm/s][e]		PPB f_b [%][f]	Metabolic stability $t_{1/2}$ [min][g]
					a→b	b→a		
1	---	1.65	> 3000	-4.89	7.0 ± 0.6	9.4 ± 0.2	81	13
10	---	2.1 ± 0.1	21 ± 1 / 7.4	-4.7 ± 0.1 / 7.4	10.0 ± 0.9	19.0 ± 1.2	93 ± 1	n.d.
5	---	2.14	33.8 / 6.51	-4.7	4.23	n.d.	93	1.0
6	3.88	< -1.5	> 3000 / 6.61	no permeation	n.d.	n.d.	73	> 60
11a	---	0.5 ± 0.1	12 ± 1 / 7.4	-6.8 ± 0.3 / 7.4	0.12 ± 0.01	0.61 ± 0.03	n.d.	n.d.
11b	---	0.8 ± 0.0	122 ± 13 / 7.4	-9.2 ± 1.4 / 7.4	1.10 ± 0.82	0.87 ± 0.15	n.d.	n.d.
11c	---	0.2 ± 0.1	> 250 / 7.4	-7.8 ± 0.3 / 7.4	0.18 ± 0.07	1.30 ± 0.03	48 ± 2	> 60
11d	---	0.4 ± 0.0	246 ± 17 / 7.4	-7.2 ± 0.0 / 7.4	0.36 ± 0.01	1.76 ± 0.12	99 ± 1	> 60
11e	---	0.7 ± 0.1	> 250 / 7.4	-8.6 ± 0.2 / 7.4	0.28 ± 0.23	1.82 ± 0.14	> 99	> 60
11f	6.5	1.1 ± 0.0	> 150 / 3.0 > 150 / 7.4	-7.7 ± 0.8 / 5.0 -8.8 ± 0.1 / 7.4	0.40 ± 0.02	1.90 ± 0.17	n.d.	n.d.
11g	---	1.4 ± 0.0	186 ± 4 / 7.6	-5.7 ± 0.0 / 7.4	2.0 ± 0.1	13.2 ± 2.1	99 ± 0	> 60
11h	3.7	-1.4 ± 0.1	11 ± 0 / 3.0 273 ± 2 / 7.4	-9.3 ± 1.4 / 5.0 -8.8 ± 1.4 / 7.4	0.17 ± 0.00	0.22 ± 0.01	n.d.	n.d.
11i	2.5	-1.1 ± 0.1	> 150 / 3.0 > 150 / 7.4	-6.8 ± 0.2 / 5.0 -7.0 ± 0.1 / 7.4	0.22 ± 0.14	0.29 ± 0.03	n.d.	n.d.
11j	---	2.1 ± 0.0	192 ± 5 / 7.4	-5.2 ± 0.0 / 7.4	2.2 ± 0.4	22.1 ± 1.5	89 ± 1	> 60

a) pK_a values were determined by NMR spectroscopy; b) Octanol-water distribution coefficients (log $D_{7.4}$) were determined by a miniaturized shake-flask procedure at pH 7.4, values represent the mean ± SD of sextuplicate measurements;[49] c) Kinetic solubility was measured in a 96-well format using the µSOL Explorer solubility analyzer at the indicated pH in triplicate; d) P_e = effective permeability: passive permeation through an artificial membrane was determined by the parallel artificial membrane permeation assay (PAMPA), values represent the mean ± SD of quadruplicate measurements performed at the indicated pH;[50] e) P_{app} = apparent permeability: permeation through a Caco-2 cell monolayer was assessed in the absorptive (a→b) and secretory (b→a) directions in triplicate;[51] f) Plasma protein binding (PPB) was determined by equilibrium dialysis in triplicate;[52] g) Metabolic

stability was determined by incubating the compounds (2 µM) with pooled rat liver microsomes (RLM, 0.5 mg/mL) in presence of NADPH (1 mM, compounds **1**, **6, 11c-e**, **g**, **j**) or without NADPH (compound **5**);[53] n.d. = not determined.

Oral Bioavailability. Oral bioavailability relies on compound dissolution in the gastrointestinal fluids, permeation through the membranes lining the intestine, and stability against first pass metabolism.[54,55] In turn, permeability and potency define the minimum aqueous solubility required for an orally dosed compound.[56] For our FimH antagonist, we therefore aimed to exceed the solubility limit of 50 µg/mL in order to achieve substantial absorption through the intestinal mucosa. Sufficient aqueous solubility was reported for *n*-heptyl α-mannopyranoside (**1**).[19] The unsubstituted biphenyl α-D-mannopyranoside **10** as well as the antagonists bearing a methylcarboxylate, carboxamide, or tetrazole substituent in its unionized state (compounds **5**, **11a** and **11h**) were found to be scarcely soluble due to the apolar and planar character of the aglycone.[24,57] By contrast, the polar carboxylic acid moiety present in antagonist **6** or the substituents in the bioisosteres **11b-j** enhanced the observed solubility beyond the limit of 50 µg/mL. Permeability data derived from PAMPA[58] and the Caco-2 model[59] suggest high permeation of the moderately lipophilic antagonists **1**, **10**, and **5** (log $D_{7.4}$ > 1.6) through the intestinal membranes. The bioisosteres **11a**-**f**, **h**, **i**, although slightly more permeable than the strongly hydrophilic carboxylic acid derivative **6**, show only moderate values of permeability compared to *n*-heptyl α-mannopyranoside (**1**) or the unsubstituted biphenyl mannoside **10**. However, the *para*-cyanobiphenyl derivatives **11g** and **11j** display elevated log $D_{7.4}$ and effective permeability (log P_e) in the range for successful intestinal absorption. Featuring both high aqueous solubility and elevated membrane permeability, the *para*-cyano substituted bioisosteres **11g** and **11j** are thus the most promising candidates for oral absorption. Moreover, combining the bioisosteric replacement with the addition of a chloro substituent in the *ortho*-position of the aromatic ring adjacent to the anomeric oxygen (→ **11j**)[24] resulted in the most advantageous physicochemical profile for oral bioavailability.

Renal Excretion. The rate of renal excretion depends on the rate of glomerular filtration and the propensity to tubular secretion and reabsorption of an antagonist.[60] Only the fraction that is not bound to plasma proteins is expected to enter the glomerular filtrate.[61] Plasma protein binding (PPB) data indicating the fraction bound

(f_b) are listed in Table 2.[52] The biphenyls **6** and **11c** were identified as moderate binders to plasma proteins ($f_b \leq 65\%$), which suggests a low impact of PPB on antagonist filtration. The f_b values of the antagonists **1**, **10**, **5**, and **11j** were between 80 and 93%, whereas the bioisosteres **11d**, **e**, and **g** showed particularly high protein binding ($f_b \geq 99\%$) implying slow compound entry into the primary urine. However, the kinetic aspects of PPB, that is, association and dissociation rate constants, remain to be determined to quantify precisely the influence of PPB on filtration.[62]

Furthermore, log $D_{7.4}$ was identified as key determinant of tubular reabsorption.[63-65] Accordingly, lipophilic compounds are predominantly reabsorbed from the renal filtrate. Given that renal clearance is the major route of elimination, this will result in a slow but steady excretion into the bladder. In contrast, hydrophilic compounds are poorly reabsorbed and thus quickly renally eliminated, which leads to high initial compound levels in the urine but narrows the time range where the minimal anti-adhesive concentration is maintained. Consequently, low log $D_{7.4}$ as shown for the antagonists **6**, **11h**, and **11i** implies low tubular reabsorption and rapid elimination of the filtered molecules by the urine. Otherwise, log $D_{7.4}$ between 0.2 and 0.7, such as determined for the bioisosteres **11a**-**e,** suggests increasing propensity to tubular reuptake, whereas log $D_{7.4} > 1$ as shown for heptyl mannoside **1** and the biphenyl mannosides **10**, **5**, **11g**, **11f**, and **11j** is optimal for tubular reabsorption from the glomerular filtrate and thus for slow renal clearance.

Metabolic Stability. Increasing lipophilicity is usually paralleled by increasing susceptibility to metabolism.[66] Liabilities towards metabolic clearance pathways which prevent the intact antagonist from reaching the target in the bladder were therefore of interest. To assess their propensity to cytochrome P450 (CYP450)-mediated metabolism, heptyl mannoside **1**, the carboxylic acid derivative **6**, and the bioiosteres **11c-e**, **g**, **j** were incubated with rat liver microsomes (RLM, 0.5 mg/mL) in presence of the cofactor β-nicotinamide adenine dinucleotide phosphate (NADPH).[53] To confirm the high propensity of the methyl ester present in antagonist **5** to carboxylesterase (CES)-mediated hydrolysis, this antagonist was incubated with RLM only. The profiles of unchanged compound versus time revealed high susceptibility of heptyl mannoside **1** to CYP450-mediated metabolism ($t_{1/2}$ = 13 min) and rapid hydrolysis of the ester **5** by the hepatic CES ($t_{1/2}$ = 1.0 min). Otherwise, the

bioisosteres **11c**-**e,g** & **j** were stable against enzyme-mediated bioconversion ($t_{1/2}$ > 60 min) suggesting lower propensity to metabolic, non-renal elimination pathways.

Considering PPB, lipophilicity, and metabolic stability data, we therefore expected (i) a steady release of compounds **11d**, **e**, **g**, **j** into the bladder because of high PPB decelerating glomerular filtration (**11d**, **e**, **g**) and/or high log $D_{7.4}$ supporting tubular reabsorption (**11g**, **j**), (ii) a fast excretion of antagonist **6** and **11c** via the urine due to low PPB and low log $D_{7.4}$, and (iii) a rapid clearance of heptyl mannoside **1** from the body by renal and metabolic pathways. Compounds featuring high propensity to renal excretion as major route of elimination (**11c**, **11e** and **11j**) were selected for *in vivo* PK studies in a mouse model.

Pharmacokinetic Studies in C3H/HeN Mice. This first part of our study explored the predicted effects of lipophilicity, PPB, and metabolic stability on antagonist disposition and elimination upon a single dose iv application (50 mg/kg) of compounds **11c** and **11e**. The PK parameters of these applications and those of the previously published carboxylate **6** are summarized in Table 4. The Table also contains the results of the iv administration of compound **11j** (0.625 mg/kg).

Table 4. Pharmacokinetic parameters determined after a single iv application of compounds **6a**, **11c**, **11e** and **11j** in female C3H/HeN mice. Values were calculated using PKSolver.[67] C_0, initial concentration; V_z, volume of distribution in terminal phase; AUC, Area under the curve; CL_{tot}, total clearance; C_{max}, maximal concentration.

Compd	**Plasma**						**Urine**
	C_0 (µg/mL)	Dose (mg/kg)	V_z (mL)	$t_{1/2}$ (h)	$AUC_{0\text{-}inf}$ (µg x h/mL)	CL_{tot} (mL/h)	C_{max} (µg/mL)
6[19]	40	50	25.2	0.33	23.5	53.1	300
11c	109.7	50	28.3	0.4	25.3	49.4	4611
11e	151.6	50	19.5	1.9	175.1	7.1	387
11j	0.36	0.625	52.8	0.17	0.07	218	10

In contrast to the fast plasma clearance of antagonists **6** and **11c** (Figure 5A), the methyl sulfonamide bioisostere **11e** attained higher initial concentration in plasma (C_0) and lower total clearance (CL_{tot}). Therefore, it could be detected until six hours post application, resulting in markedly higher plasma AUC. The observed high C_0 of compound **11e** may be attributed to a small volume of distribution (V_z) resulting from the high PPB (f_b ≥ 99%).[61] In urine (Figure 5B), the carboxylic acid **6** and the morpholinomethanone **11c** displayed high levels immediately following administration and a rapid concentration decrease within the first two hours, reflecting the rapid elimination from plasma. Fast renal excretion as major route of elimination can be rationalized by the physicochemical properties of the antagonists **6** and **11c**, that is, moderate PPB and log $D_{7.4}$, as well as high metabolic stability. Otherwise, the methyl sulfonamide bioisostere **11e** showed sustained compound levels in urine over a period of two hours and subsequent slow decrease until six hours post administration. This sustained renal excretion is a result of the interplay of the antagonist's elevated PPB and log $D_{7.4}$.

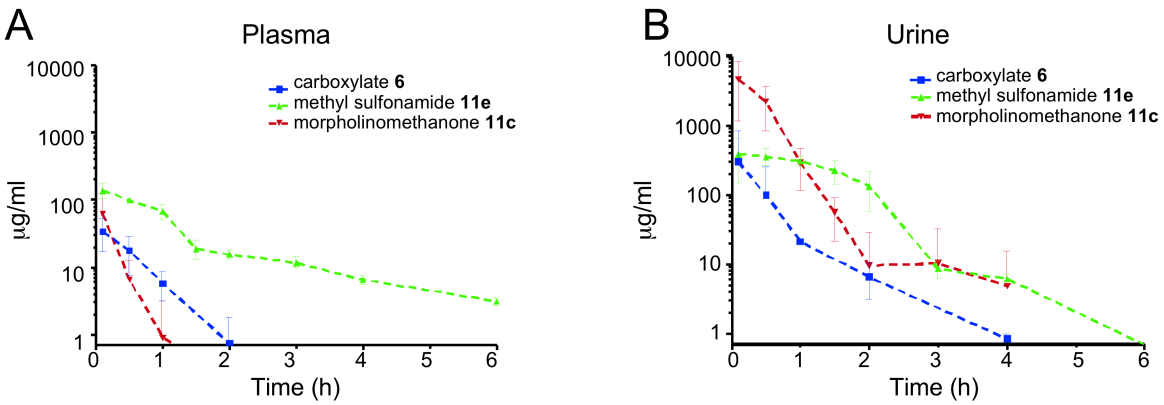

Figure 5. Antagonist concentrations in (A) plasma and (B) urine after a single iv application of **6**, **11c**, and **11e** (50 mg/kg).

In a second study, the *para*-cyano bioisostere **11j**, characterized by a high oral absorption potential, but low solubility, was administered as a single dose iv (0.625 mg/kg) and po (1.25 mg/kg). The plasma concentration curve upon iv dosing displays a steep decline within the first hour post application, while the po curve shows a prolonged period where absorption and elimination are in equilibrium (Figure 6A). The urine concentration profiles (Figure 6B) parallel the plasma curves obtained by the two modes of application, i.e. high plasma clearance upon iv bolus injection led to high initial antagonist levels in urine and a rapid concentration decline. By contrast, sustained plasma concentrations upon po administration resulted in prolonged urine levels. As a result, urine concentrations exceed the minimum level required for the anti-adhesive effect (minimal anti-adhesion concentration, MAC_{90}),[23] determined by flow cytometry[68] (0.094 µg/ml), for more than eight hours upon oral single-dose administration, proving the high potential of the *para*-cyano biphenyl mannoside for the oral treatment of UTI (Figure 6B).

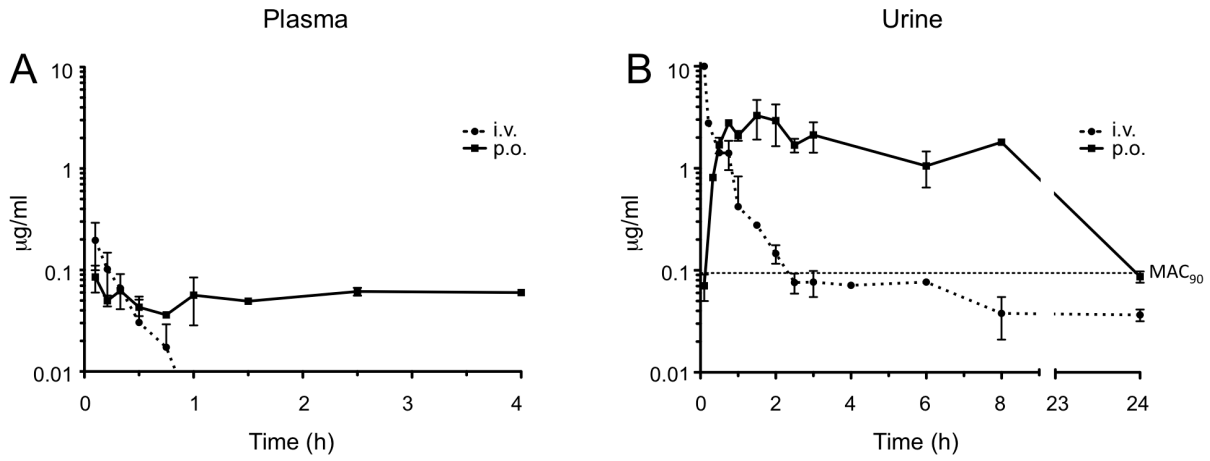

Figure 6. Antagonist concentrations in (A) plasma and (B) urine after a single iv and po application of compound **11j** (iv: 0.625 mg/kg; po: 1.25 mg/kg). MAC_{90}, minimal anti-adhesive concentration to inhibit 90% adhesion (0.094 µg/ml).

Infection study in C3H/HeN Mice. Based on the promising PK profile of **11j**, six mice were inoculated with UTI89 following an oral application of **11j** (1.25 mg/kg) 40 min prior to infection. Three hours after inoculation, animals were sacrificed and bladder and kidneys were removed. Organs were homogenized and analysed for bacterial counts. The results were compared to ciprofloxacin (CIP), used as standard antibiotic therapy against UTI89.[69] The median reduction in bacterial counts of the mice treated with **11j** and CIP compared to the control group are displayed in Figure 7.

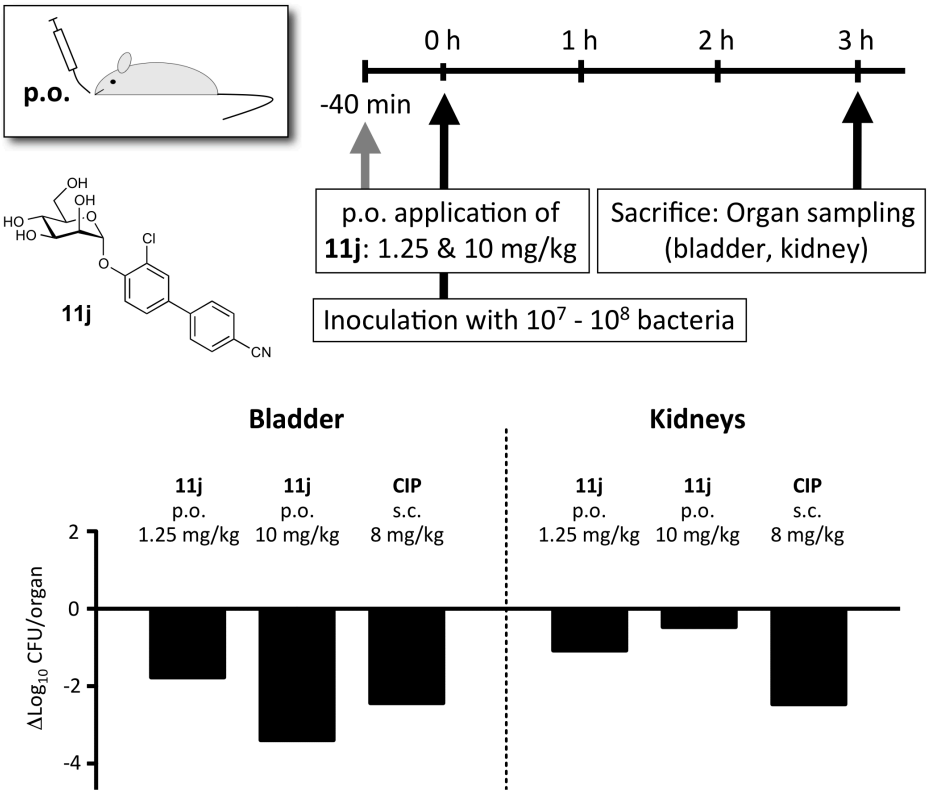

Figure 7. Treatment efficacy in the UTI mouse model 3 h after infection. The bars depict the median reduction of bacterial counts after application of 1.25 or 10 mg/kg **11j** p.o. or 8 mg/kg CIP s.c. (representing the murine dose equivalent to a human standard dose).[70] The baseline represents the median counts of the untreated control group.

The median value in the untreated control group showed bacterial counts of 6.6 Log_{10} colony forming units (CFU) in the bladder and 6 Log_{10} CFU in the kidneys. After oral application of 1.25 mg/kg of **11j**, bacterial loads in the bladder decreased by 1.7 Log_{10} CFU and 1.08 Log_{10} CFU in the kidneys. The lower reduction in the kidneys is most likely due to the differing adhesion mechanisms between bladder and kidneys (type 1 pili vs P-pili), which is not targeted by **11j**.[71] With CIP (8 mg/kg s.c.) a substantial reduction in both, bladder and kidneys (median reductions of 2.44 Log_{10} and 2.47 Log_{10}, respectively) was observed. Despite the low oral dose of **11j**, the approximately 100-fold reduction of CFU in the bladder promised en even higher effect upon dose increase. To increase solubility of **11j**, a basic formulation was used,. When 10 mg/kg were applied, bacterial loads in the bladder decreased by 3.4 Log_{10} CFU/ml, exceeding the effect of CIP, but only 0.5 Log_{10} CFU in the kidneys. Based on this large reduction after an oral application of 10 mg/kg, **11j** has a large potential for further development.

SUMMARY AND CONCLUSION

Recently, numerous monovalent alkyl and aryl α-D-mannopyranosides have been described as potent FimH antagonists. However, most of them suffer from insufficient pharmacokinetic properties, i.e. modest bioavailability and short duration of the therapeutic effect in the bladder, their site of action. As a consequence, high doses at short intervals are required to achieve anti-adhesive effects over an extended period of time. Therefore, the goal of the present study was an appropriate optimization of the pharmacokinetic profile of biphenyl α-D-mannopyranosides while keeping their high affinity to the CRD of FimH. The starting point was the biphenyl-carboxylate **6** where the critical carboxylate was replaced by bioisosteres.[29,72]
With a series of bioisosteres a three- to fivefold improvement of affinity was achieved compared to **6**. Although binding necessitates only partial desolvation of the carboxylate and its bioisosteric replacements, a reduction of the enthalpy penalty for desolvation[41] was identified as the source of the improved affinity exhibited by the bioisosteres. Thermodynamic evaluation of antagonists **11b**-**e** revealed almost identical enthalpy contribution to binding. However, for antagonists with the para-cyano substituent (**11g** & **11j**) an enhancement of up to -8.7 kJ/mol was observed, indicating a reduced desolvation penalty and an improved stacking as derived from the crystal structure of **11j** co-crystallized with the CRD of FimH (Figure 4B). On the other hand, higher affinity originating from a reduction of conformational flexibility of ligand and protein resulted in a concomitant entropy penalty of up to 6.5 kJ/mol.

In addition to the improved pharmacodynamics, the relevant pharmacokinetic parameters (solubility, permeability, renal excretion) could also be substantially improved. With 3'-chloro-4'-(α-D-mannopyranosyloxy)-biphenyl-4-carbonitrile (**11j**), a FimH antagonist with an optimal *in vitro* PK/PD profile was identified. The *para*-cyano substituent conferred lipophilicity and high binding to plasma proteins, which slowed down the rate of renal excretion. Despite higher lipophilicity, antagonist **11j** was insusceptible to CYP450 mediated metabolism, and therefore predominantly eliminated via the renal pathway. *In vivo* experiments confirmed the excellent PK-profile of **11j** with steady renal excretion for more than eight hours after oral application, suggesting a long-lasting anti-adhesive effect. Finally, orally applied **11j** (10 mg/kg) was effective in a mouse model of UTI by reducing the bacterial load

inthe bladder by over 1000-fold. Improvement of solubility, enabling the application of higher dosages of **11j**, will possibly lead to an even higher bacterial reductions, which will be the subject of future investigations.

EXPERIMENTAL SECTION

Synthesis

The synthesis of compounds **11a-f**, **11i**, **14a-f**, **16**, **19**, and **24**, including compound characterization data, can be found in the Supporting Information.

General methods. NMR spectra were recorded on a Bruker Avance DMX-500 (500.1 MHz) spectrometer. Assignment of ^{1}H and ^{13}C NMR spectra was achieved using 2D methods (COSY, HSQC, HMBC). Chemical shifts are expressed in ppm using residual $CHCl_3$, CHD_2OD or HDO as references. Optical rotations were measured using Perkin-Elmer Polarimeter 341. Electron spray ionization mass spectra (ESI-MS) were obtained on a Waters micromass ZQ. The LC/HRMS analysis were carried out using a Agilent 1100 LC equipped with a photodiode array detector and a Micromass QTOF I equipped with a 4 GHz digital-time converter. Microwave-assisted reactions were carried out with a CEM Discover and Explorer. Reactions were monitored by TLC using glass plates coated with silica gel 60 F_{254} (Merck) and visualized by using UV light and/or by charring with a molybdate solution (a 0.02 M solution of ammonium cerium sulfate dihydrate and ammonium molybdate tetrahydrate in aqueous 10% H_2SO_4). MPLC separations were carried out on a CombiFlash Companion or Rf (Teledyne Isco) equipped with RediSep normal-phase or RP-18 reversed-phase flash columns. LC-MS separations were done on a Waters system equipped with sample manager 2767, pump 2525, PDA 2525 and micromass ZQ. All compounds used for biological assays are at least of 95% purity based on HPLC analytical results. Commercially available reagents were purchased from Fluka, Aldrich, Alfa Aesar or abcr GmbH & Co. KG (Germany). Solvents were purchased from Sigma-Aldrich or Acros and were dried prior to use where indicated. Methanol (MeOH) was dried by refluxing with sodium methoxide and distilled immediately before use. Dimethoxyethane (DME) was dried by filtration over Al_2O_3

(Fluka, type 5016 A basic).

4'-(2,3,4,6-Tetra-*O*-acetyl-α-D-mannopyranosyloxy)-biphenyl-4-carbonitrile (14g). A Schlenk tube was charged with aryl iodide **12**[24] (330 mg, 0.60 mmol), 4-cyanophenylboronic acid (**13g**, 96 mg, 0.65 mmol), $Pd(dppf)Cl_2 \cdot CH_2Cl_2$ (15 mg, 0.018 mmol), K_3PO_4 (192 mg, 0.90 mmol) and a stirring bar. The tube was closed with a rubber septum and was evacuated and flushed with argon. This procedure was repeated once, and then anhydrous DMF (2 mL) was added under a stream of argon. The mixture was degassed in an ultrasonic bath and flushed with argon for 5 min, and then stirred at 80 °C overnight. The reaction mixture was cooled to rt, diluted with EtOAc (50 mL), and washed with water (50 mL) and brine (50 mL). The organic layer was dried over Na_2SO_4 and concentrated *in vacuo*. The residue was purified by MPLC on silica gel (petroleum ether/EtOAc) to afford **14g** (187 mg, 59%) as colorless oil. $[\alpha]_D^{20}$ +72.9 (*c* 0.8, MeOH); ^{1}H NMR (500 MHz, CD_3OD): δ = 7.73-7.71 (m, 2H, Ar-H), 7.65-7.64 (m, 2H, Ar-H), 7.57-7.53 (m, 2H, Ar-H), 7.21-7.19 (m, 2H, Ar-H), 5.60-5.57 (m, 2H, H-1, H-3), 5.47 (dd, *J* = 1.9, 3.4 Hz, 1H, H-2), 5.40 (t, *J* = 10.1 Hz, 1H, H-4), 4.30 (dd, *J* = 5.1, 12.2 Hz, 1H, H-6a), 4.14-4.08 (m, 2H, H-6b, H-5), 2.22, 2.07, 2.06, 2.04 (4 s, 12H, 4 $COCH_3$); ^{13}C NMR (126 MHz, CD_3OD): δ = 170.62, 170.14, 170.11, 169.83 (4 CO), 156.16, 144.87, 134.05, 132.77, 128.64, 127.46 (Ar-C), 119.05 (CN), 117.15, 110.77 (Ar-C), 95.86 (C-1), 69.42 (2C, C-2, C-5), 68.90 (C-3), 65.94 (C-4), 62.16 (C-6), 21.01, 20.84, 20.82 (4C, 4 $COCH_3$); ESI-MS: *m/z*: Calcd for $C_{27}H_{27}NNaO_{10}$ $[M+Na]^+$: 548.2, found: 548.2.

4'-(α-D-Mannopyranosyloxy)-biphenyl-4-carbonitrile (11g). To a solution of **14g** (40 mg, 0.08 mmol) in dry MeOH (5 mL) was added freshly prepared 1 M NaOMe/MeOH (0.1 eq) under argon. The mixture was stirred at rt until the reaction was complete (monitored by TLC), then neutralized with Amberlyst-15 (H^+) ion-exchange resin, filtered and concentrated *in vacuo*. The residue was purified by MPLC on silica gel (DCM/MeOH, 10:1-7:1) to afford **11g** (16 mg, 60%) as white solid. ^{1}H NMR (500 MHz, CD_3OD): δ = 7.82-7.75 (m, 4H, Ar-H), 7.69-7.63 (m, 2H, Ar-H), 7.30-7.23 (m, 2H, Ar-H), 5.58 (d, *J* = 1.7 Hz, 1H, H-1), 4.05 (dd, *J* = 1.8, 3.4 Hz, 1H, H-2), 3.94 (dd, *J* = 3.4, 9.5 Hz, 1H, H-3), 3.83-3.71 (m, 3H, H-4, H-6a, H-6b), 3.62 (ddd, *J* = 2.5, 5.3, 9.8 Hz, 1H, H-5). The spectroscopic data were in accordance with literature values.[18]

5-(4'-(2,3,4,6-Tetra-*O*-acetyl-α-D-mannopyranosyloxy)-biphenyl-4-yl)-1*H*-tetrazole (15). A Schlenk tube was charged with **14g** (30 mg, 0.06 mmol), trimethylsilyl azide (16 μL, 0.12 mmol), dibutyltin oxide (2 mg, 0.006 mmol), DME (1 mL) and a stirring bar. The mixture was heated to 150 °C for 10 min by microwave irradiation. The reaction mixture was cooled to rt, and then concentrated *in vacuo*. The residue was purified by MPLC on silica gel (DCM/MeOH, 9:1-8:1) to afford **15** (26 mg, 81%) as colorless oil. $[\alpha]_D^{20}$ +56.1 (*c* 0.3, MeOH); ^{1}H NMR (500 MHz, $CDCl_3$): δ = 8.25-8.15 (m, 2H, Ar-H), 7.75-7.65 (m, 2H, Ar-H), 7.60-7.55 (m, 2H, Ar-H), 7.20-7.17 (m, 2H, Ar-H), 5.64-5.55 (m, 2H, H-1, H-3), 5.49 (dd, *J* = 1.7, 3.3 Hz, 1H, H-2), 5.40 (t, *J* = 10.1 Hz, 1H, H-4), 4.31 (dd, *J* = 5.3, 12.4 Hz, 1H, H-6a), 4.17-4.06 (m, 2H, H-5, H-6b), 2.22, 2.07, 2.06, 2.05 (4 s, 12H, 4 $COCH_3$); ^{13}C NMR (126 MHz, $CDCl_3$): δ = 170.67, 170.14, 170.11, 169.81 (4 CO), 155.61, 128.36, 127.84, 127.49, 116.93 (Ar-C), 95.78 (C-1), 69.36 (C-5), 69.26 (C-2), 68.90 (C-3), 65.89 (C-4), 62.12 (C-6), 20.92, 20.76, 20.73 (4 $COCH_3$); ESI-MS: *m/z*: Calcd for $C_{27}H_{28}N_4NaO_{10}$ $[M+Na]^+$: 591.2, found: 591.1.

5-(4'-(α-D-Mannopyranosyloxy)-biphenyl-4-yl)-1*H*-tetrazole (11h). Prepared according to the procedure described for **11g** from **15** (26 mg, 0.03 mmol). Yield: 18 mg (quant.) as a white solid. $[\alpha]_D^{20}$ +112.1 (*c* 0.1, MeOH/H_2O, 2:1); ^{1}H NMR (500 MHz, CD_3OD): δ = 7.98-7.96 (m, 2H, Ar-H), 7.72-7.71 (m, 2H, Ar-H), 7.58-7.54 (m, 2H, Ar-H), 7.16-7.13 (m, 2H, Ar-H), 5.46 (d, *J* = 1.7 Hz, 1H, H-1), 3.94 (dd, *J* = 1.9, 3.5 Hz, 1H, H-2), 3.83 (dd, *J* = 3.4, 9.5 Hz, 1H, H-3), 3.68-3.61 (m, 3H, H-4, H-6a, H-6b), 3.52 (ddd, *J* = 2.5, 5.4, 9.7 Hz, 1H, H-5); ^{13}C NMR (126 MHz, CD_3OD): δ = 158.19, 145.07, 134.97, 129.29, 128.74, 128.55, 118.26 (Ar-C), 100.13 (C-1), 75.52 (C-5), 72.42 (C-3), 71.98 (C-2), 68.33 (C-4), 62.69 (C-6); HRMS: *m/z*: Calcd for $C_{19}H_{21}N_4O_6$ $[M+H]^+$: 401.1456, found: 401.1450.

4'-(2,3,4,6-Tetra-*O*-acetyl-α-D-mannopyranosyloxy)-3'-chloro-biphenyl-4-carbonitrile (20). Prepared according to the procedure described for **14g** from aryl iodide **19**[23] (79 mg, 0.135 mmol), **13g** (22 mg, 0.15 mmol), $Pd(dppf)Cl_2 \cdot CH_2Cl_2$ (3.3 mg, 4 μmol) and K_3PO_4 (57 mg, 0.27 mmol). Yield: 57 mg (75%) as a white solid. $[\alpha]_D^{20}$ +77.7 (*c* 0.5, $CHCl_3$); ^{1}H NMR (500 MHz, $CDCl_3$): δ = 7.72 (d, *J* = 8.3 Hz, 2H,

Ar-H), 7.63 (m, 3H, Ar-H), 7.43 (dd, *J* = 2.2, 8.6 Hz, 1H, Ar-H), 7.27 (d, *J* = 8.6 Hz, 1H, Ar-H), 5.64-5.59 (m, 2H, H-1, H-2), 5.54 (dd, *J* = 1.9, 3.2 Hz, 1H, H-3), 5.41 (t, *J* = 10.1 Hz, 1H, H-4), 4.28 (dd, *J* = 5.2, 12.3 Hz, 1H, H-6a), 4.17 (ddd, *J* = 2.1, 5.1, 10.0 Hz, 1H, H-5), 4.10 (dd, *J* = 2.2, 12.3 Hz, 1H, H-6b), 2.21 (s, 3H, $COCH_3$), 2.12-2.00 (m, 9H, 3 $COCH_3$); ^{13}C NMR (126 MHz, $CDCl_3$): *δ* = 170.54, 170.08, 169.90, 169.84, (4C, CO) 151.67, 143.61, 135.29, 132.87, 129.41, 127.53, 126.60, 125.20, 118.79, 117.36, 111.47 (Ar-C, CN), 96.72 (C-1), 70.00 (C-5), 69.39 (C-3), 68.82 (C-2), 65.86 (C-4), 62.16 (C-6), 20.98, 20.81, 20.79, 20.78 (4 CO*C*H_3); ESI-MS*: m/z*: Calcd for $C_{27}H_{26}ClNNaO_{10}$ $[M+Na]^+$: 582.1, found: 582.1.

3'-Chloro-4'-(α-D-mannopyranosyloxy)-biphenyl-4-carbonitrile (11j). Prepared according to the procedure described for **11g** from **20** (36 mg, 0.06 mmol). Yield: 12 mg (48%) as a white solid. $[\alpha]_D^{20}$ +109.4 (*c* 0.23, MeOH); ^1H NMR (500 MHz, CD_3OD): *δ* = 7.80-7.72 (m, 5H, Ar-H), 7.59 (dd, *J* = 2.2, 8.6 Hz, 1H, Ar-H), 7.48 (d, *J* = 8.7 Hz, 1H, Ar-H), 5.62 (d, *J* = 1.4 Hz, 1H, H-1), 4.12 (dd, *J* = 1.8, 3.3 Hz, 1H, H-2), 4.00 (dd, *J* = 3.4, 9.5 Hz, 1H, H-3), 3.83-3.68 (m, 3H, H-4, H-6a, H-6b), 3.63 (ddd, *J* = 2.3, 5.4, 9.6 Hz, 1H, H-5); ^{13}C NMR (126 MHz, CD_3OD): *δ* = 153.65, 145.15, 135.42, 133.86, 129.82, 128.53, 127.87, 125.47, 119.70, 118.59 (Ar-C), 111.97 (CN), 100.66 (C-1), 76.05 (C-5), 72.39 (C-3), 71.80 (C-2), 68.20 (C-4), 62.65 (C-6); IR (KBr), *ν* = 3400 (OH), 2227 (C≡N), 1606, 1487 (Ar-C=C) cm^{-1}; HRMS: *m/z*: Calcd for $C_{19}H_{18}ClNNaO_6$ $[M+Na]^+$: 414.0715, found: 414.0721.

3'-Chloro-*N*-(3',6'-dihydroxy-3-oxo-3*H*-spiro[isobenzofuran-1,9'-xanthen]-5-yl)-4'-(α-D-mannopyranosyloxy)-biphenyl-4-carboxamide (21). Compound **8** (10.0 mg, 0.024 mmol), fluoresceinamine isomer I (12.7 mg, 0.037 mmol) and COMU (20.9 mg, 0.049 mmol) were dissolved in dry DMF (1 mL), then NEt_3 (10 mL, 0.073 mmol) was added and the mixture was stirred at rt for 7 h. 1 N HCl in DMF was added until acid reaction on pH paper and the mixture was concentrated. The residue was dissolved in DCM/MeOH (3:1) and loaded onto a silica gel column. The complex mixture of compounds was only partially resolved. The fractions containing the product were collected, concentrated and purified by preparative HPLC (gradient water/MeCN containing 0.2% HCO_2H), to afford compound **21** (5 mg, 19%). $[\alpha]_D^{20}$ +21.1 (*c* 0.1, MeOH); ^1H NMR (500 MHz, CD_3OD): *δ* = 8.26 (d, *J* = 8.4 Hz, 2H, Ar-H), 7.88-7.74 (m, 3H, Ar-H), 7.66 (dd, *J* = 2.2, 8.6 Hz, 1H, Ar-H), 7.51 (d, *J* = 8.7 Hz, 1H,

Ar-H), 7.29 (dd, *J* = 1.9, 5.3 Hz, 2H, Ar-H), 7.19 (dd, *J* = 2.1, 8.3 Hz, 1H, Ar-H), 7.08-6.99 (m, 2H, Ar-H), 6.95 (d, *J* = 8.7 Hz, 1H, Ar-H), 6.72 (dd, *J* = 5.5, 10.6, Hz, 2H, Ar-H), 6.61 (dd, *J* = 2.3, 8.7 Hz, 1H, Ar-H), 5.65 (s, 1H, H-1), 4.15 (dd, *J* = 1.8, 3.2 Hz, H-2), 4.03 (dd, *J* = 3.4, 9.5, Hz, H-3), 3.87-3.72 (m, 3H, H-4, H-6a, H-6b), 3.65 (m, 1H, H-5); ^{13}C NMR (126 MHz, CD_3OD): *δ* = 137.50, 136.01, 131.90, 130.24, 130.20, 129.87, 129.24, 128.03, 127.91, 125.79, 125.46, 124.73, 118.99, 118.76, 118.65 (Ar-C), 100.73 (C-1), 76.06 (C-5), 72.42 (C-3), 71.85 (C-2), 68.24 (C-4), 62.69 (C-2); ESI-MS: *m/z*: Calcd for $C_{39}H_{31}ClNO_{12}$ $[M+H]^+$: 740.2, found: 740.2.

3'-Chloro-*N*-(2-(3-(3',6'-dihydroxy-3-oxo-3*H*-spiro[isobenzofuran-1,9'-xanthen]-5-yl)-thioureido)ethyl)-4'-(a-D-mannopyranosyloxy)-biphenyl-4-carboxamide (22). To a stirred solution of compound **8** (25 mg, 0.061 mmol) in dry DMF (1 mL), NHS (21 mg, 0.183 mmol) was added, followed by DIC (9.2 mg, 0.073 mmol). The mixture was stirred at rt for 2 h, then *N*-Boc-ethylendiamine (10.7 mg, 0.067 mmol) was added and the reaction was stirred for 10 h. It was then cooled down to 0 °C, diluted with water and concentrated. Chromatography on silica gel (DCM/MeOH) yielded 23 mg (0.042 mmol, 68%) of *tert*-butyl (3'-chloro-4'-(a-D-mannopyranosyloxy)-biphenyl-4-yl-carboxamido)ethyl)carbamate. This product was dissolved in CH_2Cl_2 (3 mL) and TFA (1 mL) was added. The solid dissolved during addition of TFA. After 10 min the reaction was complete. The mixture was evaporated and excess TFA was removed in high vacuum. The intermediate *N*-(2-aminoethyl)-3'-chloro-4'-(a-D-manno-pyranosyloxy)-biphenyl-4-carboxamide TFA salt (23 mg, 0.042 mmol, quant.) was used directly in the next step. It was dissolved in dry DMF (0.5 mL) and NEt_3 (12.8 mg, 0.127 mmol) was added. The mixture was cooled to 0 °C, then FITC (14.8 mg, 0.038 mmol) was added and the mixture was stirred for 3 h in the dark. The mixture was then co-evaporated with water, taken up in MeOH/10% aq. acetic acid and evaporated. Chromatography on silica gel (DCM/MeOH) yielded compound **22**, contaminated with triethylammonium acetate. The compound was then re-dissolved in MeOH, and 0.5 N HCl in MeOH was added. The mixture was evaporated and chromatographed on silica gel, to yield pure **22** (15 mg, 47%). $[\alpha]_D^{20}$ +12.1 (*c* 0.3, MeOH); ^{1}H NMR (500 MHz, CD_3OD): *δ* = 8.12 (s, 1H), 7.92 (d, *J* = 8.3 Hz, 2H, Ar-H), 7.70 (dd, *J* = 5.0, 13.1 Hz, 2H, Ar-H), 7.64 (d, *J* = 8.3 Hz, 2H, Ar-H), 7.54 (dd, *J* = 2.2, 8.6 Hz, 1H, Ar-H), 7.46 (d, *J* = 8.7 Hz, 1H, Ar-H), 7.09 (d, *J* = 8.2 Hz, 1H, Ar-H), 6.74 (s, 2H), 6.69 (d, *J* = 1.4 Hz, 2H, Ar-H), 6.55 (d, *J* = 8.4 Hz, 2H, Ar-H), 5.63 (d, *J* = 1.3

Hz, H-1), 4.15 (dd, *J* = 1.8, 3.1 Hz, H-2), 4.03 (dd, *J* = 3.4, 9.5 Hz, H-3), 3.94 (s, 2H, CH_2), 3.86-3.64 (m, 6H, H-4, H-5, H-6, CH_2); ^{13}C NMR (126 MHz, CD_3OD): δ = 153.21, 143.84, 136.41, 129.66, 129.18, 127.76, 127.70, 125.37, 118.64, 103.62 (Ar-C), 100.75 (C-1), 76.00 (C-5), 72.41 (C-3), 71.86 (C-2), 68.24 (C-4), 62.69 (C-6), 40.76 (CH_2); ESI-MS: *m/z*: Calcd for $C_{42}H_{37}ClN_3O_{12}S$ $[M+H]^+$: 842.2, found: 842.2.

3'-Chloro-*N*-(2-(2-(2-(3-(3',6'-dihydroxy-3-oxo-3*H*-spiro[isobenzofuran-1,9'-xanthen]-5-yl)thioureido)ethoxy)ethoxy)ethyl)-4'-(α-D-mannopyranosyloxy)-biphenyl-4-carboxamide (23). Compound **8** (280 mg, 0.68 mmol) was dissolved in dry DMF (5 mL) under argon, then NHS (235 mg, 2.04 mmol) was added, followed by DIC (0.12 mL, 0.78 mmol) and the mixture was stirred at rt for 4 h, then Boc-PEG2-NH_2 (186 mg, 0.75 mmol) was added, and the mixture was stirred at rt under argon for 10 h. It was then slowly diluted with water and concentrated. The residue was purified by chromatography on silica gel (DCM/MeOH) to give *tert*-butyl (2-(2-(2-(3'-chloro-4'-(α-D-mannopyranosyloxy)-biphenyl-4-ylcarboxamido)ethoxy)ethoxy)ethyl)carbamate (300 mg, 0.468 mmol, 69%). Then, the carbamate was suspended in DCM (3 mL) and TFA (1 mL) was added dropwise at rt. After 30 min, the solvents were evaporated and the crude mixture was dissolved in $CHCl_3$/MeOH (6:4 + 0.5% conc. NH_4OH) and transferred to a silica gel column, eluting with the same solvent mixture, to yield *N*-(2-(2-(2-aminoethoxy)ethoxy)ethyl)-3'-chloro-4'-(α-D-mannopyranosyloxy)-biphenyl-4-carboxamide (228 mg, 90 %). A fraction of the amine (10 mg, 0.018 mmol) was dissolved in dry DMF (0.5 mL) and cooled to 0 °C. FITC (6.5 mg, 0.017 mmol) was added and the mixture was stirred for 1 h. The mixture was concentrated and the residue was purified by chromatography on silica (DCM/MeOH), to yield **23** (10 mg, 65%). ^1H NMR (500 MHz, CD_3OD): δ = 8.21 (d, *J* = 1.4 Hz, 1H, Ar-H), 7.88 (d, *J* = 8.3 Hz, 2H, Ar-H), 7.68 (d, *J* = 2.2 Hz, 2H, Ar-H), 7.63 (d, *J* = 8.3 Hz, 2H, Ar-H), 7.53 (dd, *J* = 2.2, 8.6 Hz, 1H, Ar-H), 7.43 (d, *J* = 8.7 Hz, 1H, Ar-H), 7.09 (d, *J* = 8.2 Hz, 1H, Ar-H), 6.68 (d, *J* = 2.3 Hz, 2H, Ar-H), 6.65 (dd, *J* = 2.6, 8.6 Hz, 2H, Ar-H), 6.53 (dd, *J* = 1.6, 8.7 Hz, 2H, Ar-H), 5.61 (d, *J* = 1.3 Hz, 1H, H-1), 4.14 (dd, *J* = 1.8, 3.2, Hz, 1H, H-2), 4.03 (dd, *J* = 3.4, 9.5 Hz, 1H, H-3), 3.93-3.53 (m, 16H), 3.37 (s, 2H, NCH_2), 1.30 (s, 2H, CH_2); ^{13}C NMR (126 MHz, CD_3OD): δ = 170.01 (CO), 153.17, 143.72, 136.37, 134.37, 130.39, 129.69, 129.04, 127.78, 127.73, 125.35, 118.60, 103.60 (Ar-C), 100.72 (C-1), 75.97 (C-5), 72.41 (C-3), 71.86, 71.40, 70.59 (5C, C-2, OCH_2), 68.23 (C-4), 62.64 (C-6), 49.88, 45.49,

40.97 (CH_2); ESI-MS: *m/z*: Calcd for $C_{46}H_{45}ClN_3O_{14}S$ $[M+H]^+$: 930.2, found: 930.4.

Competitive Fluorescence Polarization Assay

Expression and purification of CRD of FimH. A recombinant protein consisting of the CRD of FimH linked to a 6His-tag via a thrombin cleavage site (FimH-CRD-Th-His_6) was expressed in *E. coli* strain HM125 and purified by affinity chromatography as previously described.[33]

***K*$_D$ determination of FITC-labeled ligands.** The functionalized ligands (**22**, **23**) were prepared as a 10 mM stock solution in pure DMSO (Sigma Aldrich, Buchs, Switzerland). All further dilutions of compounds and FimH-CRD-Th-His_6 protein were prepared in assay buffer (20 mM HEPES, 150 mM NaCl, 50 µg/mL BSA, pH 7.4). BSA was added to the assay buffer to prevent non-specific binding of protein to the plastic surface. Binding isotherms for the fluorescent ligands were obtained in direct binding studies by adding a constant concentration of ligand (final concentration 5 nM) and a linear dilution of protein (final concentration 0-100 nM) to a final volume of 200 µL in 96-well, black, flat bottom NBS™ plates (Corning Inc., Corning, NY, USA). After incubating the plate for 24 h at rt with gentle shaking, the fluorescence polarization was measured with the Synergy™ H1 Hybrid Multi-Mode Microplate Reader (BioTek Instruments Inc., Winooski, VT, USA) with polarized excitation at 485 nm and emission measured at 528 nm through polarizing filters parallel and perpendicularly oriented to the incident polarized light. K_D values were determined by plotting the FP readout as a function of the protein concentration and applying the following single-site binding equation (Equation 1) that accounts for ligand depletion:

$$S_{obs} = S_F + (S_B - S_F) \cdot \left(\frac{C_P + C_L + K_D - \sqrt{(C_P + C_L + K_D)^2 - 4C_P C_L}}{2C_L}\right) \quad (1)$$

where S_{obs} is the observed signal from the ligand, S_F is the signal from free ligand, S_B is the signal from bound ligand, C_P is the total concentration of protein, and C_L is the total concentration of ligand.[39]

***K*$_D$ Determination of FimH Antagonists.** The fluorescently labeled ligand **22** was used for the competitive fluorescence polarization assay. A linear dilution of non-labeled FimH antagonist with final concentrations ranging from 0-10 µM was titrated

into 96-well, black, flat bottom NBS™ plates (Corning Inc.) to a final volume of 200 µL containing a constant concentration of protein (final concentration 25 nM) and FITC-labeled ligand which was fixed at a higher concentration in competitive binding assays than in direct binding experiments to obtain higher fluorescence intensities (final concentration 20 nM). Prior to measuring the fluorescence polarization, the plates were incubated on a shaker for 24 h at rt until the reaction reached equilibrium. The IC_{50} value was determined with Prism (GraphPad Software Inc., La Jolla, CA, USA) by applying a standard four-parameter IC_{50} function. The obtained IC_{50} values were converted into their corresponding K_D values using the derivation of the Cheng-Prusoff equation.[35] This variation of the Cheng-Prusoff equation is applied to competition assays with tight-binding inhibitors, and includes terms to correct for ligand depletion effects. However, the K_D for antagonists having a higher affinity towards FimH than the labeled ligand could not be accurately determined.[35]

Isothermal Titration Calorimetry (ITC)

All ITC experiments were performed with the FimH-CRD-Th-His_6 protein using a VP-ITC instrument from MicroCal, Inc. (GE Healthcare, Northampton, MA, USA) with a sample cell volume of 1.4523 mL. The measurements were performed with 2.5 or 5% DMSO at 25 °C, a stirring speed of 307 rpm, and 10 µcal s^{-1} reference power. The protein samples were dialyzed in assay buffer prior to all experiments. Compounds **6**, **10**, and **24** were measured in a direct fashion by titration of ligand (120-2,000 µM) into protein (10-55 µM) with injections of 3-6 µL at intervals of 10 min to ensure non-overlapping peaks. The quantity $c = Mt(0)\ K_D^{-1}$, where *Mt(0)* is the initial macromolecule concentration, is of importance in titration microcalorimetry. The *c*-values of the direct titrations were below 1'000 and thus within the reliable range. For the compounds **11b**-**e, 11g** and **11j** additional competitive ITC experiments were performed due to their high affinity resulting in *c*-values above 1'000 for direct titrations. These ligands (600 µM) were titrated into protein (30 µM), which was preincubated with compound **24** (300 µM) resulting in sigmoidal titration curves. Due to slow reaction kinetics, titration intervals of 20 min were used.

Baseline correction and peak integration was performed using the Origin 7 software (OriginLab, Northampton, MA, USA). An initial 2 µL injection was excluded from data

analysis. Baseline subtraction and curve-fitting with the three variables *N* (concentration correction factor), K_D (dissociation constant), and $\Delta H°$ (change in enthalpy) was performed with the SEDPHAT software version 10.40 (National Institute of Health). A global fitting analysis was performed for the competition titration (compounds **11b-e**, **11g** or **11j** competing for the protein binding site with compound **24**) and the direct titration of the competitor (compound **24** binding to protein) to fit for K_D. $\Delta H°$ and *N* were fitted from direct titrations of compounds **11b-e**, **11g** or **11j** into protein. For the compounds **6, 10** and **24** binding to protein all variables could be determined from a global analysis of the direct titration.

The thermodynamic parameters were calculated with the following equation (Equation 2):

$$\Delta G° = \Delta H° - T\Delta S° = RT \ln K_D = -RT \ln K_A \quad (2)$$

where $\Delta G°$, $\Delta H°$, and $\Delta S°$ are the changes in free energy, enthalpy, and entropy of binding, respectively, *T* is the absolute temperature, and *R* is the universal gas constant (8.314 J mol^{-1} K^{-1}). The 95 %-confidence intervals of the measurements were calculated for the two variables K_D and $\Delta H°$ with the 1-dimensional error surface projection within the SEDPHAT software.

Calculation of the Free Energy of Desolvation. The three dimensional representation for each of the aglycons (4-methoxy biphenyl scaffold, Figure 7) was built in the Maestro[73] modeling environment and the global minimum conformation was identified by performing 500 iterations of the mixed torsional/low-mode conformational sampling in combination with the OPLS-2005 force-field and the implicit solvent model (water) as implemented in the Macromodel 9.9.[74] The global minimum structures were used as input for the AMSOL 7.1 program[76] to obtain the free energy of desolvation DG_{des} (Table 5) with the SM5.4A solvation model[76] and the AM1[77] level of theory (used keywords “AM1 SM5.4A SOLVNT=WATER TRUES”).

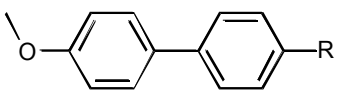

Figure 7. **The 4-methoxy biphenyl scaffold of aglycons.**

Table 5. **Aqueous free energy of desolvation.**

R	DG_{des} [kJ/mol]
neutral	
H	15.6
$CONHCH_3$	39.9
$COOCH_3$	23.0
SO_2NHCH_3	65.5
SO_2CH_3	56.4
4-morpholine amide	45.3
CN	22.0
deprotonated	
COO^-	298.2
SO_2-N^--Me	342.0

Determination of the MAC_{90} by flow cytometry

The MAC_{90} was determined in principle as in the previously published flow cytometry assay,[68] but with some modifications. The human epithelial bladder carcinoma cell line 5637 (DSMZ, Braunschweig, Germany) was grown in RPMI 1640 medium, supplemented with 10% fetal calf serum (FCS), 100 U/mL penicillin and 100 µg/mL streptomycin at 37 °C, 5% CO_2. All solutions were purchased from Invitrogen (Basel, Switzerland). The cells were subcultured 1:6 twice per week [using Trypsin/EDTA (Sigma-Aldrich) for the detachment]. Two days before infection, 1.8×10^5 cells were seeded in each well of a 24-well plate in RPMI 1640 containing 10% FCS without antibiotics. The cell density was approximately $3\text{-}5 \times 10^5$ cells/well at the assay day.
For infection, the GFP-expressing clinical *E. coli* isolate UTI89[78] (UTI89 wt) and the GFP-expressing FimA-H knock-out strain UTI89 Δ*fimA-H* were used (strains were provided by Prof. Urs Jenal, Biocenter, University of Basel, Switzerland).[68] Bacteria were cultivated at 37 °C in 10 mL Luria-Bertani (LB) broth (Becton, Dickinson and Company) overnight, harvested by centrifugation (3800 rpm, 10 min) and washed three times in phosphate buffered saline (PBS, Sigma-Aldrich) and a bacterial solution of OD_{600} of 0.75 in RPMI + 10% FCS was prepared. For the determination of

the MAC_{90} value, the IC_{90}, linear dilutions of the FimH-antagonist were prepared in 5% DMSO and PBS. Bacteria and antagonists were pre-incubated for 10 min at 37 °C, before cells were infected with either only 200 µL bacterial solution of UTI89 or UTI89 Δ*fimA-H* (positive and negative controls), or 225 µL of the pre-incubated bacteria-antagonist mixture. Infection lasted for 1.5 h, during this time infected cells were incubated at 37 °C. Then, cells were washed with PBS and detached from wells by the addition of 150 µL trypsin and incubation at 37 °C for 10 min, before flushing from wells PBS containing 2% FCS and transferred to tubes. To dilute the trypsin, cells were centrifuged at 13000 rpm, 1 min, 600 µL of the supernatant was discarded and the pellet was re-suspended in the remaining 300 µL PBS containing 2% FCS. Samples were stored on ice until measurement. Before analysis with the flow cytometer (Becton Dickinson, FACSCanto II), the samples were gently mixed and filtered using a 35 µm nylon mesh (Corning Life Sciences) to prevent cellular aggregation. Cells were gated with linear scaling for side scatter (SSC) and forward scatter (FSC) and GFP intensity of live cells was evaluated. IC_{90} values were determined by plotting the concentration of the antagonist in a logarithmic mode versus the mean fluorescence intensity (MFI) of living cells and by fitting a dose response curve (variable slope, four parameters) with the prism software (GraphPad Prism).

X-ray analysis of the antagonists 11e and 11j co-crystallized with FimH-CRD

FimH-CRD-11e co-crystallization. Initial FimH-CRD (18 mg/mL in 20 mM HEPES pH 7.4) crystals were obtained in complex with 4-(5-nitroindolin-1-yl)phenyl α-D-mannopyranoside (5 mM).[23] Crystals were grown in sitting-drop vapor diffusion at 20 °C with 200 nL of protein-antagonist mixture together with 200 nL precipitant solution in well D3 (0.2 M sodium phosphate monobasic monohydrate, 20% w/v PEG 3,350) of the PEG/Ion HT™ screen (Hampton Research, CA, USA). Cubic crystals appeared within one week, which served as cross-seeding crystals. A solution of FimH-CRD (20 mg/mL) and **11e** (5 mM) was mixed with 0.2 M sodium phosphate monobasic monohydrate, 20% w/v PEG 400 with 0.5 µL of each solution. Streak-seeding was performed after one day of incubation. Cubic FimH-CRD-**11e** crystals formed within 24 h. Crystals were flash cooled to 100 K with perfluoropolyether cryo oil (Hampton

Research, CA, USA) as cryoprotectant. Data was collected with synchrotron radiation (λ = 0.99999 Å) at the PXIII beamline, Swiss Light Source, Switzerland.

FimH-CRD-11j co-crystallization. Co-crystals were initially grown in sitting-drop vapor diffusion at 20 °C with 0.5 µL of a mixture of FimH-CRD (20 mg/mL) and **11j** (5 mM) together with 0.5 µL of 0.1 M HEPES pH 7.5, 2 M ammonium sulfate. Plate-like crystals formed within two weeks and were used as seeds for subsequent crystallization. Diffraction quality crystals were grown by streak-seeding in 0.5 µL of FimH-CRD (10 mg/mL) with **11j** (2.5 mM) and 0.5 µL of 0.1 M HEPES pH 7.5, 1.25 M ammonium sulfate. The drops were covered with perfluoropolyether cryo oil prior to flash cooling to 100 K. Data was collected with synchrotron radiation (λ = 1.00003 Å) at the PXIII beamline, Swiss Light Source, Switzerland.

Structure Determination and Refinement. Data were indexed and integrated with the XDS package[79] for the FimH-CRD-**11e** co-crystal structure, and with mosflm[807] for the FimH-CRD-**11j** co-crystal structure. Scaling was performed with XDS and SCALA included in the CCP4 suite, respectively.[81] Structures were solved by molecular replacement with PHASER[82] using the FimH-CRD-butyl α-D-mannopyranoside complex (PDB code 1UWF) as search model. The structures were iteratively built using the COOT software[83] and refined with the PHENIX software.[84] Geometric restraints for **11e** and **11j** were generated with PRODRG.[85] The models were validated using molprobity.[86] Residues 113-115 were not modeled in the **11e** structure due to disorder. Furthermore, the ligand was modeled in two possible conformations. For both ligands, electron density is reduced on the second aromatic ring due to flexibility of the ligand.

Table 6. Data Collection and Refinement Statistics for FimH-CRD-**11e** and FimH-CRD-**11j** co-crystals.

	FimH-CRD-**11e**	FimH-CRD-**11j**
PDB code	4CSS	4CST
Space group	P 2_1 2_1 2_1	P 2_1 2_1 2_1
No. of molecules in the asymmetric unit	1	1
Cell dimensions		
a, b, c (Å)	48.38, 56.23, 61.59	48.84, 55.89, 61.00
a, b, c (°)	90, 90, 90	90, 90, 90
Data Collection		
Beamline	Swiss Light Source PXIII	Swiss Light Source PXIII
Resolution range (Å)[a]	30.0 - 1.07 (1.13 – 1.07)	23.5 – 1.10 (1.12 – 1.10)
Unique observations[a]	72000 (9354)	66470 (2500)
Average multiplicity[a]	10.9 (3.7)	5.4 (2.4)
Completeness (%)	96.1 (78.0)	97.2 (76.5)
R_{merge}[a]	0.056 (0.57)	0.051 (0.305)
Mean I / σ(I)[a]	21.5 (2.22)	15.5 (2.9)
Refinement		
Resolution range (Å)	15.7 – 1.07	23.5 – 1.10
R, R_{free}	11.2, 13.2	11.4, 13.0
Rms deviation from ideal bond length (Å)	0.010	0.010
Rms deviation from ideal bond angle (deg)	1.170	1.420

[a]Values in parentheses are for highest-resolution shell.

Physicochemical and *in vitro* pharmacokinetic studies.

Materials. Dimethyl sulfoxide (DMSO), 1-propanol, 1-octanol, Dulbecco's Modified Eagle's Medium (DMEM) - high glucose, L-glutamine solution, penicillin-streptomycin solution, Dulbecco's Phosphate Buffered Saline (DPBS), trypsin-EDTA solution, magnesium chloride hexahydrate, and reduced nicotinamide adenine dinucleotide phosphate (NADPH) were purchased from Sigma-Aldrich. MEM nonessential amino acid (MEM-NEAA) solution, fetal bovine serum (FBS), and DMEM without sodium pyruvate and phenol red were bought from Invitrogen (Carlsbad, CA, USA). PRISMA HT universal buffer, GIT-0 Lipid Solution, and Acceptor Sink Buffer were ordered

from pIon (Woburn, MA, USA). Human plasma was bought from Biopredic (Rennes, France) and acetonitrile (MeCN) and methanol (MeOH) from Acros Organics (Geel, Belgium). Pooled male rat liver microsomes were purchased from BD Bioscience (Franklin Lakes, NJ, USA). Tris(hydroxymethyl)-aminomethane (TRIS) was obtained from AppliChem (Darmstadt, Germany). The Caco-2 cells were kindly provided by Prof. G. Imanidis, FHNW, Muttenz, and originated from the American Type Culture Collection (Rockville, MD, USA).

pK_a. The pK_a values were determined as described elsewhere.[87] In brief, the pH of a sample solution was gradually changed and the chemical shift of protons adjacent to ionizable centers was monitored by ^1H nuclear magnetic resonance (NMR) spectroscopy. The shift was plotted against the pH of the respective sample, and the pK_a was read out from the inflection point of the resulting sigmoidal curve.

Log $D_{7.4}$. The in silico prediction tool ALOGPS[88] was used to estimate log *P* values of the compounds. Depending on these values, the compounds were classified into three categories: hydrophilic compounds (log *P* below zero), moderately lipophilic compounds (log *P* between zero and one) and lipophilic compounds (log *P* above one). For each category, two different ratios (volume of 1-octanol to volume of buffer) were defined as experimental parameters (Table 7).

Table 7. Compound classification based on estimated log *P* values.

Compound type	**log *P***	**ratio (1-octanol / buffer)**
hydrophilic	< 0	30:140, 40:130
moderately lipophilic	0 - 1	70:110, 110:70
lipophilic	> 1	3:180, 4:180

Equal amounts of phosphate buffer (0.1 M, pH 7.4) and 1-octanol were mixed and shaken vigorously for 5 min to saturate the phases. The mixture was left until separation of the two phases occurred, and the buffer was retrieved. Stock solutions of the test compounds were diluted with buffer to a concentration of 1 µM. For each compound, six determinations, that is, three determinations per 1-octanol/buffer ratio,

were performed in different wells of a 96-well plate. The respective volumes of buffer containing analyte (1 µM) were pipetted to the wells and covered by saturated 1-octanol according to the chosen volume ratio. The plate was sealed with aluminum foil, shaken (1350 rpm, 25 °C, 2 h) on a Heidolph Titramax 1000 plate-shaker (Heidolph Instruments GmbH & Co. KG, Schwabach, Germany) and centrifuged (2000 rpm, 25 °C, 5 min, 5804 R Eppendorf centrifuge, Hamburg, Germany). The aqueous phase was transferred to a 96-well plate for analysis by LC-MS.

The log $D_{7.4}$ coefficient was calculated from the 1-octanol/buffer ratio (o:b), the initial concentration of the analyte in buffer (1 µM), and the concentration of the analyte in buffer (c_B) with Equation 3:

$$\log D_{7.4} = \log\left(\frac{1\mu M - c_B}{c_B} \times \frac{1}{o:b}\right) \tag{3}$$

Aqueous Solubility. Solubility was determined in a 96-well format using the µSOL Explorer solubility analyzer (pIon, version 3.4.0.5). For each compound, measurements were performed at pH 3.0 and 7.4 in triplicates. For this purpose, six wells of a deep well plate, that is, three wells per pH value, were filled with 300 µL of PRISMA HT universal buffer, adjusted to pH 3.0 or 7.4 by adding the requested amount of NaOH (0.5 M). Aliquots (3 µL) of a compound stock solution (10-50 mM in DMSO) were added and thoroughly mixed. The final sample concentration was 0.1-0.5 mM, the residual DMSO concentration was 1.0% (v/v) in the buffer solutions. After 15 h, the solutions were filtrated (0.2 µm 96-well filter plates) using a vacuum to collect manifold (Whatman Ltd., Maidstone, UK) to remove the precipitates. Equal amounts of filtrate and 1-propanol were mixed and transferred to a 96-well plate for UV/Vis detection (190 to 500 nm, SpectraMax 190). The amount of material dissolved was calculated by comparison with UV/Vis spectra obtained from reference samples, which were prepared by dissolving compound stock solution in a 1:1 mixture of buffer and 1-propanol (final concentrations 0.017-0.083 mM).

Parallel Artificial Membrane Permeation Assay (PAMPA). Effective permeability (log P_e) was determined in a 96-well format with the PAMPA.[50] For each compound, measurements were performed at pH 5.0 and 7.4 in quadruplicates. Eight wells of a deep well plate, that is, four wells per pH-value, were filled with 650 µL of PRISMA

HT universal buffer adjusted to pH 5.0 or 7.4 by adding the requested amount of NaOH (0.5 M). Samples (150 µL) were withdrawn from each well to determine the blank spectra by UV/Vis-spectroscopy (190 to 500 nm, SpectraMax 190). Then, analyte dissolved in DMSO was added to the remaining buffer to yield 50 µM solutions. To exclude precipitation, the optical density was measured at 650 nm, with 0.01 being the threshold value. Solutions exceeding this threshold were filtrated. Afterwards, samples (150 µL) were withdrawn to determine the reference spectra. Further 200 µL were transferred to each well of the donor plate of the PAMPA sandwich (pIon, P/N 110163). The filter membranes at the bottom of the acceptor plate were infused with 5 µL of GIT-0 Lipid Solution, and 200 µL of Acceptor Sink Buffer was filled into each acceptor well. The sandwich was assembled, placed in the GutBox^{TM}, and left undisturbed for 16 h. Then, it was disassembled and samples (150 µL) were transferred from each donor and acceptor well to UV-plates for determination of the UV/Vis spectra. Effective permeability (log P_e) was calculated from the compound flux deduced from the spectra, the filter area, and the initial sample concentration in the donor well with the aid of the PAMPA Explorer Software (pIon, version 3.5).

Colorectal Adenocarcinoma (*Caco*-2) Cell Permeation Assay. Caco-2 cells were cultivated in tissue culture flasks (BD Biosciences) with DMEM high glucose medium, containing L-glutamine (2 mM), nonessential amino acids (0.1 mM), penicillin (100 U/mL), streptomycin (100 µg/mL), and fetal bovine serum (10%). The cells were kept at 37 °C in humidified air containing 5% CO_2, and the medium was changed every second day. When approximately 90% confluence was reached, the cells were split in a 1:10 ratio and distributed to new tissue culture flasks. At passage numbers between 60 and 65, they were seeded at a density of 5.3×10^5 cells per well to Transwell 6-well plates (Corning Inc.) with 2.5 mL of culture medium in the basolateral and 1.8 mL in the apical compartment. The medium was renewed on alternate days. Permeation experiments were performed between days 19 and 21 post seeding. Prior to the experiment, the integrity of the Caco-2 monolayers was evaluated by measuring the transepithelial electrical resistance (TEER) with an Endohm tissue resistance instrument (World Precision Instruments Inc., Sarasota, FL, USA). Only wells with TEER values higher than 250 Ω cm^2 were used. Experiments were performed in the apical-to-basolateral (absorptive) and

basolateral-to-apical (secretory) directions in triplicates. Transport medium (DMEM without sodium pyruvate and phenol red) was withdrawn from the donor compartments of three wells and replaced by the same volume of compound stock solution (10 mM in DMSO) to reach an initial sample concentration of 62.5 µM. The Transwell plate was then shaken (600 rpm, 37 °C) on a Heidolph Titramax 1000 plate-shaker. Samples (40 µL) were withdrawn from the donor and acceptor compartments 30 min after initiation of the experiment and the compound concentrations were determined by LC-MS (see below). Apparent permeability (P_{app}) was calculated according to Equation 4:

$$P_{app} = \frac{dQ}{dt} \times \frac{1}{A \times c_0} \quad (4)$$

where dQ/dt is the compound flux (mol s^{-1}), A is the surface area of the monolayer (cm^2), and c_0 is the initial concentration in the donor compartment (mol cm^{-3}).[50] After the experiment, TEER values were assessed again for each well and results from wells with values below 250 Ω cm^2 were discarded.

Plasma Protein Binding (PPB). PPB was determined in a 96-well format using a high throughput dialysis block (HTD96b; HTDialysis LCC, Gales Ferry, CT, USA). For each compound, measurements were performed in triplicate. Dialysis membranes (MWCO 12-14 K; HTDialysis LCC) were hydrated according to the instructions of the manufacturer and placed into the dialysis block. Human plasma was centrifuged (5800 rpm, 5 °C, 10 min), the pH of the supernatant (without floating plasma lipids) was adjusted to 7.4 by adding the requested amount of HCl (4 M), and analyte was added to yield a final concentration of 10 µM. Equal volumes (150 µL) of plasma containing the analyte or TRIS-HCl buffer (0.1 M, pH 7.4) were transferred to the compartments separated by the dialysis membrane. The block was covered with a sealing film and left undisturbed (5 h, 37 °C). Afterwards, samples (90 µL) were withdrawn from the buffer compartments and diluted with plasma (10 µL). From the plasma compartments, samples (10 µL) were withdrawn and diluted with TRIS-HCl buffer (90 µL). The solutions were further diluted with ice-cooled MeCN (300 µL) to precipitate the proteins and centrifuged (3600 rpm, 4 °C, 10 min). The supernatants (50 µL) were retrieved, and the analyte concentrations were determined by LC-MS (see below). The fraction bound (f_b) was calculated as follows (Equation 5):

$$f_b = 1 - \frac{c_b}{c_p} \quad (5)$$

where c_b is the concentration of the analyte withdrawn from the buffer compartment before dilution and c_p is the concentration in the plasma compartment. The values were accepted if the recovery of analyte was between 80 and 120% of the initial amount.

Cytochrome P450-mediated metabolism. Incubations consisted of pooled male rat liver microsomes (0.5 mg microsomal protein/mL), test compound (2 µM), $MgCl_2$ (2 mM), and NADPH (1 mM) in a total volume of 300 µL TRIS-HCl buffer (0.1 M, pH 7.4) and were performed in a 96-well plate on a Thermomixer Comfort (Eppendorf). Compounds and microsomes were preincubated (37 °C, 700 rpm, 10 min) before NADPH was added. Samples (50 µL) at t = 0 min and after an incubation time of 5, 10, 20, and 30 min were quenched with 150 µL of ice-cooled MeOH, centrifuged (3600 rpm, 4 °C, 10 min), and 80 µL of supernatant was transferred to a 96-well plate for LC-MS analysis (see below). The metabolic half-life ($t_{1/2}$) was calculated from the slope of the linear regression from the log percentage remaining compound versus incubation time relationship. Control experiments without NADPH were performed in parallel.

LC-MS measurements. Analyses were performed using an 1100/1200 Series HPLC System coupled to a 6410 Triple Quadrupole mass detector (Agilent Technologies, Inc., Santa Clara, CA, USA) equipped with electrospray ionization. The system was controlled with the Agilent MassHunter Workstation Data Acquisition software (version B.01.04). The column used was an Atlantis® T3 C18 column (2.1 x 50 mm) with a 3-µm particle size (Waters Corp., Milford, MA, USA). The mobile phase consisted of eluent A: H_2O containing 0.1% formic acid (for **11a**-**f**, **h**-**i**), or 10 mM ammonium acetate, pH 5.0 in 95:5, H_2O/MeCN (for **11g**, **j**); and eluent B: MeCN containing 0.1% formic acid. The flow rate was maintained at 0.6 mL/min. The gradient was ramped from 95% A/5% B to 5% A/95% B over 1 min, and then hold at 5% A/95% B for 0.1 min. The system was then brought back to 95% A/5% B, resulting in a total duration of 4 min. MS parameters such as fragmentor voltage, collision energy, polarity were optimized individually for each analyte, and the molecular ion was followed for each compound in the multiple reaction monitoring mode. The concentrations of the analytes were quantified by the Agilent Mass Hunter Quantitative Analysis software (version B.01.04).

***In Vivo* Pharmacokinetic Studies.**

Materials. DMSO and PBS were purchased from Sigma-Aldrich. The 96-well plates were bought from Agilent Technologies (0.5 mL, polypropylene). The gavage was obtained from Fine Science (Heidelberg, Germany) and the syringes (BD Micro Fine, U-100 Insuline, 30 G) and needles (BD Microlance 3, 25 G) from Becton Dickinson (USA, Ireland) and Henke Sass Wolf in Germany (Soft-Ject, 1 mL syringes).

Animals. Female C3H/HeN mice weighing between 19 and 25 g were obtained from Charles River Laboratories (Sulzfeld, Germany) and were housed three or four per cage. The mice were kept under specific pathogen-free conditions in the Animal House of the Department of Biomedicine, University Hospital of Basel, and animal experimentation guidelines according to the regulations of the Swiss veterinary law were followed. After 7 d of acclimatization, 9-10 week old mice were used for the studies. Animals had free access to chow and water at any time and were kept in a 12h/12h light/dark cycle. For administration volumes and sampling the good practice guidelines were followed.[89]

Pharmacokinetic studies. The single-dose studies for the first experiment set were performed by intravenous application of FimH antagonists at a dosage of 50 mg/kg body weight, followed by plasma and urine sampling. Antagonists were diluted in PBS for injection into the tail vein. Blood and urine samples (10 µL) were taken at 6 and 30 min, and 1, 2, 4, 6, and 8 h after injection. For the PK studies with **11j**, the antagonist was dissolved in PBS with 5 % DMSO and injected into the tail vain (0.625 mg/kg) or given orally (1.25 mg/kg) using a gavage. Blood and urine were sampled (10 µL) after 7, 13, 20, 30, 45 min, and 1, 1.5, 2, 2.5, 3, 4, 6, 8, and 24 h. Both, blood and urine samples, were directly diluted after sampling with MeOH to precipitate the proteins and centrifuged for 11 min at 13000 rpm. The supernatants were transferred to a 96-well plate and the analyte concentrations were determined by LC-MS (see above).

Infection study. For all infection studies, the drinking water of the mice was replaced by 5% glucose (monohydrate from AppliChem, BioChemica) containing water, three days before the start of the experiment. **11j** was dosed at 1.25 mg/kg (in 5% DMSO

and PBS) and 10 mg/kg (5% DMSO in PBS containing 1% Tween 80) applied orally to 6 and 4 mice, respectively, as described in the pharmacokinetic studies, 40 min prior to infection. Ciprofloxacin was dosed with 8 mg/kg, which would correspond to a human dose of 400 mg,[70] subcutaneously 10 minutes prior to infection with UTI89 to 4 mice. Control values resulted from the infection of 11 mice. Before infection, remaining urine in the bladder was expelled by gentle pressure on the abdomen. Mice were anaesthetised in 2.5 vol% isoflurane/oxygen mixture (Attane, Minrad Inc, Buffalo, NY, USA) and placed on their back. Infection was performed transurethrally using a polyethylene catheter (Intramedic polyethylene tubing, inner diameter 0.28 mm, outer diameter 0.61 mm, Beckton Dickinson, Allschwil, Switzerland), on a syringe (Hamilton Gastight Syringe 50 µl, removable 30G needle, BGB Analytik AG, Boeckten, Switzerland). After gentle insertion of the catheter into the bladder, 50 µl of bacterial suspension of UTI89 ($5.5x10^9$-$2.25x10^{10}$ CFU/ml) was slowly injected. This corresponded to approximately 10^7-10^8 CFU per mouse. Mice were killed by CO_2 three hours after inoculation and bladder and kidneys were aseptically removed. Organs were homogenized in 1 ml PBS using a tissue lyser (Retsch, Haan, Germany). Serial dilutions of bladder and kidneys were plated on Levine Eosin Methylene Blue Agar plates (Beckton Dickinson, France) and CFU were counted after overnight incubation at 37°C.

Acknowledgement

The authors thank Prof. Dr. med. Radek Skoda, Department of Biomedicine, University Hospital Basel, Switzerland, for giving us access to the animal facility. The financial support by the Swiss National Science Foundation (SNF interdisciplinary grant K-32K1-120904) is gratefully acknowledged.

References

(1) Foxman, B.; Barlow, R.; D'Arcy, H.; Gillespie, B.; Sobel, J. D. Urinary tract infection: self-reported incidence and associated costs. *Ann. Epidemiol.* **2000**, *10*, 509-515.

(2) Ronald, A. The etiology of urinary tract infection: traditional and emerging pathogens. *Am. J. Med.* **2002**, *113 Suppl. 1A*, 14S-19S.

(3) Fihn, S. D. Acute uncomplicated urinary tract infection in women. *N. Engl. J. Med.* **2003**, *349*, 259-266.

(4) Hooton, T. M.; Besser, R.; Foxman, B.; Fritsche, T. R.; Nicolle, L. E. Acute uncomplicated cystitis in an era of increasing antibiotic resistance: a proposed approach to empirical therapy. *Clin. Infect. Dis.* **2004**, *39*, 75-80.

(5) Sanchez, G. V.; Master, R. N.; Karlowsky, J. A.; Bordon, J. M. In vitro antimicrobial resistance of urinary *Escherichia coli* isolates among U. S. outpatients from 2000 to 2010. *Antimicrob. Agents Chemother.* **2012**, *56*, 2181-2183.

(6) Clatworthy, A. E.; Pierson, E.; Hung, D. T. Targeting virulence: a new paradigm for antimicrobial therapy. *Nature Chem. Biol.* **2007**, *3*, 541-548.

(7) Mulvey, M. A.; Schilling, J. D.; Martinez, J. J.; Hultgren, S. J. Bad bugs and beleaguered bladders: interplay between uropathogenic *Escherichia coli* and innate host defenses. *Proc. Natl. Acad. Sci. U S A* **2000**, *97*, 8829-8835.

(8) Schilling, J. D.; Mulvey, M. A.; Hultgren, S. J. Structure and function of *Escherichia coli* type 1 pili: new insight into the pathogenesis of urinary tract infections. *J. Infect. Dis.* **2001**, *183 Suppl. 1*, S36-40.

(9) Wiles, T. J.; Kulesus, R. R.; Mulvey, M. A. Origins and virulence mechanisms of uropathogenic *Escherichia coli*. *Exp. Mol. Pathol.* **2008**, *85*, 11-19.

(10) Capitani, G.; Eidam, O.; Glockshuber, R.; Grütter, M. G. Structural and functional insights into the assembly of type 1 pili from *Escherichia coli*. *Microbes Infect.* **2006**, *8*, 2284-2290.

(11) Le Trong, I.; Aprikian, P.; Kidd, B. A.; Forero-Shelton, M.; Tchesnokova, V.; Rajagopal, P.; Rodriguez, V.; Interlandi, G.; Klevit, R.; Vogel, V.; Stenkamp, R.

E.; Sokurenko, E. V.; Thomas, W. E. Structural basis for mechanical force regulation of the adhesin FimH via finger trap-like β sheet twisting. *Cell* **2010**, *141*, 645-655.

(12) Sharon, N. Carbohydrates as future anti-adhesion drugs for infectious diseases. *Biochim. Biophys. Acta.* **2006**, *1760*, 527-537.

(13) Firon, N.; Itzhak, O.; Sharon, N. Interaction of mannose-containing oligosaccharides with the fimbrial lectin of *Escherichia coli*. *Biochem. Biophys. Res. Commun.* **1982**, *105*, 1426-1432.

(14) Firon, N.; Ofek, I.; Sharon, N. Carbohydrate specificity of the surface lectins of *Escherichia coli*, *Klebsiella pneumoniae*, and *Salmonella typhimurium*. *Carbohydr. Res.* **1983**, *120*, 235-249.

(15) Bouckaert, J.; Berglund, J.; Schembri, M.; De Genst, E.; Cools, L.; Wuhrer, M.; Hung, C.-S.; Pinkner, J.; Slättegard, R.; Zavialov, A.; Choudhury, D.; Langermann, S.; Hultgren, S. J.; Wyns, L.; Klemm, P.; Oscarson, S.; Knight, S. D.; De Greve, H. Receptor binding studies disclose a novel class of high-affinity inhibitors of the *Escherichia coli* FimH adhesin. *Mol. Microbiol.* **2005**, *55*, 441-455.

(16) Firon, N.; Ashkenazi, S.; Mirelman, D.; Ofek, I.; Sharon, N. Aromatic alpha-glycosides of mannose are powerful inhibitors of the adherence of type 1 fimbriated *Escherichia coli* to yeast and intestinal epithelial cells. *Infect. Immun.* **1987**, *55*, 472-476.

(17) Sperling, O.; Fuchs, A.; Lindhorst, T. K. Evaluation of the carbohydrate recognition domain of the bacterial adhesin FimH. Design, synthesis and binding properties of mannoside ligands. *Org. Biomol. Chem.* **2006**, *4*, 3913-3922.

(18) Han, Z.; Pinkner, J. S.; Ford, B.; Obermann, R.; Nolan, W.; Wildman, S. A.; Hobbs, D.; Ellenberger, T.; Cusumano, C. K.; Hultgren, S. J.; Janetka, J. W. Structure-based drug design and optimization of mannoside bacterial FimH antagonists. *J. Med. Chem.* **2010**, *53*, 4779-4792.

(19) Klein, T.; Abgottspon, D.; Wittwer, M.; Rabbani, S.; Herold, J.; Jiang, X.; Kleeb, S.; Lüthi, C.; Scharenberg, M.; Bezençon, J.; Gubler, E.; Pang, L.; Smiesko, M.; Cutting, B.; Schwardt, O.; Ernst, B. FimH antagonists for the oral

treatment of urinary tract infections: from design and synthesis to in vitro and in vivo evaluation. *J. Med. Chem.* **2010**, *53*, 8627-8641.

(20) Schwardt, O.; Rabbani, S.; Hartmann, M.; Abgottspon, D.; Wittwer, M.; Kleeb, S.; Zalewski, A.; Smiesko, M.; Cutting, B.; Ernst, B. Design, synthesis and biological evaluation of mannosyl triazoles as FimH antagonists. *Bioorg. Med. Chem.* **2011**, *19*, 6454-6473.

(21) Cusumano, C. K.; Pinkner, J. S.; Han, Z.; Greene, S. E.; Ford, B. A.; Crowley, J. R.; Henderson, J. P.; Janetka, J. W.; Hultgren, S. J. Treatment and prevention of urinary tract infection with orally active FimH inhibitors. *Sci. Transl. Med.* **2011**, *3*, 109-115.

(22) Han, Z.; Pinkner, J. S.; Ford, B.; Chorell, E.; Crowley, J. M.; Cusumano, C. K.; Campbell, S.; Henderson, J. P.; Hultgren, S. J.; Janetka, J. W. Lead optimization studies on FimH antagonists: discovery of potent and orally bioavailable ortho-substituted biphenyl mannosides. *J. Med. Chem.* **2012**, *55*, 3945-3959.

(23) Jiang, X.; Abgottspon, D.; Kleeb, S.; Rabbani, S.; Scharenberg, M.; Wittwer, M.; Haug, M.; Schwardt, O.; Ernst, B. Anti-adhesion therapy for urinary tract infections – a balanced PK/PD profile proved to be key for success. *J. Med. Chem.* **2012**, *55*, 4700-4713.

(24) Pang, L.; Kleeb, S.; Lemme, K.; Rabbani, S.; Scharenberg, M.; Zalewski, A.; Schädler, F.; Schwardt, O.; Ernst, B. FimH antagonists: structure-activity and structure-property relationships for biphenyl α-D-mannopyranosides. *ChemMedChem.* **2012**, *7*, 1404-1422.

(25) Choudhury, D.; Thompson, A.; Stojanoff, V.; Langermann, S.; Pinkner, J.; Hultgren, S. J.; Knight, S. D. X-ray structure of the FimC-FimH chaperone-adhesin complex from uropathogenic *Escherichia coli*. *Science* **1999**, *285*, 1061-1066.

(26) Hung, C.-S.; Bouckaert, J.; Hung, D.; Pinkner, J.; Widberg, C.; DeFusco, A.; Auguste, C. G.; Strouse, R.; Langermann, S.; Waksman, G.; Hultgren, S. J. Structural basis of tropism of *Eschrichia coli* to the bladder drug in urinary tract infection. *Mol. Microbiol.* **2002**, *44*, 903-915.

(27) Wellens, A.; Garofalo, C.; Nguyen, H.; Van Gerven, N.; Slättegard, R.; Henalsteens, J.-P.; Wyns, L.; Oscarson, S.; De Greve, H.; Hultgren, S. J.; Bouckaert, J. Intervening with urinary tract infections using anti-adhesives based on the crystal structure of the FimH-oligomannose-3 complex. *PLoS One* **2008**, *3*, e2040.

(28) Wellens, A.; Lahmann, M.; Touaibia, M.; Vaucher, J.; Oscarson, S.; Roy, R.; Remaut, H.; Bouckaert, J. The tyrosine gate as a potential entropic lever in the receptor-binding site of the bacterial adhesin FimH. *Biochemistry* **2012**, *51*, 4790-4799.

(29) Meanwell, M. A. Synopsis of some recent tactical application of bioisosteres in drug design. *J. Med. Chem.* **2011**, *54*, 2529-2591.

(30) Prieto, M.; Zurita, E.; Rosa, E.; Luñoz, L.; Lloyd-Williams, P.; Giralt, E. Arylboronic acids and arylpinacolboronate esters in Suzuki coupling reactions involving indoles. Partner role swapping and heterocycle protection. *J. Org. Chem.* **2004**, *69*, 6812-6820.

(31) Schulz, M. J.; Coats, S. J.; Hlasta, D. J. Microwave-assisted preparation of aryltetrazoleboronate esters. *Org. Lett.* **2004**, *6*, 3265-3268.

(32) Devos, A.; Remion, J.; Frisque-Hesbain, A. M.; Colens, A.; Ghosez, L. Synthesis of acyl halides under very mild conditions. *J. Chem. Soc. Chem. Commun.* **1979**, 1180-1181.

(33) Rabbani, S.; Jiang, X.; Schwardt, O.; Ernst, B. Expression of the carbohydrate recognition domain of FimH and development of a competitive binding assay. *Anal. Biochem.* **2010**, *407*, 188-195.

(34) Waetherman, R.V.; Kiessling, L.L. Fluorescence anisotropy assay reveals affinities of *C*- and *O*-glycosides for concanavalin A. *J. Org. Chem.* **1996**, *61*, 534-538.

(35) Cer, R. Z.; Mudunuri, U.; Stephens, R.; Lebeda, F. J. IC50-to-Ki: a web-based tool for converting IC50 to Ki values for inhibitors of enzyme activity and ligand binding. *Nucleic Acids Research*, **2009**, *37*, W441-W445.

(36) Lynch, B. A.; Loiacono, K. A.; Tiong, C. L.; Adams, S. E.; MacNeil, I. A. A Fluorescence Polarization Based Src-SH2 Binding Assay. *Anal. Biochem.* **1997**, 247, 77-82.

(37) Wu, P.; Brasseur, M.; Schindler, U. A High-Throughput STAT Binding Assay Using Fluorescence Polarization *Anal. Biochem*. **1997**, 249, 29-36.

(38) Huang, X. Fluorescence Polarization Competition Assay: The Range of Resolvable Inhibitor Potency Is Limited by the Affinity of the Fluorescent Ligand *J. Biomol. Screen.* **2003**, 8, 34-38.

(39) Cooper, A. *Biophysical Chemistry, 2nd Edition.* RSC Publishing. Cambridge UK. **2011**, pp. 122-123.

(40) Scharenberg, M.; Jiang, X.; Pang, L.; Navarra, G.; Rabbani, S.; Binder, F.; Schwardt, O.; Ernst, B. Kinetic properties of carbohydrate-lectin interactions: FimH antagonists. *ChemMedChem* **2014**, *9*, 78-83.

(41) Cabani, S.; Gianni, P.; Mollica, V.; Lepori, L. Group contribution to the thermodynamic properties of non-ionic solutes in dilute aqueous solution. *J. Solution Chem.* **1981**, *10*, 563-595.

(42) Hansch, C.; Leo, A.; Taft, R.W. A survey of Hammett substituent constants and resonance and field parameters. *Chem. Rev.* **1991**, *91*, 165-195.

(43) Chen, A.; Wadso, I. Simultaneous determination of delta G, delta H and delta S by an automatic microcalorimetric titration technique: application to protein ligand binding. *J Biochem Biophys Meth,* **1982**, *6*, 307-316.

(44) Freire, E.; Mayorga, O.L.; Straume, M. Isothermal titration calorimetry. *Anal Chem,* **1990**, *62*, 950A-959A.

(45) Wiseman, T.; Williston, S.; Brandts, J. F.; Lin, L.-N. Rapid measurement of binding constants and heats of binding using a new titration calorimeter. *Anal. Biochem.* **1989**, *179*, 131-137.

(46) Turnbull, W. B.; Daranas A.H. On the value of c: can low affinity systems be studied by isothermal titration calorimetry? *J. Am. Chem. Soc.* **2003**, *125*, 14859-14866.

(47) Sigurskjold B. W. Exact analysis of competition ligand binding by displacement isothermal titration calorimetry. *Anal. Biochem.* **2000**, *277*, 260-266.

(48) Velazquez-Campoy A.; Freire E. Isothermal titration calorimetry to determine association constants for high-affinity ligands. *Nat. Protoc.* **2006**, *1*, 186-191.

(49) Dearden, J. C.; Bresnen, G. M. The measurement of partition coefficients. *QSAR Comb. Sci.* **1988**, *7*, 133-144.

(50) Kansy, M.; Senner, F.; Gubernator, K. Physicochemical high throughput screening: parallel artificial membrane permeation assay in the description of passive absorption processes. *J. Med. Chem.* **1998**, *41*, 1007-1010.

(51) Hubatsch, I.; Ragnarsson, E. G. E.; Artursson, P. Determination of drug permeability and predicition of drug absorption in Caco-2 monolayers. *Nat. Protoc.* **2007**, *2*, 2111-2119.

(52) Banker, M. J.; Clark, T. H.; Williams, J. A. Development and validation of a 96-well equilibrium dialysis apparatus for measuring plasma protein binding. *J. Pharm. Sci.* **2003**, *92*, 967-974.

(53) Obach, R. S. Prediction of human clearance of twenty-nine drugs from hepatic microsomal intrinsic clearance data: an examination of in vitro half-life approach and nonspecific binding to microsomes. *Drug Metab. Dispos.* **1999**, *27*, 1350-1359.

(54) Chaturvedi, P. R.; Decker, C. J.; Odinecs, A. Prediction of pharmacokinetic properties using experimental approaches during early drug discovery. *Curr. Opin. Chem. Biol.* **2001**, *5*, 452-463.

(55) Di, L.; Kerns, E. H. Profiling drug-like properties in discovery research. *Curr. Opin. Chem. Biol.* **2003**, *7*, 402-408.

(56) Lipinski, C. A. Drug-like properties and the causes of poor solubility and poor permeability. *J. Pharmacol. Toxicol. Methods* **2000**, *44*, 235-249.

(57) Ishikawa, M.; Hashimoto, Y. Improvement in aqueous solubility in small molecule drug discovery programs by disruption of molecular planarity and symmetry. *J. Med. Chem.* **2011**, *54*, 1539-1554.

(58) Avdeef, A.; Bendels, S.; Di, L.; Faller, B.; Kansy, M.; Sugano, K.; Yamauchi, Y. PAMPA – critical factors for better predictions of absorption. *J. Pharm. Sci.* **2007**, *96*, 2893-2909.

(59) Artursson, P.; Karlsson, J. Correlation between oral drug absorption in humans and apparent drug permeability coefficients in human intestinal

epithelial (Caco-2) cells. *Biochem. Biophys. Res. Commun.* **1991**, *175*, 880-885.

(60) Feng, B.; LaPerle, J. L.; Chang, G.; Varma, M. V. S. Renal clearance in drug discovery and development: molecular descriptors, drug transporters and disease state. *Expert Opin. Drug. Metab. Toxicol.* **2010**, *6*, 939-952.

(61) Schmidt, S.; Gonzalez, D.; Derendorf, H. Significance of protein binding in pharmacokinetics and pharmacodynamics. *J. Pharm. Sci.* **2010**, *99*, 1107-1122.

(62) Weisiger, R. A. Dissociation from albumin: A potentially rate-limiting step in the clearance of substances by the liver. *Proc. Natl. Acad. Sci. USA* **1985**, *82*, 1563-1567.

(63) Smith, D. A.; Jones, B. C.; Walker, D. K. Design of drugs involving the concepts and theories of drug metabolism and pharmacokinetics. *Med. Res. Rev.* **1996**, *16*, 243-266.

(64) Van de Waterbeemd, H.; Smith, D. A.; Beaumont, K.; Walker, D. K. Property-based design: optimization of drug absorption and pharmacokinetics. *J. Med. Chem.* **2001**, *44*, 1313-1333.

(65) Varma, M. V. S.; Feng, B.; Obach, R. S.; Troutman, M. D.; Chupka, J.; Miller, H. R.; El-Kattan, A. Physicochemical determinants of human renal clearance. *J. Med. Chem.* **2009**, *52*, 4844-4852.

(66) Waring, M. J. Lipophilicity in drug discovery. *Expert Opin. Drug Discov.* **2010**, *5*, 235-248.

(67) Zhang Y.; Huo M.; Solver, P.K. An Add-in program for pharmacokinetic and pharmacodynamic data analysis in Microsoft Excel, *Computer Methods and Programs in Biomedicine* **2010**, *99*, 306-314.

(68) Scharenberg, M.; Abgottspon, D.; Cicek, E.; Jiang, X.; Schwardt, O.; Rabbani, S.; Ernst, B. Cytometry-Based Assay for Screening FimH Antagonists. *Assay and Drug Development Technologies* **2011**, *9*, 455-464.

(69) Hooton, T. M. Fluoroquinolones and resistance in the treatment of uncomplicated urinary tract infection. *Int. J. Antimicrob. Agents* **2003**, *22*, 65-72.

(70) Jakobsen, L.; Cattoir, V.; Hammerum, A. M.; Nordmann, P.; Frimodt-Møller N.; Impact of low-level fluoroquinolone resistance genes qnrA1, qnrB19, and qnrS1 on ciprofloxacin treatment of *Escherichia coli* urinary tract infection in murine model. Poster presented at ICAAC 2010. 50th Interscience Conference on Antimicrobial Agents and Chemotharapy, 2010, Sep 12–15, Boston, MA.

(71) Mulvey, M. A. Adhesion and entry of uropathogenic *Escherichia coli*. *Cell Microbiol.* **2002**, *4*, 257– 271.

(72) Ballatore, C.; Huryn, D. M.; Smith, A. B. Carboxylic acid (bio)isosteres in drug design. *ChemMedChem* **2013**, *8*, 385-395.

(73) Maestro, version 9.3, Schrödinger, LLC, New York, NY, 2012.

(74) MacroModel, version 9.9, Schrödinger, LLC, New York, NY, 2012.

(75) AMSOL, version 7.1, Hawkins, G. D.; Giesen, D. J.; Lynch, G. C.; Chambers, C. C.; Rossi, I.; Storer, J. W.; Li, J.; Thompson, J. D.; Winget, P.; Lynch, B. J.; Rinaldi, D.; Liotard, D. A.; Cramer, C. J.; Truhlar, D. G. University of Minnesota, Minneapolis, 2003; based in part on AMPAC, version 2.1, Liotard, D. A.; Healy, E. F.; Ruiz, J. M.; Dewar, M. J. S.

(76) Chambers, C. C.; Hawkins, G. D.; Cramer, C. J.; Truhlar, D. G. Model for aqueous solvation based on class IV atomic charges and first solvation shell effects. *J. Phys. Chem.* **1996**, *100*, 16385-16398.

(77) Dewar, M. J. S.; Zoebisch, E. G.; Healy, E. F.; Stewart, J. J. P. AM1 - A new general-purpose quantum-mechanical molecular-model (Vol. 107, PG 3902, 1985). *J. Am. Chem. Soc.* **1993**, *115*, 5348-5348.

(78) Mulvey, M. A.; Schilling, J. D.; Hultgren, S. J. Establishment of a persistent *Escherichia coli* reservoir during the acute phase of a bladder infection. *Infect. Immun.* **2001**, *69*, 4572-4579.

(79) Kabsch, W. Automatic Processing of Rotation Diffraction Data from Crystals of Initially Unknown Symmetry and Cell Constants. *J. Appl. Crystallogr.* **1993**, *26*, 795-800.

(80) Leslie, A. G. W. The integration of macromolecular diffraction data. *Acta Crystallogr. D* **2006**, *62*, 48-57.

(81) Winn, M. D.; Ballard, C. C.; Cowtan, K. D.; Dodson, E. J.; Emsley, P.; Evans, P. R.; Keegan, R. M.; Krissinel, E. B.; Leslie, A. G. W.; McCoy, A.; McNicholas, S. J.; Murshudov, G. N.; Pannu, N. S.; Potterton, E. A.; Powell, H. R.; Read, R. J.; Vagin, A.; Wilson, K. S. Overview of the CCP4 suite and current developments. *Acta Crystallogr. D* **2011**, *67*, 235-242.

(82) McCoy, A. J. Solving structures of protein complexes by molecular replacement with Phaser. *Acta Crystallogr. D* **2007**, *63*, 32-41.

(83) Emsley, P.; Cowtan, K. Coot: model-building tools for molecular graphics. *Acta Crystallogr D* **2004**, *60*, 2126-2132.

(84) Adams, P. D.; Grosse-Kunstleve, R. W.; Hung, L.-W.; Ioerger, T. R.; McCoy, A. J.;Moriarty, N. W.; Read, R. J.; Sacchettini, J. C.; Sauter, N. K.; Terwilliger, T. C. PHENIX: building new software for automated crystallographic structure determination. *Acta Crystallogr. D Biol. Crystallogr.* **2002**, *58***,** 1948–1954.

(85) van Aalten, D. M. F.; Bywater, R.; Findlay, J. B. C.; Hendlich, M.; Hooft, R. W. W.; Vriend, G. PRODRG, a program for generating molecular topologies and unique molecular descriptors from coordinates of small molecules. *J. Comput. Aided Mol. Des.* **1996**, *10*, 255-262.

(86) Chen, V. B.; Arendall, W. B.; Headd, J. J.; Keedy, D. A.; Immormino, R. M.; Kapral, G. J.; Murray, L. W.; Richardson, J. S.; Richardson, D. C. MolProbity: all-atom structure validation for macromolecular crystallography. *Acta Crystallogr. D* **2010,** *66*, 12-21.

(87) Bezençon, J.; Wittwer, M. B.; Cutting, B.; Smiesko, M.; Wagner, B.; Kansy, M.; Ernst, B. pK_a determination by ^{1}H NMR spectroscopy – an old methodology revisited. *J. Pharm. Biomed. Anal.* **2014**, in press; http://dx.doi.org/10.1016/j.jpba.2013.12.014.

(88) (a) VCCLAB, Virtual Computational Chemistry Laboratory, 2005, http://www.vcclab.org (accessed August 14, 2012); (b) Tetko, I. V.; Gasteiger, J.; Todeschini, R.; Mauri, A.; Livingstone, D.; Ertl, P.; Palyulin V. A.; Radchenko, E. V.; Zefirov, N. S.; Makarenko, A. S.; Tanchuk, V. Y.; Prokopenko, V. V. Virtual computational chemistry laboratory – design and description. *J. Comput. Aided Mol. Des.* **2005**, *19*, 453-463.

(89) Diehl K-H.; Hull R. A. Good Practice Guide to the Administration of Substances and Removal of Blood, Including Routes and Volumes. *J. Appl. Toxicol.* **2001**, *21*, 15-23.

Supporting Information

FimH Antagonists: Bioisosteres of a Carboxylate to Improve PK/PD Properties

Simon Kleeb,[a)] Lijuan Pang,[a)] Katharina Mayer,[a)] Deniz Eris,[a)] Anja Sigl,[a)] Roland C. Preston,[a)] Pascal Zihlmann,[a)] Timothy Sharpe,[c)] Roman P. Jakob,[b)] Daniela Abgottspon,[a)] Aline S. Hutter,[a)] Meike Scharenberg,[a)] Xiaohua Jiang,[a)] Giulio Navarra,[a)] Said Rabbani,[a)] Martin Smiesko,[a)] Nathalie Lüdin,[a)] Jacqueline Bezencon,[a)] Oliver Schwardt,[a)] Timm Maier,[b)] Beat Ernst [a)]*

[a)] Institute of Molecular Pharmacy, Pharmacenter, University of Basel, Klingelbergstrasse 50, CH-4056 Basel, Switzerland

[b)] Structural Biology, Biocenter, University of Basel, Klingelbergstrasse 70, CH-4056 Basel

[c)] Biophysical Facility, Biocenter, University of Basel, Klingelbergstrasse 70, CH-4056 Basel

* To whom correspondence should be addressed: Prof. Dr. Beat Ernst, Institute of Molecular Pharmacy, Pharmacenter, University of Basel, Klingelbergstrasse 50, CH-4056 Basel, Switzerland; Tel: +41 61 267 15 51, Fax: +41 61 267 15 52; E-mail: beat.ernst@unibas.ch

Contents

Synthesis

General methods. NMR spectra were recorded on a Bruker Avance DMX-500 (500.1 MHz) spectrometer. Assignment of ^{1}H and ^{13}C NMR spectra was achieved using 2D methods (COSY, HSQC, HMBC). Chemical shifts are expressed in ppm using residual $CHCl_3$, CHD_2OD or HDO as references. Optical rotations were measured using Perkin-Elmer Polarimeter 341. Electron spray ionization mass spectra (ESI-MS) were obtained on a Waters micromass ZQ. The LC/HRMS analysis were carried out using a Agilent 1100 LC equipped with a photodiode array detector and a Micromass QTOF I equipped with a 4 GHz digital-time converter. Microwave-assisted reactions were carried out with a CEM Discover and Explorer. Reactions were monitored by TLC using glass plates coated with silica gel 60 F_{254} (Merck) and visualized by using UV light and/or by charring with a molybdate solution (a 0.02 M solution of ammonium cerium sulfate dihydrate and ammonium molybdate tetrahydrate in aqueous 10% H_2SO_4). MPLC separations were carried out on a CombiFlash Companion or Rf (Teledyne Isco) equipped with RediSep normal-phase or RP-18 reversed-phase flash columns. LC-MS separations were done on a Waters system equipped with sample manager 2767, pump 2525, PDA 2525 and micromass ZQ. All compounds used for biological assays are at least of 95% purity based on HPLC analytical results. Commercially available reagents were purchased from Fluka, Aldrich, Alfa Aesar or abcr GmbH & Co. KG (Germany). Solvents were purchased from Sigma-Aldrich or Acros and were dried prior to use where indicated. Methanol (MeOH) was dried by refluxing with sodium methoxide and distilled immediately before use. Dimethoxyethane (DME) was dried by filtration over Al_2O_3 (Fluka, type 5016 A basic).

General procedure A for palladium-catalyzed Miyaura-Suzuki coupling. A Schlenk tube was charged with aryl iodide **12**[S1] (1.0 eq), boronic acid or boronate **13a-f** (1.1 eq), $Pd(dppf)Cl_2 \cdot CH_2Cl_2$ (0.03 eq), K_3PO_4 (1.5 eq) and a stirring bar. The tube was closed with a rubber septum and was evacuated and flushed with argon. This procedure was repeated once, and then anhydrous DMF (2 mL) was added under a stream of argon. The mixture was degassed in an ultrasonic bath and flushed with argon for 5 min, and then stirred at 80°C overnight. The reaction mixture was cooled to rt, diluted with EtOAc (50 mL), and washed with water (50 mL) and brine (50 mL). The organic layer was dried over Na_2SO_4 and concentrated in vacuo.

The residue was purified by MPLC on silica gel (petroleum ether/EtOAc) to afford **14a-f**.

General procedure B for deacetylation. To a solution of **14a-f** (1.0 eq) in dry MeOH (5 mL) was added freshly prepared 1 M NaOMe/MeOH (0.1 eq) under argon. The mixture was stirred at rt until the reaction was complete (monitored by TLC), then neutralized with Amberlyst-15 (H^+) ion-exchange resin, filtered and concentrated in vacuo. The residue was purified by MPLC on silica gel (DCM/MeOH, 10:1-7:1) to afford **11a-f** as white solids.

4'-(2,3,4,6-Tetra-*O*-acetyl-α-D-mannopyranosyloxy)-biphenyl-4-carboxamide (14a). Prepared according to general procedure A from **12** (150 mg, 0.27 mmol), (4-carbamoylphenyl)boronic acid (**13a**, 49 mg, 0.30 mmol), $Pd(dppf)Cl_2 \cdot CH_2Cl_2$ (6.6 mg, 0.008 mmol) and K_3PO_4 (86 mg, 0.41 mmol). Yield: 108 mg (73%) as yellow oil. $[\alpha]_D^{20}$ +70.7 (*c* 0.6, EtOAc); ^{1}H NMR (500 MHz, $CDCl_3$): δ = 7.89-7.87 (m, 2H, Ar-H), 7.63-7.62 (m, 2H, Ar-H), 7.57-7.55 (m, 2H, Ar-H), 7.19-7.17 (m, 2H, Ar-H), 6.18 (br, 1H, NH), 5.85 (br, 1H, NH), 5.60-5.57 (m, 2H, H-1, H-3), 5.48 (dd, *J* = 1.8, 3.5 Hz, 1H, H-2), 5.40 (t, *J* = 10.1 Hz, 1H, H-4), 4.30 (dd, *J* = 5.3, 12.4 Hz, 1H, H-6a), 4.17-4.03 (m, 2H, H-5, H-6b), 2.22, 2.07, 2.05, 2.04 (4 s, 12H, 4 $COCH_3$); ^{13}C NMR (126 MHz, $CDCl_3$): δ = 170.68, 170.17, 170.14, 169.88, 169.12 (5 CO), 155.77, 144.07, 134.85, 131.83, 128.58, 128.10, 127.04, 117.02 (Ar-C), 95.89 (C-1), 69.47 (C-5), 69.38 (C-2), 68.96 (C-3), 66.00 (C-4), 62.20 (C-6), 21.03, 20.86, 20.84, 20.83 (4 CO*C*H_3); ESI-MS: *m/z*: Calcd for $C_{27}H_{29}NNaO_{11}$ $[M+Na]^+$: 566.2, found: 566.2.

4'-(2,3,4,6-Tetra-*O*-acetyl-α-D-mannopyranosyloxy)-*N*-methyl-biphenyl-4-carboxamide (14b). Prepared according to general procedure A from **12** (50 mg, 0.09 mmol), (4-(methylcarbamoyl)phenyl)boronic acid (**13b**, 18 mg, 0.10 mmol), $Pd(dppf)Cl_2 \cdot CH_2Cl_2$ (3 mg, 0.003 mmol) and K_3PO_4 (29 mg, 0.14 mmol). Yield: 32 mg (63%) as colorless oil. $[\alpha]_D^{20}$ +76.1 (*c* 0.6, EtOAc); ^{1}H NMR (500 MHz, $CDCl_3$): δ = 7.83-7.81 (m, 2H, Ar-H), 7.60-7.53 (m, 4H, Ar-H), 7.17-7.15 (m, 2H, Ar-H), 6.30 (d, *J* = 4.8 Hz, 1H, NH), 5.58-5.56 (m, 2H, H-1, H-3), 5.46 (dd, *J* = 1.8, 3.4 Hz, 1H, H-2), 5.38 (t, *J* = 10.0 Hz, 1H, H-4), 4.28 (dd, *J* = 5.1, 12.1 Hz, 1H, H-6a), 4.12-4.06 (m, 2H, H-5, H-6b), 3.03 (d, *J* = 4.8 Hz, 3H, NHC*H*$_3$), 2.20, 2.05, 2.03, 2.02 (4 s, 12H, 4 $COCH_3$); ^{13}CNMR (126 MHz, $CDCl_3$): δ = 170.66, 170.14, 170.11, 169.86, 167.99 (5

CO), 155.65, 143.36, 134.97, 133.17, 128.51, 127.53, 126.96, 116.98 (Ar-C), 95.88 (C-1), 69.46 (C-5), 69.35 (C-2), 68.96 (C-3), 65.98 (C-4), 62.19 (C-6), 26.99 (NH*C*H_3), 21.02, 20.84, 20.82, 20.81 (4 CO*C*H_3); ESI-MS: *m/z*: Calcd for $C_{28}H_{32}NO_{11}$ $[M+H]^+$: 558.2, found: 558.3.

4'-(2,3,4,6-Tetra-*O*-acetyl-α-D-mannopyranosyloxy)-biphenyl-4-yl-(morpholino)-methanone (14c). Prepared according to general procedure A from **12** (110 mg, 0.20 mmol), pinacol 4-(morpholine-4-carbonyl)phenylboronate (**13c**, 70 mg, 0.22 mmol), Pd(dppf)Cl_2· CH_2Cl_2 (5 mg, 0.006 mmol) and K_3PO_4 (64 mg, 0.30 mmol). Yield: 139 mg (99%) as yellow oil. $[\alpha]_D^{20}$ +62.0 (*c* 0.4, MeOH); ^{1}H NMR (500 MHz, $CDCl_3$): δ = 7.60-7.47 (m, 6H, Ar-H), 7.19-7.17 (m, 2H, Ar-H), 5.60-5.58 (m, 2H, H-1, H-3), 5.47 (dd, *J* = 1.9, 3.4 Hz, 1H, H-2), 5.40 (t, *J* = 10.1 Hz, 1H, H-4), 4.30 (dd, *J* = 5.1, 12.2 Hz, 1H, H-6a), 4.14-4.08 (m, 2H, H-6b, H-5), 3.78-3.45 (m, 8H, 4 CH_2), 2.22, 2.09, 2.07, 2.04 (4 s, 12H, 4 $COCH_3$); ^{13}C NMR (126 MHz, $CDCl_3$): δ = 170.55, 170.26, 170.05, 170.01, 169.76 (5 CO), 155.50, 142.00, 135.03, 133.82, 128.36, 127.80, 126.94, 116.90 (Ar-C), 95.81 (C-1), 69.38 (C-5), 68.85 (C-2), 66.94 (C-3), 65.90 (C-4), 62.09 (C-6), 20.92, 20.74, 20.72, 20.71 (4 CO*C*H_3); ESI-MS: *m/z*: Calcd for $C_{31}H_{35}NNaO_{12}$ $[M+Na]^+$: 636.2, found: 636.3.

4'-(Methylsulfonyl)-biphenyl-4-yl 2,3,4,6-tetra-*O*-acetyl-α-D-mannopyranoside (14d). Prepared according to general procedure A from **12** (50 mg, 0.09 mmol), 4-(methylsulfonyl)-phenylboronic acid (**13d**, 20 mg, 0.10 mmol), Pd(dppf)Cl_2·CH_2Cl_2 (3 mg, 0.003 mmol) and K_3PO_4 (29 mg, 0.14 mmol). Yield: 23 mg (44%) as a yellow solid. $[\alpha]_D^{20}$ +78.3 (*c* 0.6, EtOAc); ^{1}H NMR (500 MHz, $CDCl_3$): δ = 8.00-7.99 (m, 2H, Ar-H), 7.74-7.72 (m, 2H, Ar-H), 7.59-7.56 (m, 2H, Ar-H), 7.23-7.18 (m, 2H, Ar-H), 5.60-5.56 (m, 2H, H-1, H-3), 5.47 (dd, *J* = 1.8, 3.4 Hz, 1H, H-2), 5.40 (t, *J* =10.0 Hz, 1H, H-4), 4.30 (dd, *J* = 4.9, 12.0 Hz, 1H, H-6a), 4.13-4.08 (m, 2H, H-5, H-6b), 3.10 (s, 3H, SO_2CH_3), 2.22, 2.07, 2.05, 2.04 (4 s, 12H, 4 $COCH_3$); ^{13}C NMR (126 MHz, $CDCl_3$): δ = 170.53, 170.05, 170.02, 169.73 (4 CO), 156.11, 145.82, 138.86, 133.89, 128.71, 128.00, 127.61, 117.05 (Ar-C), 95.77 (C-1), 69.32 (2C, C-2, C-5), 68.80 (C-3), 65.84 (C-4), 62.06 (C-6), 44.65 (SO_2*C*H_3), 20.91, 20.74, 20.72 (4C, 4 CO*C*H_3); ESI-MS: *m/z*: Calcd for $C_{27}H_{30}NaO_{12}S$ $[M+Na]^+$: 601.1, found: 601.1.

4'-(2,3,4,6-Tetra-*O*-acetyl-α-D-mannopyranosyloxy)-*N*-methyl-biphenyl-4-sulfonamide (14e). Prepared according to general procedure A from **12** (116 mg, 0.21 mmol), 4-(*N*-methylsulfamoyl)-phenylboronic acid (**13e**, 50 mg, 0.23 mmol), $Pd(dppf)Cl_2 \cdot CH_2Cl_2$ (5 mg, 0.006 mmol) and K_3PO_4 (67 mg, 0.32 mmol). Yield: 105 mg (84%) as a white solid. $[\alpha]_D^{20}$ +56.4 (*c* 0.5, MeOH); ^{1}H NMR (500 MHz, $CDCl_3$): δ = 7.92-7.90 (m, 2H, Ar-H), 7.70-7.68 (m, 2H, Ar-H), 7.57-7.55 (m, 2H, Ar-H), 7.21-7.19 (m, 2H, Ar-H), 5.60-5.57 (m, 2H, H-1, H-3), 5.48 (dd, *J* = 1.8, 3.4 Hz, 1H, H-2), 5.40 (t, *J* =10.0 Hz, 1H, H-4), 4.38 (dd, *J* = 5.4, 10.8 Hz, 1H, NH), 4.30 (dd, *J* = 4.9, 12.3 Hz, 1H, H-6a), 4.13-4.08 (m, 2H, H-5, H-6b), 2.72 (d, *J* = 5.4 Hz, 3H, NCH_3), 2.22, 2.07, 2.05, 2.04 (4 s, 12H, 4 $COCH_3$); ^{13}C NMR (126 MHz, $CDCl_3$): δ = 170.55, 170.06, 170.03, 169.75 (4 CO), 155.97, 144.81, 137.16, 134.09, 128.62, 127.85, 127.39, 117.01 (Ar-C), 95.78 (C-1), 69.34 (C-5), 69.31 (C-2), 68.81 (C-3), 65.86 (C-4), 62.07 (C-6), 29.44 (NH*C*H_3), 20.92, 20.74, 20.72 (4C, 4 CO*C*H_3); ESI-MS: *m/z*: Calcd for $C_{27}H_{31}NNaO_{12}S$ $[M+Na]^+$: 616.1, found: 616.1.

3',5'-Difluoro-4'-hydroxy-biphenyl-4-yl 2,3,4,6-tetra-*O*-acetyl-α-D-mannopyranoside (14f). Prepared according to general procedure A from **12** (100 mg, 0.18 mmol), pinacol (3,5-difluoro-4-hydroxyphenyl)boronate (**13f**, 51 mg, 0.20 mmol), $Pd(dppf)Cl_2 \cdot CH_2Cl_2$ (5 mg, 0.006 mmol) and K_3PO_4 (57 mg, 0.27 mmol). Yield: 57 mg (52%) as colorless oil. $[\alpha]_D^{20}$ +64.9 (*c* 0.7, MeOH); ^{1}H NMR (500 MHz, $CDCl_3$): δ = 7.44-7.38 (m, 2H, Ar-H), 7.15-7.11 (m, 2H, Ar-H), 7.10-7.02 (m, 2H, Ar-H), 5.90 (bs, 1H, OH), 5.59 (dd, *J* = 3.6, 10.1 Hz, 1H, H-3), 5.56 (d, *J* = 1.8 Hz, 1H, H-1), 5.47 (dd, *J* = 1.8, 3.5 Hz, 1H, H-2), 5.40 (t, *J* = 10.1 Hz, 1H, H-4), 4.30 (dd, *J* = 4.8, 12.0 Hz, 1H, H-6a), 4.14-4.08 (m, 2H, H-6b, H-5), 2.22, 2.07, 2.06, 2.05 (4 s, 12H, 4 $COCH_3$); ^{13}C NMR (126 MHz, $CDCl_3$): δ = 170.83, 170.31, 170.25, 169.99 (4 CO), 155.43 (Ar-C), 152.19 (d, *J* = 241.0 Hz, Ar-C), 152.14 (d, *J* = 241.0 Hz, Ar-C), 133.82 (Ar-C), 132.29 (d, *J* = 20.6 Hz, Ar-C), 127.93, 117.02 (Ar-C), 110.04 (d, *J* = 6.4 Hz, Ar-C), 109.91 (d, *J* = 6.4 Hz, Ar-C), 95.90 (C-1), 69.53 (C-5), 69.34 (C-2), 68.97 (C-3), 66.02 (C-4), 62.23 (C-6), 21.02, 20.85, 20.82, 20.81 (4 CO*C*H_3); ESI-MS: *m/z*: Calcd for $C_{26}H_{26}F_2NaO_{11}$ $[M+Na]^+$: 575.1, found: 575.2.

4'-(α-D-Mannopyranosyloxy)-biphenyl-4-carboxamide (11a). Prepared according to general procedure B from **14a** (30 mg, 0.05 mmol). Yield: 6 mg (29%) as a white solid. $[\alpha]_D^{20}$ +133.0 (*c* 0.3, dioxane/H_2O, 2:1); ^{1}H NMR (500 MHz, DMSO-d_6): δ =

7.98-7.94 (m, 2H, Ar-H), 7.72-7.70 (m, 2H, Ar-H), 7.67-7.64 (m, 2H, Ar-H), 7.27-7.23 (m, 2H, Ar-H), 5.57 (d, *J* = 1.6 Hz, 1H, H-1), 4.05 (dd, *J* = 1.8, 3.4 Hz, 1H, H-2), 3.95 (dd, *J* = 3.4, 9.4 Hz, 1H, H-3), 3.85-3.70 (m, 3H, H-4, H-6a, H-6b), 3.64 (m, 1H, H-5); ^{13}C NMR (126 MHz, DMSO-d_6): δ = 167.80 (CO), 156.39, 142.33, 132.78, 132.36, 128.13, 127.96, 125.93, 117.16 (Ar-C), 98.73 (C-1), 74.89 (C-5), 70.59 (C-3), 70.00 (C-2), 66.62 (C-4), 60.96 (C-6); HRMS: *m/z*: Calcd for $C_{19}H_{22}NO_7$ $[M+H]^+$: 376.1391, found: 376.1394.

4'-(α-D-Mannopyranosyloxy)-*N*-methyl-biphenyl-4-carboxamide (11b). Prepared according to general procedure B from **14b** (30 mg, 0.05 mmol). Yield: 13 mg (62%) as a white solid. $[\alpha]_D^{20}$ +117.0 (*c* 0.3, MeOH/H_2O, 5:1); ^{1}H NMR (500 MHz, CD_3OD): δ = 7.85-7.83 (m, 2H, Ar-H), 7.66-7.64 (m, 2H, Ar-H), 7.61-7.58 (m, 2H, Ar-H), 7.21-7.19 (m, 2H, Ar-H), 5.52 (d, *J* = 1.5 Hz, 1H, H-1), 4.00 (dd, *J* = 1.9, 3.4 Hz, 1H, H-2), 3.90 (dd, *J* = 3.4, 9.5 Hz, 1H, H-3), 3.75-3.69 (m, 3H, H-4, H-6a, H-6b), 3.59 (ddd, *J* = 2.4, 5.1, 9.7 Hz, 1H, H-5), 2.91 (s, 3H, NHC*H*$_3$); ^{13}C NMR (126 MHz, CD_3OD): δ = 170.51 (CO), 158.04, 145.09, 135.28, 133.78, 129.29, 128.80, 127.64, 118.20 (Ar-C), 100.13 (C-1), 75.49 (C-5), 72.41 (C-2), 71.98 (C-3), 68.32 (C-4), 62.67 (C-6), 26.94 (NH*C*H$_3$); HRMS: *m/z*: Calcd for $C_{20}H_{24}NO_7$ $[M+H]^+$: 390.1547, found: 390.1551.

4'-(α-D-Mannopyranosyloxy)-biphenyl-4-yl-(morpholino)methanone (11c). Prepared according to general procedure B from **14c** (50 mg, 0.08 mmol). Yield: 27 mg (75%) as a white solid. $[\alpha]_D^{20}$ +96.5 (*c* 0.4, MeOH); ^{1}H NMR (500 MHz, CD_3OD): δ = 7.71-7.70 (m, 2H, Ar-H), 7.63-7.63 (m, 2H, Ar-H), 7.52-7.50 (m, 2H, Ar-H), 7.25-7.23 (m, 2H, Ar-H), 5.56 (d, *J* = 1.7 Hz, 1H, H-1), 4.05 (dd, *J* = 1.8, 3.4 Hz, 1H, H-2), 3.95 (dd, *J* = 3.5, 9.5 Hz, 1H, H-3), 3.78-3.54 (m, 12H, H-4, H-5, H-6a, H-6b, 4 CH_2); ^{13}C NMR (126 MHz, CD_3OD): δ = 172.29 (CO), 158.00, 143.86, 135.30, 134.66, 129.25, 128.90, 127.85, 118.23 (Ar-C), 100.14 (C-1), 75.50 (C-5), 72.42 (C-3), 71.99 (C-2), 68.33, 62.69 (6C, C-4, C-6, 4 CH_2); HRMS: *m/z*: Calcd for $C_{23}H_{28}NO_8$ $[M+H]^+$: 446.1809, found: 446.1813.

4'-(Methylsulfonyl)-biphenyl-4-yl α-D-mannopyranoside (11d). Prepared according to general procedure B from **14d** (20 mg, 0.03 mmol). Yield: 12 mg (86%) as a white solid. $[\alpha]_D^{20}$ +105.8 (*c* 0.2, DCM/MeOH, 1:3); ^{1}H NMR (500 MHz, DMSO-d_6): δ = 7.90-7.88 (m, 2H, Ar), 7.76-7.74 (m, 2H, Ar), 7.58-7.56 (m, 2H, Ar-H), 7.17-

7.15 (m, 2H, Ar-H), 5.46 (d, *J* = 1.7 Hz, 1H, H-1), 3.93 (dd, *J* = 1.9, 3.5 Hz, 1H, H-2), 3.81 (dd, *J* = 3.4, 9.5 Hz, 1H, H-3), 3.69-3.61 (m, 3H, H-4, H-6a, H-6b), 3.50 (ddd, *J* = 2.5, 5.4, 9.7 Hz, 1H, H-5), 3.05 (SO_2CH_3); ^{13}C NMR (126 MHz, DMSO-d_6): δ = 156.95, 144.60, 138.94, 131.86, 128.36, 127.57, 126.98, 117.24 (Ar-C), 98.78 (C-1), 75.07 (C-5), 70.63 (C-3), 70.00 (C-2), 66.67 (C-4), 61.02 (C-6), 43.58 (SO_2CH_3); HRMS: *m/z*: Calcd for $C_{19}H_{22}NaO_8S$ $[M+Na]^+$: 433.0928, found: 433.0928.

4'-(α-D-Mannopyranosyloxy)-*N*-methyl-biphenyl-4-sulfonamide (11e). Prepared according to general procedure B from **14e** (40 mg, 0.07 mmol). Yield: 22 mg (76%) as a white solid. $[\alpha]_D^{20}$ +105.7 (*c* 0.3, MeOH); ^{1}H NMR (500 MHz, CD_3OD): δ = 7.90-7.88 (m, 2H, Ar-H), 7.80-7.79 (m, 2H, Ar-H), 7.66-7.64 (m, 2H, Ar-H), 7.26-7.25 (m, 2H, Ar-H), 5.58 (d, *J* = 1.7 Hz, 1H, H-1), 4.06 (dd, *J* = 1.8, 3.3 Hz, 1H, H-2), 3.96 (dd, *J* = 3.4, 9.5 Hz, 1H, H-3), 3.79-3.74 (m, 3H, H-4, H-6a, H-6b), 3.63 (ddd, *J* = 2.5, 5.2, 9.7 Hz, 1H, H-5), 2.57 (s, 3H, NHC*H*$_3$); ^{13}C-NMR (126 MHz, CD_3OD): δ = 158.34, 146.13, 138.67, 134.55, 129.53, 128.82, 128.21, 118.29 (Ar-C), 100.09 (C-1), 75.53 (C-5), 72.42 (C-3), 71.96 (C-2), 68.32 (C-4), 62.68 (C-6), 29.31 ($NHCH_3$); HRMS: *m/z*: Calcd for $C_{19}H_{23}NNaO_8S$ $[M+Na]^+$: 448.1037, found: 448.1038.

3',5'-Difluoro-4'-hydroxy-biphenyl-4-yl α-D-mannopyranoside (11f). Prepared according to general procedure B from **14f** (40 mg, 0.07 mmol). Yield: 21 mg (78%) as a white solid. $[\alpha]_D^{20}$ +117.6 (*c* 0.4, MeOH); ^{1}H NMR (500 MHz, CD_3OD): δ = 7.52-7.49 (m, 2H, Ar-H), 7.19-7.14 (m, 4H, Ar-H), 5.54 (d, *J* = 1.7 Hz, 1H, H-1), 4.04 (dd, *J* = 1.8, 3.4 Hz, 1H, H-2), 3.94 (dd, *J* = 3.5, 9.5 Hz, 1H, H-3), 3.78-3.73 (m, 3H, H-4, H-6a, H-6b), 3.63 (ddd, *J* = 2.5, 5.1, 9.8 Hz, 1H, H-5); ^{13}C NMR (126 MHz, CD_3OD): δ = 157.56 (Ar-C), 154.26 (d, *J* = 240.0 Hz, Ar-C), 154.21 (d, *J* = 240.0 Hz, Ar-C), 134.38 (t, *J* = 2.3 Hz, Ar-C), 132.92, 128.64, 118.16 (Ar-C), 110.59 (d, *J* = 6.6 Hz, Ar-C), 110.46 (d, *J* = 6.6 Hz, Ar-C), 100.15 (C-1), 75.44 (C-5), 72.42 (C-3), 71.99 (C-2), 68.32 (C-4), 62.66 (C-6); HRMS: *m/z*: Calcd for $C_{18}H_{18}F_2NaO_7$ $[M+Na]^+$: 407.0913, found: 407.0913.

4'-(2,3,4,6-Tetra-*O*-acetyl-α-D-mannopyranosyloxy)-biphenyl-4-carboxylic acid (16). To a solution of **6**[S2] (59 mg, 0.16 mmol) in pyridine (6 mL) was added acetic anhydride (2 mL) at 0°C under argon. The mixture was allowed to warm up to rt and stirred overnight. The mixture was concentrated and the residue was treated with

DCM/satd. aq. $NaHCO_3$ (1:1, 50 mL) for 1 h. The organic layer was washed subsequently with 1 N aq. HCl (25 mL) and water (25 mL), dried over Na_2SO_4 and concentrated in vacuo. The residue was purified by MPLC on silica gel (DCM/*i*PrOH, 15:1) to afford **16** (45 mg, 53%) as a white solid. $[\alpha]_D^{20}$ +71.9 (*c* 0.4, EtOAc); ^{1}H NMR (500 MHz, $CDCl_3$): δ = 8.25-8.15 (m, 2H, Ar-H), 7.70 - 7.63 (m, 2H, Ar-H), 7.60-7.55 (m, 2H, Ar-H), 7.20-7.17 (m, 2H, Ar-H), 5.64-5.55 (m, 2H, H-1, H-3), 5.49 (dd, *J* = 1.8, 3.4 Hz, 1H, H-2), 5.41 (t, *J* = 10.1 Hz, 1H, H-4), 4.31 (dd, *J* = 5.5, 12.5 Hz, 1H, H-6a), 4.10-4.08 (m, 2H, H-5, H-6b), 2.22, 2.07, 2.06, 2.05 (4s, 12H, 4 $COCH_3$); ^{13}C NMR (126 MHz, $CDCl_3$): δ = 171.72, 170.71, 170.16, 170.14, 169.90 (5 CO), 155.86, 145.61, 134.75, 130.87, 128.65, 128.49, 127.97, 127.18, 126.84, 122.22, 117.00 (Ar-C), 95.82 (C-1), 69.43 (C-5), 69.34 (C-2), 68.94 (C-3), 65.97 (C-4), 62.18 (C-6), 20.98, 20.80, 20.79, 20.77 (4 CO*C*H_3); ESI-MS: *m/z*: Calcd for $C_{27}H_{28}NaO_{12}$ $[M+Na]^+$: 567.1, found: 567.1.

***N*-Cyano-4'-(α-D-mannopyranosyloxy)-biphenyl-4-carboxamide (11i).** To a solution of **16** (40 mg, 0.07 mmol) in toluene was added 1-chloro-*N*,*N*-2-trimethyl-1-propenylamine (19 μL, 0.15 mmol) at 0 °C under argon. The mixture was allowed to warm up to rt in 4 h. Then the reaction mixture was concentrated and dried in vacuo overnight. The residue was dissolved in DMF (1 mL) and treated at 0 °C with a freshly prepared solution of NaNHCN in DMF [NH_2CN (6 mg, 0.15 mmol) and 60% NaH (6 mg, 0.15 mmol) in DMF (0.5 mL)]. The reaction mixture was stirred at rt overnight and then concentrated in vacuo. The residue was deacetylated according to general procedure B and the crude product was purified by MPLC (H_2O/MeOH, 1:1) on RP18 to afford **11i** (6 mg, 21% for three steps) as a white solid. $[\alpha]_D^{20}$ +44.7 (*c* 0.1, MeOH); ^{1}H NMR (500 MHz, CD_3OD): δ = 8.02-7.95 (m, 2H, Ar-H), 7.80-7.63 (m, 4H, Ar-H), 7.30-7.22 (m, 2H, Ar-H), 5.57 (s, 1H, H-1), 4.05 (s, 1H, H-2), 3.95 (dd, *J* = 3.2, 9.4 Hz, 1H, H-3), 3.84-3.71 (m, 3H, H-4, H-6a, H-6b), 3.66-3.62 (m, 1H, H-5); ^{13}C NMR (126 MHz, CD_3OD): δ = 158.37, 134.86, 130.09, 129.46, 127.82, 118.28 (Ar-C), 101.41 (CN), 100.16 (C-1), 75.54 (C-5), 72.44 (C-3), 71.98 (C-2), 68.37 (C-4), 62.71 (C-6); HRMS: *m/z*: Calcd for $C_{20}H_{20}N_2NaO_7$ $[M+Na]^+$: 423.1163, found: 423.1167.

2-Chloro-4-iodophenyl 2,3,4,6-tetra-*O*-acetyl-α-D-mannopyranoside (19). In a dry flask activated molecular sieves 4Å (300 mg), α-D-mannose pentaacetate (**17**,

390 mg, 0.77 mmol) and 2-chloro-4-iodophenol (**18**, 235 mg, 0.90 mmol) were dissolved in dry CH_2Cl_2 (3 mL) under argon. $BF_3 \cdot Et_2O$ (freshly distilled, 290 μL, 2.3 mmol) was added dropwise and the mixture was stirred for 20 h at 40 °C. After cooling to rt the mixture was diluted with CH_2Cl_2 (75 mL), filtered through celite and subsequently washed with satd. aq. $NaHCO_3$ (75 mL), water (75 mL) and brine (75 mL). The organic phase was dried over Na_2SO_4 and concentrated under reduced pressure. The crude product was purified via flash column chromatography (petroleum ether/EtOAc, 1:0 to 1:1) to yield **19** (345 mg, 76%). Spectroscopic data were in accordance with reported values.[S3]

Synthesis of *n*-heptyl 2-deoxy-α-D-mannopyranoside (24)

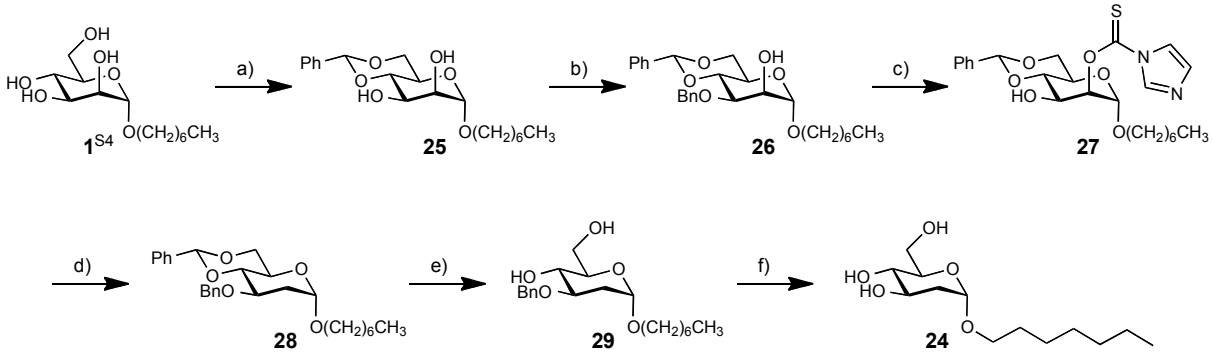

Scheme S1. a) $PhCH(OMe)_2$, *p*-TsOH, DMF, 50 °C, 5 h (94%); b) $Bu_2Sn(O)$, toluene, TBAB, BnBr, reflux (91%); c) TCDI, DCE, reflux (91%); d) Bu_3SnH, toluene, reflux, 6 h (58%); e) 80% aq. AcOH, 80 °C, 30 min (64%); f) H_2 (4 bar), cat. $Pd(OH)_2/C$, rt, (72%).

***n*-Heptyl 4,6-*O*-benzylidene-α-D-mannopyranoside (25).** To a solution of **1**[S4] (527 mg, 1.89 mmol) in dry DMF (6.0 mL) were added benzaldehyde dimethylacetal (0.56 mL) and *p*-TsOH (18 mg) at rt. The reaction mixture was stirred at 50 °C for 5 h, then diluted with DCM, washed with 5% aq. $NaHCO_3$ and brine. The organic layer was dried over Na_2SO_4 and concentrated. The residue was purified by flash chromatography on silica gel (petroleum ether/EtOAc, 3:1-3:2) to give **25** (650 mg, 94%) as a glassy solid. ^{1}H NMR (500 MHz, CD_3OD): δ = 7.51-7.49 (m, 2H Ar-H), 7.37-7.33 (m, 3H, Ar-H), 5.60 (s, 1H, C*H*Ph), 4.77 (d, *J* = 1.0 Hz, 1H, H-1), 4.18 (dd, *J* = 4.5, 10.0 Hz, 1H, H-6a), 3.95-3.90 (m, 2H, H-3, H-4), 3.88 (m, 1H, H-2), 3.81 (t, *J* = 10.0 Hz, 1H, H-6b), 3.76-3.41 (m, 2H, H-5, OCH_2), 3.46 (dt, *J* = 6.5, 9.5 Hz, 1H, OCH_2), 1.62 (m, 2H, CH_2), 1.36 (m, 8H, 4 CH_2), 0.91 (t, *J* = 7.0 Hz, 3H, CH_3); ^{13}C NMR (126 MHz; CD_3OD): δ = 139.31, 129.87, 129.02, 127.52 (Ar-C), 103.36 (*C*HPh), 102.59 (C-1), 80.20 (C-3), 72.74 (C-2), 69.87 (C-6), 69.61 (C-4), 68.77 (OCH_2), 65.25 (C-5), 33.01, 30.57, 30.17, 27.29, 23.70 (5 CH_2), 14.46 (CH_3); ESI-MS: *m/z*: Calcd for $C_{20}H_{30}NaO_6$ $[M+Na]^+$: 389.2, found: 389.1.

***n*-Heptyl 3-*O*-benzyl-4,6-*O*-benzylidene-α-D-mannopyranoside (26).** To a solution of **25** (152 mg, 0.414 mmol) in dry toluene (8 mL) was added dibutyltin oxide (112 mg, 0.456 mmol) at rt. The suspension was refluxed for 6 h and concentrated to dryness under reduced pressure. To a solution of the residue in dry toluene (8 mL) were added tetrabutylammonium bromide (TBAB) (147 mg, 0.456 mmol) and benzyl

bromide (59 μL, 0.5 mmol). The mixture was stirred at 95 °C overnight, concentrated to dryness, and purified by flash chromatography on silica gel (petroleum ether/EtOAc, 9:1-4:1) to give **26** (172 mg, 91%) as colorless oil. $[\alpha]_D^{20}$ +34.2 (*c* 1.43, MeOH); ^{1}H NMR (500 MHz, $CDCl_3$): δ = 7.51-7.49 (m, 2H, Ar-H), 7.40-7.33 (m, 8H, Ar-H), 5.62 (s, 1H, PhC*H*), 4.86 (m, 1H, H-1), 4.87 (d, *J* = 11.5 Hz, 1H, CH_2Ph), 4.73 (d, *J* = 11.5 Hz, 1H, CH_2Ph), 4.27 (m, 1H, H-6a), 4.14-4.06 (m, 2H, H-4, H-2), 3.94 (dd, *J* = 3.0, 9.5 Hz, 1H, H-3), 3.88-3.82 (m, 2H, H-5, H-6b), 3.67 (m, 1H, OCH_2), 3.41 (m, 1H, OCH_2), 2.64 (s, 1H, OH), 1.57 (m, 2H, CH_2), 1.29 (m, 8H, 4 CH_2), 0.89 (t, *J* = 7.0 Hz, 3H, CH_3); ^{13}C NMR (126 MHz, $CDCl_3$): δ = 138.05, 137.53, 128.90, 128.45, 128.22, 127.88, 127.77, 126.01 (Ar-C), 101.52 (*C*HPh), 99.87 (C-1), 78.93 (C-4), 75.79 (C-3), 73.04 (*C*H_2Ph), 70.10 (C-2), 68.92 (C-6), 67.97 (OCH_2), 63.19 (C-5), 32.75, 29.37, 29.05, 26.04, 22.61 (5 CH_2), 14.09 (CH_3); HRMS: *m/z*: Calcd for $C_{27}H_{36}NaO_6$ $[M+Na]^+$: 479.2410, found: 479.2414.

***n*-Heptyl 3-*O*-benzyl-4,6-*O*-benzylidene-2-*O*-(thiocarbonylimidazol-1-yl)-α-D-mannopyranoside (27).** A mixture of **26** (210 mg, 0.46 mmol) and *N*,*N*'-thiocarbonyldiimidazole (246 mg, 1.38 mmol) in DCE (5.0 mL) was refluxed overnight. The solution was concentrated in vacuo, the residue was diluted with DCM, and washed with 1 N aq. HCl and brine. The organic layer was dried over Na_2SO_4 and evaporated to dryness. The residue was purified by flash chromatography on silica gel (petroleum ether/EtOAc, 3:1-3:2) to afford **27** (238 mg, 91%) as yellow oil. $[\alpha]_D^{20}$ -9.8 (*c* 0.44, CH_2Cl_2); ^{1}H NMR (500 MHz, $CDCl_3$): δ = 8.39 (s, 1H, Ar-H), 7.67 (s, 1H, Ar-H), 7.51 (dd, *J* = 7.5, 2.5 Hz, 2H, Ar-H), 7.42-7.36 (m, 3H, Ar-H), 7.29-7.27 (m, 5H, Ar-H), 7.07 (d, *J* = 0.5 Hz, 1H, Ar-H), 5.90 (dd, *J* = 1.5, 3.5 Hz, 1H, H-2), 5.67 (s, 1H, C*H*Ph), 5.01 (d, *J* = 1.5 Hz, 1H, H-1), 4.73 (q, *J* = 12.0 Hz, 2H, CH_2Ph), 4.31 (dd, *J* = 4.5, 10.0 Hz, 1H, H-6a), 4.19 (dd, *J* = 3.5, 10.0 Hz, 1H, H-3), 4.04 (t, *J* = 10.0 Hz, 1H, H-4), 3.94 (td, *J* = 4.5, 10.0 Hz, 1H, H-5), 3.85 (t, *J* = 10.0 Hz, 1H, H-6b), 3.69 (dt, *J* = 6.5, 9.5 Hz, 1H, OCH_2), 3.46 (dt, *J* = 6.5, 9.5 Hz, 1H, OCH_2), 1.61 (m, 2H, CH_2), 1.31 (m, 8H, 4 CH_2), 0.90 (t, *J* = 7.0 Hz, 3H, CH_3); ^{13}C NMR (126 MHz, $CDCl_3$): δ = 183.59 (CS), 137.65, 137.17, 131.04, 129.05, 128.37, 128.24, 127.77, 127.57, 126.07, 109.96 (Ar-C), 101.75 (Ph*C*H), 97.24 (C-1), 79.24 (C-4), 78.80 (C-2), 73.91 (C-3), 72.87 (*C*H_2Ph), 68.80 (C-6), 68.54 (OCH_2), 63.68 (C-5), 31.73, 29.24, 29.00, 25.93, 22.60 (5 CH_2), 14.09 (CH_3); HRMS: *m/z*: Calcd for $C_{31}H_{38}N_2NaO_6S$ $[M+Na]^+$: 589.2348, found: 589.2351.

***n*-Heptyl 3-*O*-benzyl-4,6-*O*-benzylidene-2-deoxy-α-D-mannopyranoside (28).** A solution of **27** (238 mg, 0.419 mmol) in dry toluene (2 mL) was added dropwise over 10 min to a stirred solution of refluxing toluene (6 mL) and tributylstannane (0.169 mL, 0.63 mmol) under argon. The reaction mixture was refluxed for 6 h, then the solvent was removed in vacuo and the residue was purified by chromatography on silica gel (petroleum ether/EtOAc, 16:1-4:1) to afford **28** (107 mg, 58%) as colorless oil. $[\alpha]_D^{20}$ +49.9 (*c* 1.07, MeOH); ^{1}H NMR (500 MHz, $CDCl_3$): δ = 7.52 (dd, *J* = 7.5, 2.5 Hz, 1H, Ar-H), 7.41-7.25 (m, 9H, Ar-H), 5.63 (s, 1H, C*H*Ph), 4.90 (d, *J* = 3.5 Hz, 1H, H-1), 4.86 (d, *J* = 12.0 Hz, 1H, CH_2Ph), 4.69 (d, *J* = 12.0 Hz, 1H, CH_2Ph), 4.26 (dd, *J* = 4.5, 10.0 Hz, 1H, H-6a), 4.05 (ddd, *J* = 5.0, 9.0, 11.0 Hz, 1H, H-3), 3.83 (m, 1H, H-5), 3.77 (t, *J* = 10.0 Hz, 1H, H-6b), 3.70 (t, *J* = 9.0 Hz, 1H, H-4), 3.62 (dt, *J* = 6.5, 9.5 Hz, 1H, OCH_2), 3.35 (dt, *J* = 6.5, 9.5 Hz, 1H, OCH_2), 2.28 (ddd, *J* = 1.0, 5.0, 13.5 Hz, 1H, H-2e), 1.81 (ddd, *J* = 3.5, 11.5, 13.5 Hz, 1H, H-2a), 1.58 (m, 2H, CH_2), 1.30 (m, 8H, 4 CH_2), 0.89 (t, *J* = 7.0 Hz, 3H, CH_3); ^{13}C NMR (126 MHz, $CDCl_3$): δ = 138.76, 137.63, 128.84, 128.32, 128.21, 127.62, 127.49, 126.02 (Ar-C), 101.29 (*C*HPh), 97.93 (C-1), 83.99 (C-4), 73.12 (C-3), 72.97 (*C*H_2Ph), 69.16 (C-6), 67.65 (OCH_2), 62.89 (C-5), 36.58 (C-2), 31.75, 29.49, 29.08, 26.13, 22.61 (5 CH_2), 14.09 (CH_3); HRMS: *m/z*: Calcd for $C_{27}H_{36}NaO_5$ $[M+Na]^+$: 463.2460, found: 463.2453.

***n*-Heptyl 3-*O*-benzyl-2-deoxy-α-D-mannopyranoside (29).** A solution of **28** (66 mg, 0.15 mmol) in 80% aq. AcOH (1.25 mL) was stirred at 80 °C for 1 h and then concentrated to dryness. The residue was purified by chromatography on silica gel (petroleum ether/EtOAc, 4:1-3:2) to afford **29** (33.7 mg, 64%), which was directly used in the next step.

***n*-Heptyl 2-deoxy-α-D-mannopyranoside (24).** A suspension of **29** (30 mg, 0.085 mmol) and 10% $Pd(OH)_2$/C (5.2 mg) in MeOH (5.0 mL) was hydrogenated (4 bar H_2) in a Parr shaker at rt for 5 h. Then, the mixture was filtered through a pad of celite and the filtrate was concentrated in vacuo. The residue was purified by flash chromatography on silica gel (DCM/MeOH, 10:1) to give **24** (18 mg, 72%) as a white solid. $[\alpha]_D^{20}$ +106.1 (*c* 0.12, MeOH); ^{1}H NMR (500 MHz, CD_3OD): δ = 4.87 (d, *J* = 2.5 Hz, 1H, H-1), 3.85-3.79 (m, 2H, H-3, H-6a), 3.70-3.66 (m, 2H, H-6b, OCH_2), 3.52 (m, 1H, H-5), 3.33 (m, 1H, OCH_2), 3.23 (t, *J* = 9.5 Hz, 1H, H-4), 2.04 (dd, *J* = 5.0, 13.0

Hz, 1H, H-2a), 1.62-1.57 (m, 3H, H-2e, CH_2), 1.32 (m, 8H, 4 CH_2), 0.91 (t, J = 7.0 Hz, 3H, CH_3); ^{13}C NMR (125 MHz, CD_3OD): δ = 98.58 (C-1), 73.97 (C-5), 73.34 (C-4), 69.99 (C-3), 68.26 (OCH_2), 62.85 (C-6), 39.00 (C-2), 33.02, 30.70, 30.30, 27.40, 23.71 (5 CH_2), 14.43 (CH_3); HRMS: *m/z*: Calcd for $C_{13}H_{26}NaO_5$ $[M+Na]^+$: 285.1678, found: 285.1678.

HPLC data of the target compounds:

Method A: System: Beckman Coulter Gold, consisting of pump 126, DAD 168 (190-400 nm) and auto-sampler 508. Column: Waters Atlantis T3, 3 μm, 2.1 × 100 mm. A: H_2O + 0.1% TFA; B: MeCN + 0.1% TFA. Gradient: 0% B → 70% B (20 min); 70% B (2 min); 70% B → 5% B (3 min); 5% B → 0% B (2 min); flow rate: 0.5 mL/min.

Method B: System: Agilent 1100/1200 with UV detector (190-410 nm) and Waters 2420 ELSD. Column: Waters Atlantis T3, 3 μm, 2.1 × 100 mm. A: H_2O + 0.1% TFA; B: H_2O/MeCN (90:10) + 0.1% TFA. Detection: UV (214 nm) and light scattering (LS). ELSD parameters: Nebulizer control 70%, drift tube temperature 50°C, gas pressure 50 psi, gain 500. Gradient: 5% B (1 min), 5% B → 70% B (15 min), 70% B (1 min), 70% B → 5% B (3 min); flow rate: 0.5 mL/min.

Table S1. HPLC data of the target compounds.

Compound	Formula	Method	Retention [min]	Detection	Purity [%]
11a	$C_{19}H_{21}NO_7$	A	13.25	254 nm	> 99.5
11b	$C_{20}H_{23}NO_7$	A	15.10	254 nm	99.3
11c	$C_{23}H_{27}NO_8$	A	12.63	254 nm	98.6
11d	$C_{19}H_{22}O_8S$	A	15.78	254 nm	98.7
11e	$C_{19}H_{23}NO_8S$	A	13.17	285 nm	98.9
11f	$C_{18}H_{18}F_2O_7$	A	13.43	285 nm	> 99.5
11g	$C_{19}H_{19}NO_6$	B	10.68	LS	> 99.5
11h	$C_{19}H_{20}N_4O_6$	A	12.73	254 nm	> 99.5
11i	$C_{20}H_{20}N_2O_7$	A	14.73	296 nm	> 80[a)]
11j	$C_{19}H_{18}ClNO_6$	B	9.79	LS	> 99.5
21	$C_{39}H_{30}ClNO_{12}$	B	12.82	LS	93
22	$C_{42}H_{36}ClN_3O_{12}S$	B	9.89	LS	> 99.5
23	$C_{47}H_{46}ClN_3O_{14}S$	B	12.10	LS	> 99.5
24	$C_{13}H_{26}O_5$	B	15.12	LS	> 99.5

a) The minor peaks presumably stem from the possible tautomers of the cyanamide substituent.

HPLC traces of the target compounds:

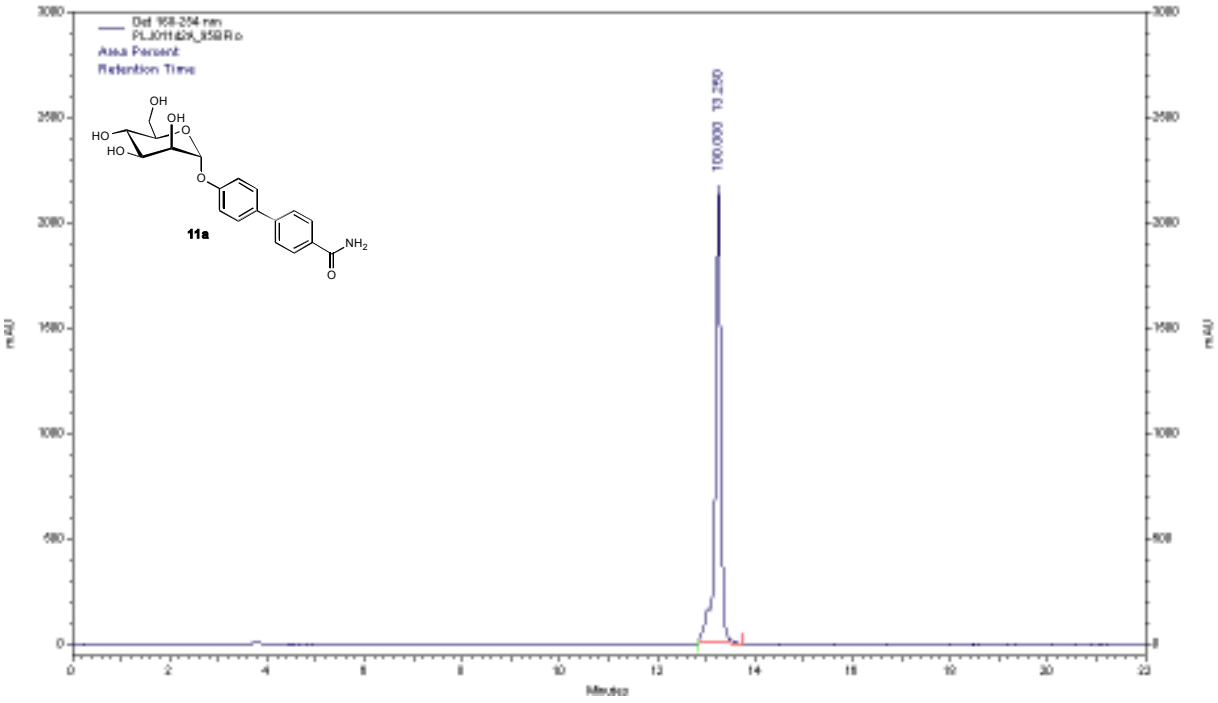

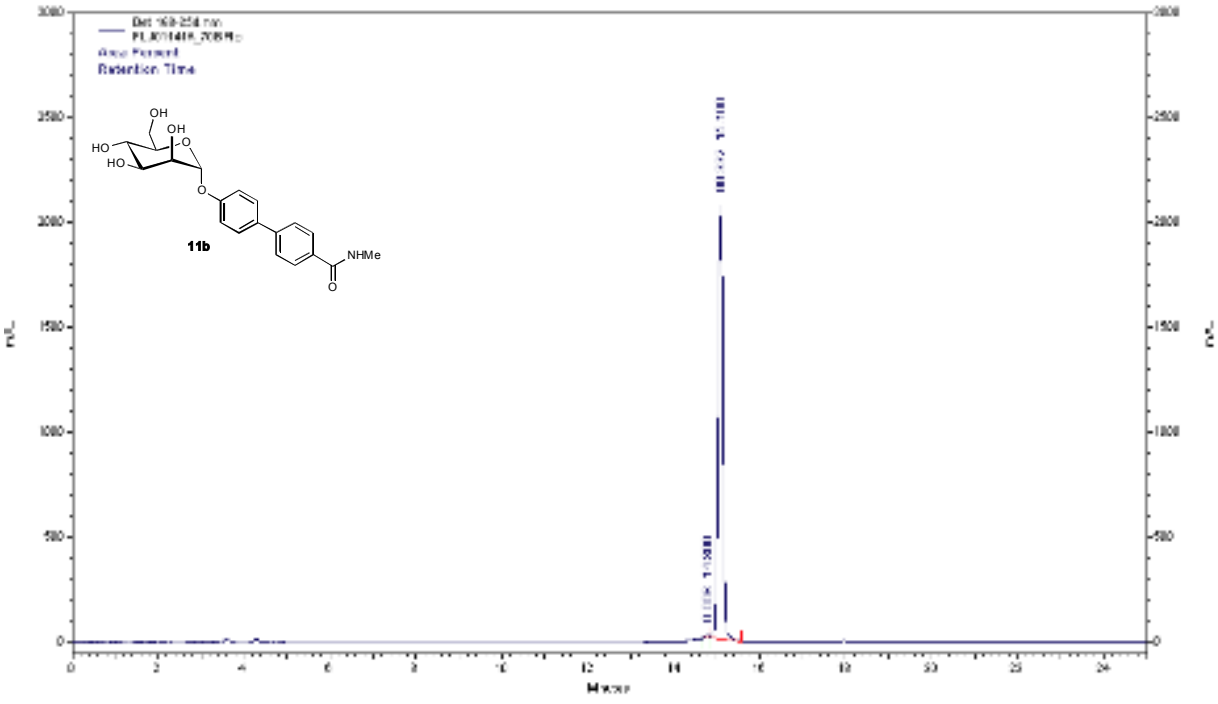

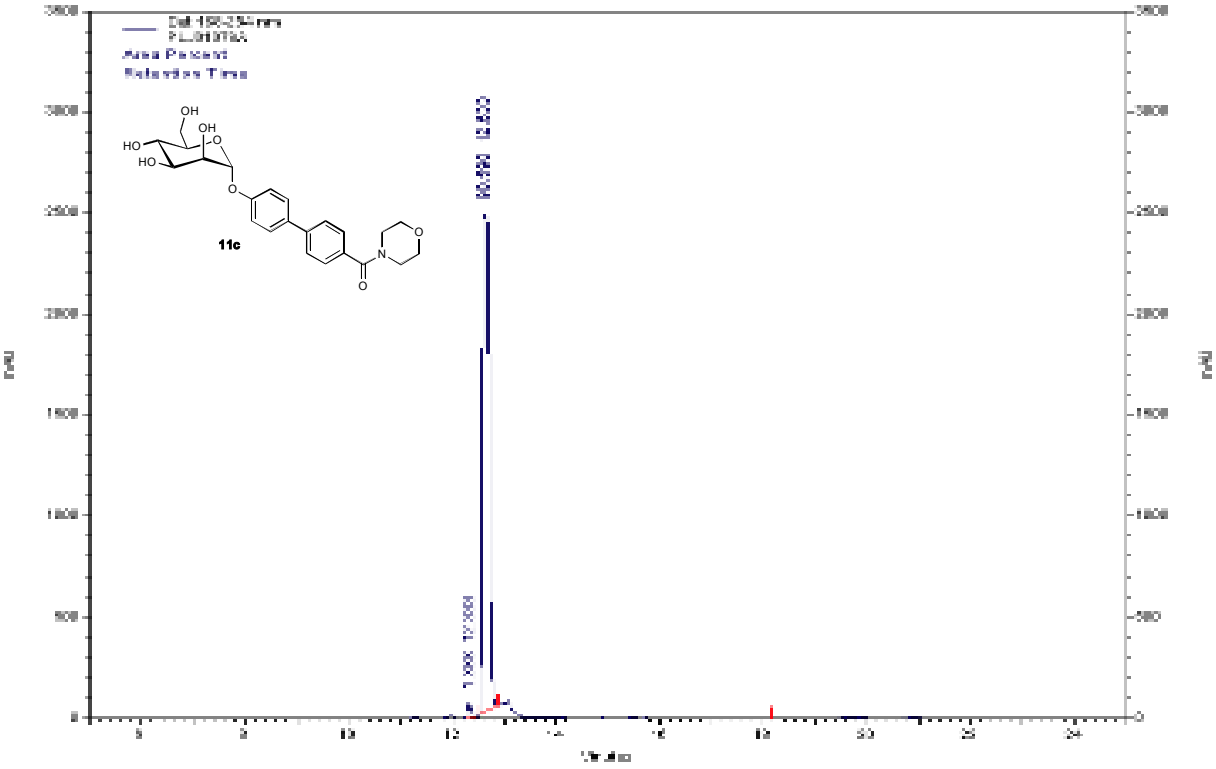
Area Percent
Retention Time
11c

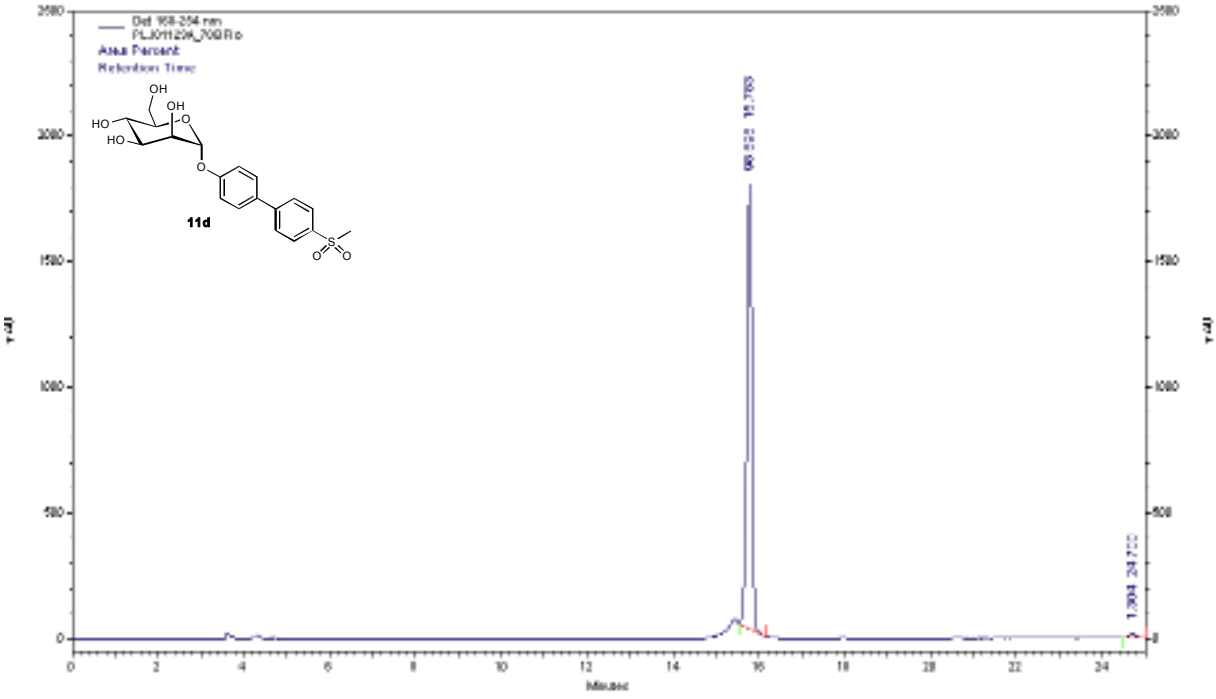
Area Percent
Retention Time
11d

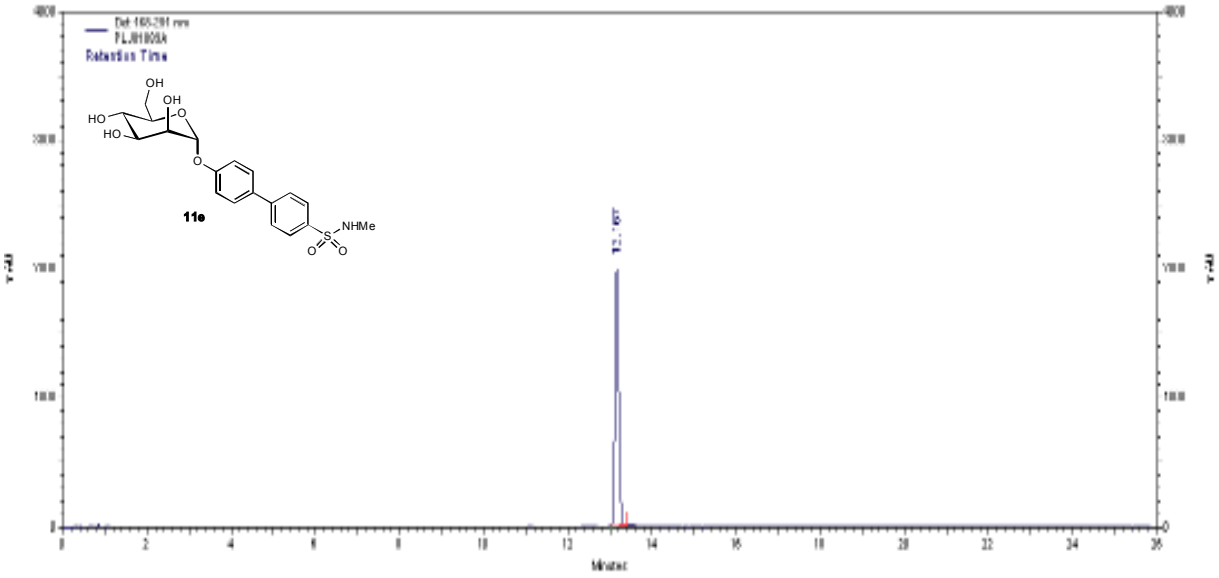
Retention Time
11e
NHMe
Minutes

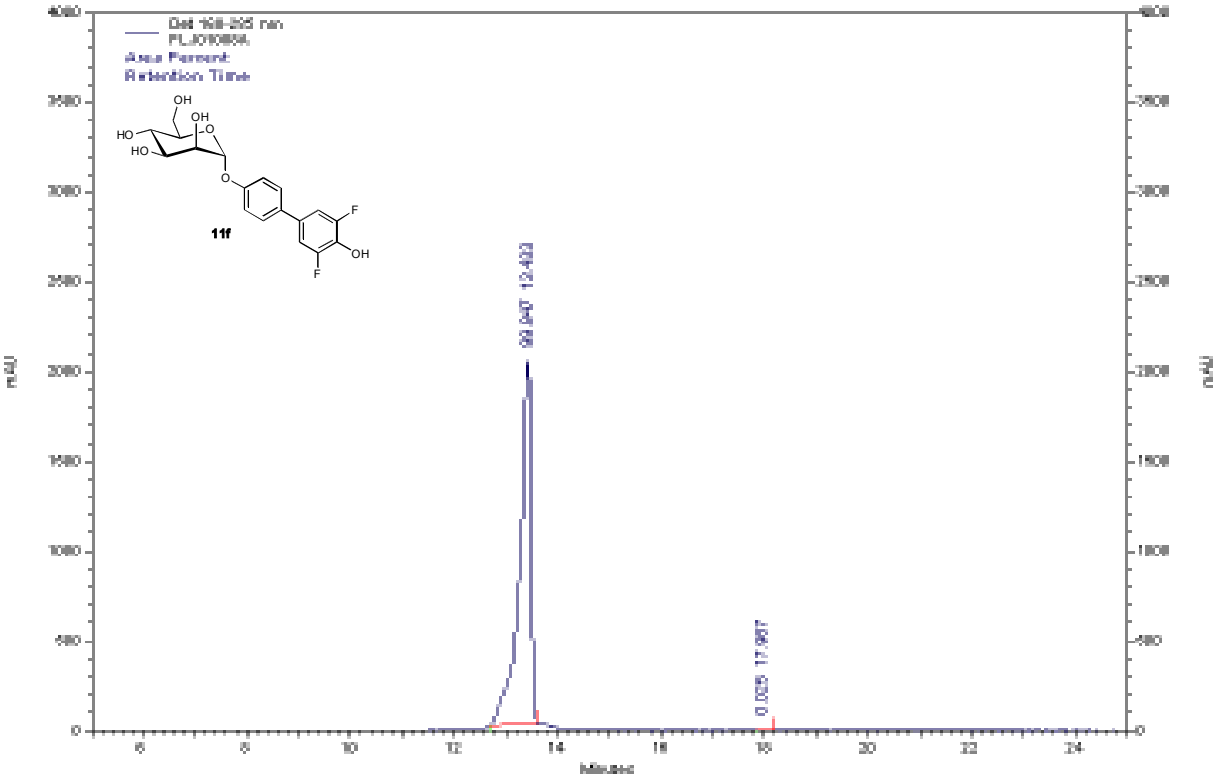
Area Percent
Retention Time
11f
F
OH
F
99.845 12.433
0.025 17.967
mAU
Minutes

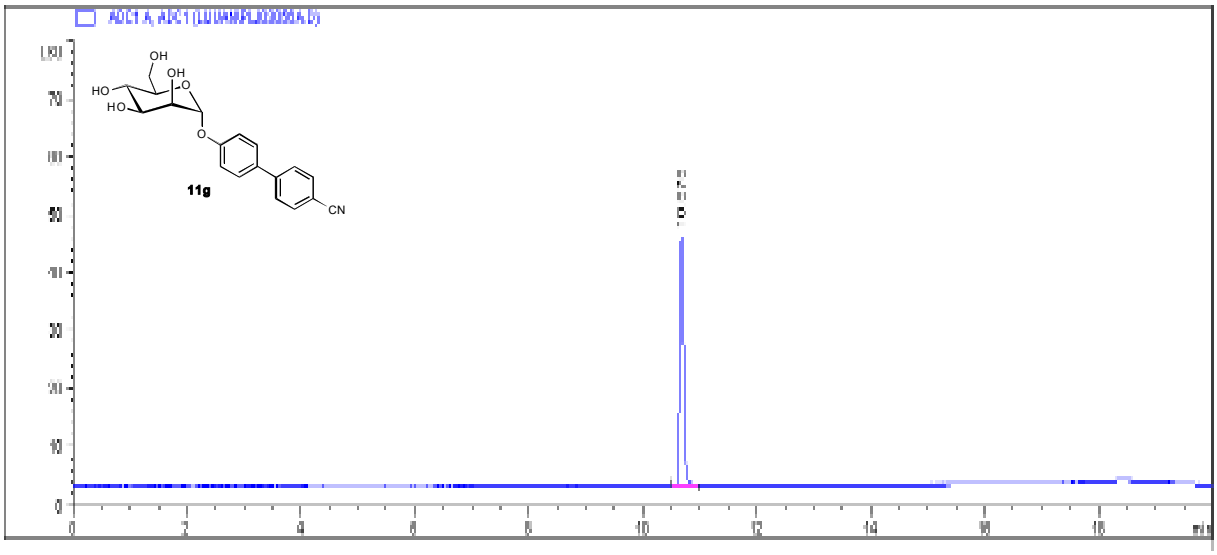
11g
CN

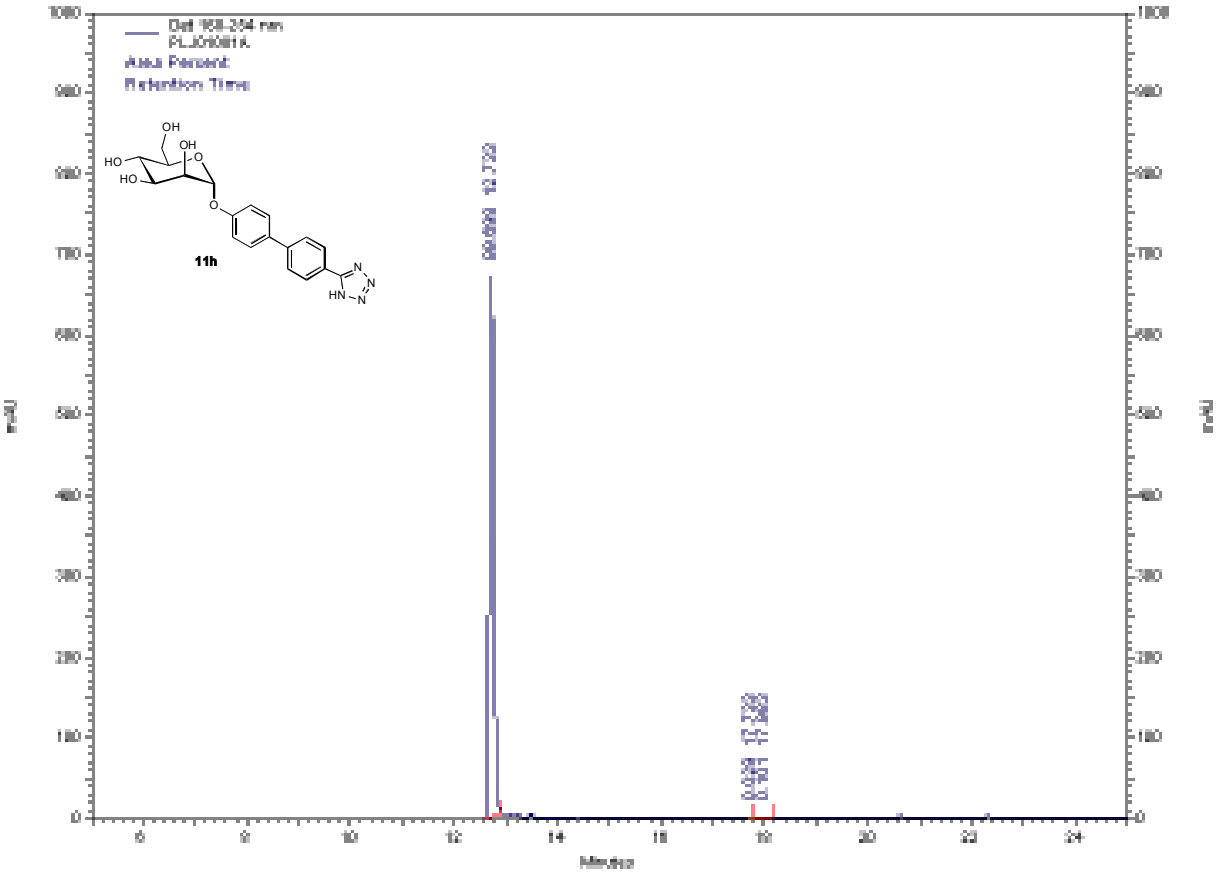
11h
HN
N

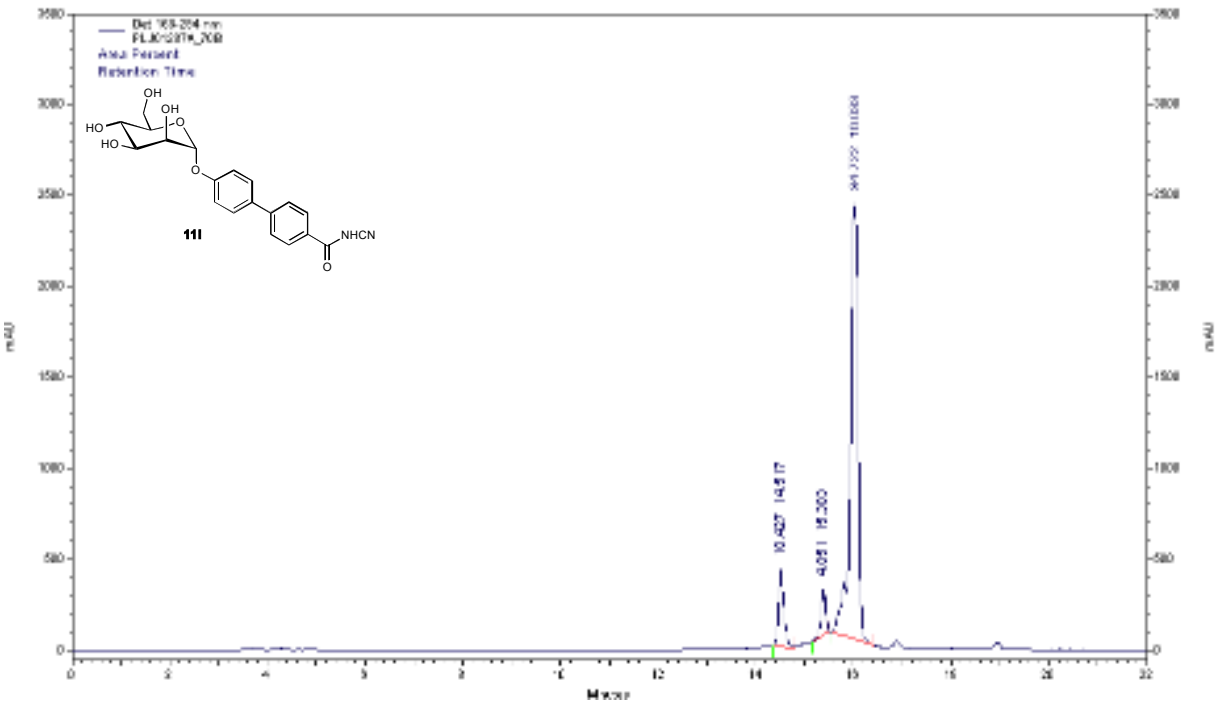
Area Percent
Retention Time
11l
NHCN
mAU
Minutes

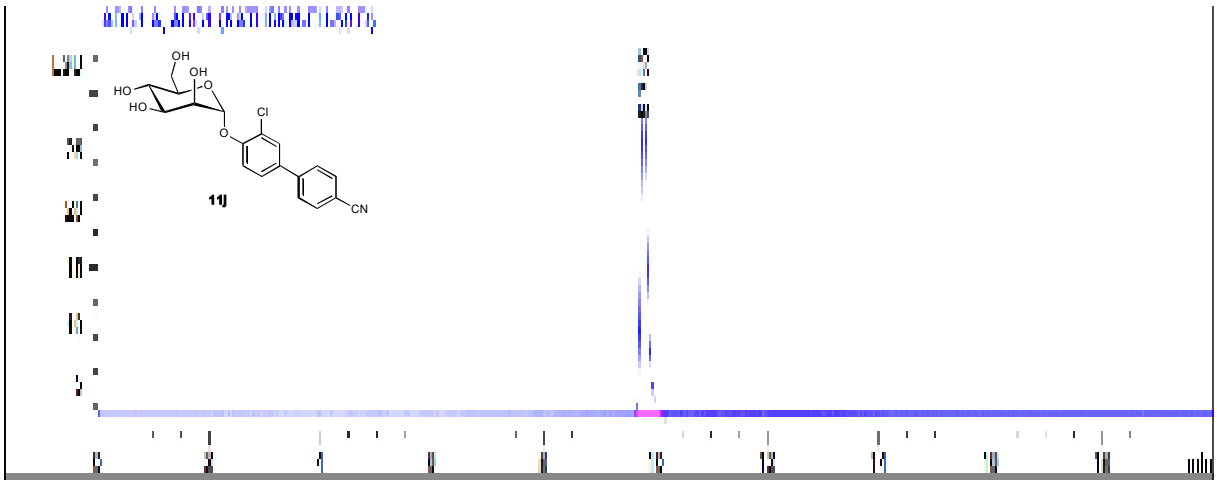
11j
Cl
CN

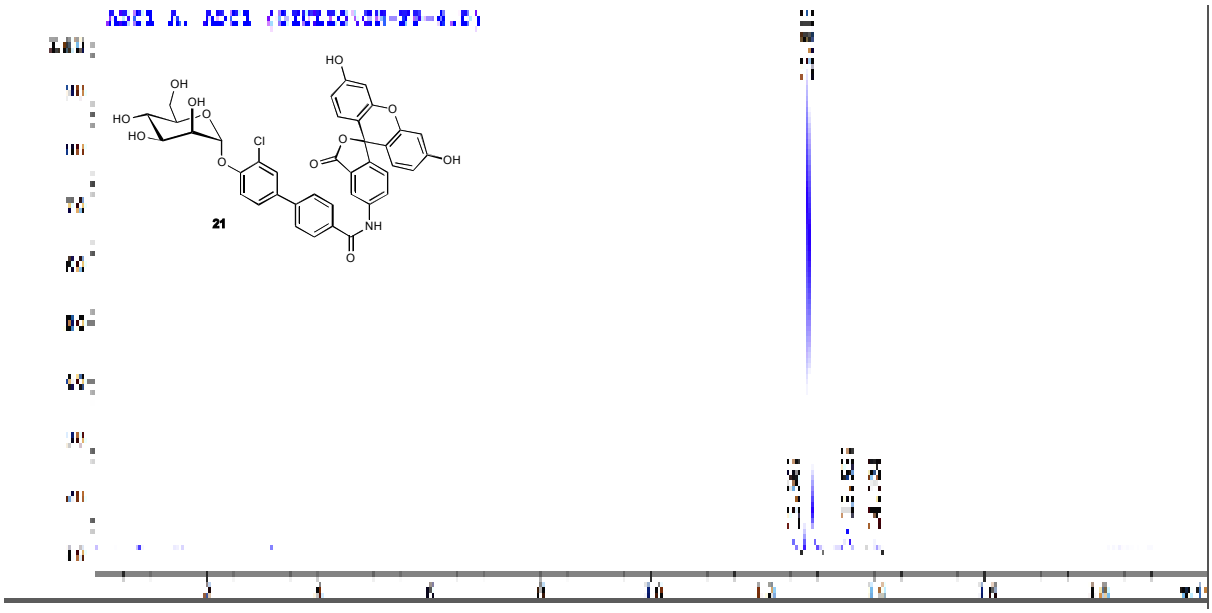
HO
OH
OH
HO
HO
O
Cl
O
O
O
OH
NH
O
21

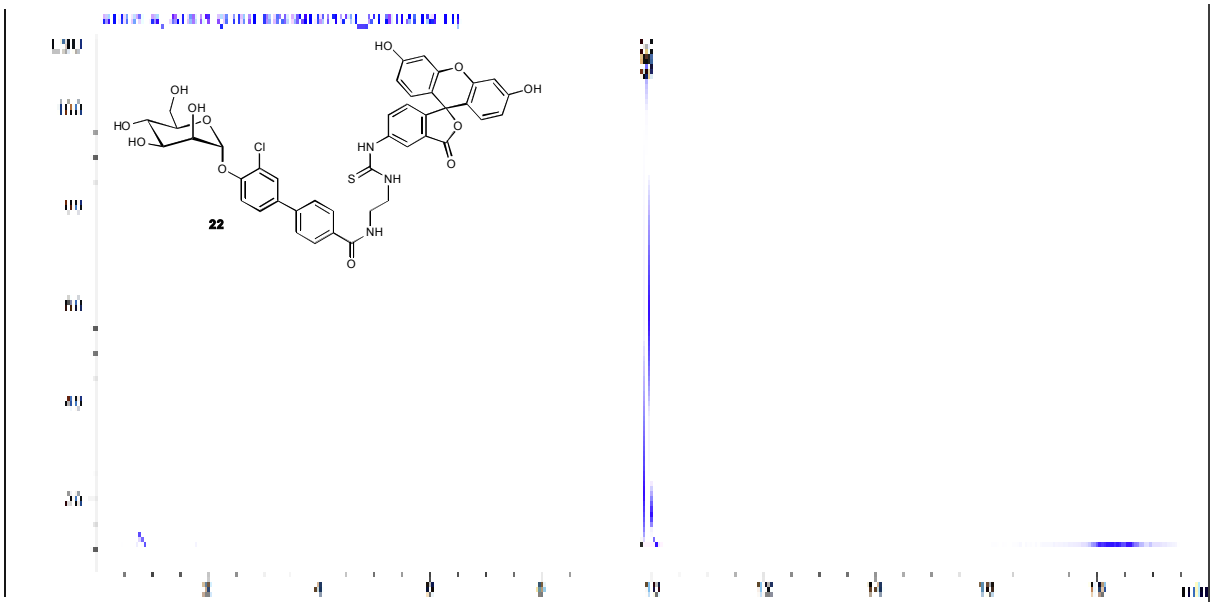
HO
OH
OH
HO
HO
O
Cl
HN
S
NH
O
O
O
OH
NH
O
22

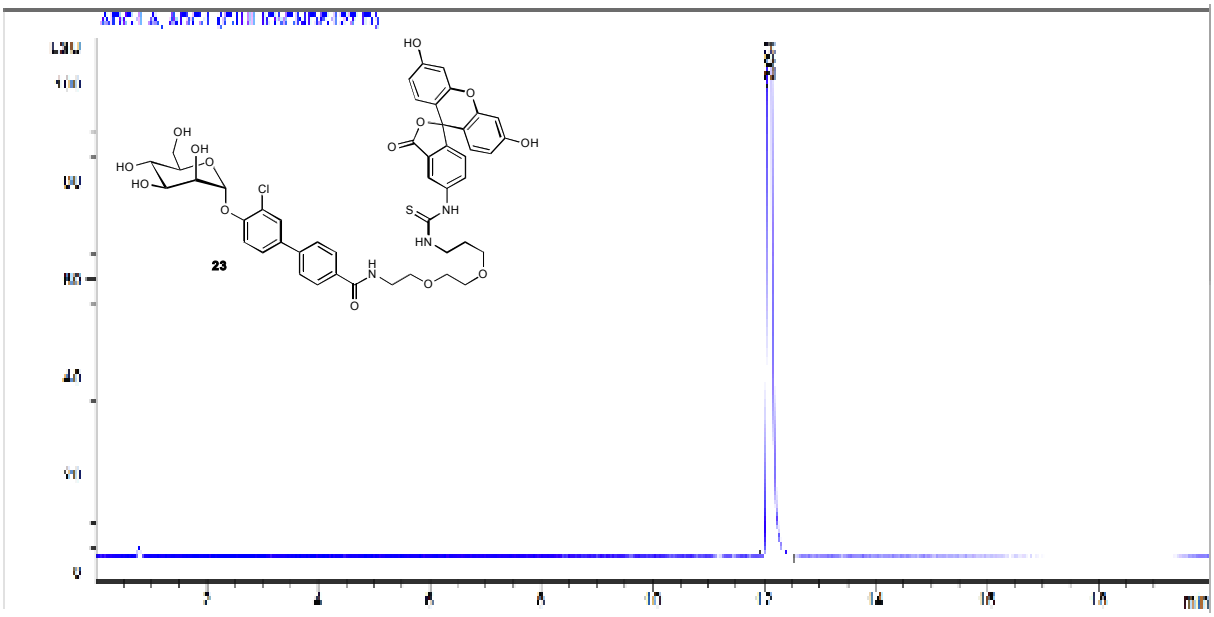
23

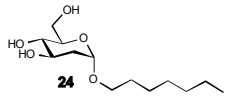
24

^{1}H NMR spectra of the synthetic compounds:

^{1}H NMR (500 MHz) of **11a**

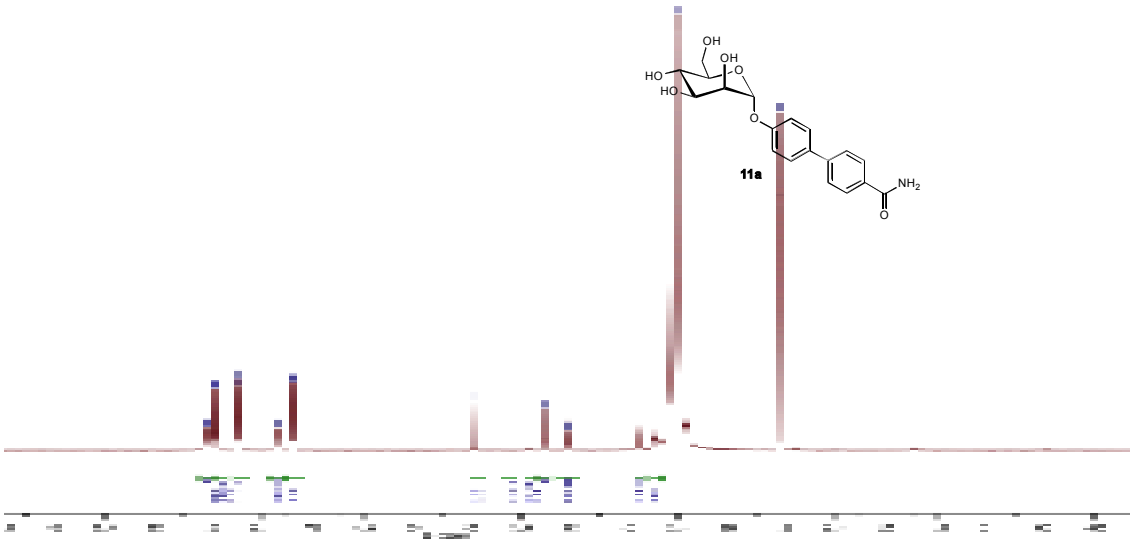

^{1}H NMR (500 MHz) of **11b**

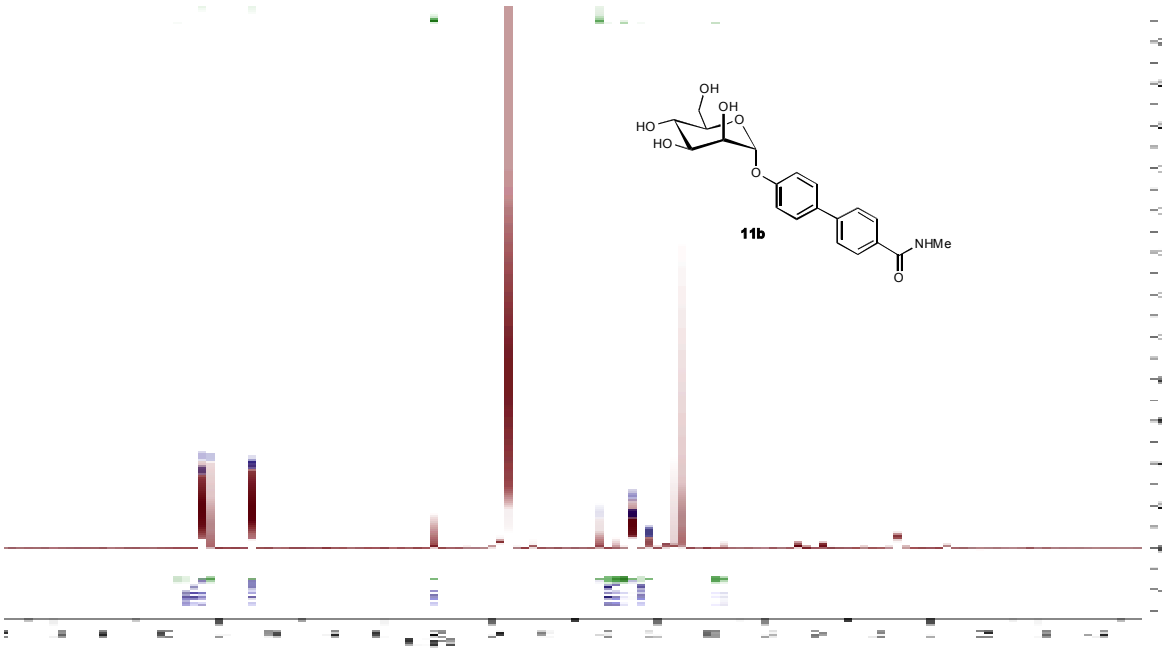

^{1}H NMR (500 MHz) of **11c**

^{1}H NMR (500 MHz) of **11d**

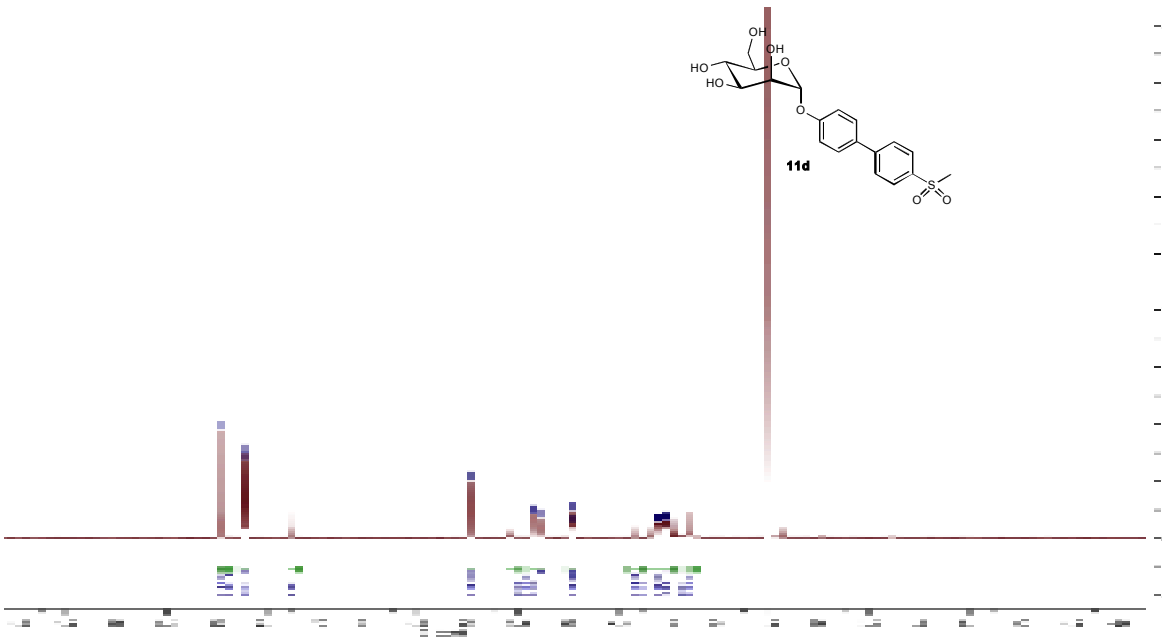

^{1}H NMR (500 MHz) of **11e**

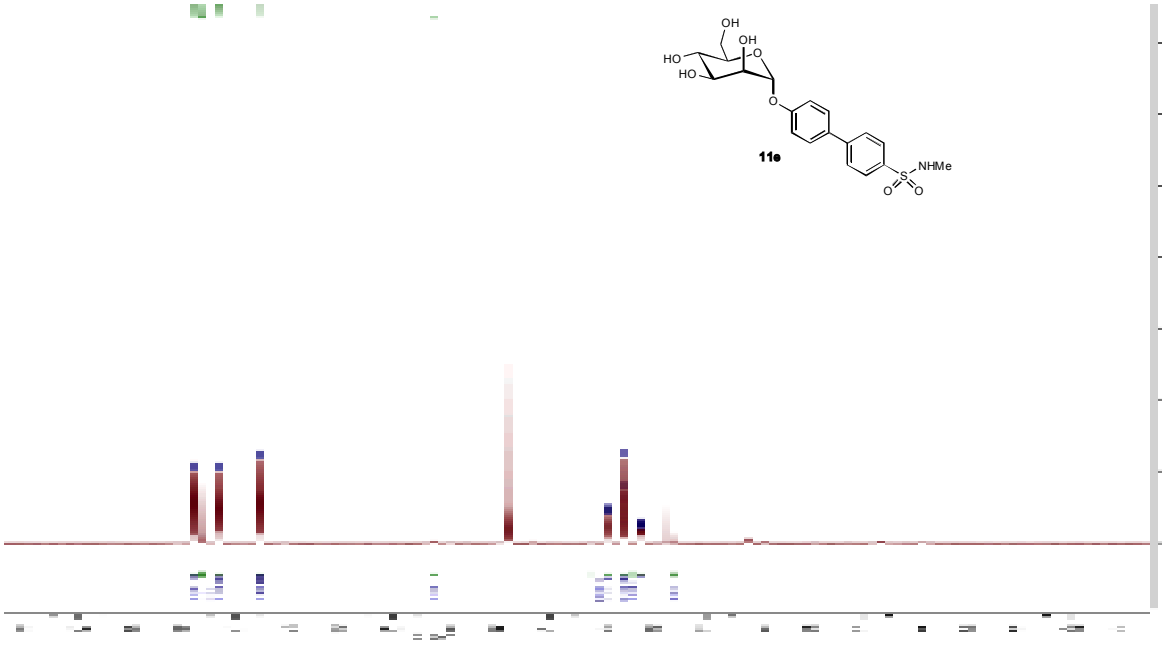

^{1}H NMR (500 MHz) of **11f**

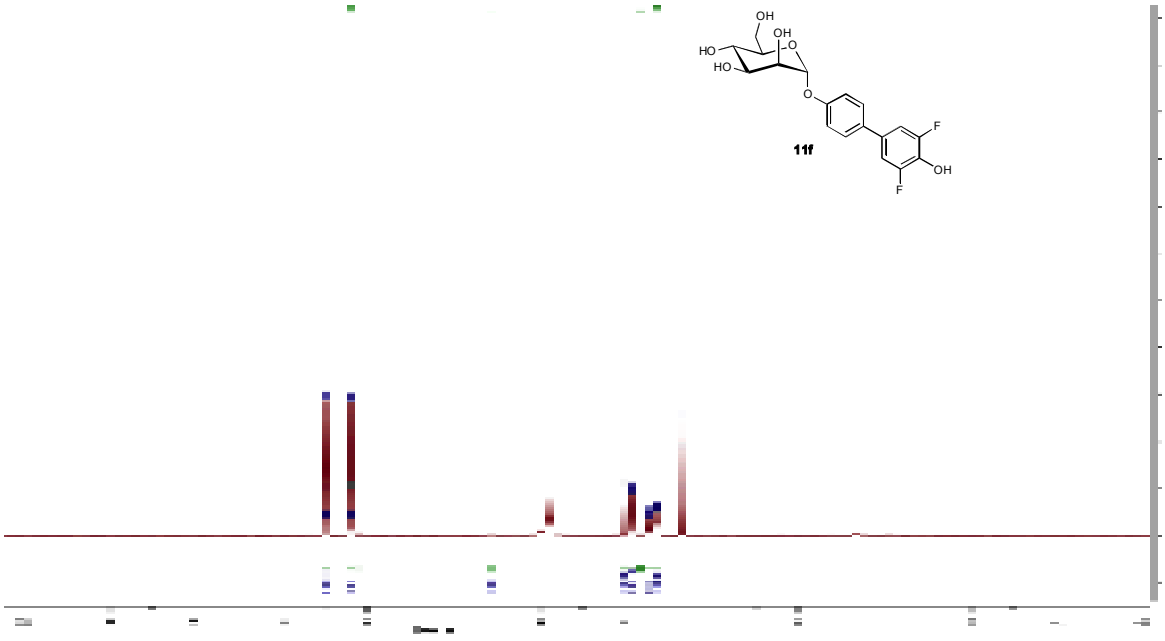

^{1}H NMR (500 MHz) of **11g**

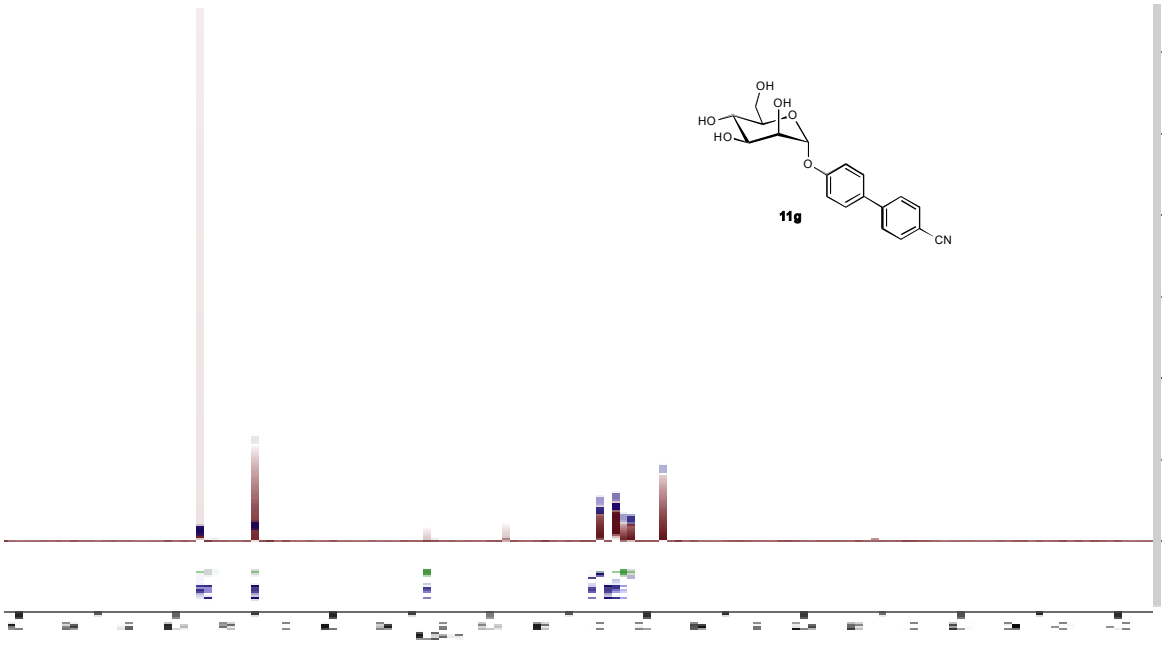

^{1}H NMR (500 MHz) of **11h**

^{1}H NMR (500 MHz) of **11i**

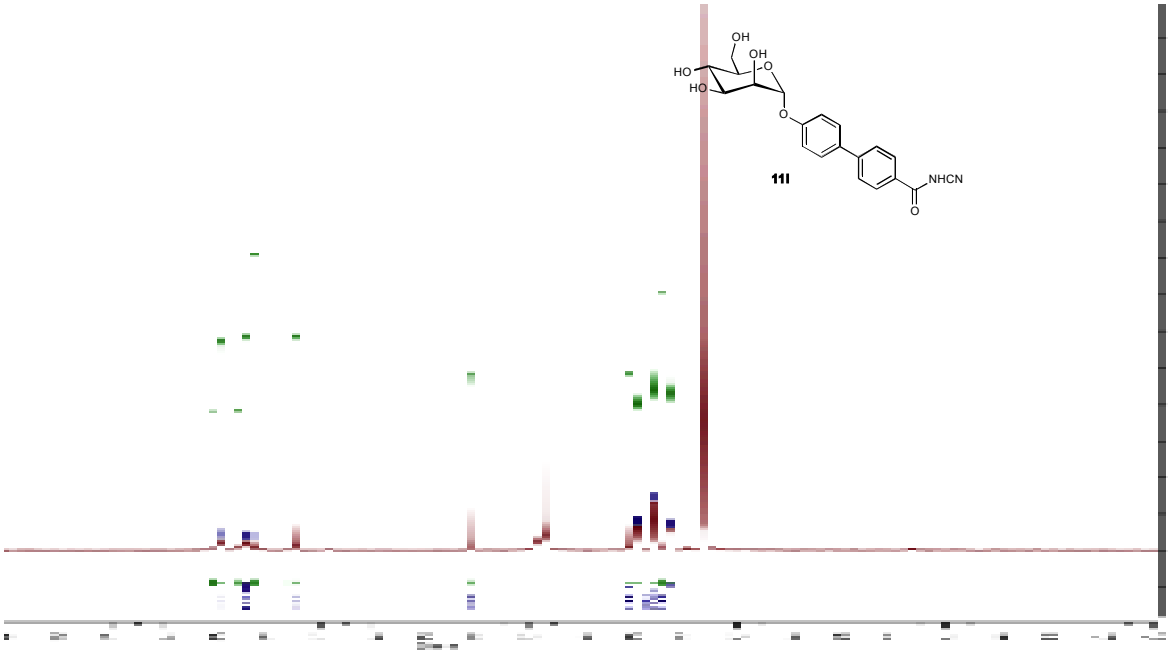

^{1}H NMR (500 MHz) of **11j**

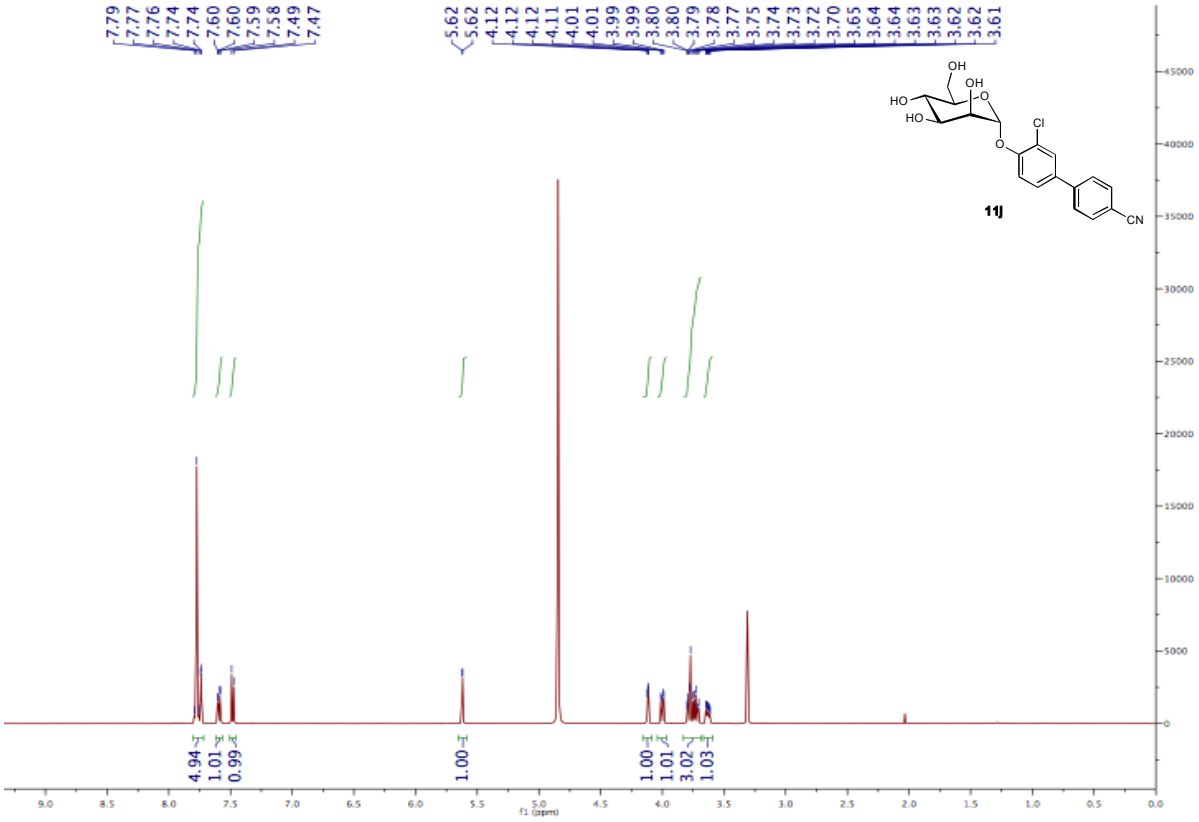

^{1}H NMR (500 MHz) of **14a**

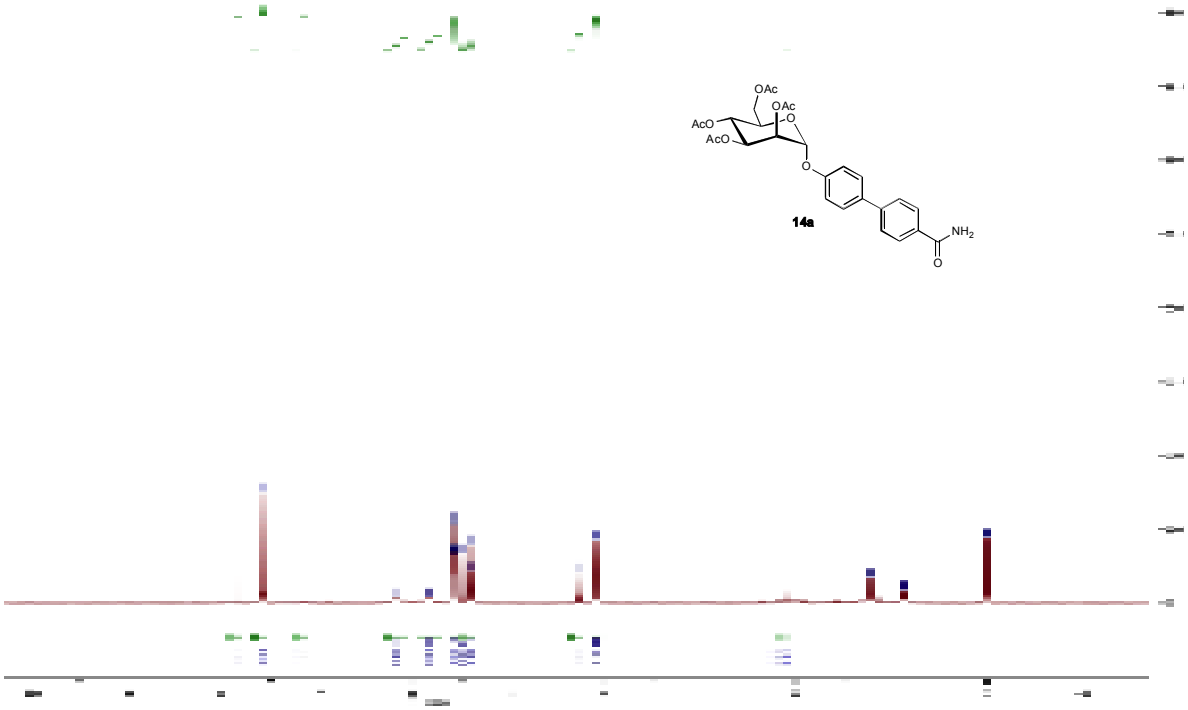

^{1}H NMR (500 MHz) of **14b**

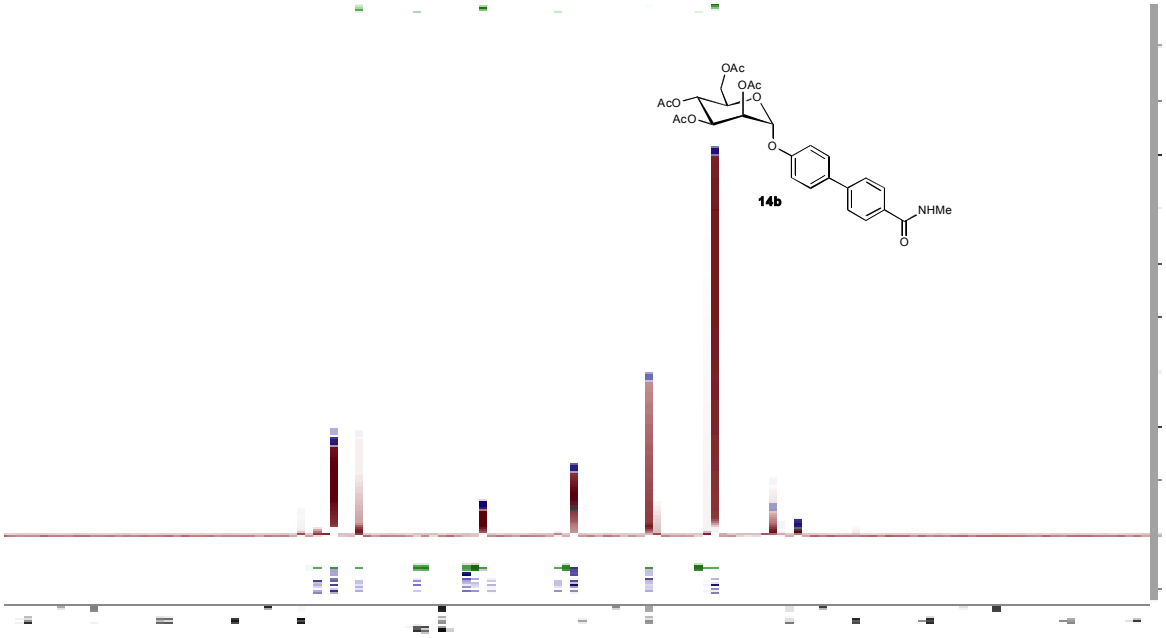

^{1}H NMR (500 MHz) of **14c**

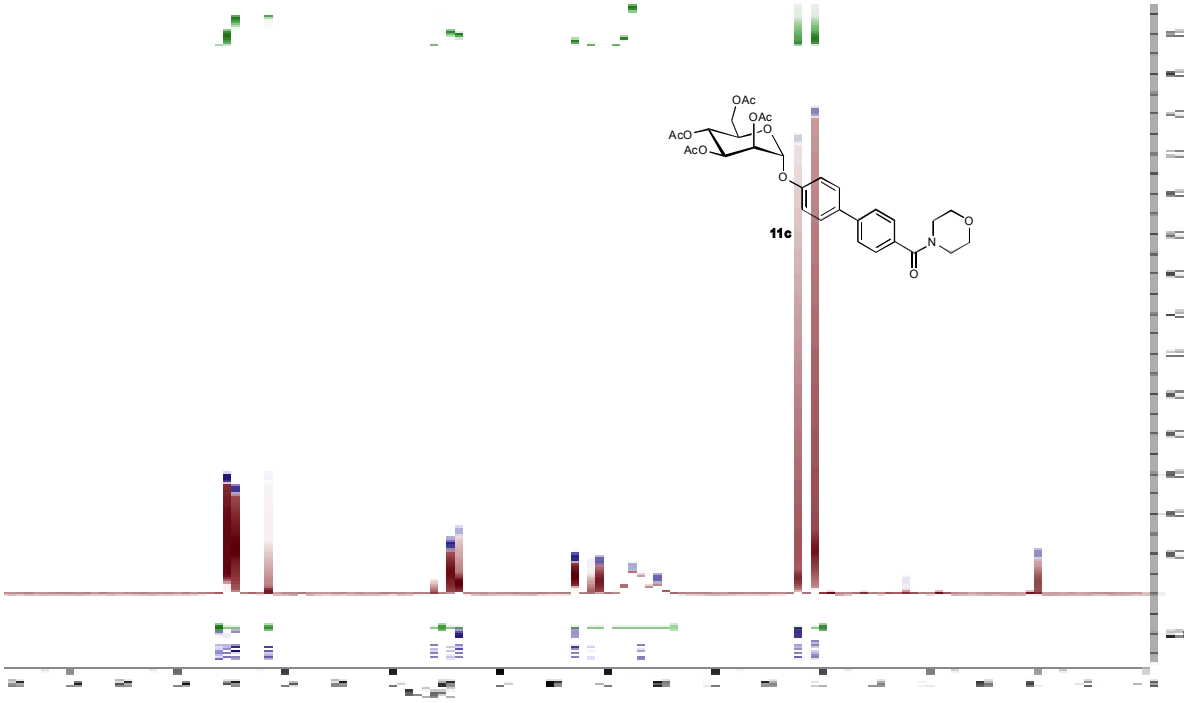

^{1}H NMR (500 MHz) of **14d**

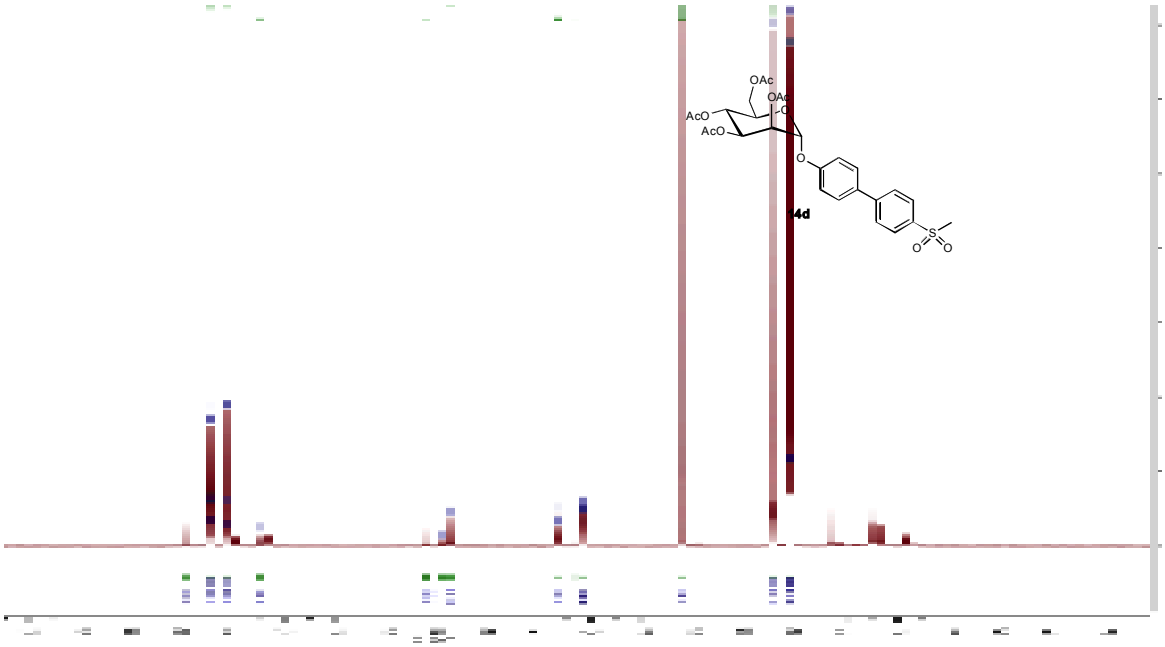

^{1}H NMR (500 MHz) of **14e**

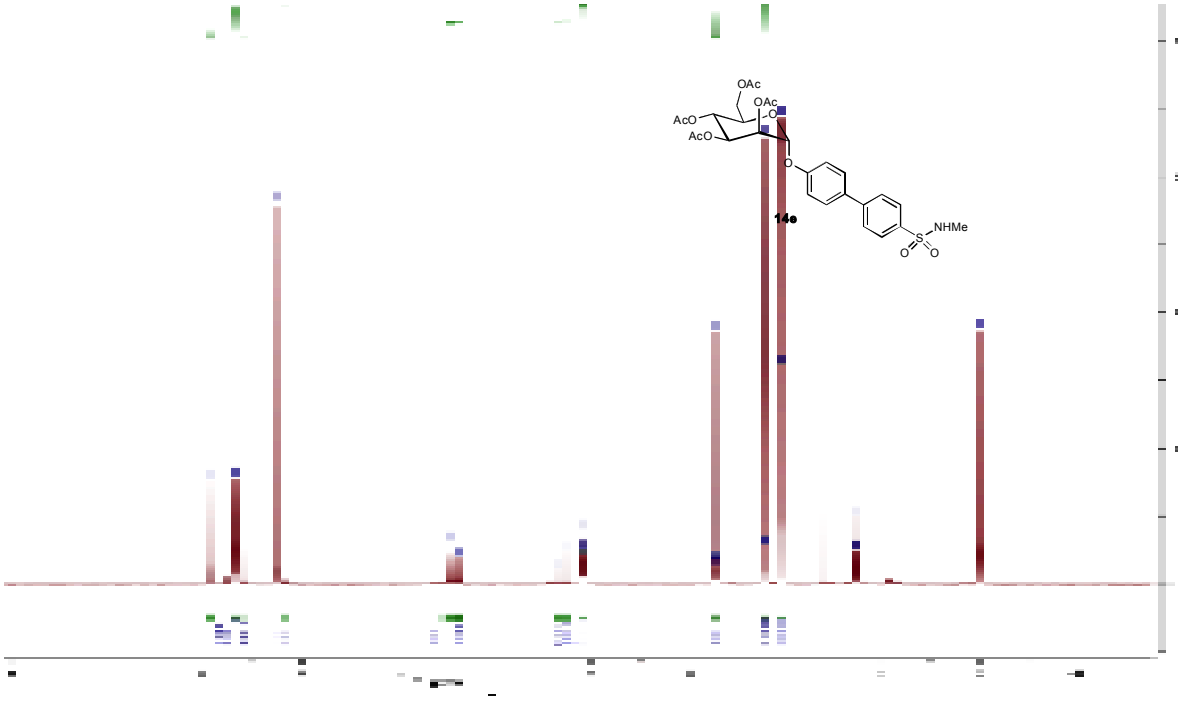

^{1}H NMR (500 MHz) of **14f**

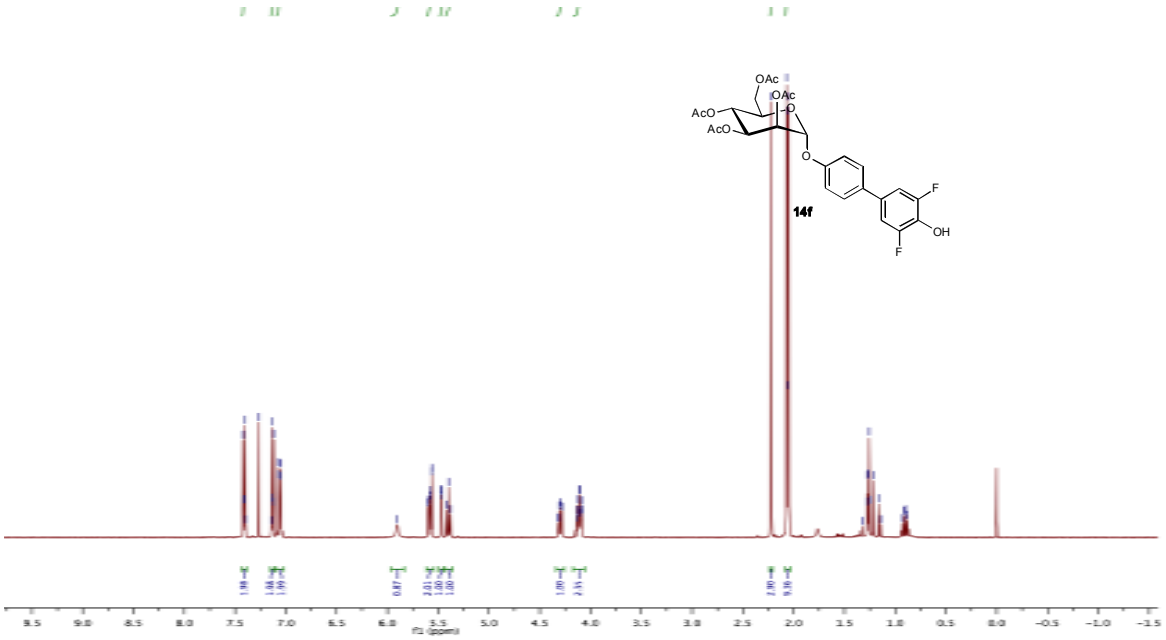

^{1}H NMR (500 MHz) of **14g**

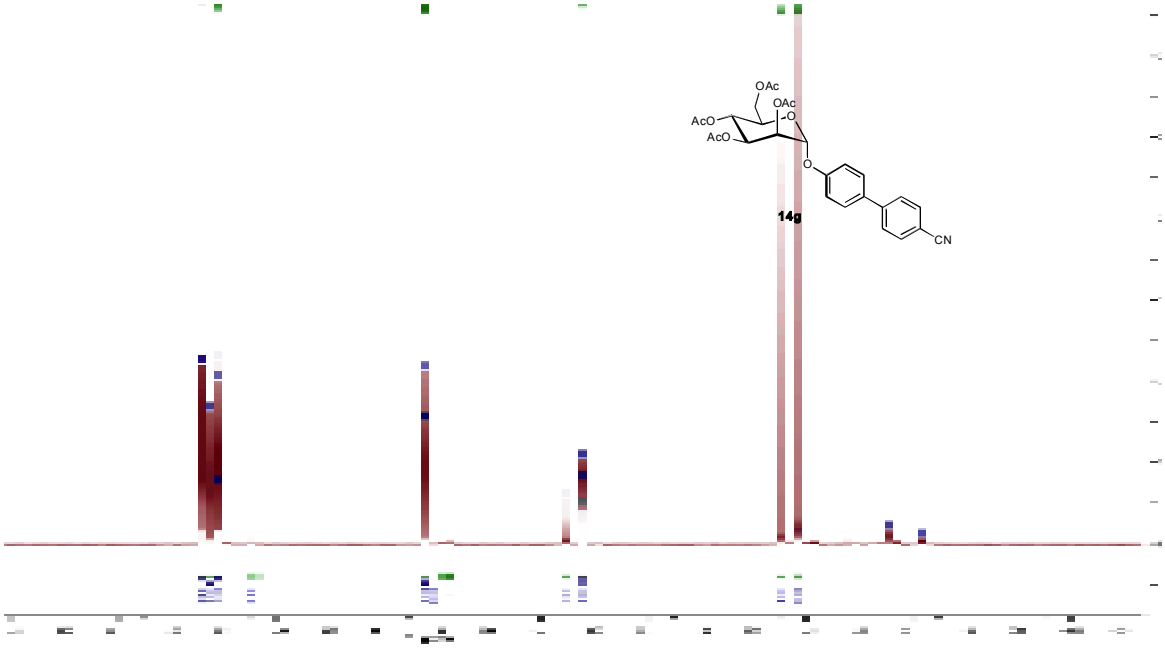

^{1}H NMR (500 MHz) of **15**

^{1}H NMR (500 MHz) of **16**

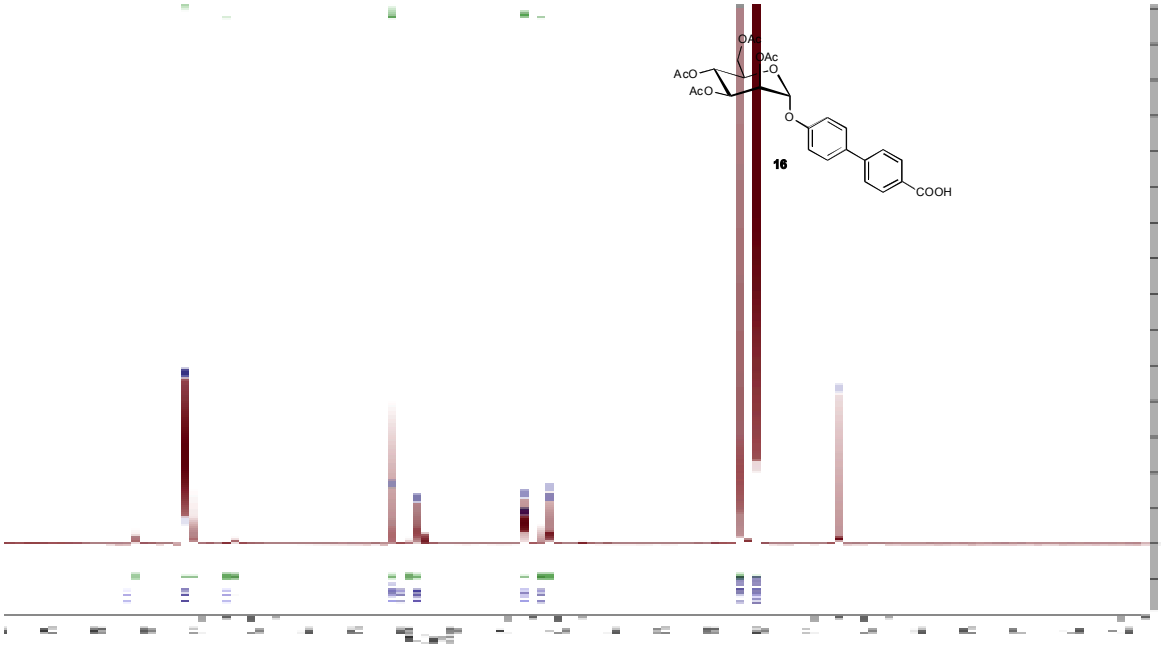

^{1}H NMR (500 MHz) of **21**

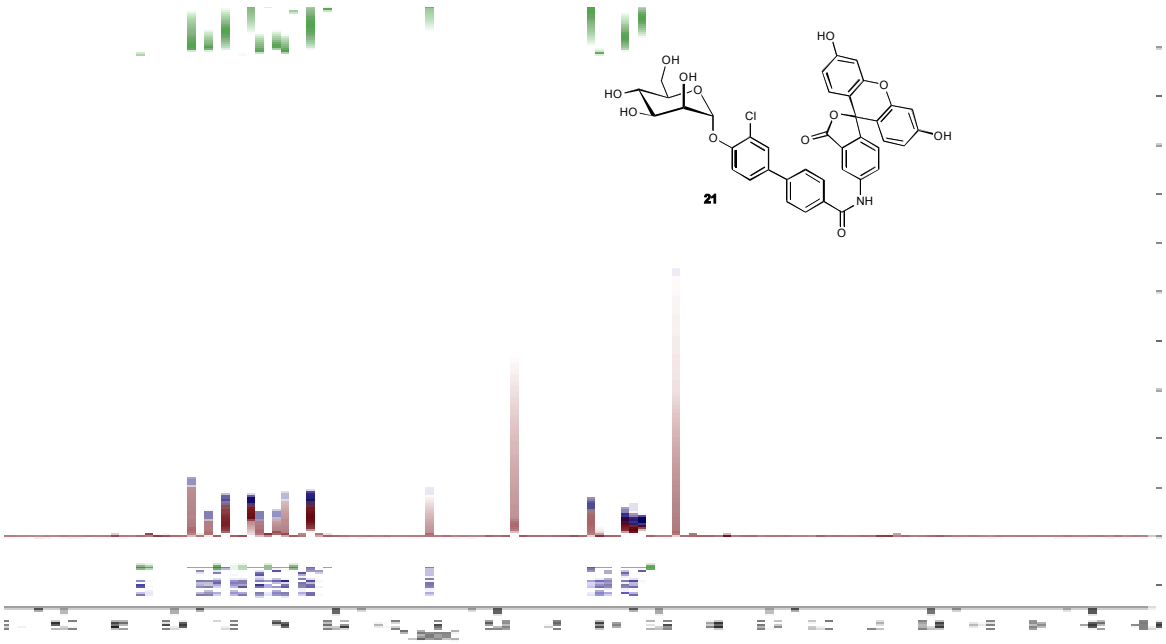

^{1}H NMR (500 MHz) of **22**

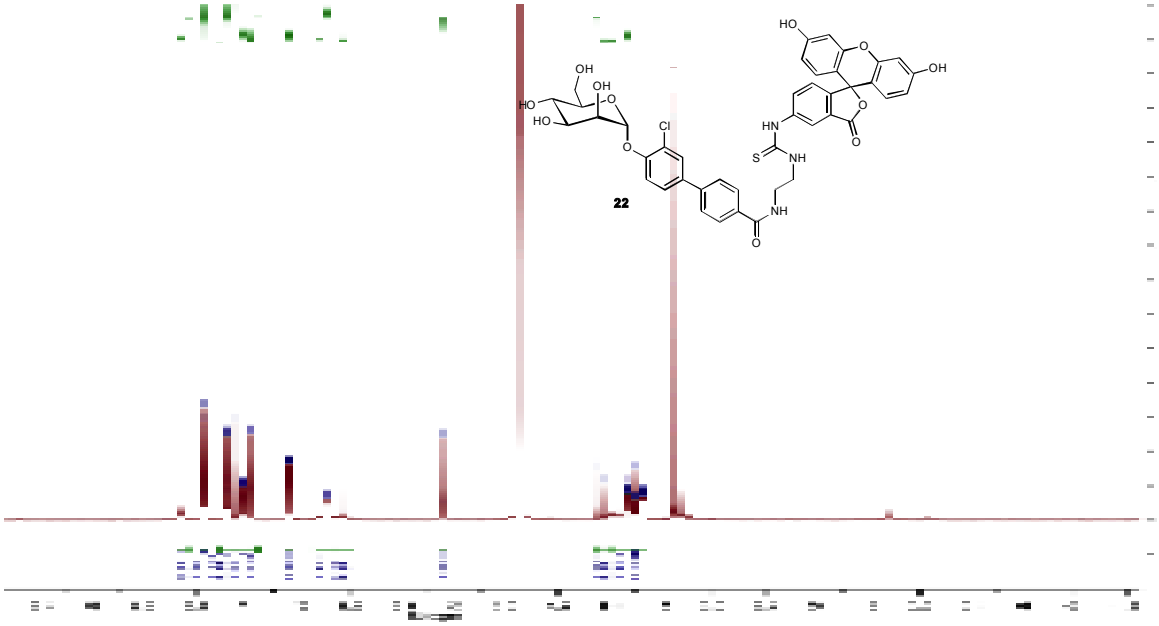

^{1}H NMR (500 MHz) of **23**

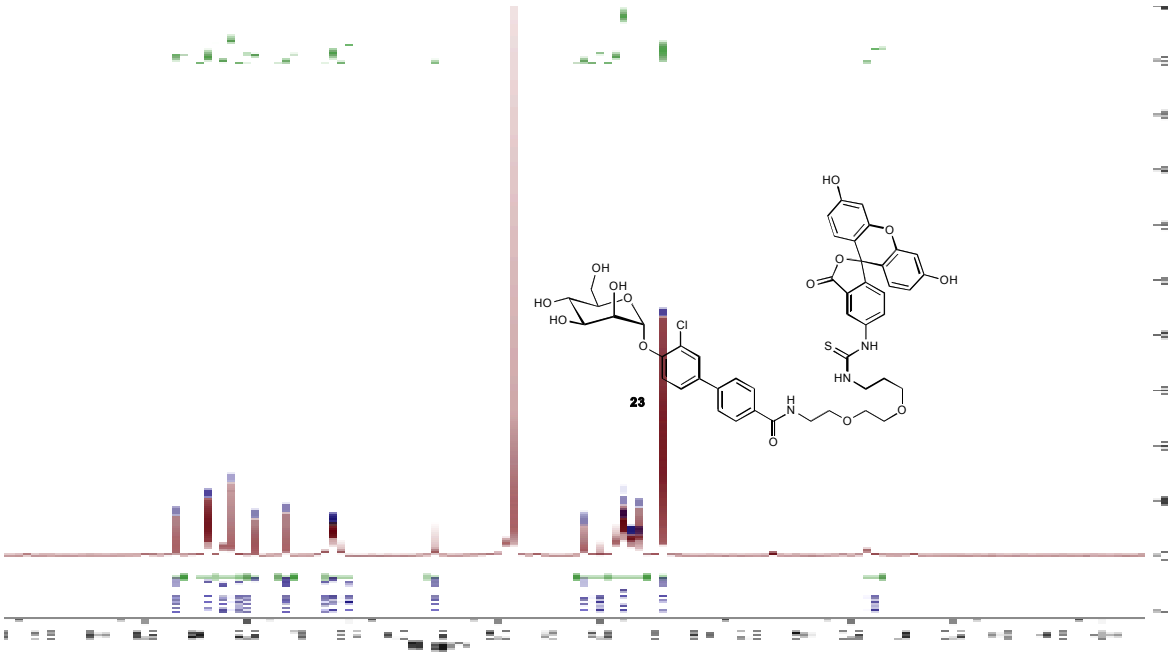

^{1}H NMR (500 MHz) of **24**

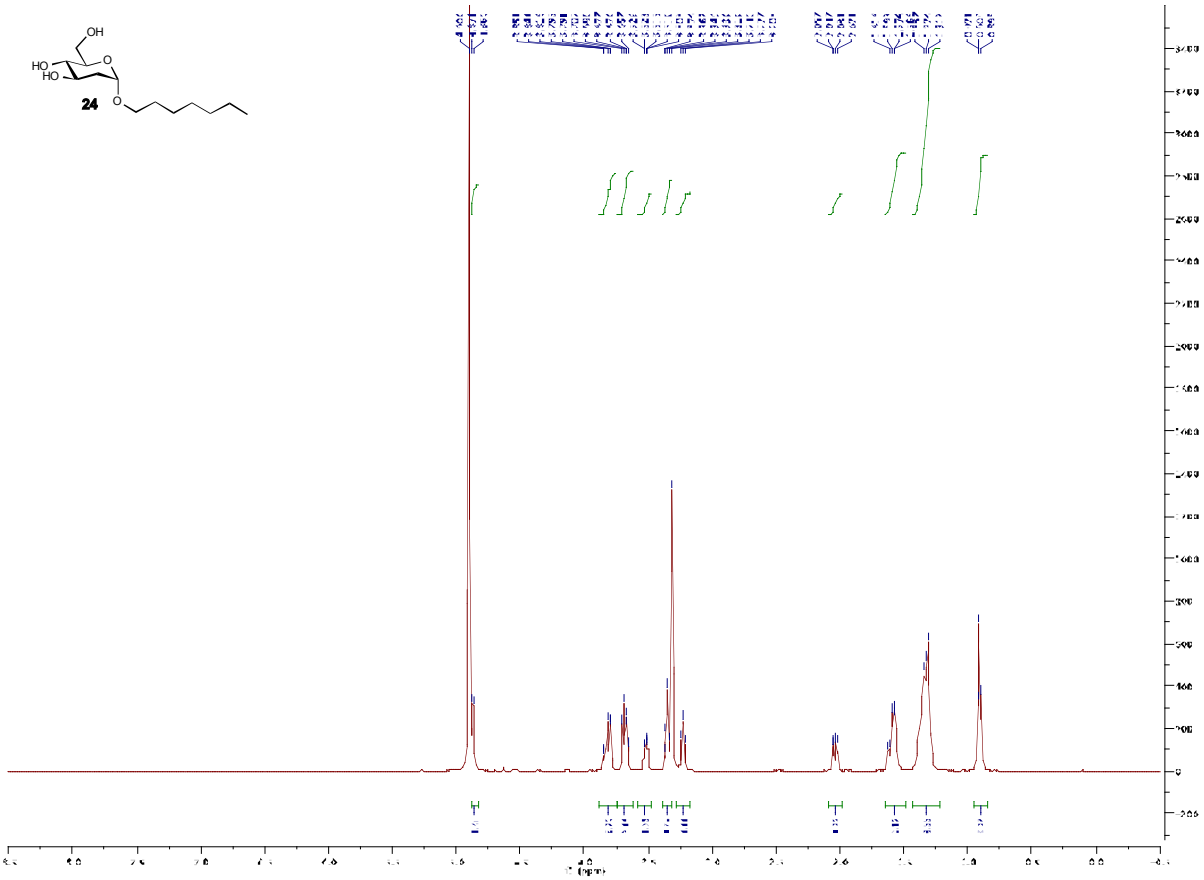

References

(S1) Pang, L.; Kleeb, S.; Lemme, K.; Rabbani, S.; Scharenberg, M.; Zalewski, A.; Schädler, F.; Schwardt, O.; Ernst, B. FimH antagonists: structure-activity and structure-property relationships for biphenyl α-D-mannopyranosides. *ChemMedChem.* **2012**, *7*, 1404-1422.

(S2) Klein, T.; Abgottspon, D.; Wittwer, M.; Rabbani, S.; Herold, J.; Jiang, X.; Kleeb, S.; Lüthi, C.; Scharenberg, M.; Bezençon, J.; Gubler, E.; Pang, L.; Smiesko, M.; Cutting, B.; Schwardt, O.; Ernst, B. FimH antagonists for the oral treatment of urinary tract infections: from design and synthesis to in vitro and in vivo evaluation. *J. Med. Chem.* **2010**, *53*, 8627-8641.

(S3) Jiang, X.; Abgottspon, D.; Kleeb, S.; Rabbani, S.; Scharenberg, M.; Wittwer, M.; Haug, M.; Schwardt, O.; Ernst, B. Antiadhesion therapy for urinary tract infections – a balanced PK/PD profile proved to be key for success. *J. Med. Chem.* **2012**, *55*, 4700-4713.

(S4) Bouckaert, J.; Berglund, J.; Schembri, M.; De Genst, E.; Cools, L.; Wuhrer, M.; Hung, C.-S.; Pinkner, J.; Slättegard, R.; Zavialov, A.; Choudhury, D.; Langermann, S.; Hultgren, S. J.; Wyns, L.; Klemm, P.; Oscarson, S.; Knight, S. D.; De Greve, H. Receptor binding studies disclose a novel class of high-affinity inhibitors of the *Escherichia coli* FimH adhesin. *Mol. Microbiol.* **2005**, *55*, 441-455.

RESULTS AND DISCUSSION

Manuscript I

Anti-Adhesion Beats Killing - *In vivo* Activity of a FimH Antagonist Against UTI in Comparison to Antibiotic Treatment.

Abgottspon D, Schwardt O, Kleeb S, Scharenberg M, Ernst B.

Preliminary manuscript: With outlook for completion.

My contributions:

In vitro evaluation of the inhibitory potency of the FimH antagonists in the flow cytometry infection assay together with Scharenberg M. and in the aggregometry assay.

In vivo pharmacokinetic and infection studies in the UTI mouse model.

Manuscript preparation.

Anti-Adhesion Beats Killing - *In vivo* Activity of FimH Antagonists Against Urinary Tract Infection in Comparison to Antibiotic Treatment

Daniela Abgottspon, Oliver Schwardt, Simon Kleeb, Meike Scharenberg, Beat Ernst*
Institute of Molecular Pharmacy, Pharmacenter, University of Basel, Switzerland

Part of this work was presented:
As poster at the Interscience Conference on Antimicrobial Agents and Chemotherapy (ICAAC), September 2011, Chicago, USA.

As oral presentation at the Swiss Chemical Society (SCS) Fall Meeting, September, 2011, Lausanne, Switzerland.

*Corresponding author: Prof. Dr. Beat Ernst, Institute of Molecular Pharmacy, Pharmacenter, University of Basel, Klingelbergstrasse 50, CH-4056 Basel, Switzerland
Tel: +41 61 267 1551, Fax: +41 61 267 1552, Email: beat.ernst@unibas.ch

Abstract

The increasing resistance against most of the currently available antimicrobials is a major challenge in public health. Therefore, new treatment strategies targeting alternative mechanisms avoiding selection pressure on bacteria and thereby implying a reduced risk of resistance are urgently needed. A promising target for an anti-virulence therapy is FimH, a mannose-binding adhesin, which is expressed on the bacterial surface and is mediating attachment to host urothelial cells. This is the initial step for a successful establishment of urinary tract infections (UTIs), predominantly caused by uropathogenic *Escherichia coli* (UPEC). Here, we present a new class of highly active anti-adhesion molecules, targeting the virulence factor FimH. All squaric acid derivatives showed very high potency in the *in vitro* cell-based assays. The *in vitro* pharmacokinetic (PK) analysis revealed a candidate with optimal PK parameters for i.v. application in the UTI mouse model. The *in vivo* PK analysis showed a dose dependent elevation of urine and plasma concentrations and in the UTI prevention study, the colony-forming units in the bladder could be reduced by 5 orders of magnitude. Results were compared to ciprofloxacin, with FimH antagonists showing a more than one order of magnitude better efficacy compared with standard antimicrobial treatment.

Introduction

Since the discovery of the first antimicrobials almost a century ago, there is a continuous battle between the development of new and the improvement of existing antimicrobial drugs and resistant pathogens. Up to date all antibiotics target essential bacterial functions (DNA, cell wall structures and their synthesis, protein expression or metabolic pathways) and therefore they impose high selection pressure upon bacteria, resulting in resistant or multidrug-resistant pathogens, which are difficult to treat [1, 2]. Targeting bacterial virulence mechanisms recently gained interest as a novel strategy to fight against bacterial infections [3 – 6]. Bacterial virulence factors actively cause damage to host tissue and consequently enhance the fitness of the infecting microorganism to successfully colonize different niches in the host [5, 6]. If these essential functions for colonization are missing, the infectivity of bacteria is often impaired.

Urinary tract infection (UTI) is one of the most common infectious disease worldwide and is primarily caused by uropathogenic *Escherichia coli* (UPEC) (70 - 95%) [7, 8]. Responsible for the initial colonization are type 1 pili, which are filamentous structures expressed on the bacterial surface. These pili allow UPEC to adhere to oligomannosides, which are part of the glycoprotein uroplakin Ia on the urinary bladder mucosa [9 – 11]. Type 1 pili consist of the four subunits, FimA, forming the pilus rod, FimF, FimG and FimH, the latter located at the tip of the pili. As a part of the FimH subunit, a carbohydrate-recognition domain (CRD) is responsible for the protein-sugar interactions between the bacteria and the host cells in the urinary tract [10, 13 – 15]. The adhesion is the first and most crucial step in the infection process and prevents the rapid clearance of *E. coli* from the urinary tract by the bulk flow of urine and at the same time, enables the invasion of host cells [9, 10]. α-D-Mannopyranosides are able to effectively prevent the FimH dependent adhesion, hence bacteria are cleared from the urinary tract and no infection can occur [16].

To date, various classes of mono- and multivalent FimH antagonists were investigated *in vitro* [17], but only a few monovalent α-D-mannopyranosides were tested *in vivo* [15, 18 – 25]. The most promising and recently presented compound families are biphenyl [20 - 24], indolinylphenyl and indolylphenyl [25] α-D-

mannopyranoside derivatives. All compound classes showed high activity in the UTI mouse model, being equally effective than antibiotic treatment (ciprofloxacin (CIP) [25] or trimethoprim-sulfamethoxazole (TMP-SMZ) [21]). Furthermore, biphenyl antagonists applied together with antibiotics were reported to have a synergistic effect on the treatment outcome and were able to improve the efficacy of TMP-SMZ treatment on catheter associated UTI [24].

In this communication, we present a new series of squaric acid derivatives, which were developed from previosly described squaric acid FimH antagonists [26] to improve their pharmacokinetic properties. The squaric acid derivatives were investigated for their *in vitro* efficacy and pharmacokinetics to evaluate their potential for *in vivo* studies. The most potent compound was selected for prevention studies in the UTI mouse model and results were compared with a standard antibiotic treatment.

Results and Discussion

Synthesis of FimH antagonists. Squaric acid derivatives were previously described as high affinity FimH antagonists [26], though their PK properties lack *in vivo* bioavailability. Besides high affinity, drug-like pharmacokinetic properties are a prerequisite for a successful *in vivo* application. In the UTI mouse model, intravenously or orally available FimH antagonists are required that, once absorbed to circulation, are metabolically stable and undergo fast renal elimination. Sufficient bioavailability requires a combination of high solubility and permeability to maximize absorption and low hepatic clearance to minimize first pass extraction. Furthermore, for efficient renal elimination, active and/or passive membrane permeability and low re-absorption in the renal tubuli is required in order to reach the target organ, the bladder. A new series of squaric acid derivatives was synthesized (Scheme 1) to improve the PK properties to allow intravenous (i.v.) and more important per oral (p.o.) application.

The mannosylated ethyl squarate **5** was synthesized according to a strategy reported by Lindhorst *et al.* [26] (Scheme 1). The known nitrophenyl mannoside **2** [27] was deacetylated (→ **3**) and reduced to aniline **4** by catalytic hydrogenation on platinum dioxide in the presence of morpholine [28]. In contrast to the results obtained by Lindhorst *et al.* [26], the use of palladium on charcoal as catalyst in our hands resulted in substantial loss of the chloro-substituent. Finally, treatment of ester **5** with primary and secondary amines yielded amides **6a**-**f** in 51-90% ready for biological testing.

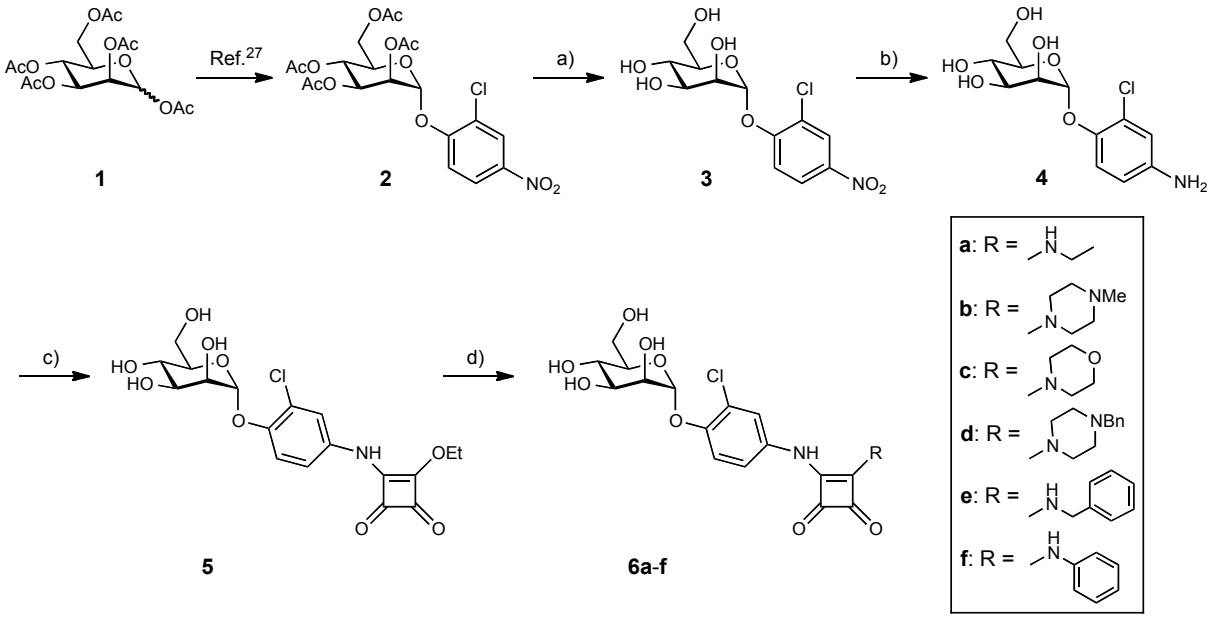

Scheme 1. a) NaOMe/MeOH, 1 h, 86%; c) H_2 (1 atm), cat. PtO_2, morpholine, MeOH, 45 min, quant; d) DES, MeOH, 1 d, 61% [26]; e) HNR^1R^2, DIPEA, MeOH, 51-90%.

***In vitro* pharmacokinetic characterization.** To evaluate wether newly synthesized squaric acid derivatives (**6a**-**f**) are suitable for *in vivo* application, their physicochemical parameters such as pK_a-values, lipophilicity (distribution coefficients, log$D_{7.4}$), solubility and permeability were determined (Table 1).

For *in vivo* studies, the application of the compound in a physiological solution (PBS) without further needs to develop suitable formulations is favorable. Furthermore, for absorption in the gastrointestinal tract and then efficient renal excretion high solubility is a prerequisite. Due to their hydrophilicity, **5**, **6b** and **6c** showed excellent solubility for all tested pH conditions (3.0, 5.0 and 7.4). **6d** is well soluble at pH of 3.0 but not at

pH of 7.4, a requirement for an i.v. application. **6a** and **6d**-**f** have a more lipophilic character, consequently they exhibited very poor solubility and are therefore not suitable for *in vivo* studies (Table 1).

For a sucessful treatment of UTI it is essential that FimH antagonists reach the target organ (bladder) by renal clearance. The estimated negative $logD_{7.4}$ in the range of -0.45 to -1.33 and pK_a values of approximately 10 for antagonists **6a**-**c** is expected to fulfill these specifications for an efficient renal elimination and a low re-absorption [29]. The $logD_{7.4}$ for all other tested antagonists (**5** and **6d**-**f**) showed positive values, predicting lower renal excretion and high re-absorption in the kidneys (Table 1).

For later use in patients, oral application is eligible. To determine oral availability of the squaric acid derivatives a parallel artificial membrane permeation assay (PAMPA) [30] was carried out. To allow oral absorption, $logP_e$ values above -5.7 and/or membrane retention above 80% [31] are required, however although compounds **6d**-**f** have a more lipophilic behavior, intended to improved their permeability, the corresponding values for all tested squaric acid derivatives (**5** and **6a**-**f**) showed that permeation is not expected.

Based on these *in vitro* PK parameters, only antagonists **6b** and **6c** fulfill the requirements for i.v. application in the UTI mouse model. The other antagonists are predicted either to be re-absorbed in the kidneys (**5**, **6d**-**f**) or insoluble (**6a, 6d**-**f**), making them unsuitable for *in vivo* studies. All tested squaric acid derivatives are not permeable and therefore not suited for oral application.

Table 1. Pharmacokinetic paramters of FimH antagonists. Passive permeation through an artificial membrane and retention were determined by PAMPA (parallel artificial membrane permeation assay). Distribution coefficients ($logD_{7.4}$ values) were measured by a miniaturized shake flask procedure. pK_a values were determined by NMR spectroscopy. Thermodynamic solubility was measured by an equilibrium shake flask approach. P_e: effective permeation; n.p.: not permeable; n.d.: not detected.

Compound	Structure	PAMPA $logP_e$ [cm/s]	$logD_{7.4}$ (mean ± SD)	pK_a	Solubility [µg/ml]/pH
5 (OS-394)	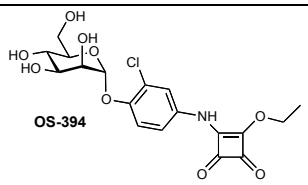	n.p.	0.09 ± 0.04	9.3	> 150 / 3.0 > 150 / 5.0 > 150 / 7.4
6a (OS-420)	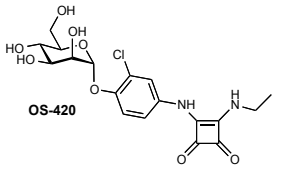	n.p.	-0.45 ± 0.07	10.1	42.8±4.2 / 3.0 42.0±1.3 / 5.0 40.8±2.1 / 7.4
6b (OS-421)	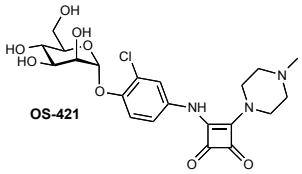	n.p.	-1.33 ± 0.14	6.4 9.3	> 150 / 3.0 > 150 / 5.0 > 150 / 7.4
6c (OS-464)	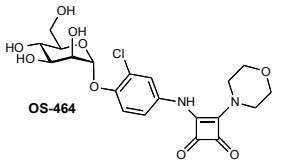	n.p.	-1.13 ± 0.12	9.4	> 150 / 3.0 > 150 / 5.0 > 150 / 7.4
6d (OS-396)	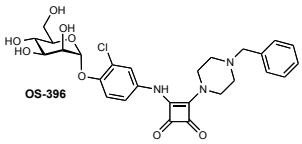	n.p.	0.80 ± 0.10	5.7 9.2	> 150 / 3.0 90.2±8.6 / 5.0 23.0±1.0 / 7.4
6e (OS-395)	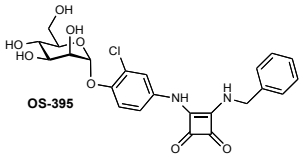	n.p.	1.05 ± 0.04	10.0	14.6±1.2 / 3.0 15.8±1.4 / 5.0 15.9±0.9 / 7.4
6f (OS-397)	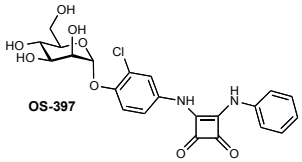	n.p.	1.12 ± 0.04	n.d.	4.3±0.4 / 3.0 4.2±0.1 / 5.0 3.9±0.2 / 7.4

Evaluation of the *in vitro* potency. For the evaluation of the *in vitro* potency of the squaric acid derivatives two cell-based assay formats have been developed, an aggregation assay [32] and a flow cytometry based infection assay [33]. In the aggregometry assay, the potential of the FimH antagonists to disaggregate *E. coli* from guinea pig erythrocytes (GPE) was determined. Antagonists were measured in

triplicates and the corresponding IC_{50} values were calculated by plotting the area under the curve (AUC) of disaggregation against the concentration of the antagonists. In the flow cytometry based infection assay, human bladder cells (5637) were infected with GFP labeled UPEC (UTI89), which were pre-incubated with FimH antagonists, followed by flow cytomertry analysis of 10'000 bladder cells. The IC_{50} values were calculated by plotting the mean fluorescent intensity (MFI) of the cells against the concentration of the antagonists. The background was determined using the GFP labeled type 1 pili deficient UPEC strain UTI89 Δ*fimA-H.*

Table 2. IC_{50} values of the squaric acid derivatives measured by aggregometry (hemagglutination) and flow cytometry based infection assay. The relative inhibitory potencies (RIPs) were calculated compared to the reference compound **7** (*n*-heptyl α-D-mannopyranoside). RIP_{agg}: relative inhibitory potency of the aggregometry assay, RIP_{fc}: relative inhibitory potency of the flow cytometry infection assay, n.d.: not determined.

Compound	Aggregometry [μM]	RIP_{agg}	Flow Cytometry [μM]	RIP_{fc}
7	77.1 ± 8.7	1	3.9 ± 1.6	1
5 (OS-394)	0.85 ± 0.13	91	0.035 ± 0.008	111
6a (OS-420)	3.3 ± 1.3	23	0.13 ± 0.02	30
6b (OS-421)	5 ± 1.3	15	0.11 ± 0.2	35
6c (OS-464)	5.3 ± 2.3	15	0.12 ± 0.06	33
6d (OS-396)	4.5 ± 1.2	17	n.d.	-
6e (OS-395)	4.4 ± 0.5	18	n.d.	-
6f (OS-397)	1.9 ± 0.5	41	0.09 ± 0.01	44

n-Heptyl α-D-mannopyranoside (**7**) was used as reference compound [15]. All squaric acid derivatives showed high activity in the low μM range in the aggregometry and in the nM range in the flow cytometry assay, respectively (Table 2). Results of the two assay formats correlate well.

The aim of our project was the identification of FimH antagonists suitable for intravenous (i.v.) or preferably oral (p.o.) application in the UTI mouse model. *In vitro* PK studies revealed that this series of squaric acid derivatives are not orally available but once in circulation they are predicted to be highly renally excreted and are therefore suitable for i.v. application. All antagonists exhibit similar binding potencies.

However, compound **6b** was chosen for *in vivo* studies because of its optimal *in vitro* PK properties (high solubility and renal permeation).

***In vivo* pharmacokinetics and efficacy.** To evaluate the availability of the antagonist in the bladder, the *in vivo* pharmacokinetic parameters were determined. Therefore, plasma and urine concentrations of **6b** after single i.v. applications were measured. With dosages of 25, 50 and 100 mg/kg, **6b** showed an availability in the bladder over a period of 4 h after administration (Figure 1). Higher availability of the antagonist in the urine was observed compared to the plasma indicating the fast renal clearance.

Dosage	**Compartment**	**$AUC_{0\text{-}24\ i.v.}$ [µg x h/mL]**
25 mg/kg	Plasma	6.6 ± 3.3
	Urine	3518 ± 2083
50 mg/kg	Plasma	23.4 ± 11.9
	Urine	4660 ± 1909
100 mg/kg	Plasma	6.7 ± 1.8
	Urine	11183 ± 2386

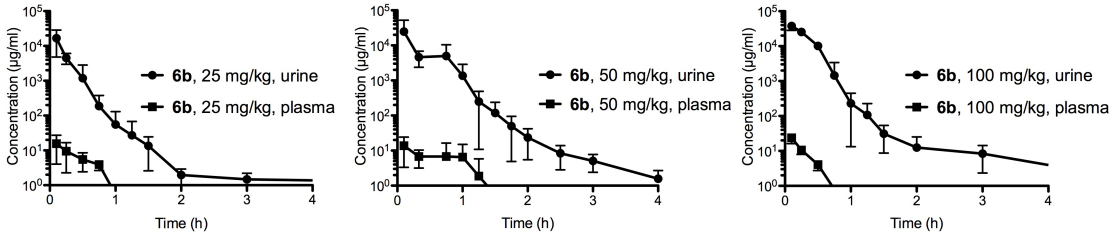

Figure 1. Determination of antagonist concentration in urine and plasma after a single i.v. application of 25, 50 and 100 mg/kg of **6b**. The data (table and graphs) show time-dependent urine and plasma concentrations.

A dose dependent elevation of the $AUC_{0\text{-}24\ i.v.}$ values in urine was observed, however although there is a linear correlation between 50 and 100 mg/kg (4660 vs. 11183 µg x h/mL), no correlation between 25 and 50 mg/kg (3518 vs. 4660 µg x h/mL) was observed. Once applied, the antagonist is rapidly renally excreted, which is favored for the treatment of UTI, because it enables high availability in the target organ.

Simultaneously, fast renal excretion is also a drawback, because it limits the exposure time in the bladder.

For the *in vivo* UTI treatment studies, different concentrations of **6b** (25, 50 and 100 mg/kg) were applied 10 minutes prior to infection with UPEC (UTI89). The results were compared to ciprofloxacin (CIP), used as a standard antibiotic therapy against UTI [34] at a dosage of 8 mg/kg, representing the murine dose equivalent to a human standard dose [35]. For each treatment study, a group of 6 animals were used. The animals were sacrificed 3 h after inoculation and urine and homogenized organs (bladder, kidneys) were examined for bacterial counts. The mean values in the untreated reference group showed 1.6 x 10^7 CFU/ml in the urine, 7.8 x 10^7 CFU in the bladder and 6.7 x 10^6 CFU in the kidneys. The bar diagram in Figure 2 summarizes the reduction of bacterial counts after i.v. treatment of **6b** and CIP. The baseline represents the values obtained for the control group and was used as reference for CFU reductions.

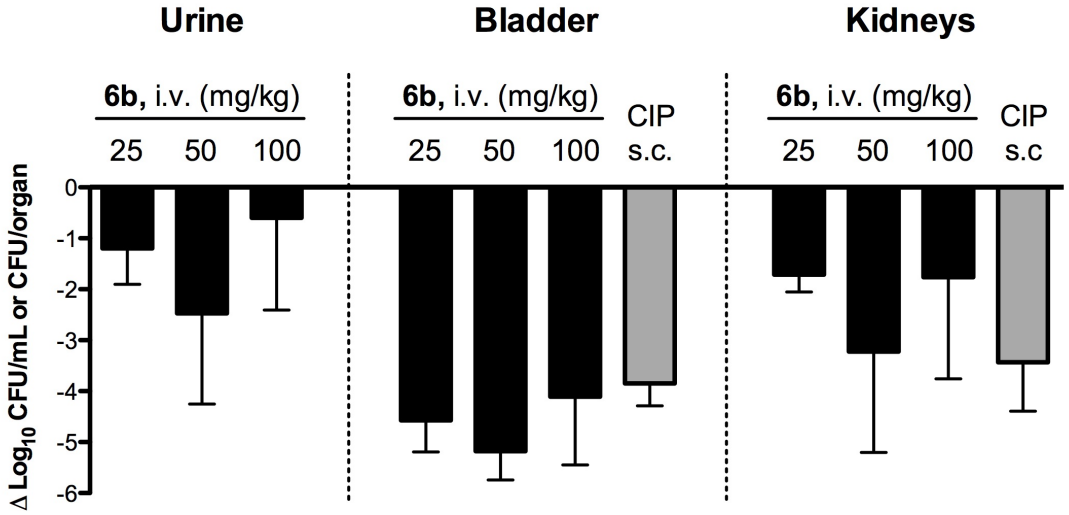

Figure 2. Treatment efficacy of **6b** (25, 50, 100 mg/kg) and CIP (8 mg/kg) in the UTI mouse model after 3 hours of infection (n = 6). **6b** was applied i.v. into the tail vein, whereas CIP was applied subcutaneously (s.c) into the neck. As baseline (reference), the mean counts of mice treated with PBS only were subtracted from the results of the tested antagonists.

Infection studies (Figure 2) showed that antagonist **6b** at a dosage of 25 mg/kg exhibited -1 $\log_{10}$ CFU in the urine, -4.5 $\log_{10}$ CFU in the bladder and -2 $\log_{10}$ CFU in the kidneys. 50 mg/kg resulted in a reduction of bacterial counts of -2.5 $\log_{10}$ CFU in

the urine, a substantial decrease of bacteria in the bladder of -5 $\log_{10}$ CFU and -3.8 $\log_{10}$ CFU in the kidneys. Surprisingly, the highest dosage of **6b** (100 mg/kg) showed only a minor reduction of bacterial counts in the urine (-0.5 $\log_{10}$ CFU), -4 $\log_{10}$ CFU in the bladder and -2.5 $\log_{10}$ CFU in the kidneys. The comparison with standard antibiotic treatment with CIP [34, 35] showed a reduction of the bacterial counts in the bladder by -3.7 $\log_{10}$ CFU, thus being less potent than all tested concentrations of **6b**, and -4 $\log_{10}$ CFU in the kidneys. The large differences in CFU counts in urine, bladder and kidneys were found probably due to sampling problems and different adhesion mechanisms (see below).

Our *in vivo* PK studies revealed high availability of **6b** in the urine of mice and treatment studies resulted in a substantial decrease of bacteria in the bladder. As mentioned in previous publications [20, 25], urine samples showed higher bacterial counts and larger standard deviations compared to the bladder (Figure 2). This could be due to difficulties during urine sampling and varying urine volumes, leading to either a concentration or dilution of bacteria in the samples. Consequently, the lower urine volume leads to a higher concentration of bacteria in the collected urine and furthermore, non-adherent bacteria, which were detached from the bladder and kidneys after application of the FimH antagonists, accumulate in the urine. The bacterial concentration in the urine of mice treated with antibiotics was excluded, because of the bactericidal activity of CIP no viable bacteria were found in the urine.

Also kidney counts were reduced to a lower extend in all treated animals (Figure 2), probably due to different bacterial adhesion mechanisms in bladder and kidneys (mannose dependent type 1 pili vs. galactose dependent P pili interactions) [12]. Furthermore, in patients, UTI is an ascending infection, which is usually initiated by bacteria ascending from the periurethral area into the urinary tract [36] or by spreading of quiescent intracellular bacteria in the bladder [37]. If a FimH antagonist is applied at this stage of infection, ascending bacteria are hindered, hence less kidney infections should occur. In the UTI mouse model, the application of bacteria directly into the bladder and concomitantly also into the kidneys (vesicourethral reflux (VUR)) during the inoculation process is a prevalent problem [38], hence high kidney counts were already observed 3 h after infection (negative control, 6.7 x 10^6 CFU).

Due to the above mentioned problems with bacterial counts in urine and kidneys, evaluation of the efficacy of FimH antagonists was exclusively limited to bladder counts. Organs were immediately frozen on dry ice after collection and plated within 1 h after thawing. Within this hour of organ processing (homogenization, plating) CIP was also present in the samples and able to further kill extra cellular bacteria in the organ samples, which could additionally reduce bacterial counts in the bladder and kidneys compared to FimH antagonists.

6b at a dosage of 50 mg/kg, reduced bacterial counts in the bladder by -5 $\log_{10}$ CFU (Figure 2), which is an over 1 $\log_{10}$ more efficient reduction than standard antibiotic treatment (CIP). One reason could be the more direct mode of action of FimH antagonists, that once present in the bladder, are able to immediately bind to their target (FimH), detaching bacteria from the bladder wall and inhibiting further adhesion. In comparison, ciprofloxacin needs longer time to deploy its mode of action, because it first has to penetrate the cell wall of the bacteria to reach its intracellular target (bacterial DNA gyrase). The direct mode of action is a key advantage of the FimH antagonists compared to antibiotics for treatment of UTI and might explain their higher efficacy in the mouse model.

Conclusion

Therapeutic targeting of bacterial virulence factors gained interest during the last few years as an alternative to antibiotics. Aiming the development of a new treatment against UTI targeting type 1 pili, we have synthesized a series of potent small molecular weight FimH antagonists. Starting from the known squaric acid derivative (**5**), six equally potent derivatives were synthesized (**6a**-**f**). According to their pharmacokinetic properties, all the squaric acid derivatives were predicted not to be orally available. **6b** was chosen for i.v. application in animal studies (PK and infection) because of ist superior pharmacokinetic properties, i.e. high solubility and was predicted to be renally permeable. *In vivo* PK studies in mice exhibited a fast renal excretion of **6b** to the target organ, the bladder. In the UTI mouse model, the colony forming units (CFU) in homogenized bladders were reduced by five orders of magnitude. Furthermore, a comparison with ciprofloxacin, used as standard

antimicrobial in the clinics, showed, that **6b** was more than one $\log_{10}$ unit more potent. This indicates the therapeutic potential of α-D-mannopyranosides for a successful treatment of UTI, resulting in less resistance problems.

However, the drawback of the squaric acid family of FimH antagonists, is their missing oral availability. In addition, due to fast renal elimination, the exposure time of **6b** in the bladder is limited to approximately 4 h. An improvement of the corresponding pharmacokinetic parameters should allow the oral application and positively influence the duration of action for an optimal treatment of urinary tract infection.

Experimental Section

Methods

FimH antagonist. *n*-Heptyl α-D-mannopyranoside was synthesized as described in [32].

Synthesis

2-Chloro-4-nitrophenyl α-D-mannopyranoside (3). To a solution of **2** (748 mg, 1.49 mmol) in MeOH (15 mL) was added 0.5 M NaOMe/MeOH (1.0 mL) under argon. The mixture was stirred at rt for 1 h, then neutralized with Dowex 50X8 (H^+) ion-exchange resin, filtered, and concentrated *in vacuo*. The residue was purified by MPLC on silica (DCM/MeOH) to afford **3** (430 mg, 86%) as a yellowish solid.

^{1}H NMR (500 MHz, CD_3OD): δ 3.49 (ddd, *J* = 2.3, 5.9, 9.6 Hz, 1H, H-5), 3.68 (dd, *J* = 5.9, 12.1 Hz, 1H, H-6a), 3.74 (t, *J* = 9.7 Hz, 1H, H-4), 3.77 (dd, *J* = 2.3, 12.1 Hz, 1H, H-6b), 3.97 (dd, *J* = 3.4, 9.5 Hz, 1H, H-3), 4.11 (dd, *J* = 1.9, 3.3 Hz, 1H, H-2), 5.75 (d, *J* = 1.5 Hz, 1H, H-1), 7.57 (d, *J* = 9.2 Hz, 1H, C_6H_3), 8.19 (dd, *J* = 2.7, 9.2 Hz, 1H, C_6H_3), 8.32 (d, *J* = 2.7 Hz, 1H, C_6H_3); ^{13}C NMR (125 MHz, CD_3OD): δ 62.6 (C-6), 68.0 (C-4), 71.5 (C-2), 72.3 (C-3), 76.5 (C-5), 100.6 (C-1), 117.0, 124.9, 124.9, 126.7, 143.6, 158.1 (C_6H_3); ESI-MS Calcd for $C_{12}H_{14}ClNNaO_8$ $[M+Na]^+$: 358.03, Found: 357.98.

4-Amino-2-chlorophenyl α-D-mannopyranoside (4). A suspension of **3** (430 mg, 1.28 mmol), morpholine (30 μL) and PtO_2 (50 mg) in MeOH (20 mL) was hydrogenated (1 atm H_2) for 45 min. Then the mixture was filtered and concentrated *in vacuo* to give crude **4** (443 mg) as a colorless oil, which contained approx. 15% morpholine and was used in the next step without further purification.

^{1}H NMR (500 MHz, CD_3OD): δ 3.71-3.81 (m, 3H, H-4, H-5, H-6a), 3.83 (dd, *J* = 1.7, 12.7 Hz, 1H, H-6b), 3.95 (dd, *J* = 3.4, 9.1 Hz, 1H, H-3), 4.11 (dd, *J* = 1.8, 3.4 Hz, 1H, H-2), 5.27 (d, *J* = 1.7 Hz, 1H, H-1), 6.61 (dd, *J* = 2.7, 8.7 Hz, 1H, C_6H_3), 6.78 (d, *J* = 2.7 Hz, 1H, C_6H_3), 7.09 (d, *J* = 8.7 Hz, 1H, C_6H_3); ^{13}C NMR (125 MHz, CD_3OD): δ 62.6 (C-6), 68.4 (C-4), 71.9 (C-2), 72.3 (C-3), 75.7 (C-5), 102.1 (C-1), 115.7, 117.4, 121.2, 153.2 (6C, C_6H_3); ESI-MS Calcd for $C_{12}H_{17}ClNO_6$ $[M+H]^+$: 306.07, Found: 306.02.

2-Chloro-4-[(2-ethoxy-3,4-dioxocyclobuten-1-yl)amino]phenyl α-D-mannopyranoside (5) [26]. To a solution of **4** (443 mg) in MeOH (15 ml) was added diethyl squarate (379 μL, 2.56 mmol) under argon and the reaction mixture was stirred at rt for 1 d. Then, the solvent was removed *in vacuo* and the residue was purified by MPLC on RP-18 (H_2O/MeOH) to yield **5** (337 mg, 61% from **3**) as a yellow solid.

^{1}H NMR (500 MHz, CD_3OD): δ 1.47 (t, *J* = 7.1 Hz, 3H, OCH_2CH_3), 3.66 (dt, *J* = 3.7, 9.9 Hz, 1H, H-5), 3.75 (d, *J* = 3.7 Hz, 2H, H-6), 3.79 (t, *J* = 9.8 Hz, 1H, H-4), 4.00 (dd, *J* = 3.4, 9.6 Hz, 1H, H-3), 4.16 (dd, *J* = 1.8, 3.3 Hz, 1H, H-2), 4.81 (q, *J* = 7.1 Hz, 2H, OCH_2CH_3), 5.56 (d, *J* = 1.5 Hz, 1H, H-1), 7.23 (m, 1H, C_6H_3), 7.32 (d, *J* = 9.0 Hz, 1H, C_6H_3), 7.47 (s, 1H, C_6H_3); ^{13}C NMR (125 MHz, CD_3OD): δ 15.7 (OCH_2CH_3), 61.4 (C-6), 67.2 (C-4), 70.8 (C-2), 71.4 (C-3), 71.6 (OCH_2CH_3), 74.9 (C-5), 100.0 (C-1), 119.2, 120.2, 122.4, 124.7, 134.6, 152.5 (C_6H_3), 168.9, 176.2 (C=C), 183.3, 186.9 (2 CO); ESI-MS Calcd for $C_{18}H_{21}ClNO_9$ $[M+H]^+$: 430.09, Found: 430.13.

General procedure for the synthesis of mannosylated squaric acid amides 6a-f. The squaric acid monoester **5** (1.0 eq) was dissolved in MeOH (1 mL/10 mg of **5**) at 50°C. After cooling to rt, the amine (1.5 eq) and DIPEA (20 μL/10 mg of **5**) were added and the reaction mixture was stirred overnight at rt. Then the solvent was removed *in vacuo* and the residue was purified by MPLC on RP-18 (H_2O/MeOH) or by LC-MS (RP-18, H_2O/MeCN + 0.2% HCO_2H) to give compounds **6a-f** as a white powder after a final lyophilization from H_2O/dioxane.

2-Chloro-4-[(2-(ethylamino)-3,4-dioxocyclobuten-1-yl)amino]phenyl α-D-mannopyranoside (6a). Following the general procedure, **5** (30.0 mg, 69.6 μmol) was treated with ethylamine hydrochloride (8.51 mg, 104 μmol) and DIPEA (60 μL) in MeOH (3 mL) to yield **6a** (15.4 mg, 51%) after purification by LC-MS.

$[\alpha]_D$ +84.4 (*c* 0.10, MeOH); ^{1}H NMR (500 MHz, CD_3OD): δ 1.30 (t, *J* = 7.2 Hz, 3H, CH_3), 3.65-3.75 (m, 5H, H-4, H-5, H-6a, NCH_2), 3.80 (dd, *J* = 2.0, 11.8 Hz, 2H, H-6b), 3.95 (dd, *J* = 3.4, 9.3 Hz, 1H, H-3), 4.09 (dd, *J* = 1.8, 3.3 Hz, 1H, H-2), 5.46 (d, *J* = 1.4 Hz, 1H, H-1), 7.27 (dd, *J* = 2.6, 8.9 Hz, 1H, C_6H_3), 7.34 (d, *J* = 8.9 Hz, 1H, C_6H_3), 7.61 (bs, 1H, C_6H_3); ^{13}C NMR (125 MHz, CD_3OD): δ 16.3 (CH_3), 40.2 (NCH_2), 62.2 (C-6), 67.7 (C-4), 71.3 (C-2), 71.9 (C-3), 75.5 (C-5), 100.8 (C-1), 119.0, 119.3, 121.2,

125.0, 135.8, 150.1 (C_6H_3), 164.6, 169.1 (C=C), 183.0, 185.8 (2 CO); HR-MS Calcd for $C_{18}H_{21}ClN_2NaO_8$ $[M+Na]^+$: 451.0884, Found: 451.0882.

2-Chloro-4-[(2-(4-methylpiperazin-1-yl)-3,4-dioxocyclobuten-1-yl)amino]phenyl α-D-mannopyranoside (6b). Following the general procedure, **5** (72.5 mg, 0.169 mmol) was treated with 1-methylpiperazine (28.0 μL, 0.252 mmol) and DIPEA (145 μL) in MeOH (7.5 mL) to yield **6b** (73.9 mg, 90%) after purification by MPLC on RP-18 (H_2O/MeOH).

$[\alpha]_D$ +74.5 (*c* 1.00, MeOH); ^{1}H NMR (500 MHz, CD_3OD): δ 2.47 (s, 3H, NCH_3), 2.76 (m, 4H, 2 CH_2), 3.66 (ddd, *J* = 2.1, 5.6, 9.8 Hz, 1H, H-5), 3.71 (dd, *J* = 5.6, 11.8 Hz, 2H, H-6a), 3.74 (t, *J* = 9.7 Hz, 1H, H-4), 3.79 (dd, *J* = 2.1, 11.8 Hz, 2H, H-6b), 3.88 (m, 4H, 2 CH_2), 3.96 (dd, *J* = 3.4, 9.4 Hz, 1H, H-3), 4.09 (dd, *J* = 1.8, 3.3 Hz, 1H, H-2), 5.48 (d, *J* = 1.4 Hz, 1H, H-1), 7.15 (dd, *J* = 2.7, 8.9 Hz, 1H, C_6H_3), 7.33 (d, *J* = 8.9 Hz, 1H, C_6H_3), 7.35 (d, *J* = 2.7 Hz, 1H, C_6H_3); ^{13}C NMR (125 MHz, CD_3OD): δ 45.4 (NCH_3), 47.4 (2C, 2 CH_2), 55.0 (2C, 2 CH_2), 62.7 (C-6), 68.2 (C-4), 71.8 (C-2), 72.3 (C-3), 76.0 (C-5), 101.2 (C-1), 119.0, 121.6, 123.8, 125.0, 135.1, 150.2 (C_6H_3), 164.9, 169.2 (C=C), 183.3, 185.9 (2 CO); HR-MS Calcd for $C_{21}H_{26}ClN_2NaO_8$ $[M+Na]^+$: 506.1306, Found: 506.1303.

2-Chloro-4-[(2-morpholino-3,4-dioxocyclobuten-1-yl)amino]phenyl α-D-mannopyranoside (6c). Following the general procedure, **5** (18.1 mg, 42.2 μmol) was treated with morpholine (5.6 μL, 63 μmol) and DIPEA (50 μL) in MeOH (2.5 mL) to yield **6c** (14.5 mg, 73%) after purification by MPLC on RP-18 (H_2O/MeOH).

$[\alpha]_D$ +82.2 (*c* 0.52, MeOH); ^{1}H NMR (500 MHz, CD_3OD): δ 3.66 (ddd, *J* = 2.0, 5.4, 9.6 Hz, 1H, H-5), 3.70-3.84 (m, 11H, H-4, H-6, 4 CH_2), 3.96 (dd, *J* = 3.3, 9.5 Hz, 1H, H-3), 4.09 (dd, *J* = 1.8, 3.0 Hz, 1H, H-2), 5.47 (d, *J* = 1.2 Hz, 1H, H-1), 7.14 (dd, *J* = 2.7, 8.8 Hz, 1H, C_6H_3), 7.31 (d, *J* = 9.0 Hz, 1H, C_6H_3), 7.34 (d, *J* = 2.7 Hz, 1H, C_6H_3); ^{13}C NMR (125 MHz, CD_3OD): δ 48.9 (2C, 2 NCH_2), 62.7 (C-6), 67.7 (2C, 2 OCH_2), 68.2 (C-4), 71.9 (C-2), 72.4 (C-3), 76.0 (C-5), 101.2 (C-1), 118.9, 121.5, 123.7, 125.0, 135.2, 150.1 (C_6H_3), 164.5, 169.3 (C=C), 183.0, 186.0 (2 CO); HR-MS Calcd for $C_{20}H_{23}ClN_2NaO_9$ $[M+Na]^+$: 493.0990, Found: 493.0990.

4-[(2-(4-Benzylpiperazin-1-yl)-3,4-dioxocyclobuten-1-yl)amino]-2-chlorophenyl α-D-mannopyranoside (6d). Following the general procedure, **5** (50.0 mg, 0.116 mmol) was treated with 1-benzylpiperazine (30.2 μL, 0.174 mmol) and DIPEA (100 μL) in MeOH (5 mL) to yield **6d** (46.9 mg, 72%) after purification by LC-MS.
$[\alpha]_D$ +72.3 (*c* 0.40, MeOH); ^{1}H NMR (500 MHz, CD_3OD): δ 2.74 (m, 4H, 2 CH_2), 3.66 (ddd, *J* = 2.3, 5.5, 9.8 Hz, 1H, H-5), 3.70-3.75 (m, 4H, H-4, H-6a, C*H*$_2$Ph), 3.78 (dd, *J* = 2.2, 12.4 Hz, 2H, H-6b), 3.85 (m, 4H, 2 CH_2), 3.96 (dd, *J* = 3.4, 9.4 Hz, 1H, H-3), 4.10 (dd, *J* = 1.8, 3.3 Hz, 1H, H-2), 5.46 (d, *J* = 1.5 Hz, 1H, H-1), 7.12 (dd, *J* = 2.6, 8.9 Hz, 1H, C_6H_3), 7.28 (d, *J* = 8.9 Hz, 1H, C_6H_3), 7.30-7.38 (m, 6H, C_6H_3, C_6H_5); ^{13}C NMR (125 MHz, CD_3OD): δ 48.0 (2C, 2 CH_2), 53.4 (2C, 2 CH_2), 62.7 (C-6), 63.3 (*C*H_2Ph), 68.2 (C-4), 71.8 (C-2), 72.4 (C-3), 75.9 (C-5), 101.2 (C-1), 118.9, 121.5, 123.7, 125.0, 129.0, 129.6, 130.8, 135.9, 136.8, 150.1 (12C, C_6H_3, C_6H_5), 164.6, 169.1 (C=C), 183.0, 185.8 (2 CO); HR-MS Calcd for $C_{27}H_{30}ClN_2NaO_8$ $[M+Na]^+$: 582.1619, Found: 582.1619.

4-[(2-(Benzylamino)-3,4-dioxocyclobuten-1-yl)amino]-2-chlorophenyl α-D-mannopyranoside (6e). Following the general procedure, **5** (50.0 mg, 0.116 mmol) was treated with benzyl amine (19.0 μL, 0.174 mmol) and DIPEA (100 μL) in MeOH (5 mL) to yield **6e** (38.9 mg, 68%) after purification by LC-MS.
$[\alpha]_D$ +74.0 (*c* 0.20, MeOH); ^{1}H NMR (500 MHz, CD_3OD): δ 3.66 (ddd, *J* = 2.2, 5.6, 9.8 Hz, 1H, H-5), 3.70 (dd, *J* = 5.6, 11.8 Hz, 2H, H-6a), 3.73 (t, *J* = 9.7 Hz, 1H, H-4), 3.79 (dd, *J* = 2.2, 11.8 Hz, 2H, H-6b), 3.94 (dd, *J* = 3.4, 9.3 Hz, 1H, H-3), 4.09 (dd, *J* = 1.8, 3.4 Hz, 1H, H-2), 4.87 (s, 2H, C*H*$_2$Ph), 5.45 (d, *J* = 1.7 Hz, 1H, H-1), 7.25 (dd, *J* = 2.7, 8.9 Hz, 1H, C_6H_3), 7.30-7.33, 7.37-7.39 (m, 6H, C_6H_3, C_6H_5), 7.58 (d, *J* = 2.0 Hz, 1H, C_6H_3); ^{13}C NMR (125 MHz, CD_3OD): δ 49.3 (*C*H_2Ph), 62.7 (C-6), 68.3 (C-4), 71.9 (C-2), 72.4 (C-3), 76.0 (C-5), 101.3 (C-1), 119.6, 121.8, 125.7, 128.8, 129.0, 130.0, 135.5, 139.4, 149.8 (12C, C_6H_3, C_6H_5), 165.1, 173.3 (C=C), 182.4, 183.8 (2 CO); HR-MS Calcd for $C_{23}H_{23}ClN_2NaO_8$ $[M+Na]^+$: 513.1041, Found: 513.1039.

2-Chloro-4-[(3,4-dioxo-2-(phenylamino)cyclobuten-1-yl)amino]phenyl α-D-mannopyranoside (6f). Following the general procedure, **5** (50.0 mg, 0.116 mmol) was treated with aniline (15.9 μL, 0.174 mmol) and DIPEA (100 μL) in MeOH (5 mL) to yield **6f** (30.7 mg, 56%) after purification by LC-MS.

$[\alpha]_D$ +75.0 (*c* 0.19, MeOH); ^{1}H NMR (500 MHz, CD_3OD): δ 3.67 (ddd, *J* = 2.3, 5.5, 9.6 Hz, 1H, H-5), 3.73 (dd, *J* = 5.5, 11.8 Hz, 2H, H-6a), 3.75 (t, *J* = 9.7 Hz, 1H, H-4), 3.80 (dd, *J* = 2.3, 11.9 Hz, 2H, H-6b), 3.96 (dd, *J* = 3.4, 9.4 Hz, 1H, H-3), 4.10 (dd, *J* = 1.8, 3.3 Hz, 1H, H-2), 5.48 (d, *J* = 1.6 Hz, 1H, H-1), 7.11 (t, *J* = 7.4 Hz, 1H, C_6H_5), 7.34-7.37 (m, 4H, C_6H_3, C_6H_5), 7.49 (d, *J* = 7.8 Hz, 2H, C_6H_5), 7.67 (s, 1H, C_6H_3); ^{13}C NMR (125 MHz, CD_3OD): δ 61.0 (C-6), 66.6 (C-4), 70.0 (C-2), 70.6 (C-3), 75.4 (C-5), 99.9 (C-1), 118.4, 118.6, 118.7, 120.2, 123.3, 123.4, 129.4, 133.9, 138.6, 147.7 (12C, C_6H_3, C_6H_5), 165.4, 165.6 (C=C), 181.5, 181.8 (2 CO); HR-MS Calcd for $C_{22}H_{21}ClN_2NaO_8$ $[M+Na]^+$: 499.0884, Found: 499.0883.

In vitro pharmacokinetics

Materials

Dimethyl sulfoxide (DMSO), 1-propanol, and 1-octanol were purchased from Sigma-Aldrich (Sigma-Aldrich, St. Louis MI, USA). PAMPA System Solution, GIT-0 Lipid Solution, and Acceptor Sink Buffer were ordered from pIon (pIon, Woburn MA, USA). Acetonitrile (MeCN) was bought from Acros (Acros Organics, Geel, Belgium).

$LogD_{7.4}$ determination. The *in silico* prediction tool ALOGPS [39] was used to estimate the logP values of the compounds. Depending on these values, the compounds were classified into three categories: hydrophilic compounds (logP below zero), moderately lipophilic compounds (logP between zero and one) and lipophilic compounds (logP above one). For each category, two different ratios (volume of 1-octanol to volume of buffer) were defined as experimental parameters (Table 3).

Table 3

Compound type	logP	Ratios (1-octanol: buffer)
hydrophilic	< 0	30:140, 40:130
moderately lipophilic	0 - 1	70:110, 110:70
lipophilic	> 1	3:180, 4:180

Equal amounts of phosphate buffer (0.1 M, pH 7.4) and 1-octanol were mixed and shaken vigorously for 5 min to saturate the phases. The mixture was left until separation of the two phases occurred, and the buffer was retrieved. Stock solutions of the test compounds were diluted with buffer to a concentration of 1 µM. For each compound, six determinations, i.e., three determinations per 1-octanol:buffer ratio, were performed in different wells of a 96-well plate. The respective volumes of buffer containing analyte (1 µM) were pipetted to the wells and covered by saturated 1-octanol according to the chosen volume ratio. The plate was sealed with aluminium foil, shaken (1350 rpm, 25 °C, 2 h) on a Heidoph Titramax 1000 plate-shaker (Heidolph Instruments GmbH & Co. KG, Schwabach, Germany) and centrifuged (2000 rpm, 25 °C, 5 min, 5804 R Eppendorf centrifuge, Hamburg, Germany). The aqueous phase was transferred to a 96-well plate for analysis by liquid chromatography-mass spectrometry (LC-MS).

$\log D_{7.4}$ was calculated from the 1-octanol:buffer ratio (o:b), the initial concentration of the analyte in buffer (1 µM), and the concentration of the analyte in buffer (c_B) with equation:

$$\log D_{7.4} = \log\left(\frac{1\mu M - c_B}{c_B} \times \frac{1}{o:b}\right)$$

The average of the three $\log D_{7.4}$ values per 1-octanol:buffer ratio was calculated. If the two mean values obtained for a compound did not differ by more than 0.1 unit, the results were accepted.

Parallel artificial membrane permeation assay (PAMPA). $\log P_e$ was determined in a 96-well format with the PAMPA [30] permeation assay. For each compound, measurements were performed at three pH values (5.0, 6.2, 7.4) in quadruplicates. For this purpose, 12 wells of a deep well plate, i.e., four wells per pH-value, were filled with 650 µL System Solution. Samples (150 µL) were withdrawn from each well to determine the blank spectra by UV-spectroscopy (SpectraMax 190, Molecular Devices, Silicon Valley Ca, USA). Then, analyte dissolved in DMSO was added to the remaining System Solution to yield 50 µM solutions. To exclude precipitation, the optical density was measured at 650 nm, with 0.01 being the threshold value. Solutions exceeding this threshold were filtrated. Afterwards, samples (150 µL) were withdrawn to determine the reference spectra. Further 200 µL were transferred to

each well of the donor plate of the PAMPA sandwich (pIon, Woburn MA, USA, P/N 110 163). The filter membranes at the bottom of the acceptor plate were impregnated with 5 µL of GIT-0 Lipid Solution and 200 µL of Acceptor Sink Buffer were filled into each acceptor well. The sandwich was assembled, placed in the GutBox^{TM}, and left undisturbed for 16 h. Then, it was disassembled and samples (150 µL) were transferred from each donor and acceptor well to UV-plates. Quantification was performed by both UV-spectroscopy and LC-MS. logP_e-values were calculated with the aid of the PAMPA Explorer Software (pIon, version 3.5).

pK_a values. The pK_a values were determined as described elsewhere [40]. Briefly, the pH of a sample solution was gradually changed and the chemical shift of protons adjacent to ionizable centers was monitored by ^{1}H nuclear magnetic resonance (NMR) spectroscopy. The shift was plotted against the pH of the respective sample and the pK_a was read out from the inflection point of the resulting sigmoidal curve.

Solubility. Solubility was determined in a 96-well format using the µSOL Explorer solubility analyzer (pIon, version 3.4.0.5). For each compound, measurements were performed at three pH values (3.0, 5.0, 7.4) in triplicates. For this purpose, nine wells of a deep well plate, i.e. three wells per pH value, were filled with 300 µL of an aqueous universal buffer solution. Aliquots (3 µL) of a compound stock solution (40-100 mM in DMSO) were added and thoroughly mixed. The final sample concentration was 0.4-1.0 mM, the residual DMSO concentration was 1.0% (v/v) in the buffer solutions. After 15 h, the solutions were filtrated (0.2 µm 96-well filter plates) using a vacuum to collect manifold (Whatman Ltd., Maidstone, UK) to remove any precipitates. Equal amounts of filtrate and n-propanol were mixed and transferred to a 96-well plate for UV detection (190 to 500 nm). The amount of material dissolved was calculated by comparison with UV spectra obtained from reference samples, which were prepared by dissolving compound stock solution in a 1:1 mixture of buffer and n-propanol (final concentrations 0.067-0.167 mM).

LC-MS measurements. Analyses were performed using a 1100/1200 Series HPLC System coupled to a 6410 Triple Quadrupole mass detector (Agilent Technologies, Inc., Santa Clara CA, USA) equipped with electrospray ionization. The system was controlled with the Agilent MassHunter Workstation Data Acquisition software

(version B.01.04). The column used was an Atlantis® T3 C18 column (2.1 x 50 m) with a 3-µm particle size (Waters Corp., Milford MA, USA). The mobile phase consisted of two eluents: solvent A (H_2O, containing 0.1% formic acid, v/v) and solvent B (acetonitrile, containing 0.1% formic acid, v/v), both delivered at 0.6 mL/min. The gradient was ramped from 95% A/5% B to 5% A/95% B over 1 min, and then hold at 5% A/95% B for 0.1 min. The system was then brought back to 95% A/5% B, resulting in a total duration of 4 min. MS parameters such as fragmentor voltage, collision energy, polarity were optimized individually for each drug, and the molecular ion was followed for each compound in the multiple reaction monitoring mode. The concentrations of the analytes were quantified by the Agilent Mass Hunter Quantitative Analysis software (version B.01.04).

***In vitro* activity**

Bacteria and growth. The clinical *E. coli* isolate UTI89 [41] (UTI89wt) and the FimA-H knock-out strain UTI89 Δ*fimA-H* were kindly provided by the group of Prof. Urs Jenal, Biocenter, University of Basel. Bacterial strains (UTI89 *wt* and UTI89 Δ*fimA-H*) labeled with green fluorescence protein (GFP) were prepared as previously described by Scharenberg et al. [33]. Microorganisms were stored at -70 °C and before experiments incubated for 24 h under static conditions at 37 °C in 10 mL Luria-Bertani broth (Becton, Dickinson and Company, Le Pont de Claix, France) using 50 mL tubes. Prior to each experiment, the microorganisms were washed twice and re-suspended in phosphate buffered saline (PBS, Sigma, Steinheim, Germany) for aggregometry measurements or in RPMI 1640 without supplements for infection experiments. Bacterial concentration was determined by plating serial 1:10 dilutions on blood agar, followed by colony counting with 20 - 200 colonies after overnight incubation at 37 °C.

Cultivation of 5637 cells. The human epithelial bladder carcinoma cell line 5637 was obtained from the German Collection of Microorganisms and Cell Cultures (DSMZ, Braunschweig, Germany). The cells were grown in RPMI 1640 medium, supplemented with 10% fetal calf serum (FCS), 100 U/mL penicillin and 100 µg/mL streptomycin at 37 °C, 5% CO_2. All solutions were purchased from Invitrogen (Basel, Switzerland). The cells were sub-cultured 1:5 twice per week for six passages before using them in the infection assay. Two days before infection, 1.8 x 10^5 cells were

seeded in each well of a 24-well plate in RPMI 1640 containing 10% FCS without antibiotics. The cell density was approximately 3-5 x 10^5 cells/well prior the infection.

Aggregometry assay. The aggregometry assay was carried out as previously described [32]. In short, the percentage of aggregation of *E. coli* UTI89 with guinea pig erythrocytes (GPE) was quantitatively determined by measuring the optical density at 740 nm and 37 °C under stirring at 1000 rpm using an APACT 4004 aggregometer (Endotell AG, Allschwil, Switzerland). Bacteria were cultivated as described above. GPE were separated from guinea pig blood (Charles River Laboratories, Sulzfeld, Germany) using Histopaque (density of 1.077 g/mL at 24 °C, Sigma-Aldrich, Buchs, Switzerland). Prior to the measurements, the cell densities of *E. coli* and GPE were adjusted to an OD_{600} of 4, corresponding to 1.9×10^8 CFU/mL and 2.2×10^6 cells/mL respectively. For the calibration of the instrument, the aggregation of protein poor plasma (PPP) using PBS alone was set as 100% and the aggregation of protein rich plasma (PRP) using GPE as 0%. After calibration, measurements were performed with 250 μL GPE and 50 μL bacterial suspension and the aggregation monitored over 600 s. After the aggregation phase of 600 s, 25 μL of antagonist in PBS was added to each cuvette and disaggregation was monitored for 1400 s. UTI89 Δ*fimA-H* was used as negative control. IC_{50} values were determined by plotting the concentration of the antagonist in logarithmic mode versus the area under the disaggregation curves ($AUC_{600\text{-}2000s}$) by fitting the curve log c with the prism software (GraphPad, inhibition curve, variable slope).

Flow cytometry infection assay. The infection assay was carried out as previously described [33]. Briefly, 5637 cells, grown in 24-well plates (as described above), were infected with 200 µL bacterial suspension at a multiplicity of infection (MOI) of 1:50 (cell:bacteria). To homogenize the infection, plates were centrifuged at room temperature for 3 min at 600 g. After an incubation of 1.5 h at 37 °C, infected cells were washed four times with RPMI 1640 medium and suspended in ice-cold PBS for 5-20 min. Cells were then kept in the dark until analysis. All measurements were made within 1 h after the termination of the infection. Samples were acquired in a CyAn ADP flow cytometer (Becton Dickinson, San Jose, CA) and analyzed by gating on the eukaryotic cells based on forward (FSC) and side scatter (SSC), which excludes unbound labeled bacteria and debris from analysis. A total of 10^4 cells were

measured per sample. Data were acquired in a linear mode for the side scatter (SSC) and logarithmic mode for the forward scatter (FSC), and the green fluorescent channel FL1-H (e.g. GFP). The mean fluorescence intensity (MFI) of FL1-H was counted as a surrogate marker for the adherence of bacteria. Quantification of adhesion was evaluated with the FlowJow software 9.0.1 (Tree Star, Inc., Ashland, OR, USA).

Inhibition assay. To evaluate FimH antagonists, a serial dilution of the antagonists in 5% DMSO was prepared. Before infection, bacterial suspension (200 µL) and 25 µL of the test compound were pre-incubated for 10 min at room temperature. The bacteria-antagonist mixture was then added to the monolayer of 5637 cells. Infection, measurement, and quantification of adhesive bacteria were performed as described above. IC_{50} values were determined by plotting the concentration of the antagonist in logarithmic mode versus the MFI and by fitting the curve log c with the prism software (GraphPad, inhibition curve, variable slope), (n=2-3, in duplicates/ triplicates).

***In vivo* pharmacokinetic and disease model**

Animals. Female C3H/HeN mice weighting between 19 and 25 g were obtained from Charles River (Sulzfeld, Germany) and were housed three to a cage. Mice were kept under specific-pathogen-free conditions in the Animal House of the Department of Biomedicine, University Hospital Basel, and animal experimentation guidelines according to the regulations of Swiss veterinary law were followed. After seven days of acclimatization, 9- to 10-week old mice were used for the PK and infection studies. During the studies, animals were allowed free access to chow and water. Three days before infection studies and during infection, 5 % D-(+)-glucose (AppliChem, Baden-Dättwil, Switzerland) was added to the drinking water [43].

Pharmacokinetic studies. Single-dose pharmacokinetic studies were performed by i.v. application of the FimH antagonist (**6b**) at concentrations of 25, 50 and 100 mg/kg. The antagonist was diluted in 100 µL PBS and injected into the tail vein, followed by blood and urine sampling (10 µL) after 6 min, 30 min, 45 min, 1 h, 1 h 15 min, 1 h 30 min, 1 h 45 min, 2 h, 2 h 30 min, 3 h, 4 h, 5 h 6 h, 8 h and 24 h. Before analysis, proteins in blood and urine samples were precipitated using methanol (Acros Organics, Basel, Switzerland) and centrifuged for 11 min at 13’000 rpm. The

supernatant was transferred into a 96-well plate (0.5 mL, polypropylene, Agilent Technologies, Basel, Switzerland) and analyzed by LC-MS as described above.

UTI mouse model. Mice were infected as previously described [42]. In brief, before infection all remaining urine was depleted form the bladder by gentle pressure on the abdomen. Mice were anesthetized with 1.1 vol% isoflurane/oxygen mixture (Attane, Minrad Inc, Buffalo, NY, USA) and placed on their back. Anesthetized mice were inoculated transurethrally with the bacterial suspension by use of a 2 cm polyethylene catheter (Intramedic polyethylene tubing, inner diameter 0.28 mm, outer diameter 0.61 mm, Beckton Dickinson, Allschwil, Switzerland), which was placed on a syringe (Hamilton Gastight Syringe 50 µL, removable 30G needle, BGB Analytik AG, Boeckten, Switzerland). The catheter was gently inserted through the urethra until it reached the top of the bladder, followed by slow injection of 50 µL bacterial suspension at a concentration of approximately 10^9 to 10^{10} CFU/mL.

Treatment studies. Three concentrations of **6b** (25, 50, 100 mg/kg) were applied i.v. in 100 - 200 µL PBS into the tail vein and ciprofloxacin (8 mg/kg, Bayer Scherig Pharma, Germany) was injected subcutaneously. Both, the FimH antagonist and antibiotic were applied 10 minutes before infection. 3 h after the onset of infection, urine was collected by gentle pressure on the abdomen and then the mouse was sacrificed with CO_2. Organs were removed aseptically and homogenized in 1 mL PBS by using a tissue lyser (Retsch, Haan, Germany). Serial dilutions of urine, bladder and kidneys were plated on Levine Eosin Methylene Blue Agar plates (Beckton Dickinson, Le Pont de Claix, France). CFU counts were determined after over night incubation at 37 °C and expressed as CFU/mL for the urine and CFU/bladder and CFU/2 kidneys for the organs.

References

1 Hamad, B. The antibiotics market. *Nat. Rev. Drug Discov.* **2010**, 9, 675.

2 Fischbach, M. A.; Walsh, C. T. Antibiotics for emerging pathogens. *Science* **2009**, 325, 1089.

3 Rasko, D. A.; Sperandio, V. Anti-virulence strategies to combat bacteria-mediated disease. *Nat Rev Drug Discov*. **2010**, 9, 117-128.

4 Lee, Y. M.; Almqvist, F,; Hultgren, S. J. Targeting virulence for antimicrobial chemotherapy. *Curr Opin Pharmacol* **2003**, 3, 513–519.

5 Alksne, L. E.; Projan, S. J. Bacterial virulence as a target for antimicrobial chemotherapy. *Curr Opin in Biotech* **2000**, 11, 625–636.

6 Clatworthy, A. E.; Pierson, A.; Hung, D. T. Targeting virulence: a new paradigm for antimicrobial therapy. *Nat Chem Biol* **2007**, 3, 541–548.

7 Fihn, S. D. Clinical practice. Acute uncomplicated urinary tract infection in women. *N. Engl. J. Med.* **2003**, *349*, 259-266.

8 Hooton, T. M. Recurrent urinary tract infection in women. *Int. J. Antimicrob. Agents* **2001**, *17*, 259-268.

9 Wiles, T. J.; Kulesus, R. R.; Mulvey, M. A. Origins and virulence mechanisms of uropathogenic *Escherichia coli*. *Exp. Mol. Pathol.* **2008**, *85*, 11-19.

10 Gouin, S. G.; Wellens, A.; Bouckaert, J.; Kovensky, J. Synthetic Multimeric Heptyl Mannosides as Potent Antiadhesives of Uropathogenic *Escherichia coli*. *ChemMedChem* **2009**, *4*, 749-755.

11 Rosen, D. A.; Hung, C. S.; Kline, K. A.; Hultgren, S. J. Streptozocin-induced diabetic mouse model of urinary tract infection. *Infect. Immun.* **2008**, *76*, 4290-4298.

12 Mulvey, M. A. Adhesion and entry of uropathogenic *Escherichia coli. Cell Microbiol.* **2002**, 4, 257-271.

13 Capitani, G.; Eidam, O.; Glockshuber, R.; Grutter, M. G. Structural and functional insights into the assembly of type 1 pili from *Escherichia coli*. *Microbes Infect.* **2006**, *8*, 2284-2290.

14 Choudhury, D.; Thompson, A.; Stojanoff, V.; Langermann, S.; Pinkner, J.: Hultgren, S. J.; Knight, S. D. X□ray structure of the FimC–FimH chaperone–adhesin complex from uropathogenic *Escherichia coli*. *Science* **1999**, *285*, 1061-1066.

15 Wellens, A.; Garofalo, C.; Nguyen, H.; Van Gerven, N.; Slättergård, R.; Hernalsteens, J.-P.; Wyns, L.; Oscarson, S.; De Greve, H.; Hultgren, S.; Bouckaert, J. Intervening with urinary tract infections using anti-adhesives based on the crystal structure of the FimH-oligomannose-3 complex. *PLoS ONE* **2008**, *3*, 4-13.

16 Bouckaert, J.; Mackenzie, J.; de Paz, J. L.; Chipwaza, B.; Choudhury, D.; Zavialov, A.; Mannerstedt, K.; Anderson, J.; Pierard, D.; Wyns, L.; Seeberger, P. H.; Oscarson, S.; De Greve; H., Knight, S. D. The affinity of the FimH fimbrial adhesin is receptor-driven and quasi-independent of *Escherichia coli* pathotypes. *Mol. Microbiol.* **2006**, *61*, 1556-1568.

17 Hartmann, M. and Lindhorst, T. K. The Bacterial Lectin FimH, a Target for Drug Discovery – Carbohydrate Inhibitors of Type 1 Fimbriae-Mediated Bacterial Adhesion. *Eur J Org Chem* **2011**, 3583-3609.

18 Aronson, M.; Medalia, O.; Schori, L.; Mirelman, D.; Sharon, N.; Ofek, I. Prevention of colonization of the urinary tract of mice with *Escherichia coli* by blocking of bacterial adherence with methyl α-D-mannopyranoside. *J. Infect. Dis.* **1979**, *139*, 329-332.

19 Svanborg Eden, C.; Freter, R.; Hagberg, L.; Hull, R.; Leffer, H.; Schoolnik, G. Inhibition of experimental ascending urinary tract infection by an epithelial cell-surface receptor analog. *Nature* **1982**, *298*, 560-562.

20 Klein, T.; Abgottspon, D.; Wittwer, M.; Rabbani, S.; Herold, J.; Jiang, X.; Kleeb, S.; Lüthi, C.; Scharenberg, M.; Bezenc¸on, J.; Gubler, E.; Pang, L.; Smiesko, M.; Schwardt, O.; Ernst, B. FimH Antagonists for the oral treatment of urinary tract infections: from design and synthesis to in vitro and in vivo evaluation. *J Med Chem* **2010**, 53, 8627–8641.

21 Han Z, Pinker JS, Ford B, Obermann R, Nolan W, Wildman SA, Hobbs D, Ellenberger T, Cusumano CK, SJ, Janetka JW. Structure-based drug design and optimization of mannoside bacterial FimH antagonists. *J. Med. Chem.* **2010**, *53*, 4779.

22 Cusumano, C. K.; Pinkner, J. S.; Han, Z.; Greene, S. E.; Ford, B. A.; Crowley, J. R.; Henderson, J. P.; Janetka, J. W.; Hultgren, S. J. Treatment and prevention of urinary tract infection with orally active FimH inhibitors. *Sci Transl Med* **2011**, 3, 109-115.

23 Han, Z.; Pinkner, J. S.; Ford, B.; Chorell, E.; Crowley, J. R.; Cusumano, C. K.; Campbell, S.; Henderson, J. P.; Hultgren, S. J. Lead optimization studies on FimH antagonists: discovery of potent and orally bioavailable ortho-substituted biphenyl mannosides. *J Med Chem* **2012**, 55, 3945-3959.

24 Guiton, P. S.; Cusumano, C. K.; Kline, K. A.; Dodson, K. W.; Han, Z.; Janetka, J. W.; Henderson, J. P.; Caparon, M. G.; Hultgren, S. J. Combination small molecule therapy prevents uropathogenic Escherichia coli catheter-associated urinary tract infections in mice. *Antimicrob Agents Chemother* **2012**, 56, 4738-4745.

25 Jiang, X.; Abgottspon, D.; Kleeb, S.; Rabbani, S.; Scharenberg, M.; Wittwer, M.; Haug, M.; Schwardt, O.; Ernst, B. Antiadhesion Therapy for Urinary Tract Infections – A Balanced PK/PD Pofile Proved to be Key for Success. *J Med Chem* **2012**, 55, 4700-4713.

26 Sperling, O., Fuchs, A. & Lindhorst, T. K. Evaluation of the carbohydrate recognition domain of the bacterial adhesin FimH: design, synthesis and binding properties of mannoside ligands. Org. Biomol. Chem. **2006,** 4, 3913–3922.

27 (a) A. Vervoort, C. K. De Bruyne, *Carbohydr. Res.* **1970**, *12*, 277-280; (b) J. De Prijcker, A. De Bock, C. K. De Bruyne, *Carbohydr. Res.* **1978**, *60*, 141-53.

28 J. R. Kosak, *Ann. N. Y. Acad. Sci.* **1970**, *172*, 175-185.

29 Varma, M. V. S.; Feng, B.; Obach, R. S.; Troutman, M. D.; Chupka, J.; Miller, H. R.; El-Kattan, A. Physicochemical Determinants of Human Renal Clearance. *J. Med. Chem.* **2009**, *52*, 4844-4852.

30 Kansy, M.; Senner, F.; Gubernator, K. Physicochemical High Throughput Screening: Parallel Artificial Membrane Permeation Assay in the Description of Passive Absorption Processes. *J. Med. Chem.* **1998**, *41*, 1007-1010.

31 Avdeef, A.; Bendels, S.; Di, L.; Faller, B.; Kansy, M.; Sugano, K.; Yamauchi, Y. Parallel artificial membrane permeability assay (PAMPA)-critical factors for better predictions of absorption. *J. Pharm. Sci.* **2007**, *96*, 2893-2909.

32 Abgottspon, D.; Rölli, G.; Hosch, L.; Steinhuber, A.; Jiang, X.; Schwardt, O.; Cutting, B.; Smiesko, M.; Jenal, U.; Ernst, B.; Trampuz, A. Development of an Aggregation Assay to Screen FimH Antagonists. *J. Microbiol. Methods* **2010**, 82, 249**–**255.

33 Scharenberg, M.; Abgottspon, D.; Ciceck, E.; Jiang, X., Schwardt, O.; Rabbani, S.; Ernst, B. Flow Ctometry-Based Assay for Screening FimH Antagonists. *Assay Drug Dev Technol.* **2011**, 9, 455-464.

34 Hooton, T. M.Fluoroquinolones and resistance in the treatment of uncomplicated urinary tract infection. *Int. J. Antimicrob. Agents* 2003, 22, 65–72

35 Jakobsen, L.; Cattoir, V.; Hammerum, A. M.; Nordmann, P.; Frimodt-Møller, N. Impact of low-level fluoroquinolone resistance genes qnrA1, qnrB19, and qnrS1 on ciprofloxacin treatment of *Escherichia coli* urinary tract infection in murine model. Poster presented at the 50th Interscience Conference on Antimicrobial Agents and Chemotharapy, **2010**, Sep 12–15, Boston, MA.

36 Langermann, S.; Palaszynski, S.; Barnhart, M.; Auguste, G.; Pinkner, J. S.; Burlein, J.; Barren, P.; Koenig, S.; Leath, S.; Jones, C. H.; Hultgren, S. J. Prevention of mucosal *Escherichia coli* infection by FimH-adhesin-based systemic vaccination. *Science* **1997**, 276, 607-611.

37 Mulvey, M. A.; Schilling, J. D.; Martinez, J. J.; Hultgren, S. J. Bad bugs and beleaguered bladders: interplay between uropathogenic *Escherichia coli* and innate host defense. *Proc. Natl. Acad. Sci. USA* **2000**, 97, 8829-8835.

38 Johnson, J. R. and Brown J. J. Defining Inoculation Conditions fort he Mouse Model of Ascending Urinary Tract Infection that Avoidf Immediate Vesicourethral Reflux yet Produce Renal and Bladder Infection. *J. Inf. Dis.* **1996**, 173, 746-749.

39 (a) VCCLAB, Virtual Computational Chemistry Laboratory; http://www.vcclab.org, 2005; (b) Tetko,I. V.; Gasteiger, J.; Todeschini, R.; Mauri, A.; Livingstone, D.; Ertl, P.; Palyulin, V. A.; Radchenko, E. V.; Zefirov, N. S.; Makarenko, A. S.; Tanchuk, V. Y.; Prokopenko, V. V. Virtual computational chemistry laboratory – design and description. *J. Comput. Aid. Mol. Des.* **2005**, 19, 453-463.

40 Wittwer, M.; Bezençon, J.; Cutting, B.; Wagner, B.; Kansy M.; Ernst, B. pK_a determination by ^{1}H-NMR spectroscopy – an old methodology revisited. Unpublished results.

41 Mulvey, M. A.; Schilling, J. D.; Hultgren, S. J. Establishment of a persistent *Escherichia coli* reservoir during the acute phase of a bladder infection. *Infect. Immun.* **2001**, 69, 4572-4579.

42 Kerrn, M. B.; Frimodt-Møller, N.; Espersen, F. Effects of Sulfomethizole and Amdinocillin against *Escherichia coli* Strains (with Various Susceptibilities) in an Ascending Urinary Tract Infection Model. *Antimicrob. Agents Chemother.* **2003**, 47, 1002-1009.

RESULTS AND DISCUSSION

Manuscript II

In vivo Pharmacokinetic/Pharmacodynamic Evaluation of JXH2372 – A Biphenyl FimH Antagonist for the Prevention of Urinary Tract Infection.

Abgottspon D, Skovbo Jensen K, Jiang X, Ernst B.

Preliminary manuscript: With outlook for completion.

My contributions:

In vitro evaluation of the inhibitory potency of the FimH antagonists in the flow cytometry infection assay together with Scharenberg M.
In vivo pharmacokinetic and infection studies in the UTI mouse model.
Manuscript preparation.

In vivo Pharmacokinetic/Pharmacodynamic Evaluation of JXH2372 – A Biphenyl FimH Antagonist for the Prevention of Urinary Tract Infection

Daniela Abgottspon[1], Klaus Skovbo Jensen[2], Xiaouah Jiang[1], Beat Ernst*[1]

[1]Institute of Molecular Pharmacy, Pharmacenter, University of Basel, Klingelbergstrasse 50, CH-4056 Basel, Switzerland, [2]CANDOR Simulation, Denmark.

Part of this work was presented at:

As poster (A2-039) at the Interscience Conference on Antimicrobial Agents and Chemotherapy (ICAAC), September 2011, Chicago, USA.

As poster (F2-2057) at the Interscience Conference on Antimicrobial Agents and Chemotherapy (ICAAC), September 2012, San Francisco, USA.

*Correspondence to Prof. Dr. Beat Ernst, Institute of Molecular Pharmacy, Pharmacenter, University of Basel, Klingelbergstrasse 50, CH-4056 Basel, Switzerland

Tel: +41 61 267 1551, Fax: +41 61 267 1552, Email: beat.ernst@unibas.ch

Abstract

Background and aims: Urinary tract infection (UTI) is one of the most common bacterial infections worldwide. UTI is commonly treated with antibiotics, leading to increasing development of resistance. Therefore, alternative treatment options are urgently needed. FimH antagonists represent a new class of antimicrobials, targeting bacterial adhesion. Our aim was to evaluate the pharmacokinetic/pharmacodynamic (PK/PD) index of the biphenyl FimH antagonist JXH2372, which best correlates with therapeutic outcome.

Methods: Cell-based infection assay to determine the minimal anti-adhesion concentration (MAC). PK studies of three different concentrations (25, 50 and 100 mg/kg) of JXH2372 were performed in uninfected mice to determine the AUC and the C_{max}. PD studies were carried out in the UTI mouse model, using the uropathogenic *Escherichia coli* strain UTI89. Determination of the predictive PK/PD parameter (T>MAC, AUC_{0-24}/MAC, C_{max}/MAC) for the therapeutic outcome.

Results: PK studies showed high availability of all three concentrations of JXH2372 in the urine. PD studies resulted in a dose dependent reduction of bacterial counts in the bladder. The best correlation with the infection outcome in the PK/PD evaluation was observed by looking at the AUC_{0-24}/MAC in the bladder (R^2 = 43%).

Conclusion: The FimH antagonist JXH2372 showed hight activity in the UTI mouse model. The most predictive PK/PD parameter suggests, that a constant mean level of antagonist over the MAC is required for an optimal treatment outcome.

Keywords: Uropathogenic *Escherichia coli*, urinary tract infection, FimH antagonist, pharmacokinetics/pharmacodynamics

Introduction

Urinary tract infection (UTI) is one of the most common bacterial infections worldwide. Women are the most affected population and every second woman will experience at least one UTI during her lifetime. Furthermore, catheter-associated UTI accounts for the most common hospital acquired (nosocomial) infection and UTI is the third most acquired infection in intensive care units (ICUs) in Europe.[1] Although UTI is not a life threatening disease, all symptomatic infections should be treated with antibiotics to prevent potential devastating complications, like kidney infections (pyelonephritis), irreversible kidney damage and dissemination from the kidneys to the bloodstream (urosepsis).[2]

The leading pathogen causing UTI is uropathogenic *Escherichia coli* (UPEC), responsible for over 90% of all infections.[3] UPEC colonize the normally sterile urinary tract in an ascending manner. The decisive virulence mechanism of UPEC colonization is their adhesion capability, using filamentous multi-subunit membrane proteins (pili or fimbriae).[4] The first and most important pili employed for the initial entry into the urethra (urethritis) and the bladder (cystitis) are type 1 pili, where the mannose-dependent attachment to the glycosylated uroplakin Ia (UPIa) present on bladder cells is mediated by the fimbrial adhesin H (FimH). Furthermore, bacteria can ascend through the urethers into the kidneys (pyelonephritis), where the adhesion is specifically mediated via P pili in a galactose dependent manner.[5-8]

Type 1 pili are filamentous multi-subunit appendages (consisting of FimA, FimF, FimG and FimH), able to bind to α-mannoside containing glycoprotein receptors on the surface of uroepithelial cells, such as uroplakin 1a (UP1a).[9,10] Adhesion is mediated via the carbohydrate-recognition domain (CRD) of FimH, a protein located on the distal tip of the type 1 pilus. This initial step of the infection process prevents the rapid clearance of *E. coli* from the urinary tract by the bulk flow of urine and enables bacteria to invade the target cells.[3,11-16] FimH antagonists such as α-D-mannopyranosides are able to effectively prevent the FimH dependent adhesion and invasion of host cells. No infection can occur and bacteria are cleared from the urinary tract by the flow of urine.[17] Hence, they provide a novel therapeutic

opportunity for the treatment and prevention of UTIs as an alternative to conventional antibiotic treatment.[2,18,19]

Different classes of FimH antagonists were identified as potential new anti-adhesion compounds, able to prevent and treat UPEC associated UTIs in mice.[20-25] A promising compound family is a series of biphenyl α-D-mannopyranoside derivatives. We previously described the design, synthesis and biological evaluation (*in vitro* and *in vivo*) of the biphenyl FimH antagonist JXH2372 (Figure 1).[20] JXH2372 showed high activity in the *in vitro* cell-based assays and resulted in a significant reduction of bacterial counts of over 4 orders of magnitude in the bladder of mice after a single i.v. application of 50 mg/kg.

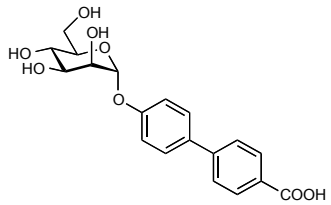

Figure 1. The chemical structure of the biphenyl α-D-mannopyranoside JXH2372 used through out these studies.

The activity of antibiotics against a pathogen is traditionally determined as the minimal inhibitory concentration (MIC) and is defined as the lowest concentration of a drug that inhibits visible growth of an organism.[26] Although FimH antagonists are antimicrobial agents, the MIC is not applicable for the determination of their activity, due to their different mode of action (they neither kill nor inhibit the growth of bacteria). Therefore, we express the activity of FimH antagonists as the minimal anti-adhesion concentration (MAC), which can be used for the determination of the therapeutic dosage *in vivo*. The MAC is defined as the concentration of antagonist leading to 90% inhibition of adhesion of the pathogen to the target cells (IC_{90}) and was evaluated in a cell-based infection assay.[27]

The traditional MIC is a valuable index to determine the antimicrobial potency of a drug. However, it lacks the ability to inform about the time course needed for an optimal antimicrobial activity, which is a key factor for the choice of a successful therapy.[28,29] To choose the optimal treatment regimen (dosage and time course),

pharmacokinetic/pharmacodynamic (PK/PD) studies are needed, combining the results from the drug concentration over time (PK) with the activity over time (PD). PK/PD studies are applicable and often used for antibiotics, however, nothing is known about the PK/PD correlation for anti-adhesion therapy using FimH antagonists. Therefore, we performed PK/PD studies of various dosages and dosage regimens of JXH2372 in the UTI mouse model.[30] With these experiments, we aimed for the identification of the PK/PD index, which most closely predicts the efficacy of the FimH antagonist.

Material and Methods

Bacterial strains and growth conditions

The clinical *E. coli* isolate UTI89 (UTI89wt)[31] was kindly provided by the group of Prof. Urs Jenal, Biocenter, University of Basel. Microorganisms were stored at -70 °C and before experiment incubated for 24 h under static conditions at 37 °C in 10 mL Luria-Bertani broth (Becton, Dickinson and Company, Le Pont de Claix, France) using 50 mL tubes. Prior to each experiment, the microorganisms were washed twice and re-suspended in phosphate buffered saline (PBS, Sigma, Steinheim, Germany). Bacterial concentration was determined by plating serial 1:10 dilutions on blood agar, followed by colony counting with 20 - 200 colonies after overnight incubation at 37 °C.

Cultivation of 5637 cells

The human epithelial bladder carcinoma cell line 5637 was obtained from the German Collection of Microorganisms and Cell Cultures (DSMZ, Braunschweig, Germany). The cells were grown in RPMI 1640 medium, supplemented with 10% fetal calf serum (FCS), 100 U/mL penicillin and 100 µg/mL streptomycin at 37°C, 5% CO_2. All solutions were purchased from Invitrogen (Basel, Switzerland). The cells were sub-cultured 1:5 twice per week for six passages before using them in the infection assay. Two days before infection, 1.8 x 10^5 cells were seeded in each well of a 24-well plate in RPMI 1640 containing 10% FCS without antibiotics. The cell density was approximately 3-5 x 10^5 cells/well prior the infection.

Flow cytometry infection assay for the determination of the minimal anti-adhesion concentration (MAC)

The infection assay was carried out as previously described.[27] Briefly, to evaluate FimH antagonists, a serial dilution of the antagonists in 5% DMSO was prepared. Before infection, a suspension of green fluorescently labeled (GFP) bacteria (UTI89, 200 µL) and 25 µL of the test compound were pre-incubated for 10 min at room temperature. The bacteria-antagonist mixture was then added to the monolayer of 5637 cells (grown in 24-well plates, as described above) at a multiplicity of infection (MOI) of 1:50 (cell:bacteria). To homogenize the infection, plates were centrifuged at room temperature for 3 min at 600 g. After an incubation of 1.5 h at 37°C, infected cells were washed four times with RPMI 1640 medium and suspended in ice-cold PBS for 5-20 min. Cells were then kept in the dark until analysis. All measurements were made within 1 h after the termination of the infection. Samples were acquired in a CyAn ADP flow cytometer (Becton, Dickinson and Company) and analyzed by gating on the eukaryotic cells based on forward (FSC) and side scatter (SSC), which excludes unbound GFP-labeled bacteria and debris from analysis. A total of 10^4 cells were measured per sample. Data were acquired in a linear mode for the side scatter (SSC) and in a logarithmic mode for the forward scatter (FSC), and the green fluorescent channel FL1-H (e.g. GFP). The mean fluorescent intensity (MFI) of FL1-H was counted as a surrogate marker for the adherence of bacteria. Quantification of adhesion was evaluated with the FlowJo software 9.0.1 (Tree Star, Inc., Ashland, OR, USA). IC_{50} values were determined by plotting the concentration of the antagonist in logarithmic mode versus the MFI and by fitting the curve with the prism software (GraphPad, inhibition curve, nonlinear regression, variable slope, n = 4). The IC_{90} (F=90) was calculated from the determined IC_{50} value and the hill slope (H) as follows:

$$IC_F = \left(\frac{F}{100 - F}\right)^{1/H} \bullet IC_{50}$$

Animals

Female C3H/HeN mice weighting between 19 and 25 g were obtained from Charles River (Sulzfeld, Germany) and were housed three to a cage. Mice were kept under specific-pathogen-free conditions in the Animal House of the Department of Biomedicine, University Hospital Basel, and animal experimentation guidelines according to the regulations of Swiss veterinary law were followed. After seven days

of acclimatization, 9- to 10-week old mice were used for the PK and infection studies. During the studies, animals were allowed free access to chow and water. Three days before infection studies and during infection, 5 % D-(+)-glucose (AppliChem, Baden-Dättwil, Switzerland) was added to the drinking water.[30]

Pharmacokinetic studies

Single-dose pharmacokinetic studies were performed by i.v. application of the FimH antagonist JXH2372 at increasing concentrations of 25, 50 and 100 mg/kg. The antagonist was diluted in 100 - 200 µL PBS and injected into the tail vein, followed by blood and urine sampling (10 µL at each time point) after 6 min, 15 min, 30 min, 45 min, 1 h, 1 h 30 min, 2 h, 2 h 30 min, 3 h, 4 h, 5 h 6 h, 8 h and 24 h. Before analysis, proteins in blood and urine samples were precipitated using methanol (Acros Organics, Basel, Switzerland) and centrifuged for 11 min at 13'000 rpm. The supernatant was transferred into a 96-well plate (0.5 mL, polypropylene, Agilent Technologies, Basel, Switzerland) and analyzed by LC-MS as previously described.[20]

A linear 1-compartment model was fitted to the plasma concentration data and thereafter expanded into a 2-compartment model (a "bladder compartment" was added) to be fitted to the urine concentration data.

UTI mouse model

Mice were infected as previously described.[30] In brief, before infection all remaining urine was depleted form the bladder by gentle pressure on the abdomen. Mice were anesthetized with 1.1 vol% isoflurane/oxygen mixture (Attane, Minrad Inc, Buffalo, NY, USA) and placed on their back. Anesthetized mice were inoculated transurethrally with the bacterial suspension by use of a 2 cm polyethylene catheter (Intramedic polyethylene tubing, inner diameter 0.28 mm, outer diameter 0.61 mm, Beckton Dickinson, Allschwil, Switzerland), which was placed on a syringe (Hamilton Gastight Syringe 50 µL, removable 30G needle, BGB Analytik AG, Boeckten, Switzerland). The catheter was gently inserted through the urethra until it reached the top of the bladder, followed by slow injection of 50 µL bacterial suspension at a concentration of approximately 10^9 to 10^{10} CFU/mL.

Pharmacodynamic studies

Various dosage regimens of length T = 3 hours were applied, starting 10 minutes before infection (JXH2372 bolus doses of 25, 50, or 100 mg/kg in 100 - 200 μL PBS were injected i.v. into the tail vein). Three hours after the onset of infection, urine was collected by gentle pressure on the abdomen and then the mouse was sacrificed with CO_2. Organs were removed aseptically and homogenized in 1 mL PBS by using a tissue lyser (Retsch, Haan, Germany). Serial dilutions of urine, bladder and kidneys were plated on Levine Eosin Methylene Blue Agar plates (Beckton Dickinson, Le Pont de Claix, France). CFU counts were determined after over night incubation at 37 °C and expressed as CFU/bladder and CFU/2 kidneys for the organs.

Results

Determination of the minimal anti-adhesion concentration (MAC)

The MAC was determined in the flow cytometry infection assay. Therefore, human bladder cells were infected with GFP labeled UPEC (strain UTI89) in the presence of different concentrations of FimH antagonists and analyzed by flow cytometry.[25,27] The half-maximal inhibitory concentration (IC_{50}) was calculated by plotting the mean fluorescent intensity (MFI) of the cells versus the concentration of the antagonist. From this plot, the concentration where 90% bacterial adhesion to human bladder cells is inhibited (IC_{90}) can be deduced and is defined as the minimal anti-adhesion concentration (MAC).[25] The FimH antagonist JXH2372 exhibited an IC_{50} of 0.82 ± 0.6 µM in the flow cytometry infection assay. The calculated IC_{90} is 11.5 µM and the corresponding MAC is 4.6 µg/mL. The MAC value of JXH2372 is substituting the MIC for the PK/PD studies during this work.

PK/PD studies

The studies described here, were carried out to determine the PK/PD index (T>MAC, $AUC_{0\text{-}24}$/MAC, C_{max}/MAC) which best correlates with the therapeutic outcome in the UTI mouse model. The single dose PK studies showed dose-dependent elevations of plasma and urine concentrations of JXH2372 in mice (Figure 2), except for urine concentrations of 50 mg/kg. Peak levels in both, plasma and urine were observed within 6 minutes after application and also show increased values for higher concentrations.

Dosage [mg/kg]	**Compartment**	**AUC_{0-24}** [µg x h/mL]	**T>MAC** [h]	**C_{max}** [µg/mL]
25	Plasma	6.3	0.52	20
	Urine	716	1.9	3620
50	Plasma	20	1.2	34
	Urine	49	2.3	40
100	Plasma	35	1.1	104
	Urine	4050	2.9	8520

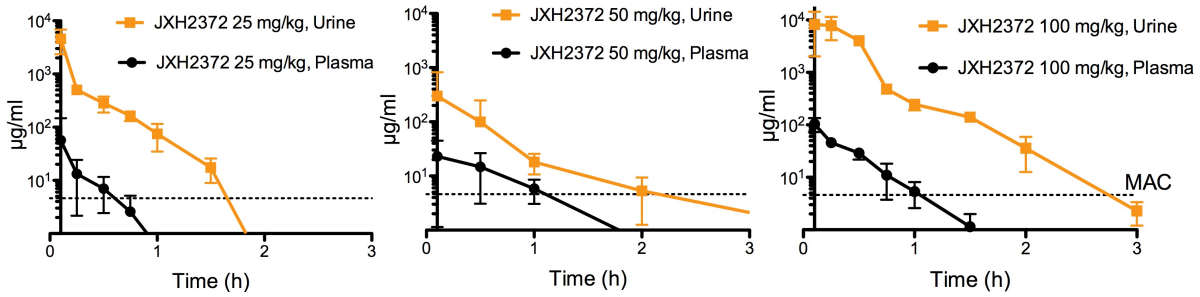

Figure 2. PK/PD study of three different dosages (25, 50, 100 mg/kg) of JXH2372. The concentration of antagonist in urine and plasma after a single i.v. application was determined using LC-MS (*n* = 6). Graphs show time dependent urine and plasma concentrations. T: time; MAC: minimal anti-adhesion concentration; AUC_{0-24}: area under the curve over 24 hours; C_{max}: peak concentration.

The PD studies were carried out in the UTI mouse model. The compound was applied 10 minutes prior to inoculation with UPEC and infection was terminated after 3 h. Urine, bladder and kidneys were collected for determination of bacterial concentration. The mean bacterial counts of the untreated control group showed values of 1.4 x 10^8 colony forming units (CFU) in the bladder and 9.7 x 10^6 CFU in the kidneys. The bar diagram in Figure 3 b shows the bacterial reduction compared to the control group after treatment with JXH2372. A dose dependent decrease of bacterial counts in the bladder was observed, with 25 mg/kg resulting in a -2.1 $\log_{10}$ CFU reduction, 50 mg/kg resulting in -4.6 $\log_{10}$ CFU and 100 mg/kg resulting in -5.1 $\log_{10}$ CFU. No dose dependent reduction of bacterial counts was observed in the kidneys (- 2.8 $\log_{10}$ CFU for 25 mg/kg, -1.9 $\log_{10}$ CFU for 50 mg/kg, -2.8 $\log_{10}$ CFU for 100 mg/kg).

Testing of various dosage regimens in the UTI mouse model for prediction of the significant PK/PD parameter

Based on the PK studies (Figure 2), a selection of dosage regimens was chosen for the PD studies in the UTI mouse model (Figure 3 a). The first bolus dose in a regimen was always administered 10 minutes prior to infection. Regimen Y showed the highest efficacy with a bacterial reduction of -4.7 log_{10} units (Figure 3 b). Regimens L and Z resulted both in a -4.4 log_{10} CFU reduction, whereas regimens M and X were less effective with -3.7 log_{10} CFU and -2.6 log_{10} CFU, respectively.

(a)

Dosage regimen	Dose [mg/kg]	Dosing interval [h]	Total dose [mg/24 kg•h]	PK/PD parameter values					
				T>MAC (%)		AUC_{0-24}/MAC (h)		C_{max}/MAC	
				P	U	P	U	P	U
D	25	every 3.0	25	20	76	17	1913	7	435
E	50	every 3.0	50	28	83	34	3826	13	870
F	100	every 3.0	100	36	91	68	7651	26	1739
L	50	every 1.5	100	56	100	68	7596	13	882
M	100	every 1.5	200	71	100	136	15192	26	1764
X	12.5	every 0.75	50	54	100	33	3672	4	253
Y	25	every 0.75	100	85	100	66	7344	7	506
Z	50	every 0.75	200	100	100	133	14688	14	1012

(b)

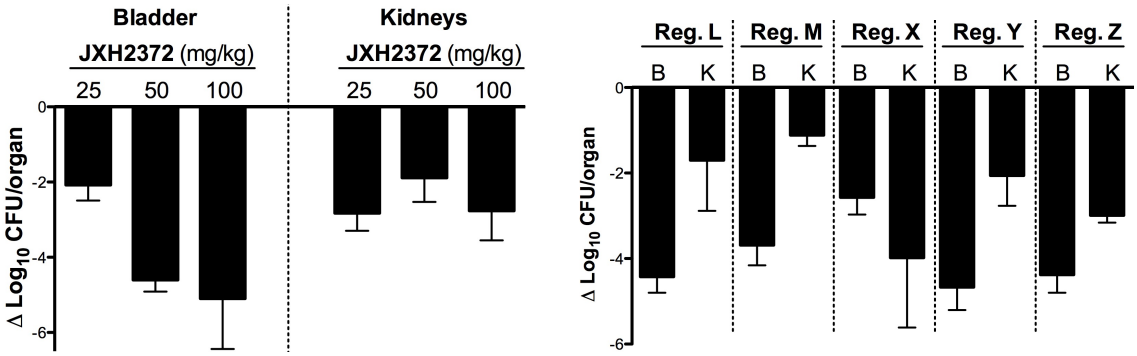

Figure 3. Pharmacodynamic study in the UTI mouse model. (a) Dosage regimens selected for *in vivo* PD studies in the UTI mouse model. T: time; MAC: minimal anti-adhesion concentration; AUC_{0-24}: area under the curve over 24 hours; C_{max}: peak concentration; P: plasma; U: urine. (b) The bar diagram represents the reduction of bacterial counts (*n* = 4) resulting from the i.v. application of JXH2372 at the indicated dosage regimen (D, E, F, L, M, X, Y, Z). The baseline represents the mean bacterial counts of the untreated control group. Reg: dosage regimen, B: bladder; K: kidneys.

The PK/PD index most predictive for the treatment outcome was evaluated by correlating the bacterial counts in the bladder and kidneys of mice after 3 h of infection with the applied dosage regimens (Figure 4). The best correlation for the infection outcome was observed by looking at the total AUC over the MAC in the bladder ($AUC_{0\text{-}24}$/MAC) with an R^2 value of 43% (Figure 4 a and b). Less correlation was found for the T>MAC index (R^2 = 29% for plasma and 39% for urine) and very poor correlation for C_{max}/MAC (R^2 = 20% for plasma and 21% for urine). No correlation was observed in the kidneys (R^2 < 0.1).

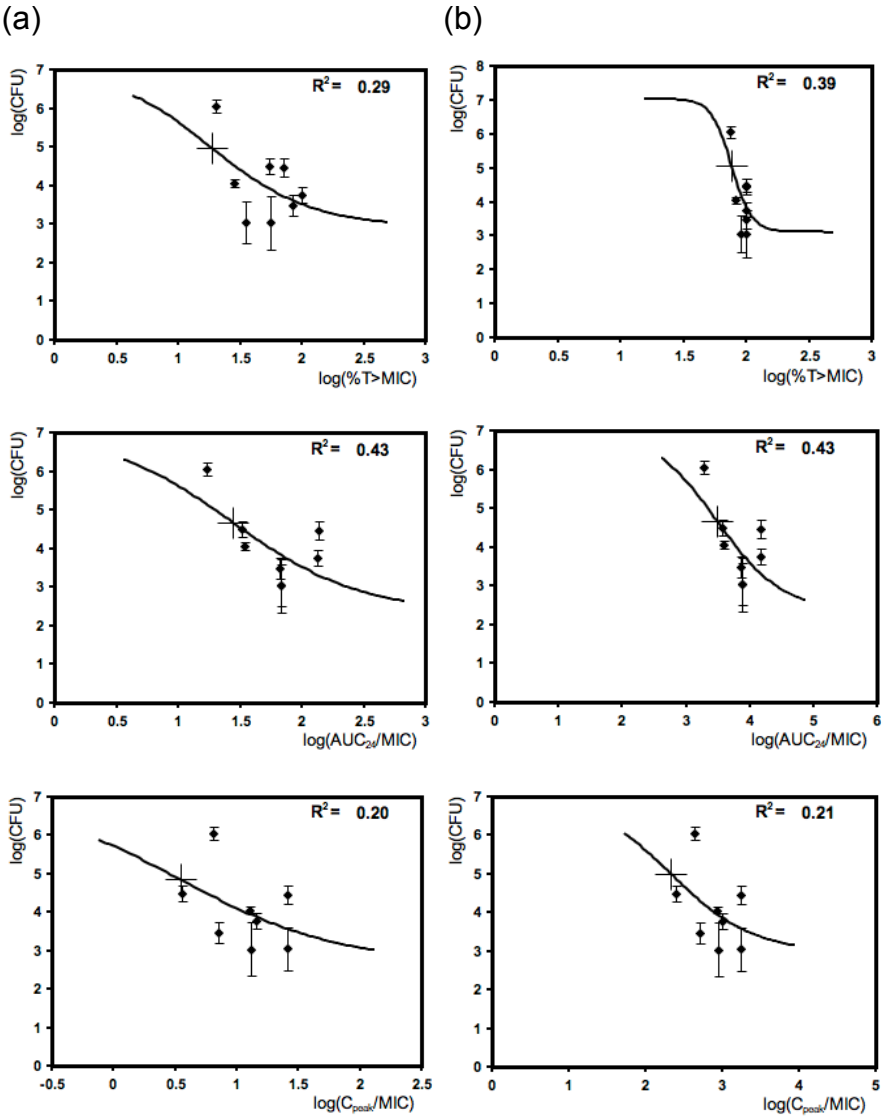

Figure 4. Correlation of the 24 h drug concentration in plasma and urine and the anti-adhesion activity of JXH2372 in the UTI mouse model. PK/PD parameters (T>MAC, $AUC_{0\text{-}24}$/MAC, C_{max}/MAC) for (a) plasma and (b) urine concentration-activity correlation in the bladder. The activity is displayed in the ordinates as change in CFU.

Discussion

In this study we described for the first time the PK/PD evaluation of a FimH antagonist in the UTI mouse model. The goal of the study was to determine the PK/PD index, best correlating with the infection outcome, in order to better understand the *in vivo* behavior of this new antimicrobial.

Traditionally the efficacy of antibiotics is expressed using the MIC. FimH antagonists exhibit a different mode of action compared to antibiotics (they neither kill nor inhibit growth of microorganisms), therefore, a modified definition of the MIC had to be elaborated. The activity of a FimH antagonist can be determined by testing its anti-adhesion property in a cell-based assay. There we evaluated the concentration of antagonist needed, to totally inhibit bacterial adhesion to human bladder cells and we defined this concentration as the minimal anti-adhesion concentration (MAC). With the MAC, we were able to conduct and evaluate the results of the PK/PD studies.

The *in vivo* PK/PD studies were carried out in the UTI mouse model using the UPEC strain UTI89. Due to the mode of action of FimH antagonists, the anti-adhesion activity is exclusively achieved by α-D-mannopyranosides present in the urine of mice (extracellular). There they bind to the bacterial FimH, preventing adhesion and invasion and concomitantly also infection. Therefore, the antagonist was always applied 10 minutes prior to inoculation (prevention study) and infection was terminated after 3 hours.

As previously described,[20,25] urine samples showed in general higher bacterial counts compared to the bladder. This could result due to difficulties during urine sampling and varying urine volumes of mice during experiments, leading to either a concentration or dilution of bacteria in urine samples. Hence, lower urine volumes lead to an increased concentration of bacteria in the collected urine and furthermore, non-adherent and detached bacteria accumulate in the urine. The same applies for kidney counts, which were also reduced to a lower extend in all treated animals (Figure 3 b). One reason could be, that compared to the bladder, bacteria exhibit a different adhesion mechanism in the kidneys (mannose dependent type 1 pili in the bladder, galactose dependent P pili interactions in the kidneys).[13] Furthermore, in the UTI mouse model, the application of bacteria directly into the bladder and

concomitantly also into the kidneys (vesicourethral reflux (VUR)) during the inoculation process is a prevalent problem,[32] hence high kidney counts were already observed 3 h after infection (negative control, 6.7 x 10^6 CFU).

The PK/PD studies of the three increasing dosages (25, 50 100 mg/kg) of JXH2372 showed a dose dependency for both, PK parameters (in plasma and urine samples) and CFU reductions (in bladder and kidneys) (Figure 2 and Figure 3 b). Except for the $AUC_{0\text{-}24}$ of the middle concentration (50 mg/kg), which showed a lower value compared to 25 mg/kg. Since plasma values of all three concentrations are in good agreement, the outlying urine $AUC_{0\text{-}24}$ for the dosage of 50 mg/kg could be explained by the problems mentioned above, that urine sampling in mice can be difficult. With these studies, a series of dosage regimes for further PD studies were selected, to be able to elicit the most predictive PK/PD index for the therapeutic outcome.
The results of the PK and PD correlations (Figure 4) shows, that the $AUC_{0\text{-}24}$/MAC in the bladder (for plasma and urine concentrations) is the most predictive PK/PD parameter for the therapeutic outcome. It indicates that the compound is binding loosely to the receptor, therefore continuous availability of the compound is needed for an effective treatment. As expected, no correlations were found for the kidneys, probably because of the reasons mentioned above (different adhesion mechanism).

In this study we focused on the application of the antagonist in a preventive manner. The evaluation of the optimal PK/PD parameter suggests, that a constant mean level of antagonist over the MAC is the optimal for treatment. Therefore, we will improve the PK parameters and use an adapted dosage regimen of the compound to avoid high peak levels and to achieve a prolonged presence of the FimH antagonist in the urine. Furthermore, to elucidate the binding mode of FimH antagonists to their target (FimH-carbohydrate recognition domain (CRD) on UPEC), additional cell-based *in vitro* and *in vivo* studies in the UTI mouse model will be performed.

Experimental PK/PD studies are usually conducted in animal models and decrease the risk (dose guessing in patients) and cost in drug development. The preclinical determination of the PK/PD indices for FimH antagonists provides valuable information for optimization and later on clinical outcome of the anti-adhesive therapy against UTI.

References

1 Foxman B. Epidemiology of urinary tract infections: incidence, morbidity, and economic costs. *Am J Med* 2002; **113**: 5S-13S.

2 Sharon N. Carbohydrates as future anti-adhesion drugs for infectious diseases. *Biochim Biophys Acta* 2006; **1760**: 527-37.

3 Wiles TJ, Kulesus RR, Mulvey MA. Origins and virulence mechanisms of uropathogenic *Escherichia coli*. *Exp Mol Pathol* 2008; **85**: 11-9.

4 Langermann S, Palaszynski S, Barnhart M *et al.* Prevention of mucosal *Escherichia coli* infection by FimH-adhesin-based systemic vaccination. *Science* 1997; **276**: 607-11.

5 Croxen MA, Finlay BB. Molecular mechanisms of *Escherichia coli* pathogenicity. *Nat Rev Microbiol* 2010; **8**: 26-38.

6 Lane MG, Alteri CJ, Smith SN *et al.* Expression of flagella is coincident with uropathogenic *Eschericia coli* ascencion to the upeer urinary tract. *Proc Natl Acad Sci USA* 2007; **104**: 16669-74.

7 Connell H, Agace W, Klemm P *et al.* Type 1 fimbrial expression enhances *Escherichia coli* virulence for the urinary tract. *Proc Natl Acad Sci USA* 1996; **93**: 9827-32.

8 Hunstad DA, Justice SS. Intracellular lifestyle and immune evasion strategies of uropathogenic *Escherichia coli*. *Annu Rev Microbiol* 2010; **64**: 203-21.

9 Fihn SD. Clinical practice. Acute uncomplicated urinary tract infection in women. *N Engl J Med* 2003; **349**: 259-66.

10 Hooton TM. Recurrent urinary tract infection in women. *Int J Antimicrob Agents* 2001; **17**: 259-68.

11 Gouin SG, Wellens A, Bouckaert J *et al*. Synthetic Multimeric Heptyl Mannosides as Potent Antiadhesives of Uropathogenic *Escherichia coli*. *ChemMedChem* 2009; **4**: 749-55.

12 Rosen DA, Hung CS, Kline KA *et al*. Streptozocin-induced diabetic mouse model of urinary tract infection. *Infect Immun* 2008; **76**: 4290-98.

13 Mulvey MA. Adhesion and entry of uropathogenic *Escherichia coli*. *Cell Microbiol* 2002; **4**: 257-71.

14 Capitani G, Eidam O, Glockshuber R *et al.* Structural and functional insights into the assembly of type 1 pili from *Escherichia coli*. *Microbes Infect* 2006; **8**: 2284-90.

15 Choudhury D, Thompson A, Stojanoff V *et al.* X‐ray structure of the FimC–FimH chaperone–adhesin complex from uropathogenic *Escherichia coli*. *Science* 1999; **285**: 1061-6.

16 Wellens A, Garofalo C, Nguyen H *et al.* Intervening with urinary tract infections using anti-adhesives based on the crystal structure of the FimH-oligomannose-3 complex. *PLoS ONE* 2008; **3**: 4-13.

17 Bouckaert J, Mackenzie J, de Paz JL *et al.* The affinity of the FimH fimbrial adhesin is receptor-driven and quasi-independent of *Escherichia coli* pathotypes. *Mol Microbiol* 2006; **61**: 1556-68.

18 Ofek I, Hasy DL, Sharon N. Anti-adhesion therapy of bacterial diseases: prospects and problems. *FEMS Immunol Med Microbiol* 2003; **38**: 181-91.

19 Ernst B, Magnani JL. From carbohydrate leads to glycomimetic drugs. *Nat Rev Drug Discov* 2009; **8**: 661-77.

20 Klein T, Abgottspon D, Wittwer M *et al.* FimH Antagonists for the oral treatment of urinary tract infections: from design and synthesis to in vitro and in vivo evaluation. *J Med Chem* 2010; **53**: 8627–41.

21 Han Z, Pinker JS, Ford B *et al.* Structure-based drug design and optimization of mannoside bacterial FimH antagonists. *J Med Chem* 2010; **53**: 4779-92.

22 Cusumano CK, Pinkner JS, Han Z *et al.* Treatment and prevention of urinary tract infection with orally active FimH inhibitors. *Sci Transl Med* 2011; **3**: 109-15.

23 Han Z, Pinkner JS, Ford B *et al.* Lead optimization studies on FimH antagonists: discovery of potent and orally bioavailable ortho-substituted biphenyl mannosides. *J Med Chem* 2012; **55**: 3945-59.

24 Guiton PS, Cusumano CK, Kline KA *et al.* Combination small molecule therapy prevents uropathogenic *Escherichia coli* catheter-associated urinary tract infections in mice. *Antimicrob Agents Chemother* 2012; **56**: 4738-45.

25 Jiang X, Abgottspon D, Kleeb *et al.* Antiadhesion Therapy for Urinary Tract Infections – A Balanced PK/PD Pofile Proved to be Key for Success. *J Med Chem* 2012; **55**: 4700-13.

26 Andrews JM. Determination of minimum inhibitory concentrations. *J Antimicrob Chemother* 2001; **48** (Suppl 1): 5-16.

27 Scharenberg M, Abgottspon D, Ciceck E *et al.* Flow cytometry-based assay for screening FimH antagonists. *Assay Drug Dev Technol* 2011; **9**: 455-64.

28 Craig WA. Pharmacokinetic/pharmacodynamic parameters: rational for antibacterial dosing of mice and men. *Clin Infect Dis* 1998; **26**:1-10.

29 Frimodt-Møller N. How predictive is PK/PD for antibacterial agents? *Int J Antimicrob Agents* 2002; **19**: 333-9.

30 Kerrn MB, Frimodt-Møller N, Espersen F. Effects of Sulfomethizole and Amdinocillin against *Escherichia coli* Strains (with Various Susceptibilities) in an Ascending Urinary Tract Infection Model. *Antimicrob Agents Chemother* 2003; **47**: 1002-9.

31 Mulvey MA, Schilling JD, Hultgren SJ. Establishment of a persistent *Escherichia coli* reservoir during the acute phase of a bladder infection. *Infect Immun* 2001; **69**: 4572-9.

32 Johnson JR, and Brown JJ. Defining Inoculation Conditions fort he Mouse Model of Ascending Urinary Tract Infection that Avoidf Immediate Vesicourethral Reflux yet Produce Renal and Bladder Infection. *J Inf Dis* 1996; **173**: 746-9.

RESULTS AND DISCUSSION

Manuscript III

Characterization of Type 1 Pili-Dependent Binding Properties of Clinical Uropathogenic *Escherichia coli* Isolates.

Scharenberg M*, Abgottspon D*, Zimmermann S, zur Werra S, Preston R, Rabbani S, Ernst B.

* These authors contributed equally to the project.

Preliminary manuscript: With outlook for completion.

My contributions:

Evaluation of the aggregation potential and type 1 pili expression profiling of the clinical isolates together with Scharenberg M. and the master students Zimmermann S. and Zur Werra S.

In vivo infection studies in the UTI mouse model with the clinical isolates.

Preparation of the results and discussion of the *in vivo* studies for the manuscript.

Characterization of Type 1 Pili-Dependent Binding Properties of Clinical Uropathogenic *Escherichia coli* Isolates

Meike Scharenberg*, Daniela Abgottspon*, Sabine Zimmermann, Sirin zur Werra, Roland Preston, Said Rabbani, Beat Ernst

Institute of Molecular Pharmacy, Pharmacenter, University of Basel, Switzerland

* These authors contributed equally to the project.

Correspondence to Prof. Dr. Beat Ernst, Institute of Molecular Pharmacy, Pharmacenter, University of Basel, Klingelbergstrasse 50, CH-4056 Basel, Switzerland

Tel: +41 61 267 1551, Fax: +41 61 267 1552, Email: beat.ernst@unibas.ch

Abstract

Urinary tract infections are caused in 70-90% of all the cases by uropathogenic *Escherichia coli* (UPEC), which express type 1 pili presenting the adhesin FimH. The interaction of FimH with mannose glycans expressed by urothelial cells allows UPECs to adhere and to invade host cells within the urinary tract epithelium. In this study, we investigated 72 clinical human UPEC isolates on their binding behavior, their *fimH* gene sequence similarities, and type 1 pili expression profile. Differences in agglutination to yeast and guinea pig erythrocytes were observed. Although numerous natural occurring point mutations were found in the *fimH* gene, we show that it is the type 1 pili expression profile that determines the general agglutination of the investigated *E. coli* isolates. Furthermore, *in vivo* mouse infection studies of two initially non-fimbriated clinical strains showed that while one strain was capable of initiating type 1 pili expression within 4 h after injection followed by infection, the other was not. Our study demonstrates that the rate of type 1 pili expression is determinant for the initiation and severity of a urinary tract infection. Consequently, FimH antagonists capable of blocking the initial adhesion step of UPECs to host tissues can be considered as potential anti-infectives.

Introduction

Urinary tract infection (UTI) is one of the most common infection, with millions of people affected every year. Besides women, who bear a risk of 40 - 50% to experience at least one symptomatic UTI episode during a life-time [1], patients with diabetes, spinal cord injuries, and suppressed immune system are particularly at risk [2, 3]. An untreated UTI may lead to a bladder infection (cystitis) and, in a later infection state, to a kidney infection (pyelonephritis) [4]. The initial and most fundamental step in the pathogenesis of UTIs is the type 1 pili dependent adhesion of uropathogenic *Escherichia coli* (UPEC) to α-mannoside containing glycoprotein receptors on the surface of uroepithelial cells, such as uroplakin 1a (UP1a) [5]. The bacterial adhesion is mediated by the lectin FimH, localized at the tip of type 1 pili, which recognizes mono- as well as oligomannosides. The adhesion triggers a bacterial cell invasion, resulting in the development of an infection. FimH antagonists such as α-D-mannopyranosides have been shown to interfere with the attachment of UPEC to their host cells, thus providing a novel therapeutic opportunity for the treatment and prevention of UTIs as an alternative to conventional antibiotic treatment [6-8].

Type 1 fimbriae are 1-3 µm long, filamentous organelles [9, 10]. These helical rods with a diameter of 7 nm consist of up to 3000 FimA subunits, forming the pilus rod, followed by the subunits FimF, FimG and FimH, forming the tip of the fimbrium. The adhesin FimH, which is located at the distal end of the linear fimbrium, contains the mannose-specific carbohydrate recognition domain (FimH-CRD) [11-13]. FimH is composed of two domains, the pilin domain, which connects the fimbrial rod, and the lectin domain, which exhibits the carbohydrate recognition domain (CRD). The highly conserved CRD enables the adhesion of bacteria to the mannosylated urothelial cell surfaces.

FimH mediates binding to these mannosylated surfaces in a shear-dependent manner, facilitated by force-enhanced allosteric catch bonds [14, 15]. Catch bonding of FimH is thought to allow sustained adhesion under flow conditions as found in the urinary tract, and to allow mobility under no-flow conditions. The catch-bond mechanism is achieved by a switch between two conformational states, the low-

affinity state and the high-affinity state. Only recently, the crystal structures of both FimH conformations have become available [16]. These revealed that in the low-affinity state, an interaction between the pilin and the lectin domain allosterically widens the binding site, thus weakening the interaction with mannose. In the high-affinity state, the lectin and the pilin domain are separated, and the binding site is tightened. The equilibrium between the two states is shifted towards the high-affinity conformation by tensile force along the bond, and by interaction with a ligand [16].

Naturally occurring mutations of FimH usually arise outside of the highly conserved mannose-binding site, but may nonetheless invoke enhanced mannose-binding affinity. This is known for the S62A and the A27V mutation [17, 18]. It is presumed that these mutations alter the interdomain interaction, thus shifting the equilibrium from the low-affinity to the high-affinity state. With a specific antibody for the high-affinity state of FimH, Tchesnokova *et al.* proved the allosteric link between the high-affinity state of the mannose-binding site and the open conformation of the interdomain region. These mutant FimH variants evolved under positive selection, benefiting from augmented mannose-binding affinity even under static conditions [19].

In a recent study using clinical isolates obtained from urine and feces of individuals with acute and recurrent UTIs, distinct mutations evolving under positive selection were identified, all of which were located outside of the mannose-binding pocket [20]. Based on the found mutations, six mutant strains with the same isogenic background were generated and investigated, showing differences in their affinity for mannose as well as in their *in vivo* fitness. However, in this study the clinical isolates were not directly investigated on their binding behavior to ligands or their *in vivo* pathogenicity, hence their biological properties remained unknown. Analyzing these properties can be of high importance when predicting the actual anti-infective potencies of FimH antagonists. Investigations on the infection mechanisms of clinical UPEC strains can provide crucial information, especially when considering exclusive treatment with FimH antagonists for the prevention of infections.

In this study, we evaluated the binding properties of 72 clinical UPEC isolates of patients suffering from acute cystitis, by performing yeast and guinea pig

erythrocytes (GPE) aggregation assays. Furthermore, type 1 pili immunostaining assays together with mutational analysis of the *fimH* gene were performed to examine if variations in pili expression or mutations in the *fimH* gene are responsible for differential binding behavior of the UPEC isolates, as observed in the aggregation studies. *In vivo* infection studies together with concurrent pili expression studies allowed an *in vivo* time-dependent type 1 pili expression profiling within 24 h post infection.

Material and methods

Bacteria and growth. The *E. coli* isolate UTI89 [21] (UTI89wt) and the FimA-H knock-out strain UTI89Δ*fimA-H* were kindly provided by the group of Prof. Urs Jenal (Biocenter, University of Basel, Switzerland). The laboratory K12/J96 (ELT115) strain was used as reference strain and was kindly provided by the group of Prof. Sokurenko (University of Washington, USA). 72 clinical *E. coli* isolates were collected at the University Hospital Basel, Switzerland during 2009 and were selectively cultivated. Age and sex of the patient and the antibiotic resistances are known. Microorganisms were stored at -70 °C and before experiment incubated for 24 h under static conditions at 37 °C in 10 mL Luria-Bertani broth (Becton, Dickinson and Company, Le Pont de Claix, France) using 50 mL tubes. Prior to each experiment, the microorganisms were washed twice and resuspended in phosphate buffered saline (PBS, Sigma, Steinheim, Germany). CFUs were determined by plating serial 1:10 dilutions on blood agar, followed by colony counting with 20-200 colonies after overnight incubation at 37 °C.

Aggregometry assay. The aggregometry assay was carried out as previously described [22]. In short, the percentage of aggregation of *E. coli* with guinea pig erythrocytes (GPE) or *Saccharomyces cerevisia* (yeast) was quantitatively determined by measuring the optical density at 740 nm and 37 °C under stirring at 1000 rpm using an APACT 4004 aggregometer (Endotell AG, Allschwil, Switzerland). Bacteria were cultivated as described above. GPE were separated from guinea pig blood (Charles River Laboratories, Sulzfeld, Germany) using Histopaque (density of 1.077 g/mL at 24 °C, Sigma-Aldrich, Buchs, Switzerland). Yeast was prepared by

dissolving commercially available dried bakers yeast in PBS. Prior to the measurements, the cell densities of *E. coli* and GPE were adjusted to an OD_{600} of 4, corresponding to 1.9×10^8 CFU/mL and 2.2×10^6 cells/mL respectively and the OD_{600} of yeast to 2, corresponding to 1.7×10^6 cells/mL. For the calibration of the instrument, the aggregation of protein poor plasma using PBS alone was set as 100% and the aggregation of protein rich plasma using GPE or yeast as 0%. After calibration, measurements were performed with 250 μL GPE or yeast and 50 μL bacterial suspension and the aggregation monitored over 600 s. After the aggregation phase of 600 s, 25 μL of antagonist *n*-heptyl α-D-mannopyranoside (HM) [22], 385 μM in PBS was added to each cuvette and disaggregation was monitored for 1400 s. UTI89Δ*fimA-H* was used as negative control. All measurements were performed in triplicates on different days. The aggregation behavior was evaluated by calculating the maximal aggregation (%) and the maximal slope (%/min). The inhibitory potential was determined by calculating the area under the disaggregation curves ($AUC_{600\text{-}2000s}$).

Sequence analysis of the *fimH* gene. The *fimH* gene was amplified in PCR reactions using either bacterial colonies or purified genomic DNA (Wizard Genomic DNA Purification Kit, Promega, Madison, USA) as template. The primers used to amplify *fimH* were the *fimH*seq fv: 5`-ACC GCG CAA AAC ATC CAG-3` and the *fimH*seq rv: 5`-GAT CGT TTG GGC CGT ACC AC-3`, located outside of the *fimH* genes in adjacent conserved DNA sequences. PCRs were performed using the iProof high-fidelity DNA polymerase (Bio Rad, Caboratories, Canada) as described in the instruction manual. Products were separated by agarose gel electrophoresis, purified (GenEluate Gel extraction Kit, Sigma-Aldrich, Steinheim, Germany) and submitted to sequence analysis (Mycrosynth, Balgach, Switzerland). Sequencing primers include the PCR primers as well as the *fimH*seq int: 5`-CCG GTG GCG CTT TAT TTG AC-3` primer. Obtained sequences were analyzed with FinchTV and Expasy and aligned with ClustalW2-Multiple Sequence Alignment. All sequences were compared to the *fimH* in the K12/J96 strain.

Type 1 pili immunostaining. With an immunostaining assay, type 1 pili expression of the strains was veryfied. Washed bacteria (with PBS) were incubated with rabbit serum raised against type-1 pili (1:300) for 1 h at 4 °C (kindly provided by Prof. Karen

Krogfelt, Staten Serum Institute, Copenhagen, Denmark). After washing the cells, the bacteria were treated with the secondary anti rabbit Alexa647 conjugated antibody (1:200, Invitrogen, Lucerne, Switzerland) for 1 h at 4 °C. After a thorough washing step, the bacteria were resuspended in 300 µL PBS. Bacteria were then kept in the dark until analysis. Samples were measured with a CyAn ADP flow cytometer (Beckman-Coulter, CA, USA) and analyzed by gating on the bacterial cells based on forward (FSC) and side scatter (SSC). A total of 1 x 10^4 – 5 x 10^4 bacteria were measured per sample. Data were acquired in a linear mode for the SSC and logarithmic mode for FSC and the red fluorescent channel FL8-H. Quantification of fluorescent labeling was evaluated with the FlowJo software 7.6.3 (Tree Star, Inc., Ashland, OR, USA). The UTI89Δ*fimA-H* strain was used as negative control.

Animals. Female C3H/HeN mice weighing between 19 and 25 g were obtained from Charles River (Sulzfeld, Germany) and were housed three to a cage. Mice were kept under specific-pathogen-free conditions in the Animal House of the Department of Biomedicine, University Hospital Basel, and animal experimentation guidelines according to the regulations of Swiss veterinary law were followed. After seven days of acclimatization, 9- to 10-week old mice were used for infection studies. During the studies, animals were allowed free access to chow and water. Three days before infection studies and during infection, 5 % D-(+)-glucose (AppliChem, Baden-Dättwil, Switzerland) was added to the drinking water [23].

UTI mouse model. Mice were infected as previously described [23]. In brief, before infection all remaining urine was depleted form the bladder by gentle pressure on the abdomen. Mice were anesthetized with 1.1 vol% isoflurane/oxygen mixture (Attane, Minrad Inc, Buffalo, NY, USA) and placed on their back. Anesthetized mice were inoculated transurethrally with the bacterial suspension by use of a 2 cm polyethylene catheter (Intramedic polyethylene tubing, inner diameter 0.28 mm, outer diameter 0.61 mm, Beckton Dickinson, Allschwil, Switzerland), which was placed on a syringe (Hamilton Gastight Syringe 50 µL, removable 30G needle, BGB Analytik AG, Boeckten, Switzerland). The catheter was gently inserted through the urethra until it reached the top of the bladder, followed by slow injection of 50 µL bacterial suspension at a concentration of approximately 10^9 to 10^{10} CFU/mL.

Results and discussion

Aggregometry screening of the clinical UPEC isolates. All strains were cultivated for 24 h under static conditions prior to aggregometry measurements, as recommended for enhanced type 1 pili expression [24]. GPE hemagglutination and yeast aggregation assays with the clinical UPEC isolates were performed to investigate their binding properties. Major differences in the aggregation behavior of the UPEC isolates were observed (Figure 1). The strains were classified into three groups, based on their aggregation capability of GPE and yeast (Figure 1 and 2). A maximal aggregation rate of more than 15% was considered as positive aggregation.

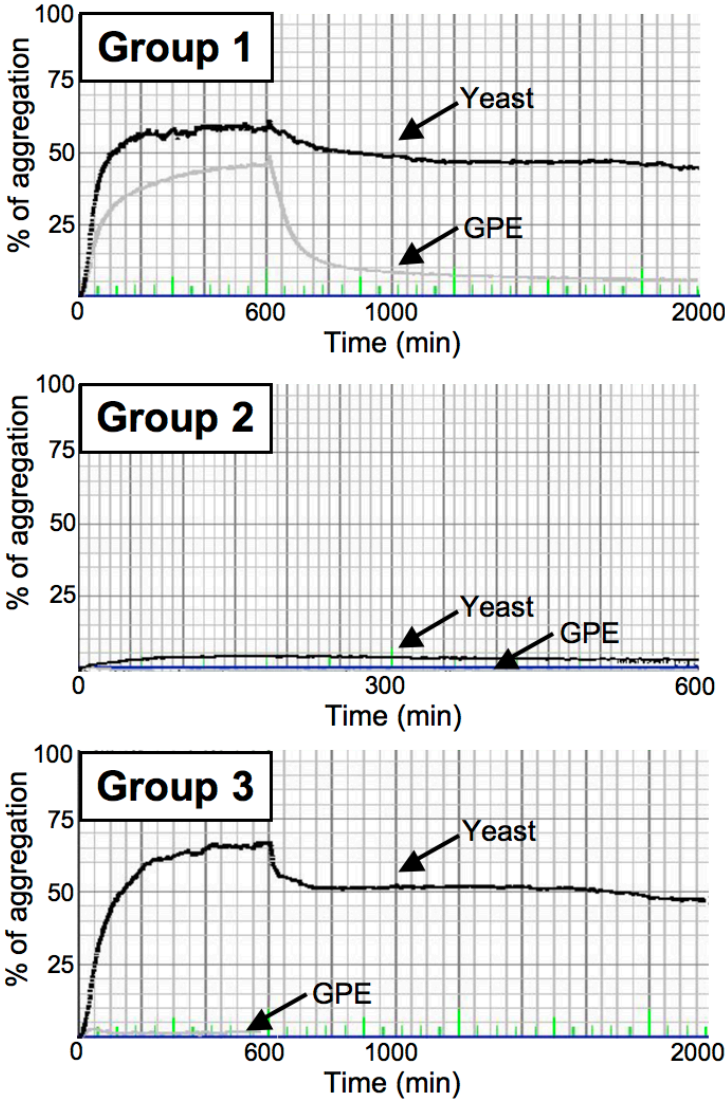

Figure 1. Aggregation and disaggregation curves of clinical isolates from group 1, 2, and 3. Disaggregation was triggered after 600s by the addition of *n*-heptyl α-D-mannopyranoside (385 μM).

Isolates of group 1 (16 isolates, 22%) showed pronounced aggregation of both GPE and yeast, whereas isolates of group 2 (19 isolates, 26%) aggregated neither with GPE nor with yeast. Group 3, representing the largest group with 37 isolates (52%), aggregated exclusively with yeast, and not with GPE. No isolate showed aggregation only with GPE and not with yeast. The highly virulent clinical isolate UTI89 belongs to group 1.

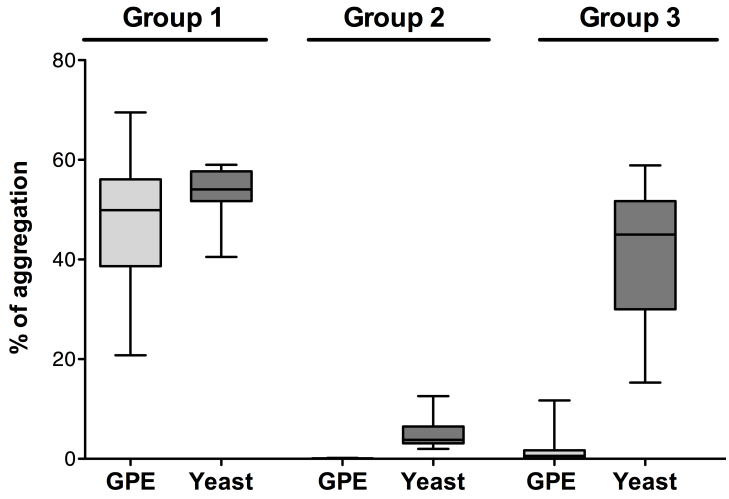

Figure 2. Aggregometry screening of the clinical *E. coli* isolates (n_{tot}= 72). Group 1: Isolates aggregating with GPE and yeast (n_{G1}= 16). Group 2: Isolates aggregating neither with GPE, nor with yeast (n_{G2}= 19). Group 3: Isolates exclusively aggregating with yeast (n_{G3}= 37). GPE: guinea pig erythrocytes, yeast: *Saccharomyces cerevisiae*.

Aggregating isolates (max. aggregation ≥15%) were further analyzed by their disaggregation behavior after the addition of the FimH antagonist *n*-heptyl α-D-mannopyranoside (385 µM final concentration, Figure 1). Disaggregation was monitored over 1400 s and the area under the disaggregation curve (AUC) was determined. The relative amount of disaggregated bacteria was calculated and expressed in % disaggregation effect ($AUC_{no\ antagonist}$ = 100% aggregation, 0% disaggregation effect, 100% - (100% • $AUC_{with\ antagonist}$ /$AUC_{no\ antagonist}$)). The aggregation of all tested strains was reverted with *n*-heptyl α-D-mannopyranoside, implying that aggregation of GPE and yeast was solely FimH dependent. For the bacteria-GPE aggregates, *n*-heptyl α-D-mannopyranoside showed an average disaggregation effect of 73%. For bacteria-yeast aggregates, disaggregation was reduced to 30% in group 1 and 23% in group 3. The aggregation results demonstrate

that the affinity of type 1 pili is higher for yeast than for GPE, since higher concentrations of antagonist are required to revert yeast aggregation, as will be discussed.

***fimH* gene sequencing**. Since it is known that point mutations in the *fimH* gene dramatically affects binding properties of type I fimbriated bacteria [17, 19, 25], *fimH* genes of 58 isolates were sequenced, i.e. 16, 15, and 27 strains of group 1, 2, and 3, respectively. The sequences were aligned to the *fimH* gene of the UPEC strain J96. We identified 26 naturally occurring amino acid mutations within the *fimH* gene, occurring with different frequencies (Table 1).

Table 1. Mutation frequencies of the *fimH* gene sequencing, subdivided into group 1, 2 and 3. *fimH* gene sequences were compared to UPEC strain J96, used as reference throught this study. The total number of sequenced isolates of each group is indicated in brackets. The most frequently occurring mutations and the corresponding amino acids are highlighted in red.

	Amino acids with Mutations												
	7	**V27A**	**41**	**62**	**66**	**68**	**N70S**	**74**	**S78N**	**101**	**106**	**117**	**118**
Group 1 (16 isolates)	-	12	-	1	3	1	6	3	7	-	-	-	-
Group 2 (15 isolates)	-	10	-	-	1	-	1	-	1	-	-	1	1
Group 3 (27 isolates)	1	25	1	-	1	-	10	-	12	1	2	-	-
Total (58 isolates)	**1**	**47**	**1**	**1**	**5**	**1**	**17**	**3**	**20**	**1**	**2**	**1**	**1**

	Amino acids with Mutations												
	119	**122**	**V128M**	**130**	**147**	**163**	**R166H**	**192**	**202**	**238**	**242**	**273**	**279**
Group 1 (16 isolates)	-	-	1	-	1	1	1	-	1	1	1	-	-
Group 2 (15 isolates)	2	-	-	1	-	1	4	-	-	-	-	1	-
Group 3 (27 isolates)	1	1	4	-	-	1	1	1	-	-	1	1	1
Total (58 isolates)	**3**	**1**	**5**	**1**	**1**	**3**	**6**	**1**	**1**	**1**	**2**	**2**	**1**

As expected, none of the mutations was directly located within the mannose binding site, which was rather conserved among all sequenced strains. The mutations were either located in the interdomain region between the lectin and the pilin domain of FimH, or in spatial proximity to amino acids that were already associated with a conformational change of the protein (Figure 3). As mentioned before, the disruption of the interdomain interactions by structural mutations leads to a shift in the equilibrium towards the high-affinity state.

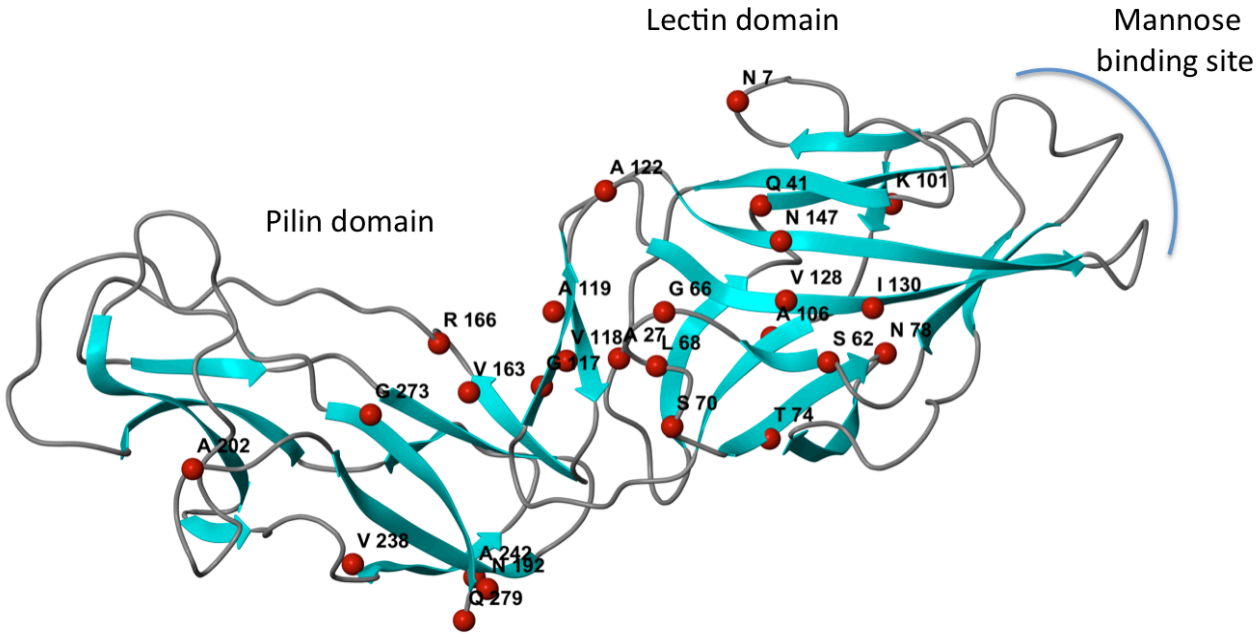

Figure 3. Structure of the FimH pilin and lectin domains with all mutations found in the 58 sequenced clinical isolates (red balls). The mannose-binding site was conserved in all strains. (PDB entry 3jwn, FimH low-affinity conformation).

The most frequently identified mutations were V27A, N70S, S78N, V128M, and R166H. 12 strains contained a valine in position 27 as in the pathogenic strain J96. This mutation has been shown to increase adhesion to mannose and to lower the threshold for catch-bond activation, implying a disruption of the interdomain region and shifting FimH towards the high-affinity state. It is assumed that this mutation is responsible for the high pathogenicity of the J96 strain [26]. The R166H mutation, which is also known to enhance mannose binding [27], was observed in six clinical isolates. The V128M mutation that was found in 5 clinical isolates was also shown to

weaken the interaction between pilin and lectin domains [15]. To date, this mutation was not further analyzed. However, residue 128 is located on the adjacent β-strand to amino acid 62, which is mutated (S62A) in the highly uropathogenic UTI89 strain and is known for its enhancing effect on mannose binding [28]. Therefore, it would be interesting to directly compare both mutations on their influence on ligand binding and pathogenicity. The mutations N70S and S78N have been shown to occur frequently, but no biological effect was associated with these mutations to date [15, 26]. Mutations that shift the equilibrium towards the high-affinity conformation emerged upon pathogenic adaptation of the *fimH* gene in nature, providing an advantage for bladder colonization during the course of an acute cystitis [17]. Although mutations can alter the binding behavior of UPECs, we did not observe a correlation between aggregation/disaggregation behavior and distinct mutations in the *fimH* genes of our isolates. Binding enhancing mutations were found in all three groups. Therefore, the general aggregation/disaggregation properties of the analyzed UPEC strains cannot be attributed to polymorphisms within the *fimH* gene.

Type 1 pili expression profiling. To evaluate the possibility that the differential binding to yeast and GPEs originates from distinct expression rates of type 1 pili, we quantified the pili expression of UPEC strains by immunostaining assays. The expression of type 1 pili is phase variable and switches between fimbriated and non-fimbriated states in individual cells. The invasion is regulated by the two recombinases FimB and FimE, which are both encoded upstream of the invertible element within the *fim* gene cluster. Several factors such as growth conditions [24] (pH, osmolarity, temperature, shaking/static incubation) and the infection state [29, 30] influence the activity of these recombinases. This enables the bacteria to switch between different fimbriation states under varying environmental conditions, which is crucial for their survival and pathogenicity [29]. The investigated strains exhibited differential pili expression profiles (Figure 4), even though the strains were cultured identically with optimal conditions for pili expression (24 h, non-shaking [31]).

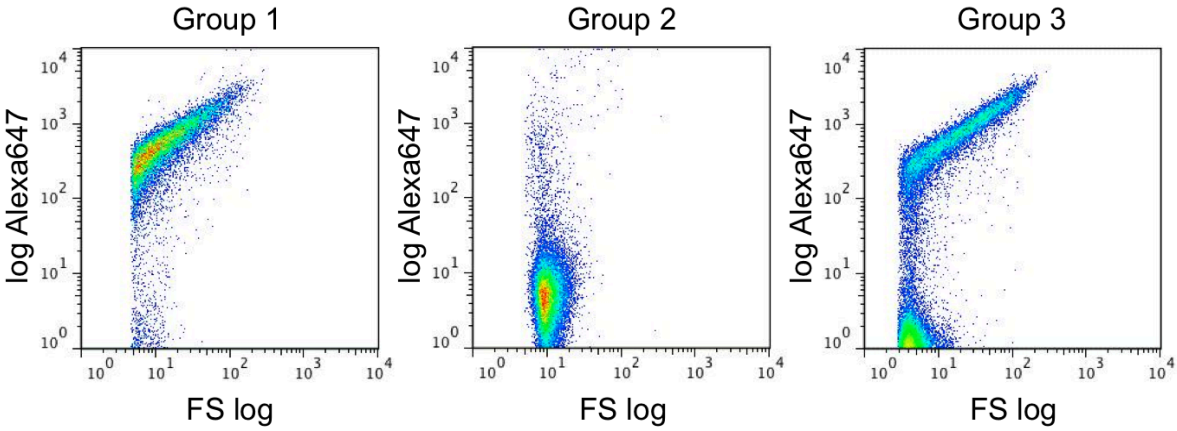

Figure 4. Examples of type 1 pili immunostaining assays for clinical isolates, belonging to group 1, 2, and 3. Group 1: Isolates aggregating with yeast and GPE; Group 2: Isolates aggregating neither with GPE, nor with yeast; Group 3: Isolates exclusively aggregating with yeast. Pili were stained with a rabbit anti-type 1 pili antibody and an anti-rabbit-Alexa647 antibody. The samples were measured in a flow cytometer and analyzed with the FlowJo software.

Clinical isolates from the first group binding to yeast and GPE, showed a strong and homogeneous expression profile. Strains from the second group, which aggregated neither with yeast nor with GPE, showed no type 1 pili expression. And finally, strains from the third group aggregating with yeast but not with GPE, either consisted of distinct piliated and non-piliated subpopulations, or of a single population with homogenously low pili density. These results indicate that the pili expression rate determines the aggregation properties of UPECs, with a higher percentage of piliated bacteria being necessary for GPE aggregation but not for yeast aggregation. This observation, together with the high disaggregation properties of *n*-heptyl α-D-mannopyranoside implies that FimH binds with a lower affinity to carbohydrate ligands on GPE than on yeast. Mannan present on yeast is composed of a core (1→6) mannose chain with branched side chains of up to 200 mannose residues [32] and was shown to be a high-affinity receptor for type 1 fimbriae [33]. For GPEs, a single glycoprotein as putative type 1 fimbriae ligand was isolated to date. It was suggested that this glycoprotein bears N-linked high-mannose glycans [34], with the density of this glycoprotein on the cell surface of GPEs being rather low. The differences in mannose ligand densities and affinities for type 1 fimbriae may account for the distinct aggregation capabilities of clinical isolates with GPE and yeast. Only

strains with a high density of fimbriae were able to agglutinate GPEs. These results prove the importance to first determine the recombinant isogenic background of the mutants and to quantify type 1 pili expression before comparing the binding behavior of different strains, or e.g. judging the influence of mutations on the binding behavior of FimH variants. Only when the pili expression profile of different strains is comparable, one can directly compare and interpret their binding behavior in aggregation or binding assays.

***In vivo* type 1 pili expression and infection study.** UPECs do not constantly express type 1 pili. Some strains require special growth conditions or even express type 1 pili only under *in vivo* conditions [24, 29 - 31]. Therefore, we performed infection studies in mice with the highly uropathogenic UTI89 strain, the FimA-H deficient UTI89 strain (UTI89Δ*fimA-H*), and two different strains from group 2, which do not express type 1 pili under the tested *in vitro* conditions (B1_39 and B1_59). After bacterial inoculation in the UTI mouse model, urine samples were collected after 0, 2, 4, 6, 8, and 24 hours, and analyzed for pili expression using immunostaining assays. The bladder and the kidneys were taken after 24 h, homogenized and plated in serial dilutions for analyis of bacterial counts.

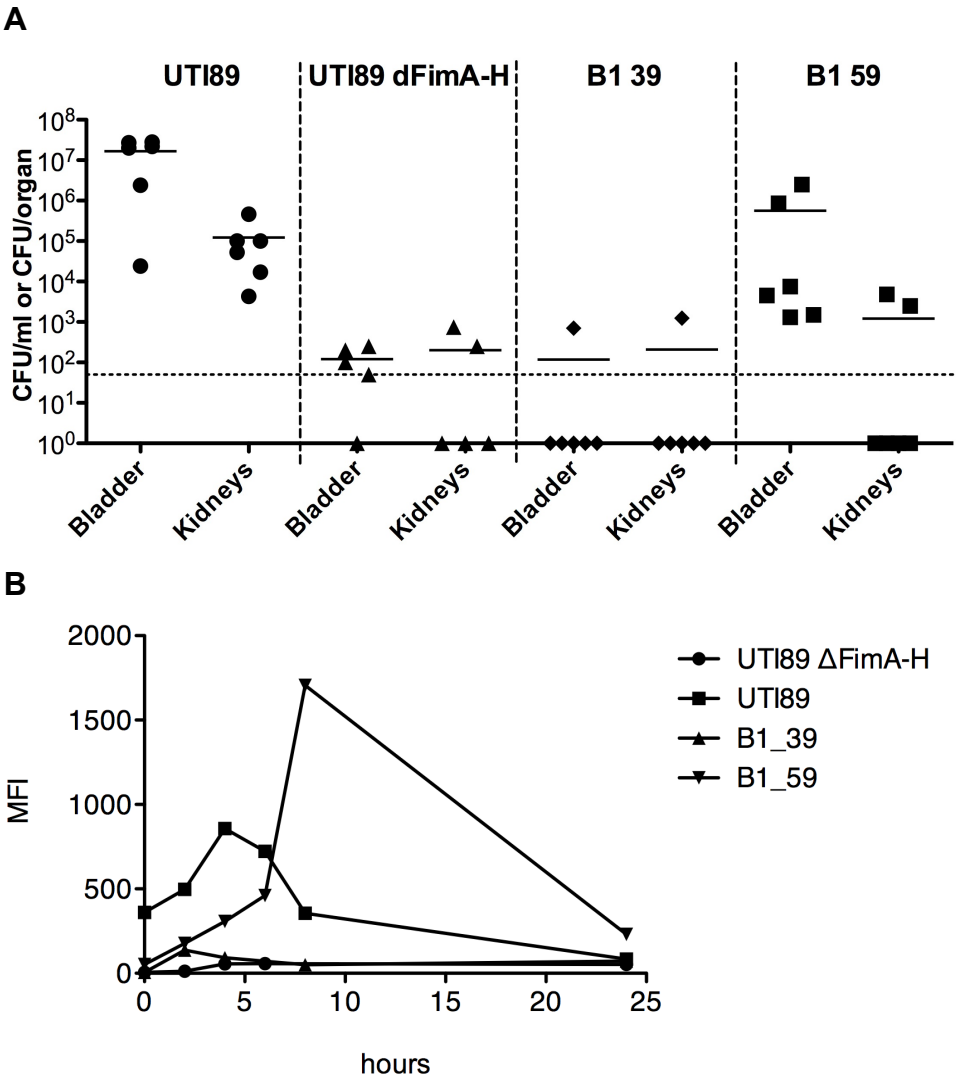

Figure 5. 24 h infection study in the UTI mouse model and type 1 pili immunostaining of bacteria present in the urine of infected mice after 0, 2, 4, 6, 8, and 24 hours. **A.** Bacterial counts in organs (bladder and kidneys) as colony forming units (CFU) after 24 hours of infection. **B.** Type 1 pili expression profiling of the urine samples collected from mice every 2 hours. The MFI (mean fluorescence intensity) level reflects the density of type 1 pili expressed by the bacteria.

The infection and type 1 pili expression study revealed differences in the expression profile between the strains in urine samples, which correlated well with the bacterial load in the organs (Figure 5). The negative control UTI89Δ*fimA-H* showed no type 1 pili expression (Figure 5 B). The positive control UTI89 expressed high levels of type 1 pili after *in vitro* cultivation, indicated by a high mean fluorescence intensity (MFI) at the beginning of the infection (0 h). The density of pili further increased during the first 4 h of infection. Isolate B1_39 showed no pili expression during the course of the

experiment, whereas isolate B1_59 showed a significant pili expression rate, starting at 2 h post-infection. Bacteria of both non-type 1 pili expressing strains, UTI89Δ*fimA-H* and B1_39, were hardly detectable in the bladder and in the kidneys (Figure 5 A). The few bacteria present in the organs were most likely able to invade via non-specific binding, and would probably be cleared after a longer study time period (e.g. 36 or 48 h). For UPEC strain B1_59 we found a lower number of bacteria in the bladder and the kidneys compared to UTI89, representing an early stage of infection. The results from the expression profile and the infection outcome correlate very well (Figure 5 B). UPEC strain UTI89 resulted in the highest bacterial load, because it had already been expressing type 1 pili before infection. The B1_59 strain, which first had to up-regulate the expression of type 1 pili, was not instantly able to adhere to bladder cells after inoculation and parts of the injection load were washed out with the flow of urine before pili expression was initiated. Therefore, only a reduced number of bacteria were able to initiate an infection, which was as a consequence weaker than for UTI89.

The type 1 pili expression rates of the pathogenic strains (UTI89 and B1_59) were down-regulated to low levels after 24 h, confirming the essential role of type 1 pili only for the initial infection process. The expression of other virulence factors, such as P fimbriae, which are crucial for the establishment of pyelonephritis in the later stages of a UTI, influences the expression rate of type 1 pili. Cross-talk between the adhesin gene clusters [30] and the activation of P fimbriae switch the *fim* gene to phase-off orientation, preventing type 1 pili expression [29]. The low type 1 pili expression rate 24 h post-infection indicates that the switch of type 1 pili to P fimbriae already occurred. P pili expression profiling would complement these observations.

This study demonstrates that type 1 pili are crucial for the establishment of a severe infection, since the UTI89Δ*fimA-H* and the B1-39 strain only caused minor bacterial counts in the kidneys and in the bladder. Furthermore, it was shown that some strains are capable of resetting their pili expression when subjected to the host tissue milieu, whereas others might have lost this capability. The initiation of an infection by the tested clinical isolates seemed to be exclusively mediated by type 1 pili, and not by other mechanisms. Treatment with FimH antagonists in the early stages of an infection should therefore allow preventing UPECs from adhering to host cells, and thus prevent UTIs.

Conclusion

Our study of 72 clinical UPEC isolates of patients with acute cystitis on their aggregation properties to yeast and GPE revealed major differences in binding behavior. The isolates were classified into three distinct groups, depending on their aggregation behavior and pili expression profile. GPE agglutination required a high and homogenous expression profile, implying that the binding properties of each individual strain to GPE are determined by its pili expression rate. Sequence analysis of 58 strains revealed a highly conserved mannose-binding site, with variations being located predominantly in the interdomain region between pilin and lectin domain. Most of the mutations were already described to influence the conformational state of FimH by disrupting the interdomain interaction. This disruption results in a shift from the low-affinity to the high-affinity state, suggesting that these mutations emerged from pathogenic adaption. This study shows that the severity of an infection is not only determined by the *fimH* variant, but rather by the pili expression rate of the individual isolates. Furthermore, we were able to confirm that type 1 pili are critical for the establishment of an infection *in vivo*. Consequently, quantification of type 1 pili for each individual strain is essential when comparing binding or infection capabilities of different strains or *fimH* variants.

Outlook

In the present study we evaluated the effect of mutations in the *fimH* gene on the binding profile of various clinical UPEC isolates. Since only the *fimH* was analysed, other influencing factors of the *E. coli* pathogenesis were not considered (e.g. other virulence factor expressions). To determine if the observed effect is exclusively due to the mentioned mutations in the *fimH* gene, isogenic mutants will be constructed and analyzed.

Literature

1. Mulvey MA, Lopez-Boado YS, Wilson CL, Roth R, Parks WC, Heuser J, Hultgren SJ, *Science* **1998**, *282*(5393):1494-1497.
2. Patterson JE, Andriole VT, *Infect. Dis. Clin. North Am.* **1997**, *11*(3):735.
3. Mahan KT, Wang J, *J Am Podiatr Med Assoc* **1993**, *83*(11):607-614.
4. Ronald A, *American Journal of Medicine* **2002**, *113*:14S-19S.
5. Mulvey MA, *Cell Microbiol.* **2002**, *4*:257-271.
6. Ofek I, Hasy DL, Sharon N, *FEMS Immunol. Med. Microbiol* **2003**, *38*(3):181-191.
7. Sharon N, *Biochim. Biophys. Acta -General Subjects* **2006**, *1760*(4):527-537.
8. Ernst B, Magnani JL, *Nat Rev Drug Discov* **2009**, *8*(8):661-677.
9. Russell PW, Orndorff PE, *J Bacteriol* **1992**, *174*(18):5923-5935.
10. Jones CH, Pinkner JS, Roth R, Heuser J, Nicholes AV, Abraham SN, Hultgren SJ, *Proc. Natl. Acad. Sci. U.S.A.* **1995**, *92*(6):2081-2085.
11. Hung C, Bouckaert J, Hung DL, Pinkner J, Widberg C, DeFusco A, Auguste G, Strouse R, Langermann S, Hultgren SJ, Mol. Microbiol. **2002,** *44*(4), 903–915
12. Hanson MS, Brinton CC, *Nature* **1988**, *332*(6161):265-268.
13. Choudhury D, Thompson A, Stojanoff V, Langermann S, Pinkner J, Hultgren SJ, Knight SD, *Science* **1999**, *285*(5430):1061-1066.
14. Yakovenko O, Sharma S, Forero M, Tchesnokova V, Aprikian P, Kidd B, Mach A, Vogel V, Sokurenko E, Thomas WE, *J Biol Chem*. **2008,** 25;283(17):11596-605.
15. Tchesnokova V, Aprikian P, Yakovenko O, Larock C, Kidd B, Vogel V, Thomas W, Sokurenko E, *J Biol Chem* **2008**, *283*(12):7823-7833.
16. Le Trong I, Aprikian P, Kidd BA, Forero-Shelton M, Tchesnokova V, Rajagopal P, Rodriguez V, Interlandi G, Klevit R, Vogel V *et al., Cell* **2010**, *141*(4):645-655.
17. Sokurenko EV, Chesnokova V, Dykhuizen DE, Ofek I, Wu XR, Krogfelt KA, Struve C, Schembri MA, Hasty DL, *Proc. Natl. Acad. Sci. U.S.A.* **1998**, *95*(15):8922-8926.
18. Sokurenko EV, Feldgarden M, Trintchina E, Weissman SJ, Avagyan S, Chattopadhyay S, Johnson JR, Dykhuizen DE, *Mol Biol Evol* **2004**, *21*(7):1373-1383.

19. Chen SL, Hung CS, Pinkner JS, Walker JN, Cusumano CK, Li Z, Bouckaert J, Gordon JI, Hultgren SJ, *Proc. Natl. Acad. Sci. U.S.A.* **2009**, *106*(52):22439-22444.
20. Sokurenko EV, Feldgarden M, Trintchina E, Weissman SJ, Avagyan S, Chattopadhyay S, Johnson JR, Dykhuizen DE, *Mol. Biol. Evol.* **2004**, 21(7):1373-83.
21. Mulvey MA, Schilling JD, Hultgren SJ, *Infect. Immun.* **2001**, *69*(7): 4572-4579.
22. Abgottspon D, Roelli G, Steinhuber A, Ernst B, Trampuz A, *J, Microbiol Methods.* **2010** *82*(3):249-55.
23. Kerrn MB, Frimodt-Møller N, Espersen F, *Antimicrob. Agents Chemother.* **2003**, *47*(3):1002-1009.
24. Tsai K-W, Lai H-T, Tsai T-C, Wu Y-C, Yang Y-T, Chen K-Y, Chen C-M, Li Y-SJ, Chen C-N, *J Biomed Sci* **2009**, *3*:16-91.
25. Yakovenko O, Sharma S, Forero M, Tchesnokova V, Aprikian P, Kidd B, Mach A, Vogel V, Sokurenko E, Thomas WE, *J Biol Chem* **2008**, *283*(17):11596-11605.
26. Hommais F, Gouriou S, Amorin C, Bui H, Rahimy MC, Picard B, Denamur E, *Infect. Immun*. **2003**, *71*(6):3619-3622.
27. Weissman SJ, Beskhlebnaya V, Chesnokova V, Chattopadhyay S, Stamm WE, Hooton TM, Sokurenko EV, *Infect. Immun* **2007**, *75*(7):3548-3555.
28. Aprikian P, Tchesnokova V, Kidd B, Yakovenko O, Yarov-Yarovoy V, Trinchina E, Vogel V, Thomas W, Sokurenko E, *J Biol Chem* **2007**, *282*(32):23437-23446.
29. Xia Y, Gally D, Forsman-Semb K, Uhlin BE: Regulatory cross-talk between adhesin operons in Escherichia coli, *EMBO J*. **2000**, *19*(7):1450-1457.
30. Lindberg S, Xia Y, Sonden B, Goeransson M, Hacker J, Uhlin BE, *Infect. Immun.* **2008**, *76*(2):771-780.
31. Gally DL, Rucker TJ, Blomfield IC, *J Bacteriol* **1994**, *176*(18):5665-5672.
32. Cabib E, Roberts R, Bowers B, *Annu. Rev. Biochem*. **1982**, *51*:763-793.
33. Sokurenko EV, Courtney HS, Maslow J, Siitonen A, Hasty DL, *J Bacteriol* **1995**, *177*(13):3680-3686.
34. Giampapa CS, Abraham SN, Chiang TM, Beachey EH, *J Biol Chem* **1988**, *263*(11):5362-5367.

SUPPLEMENTARY

Aggregometry and Flow Cytometry Assay Results

Results obtained from aggregometry and flow cytometry experiments of the different compound classes are listed below in Tables 1 to 7. rIC_{50}s were calculated by dividing the IC_{50} of the compound of interest by the IC_{50} of the reference compound *n*-heptyl α-D-manno-pyranoside. This leads to rIC_{50} values below 1.0 for derivatives with higher activity than the reference compound and rIC_{50} values above 1.0 for compounds with lower activity than the reference compound.

Table 1. IC_{50} values obtained for **CL** compounds using aggregometry and flow cytometry. n.a.: not active; dash (-): not measured.

Compound	Structure	Aggregometry		Flow cytometry	
		IC_{50} [µM]	rIC_{50}	IC_{50} [µM]	rIC_{50}
***n*-heptyl α-D-manno-pyranoside (reference)**	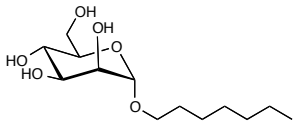	77.1 ± 8.7	1	3.9 ± 1.6	1
α-D-methyl mannoside	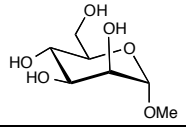	n.a.	-	249.2 ± 62.3	63.8
pNpα mannoside	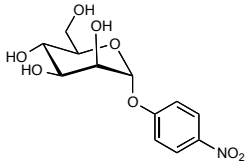	45.1 ± 7.8	0.6	3.2 ± 0.7	0.8
CL14	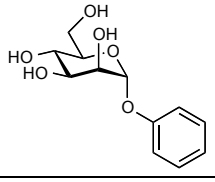	n.a.	-	-	-
CL15	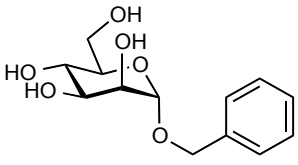	n.a.	-	-	-
CL16	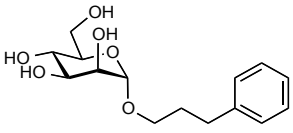	n.a.	-	-	-

Table 2. IC_{50} values obtained for **JH** compounds using aggregometry and flow cytometry. n.a.: not active; dash (-): not measured.

Compound	Structure	Aggregometry		Flow cytometry	
		IC_{50} [µM]	**rIC_{50}**	**IC_{50} [µM]**	**rIC_{50}**
***n*-heptyl α-D-manno-pyranoside (reference)**	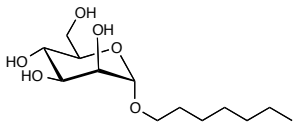	77.1 ± 8.7	1	3.9 ± 1.6	1
JH14.2	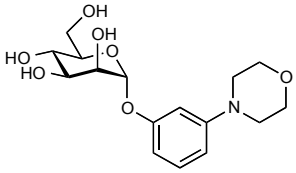	n.a.	-	-	-
JH16.2	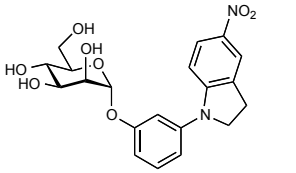	19.2	0.2	-	-
JH17.2	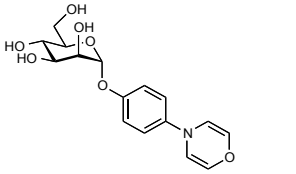	n.a.	-	-	-
JH18.2	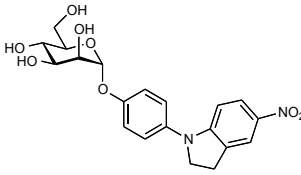	8.7	0.1	-	-

Table 3. IC_{50} values obtained for **JXH** compounds using aggregometry and flow cytometry. n.a.: not active; dash (-): not measured.

Compound	Structure	Aggregometry		Flow cytometry	
		IC_{50} [µM]	rIC_{50}	IC_{50} [µM]	rIC_{50}
***n*-heptyl α-D-manno-pyranoside (reference)**	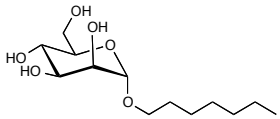	77.1 ± 8.7	1	3.9 ± 1.6	1
JXH001	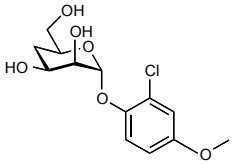	n.a.	-	-	-
JXH016	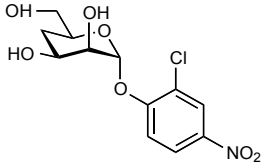	n.a.	-	-	-
JXH031	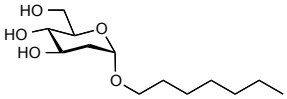	n.a.	-	-	-
JXH039	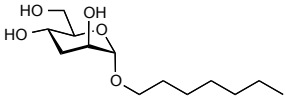	n.a.	-	-	-
JXH041	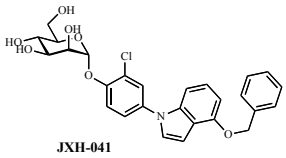	n.a.	-	-	-
JXH046	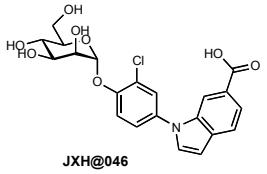	26.8	0.3	-	-
JXH065	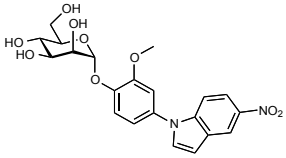	4.1	0.05	-	-
JXH067	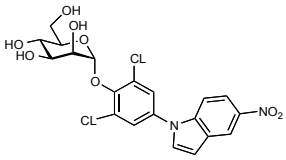	7.1	0.09	-	-

JXH073	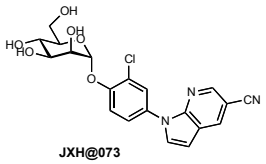 JXH@073	12.8	0.2	-	-
JXH081	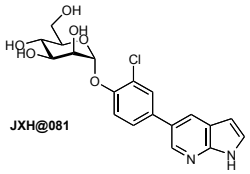 JXH@081	30.9 ± 3.7	0.4	-	-
JXH087	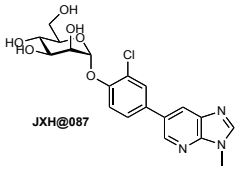 JXH@087	25.3	0.3	-	-
JXH097	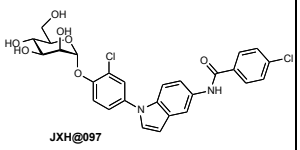 JXH@097	n.a.	-	-	-
JXH099	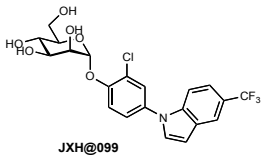 JXH@099	6.4	0.8	-	-
JXH0192	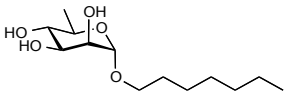	n.a.	-	-	-
JXH0682	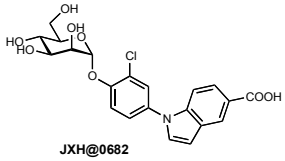 JXH@0682	3.1	0.04	-	-
JXH0751	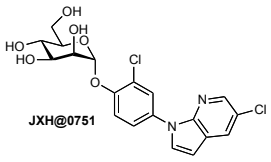 JXH@0751	23	0.3	-	-
JXH101	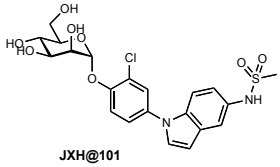 JXH@101	5.6	0.07	-	-
JXH224	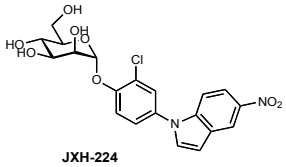 JXH-224	1.3	0.02	0.6 ± 0.05	0.2

JXH232	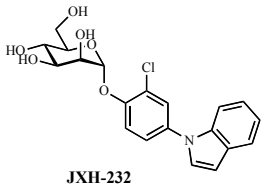 JXH-232	8.3	0.1	-	-
JXH2372	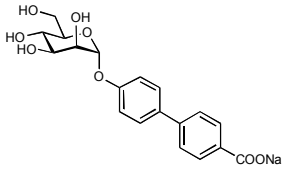	45.1 ± 7.8	0.6	0.9 ± 0.6	0.2
JXH2431	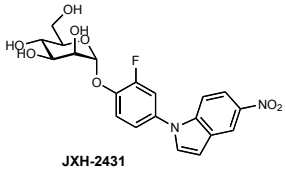 JXH-2431	5	0.06	1	0.3
JXH2432	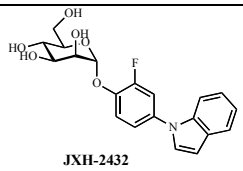 JXH-2432	29.9	0.4	-	-

Table 4. IC_{50} values obtained for **MH** compounds using aggregometry and flow cytometry. n.a.: not active; dash (-): not measured.

Compound	Structure	Aggregometry		Flow cytometry	
		IC_{50} [µM]	**rIC_{50}**	**IC_{50} [µM]**	**rIC_{50}**
***n*-heptyl α-D-manno-pyranoside (reference)**	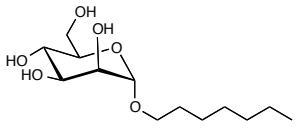	77.1 ± 8.7	1	3.9 ± 1.6	1
MH17	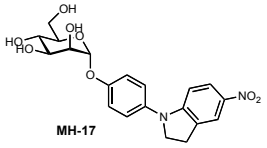 MH-17	25.4 ± 7	0.3	-	-
MH35	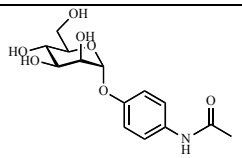 MH-35	105.3	1.4	-	-
MH36	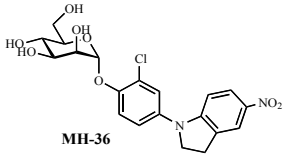 MH-36	n.a.	-	-	-
MH39	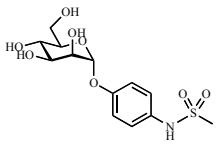 MH-39	225.1	2.9	-	-

Table 5. IC_{50} values obtained for **Mha** compounds using aggregometry and flow cytometry. n.a.: not active; dash (-): not measured.

Compound	Structure	Aggregometry		Flow cytometry	
		IC_{50} [µM]	rIC_{50}	IC_{50} [µM]	rIC_{50}
***n*-heptyl α-D-manno-pyranoside (reference)**	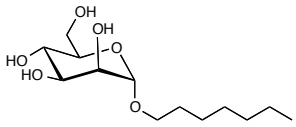	77.1 ± 8.7	1	3.9 ± 1.6	1
Mha8	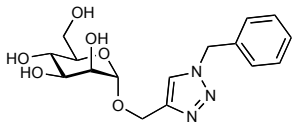	n.a.	-	-	-
Mha10	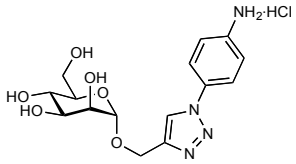	299.1	3.9	-	-
Mha11	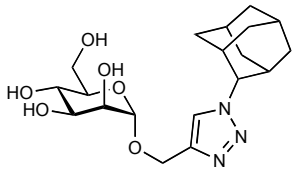	n.a.	-	-	-
Mha19.2	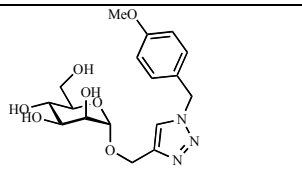	n.a.	-	-	-
Mha20	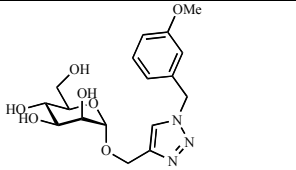	n.a.	-	-	-
Mha28	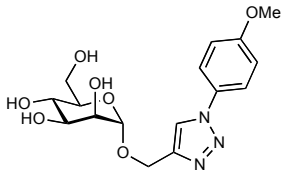	376.4	4.9	-	-
Mha29	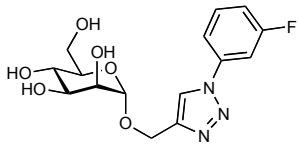	373.8	4.9	-	-
Mha31	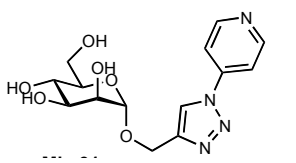	n.a.	-	21.5 ± 1.5	5.5

Mha52	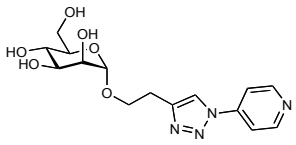	339.1	4.4	-	-
Mha53	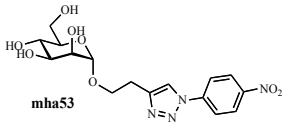	n.a.	-	-	-
Mha54	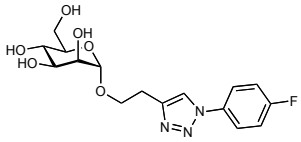	216.2	2.8	-	-

Table 6. IC_{50} values obtained for **OS** compounds using aggregometry and flow cytometry. n.a.: not active; dash (-): not measured.

Compound	**Structure**	**Aggregometry**		**Flow cytometry**	
		IC_{50} [µM]	**rIC_{50}**	**IC_{50} [µM]**	**rIC_{50}**
***n*-heptyl α-D-manno-pyranoside (reference)**	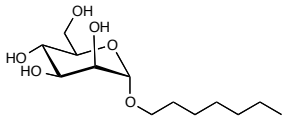	77.1 ± 8.7	1	3.9 ± 1.6	1
OS373	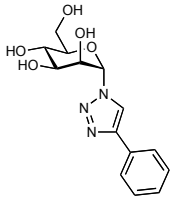	298.6	3.9	-	-
OS376	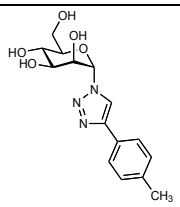	188.3	2.4	-	-
OS377	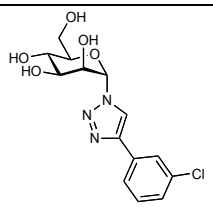	122.9	1.6	-	-
OS380	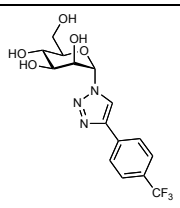	280.9	3.6	-	-

OS381	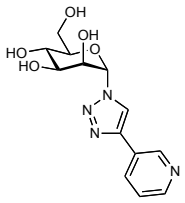	248.5	3.2	-	-
OS383	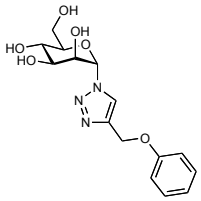	n.a.	-	-	-
OS386	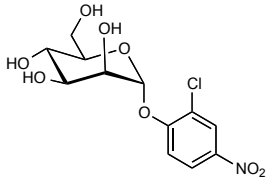	14 ± 1	0.2	1.1 ± 0.5	0.3
OS394	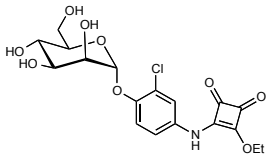	0.85 ± 0.13	0.01	0.04 ± 0.008	0.009
OS395	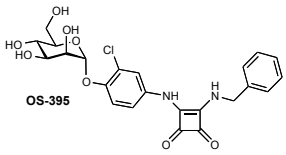	4.4 ± 0.5	0.06	-	-
OS396	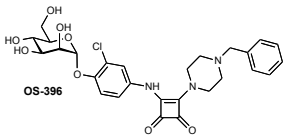	4.5 ± 1.2	0.06	-	-
OS397	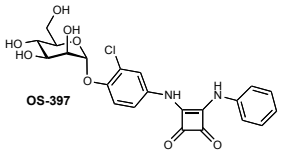	2.1 ± 0.8	0.03	-	-
OS405	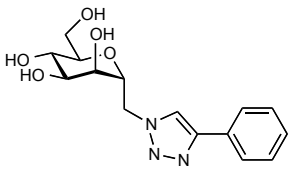	n.a.	-	-	-
OS412	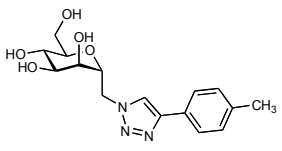	n.a.	-	-	-

OS413	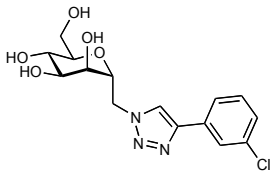	n.a.	-	-	
OS416	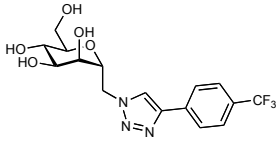	n.a.	-	-	-
OS417	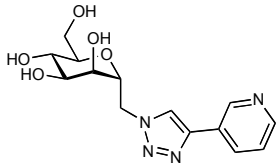	n.a.	-	-	-
OS419	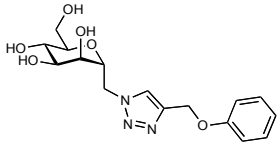	n.a.	-	-	-
OS420	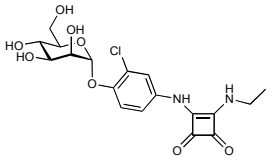	3.3 ± 1.3	0.04	0.1 ± 0.02	0.03
OS421	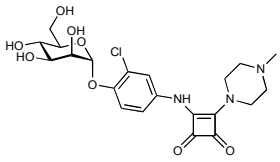	5 ± 1.3	0.06	0.1± 0.2	0.03

Table 7. IC_{50} values obtained for **PLJ** compounds using aggregometry and flow cytometry. n.a.: not active; dash (-): not measured.

Compound	Structure	Aggregometry		Flow cytometry	
		IC_{50} [µM]	**rIC_{50}**	**IC_{50} [µM]**	**rIC_{50}**
***n*-heptyl α-D-manno-pyranoside (reference)**	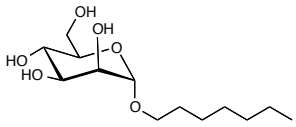	77.1 ± 8.7	1	3.9 ± 1.6	1
PLJ01066A	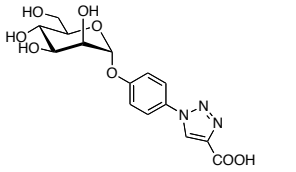	-	-	2.7 ± 0.3	0.7
PLJ01076A	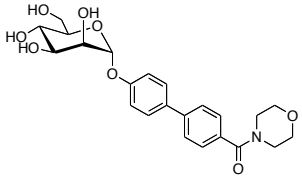	27.2 ± 1.5	0.4	0.8 ± 0.2	0.2
PLJ01089A	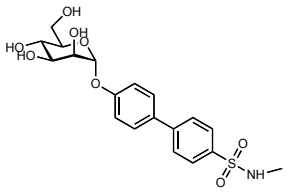	-	-	4.9	1.3
PLJ01089B	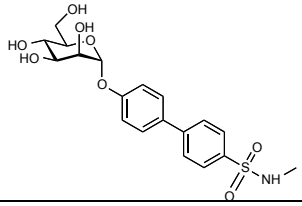	16.8 ± 1.2	0.2	-	-
PLJ01179B	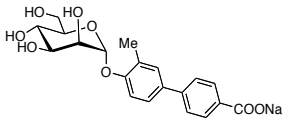	9.1 ± 2.7	0.1	1.8 ± 0.1	0.5
PLJ01178B	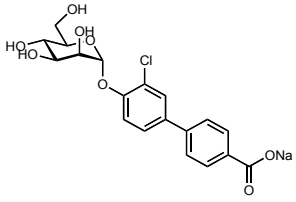	24.5 ± 2.8	0.3	2 ± 0.4	0.5
PLJ01181B	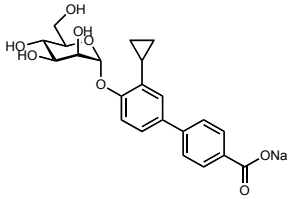	9.5 ± 8.1	0.1	4.9 ± 0.8	1.2

PLJ01194B	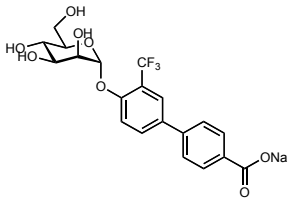	3.4 ± 0.4	0.04	0.9 ± 0.1	0.2
PLJ01175B	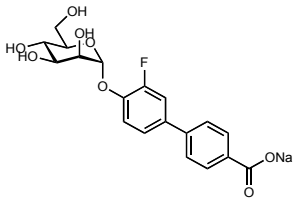	34.4 ± 4.2	0.4	1.5 ± 0.3	0.4

Table 8. IC_{50} values obtained for **TK** compounds using aggregometry and flow cytometry. n.a.: not active; dash (-): not measured.

Compound	**Structure**	**Aggregometry**		**Flow cytometry**	
		IC_{50} [µM]	**rIC_{50}**	**IC_{50} [µM]**	**rIC_{50}**
***n*-heptyl α-D-manno-pyranoside (reference)**	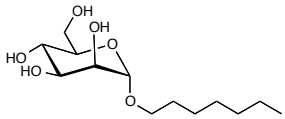	77.1 ± 8.7	1	3.9 ± 1.6	1
TK05	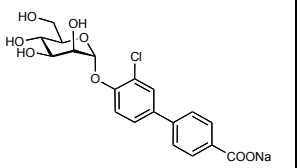	9.2 ± 3.9	0.1	0.3 ± 0.05	0.09
TK14	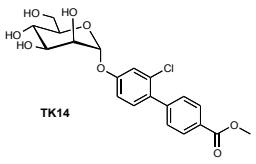	41.6	0.5	-	-
TK15	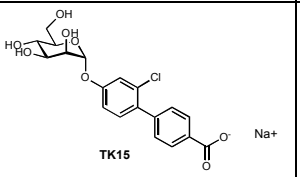	16.8	0.2	0.5 ± 0.06	0.1
TK 16	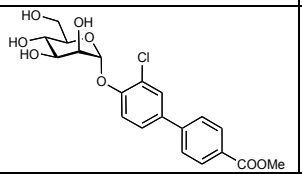	9.2 ± 2.7	0.1	0.2 ± 0.04	0.06
TK17	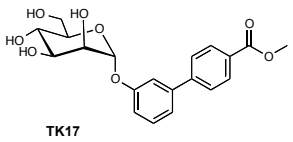	32.8	0.4	-	-

TK18	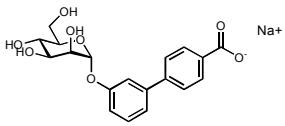	50.6 ± 1.7	0.7	4.5 ± 1.9	1.1
TK19	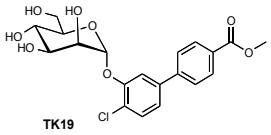	31.2	0.4	-	-
TK20	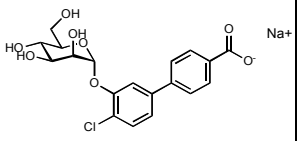	n.a.	-	0.8 ± 0.2	0.2
TK22	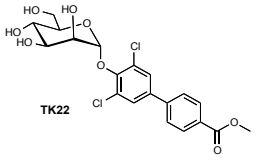	13.8	0.2	-	-

In vivo Pharmacokinetic Study Results

Results obtained from the *in vivo* pharmacokinetic studies in mice of the different classes of FimH antagonists are summarized in the data-sheets below.

Pharmacokinetic Study of TK05 and TK16

Compound	No of animals	Age (weeks)	Dosage	Application
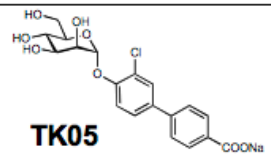 **TK05**	12	9-10	50 mg/kg	p.o. + i.v.
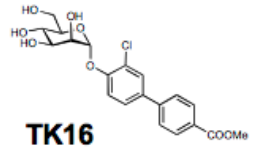 **TK16**	12	9-10	50 mg/kg	p.o. + i.v.

Plasma concentration of **TK05** (applied p.o. as **TK16**)

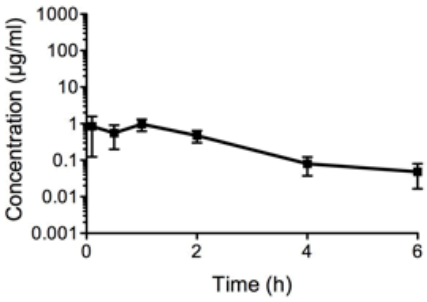

Urine concentration of **TK05** (applied p.o. as **TK16**)

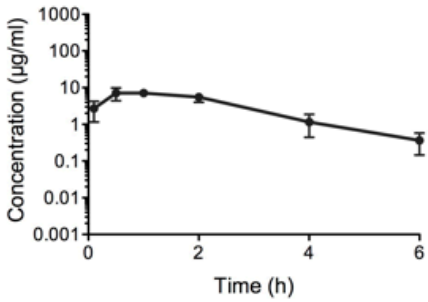

Plasma concentration of **TK05** (i.v.)

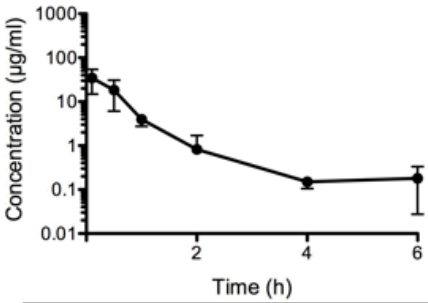

Urine concentration of **TK05** (i.v.)

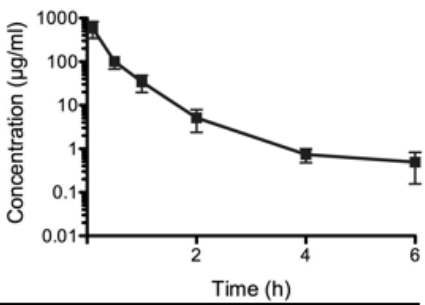

Detected Antagonist	Compartment	AUC_{0-24} (µg x h/ml)
TK05 (p.o.)	**Plasma**	0
	Urine	2.7 ± 3.2
TK05 (applied p.o. as **TK16**)	**Plasma**	2.1 ± 0.6
	Urine	21.7 ± 3.9
TK05 (i.v.)	**Plasma**	22.4 ± 7.2
	Urine	235 ± 58.7

Pharmacokinetic Study of MH17 and MH36

Compound	No of animals	Age (weeks)	Dosage	Application
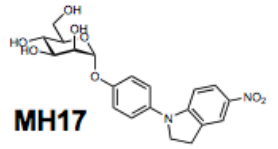 **MH17**	4	10	1 mg/kg	i.v.
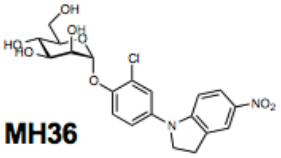 **MH36**	4	10	0.05 mg/kg	i.v.

Plasma concentration of **MH17**

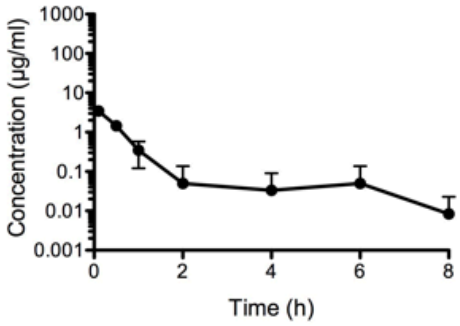

Urine concentration of **MH17**

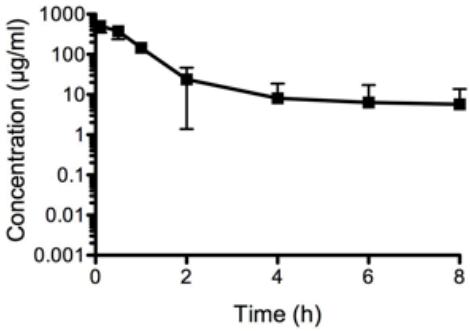

Plasma concentration of **MH36**

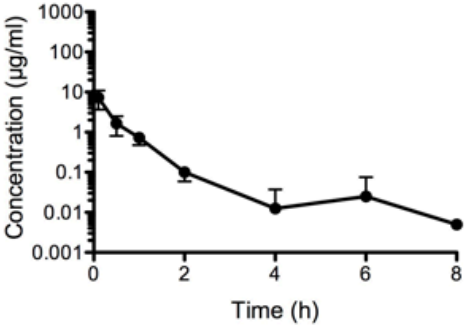

Urine concentration of **MH36**

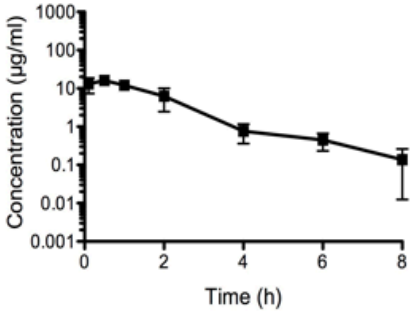

Antagonist	Compartment	AUC_{0-24} (µg x h/ml)
MH17	**Plasma**	2.2 ± 0.8
	Urine	586.4 ± 251.6
MH36	**Plasma**	3.5 ± 1.2
	Urine	33.4 ± 11

Pharmacokinetic Study of JXH224 and JXH232

Compound	No of animals	Age (weeks)	Dosage	Application
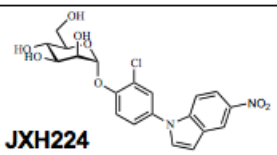 JXH224	4	10	25 mg/kg	i.v.
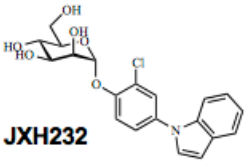 JXH232	4	10	5 mg/kg	i.v.

Plasma concentration of **JXH224**

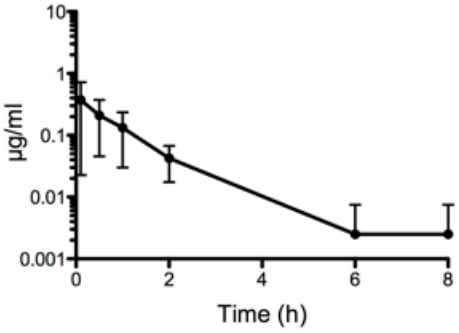

Urine concentration of **JXH224**

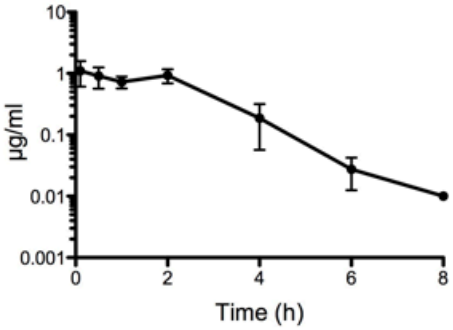

Plasma concentration of **JXH232**

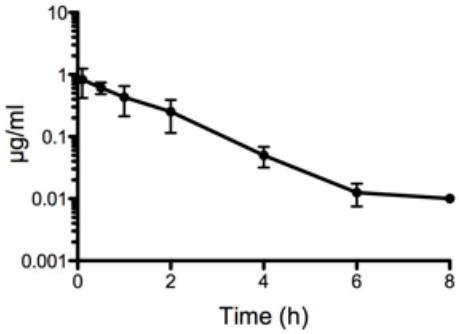

Urine concentration of **JXH232**

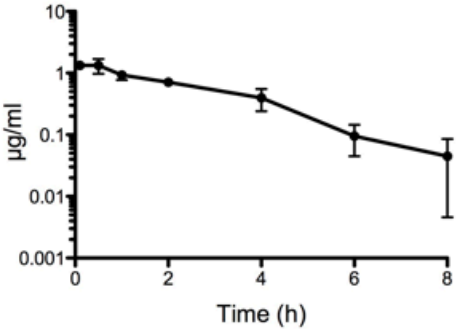

Antagonist	Compartment	AUC_{0-24} (µg x h/ml)
JXH224	**Plasma**	8.2 ± 3.2
	Urine	19.3 ± 3.9
JXH232	**Plasma**	2.3 ± 1.1
	Urine	13.2 ± 4.2

Pharmacokinetic Study of PLJ01076A and PLJ01089A

Compound	No of animals	Age (weeks)	Dosage	Application
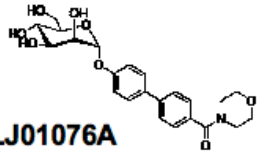 PLJ01076A 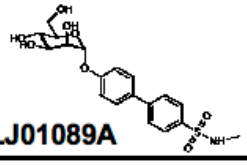 PLJ01089A	6	9	50 mg/kg	i.v.

Plasma concentration of **PLJ01076A**

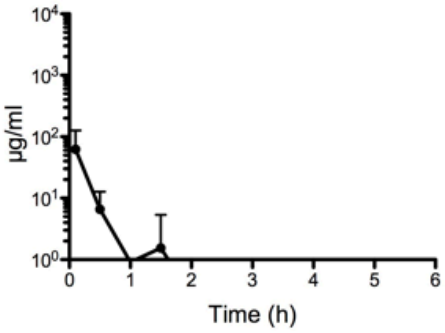

Urine concentration of **PLJ01076A**

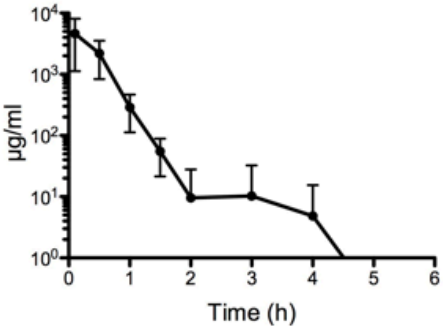

Plasma concentration of **PLJ01089A**

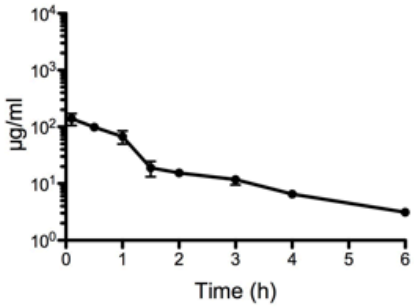

Urine concentration of **PLJ01089A**

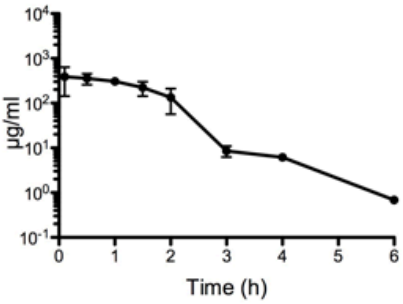

Antagonist	Compartment	AUC_{0-24} (µg x h/ml)
PLJ01076A	**Plasma**	21 ± 18.6
	Urine	2178.8 ± 978.8
PLJ01089A	**Plasma**	175.7 ± 21.6
	Urine	576.6 ± 115.2

Pharmacokinetic Study of the Prodrug WS067

Compound	No of animals	Age (weeks)	Dosage	Application
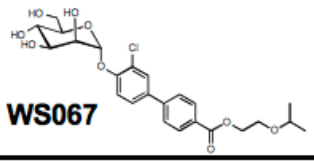 **WS067**	12	9-10	1.3 mg/kg	p.o. + i.v.

Plasma concentration of **TK05** (applied i.v. as **WS067**)

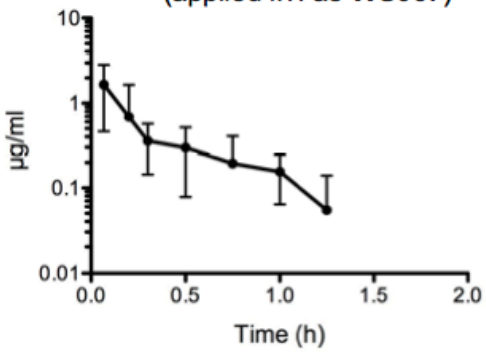

Urine concentration of **TK05** (applied i.v. as **WS067**)

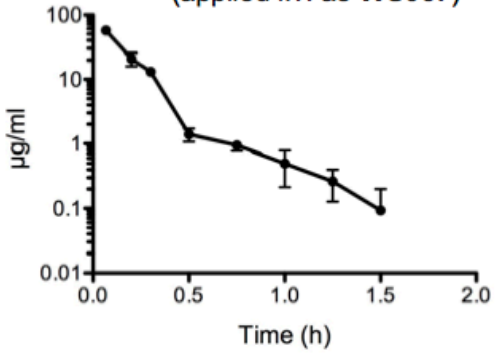

Detected Antagonist	Compartment	AUC_{0-24} (µg x h/ml)
WS067 (p.o.)	**Plasma**	0
	Urine	0
TK05 (applied p.o. as **WS067**)	**Plasma**	0
	Urine	0
WS067 (i.v.)	**Plasma**	0
	Urine	0
TK05 (applied i.v. as **WS067**)	**Plasma**	0.5 ± 0.33
	Urine	9.44 ± 2.5

In vivo Infection Study Results

Results obtained from the *in vivo* infection studies in the UTI mouse model of the different classes of FimH antagonists are summarized in the data-sheets below.

Infection Experiment with UTI89 dFimA-H

Compound	No of animals	Age (weeks)	Dosage and Application
-	6	9	-

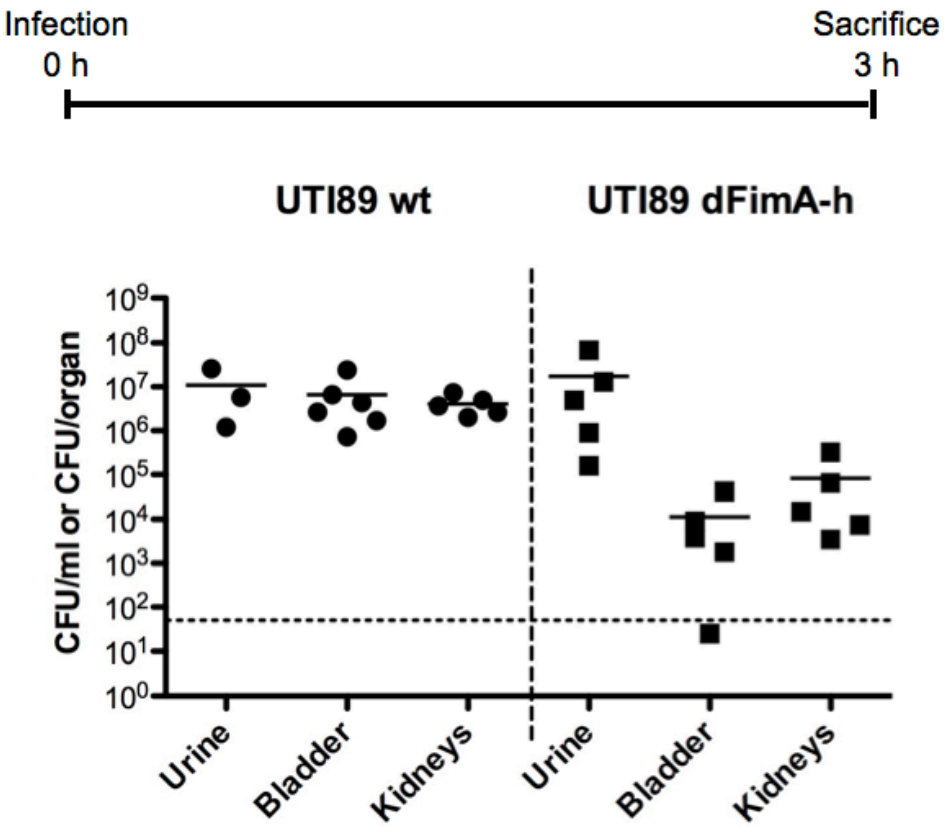

Mean bacterial counts (CFU/ml or CFU/organ)

	UTI89 wt	UTI89 dFimA-H
Urine	1.1×10^7	1.7×10^7
Bladder	6.7×10^6	3.7×10^3
Kidneys	4.1×10^6	8.2×10^4

UTI Prevention Study of TK05 and TK16

Compound	No of animals	Age (weeks)	Dosage	Application
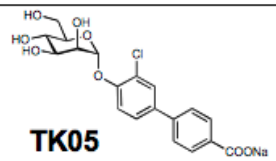 TK05	6	9	50 mg/kg	i.v.
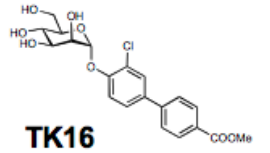 TK16	6	9	50 mg/kg	p.o.

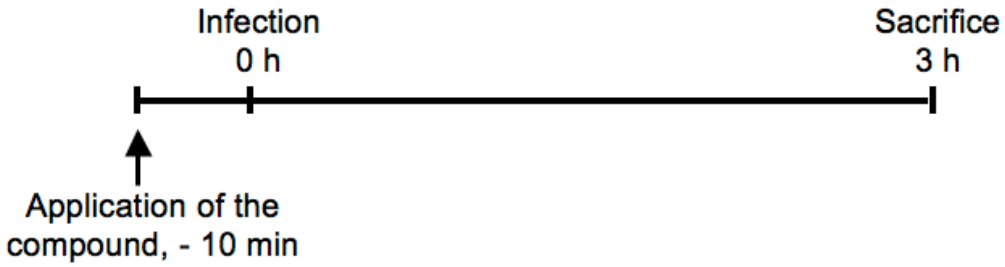

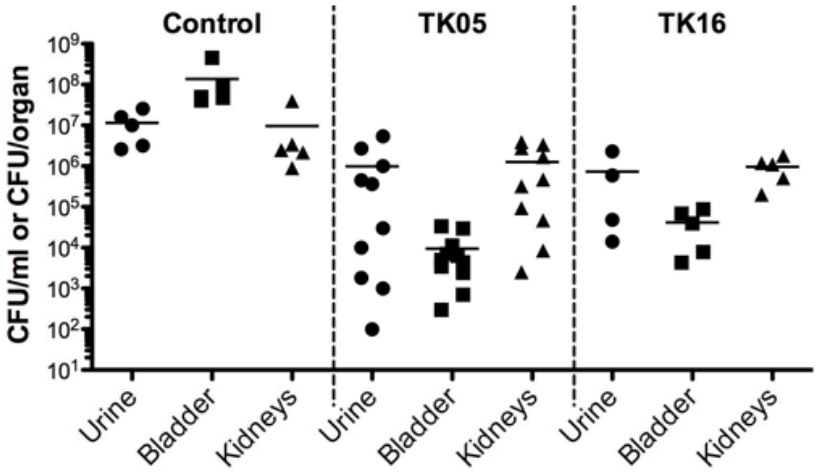

Mean bacterial counts (CFU/ml or CFU/organ)

	Control	TK05	TK16
Urine	1.2×10^7	9.9×10^5	7.4×10^5
Bladder	1.2×10^8	9.4×10^3	4.1×10^4
Kidneys	9.7×10^6	1.3×10^6	9.6×10^5

UTI Prevention Study of MH17

Compound	No of animals	Age (weeks)	Dosage	Application
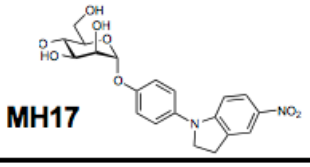 MH17	14	9	10 mg/kg	i.v.

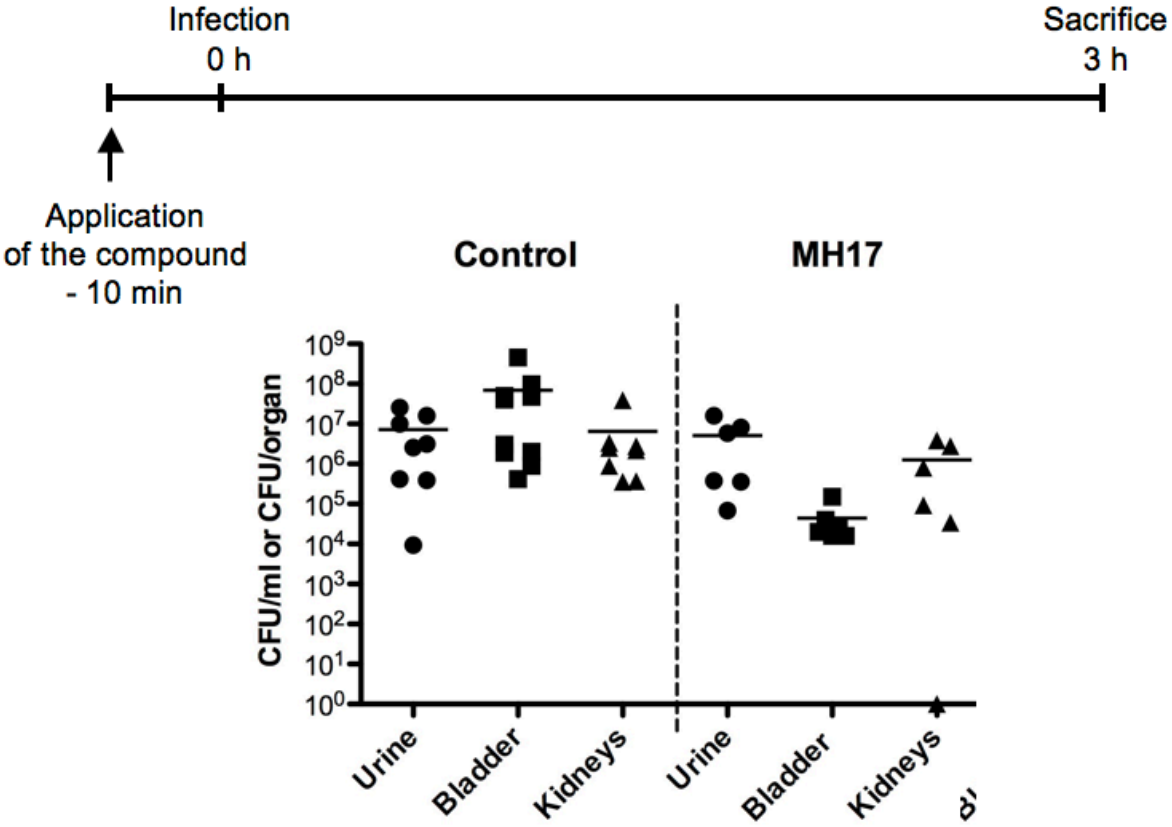

Mean bacterial counts (CFU/ml or CFU/organ)

	Control	MH17
Urine	7.3×10^7	5.1×10^6
Bladder	7×10^7	4.5×10^4
Kidneys	6.5×10^6	1.3×10^6

Multiple Dosage UTI Treatment Experiment of MH17

Compound	No of animals	Age (weeks)	Dosage	Application
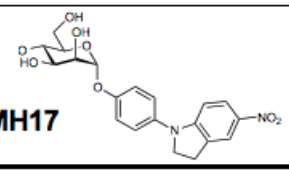 MH17	14	9	10mg/kg	i.v.

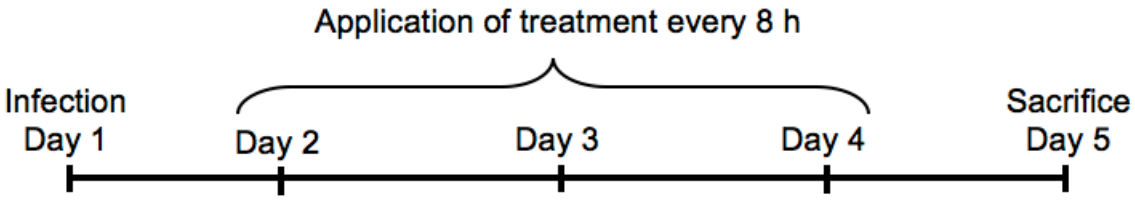

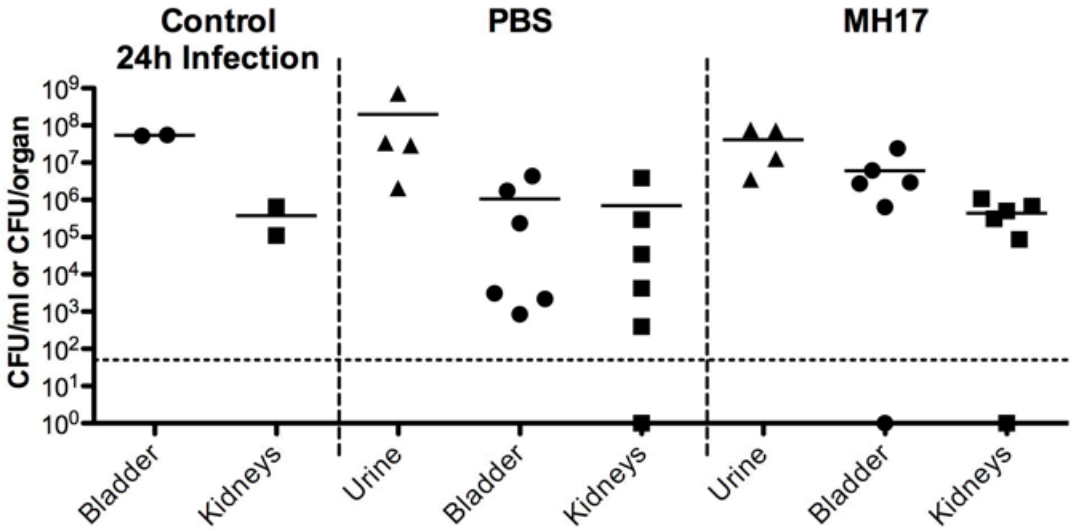

Mean bacterial counts (CFU/ml or CFU/organ)

	Control 24 h	PBS	MH17
Urine	-	2×10^8	4.2×10^7
Bladder	5.4×10^7	1.1×10^6	6.1×10^6
Kidneys	3.8×10^5	7.1×10^5	4.4×10^5

UTI Prevention Study of Ciprofloxacin (CIP)

Compound	No of animals	Age (weeks)	Dosage	Application
CIP 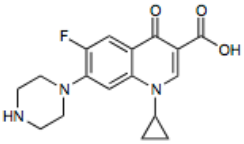	6	9	8 mg/kg	s.c.

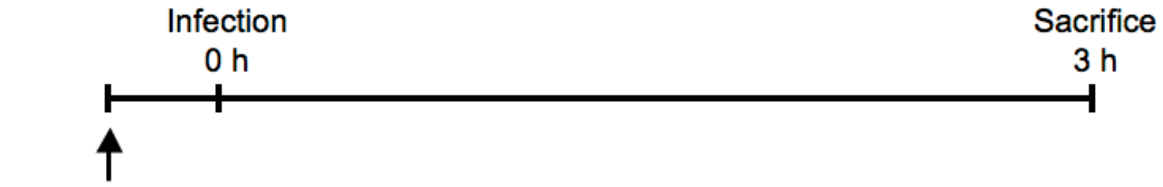

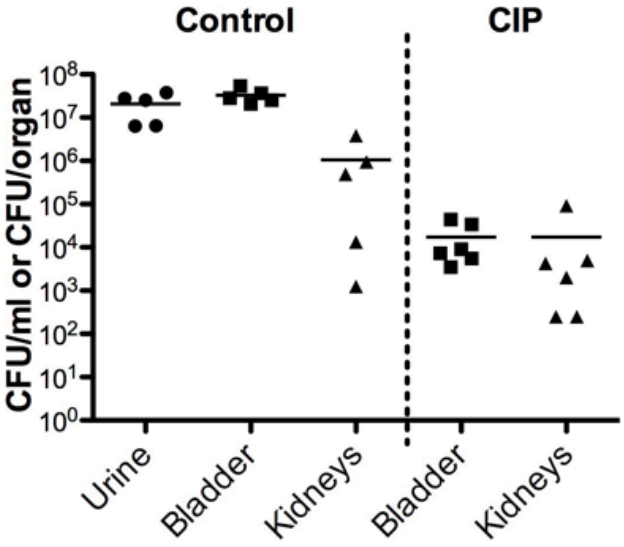

Mean bacterial counts (CFU/ml or CFU/organ)

	Control	CIP
Urine	2.1×10^7	-
Bladder	3.3×10^7	1.7×10^4
Kidneys	1.1×10^6	1.7×10^6

UTI Treatment Experiment - Application of OS421 and Ciprofloxacin (CIP) 1 h after Infection

Compound	No of animals	Age (weeks)	Dosage and Application
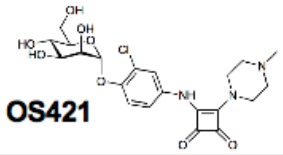 OS421	18	9	OS421: 50 mg/kg i.v. CIP: 8 mg/kg s.c.

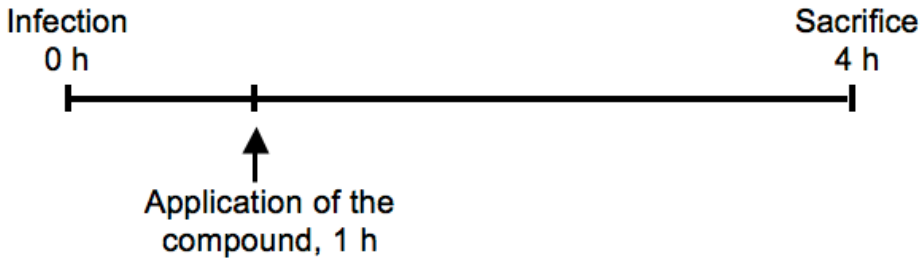

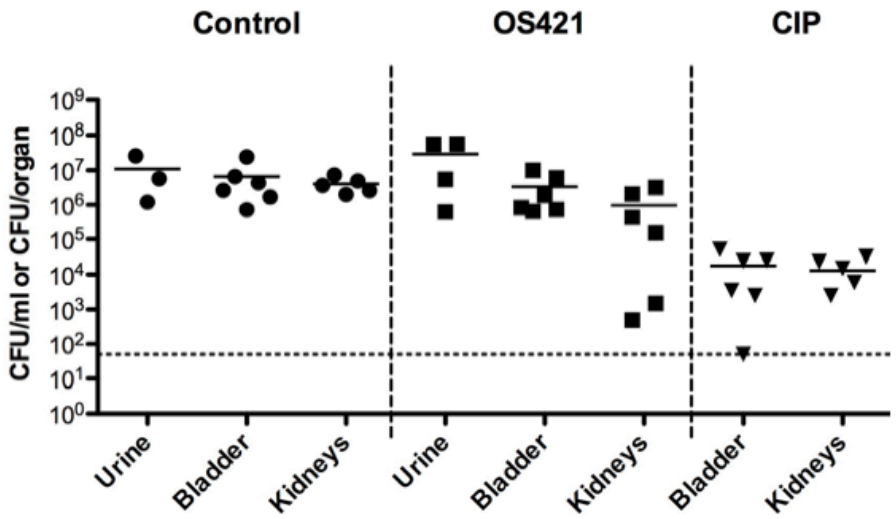

Mean bacterial counts (CFU/ml or CFU/organ)

	Control	OS421	CIP
Urine	1.1×10^7	2.9×10^7	-
Bladder	6.7×10^6	3.4×10^6	1.8×10^4
Kidneys	4.1×10^6	9.6×10^5	1.3×10^4

In vivo Type 1 pili Expression Analysis of the Clinical Isolates B1 39 and B1 59

Compound	No of animals	Age (weeks)	Dosage	Application
-	12	9	-	-

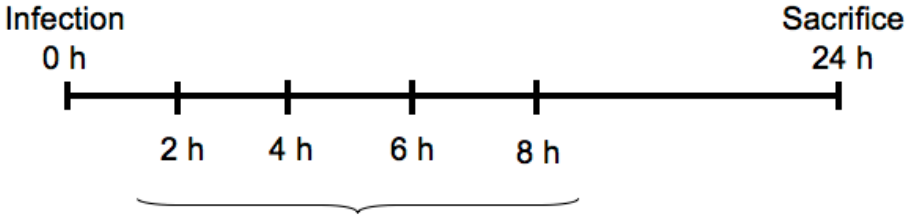

Urine sampling for immunostaining followed by flow cytometry analysis for the determination of *in vivo* type 1 pili expression.

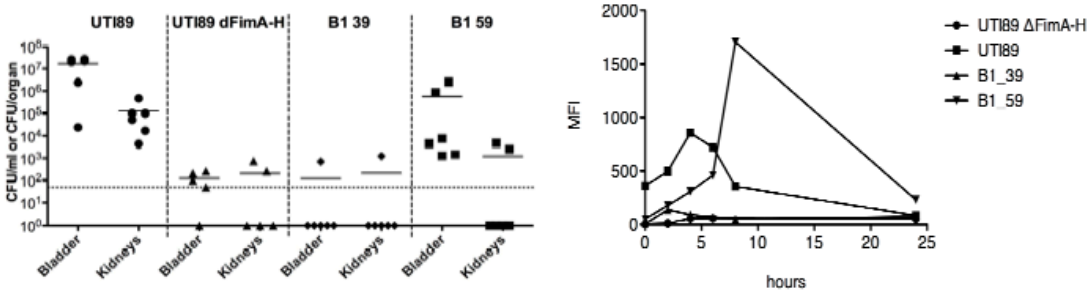

Mean bacterial counts (CFU/ml or CFU/organ)

	UTI89	UTI89 dFimA-H	B1 39	B1 59
Bladder	1.7×10^7	120	120	5.6×10^5
Kidneys	1.2×10^5	200	210	1200

In vivo Pharmacokinetic/Pharmacodynamic Study Results

Results obtained from the *in vivo* pharmacokinetic/pharmacodynamic studies in mice of the different classes of FimH antagonists are summarized in the data-sheets below.

PK/PD Study of HM

Compound	No of animals	Age (weeks)	Dosage	Application
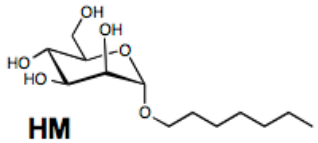 HM	16	9 - 10	25, 50 and 100 mg/kg	i.v.

Plasma concentration of **HM** 25 mg/kg

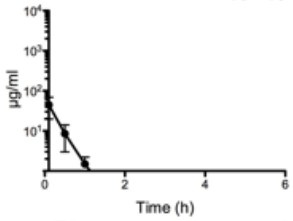

Urine concentration of **HM** 25 mg/kg

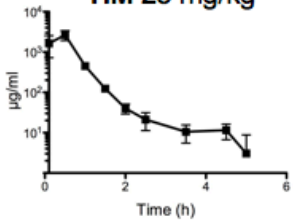

Plasma concentration of **HM** 50 mg/kg

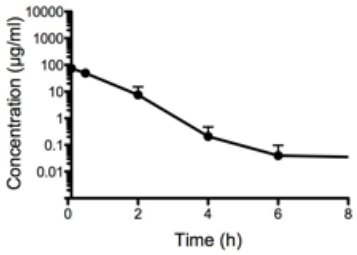

Urine concentration of **HM** 50 mg/kg

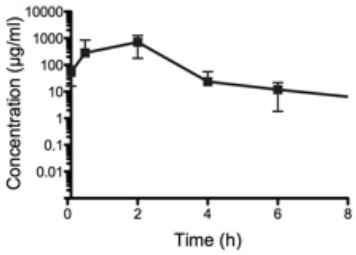

Plasma concentration of **HM** 100 mg/kg

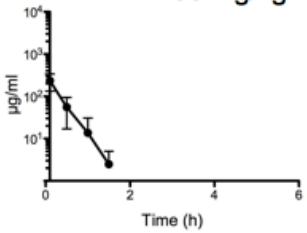

Urine concentration of **HM** 100 mg/kg

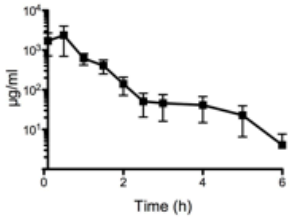

Detected Antagonist	Compartment	AUC_{0-24} (µg x h/ml)
HM 25 mg/kg	Plasma	16 ± 8.8
	Urine	1902 ± 487
HM 50 mg/kg	Plasma	97.9 ± 88.1
	Urine	1974 ± 1398
HM 100 mg/kg	Plasma	91.9 ± 35
	Urine	2115 ± 752

PK/PD Study of HM

Compound	No of animals	Age (weeks)	Dosage	Application
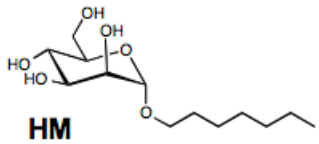 HM	18	9 - 10	25, 50 and 100 mg/kg	i.v.

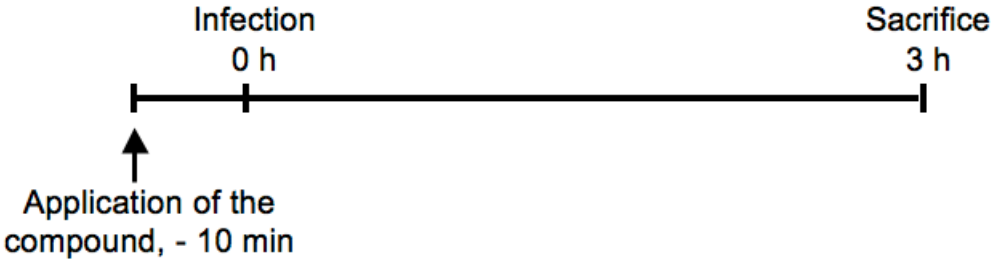

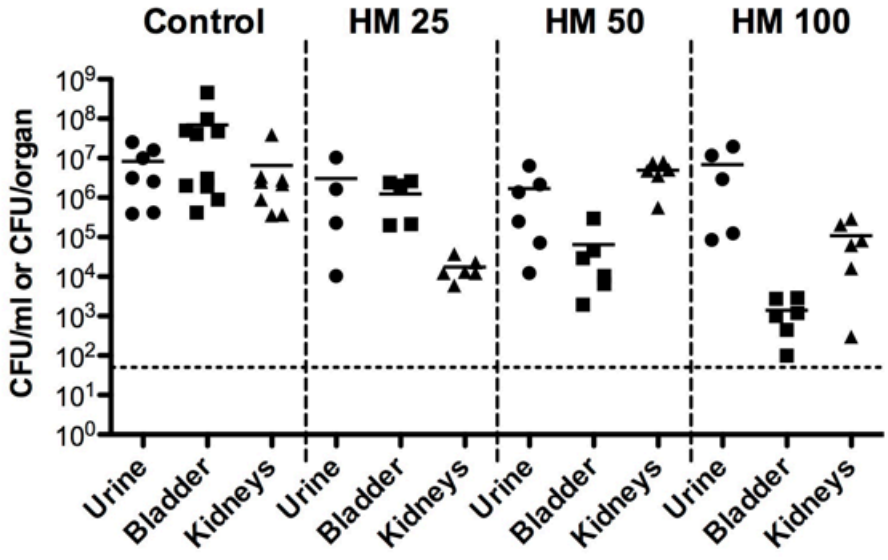

Mean bacterial counts (CFU/ml or CFU/organ)

	Control	HM 25 mg/kg	HM 50 mg/kg	HM 100 mg/kg
Urine	8.3×10^6	3.1×10^6	1.7×10^6	6.9×10^6
Bladder	7×10^7	1.2×10^6	6.5×10^4	1.4×10^3
Kidneys	6.5×10^6	1.7×10^4	5×10^6	1.1×10^5

PK/PD Study of OS421

Compound	No of animals	Age (weeks)	Dosage	Application
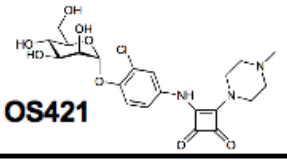 OS421	18	9 - 10	25, 50 and 100 mg/kg	i.v.

Plasma concentration of **OS421** 25 mg/kg

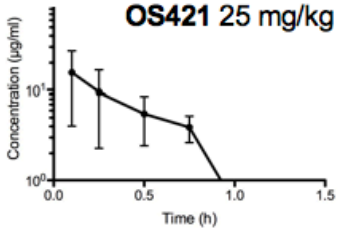

Urine concentration of **OS421** 25 mg/kg

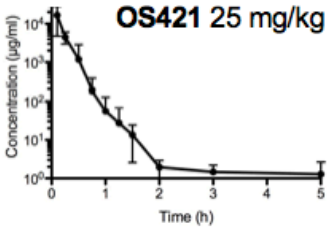

Plasma concentration of **OS421** 50 mg/kg

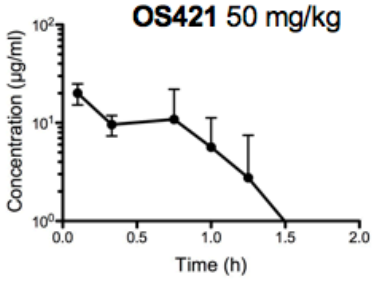

Urine concentration of **OS421** 50 mg/kg

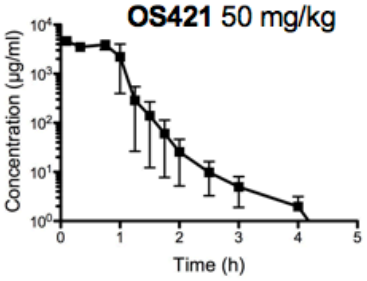

Plasma concentration of **OS421** 100 mg/kg

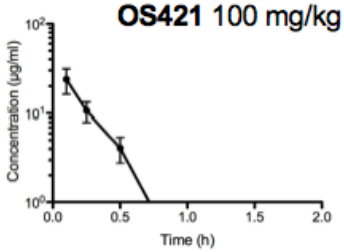

Urine concentration of **OS421** 100 mg/kg

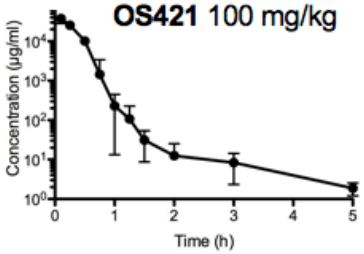

Detected Antagonist	Compartment	AUC_{0-24} (µg x h/ml)
OS421 25 mg/kg	**Plasma**	6.6 ± 3.3
	Urine	3518 ± 2083
OS421 50 mg/kg	**Plasma**	23.4 ± 11.9
	Urine	4660 ± 1909
OS421 100 mg/kg	**Plasma**	6.7 ± 1.8
	Urine	11183 ± 2386

PK/PD Study of OS421

Compound	No of animals	Age (weeks)	Dosage	Application
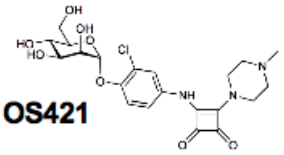 OS421	18	9 - 10	25, 50 and 100 mg/kg	i.v.

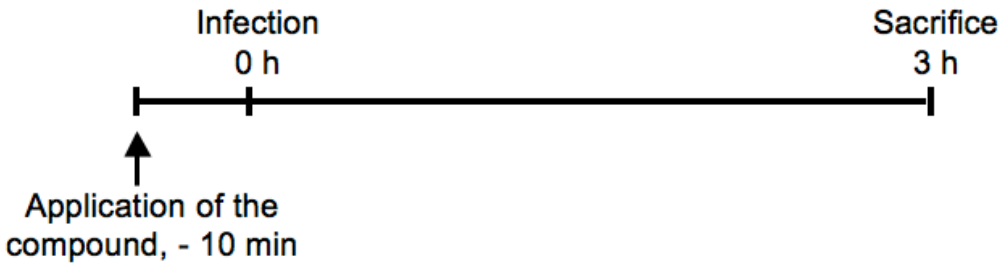

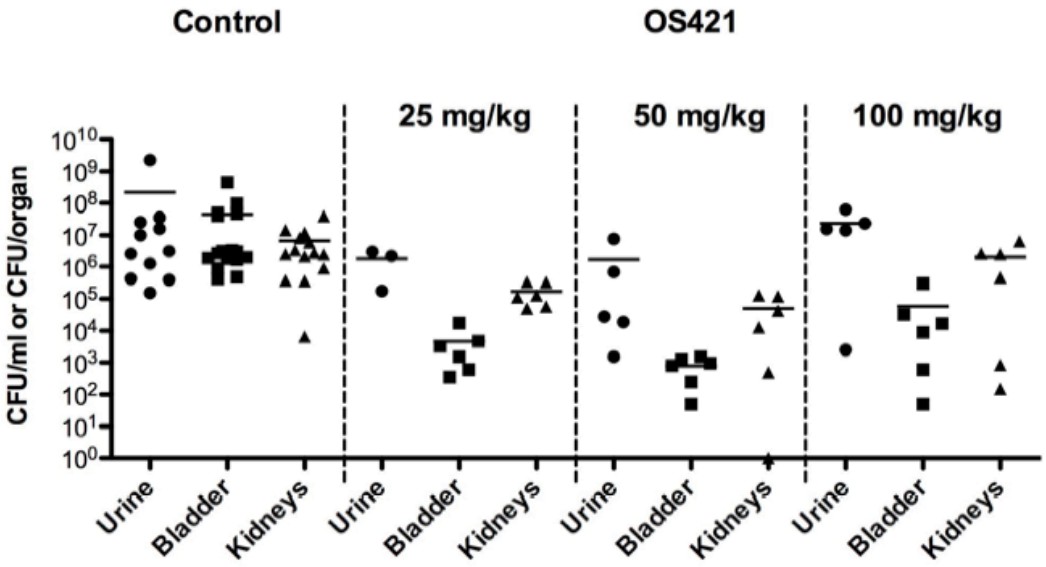

Mean bacterial counts (CFU/ml or CFU/organ)

	Control	OS421 25 mg/kg	OS421 50 mg/kg	OS421 100 mg/kg
Urine	2.0×10^8	1.8×10^6	1.7×10^6	2.3×10^7
Bladder	4.5×10^7	4.6×10^3	7.9×10^2	5.9×10^4
Kidneys	6.8×10^6	1.7×10^5	5.1×10^4	2×10^6

PK/PD Study of JXH2372

Compound	No of animals	Age (weeks)	Dosage	Application
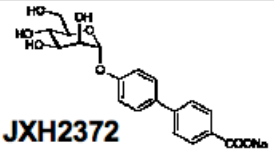 JXH2372	18	9 - 10	25, 50 and 100 mg/kg	i.v.

Plasma concentration of **JXH2372** 25 mg/kg

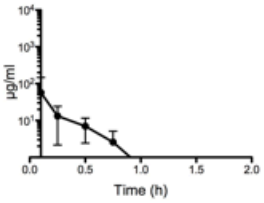

Urine concentration of **JXH2372** 25 mg/kg

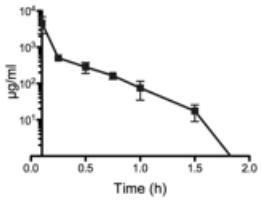

Plasma concentration of **JXH2372** 50 mg/kg

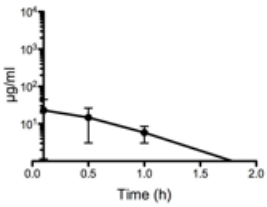

Urine concentration of **JXH2372** 50 mg/kg

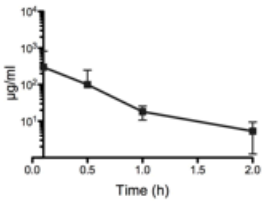

Plasma concentration of **JXH2372** 100 mg/kg

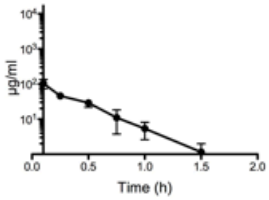

Urine concentration of **JXH2372** 100 mg/kg

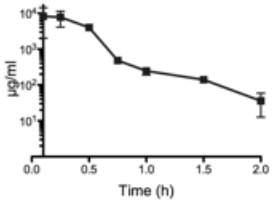

Detected Antagonist	Compartment	AUC_{0-24} (µg x h/ml)
JXH2372 25 mg/kg	**Plasma**	7.6 ± 4.2
	Urine	1056 ± 548
JXH2372 50 mg/kg	**Plasma**	18.6 ± 6.3
	Urine	139.6 ± 118.8
JXH2372 100 mg/kg	**Plasma**	35 ± 5.8
	Urine	3737 ± 1268

PK/PD Study of JXH2372

Compound	No of animals	Age (weeks)	Dosage	Application
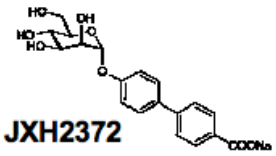 JXH2372	18	9 - 10	25, 50 and 100 mg/kg	i.v.

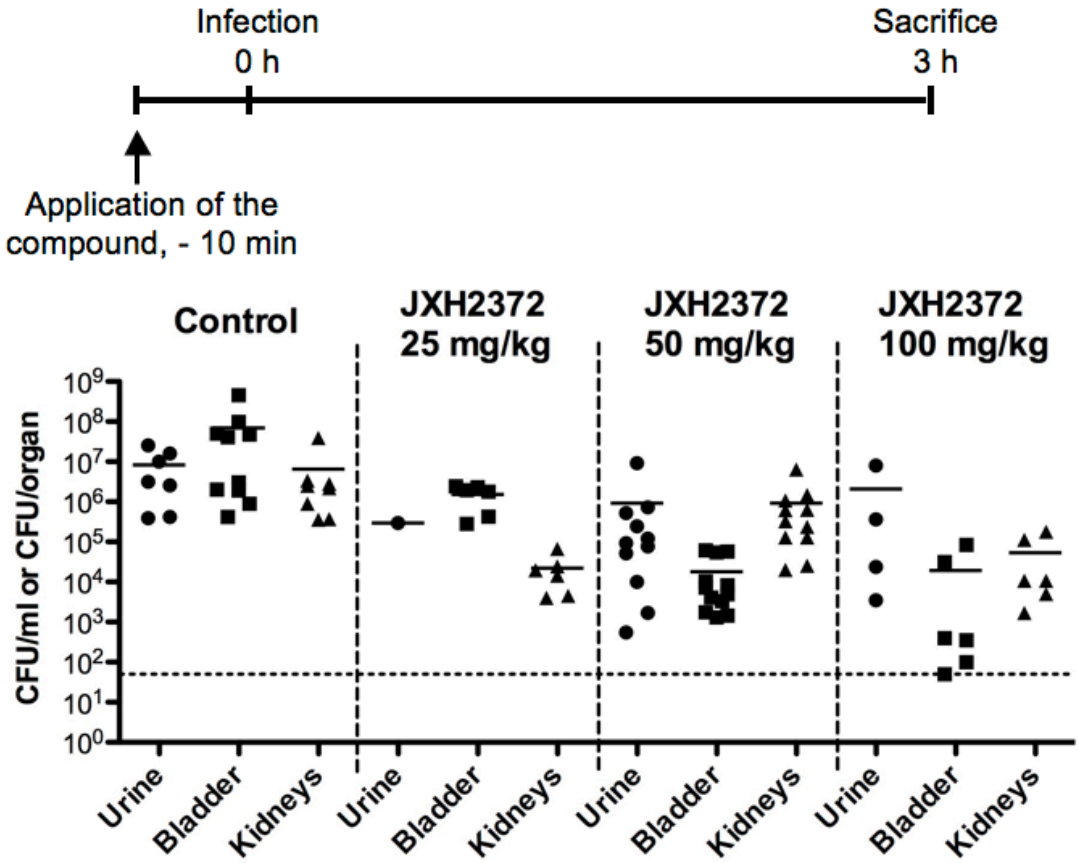

Mean bacterial counts (CFU/ml or CFU/organ)

	Control	JXH2372 25 mg/kg	JXH2372 50 mg/kg	JXH2372 100 mg/kg
Urine	8.3×10^6	3×10^5	9.2×10^5	2.1×10^6
Bladder	7×10^7	1.5×10^6	1.8×10^4	1.9×10^4
Kidneys	6.5×10^6	2.2×10^4	9.2×10^5	5.3×10^4

PK/PD Dosefraction Study of JXH2372

Compound	No of animals	Age (weeks)	Dosage	Application
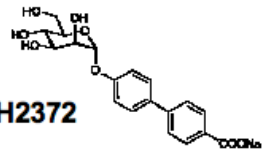 JXH2372	6	9	3x 16.7 mg/kg (total 50 mg/kg)	i.v.

Plasma and urine sampling at following time points: 4 min, 8 min, 12 min, 18 min, 30 min, 45 min, 1 h, 1 h 4 min, 1 h 8 min, 1 h 12 min, 1 h 16 min, 1 h, 30 min, 1 h 45 min, 2 h, 2 h 4 min, 2 h 8 min, 2 h 12 min, 2 h 16 min, 2 h, 30 min, 2 h 45 min, 3 h, 3 h 15 min, 3 h 30 min, 4 h, 4 h 30 min, 5 h, 6 h, 7 h, 8 h, 24 h.

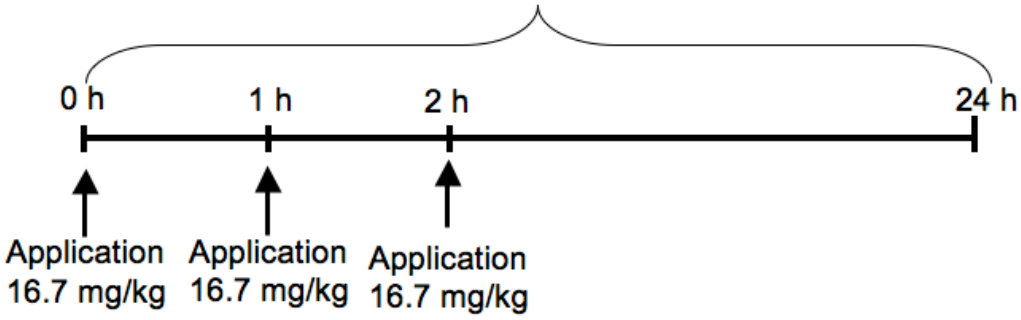

Plasma concentration of **JXH2372**

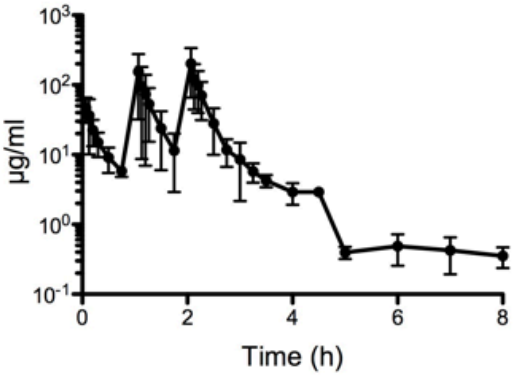

Urine concentration of **JXH2372**

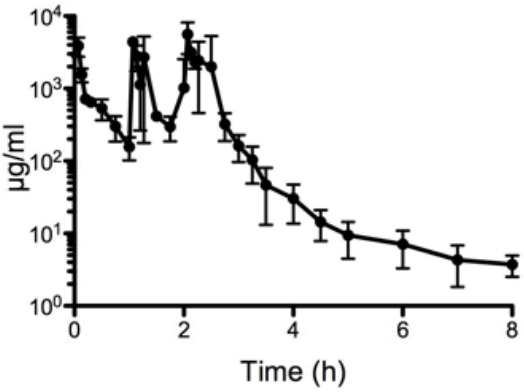

Antagonist	Compartment	AUC_{0-24} (µg x h/ml)
JXH2372	Plasma	162.05 ± 77.42
	Urine	3553.5 ± 906.3

PK/PD Dosefraction Study of JXH2372

Compound	No of animals	Age (weeks)	Dosage	Application
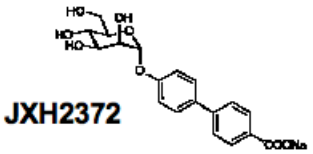 JXH2372	6	9	3x 16.7 mg/kg (total 50 mg/kg)	i.v.

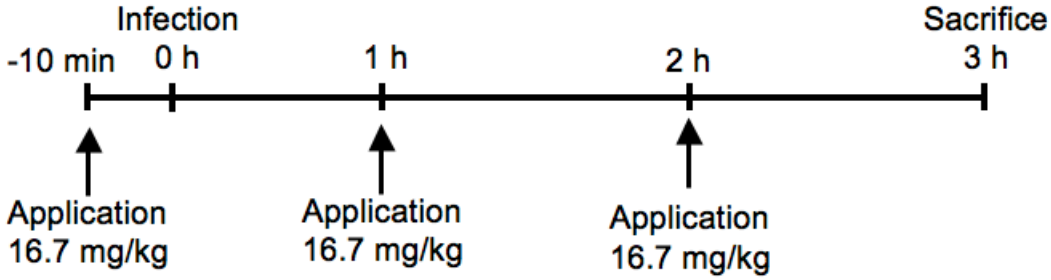

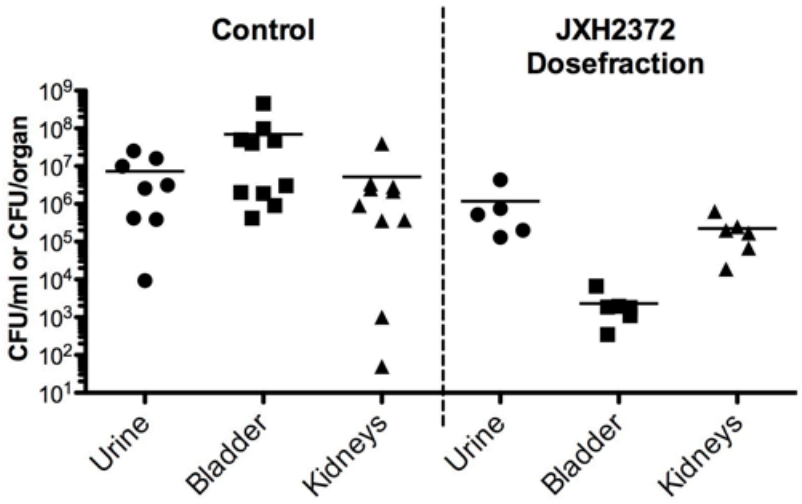

Mean bacterial counts (CFU/ml or CFU/organ)

	Control	JXH2372
Urine	8.3×10^6	1.18×10^6
Bladder	7×10^7	2292
Kidneys	6.47×10^6	2.25×10^5

PK/PD Study - Dosage Regimens of JXH2372

Compound	No of animals	Age (weeks)	Dosage	Application
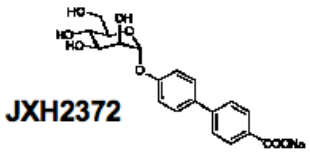 JXH2372	24	10	Dosage Regimen E, L, M, X, Y, Z	i.v.

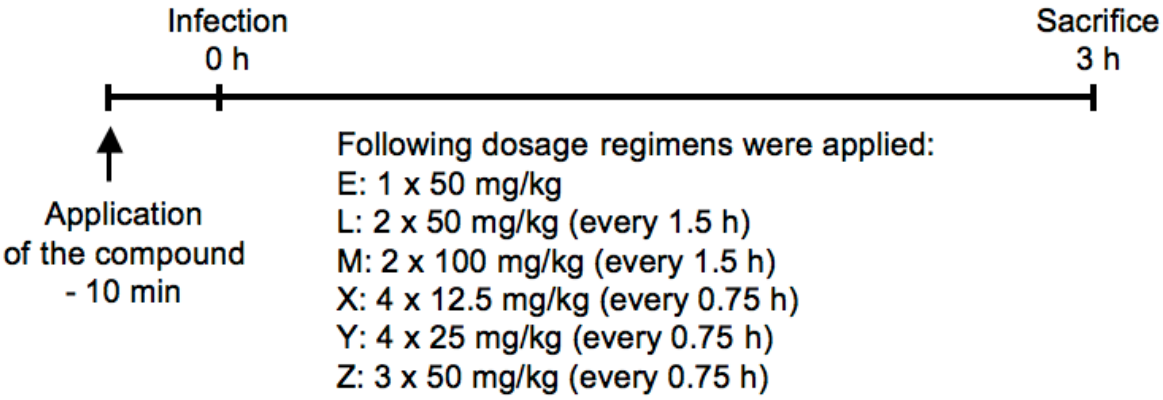

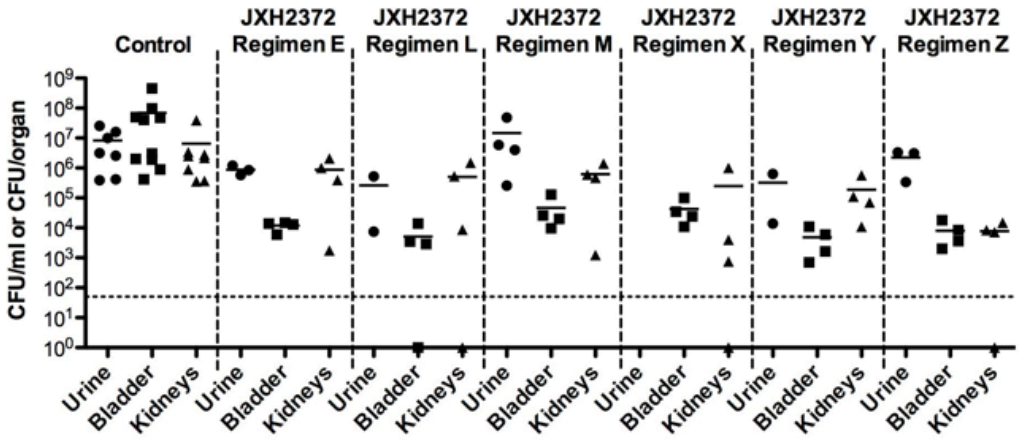

Mean bacterial counts (CFU/ml or CFU/organ)

	Control	Reg. E	Reg. L	Reg. M	Reg. X	Reg. Y	Reg. Z
U	8.29×10^6	8.77×10^5	2.64×10^5	1.45×10^7	-	3.22×10^5	2.25×10^6
B	6.99×10^7	1.2×10^4	5100	4.64×10^4	4.25×10^4	4838	8038
K	6.47×10^6	8.75×10^5	5.1×10^5	6.18×10^5	2.51×10^5	1.9×10^5	7688